Chemical Investigation

of

Streptomyces Albus Heterologous Expression Strains

and

The Biosynthesis of the Aromatic Polyketide Griseorhodin A

Dissertation

zur Erlangung des Doktorgrades (Dr. rer. nat.)

der

Mathematisch-Naturwissenschaftlichen Fakultät

der

Rheinischen Friedrich-Wilhelms-Universität Bonn

vorgelegt von

Zeynep Sabahat Yunt

aus

İstanbul, Türkei

Bonn 2012

Angefertigt mit Genehmigung der Mathematisch-Naturwissenschaftlichen Fakultät der Rheinischen Friedrich-Wilhelms-Universität Bonn.

Gutachter:
1. Prof. Dr. Jörn Piel
2. Prof. Dr. Arne Lützen
3. Prof. Dr. Ulrich Kubitscheck
4. Prof. Dr. Gabriele König

Tag der Promotion: 15.05.2012.

Erscheinungsjahr:2012

Für meine Eltern

DANKSAGUNG

Die vorliegende Arbeit wurde am Kekulé-Institut für Organische Chemie und Biochemie der Rheinischen Friedrich-Wilhelms-Universität Bonn unter Leitung von Prof. Dr. Jörn Piel angefertigt.

An erster Stelle gilt mein Dank Prof. Dr. Jörn Piel, der mir die Gelegenheit gab, die vorliegende Arbeit anzufertigen und mir durch viele wertvolle Ratschläge eine erfolgreiche Durchführung ermöglichte. Des Weiteren möchte ich mich bei ihm für das mir entgegengebrachte Vertrauen sowohl hinsichtlich fachlicher als auch organisatorischer Fragestellungen bedanken. Ganz besonders bedanke ich mich für seine Geduld und Unterstützung beim Schreiben meiner Dissertation.

Außerdem möchte ich mich bei Prof. Dr. Arne Lützen für die Übernahme des Zweitgutachtens meiner Dissertation bedanken.

Mein Dank gilt auch den weiteren Mitgliedern der Prüfungskommission Prof. Dr. Ulrich Kubitscheck und Prof. Dr. Gabriele König.

Der Abteilung für Massenanalytik des Kekulé-Instituts möchte ich für die Durchführung der zahlreichen HPLC-MS-Messungen danken, insbesondere Dr. Marianne Engeser für die Hilfe bei den MS/MS-Auswertungen.

Der NMR-Abteilung des Kekulé-Instituts und Prof. Dr. Arne Lützen, Dr. Harald Gross von der Pharmazeutischen Fakültät der Universität Bonn und Doz. Dr. Michael Lalk von der Pharmazeutischen Fakültät der Universität Greifswald möchte ich für die Hilfe bei der Durchführung der NMR-Experimente danken.

Prof. Dr. Gerhard Bringmann von der Universität Würzburg und seinen Mitarbeitern Dr. Torsten Bruhn und Anu Schaumlöffel danke ich für die Kooperation bei der Bestimmung der absoluten Konfiguration der Substanzen Griseorhodin A, Collinone und Precollinone.

Prof. Dr. Michael Gütschow von der Universität Bonn und seiner Mitarbeiterin Stephanie Hautmann danke ich für die Kooperation bei der Bestimmung der Serinproteasen-Hemmung der Substanzen Griseorhodin A, Collinone,

Lenticulone und Didesoxygriseorhodin C und die Kooperation bei den Untersuchungen von der Serine-Proteasen-Hemmung diverser Extrakte.

Prof. Dr. Hans-Martin Dahse von der Leipniz-Institut für Naturstoff-Forschung in Jena danke ich für die Kooperation bei der Bestimmung der Zytotoxizität und der antiproliferativen Wirkung der Substanzen Griseorhodin A, Collinone, Lenticulone und Didesoxygriseorhodin C.

Bei allen derzeitigen und ehemaligen Mitgliedern des Arbeitskreises Piel möchte ich mich für das gute Arbeitsklima bedanken.

Dr. Kathrin Reinhardt danke ich besonders für die molekularbiologische Herstellung vieler interessanter Stämme, sowie Minna Eklund für die gute Zusammenarbeit bei der Aufklärung von Genen der Griseorhodin-Cluster. Dr. Holger Niederkrüger danke ich für die Expression der Proteine für den Grh06 Assay. Zusätzlich möchte ich mich im Speziellen bei Dr. Marija Avramovich, Martina Heycke, Minna Eklund, Thomas Hochmuth, Daniel Flachshaar, Dr. Jana Moldenhauer, Dr. Kathrin Reinhardt, Dr. Cristian Gurgui, Dr. Jing He und Dr. Katrin Zimmermann für die gute gemeinsame Zeit, auch außerhalb des Labors, bedanken.

Für das Korrekturlesen der Arbeit möchte ich mich ganz herzlich bei meinem Professor Dr. Piel, meinem Bruder Dr. Mehmet Yunt, Dr. Simla Başar, und meiner Schwester Elif Yunt bedanken.

Besonderer Dank gilt meinen Eltern, meinem Bruder Mehmet, meiner Schwester Elif, Dr. Marija Avramovich, Dr. Simla Başar sowie meinen Freunden für ihre fortwährende Unterstützung und Hilfe.

Mein größter Dank gilt jedoch Allah, der mir stets den nötigen Willen und die Geduld gab, meine Arbeit zu Ende zu bringen.

CONTENTS

ABBREVIATIONS

ACP	Acyl carrier protein
AN	Acetonitrile
Apr	Apramycin sulfate
Asn synth	Asparagin-synthetase
AT	Acyl-transferase
ATP	Adenosine triphosphate
BLAST	Basic Local Alignment Search Tool
CC_{50}	Half maximal cytotoxicity concentration
CD	Circular dichroism
CID	Collision-induced dissociation
CLF	Chain elongation factor
CYC	Cyclase
^{13}C-NMR	Carbon 13 NMR
CoA	Co enzyme A
COSY	Correlation spectroskopy
CYP450	Cytochrome P-450 monooxygenase
DEPT	Distortionless enhancement by polarization transfer
DH	Dehydratase
DMS	Dimethyl sulfate
DMSO	Dimethyl sulfoxide
ER	Enoyl reductase
ESI-HRMS	Electrospray high-resolution mass spectra
EtAc	Ethyl acetate
FAD	Flavin adenine dinucleotide
FD	Ferrodoxin
GI_{50}	Half maximal growth inhibitory concentration
Grh	Griseorhodin A cluster
GT	Glycosyl transferase
HeLa	Henrietta Lacks (cervical cancer cell line)
HIV	Human immunodeficiency virus
HLE	Human leukocyte elastase
HMBC	Heteronuclear multiple bond correlation
HMQC	Heteronuclear multiple quantum correlation
^{1}H-NMR	Proton NMR
HPLC	High pressure liquid chromatography
HRMS	High resolution mass spectrometry
Huvec	Human umbilical vein endothelial cells
IC_{50}	Half maximal inhibitory concentration
IR	Infrared and raman spectroscopy
K562	Myelogenous leukemia cell line
KR	β-Keto reductase
KS	β-Keto-acyl synthase
LB	Luria Bertani
LC	Liquid chromatography
MAT, MCAT	Malonyl-CoA: ACP transferase
MeOH	Methanol
MS	Mass spectrometry

MT	Methyl transferase
m/z	Mass to charge ratio
NADP	Nicotin adenine dinucleotide
NDP	Nucleoside diphosphate
NMR	Nuclear magnetic resonance
NOE	Nuclear overhauser effect
ORF	Open reading frame
OXY	Oxygenase
P450	Cytochrome P-450 monooxygenase
PKS	Polyketide synthase
PPTase	Phosphopantetheinyl transferase
RP-18	Reverse phase with $SiOC_{18}H_{37}$ material
SAM	S-Adenosylmethionine
SARP	Secreted apoptosis-related protein
TE	thioesterase
TFA	Trifluor acetic acid
TLC	Thin layer chromatographi
Tris	Tris-(hydroxymethyl)-amino methane
TSB	Tryptic soy broth
UV	Ultraviolet

1 INTRODUCTION

1.1 Natural Products as a Source for New Lead Structures

Since the beginning of human civilization, the structurally diverse metabolites of plants and microorganisms have bean a main source for medicals, pigments, dyes, flavors and even poisons. Many of the currently known lead structures for therapeutic agents and pesticides are natural products or their derivatives. Recently discovered marine environment and symbiont microorganisms constitute exciting new sources of pharmacologically active natural products[1] Novel structures observed in all these sources allowed scientists to gain new insight into the structural and functional relationships of active compounds.

For several natural products, efficient synthetic methods were developed for therapeutical and industrial applications. However, in general, the structural complexities of many compounds represent a challenge for long term synthetic supply. Usually many synthetic reaction steps are necessary and the final yield is unsatisfactory. Therefore many promising drug candidates can not be produced on industrial scale using this method. Using the natural source can often be problematic too, since the amount of the metabolite produced is insufficient and the source organisms cannot be cultured to increase production. [2]

Recent developments in the biosynthesis of natural products, combined with advanced techniques in molecular biology, analytical chemistry and genetic engineering, provide promising approaches to overcome these problems and open new possibilities to use Nature's biochemical machineries as tools of discovery and production. These methods and techniques are used to derivatize compounds, investigate the function of genes and construct candidate substance libraries for front line drugs.[3] Metagenomic analysis of species is used to identify and isolate biosynthetic gene clusters of these novel compounds.[4] Then molecular biological methods are employed for the expression of these gene clusters in culturable host species to obtain sufficient amounts of compounds and enzymes in a laboratory environment. Finally, biotechnollogy provides an

opportunity to manipulate gene clusters and to investigate derivatives of the original compound. [5,6]

The focus of this study is polyketide natural products of bacterial origin and their biosynthetic pathways. In the remainder of this Chapter 1, the necessary background to the origin and the biosynthesis of bacterial polyketides is presented.

1.2 Polyketides

Thousands of polyketide metabolites, exhibiting remarkable structural and functional diversity, are reported from various sources such as bacteria, fungi, plants, insects, dinoflagullates, mollusks and sponges.[7] Their wide clinical and industrial applicability makes them one of the most demanded classes of substances. The antibiotic antitumor agent doxorubicin **(1)**,[8,9] the immunosuppressant rapamycin **(2)**,[8,10] the antimalarial ionophore monensin **(3)**, and the erythromycin A **(4)**[11,12] are examples of commercially available polyketide drugs of microbial origin. Figure 1.1 shows the structures of these polyketides having useful pharmacological activities.

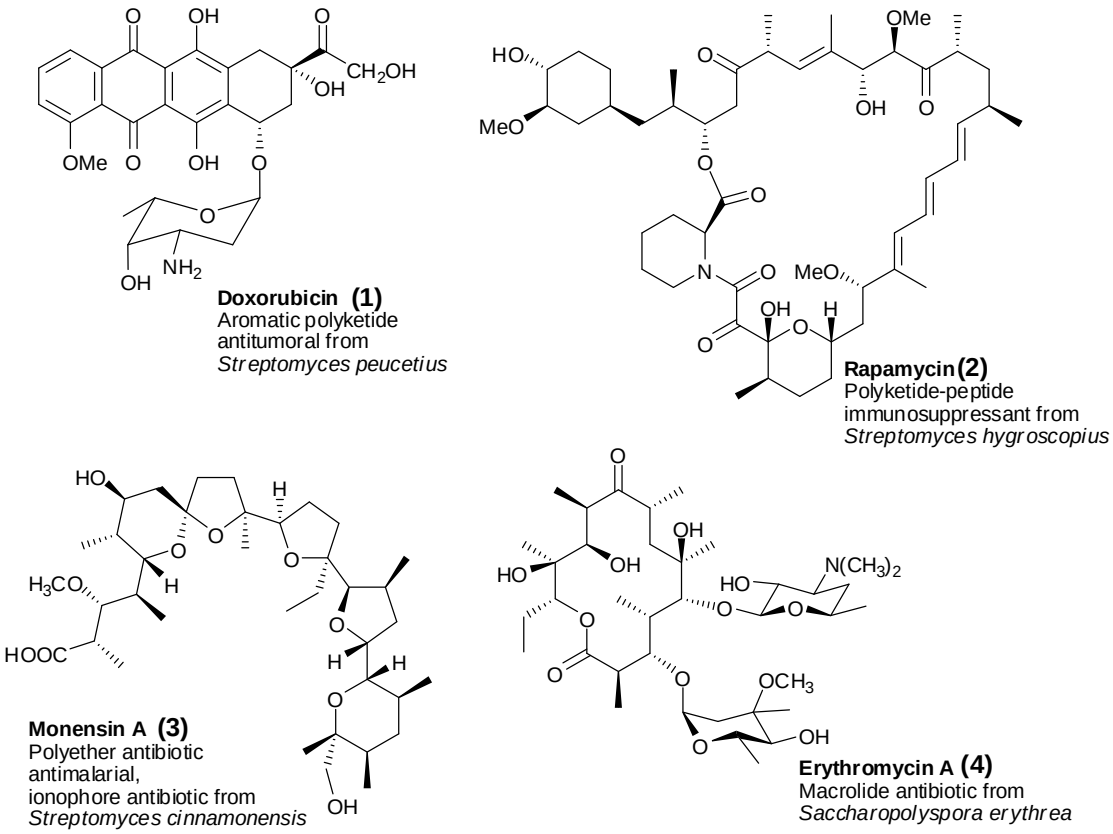

Figure 1.1 Representative structures of commercially used polyketides.[12]

Polyketides are loosely categorized based on their structure as *complex* or *aromatic*, and based on their biosynthesis as *reduced* or *non-reduced.* The biosyntheses of these two classes of polyketides differ significantly.

Polyketides like the polyaromatic compound doxorubicin **(1)** in Figure 1.1 are usually derived from an unreduced form of a poly-β-keto-chain biosynthetic precursor. Hence they are classified as non-reduced. In the case of reduced polyketides, the carbonyl functions of the poly-β-keto-chain have been reduced similar as in fatty acid biosynthesis. The two main classes of *reduced polyketides* are macrolides, such as erythromycin **(4)** and rapamycin **(2)**, and polyethers, such as monensin A **(3)**.[13, 11]

In this thesis, the compound griseorhodin A **(5)**, a rare bacterial aromatic polyketide with a highly complex aromatic spiro ketal structure, is investigated. It was isolated from *Streptomyces californicus* JA2640[14] and *Streptomyces sp.* JP95.[15] Figure 1.2 shows the structure of the polyketide.

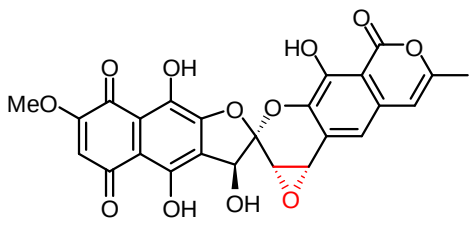

Griseorhodin A (5)

Figure 1.2 Structure of griseorhodin A (5).

1.3 Biosynthesis of Polyketides and Different Types of Polyketide Synthases

The biosynthesis of polyketides involves the stepwise formation of a functionalized chain derived from simple carbon building blocks via decarboxylative Claisen condensation analogous to classical fatty acid biosynthesis. This chain synthesis requires CoA **(6)** activated starter unit and extender units. In addition, enzymes catalyzing and directing the polyketide biosynthesis called *polyketide synthases* (PKSs), which are functioning with an activated acyl carrier protein (ACP) unit, are required.[16,17] The inactive form of ACP, which is called *apo*-ACP, needs to be transformed into the *holo*-ACP form by a phosphopantetheinyl transferase (PPTase) as shown in Figure 1.3. During the chain elongation steps of the polyketide synthesis, the growing chain stays attached to the *holo*-ACP arm. The phosphopantetheine **(7)** residue functions as

an arm reaching the polyketide intermediate to the catalytic centers of the PKS complexes.[16,18]

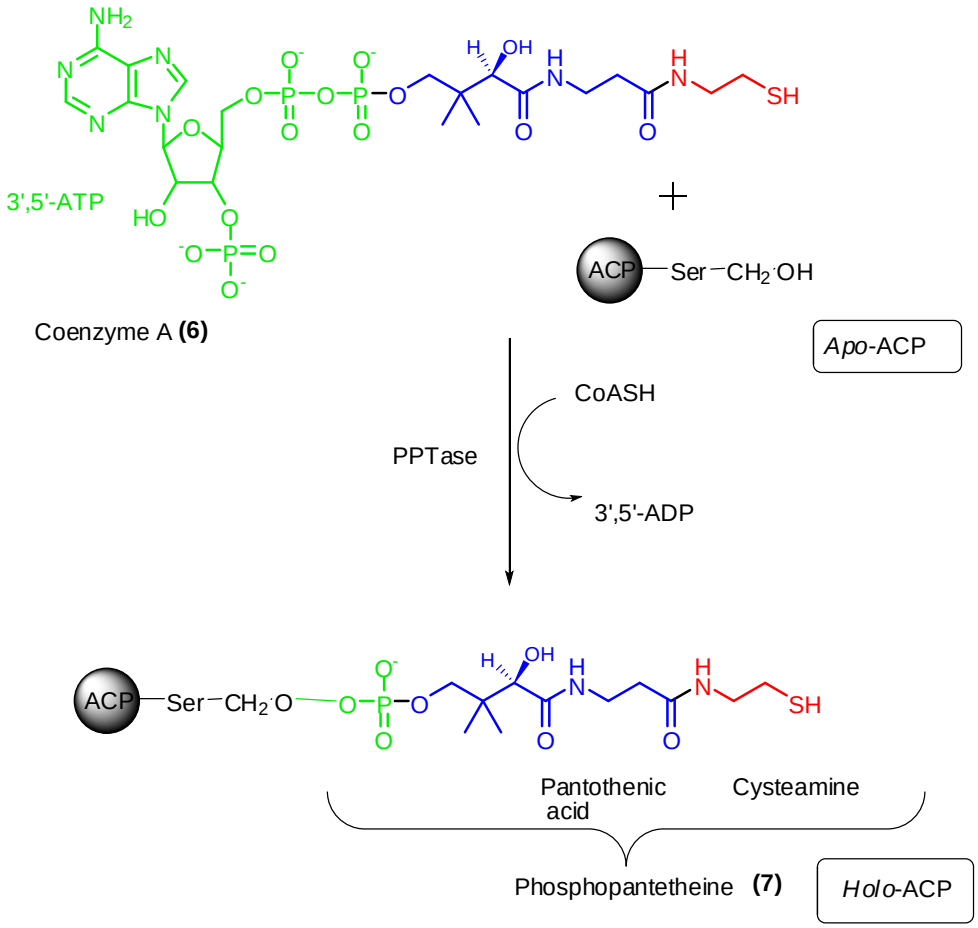

Figure 1.3 Phosphopantetheinyl transferase catalyzed posttranslational modification of *apo*-ACP into *holo*-ACP. [18]

After each condensation step, either the resulting poly-β-keto chain intermediate is elongated further or the keto groups of the chain intermediate are modified and reduced prior to the next elongation. In classical fatty acid biosynthesis, each successive chain elongation step is followed by a fixed sequence of keto reduction, dehydration and enoyl reduction. However, the individual chain elongation intermediates of modular polyketide biosynthesis may undergo all, some or none of these functional group modifications. In addition, usage of tailoring enzymes for further processing results in highly chemically complex products. Schematics of the biosynthetic pathways showing

the difference between fatty acid, aromatic polyketide, and reduced polyketide syntheses are shown in Figure 1.4.[2,19,20]

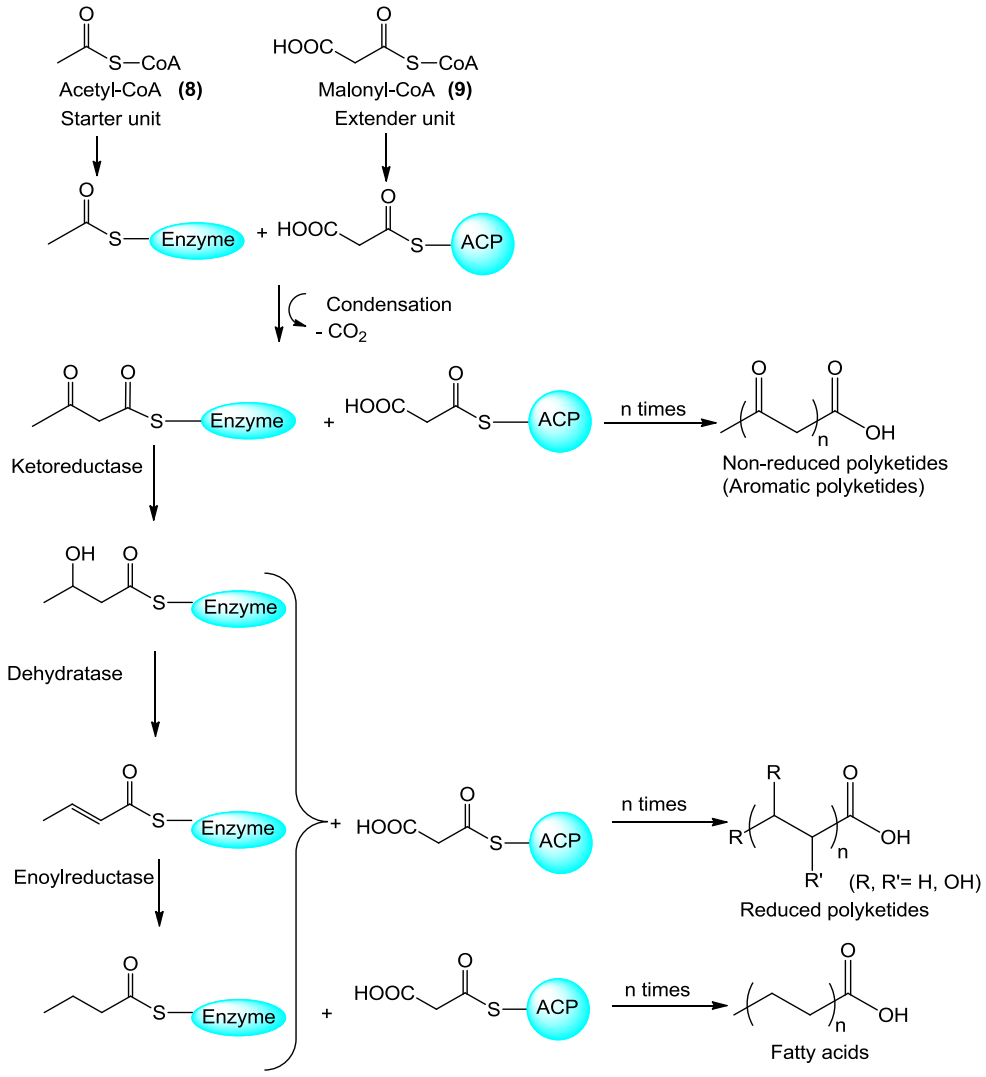

Figure 1.4 Biosynthetic pathways for fatty acid and polyketides. Starter unit and extender units are the building blocks. The processing of the elongation intermediates for fatty acids, aromatic polyketides, and reduced polyketides differ in the processing of chain intermediate.[20,2]

The biosynthetic pathway of aromatic polyketides branch from fatty acid synthesis in the earlier stages. [16] The chain extension process continues usually without reduction for aromatics, generating a highly reactive poly-β-keto chain. The intermediate has to be stabilized during enzyme processing until the entire chain assembly is complete. Subsequent cyclization reactions of the chain

intermediate result in an aromatic precursor for the biosynthesis of the aromatic scaffold.

Additional degrees of complexity arise from the use of various starter and chain elongation units.[21] Figure 1.5 exemplifies some of the starter and extender building units used in polyketide synthesis by different types of PKS enzyme complexes.

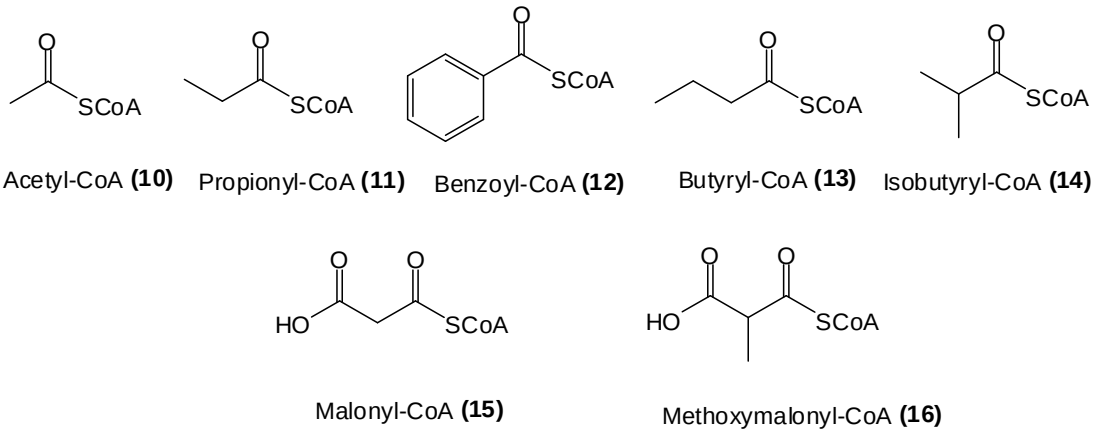

Figure 1.5 Some starter (upper row) and extender units (lower row) of polyketide biosynthesis.[21]

Three structurally different main classes of PKSs have been discovered in the microbial world until now.

These classes are:

- Modular type I PKSs and modular iterative type I in bacteria and fungi
- Iterative type II PKSs of bacteria
- Iterative type III PKSs of plants

Modular type I PKSs consist of multiple active domains organized into modules. Component domains of polyketides are acyl-transferases (ATs) to load starter, extender and intermediate acyl units; acyl carrier proteins (ACPs) to bind the growing chain as a thiol ester; β-keto-acyl synthases (KSs) to catalyze chain extension; β-keto reductases (KRs) to achieve the reduction at a keto to an alcohol functionality; dehydratases (DHs) to eliminate water to give an

unsaturated thioester; enoyl reductases (ERs) to catalyze the final reduction to reach full saturation; and finally a thioesterase (TE) to catalyze macrolide release to complete the cyclic structure.

Each module is responsible for the construction of a carbon-carbon bond, via decarboxylative condensation of a ketide extender unit with the growing polyketide chain, followed by a programmed reductive cycle. In addition, there is a loading module for the starter unit at the front of the first module and TE responsible to unload the product at the end of the last module. To process a type I polyketide, a functional module is required for each extension step, whose domain architecture usually precisely matches the functionality introduced into the growing intermediate. Thus, the order of modules is generally collinear with the order of functional groups in a polyketide. For this assembly line-like process the term *colinearity rule* has been introduced.[22,12,11]

At this point, it is important to discuss the linker regions. It is believed that dynamic linkers between modules, domains and the N- and C-terminus of the polypeptide chain establish communication by influencing correlated movements of various domains.[23,24,12]

The modular type I polyketide assembly line is exemplified by the biosynthesis of the antibiotic erythromycin **(4)**. Its biosynthesis was mainly investigated in the works of Prof. Peter Leadly's[25], Leonard Katz's and Khoshla's groups[22,26] and the schematic of the pathway is shown in the Figure 1.6.[22]

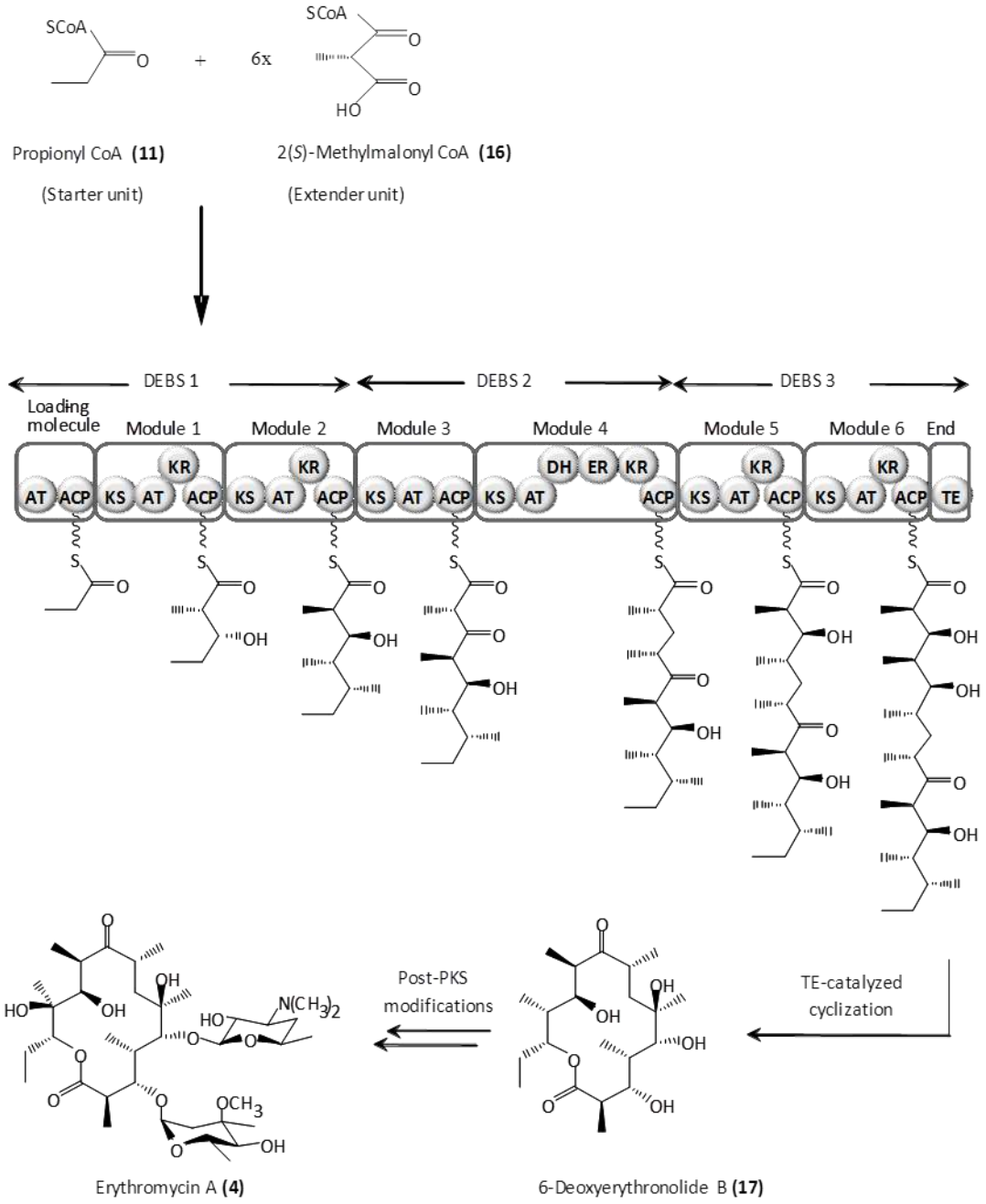

Figure 1.6 Modular polyketide biosynthesis with PKS I type assembly. In this figure erythromycin biosynthesis is used to illustrate modular PKS function.

Type I PKS systems can use modules linearly as described for erythromycin biosynthesis in Figure 1.6, or they can use modules iteratively. Iterative type I synthases are typically involved in the biosynthesis of fungal polyketides such as the compounds shown in the Figure 1.7, 6-methyl salicylic acid **(18)** and the fungal carcinogenic mykotoxine aflotoxin **(19)**[27,28] The biosynthesis of these

fungal aromatic polyketides differ from the biosynthesis of aromatic polyketides isolated from bacteria because bacteria use iterative type II PKSs instead.

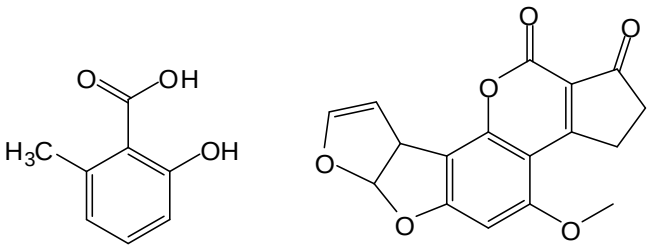

6-Methylsalicylic acid **(18)** *Aspergillus terreus*

Aflatoxin B_1 **(19)** *Aspergillus flavus*

Figure 1.7. Fungal aromatic polyketides.[28]

The biosynthesis by bacterial iterative type II systems is exemplified by the actinorhodin PKS from *Streptomyces coelicolor*. [29,30] In these synthases, active sites are contributed by several smaller, usually monofunctional polypeptides. Regarding the condensation steps, the PKSs are analogous to bacterial fatty acid synthases (FASs) and are responsible for the biosynthesis of bacterial aromatic polyketides. Type II synthases catalyze aromatization and cyclization of the poly-β-keto intermediate, but do not perform extensive reduction or reduction/dehydration cycles as the modules in type I PKSs do. The detailed enzymology of type II PKSs will be further discussed in the next section, since they are the main focus of this work.

Type III polyketide synthases are usually involved in the biosynthesis of chalcones and stilbenes in plants and some polyhydroxy phenols in bacteria.[7,16,31,32] They are comparatively small proteins with single polypeptide chains and act in the biosynthesis of flavonoids. Unlike the FASs, type I and type II PKSs, these enzymes do not use a phosphopantetheinyl cofactor, and the biosynthesis is significantly different than a bacterial type II PKS because of the organization of the genes on genome and construction of the biosynthetic machinery.[27,32]

1.4 Bacterial Aromatic Polyketides

Bacterial aromatic polyketides, which usually have polycyclic condensed aromatic structures, have been mostly encountered in actinomycetes.[32] Actinomycetes belong to Gram-positive bacteria and are a rich source of secondary metabolites. These compounds are assumed to be used in self-defense and bacterial communication.[32] The structural diversity, the biosynthesis and the organization of the related genes of these natural products have been attracting significant interest. Various type II PKS systems are encoded in organized gene clusters that contain homologous genes, which help identify the gene clusters on the genome of a bacteria. This features is important for the discovery and investigation of these systems.[33,7,34,35]

Major structural classes of bacterial aromatic polyketides are anthracyclines, angucyclines, aureolic acids, tetracyclines, tetracenomycins, pradimicin-type polyphenols **(29)**, and benzoisochromanequinones **(20)**.[36] Figure 1.8 shows actinorhodin **(20)**,[29,30,37] tetracyclin **(22)**[38], tetracenomycine **(21)**[39,40] doxorubicin **(24)**[41,42], landomycin **(25)** and mitramycin **(23)** [43,44] as some of the genetically best-studied examples of aromatic polyketides.[36,12] However, there are also several compounds produced by type II PKSs, that have novel scaffolds and do not belong to any of these groups, such as enterocin **(27),**[45,46] resistomycin **(28),**[47,48] fredericamycin A **(26)**,[42] and griseorhodin A **(5)**.[15]

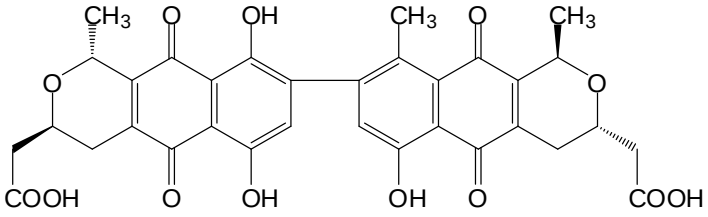

Actinorhodin **(20)**
Benzoisochromanequinone-type antibiotic

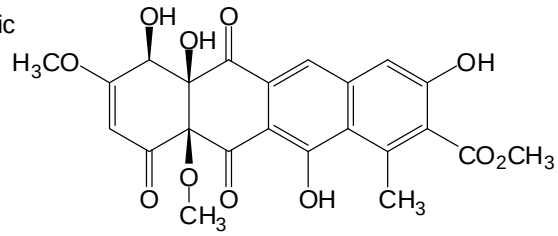

Tetracenomycin **(21)**

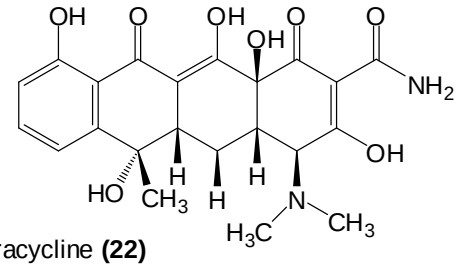

Tetracycline **(22)**

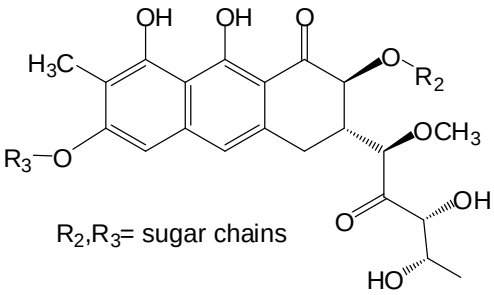

R_2,R_3= sugar chains

Mithramycin **(23)**
Aurolic acid-type glycosid anticancer drug

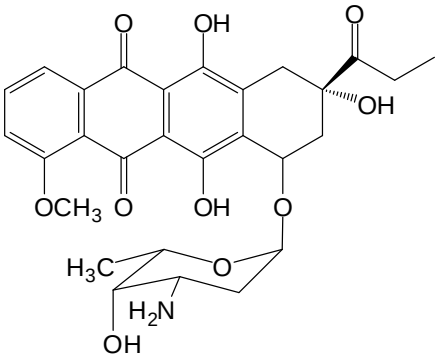

Doxorubicin **(24)**
Antracycline-type antitumore agent

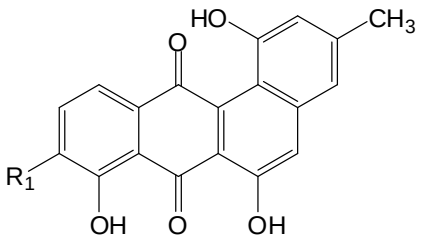

R_1= sugar chain

Landomycin A **(25)**
Angucycline type glycosid antibiotic

Figure 1.8.a Representative structures of aromatic polyketide metabolites falling into major structural types.

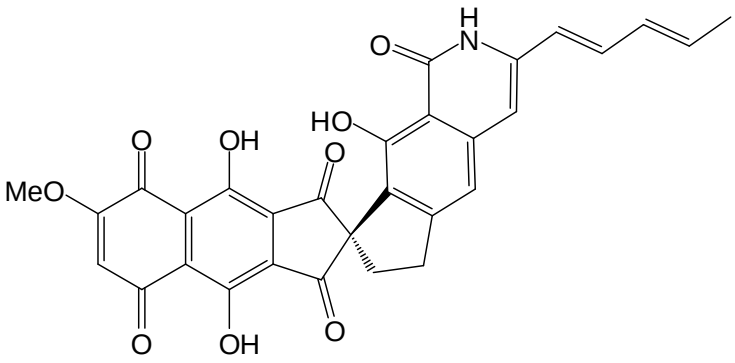

Fredericamycin A **(26)**

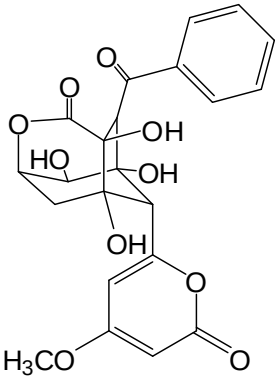

Enterocin **(27)**

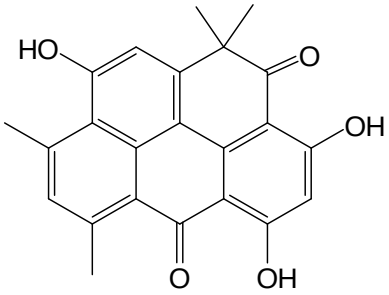

Resistomycin **(28)**

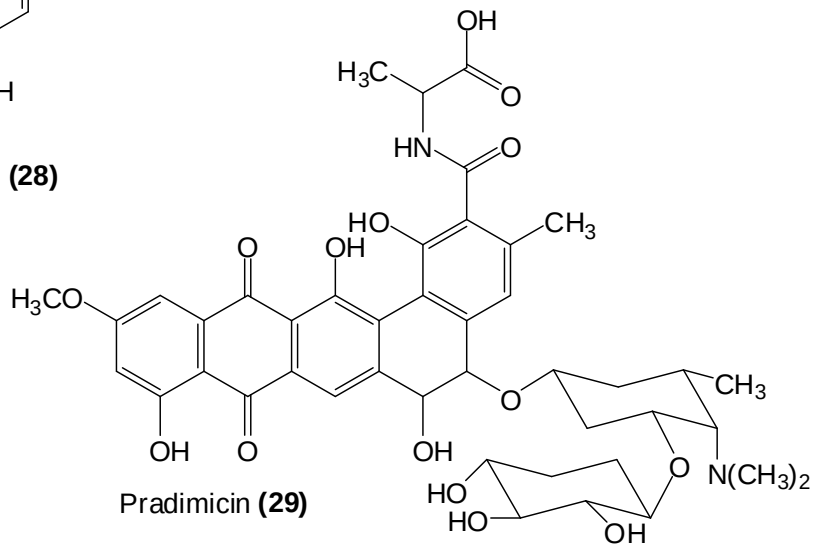

Pradimicin **(29)**

Figure 18.b Representative structures of aromatic polyketide metabolites with divergent carbon skeletons.

1.5 Enzymology of Bacterial Type II Aromatic Polyketide Biosynthesis

1.5.1 Minimal PKS

Polyketide synthesis by type II PKSs is a process comprising of several types of enzymes with individual activities organized as a multi-enzyme complex. The machinery responsible for the assembly of the poly-β-keto intermediate is the so-called *minimal PKS*, which is made up of a heterodimer ketosynthase unit and an ACP. The first ketosynthase unit KS_α possesses a cysteine reactive site, which plays an essential role in the catalysis of the condensation reactions for chain elongation. The second unit KS_β, also called the *chain elongation factor* (CLF), affects the chain length and plays an important role during the selection of the starter units.[17,29,36] KS_α and KS_β units form a cavity, where the growing polyketide chain, attached to the ACP, undergoes folding reactions.[36,49,50] Figure 1.9 illustrates a model of this enzyme complex. The size of the cavity limits the chain length and determines the folding pattern of the poly-β-keto chain.[36]

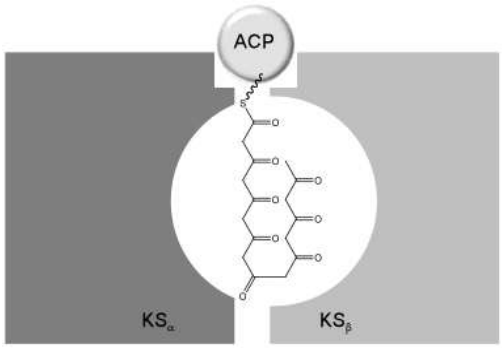

Figure 1.9 Model for a minimal PKS complex.[36]

The acyl carrier protein (ACP) is another key component of the assembly. It has a phosphopantetheine arm, to which the poly-β-keto chain is attached during synthesis. Studies have shown that, malonyl-CoA: ACP transferase (MAT, MCAT) enzymes have an important role at priming and allow the usage of starter units other than the commonly used acetyl-CoA. [36]

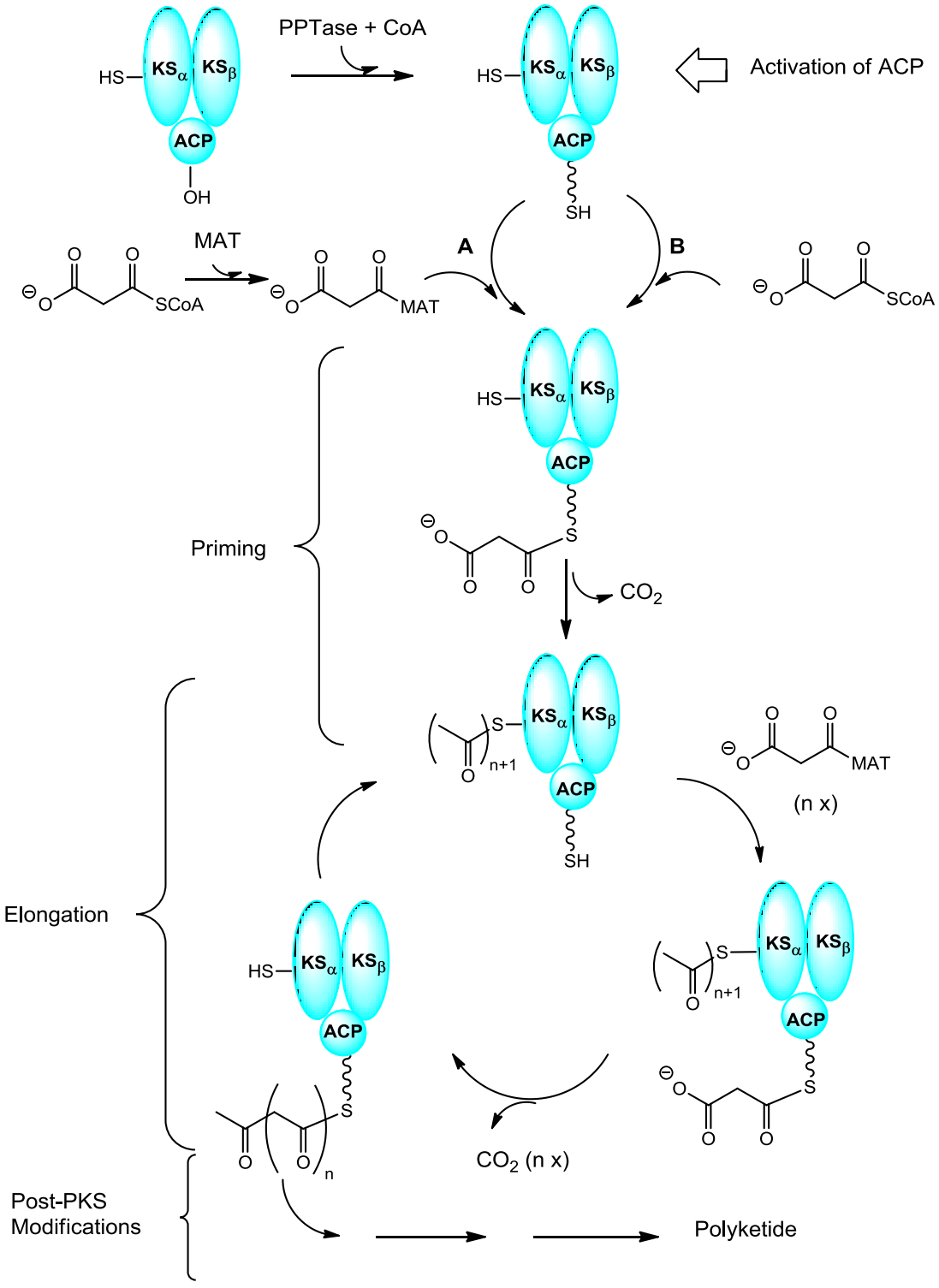

Figure 1.10 Stepwise mechanisms for type II PKS catalyzed biosynthesis of aromatic polyketides from malonyl CoA.[20]

Figure 1.10 shows the mechanism for the activation of the ACP and priming, chain elongation, and termination reactions of the poly-β-keto chain by the minimal PKS enzymes.[50,20]

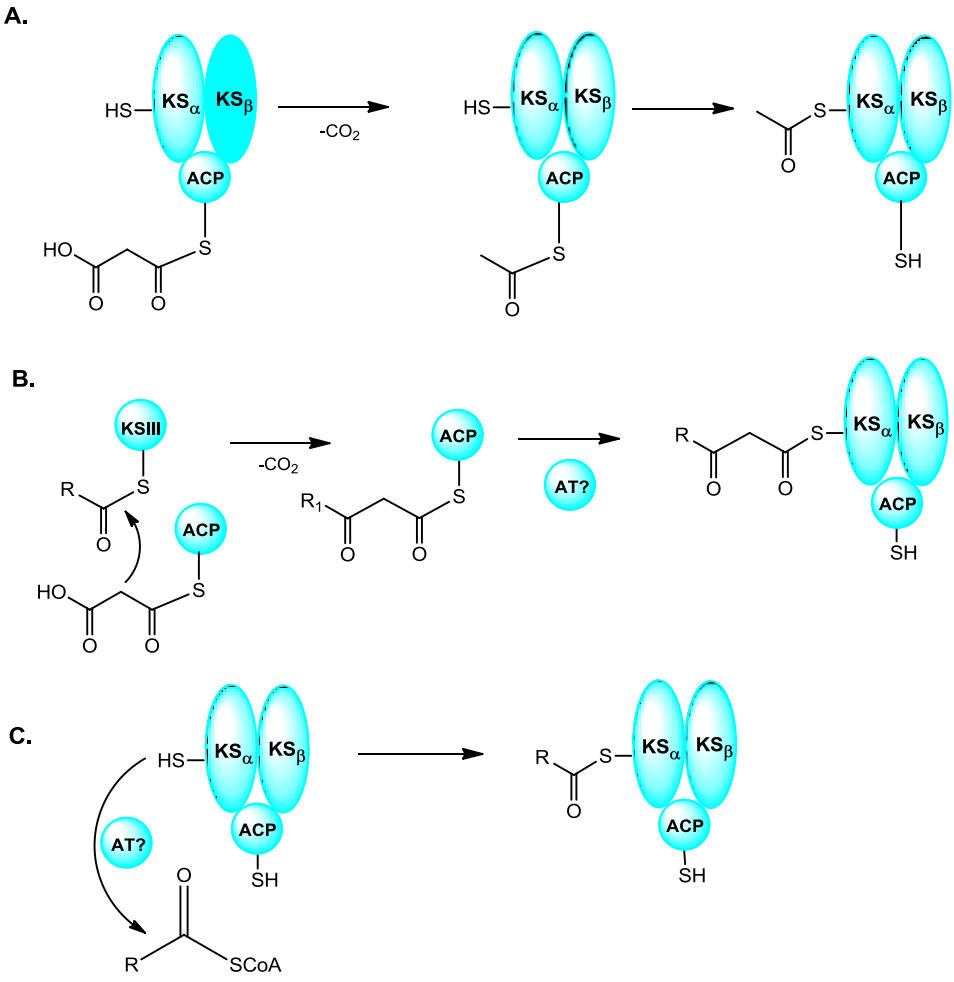

Figure 1.11 Mechanism of type II PKS priming. A. Priming involving decarboxylation. B. Priming involving a KSIII/ACP module. C. Priming involving direct loading of an acetyl-CoA starter.[36]

In most cases aromatic polyketide synthases are primed with acetate as in actinorhodin **(20)** and tetracenomycin **(21)** biosynthesis.[37,39] The PKS is primed by decarboxylation of a malonyl unit as shown in Figure 1.11A. In addition to decarboxylation of malonates, two alternative pathways have been proposed for non-acetate PKS primers. The alternative for the biosynthesis and attachment of short-chain fatty acids, such as propionate on the benastatins, involves an

additional KSIII (and ACP) as shown in Figure 1.11B.[51,52] The second alternative pathway in Figure 1.11C, which has been proposed for malonamate and benzoate starters in tetracycline **(22)** and enterocin **(27)** pathways, is the direct loading by an acyl-CoA ligase and an acyltransferase (AT).[46,21,36]

1.5.2 Accessory Enzymes

Accessory enzymes including ketoreductases (KR), cyclases and aromatases are crucial for the synthesis of the core aromatic structure because they manage the cyclization and folding patterns of the growing chain. The presence of these enzymes suppresses the occurrence of spontaneous aldol condensations. The so-called cyclases (CYCs), which function in a 'chaperone-like' manner, help in directing the nascent polyketide intermediates into particular reaction channels.[36,53] An interesting example of varying folding patterns in the context of bacterial accessory enzyme activities are presented in Figure 1.12. The folding pattern of the growing decaketide chain produces angular, linear and discoid scaffolds as in the case of dehydrorabelomycine **(29)**[54,55] tetracenomycin F1 **(30)**[39,40] and resistomycin **(28).**[47.36]

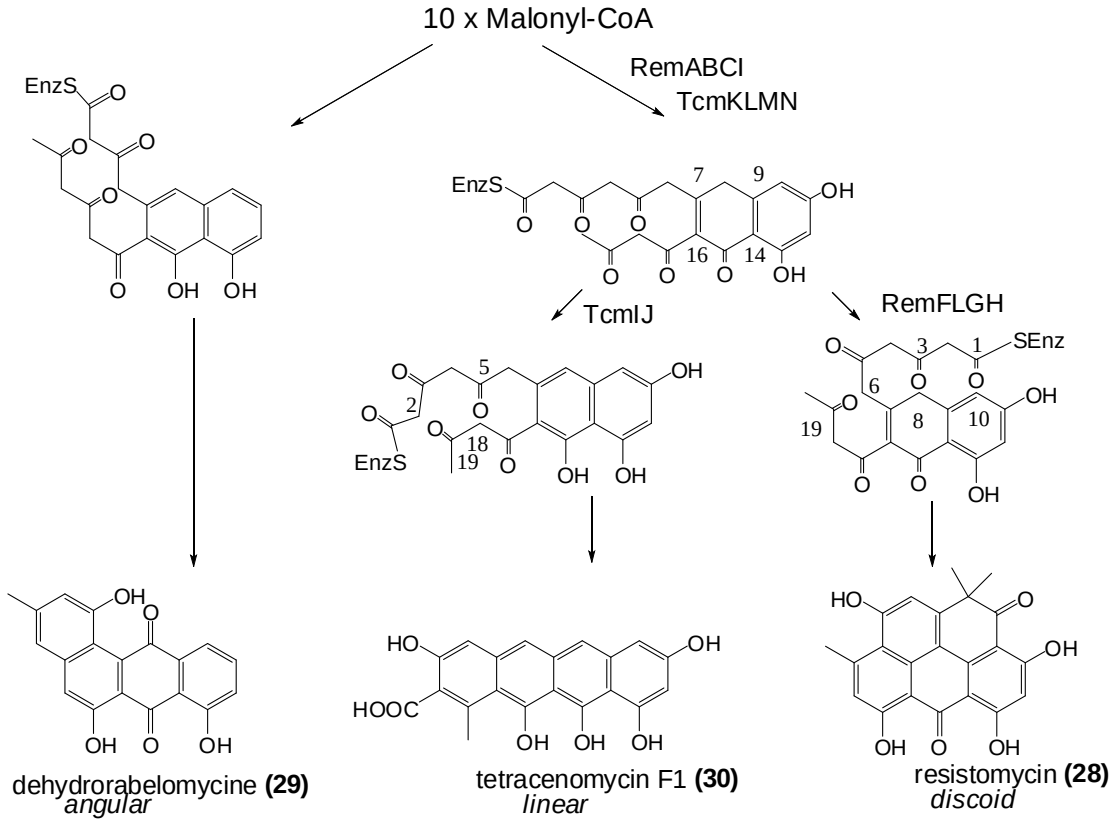

Figure 1.12 U-shape and S-shape folding in angular, linear and discoid polyketide pathways.[36]

Post-PKS modifications are the next step in the biosynthesis of the aromatic polyketides. A wide variety of tailoring enzymes, mainly group transferases such as methyl transferases and glycosidases, oxidoreductases and halogenases act at the final stages of the biosynthesis and decorate the aromatic core with substantial functional groups necessary for the biological activity of the compounds. Before proceeding with the details of the post PKS modifications, Figure 1.13 depicts an overview of actinorhodin **(20)** biosynthesis for a better understanding of the PKS type II biosynthesis. Note that, the organization of the genes encoding PKS type II systems (Figure 1.13) differ vastly from the organization of the genes encoding PKS type I systems (Figure 1.6) because they do not follow the co-linearity rule.

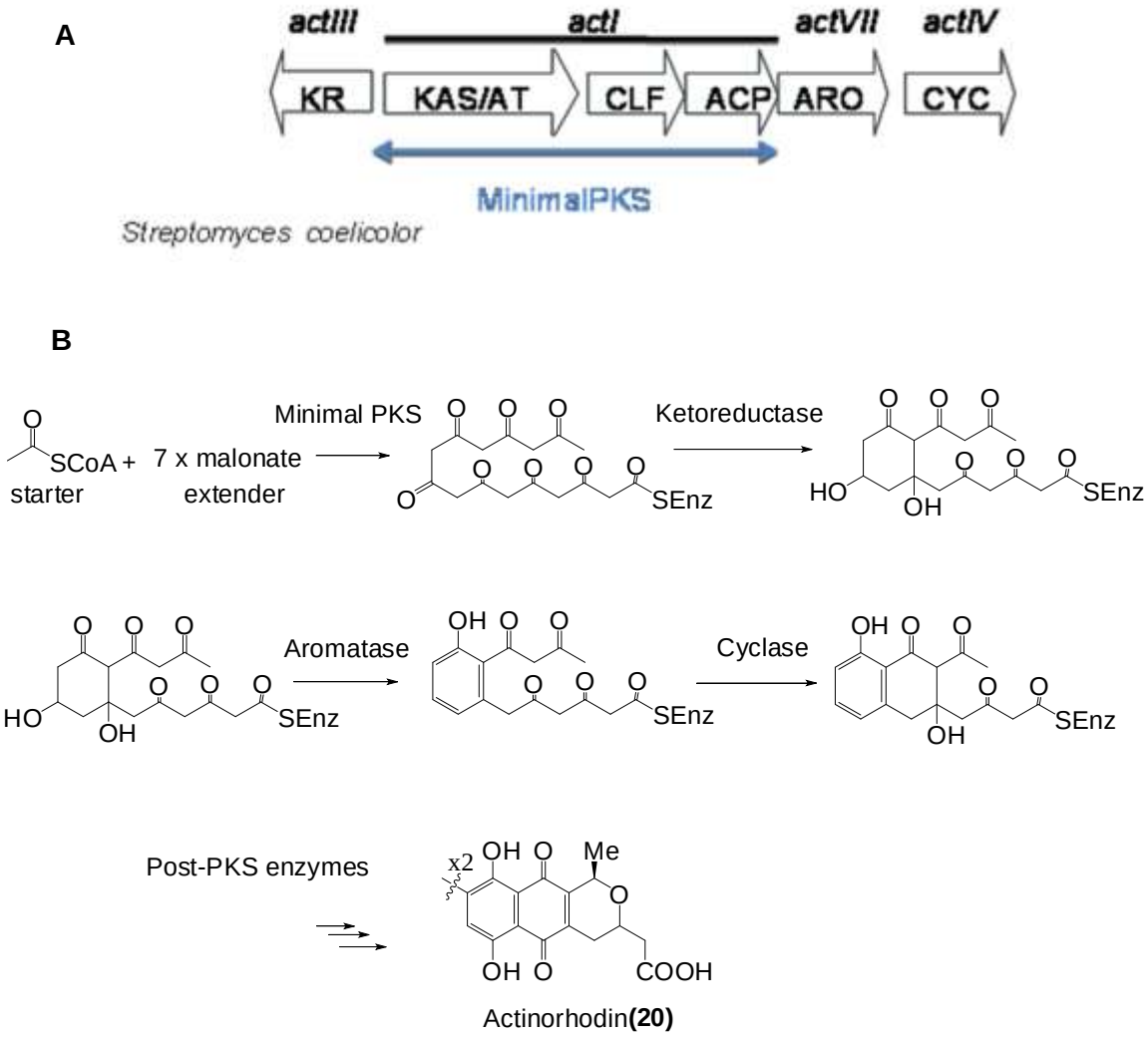

Figure 1.13 A. Actinorhodin minimal PKS gene cluster isolated from *S. coelicolor*. B. Actinorhodin biosynthesis illustrating the aromatic polyketide biosynthesis.[11,56]

1.5.3 Tailoring Enzymes

Tailoring enzymes, also called post-PKS enzymes, provide the aromatic core with new functionalities and alter the physical-chemical and stereo-chemical properties of the molecule by changing polarity and/or adding new chiral centers to it.[57] For example, glycosidases change the steric properties and solubility of molecules by adding bulky sugar chains. Several oxidases have the remarkable ability to reconstruct the whole aromatic core during the post-PKS processing via oxidative reactions.[36,58] These activities of the post-PKS enzymes have also tremendous impact on the binding properties of the polyketide to a biological ligand molecule. The possibility to change the binding ability attracts research to find new approaches to utilize these enzymes for combinatorial

biosynthesis in order to improve the pharmacological profile of certain polyketides.[59,60]

1.5.3.1 Group Transferases

The major subgroups of these enzymes are glycosyl transferases, amino transferases, alkyl transferases (usually methyl) and acyl transferases. Many enzymes are in need of co-factors to activate the donor substrates and transfer to new functionalities onto the molecule. For methyl transferases (MTs), use usually *S*-adenosylmethionine (SAM), and most amino transferases use alanine or glutamic acid as amino group donors. Glycosyl transferases (GTs) use NDP (nucleoside diphosphate) activated sugars as donor substrates. Typical nucleosides are TDP (thymine diphosphate), UDP (uracil diphosphate) and GDP (guanin diphosphate). TDP is by far the most common in the context of post-PKS modifications through glycosyl transferases.[58,61] The NDP-activated sugars are also called sugar co-substrates. For many of these sugar co-substrates, e.g. the NDP-deoxysugars, special biosynthetic pathways exist. The genes encoding these special pathways usually cluster with the genes of the metabolites to whose biosyntheses the GTs contribute.[59] It has been shown that many GTs exhibit substrate flexibility either towards their acceptor substrate or their sugar donor co-substrates, which makes them even more important for the combinatorial biosynthesis of new drug candidate glycosides.[61] Possible effects of group transfer reactions on the polyketide substrate are shown in the Figure 1.14.[60]

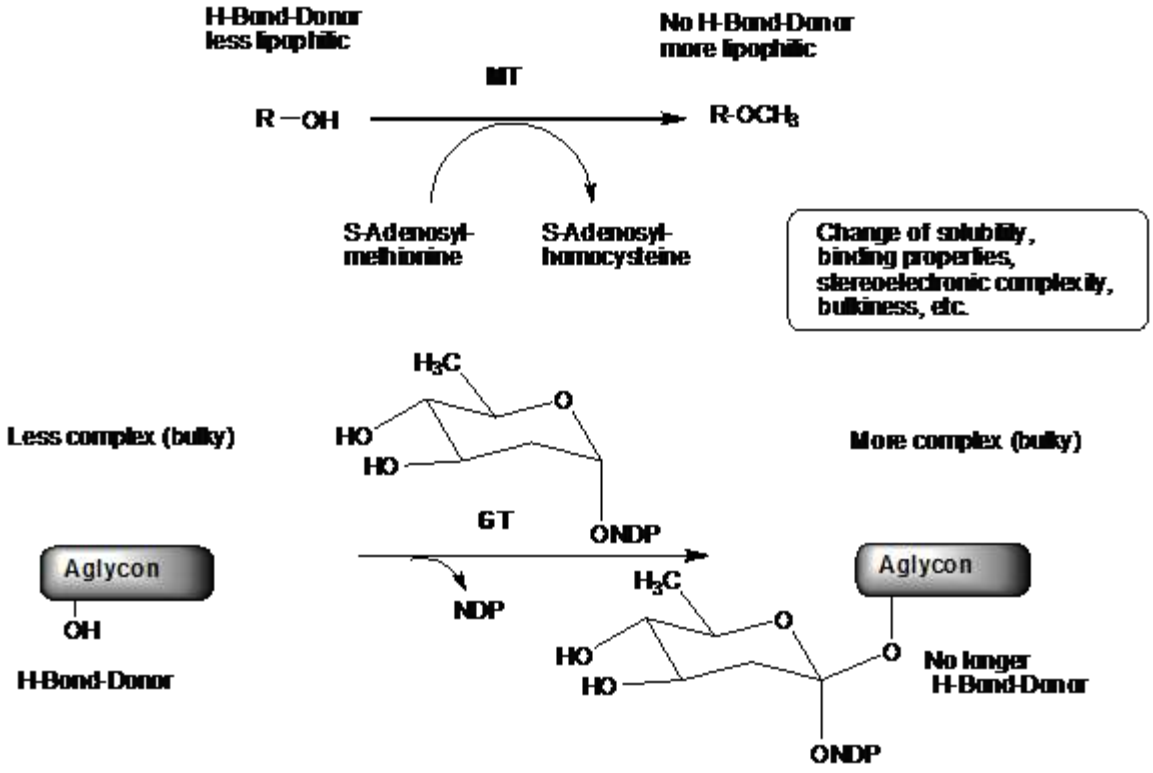

Figure 1.14 Possible effects of group transferases, such as methyl- and glycosyltransferases, MT=methyl transferase, GT=glycosyl transferase.[60]

1.5.3.2 Oxidoreductases

Oxidation reactions are the most frequently occurring post PKS-modifications occurring in the aromatic polyketide biosynthesis. Oxygenases, oxidases and peroxidases, (keto) reductases and dehydrogenases are the enzymes controlling these reactions. Oxygenase actions involve adding and transforming oxygen containing functional groups.[60,62] These modifications make the molecules more polar, change chemical properties, reactivity, and insert new stereo centers as illustrated in figure 1.15. Furthermore, oxygenases can catalyze exquisite rearrangement reactions, C-C bond cleavages, and complex decarboxylations.[60,63] On the other hand, reductases generally transform aldehydes, ketones, carboxylic acids and alcohols by adding hydrogen atoms. [60,62,64]

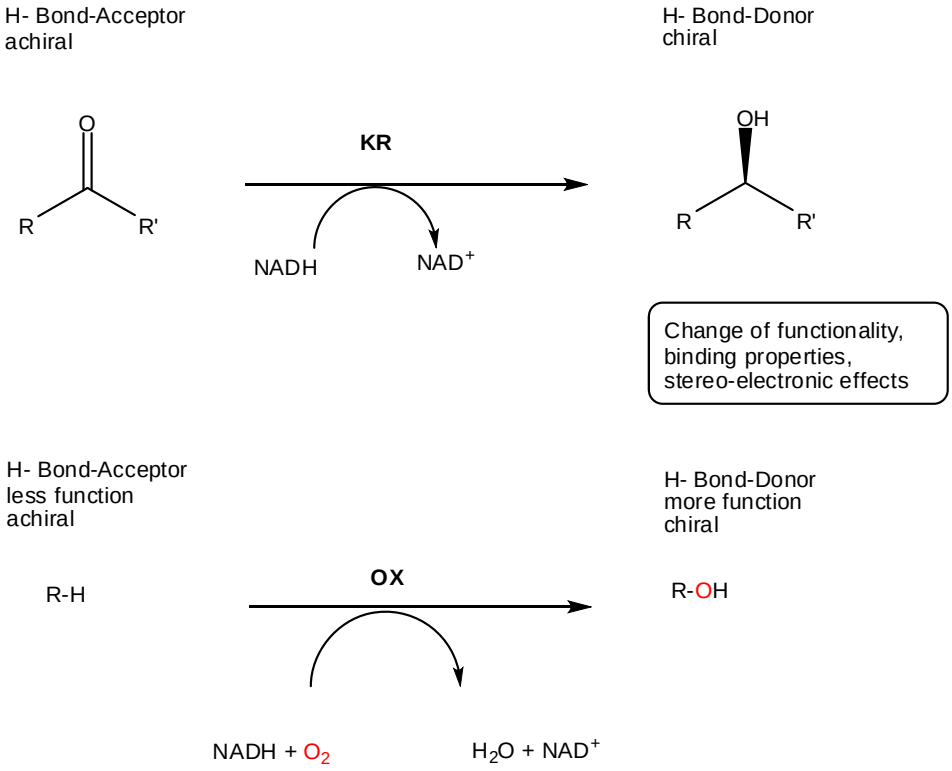

Figure 1.15 Possible effects of oxidoreductases on the biological activity.[60] KR = Ketoreductase, OX = oxygenase

Oxygenases are classified as either monooxygenases or dioxygenases. Monooxygenases incorporate an oxygen atom to the product, whereas dioxygenases incorporate both atoms of dioxygen into the final product. Catechol dioxygenases and the aromatic dihydroxylating dioxygenases are interesting examples of dioxygenases. Mono- and dioxygenases are often involved in the bacterial degradation of aromatic compounds in the environment.[65,66] Commonly occurring reactions of monooxygenases and dioxygenases are shown in Figure 1.16. [60]

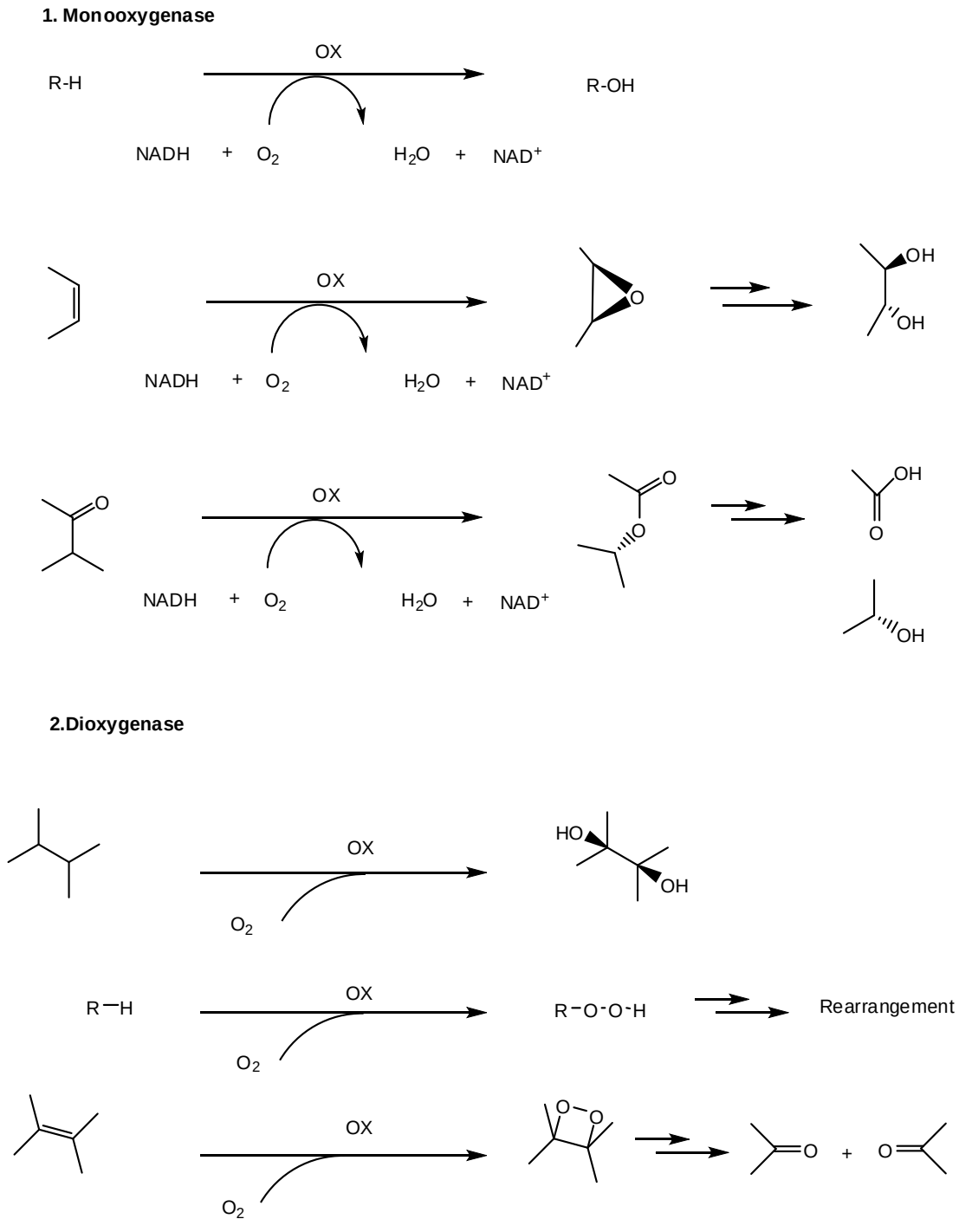

Figure1.16 Generation of structural diversity by oxygenases. Examples of products observed during mono- and dioxygenases reactions.[60]

These enzymes usually contain a redox-active transition metal or a non-metal cofactor. The used cofactor distinguishes between the classes of these enzymes.[60] The most common classes in aromatic polyketide synthesis are:

- Cytochrome P-450 monooxygenases (CYP450)
- Flavin dependent mono- and dioxygenases
- Anthrone oxygenases

Cytochrome P-450 monooxygenases (CYP450) are heme-containing enzymes and usually require a NADP dependent reductase and a ferrodoxin-like iron sulfur protein for the regeneration of the cofactor. These enzymes are involved in several essential metabolic pathways, and the genes of the regenerative enzymes are not necessarily clustered with the other oxygenase-encoding genes.[60] The mechanism of hydroxylation by P450 enzymes is shown in Figure 1.17 and is as follows: The heme cofactor **(31)** has an iron center resting in the enzyme ın the formal oxidation state +3, that is reduced to the +2 oxidation state upon substrate binding. This reduction is carried out by a reductase subunit of the enzyme. The reduced iron (II) is able to donate a single electron to the dioxygen, forming an iron (III) superoxide. Transfer of a second electron to the reductases subunit via the iron center generates iron (III) peroxide. Cleavage of the dioxygen bond occurs through protonation and results in an iron (IV) oxo species, which is believed to exist as an iron (IV) oxo/porphyrin radical cation. Oxygen insertion into the substrate can occur over a substrate radical or through a concerted mechanism involving oxygen insertion into the C-H bond of the substrate.[67]

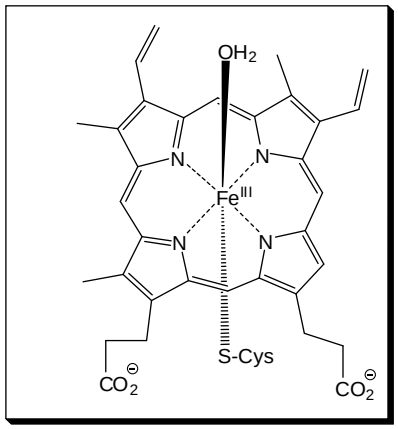

Heme cofactor **(31)**

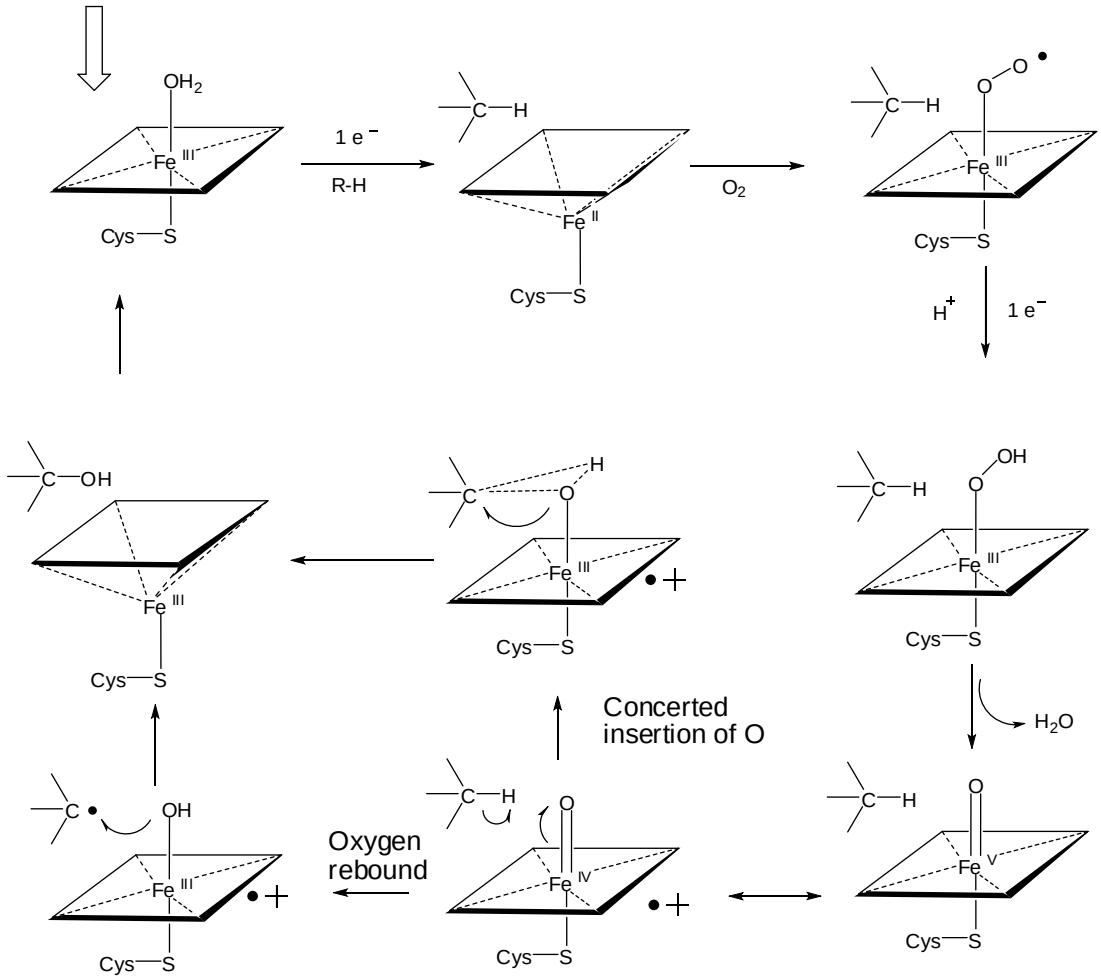

Figure 1.17 Mechanism for P_{450}-dependent hydroxylation.[67]

Flavin-dependent oxygenases use a flavin cofactor **(32)** that is in some cases covalently bound to the enzyme. Genes encoding flavin-dependent enzymes usually have similarities with each other at the binding sites of their cofactors. This property enables their identification. Figure 1.18 shows the structures of common flavin redox cofactors.[67]

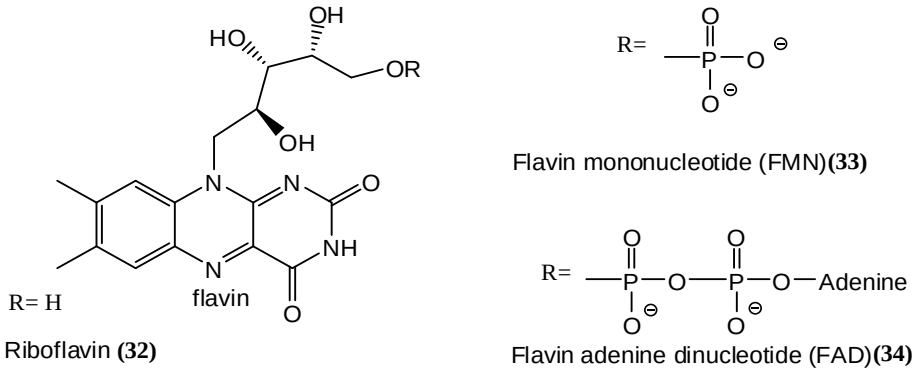

Figure 1.18 Structures of flavin redox cofactors.[67]

Flavin cofactors can exist as FAD **(34)**, as reduced $FADH_2$, or as a semiquinone radical species as shown in Figure 1.19A. The semiquinone form undergoes a single-electron transfer reaction after which the flavin molecule can react with molecular oxygen. The cofactor FAD must be regenerated at the end of each catalytic cycle by external redox reagents. *In vivo,* molecular oxygen is used to generate FAD from $FADH_2$ as shown in Figure 1.19B. For *in vitro* studies, usually chemical oxidants like benzoquinones are used.[67]

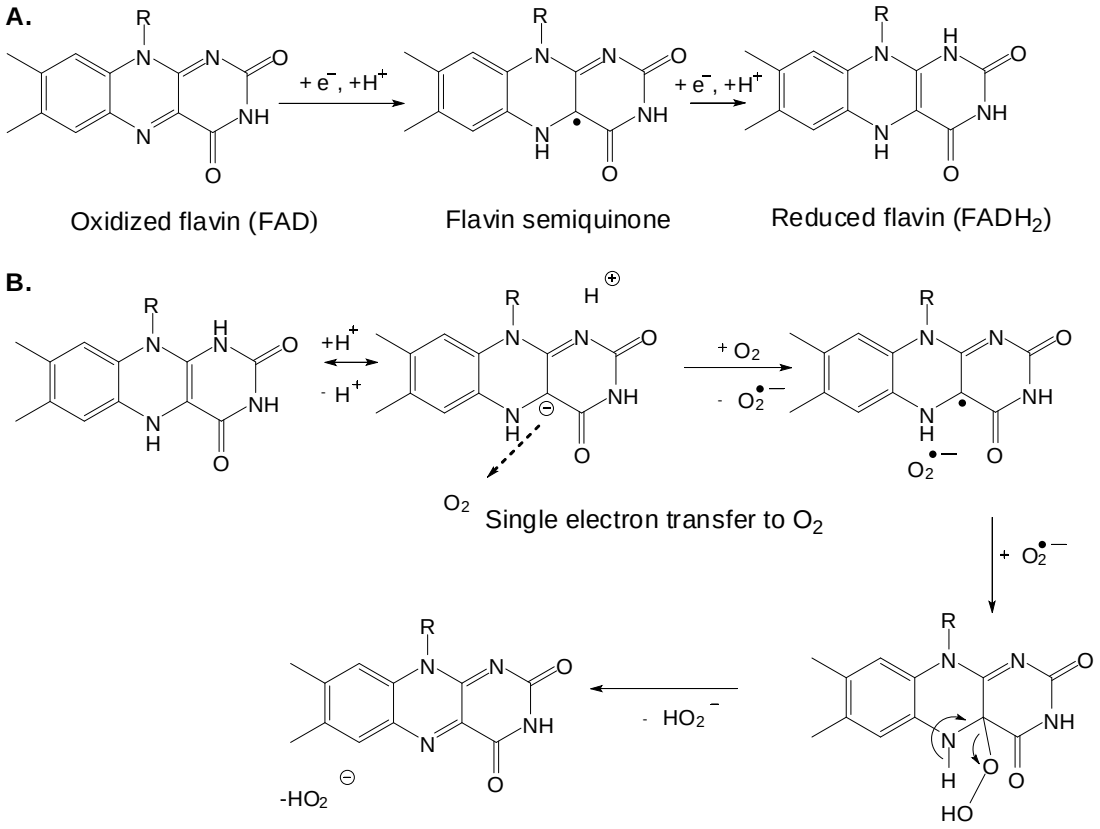

Figure 1.19 A. Redox states of riboflavin. B. Regeneration of oxidized flavin by molecular oxygen.[67]

Anthrone oxygenases occur very often in aromatic polyketide biosynthesis. Their most important property is to carry out oxidation reactions without cofactors. They are also called *"internal monooxygenases"*. They form quinone functionalities of the aromatic core by performing an oxidation in which a dioxygen molecule is reduced to water.[36,60]

Besides the various oxygenases catalyzing hydroxylation, epoxidation and anthrone oxidation reactions, there exist unique oxygenases catalyzing reactions such as Baeyer-Villiger-[68,69] or Favorskii-type[46,63] oxidative rearrangements. The flavin-dependent enzymes involved in the biosynthesis of mithramycin **(23)** and enterocin **(27)** are examples of this kind of reactions and are shown in Figure 1.20. There are also oxidative reaction cascades observed in several biosynthetic pathways.[70] Enzymes directing these reactions vary widely in their substrate-specificity and requirement of cofactors.

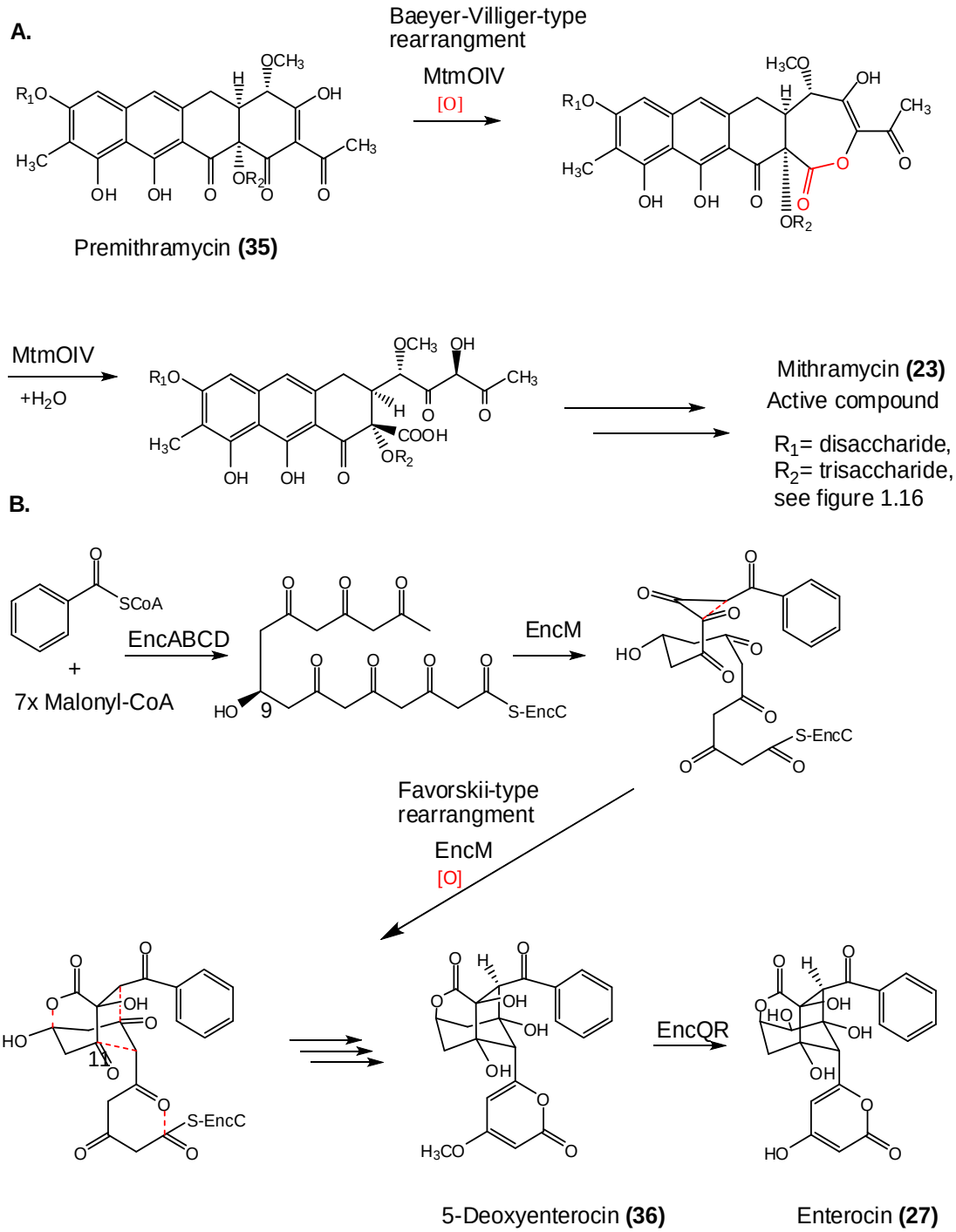

Figure 1.20 Oxidative rearrangements catalyzed by unique enzymes. A. Baeyer-Villiger oxygenase MtmOIV acting at the biosynthesis of mitramycin (23).[68] B. Enterocin (27) biosynthesis in which the gen EncM controls a Favorskii-Typ-rearrangment.[46,63]

1.6 Secondary Metabolite Production and Heterologous Expression in Streptomycetes

Streptomycetes are Gram-positive bacteria that exhibit a complex growth cycle consisting of filamentous vegetative growth, the formation of aerial hyphae (aerial mycelia) and differentiation of these hyphae into spore chains. An important feature of these bacteria is the production of secondary metabolites, which is regulated in coordination with morphological differentiation. Among these secondary metabolites are several pharmaceutically relevant compounds such as streptomycin (from *S. griseus*), vancomycin (from *S. orientalis),* tetracycline **(22)** (from *S. rimosus*), nystatin (from *S. noursei*), and avermectin (from *S. avermitilis)*. In addition, they produce a large number of extracellular enzymes that enable them to compete for nutrients in their habitat like many other actinomycetes. Streptomycetes have also the ability to sense and respond to a variety of environmental physiological signals, making them uniquely suitable to a life in a highly competitive soil environment. [71,72]

Figure 1.21 shows an overview of the complex growth cycle of *S. coelicolor* as an example. Under favorable conditions, one or two germ tubes emerge from a spore, grow by tip extention and branch formation to give rise to a mycelium. After 3-4 days, aerial hyphae, which have apical compartments, grow up, forming a spiral syncytium containing many tens of genomes. After aerial hyphae growth stops, multiple septa subdivide the apical compartment into unigenomic prespore compartments. These compartments change their shapes. Wall thickening occurs and grey spore pigments are deposited.[72]

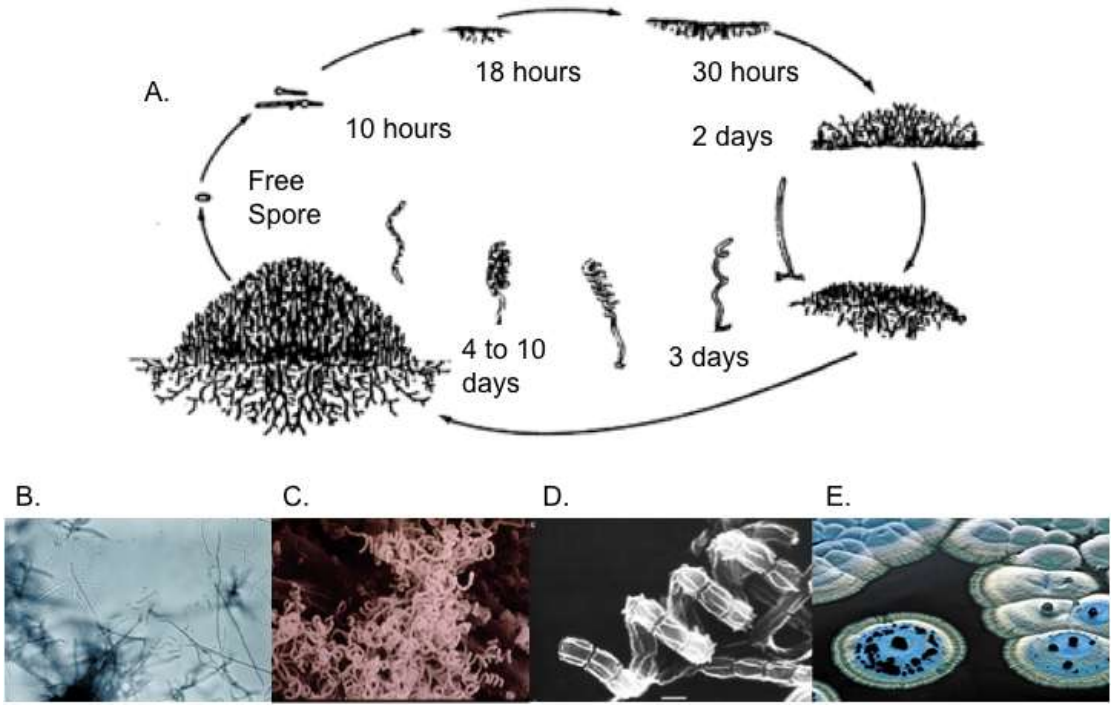

Figure 1.21 Life cycle and natural product production in Streptomycetes. A. The complex life cycle of Steptomycetes[51]. B. & C. Filamentous growth structure of Streptomycetes mycelium D. *Streptomyces plicatospours* spiral syncytium containing various genomes. E. *Streptomyces coelicolor* colonies producing actinorhodin (20). [72,73,74] Pictures from: http://microbewiki.kenyon.edu/index.php/Streptomyces

The genetic and physiological causes for differentiation, antibiotic and enzyme production of streptomycetes have been the subjects of research since the 1950s. Notably, Sir David Hopwood's research on the *Streptomyces coelicolor* A3 strain contributed significantly to the understanding of streptomycetes genetics.

Streptomycetes posses large (>8 Mb), high-(G+C), linear chromosomes. These large linear chromosomes provide twice as much coding capacity than *E. coli* chromosomes and contain more open reading frames (ORFs) than the chromosomes of the eukaryote *Saccharomyces cerevisiae*. Several secondary metabolite pathway clusters can be encoded in their genome. The size of the clusters in their genome range from 15 kb up to more than 120 kb.[75]

In addition, recent whole genome analysis of several streptomycetes strains showed the presence of cryptic or silent secondary metabolite pathway genes that either do not provide compounds at detectable levels or are non-functional under standard culture conditions. The genome sequence of *S. coelicolor* revealed 18 putative secondary metabolic gene clusters in addition to those belonging to the previously known compounds, actinorhodin (ACT) **(20)**, undecylprodigiosin (RED), calcium dependent antibiotic (CDA), and the gray spore pigment (WhiE). [76]

Genes encoding secondary metabolic pathways in streptomycetes are organized in clusters on the chromosome. Regulatory and resistance genes are usually found within the gene cluster. Because of gene clustering, once a single gene of the pathway is identified, entire pathways can be analyzed by searching the adjacent chromosomal region. This feature greatly simplifies the search for biosynthetic genes. Up to now, more than 100 secondary metabolite gene clusters from streptomycetes have been described.[77]

The functionality of the genes in the identified and isolated clusters needs to be studied in order to explain the biosynthesis of the metabolites. The wide variety of isolated clusters requires a wide variety of gene expression methods. Cloning and heterologous expression of gene clusters in genetically improved laboratory strains provides a viable solution. The method of heterologous expression is based on the idea of introduce the isolated cluster or modified gene cluster of the compound into a compatible host, in order to have the host specie express it. One option is to integrate the new genes into the genome of the host strain and another option is to use an expression vector. An important requirement of heterologous expression is that the native strain and the chosen strain for expression must have certain genetic compatibilities such as their codon usage. [77]

Many natural producer Streptomycetes strains cannot be used effectively to express a specific gene cluster for research purposes. In addition to the desired metabolite, a family of structurally related but unwanted compounds can also be produced. As exemplified by *S. coelicolor,* these bacteria can even produce more than one biochemically distinct secondary metabolite.

Therefore, a wide range of genetically modified actinomycetes including *S. coelicolor*, *S. lividans*, *S. parvulus*, and *S. albus* were developed as host species for the production of polyketides efficiently via heterologous expression.[71,78] These strains do not contain unknown or unwanted clusters and they can be manipulated systematically to increase precursor availability or to eliminate compounds that may interfere with downstream processing. This eliminates undesirable metabolites from fermentation broths. These strains can also be manipulated to increase the yield of the expressed antibiotic or protein. [71,75]

Heterologous expression with these strains increases the ease with which PKSs can be genetically engineered for production of new natural products. Secondary metabolites whose sources can hardly be cultivated or which are produced in unsatisfactory amounts can be obtained by these methods in sufficient amounts.

1.7 Recent Advances in Aromatic Polyketide Research

The first genetic level biosynthesis study of organisms producing aromatic polyketides was carried out by Hopwood *et al*. using the model species *S. coelicolor* in the 1980's.[79,30,37] *In vivo* and *in vitro* expression studies on the gene cluster of the blue pigment actinorhodin **(20)** produced by *S. coelicolor*, led to the research on organisms making aromatic polyketides with important pharmacological activity such as tetracycline **(22)**, doxorubicin **(24)**, tetracenomycin **(21)**.[33,39,41,80,81] Experience gained on the sequential analysis of the genes encoding PKS enzymes enabled the latter rapid developments in the isolation and expression of dozens of gene clusters of aromatic polyketides. Recently developed molecular biology tools such as recombinant DNA modification methods, allowed the *in vitro* and *in vivo* investigation of the biosyntheses of the metabolites at the genetic level via the expression of PKS genes and total biosynthesis clusters in host bacteria.[34,79,82] Achievements in efficient heterologous expression of polyketide gene clusters in host strains and advances in methods to manipulate the gene clusters by adding and deleting genes, opened the way for the combinatorial biosynthesis of several unique

compounds and compound libraries.[12,83] An important example of combinatorial biosynthesis is provided by the works of Hopwood and Foss.[84,85] The successful combination of genes from the biosynthesis clusters of actinorhodin **(20)** and medermycin showed that the enzymes of structurally and genetically related polyketides could work together to form new "unnatural" polyketides.[82] These results encouraged research in the field of aromatic polyketides because they suggested new ways to obtain unprecedented aromatic substances. Today, combinatorial biosynthesis is an inseparable part of natural product chemistry.

In addition to *in vivo* studies, *in vitro* reconstruction of aromatic PKSs has contributed to the understanding of the detailed mechanics of PKS machinery.[86,87] In order to engineer targeted aromatic polyketides, efforts have been made to unravel the molecular recognition features and structure-function relationships of these biosynthetic systems. However, there are still significant challenges to overcome to achieve specifically targeted metabolites. The most outstanding problems are the substrate specificity and compatibility of individual PKS components and their organizational tolerance to each other.[4,83,84] In order to find compatible components for combinatorial biosynthesis, a large PKS gene repertoire encoding diverse polyketide structures is necessary. Additional methods to develop these repertoires via search for new interesting gene clusters in microbial genomes were reported. Among these methods is mining and activat on of cryptic gene clusters. These novel approaches look highly promising for the further development of natural product libraries.[4,88,89]

Using tailoring enzymes to achieve targeted derivatisation of complex molecules is a novel idea to obtain diverse compounds whose implementation is currently investigated. Heterologous expression of polyketide genes furnishes an opportunity to develop new genetic-based strategies to implement this idea.[56,60,90] Glycosyl transferases that possess substrate flexibility have been successfully utilized for the *in vivo* synthesis of novel glycosylated polycyclic aromatic polyketides.[89,91-93] Novel oxygenases and methyl transferases are also

important tools for the research of new and efficient bio-combinatorial lead structure development.[94]

On a different front, semisynthetic approaches to improve pharmacological activity of heterologously expressed polyketides were investigated e.g. the semisynthetic derivatives of fredericamycin **(26).**[95]

1.8 Rubromycins and Griseorhodin A (5)

Rubromycins are structurally unique among aromatic polyketides. They are quinone antibiotics possessing benzotetrahydrofuran and benzotetrahydrodipyran rings, linked in a spiroketal moiety wıth non-planar molecular architecture. Heliquinomycin **(39)** and β- and γ-rubromycin **(37)** are among the most potent known human telomerase inhibitors and they exhibit activity against HIV reverse transcriptase according to Goldmann *et al.* and Ueno *et al.*[96,97] Compounds with opened spiroketal functionality, such as α-rubromycin **(40)** are found to be inactive in telomerase assays. [97] These observations suggest that, pharmacological activity of the rubromycins depends strongly on their highly unusual spiroketal moiety. [97]In addition, some members of the rubromycin family inhibit growth of bacterial strains remarkably.[98] Well-known representatives of the rubromycin family are shown in Figure 1.22.

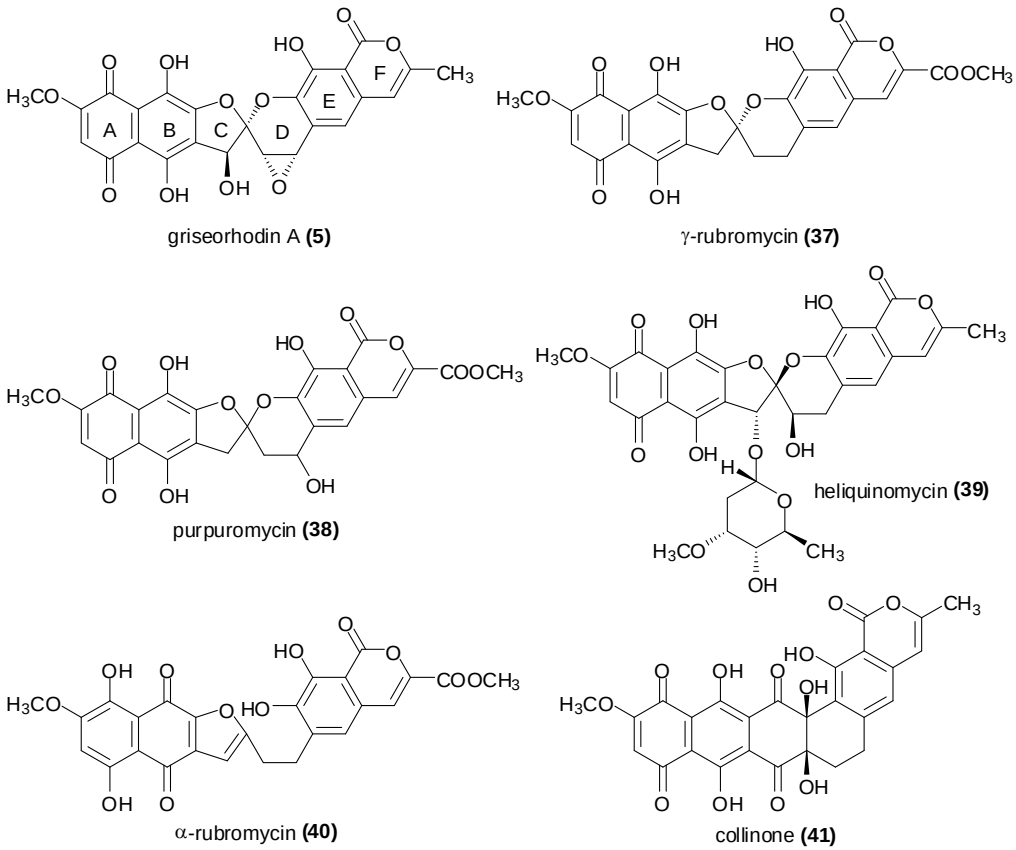

Figure 1.22 Aromatic polyketides representing the rubromycin family.[99]

The red pigment γ-rubromycin **(37)** was first isolated from cultures of a *Streptomyces* species by H. Brockmann *et al.* in 1970.[100] Subsequently its structure was determined using chemical degradation and transformation reactions.[100-102] Further structural investigations with modern spectroscopic methods were performed by C. L. Puder *et al.* in 2000.[98] The absolute configurations of γ-rubromycin **(37)** and heliquinomycin **(39)** were determined by using quantum chemical CD calculations by G. Bringmann *et al.* in 2000.[103]

Initial insights into the biosynthesis of rubromycins were obtained through feeding experiments of *Streptomyces sp.* A1, a native rubromycin producer, by Zeeck *et al*.[98] The molecule was shown to be composed of twelve acetate units and a methoxy group that had been derived from L-methionine **(42).** However, the resultant labeling pattern of the molecule could not answer the question

whether the molecule was formed from one or two polyketide chains. Figure 1.23 shows these results of the feeding experiments for rubromycin **(37).**[98]

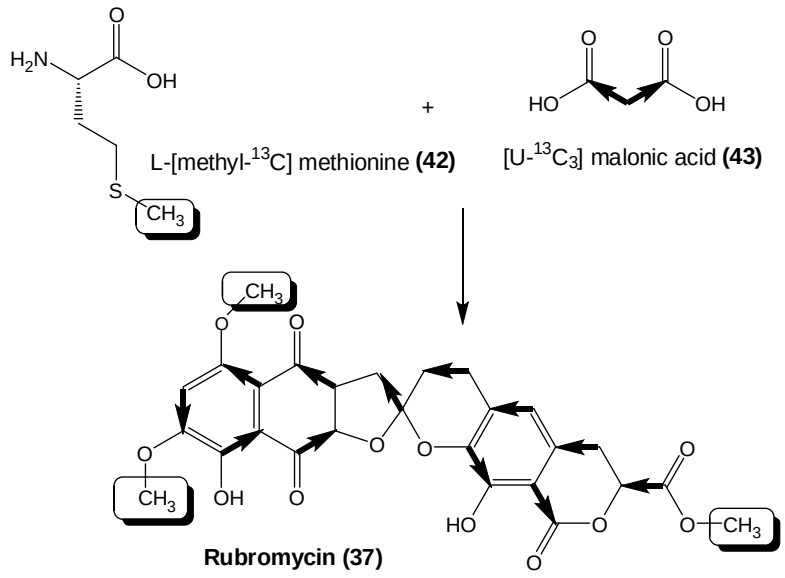

Figure 1.23 Labeling pattern of γ-rubromycin via feeding experiments with [U-$^{13}C_3$]malonic acid.[98]

The interesting structural and pharmacological features of the rubromycins motivated several synthetic approaches for the formation of the aromatic spiroketal moiety to be tried out. However the successful total synthesis of γ-rubromycin **(37)** has not yet been achieved. Thus, placing the spiroketal function into a highly oxidized aromatic core is still an ongoing synthetic chemistry challenge. [104-108]

An important study that provides insights into the biosynthesis of rubromycins was performed by Minas, Bailey, and coworkers.[109] They isolated a hexacyclic tridecaketid called collinone **(41),** a possible precursor of rubromycins. This compound was produced by heterologous expression of randomly chosen 30-50 kb sized genomic DNA fragments of a putative rubromycin **(37)** gene cluster from the strain *S. collinus* DSM 2012 using *S. coelicolor* CH999 as a host. The compound collinone **(41)** has two more carbon atoms than the unmethylated core of rubromycins. This structural difference suggests that tailoring enzymes remove these carbons from collinone in order to construct the spiroketal moiety in the latter stages of biosynthesis. (Figure 1.24) However, their results could

not exclude the possibility that the expressed DNA belonged to another pathway unrelated to rubromycin **(37)** biosynthesis. [109]

The structure of collinone **(41)** with 26 carbon atoms suggests the hypothesis that the rubromycins **(37)** use a highly oxidized pradimicin-type aromatic core as a precursor for the construction of the spiroketal moiety. Pradimicin-type aromatic compounds have an angular aromatic core comprising of five aromatic rings in an arrangement called *pentangular* formation.[110] (Figure 1.24) The enzymes and their gene sequences involved in the synthesis of the pentangular aromatic core of pradimicin **(29)** show significant similarities to the enzymes and genes involved in the biosynthesis of rubromycin **(37)** and fredericamycin A **(26)**. Rubromycins and fredericamycins are aromatic bacterial polyketides with unique spiro centers distorting their aromatic cores. The biosynthetic pathways postulated for bacterial aromatic spiro compounds assume the presence of a key pentangular aromatic intermediate that acts as a substrate for the tailoring enzymes forming the spiro centers by complex oxidative modifications.[15] Figure 1.24 shows the postulated intermediate and the aromatic polyketides exhibiting structural and biosynthetic similarities.

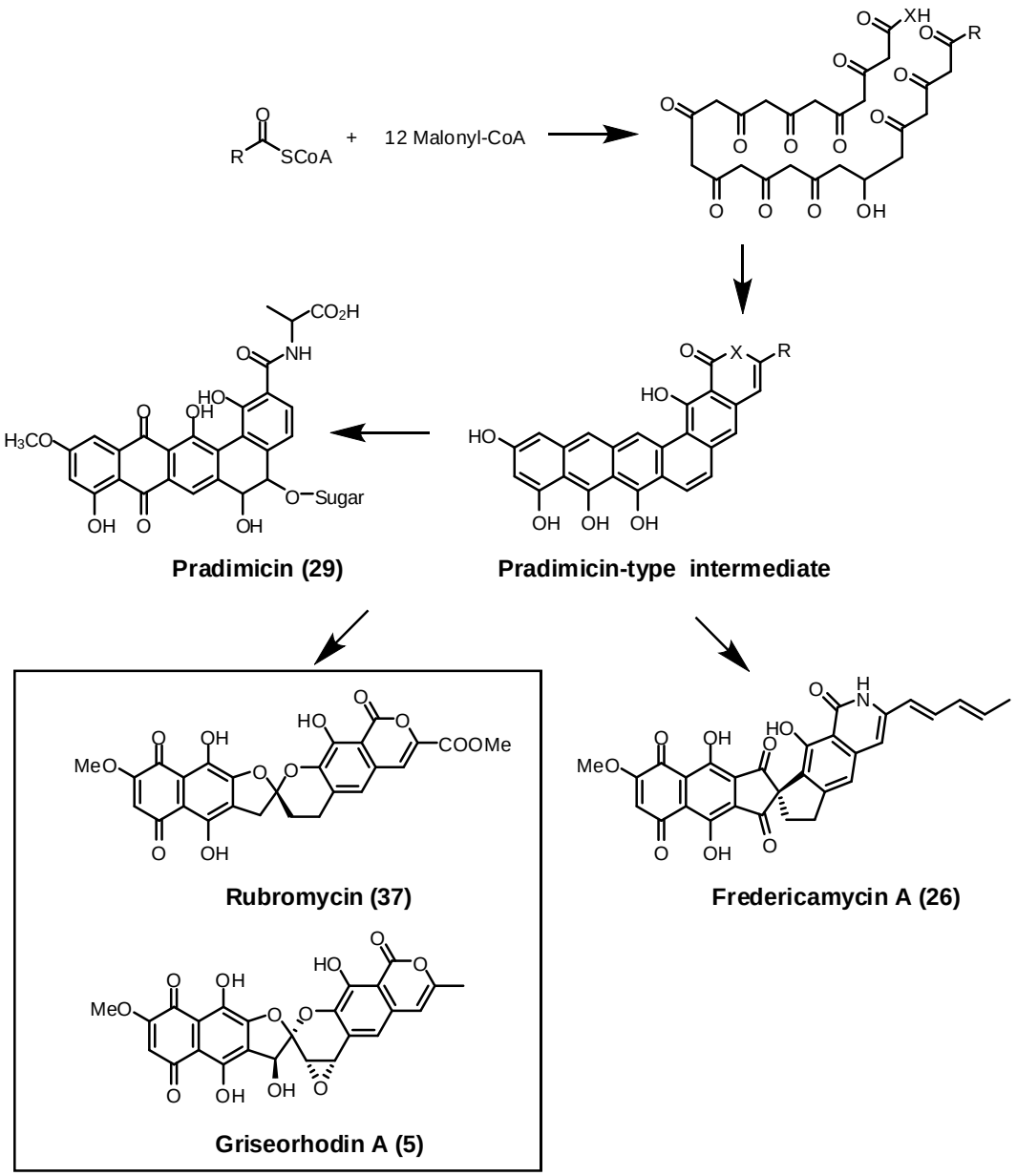

Figure 1.24 Postulated biosynthesis of aromatic polyketides involving a pradimicin type pentangular intermediate for the construction of aromatic spiro polyketides.[15] Figure shows members of aromatic spiro compounds such as rubromycins with a spiroketal moiety and fredericamycines with a carbaspiro center.

Griseorhodin A **(5)** is the most heavily oxidized member of the rubromycin family. It has human telomerase inhibition property and antibiotic activity like the other rubromycins.[97] Its unusually heavily oxidized structure makes the biosynthesis even more interesting for research. Griseorhodin A **(5)** was discovered by Treibs *et al.* in 1961 during his work in the group of K. Eckardt.[111] The compound was isolated from *Streptomyces californicus* JA2640 and the

structure was elucidated in 1978.[14,111-113] The griseorhodin A **(5)** biosynthetic gene cluster (Fig. 1.24) was isolated and sequenced by Piel *et al*.[15] The producer was the marine bacterium *Streptomyces sp.* JP95, which was isolated from the marine tunicate *Aplidium lenticulum* in the Great Barrier Reef, Australia. This bacterium produces mainly griseorhodin A **(5)** and a number of other rubromycin- type compounds. Knockout studies on the natural producer to prove that the isolated genes were involved in griseorhodin A production were not successful. The natural producer was not compatible with the methods that had to be used. In order to overcome this problem, the isolated cluster was transferred into the heterologuous host *Streptomyces lividans.*[15] The gene cluster was successfully expressed. This developed expression system proved that the isolated cluster contained all the necessary genes for the biosynthesis of the compound, opening the way for further gene deletion experiments.[15]

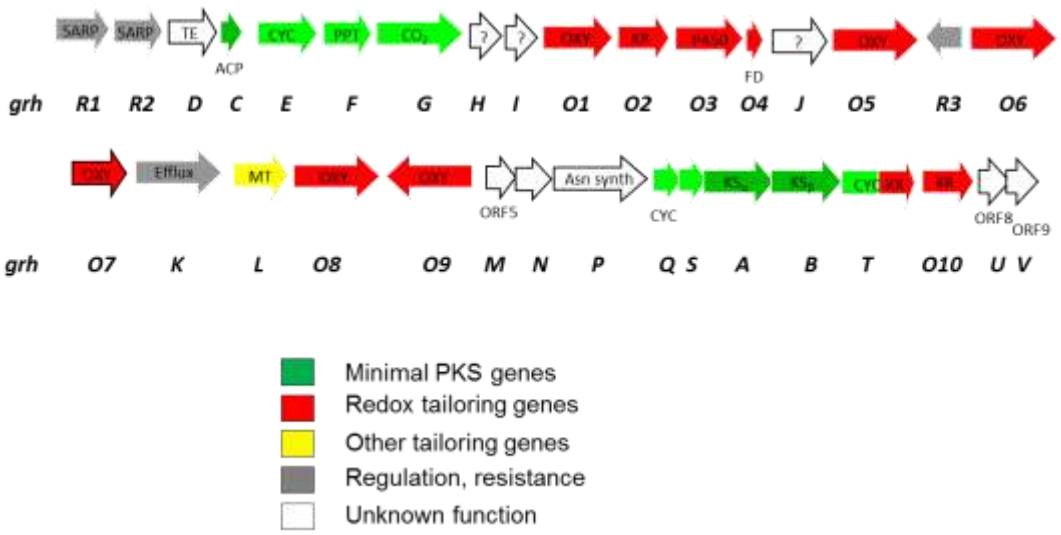

Figure 1.25. Griseorhodin A gene cluster and the suggested function of the genes assigned by the alignment results. [15] The alignment of the genes are shown in Table 1.1.

The cluster shown in Figure 1.25 has a size of 34.2 kb and contains 33 ORFs. According to database homologies, 9 ORFs are core PKS genes, 11 ORFs are tailoring genes, 4 ORFs are involved in regulation and resistance, and 9 genes have unknown functions.[15] Table 1.1 lists the alignment results for the 33 ORFs of the cluster and the proposed functions of the encoded proteins.

Table 1.1 Deduced functions of the open reading frames (ORF) of the *grh* cluster. [15]

Protein	Proposed Function	Sequence Similarity	Similarity /Identitiy
GrhR1	Transcriptonal activator	TylS, *Streptomyces fradiae*[114]	77%/65%
GrhR2	Transcriptonal activator	SAR,	85%/74%
GrhD	Thioesterase	ORF5, *Streptomyces rochei*[115]	68%/58%
GrhC	ACP	ORF3, *Streptomyces rochei*[115]	63%/52%
GrhE	CYC	SimA5, *Streptomyces antibioticus*[116]	51%/35%
GrhF	Phosphopantetheinyl transferase	Gra-ORF32, *Streptomyces violaceoruber*[117]	48%/39%
GrhG	Acetyl-CoA carboxylase	PgaI, S. sp. Pga64	88%/81%
GrhH	Unknown		
GrhI	Unknown		
GrhO1	FAD-dependent oxygenase	MitR, *Streptomyces lavendulae*[118]	57%/44%
GrhO2	2-oxoacyl-ACP reductase	Mtm TII, *Streptomyces rimosus*[68]	61%/50%
GrhO3	Cytochrome P450	PteD, *Streptomyces avermitilis*	70%/55%
GrhO4	Ferredoxin	PteE, *Streptomyces avermitilis*	73%/60%
GrhJ	Unknown	Dra0019, *Deinococcus radiodurans*	41%/31%
GrhO5	FAD-dependent	DntB, *Burkholderia sp.* RASC[119]	56%/44%
GrhR3	MarR family regulatory	2SCD64.11, *Streptomyces*	57%/44%
GrhO6	FAD-dependent	MtmOIV, *Streptomyces*	56%/45%
GrhO7	NADPH:quinone	ActVI ORF2[121]	59%/43%
GrhK	Efflux protein	UrdJ, *Streptomyces fradiae*[122]	58%/40%
GrhL	Methyltransferase	TcmO, *Streptomyces argillaceus*[123]	60%/47%
GrhO8	FAD-dependent	DntB, *Burkholderia sp.* RASC[119]	55%/40%
GrhO9	FAD-dependent	DntB, *Burkholderia sp.* RASC[119]	57%/44%
GrhM	Unknown	ORF5, *Actinomadura hibisca*[124]	47%/36%
GrhN	Unknown	Rv0580c, *Mycsobacterium tuberculosis*	48%/30%
GrhP	Asparagine synthase	TcsG, *Streptomyces aureofaciens*	58%/46%
GrhQ	CYC	RubE, *Streptomyces collinus*	89%/78%
GrhS	Unknown	RubD, *Streptomyces collinus*	81%/75%
GrhA	KS_α	RubA, *Streptomyces collinus*	91%/85%
GrhB	KS_β	RubB, *Streptomyces collinus*	83%/77%
GrhT	Bifunctional CYC-3-oxoacyl-transferase	RubF, *Streptomyces collinus*	77%/69%
GrhO10	3-oxoacyl-ACP reductase	RubG, *Streptomyces collinus*	87%/79%
GrhU	Unknown	RubH, *Streptomyces collinus*	83%/72%
GrhV	Unknown	ORF9, *Actinomadura hibisca*[124]	54%/38%

According to alignment results (Table 1.1), genes encoding the minimal PKS of the griseorhodin A cluster are *grhA*, *grhB*, and *grhC*, which can be identified by

their sequence homology to the other PKS II systems. These genes are responsible for the synthesis of the open-chain polyketide precursor. An interesting feature of the cluster is that the ACP gene *grh*C is located 26 kb upstream from the two KS/ORFs, representing a rare case of disconnected minimal PKS compared to the grouped minimal PKS of rubromycin sequence.

There are twelve putative redox-tailoring enzymes. *grhO1* is a rare oxidoreductase gene. The enzyme has a covalently bound flavin-adenine dinucleotide (FAD) as a cofactor.[15] GrhO3 is a similar to oxygenase of the cytochrome P450 family. GrhO4 is very similar to many ferrodoxin proteins and it functions as a component of the P450 oxygenase. GrhO3. GrhO5, GrhO6, GrhO8, GrhO9 have homologies to FAD-dependent monooxygenases. GrhO6 has a very close homology to a rare Baeyer-Villiger-type monooxygenase of the mitramycin cluster (MtmOIV) [120]. *GrhO7* gene aligns well with the genes of the enzymes of the NADPH:quinone oxidoreductase/ζ- crystalline (QOR) group which catalyze one-electron transfer reactions from quinone to semiquinone radicals. GrhO2, GrhO10, and the C-terminal half of GrhT have end to end similarities to enzymes of the short chain dehydrogenase/reductase (SDR) family. Other proteins structurally related to these redox enzymes are FabG enzymes from fatty acid biosynthesis that have 3-oxoacyl-ACP reductase function.[15] Regulatory genes, *grhR1* and *grhR2* have functions in the transcription control of the metabolites. Their sequences are similar to the sequences of the transcriptional activators of the Streptomyces antibiotic regulatory protein (SARP) family. GrhR3 has high homology to transcriptional repressors of the MarR family.[15] The proposed function of this protein is to control the transport of the synthesized antibiotic and impart self-resistance to the producer.

There are several genes on the cluster encoding proteins with unknown functions. Alignment studies did not provide any clues about the functions of the proteins encoded by the genes *grhH*, *grhI*, *grhJ*, *grhM*, *grhN*, *grhP*, *grhT*, *grhU* and *grhV.*[15]

For the accessory genes, a more recent alignment study was carried out by Kathrin Rheinhardt in the Piel group in order to determine sequence

similarities to other structurally similar polyketides such as rubromycins **(37)**, fredericamycin **(26)** and pradimicin **(29)**.[125] Accessory enzymes are responsible for the cyclization of the open chain precursor. The involvement of at least two cyclases is expected. In addition, the genes *grh*S, *grh*T and *grh*Q are possible candidates to encode the cyclases and aromatases function. Recent research on fredericamycin **(26)** and pradimicin **(29)** cluster genes suggests that the proteins GrhU and GrhV could also be involved in cyclization and oxygenation steps for the formation of the pentangular aromatic precursor.[15,125]

Another result of this study is that the protein GrhJ has a sequence similar to a N-Acetyl-transferase GNAT protein. [125] It is reported that type-I PKSs sometimes use GNATs to incorporate acetyl starter-unit into complex polyketides.[147]

Based on these homologies, it is hypothesized that griseorhodin A **(5)** could be synthesized by a large number of complex oxidative steps acting on a tridecaketide aromatic precursor. The biosynthesis postulated in 2002 is shown in the Figure 1.26.[15]

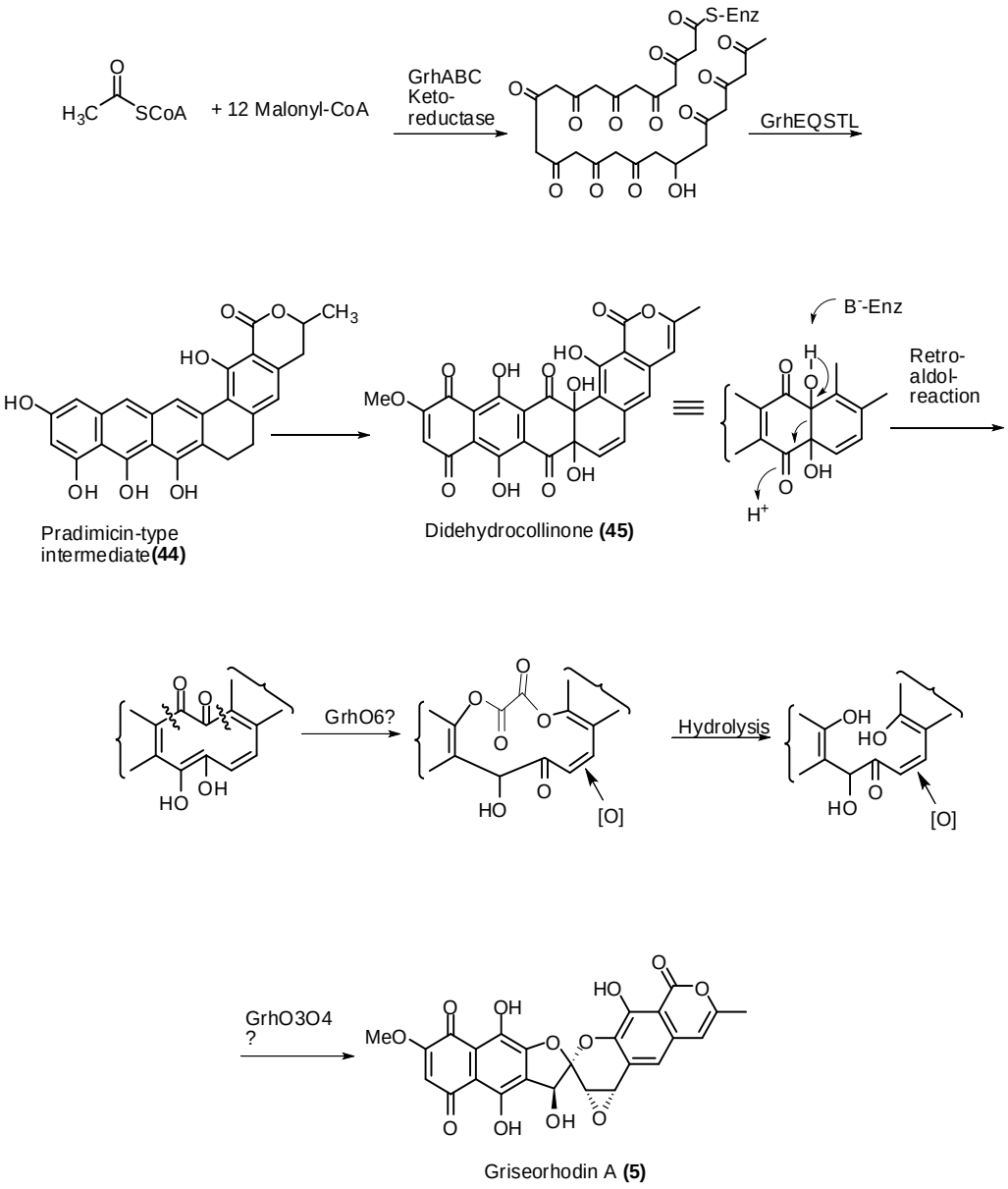

Figure 1.26.Initially postulated biosynthetic pathway leading to the formation of griseorhodin A via the hypothetical intermediate didehydrocollinone (45).[15]

2 GOALS OF THE THESIS

The main objective of this work is the testing of the hypotheses on the biosynthesis of the bacterial aromatic polyketide griseorhodin A **(5)**, shown in Figure 2.1. Background information about the aromatic polyketide griseorhodin A can be found in the introduction. The most important and pertinent characteristics of this compound are its highly oxidized nature and its pharmacologically important spiroketal moiety. The biosynthesis of this polyketide is a current research topic of the research group Piel.

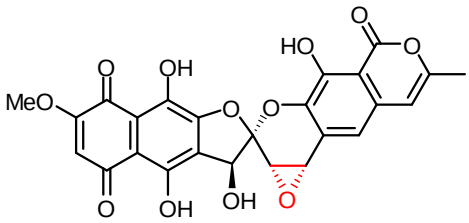

Griseorhodin A **(5)**

Figure 2.1 The structure of the aromatic polyketide griseorhodin A (5).

The griseorhodin A gene cluster was isolated and heterologously expressed by A. Li. [15]In addition, she reported a bioinformatic analysis of the genes on the cluster. Assuming the functions of several genes, the biosynthetic pathway investigated in this thesis was postulated.[15] The postulated biosynthesis involves the actions of several tailoring enzymes.

In order to prove the functions of the genes encoding the tailoring enzymes and to investigate the role of the genes with unknown functions, heterologous expression systems of individual single gene deletion mutants of the griseorhodin A cluster in *S. albus* host strain had to be obtained and the produced metabolites had to be chemically investigated. This chemical investigation is summarized in this thesis. For this investigation, 19 single gene knockout strains were used, which were successfully produced via λ-red-mediated gene deletion and the conjugation of these clusters into the expression strain *Streptomyces albus* J1074 in a concomitant work by K. Reinhardt.[99,125] In

each mutant strain a different protein involved in the biosynthesis was deactivated by deleting the corresponding gene. To obtain insights into the biosynthesis of griseorhodin A **(5)**, the metabolites produced by each single gene deletion strain had to be investigated to deduce the function of the deleted gene and its corresponding protein in the biosynthetic pathway. Figure 2.2 shows the griseorhodin A gene cluster and the pictures of the 19 one-gene knockout strains used for the studies of the pathway.

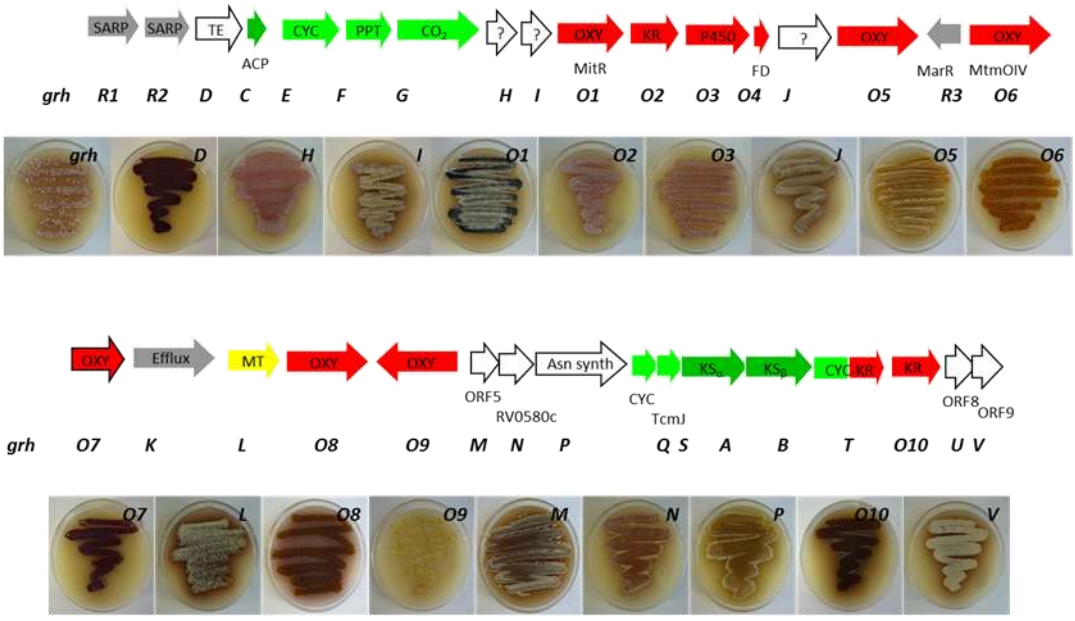

Figure 2.2 The Griseorhodin A gene cluster and the pictures of the 19 single gene-knockout strains of the cluster. The cluster contains 33 ORFs. In order to investigate the functions of the proteins and the biosynthesis of the compound, 19 single genes of the cluster were deactivated by deletion, and the modified clusters were heterologously expressed in *S. albus* host strain. The picture shows the position of each gene on the cluster and the heterologous expression strains carrying the deletion of the corresponding gene. In the picture of each mutant strain, the deactivated gene is indicated.

In order to achieve the objective of testing the hypothesized pathway, this study focuses on the identification of the enzymes involved in the construction of the highly unusual spiroketal moiety, the determination of the enzymes essential for the epoxidation, the investigation of functions of the genes that were formerly reported to have unknown functions and the detailed discussion of the

biosynthetic route of griseorhodin A **(5)** with emphasis on the compounds isolated during this study.

Specifically, the goals of this study were to investigate the metabolites of the aforementioned single gene deletion strains, to provide optimized analytical methods for screening the extracts using different techniques such as HPLC and LC-MS/MS, to develop isolation and purification steps for intermediates and to elucidate their structures using HRMS and NMR techniques as well as other spectroscopic methods.

An inseparable part of this project was the examination of better fermentation conditions for *Streptomyces albus* mutants using baffled flasks. The fermentations had to be performed in 10-20 L scale in order to obtain 10-20 mg of pure compounds for structure elucidation. These amounts were necessary for analytical measurements and also for further pharmacological activity assays of the compounds, which were partially performed by different collaborators.

During this work an assay with the overexpressed unusual oxygenase GrhO6 related to Baeyer-Villigarases also had to be performed to investigate its enzymatic activity

The absolute configurations of griseorhodin A **(5)** and of some of the other novel isolated polyketides had to be determined in collaboration with the group of Prof. Dr. G. Bringmann at the University of Würzburg.

3 RESULTS AND DISCUSSION

3.1 Heterologous Expression in the *Streptomyces albus* Host

Functional studies of the griseorhodin A **(5)** gene cluster were performed after the entire cluster was heterologously expressed in the host expression strain *Streptomyces albus* J1074.[99,125] The use of *Streptomyces albus* J1074 enables the integration of the entire cluster as well as the engineered variants into the host strain's genome red-mediated gene deletion and the conjugation of these clusters into the expression strain. This allowes the production of sufficient amounts of complex metabolites heterologously not only on agar plates, as is the case for other Streptomyces hosts, but also in liquid media. [74]

This property of the host strain facilitates the production of large amounts of metabolites. However, in order to obtain the desired quantities, a few challenging issues needed to be resolved. The production efficiency of the *S. albus* mutants varies significantly according to the growth conditions such as growth medium, temperature, time and the genes inserted into the genome. Moreover, the metabolism of the cultured organism switches at a certain stage of the life cycle to sporulation mode inhibiting the production of secondary metabolites.[74] Finally, the expression of highly oxidized secondary metabolites necessitates an adequate oxygen supply from the environment. Therefore, either baffled or normal Erlenmeyer flasks containing spiral-steel wires were used in order to provide sufficient oxygen to the growth medium during the fermentation process in the experiments discussed in this thesis.

3.1.1 Determination of the Growth- and Production Curve of *S. albus* MP66

An experiment with the *grhO6* gene deletion strain *S. albus* MP66 was conducted to obtain insights into the fermentation process. During the experiment, the expression of metabolites and the growth of the bacteria were monitored. Since various pigments produced by the strain show strong UV absorptions in a broad range, the expression of polyketides related to the aromatic quinone compound griseorhodin A **(5)** were monitored by measuring

their absorption at 488 nm. This wavelength is chosen because it is a specific absorption maximum of the aromatic quinone function of griseorhodin-type compounds. The cell density (OD) of *S. albus* MP66 was monitored by measuring the absorption at the wavelength of 600 nm, which is the wavelength generally used to observe bacterial growth. However, the strong absorption of the produced pigments and the occurrence of cell clumping during growth prevented the accurate determination of bacterial density. Therefore, to monitor bacterial growth more accurately, the biomass of the mycelium was determined. The bacterium was separated by centrifugation, freeze-dried, and weighed so that for each measuring point, the biomass of the bacteria could be determined. The details of the experimental procedure are explained in Section 4.1.5.1. Table 3.1 shows the results of the experiments.

Table 3.1 Biomass and expression data during the growth of *S. albus* MP66.

Measuring point	ΔT time [h]	OD_{600} [nm]	OD_{488} [nm]	Δ Biomass [mg]
0	0	0.035	0.05	18
1	17	0.06	0.11	120
2	20.5	0.12	0.27	183
3	40.5	0.88	1.94	327
4	44.5	1.18	2.99	346
5	63	1.46	3	342
6	68.5	1.68	3	362
7	88.5	1.80	3	389
8	100	2.55	3	485

Figure 3.1 shows the absorption at 488 nm of the pigments during the incubation period. As a result of this experiment, it was concluded that the expression reaches a maximum after two days and remains constant up to the last measuring point at 88 hours.

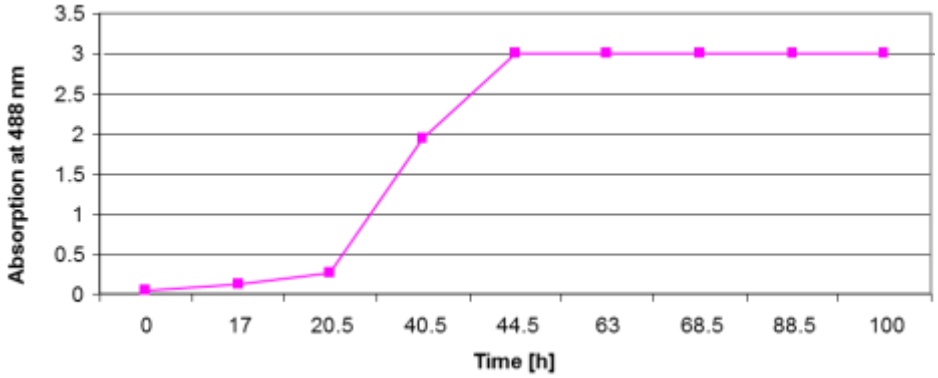

Figure 3.1 Absorption at 488 nm of the pigments expressed by *S. albus* MP66 with respect to the incubation period .

The growth curve in Figure 3.1 shows that the strain needs two days to achieve maximum production of the metabolites. After four days of incubation, the bacteria enter the sporulation phase, during which the secondary metabolite production of the strain is suppressed. (Figure 3.2B) The growth curve of the cell density values at OD_{600} shows a steady increase up to the fourth day and a rapid increase in growth after that. (Figure 3.2A) The biomass increases rapidly in the first two days. The biomass production slows down in the following two days. During this period, the absorption measured at 488 nm attains its maximum value. This behavior is additional evidence that the strain slows down its growth while expression of secondary metabolites occurs. At the last measuring point, which shows the amount of bacteria after 100 hours of incubation, an increase in the biomass can be observed. At this point, the bacterium starts sporulation, suppressing the expression of the secondary metabolites. (Figure 3.2B) As a result of these observations, it was concluded that four days was a reasonable time period for the incubation of the test strain *S. albus* MP66 in order to obtain the maximum amount of secondary metabolites and start the extraction procedure to isolate the compounds in the fermentation broth.

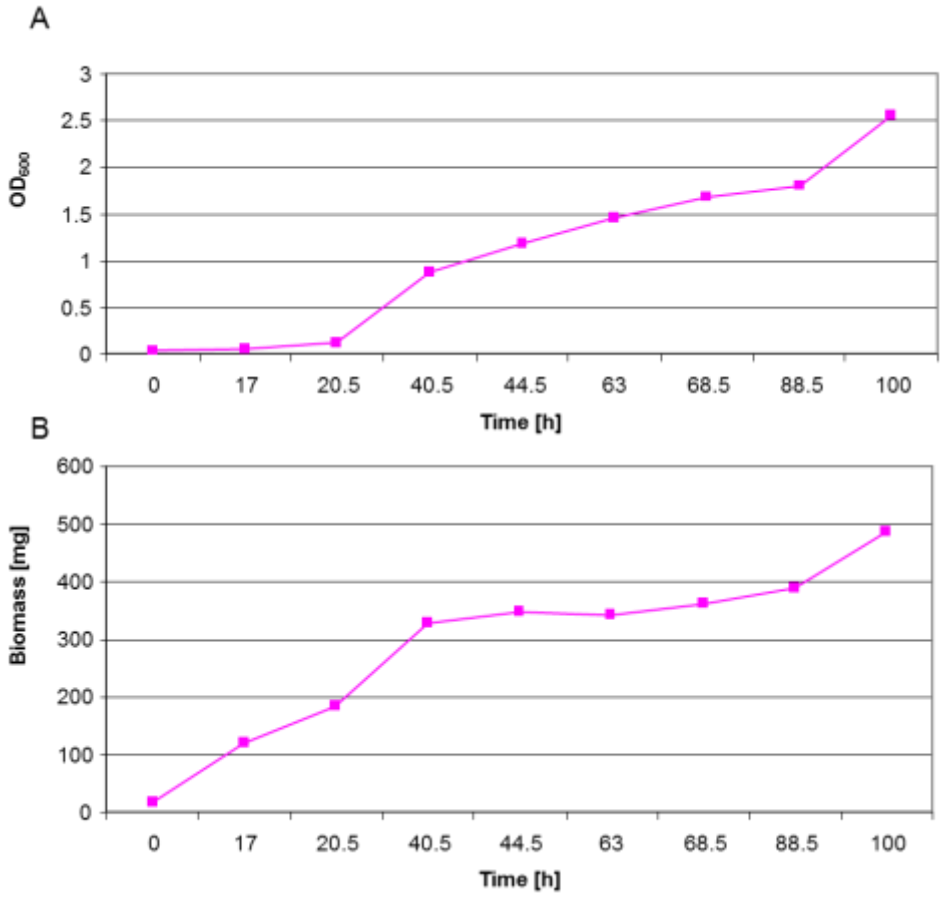

Figure 3.2 Growth of *S. albus* MP66. A. Growth of the strain with respect to the incubation time measured using absorption at 600 nm. (OD_{600} values) B. Biomass of the strain with respect to incubation time

3.1.2 Fermentation Media of the Mutant Strains

The yields of secondary metabolites vary according to growth media. In the literature, six different types of media for *S. albus* can be found. A. Li *et al.* [15] reports that LB and TSB growth media are the most efficient media for the fermentation of *S. albus*. On the other hand, for cultivation on plates, 2CM and MS agar plates are recommended. To determine the appropriate fermentation medium, small-scale fermentations of each strain in LB and TSB were performed. The medium providing the best expression was chosen, and the yield of the crude extract was determined. Table 3.2 summarizes the results. The amounts of crude extract obtained for each mutant strain vary significantly. The difference between masses could also be due to the metabolites other than

griseorhodin-type metabolites such as lipids. Table 3.2 shows the best growth medium for each strain for fermentation. Additionally, yields of the crude extracts obtained from small-scale fermentations in 400 mL after extraction with ethyl acetate in acidic conditions are listed. The ingredients of various growth media are listed in Section 4.1.1. The fermentation procedures are in Section 4.1.2.3 and 4.1.2.4.

Table 3.2 Fermentation conditions and yields of the crude extracts of the strains.

S. albus **mutants**	**Growth medium**	**Medium extract (mg/400 mL)**	**Mycelium extract (mg/400 mL)**
S. albus MP31	LB	28	20
S. albus KR13	LB	50	20
S. albus KR5	TSB	108	30
S. albus KR42	LB	83	9
S. albus KR8	TSB	123	49
S. albus MP66	LB	83	59
S. albus KR7	LB	99	56
S. albus KR40	LB	95	16
S. albus KR11	TSB	73	50
S. albus KR53	LB	54	28
S. albus KR41	LB	99	24
S. albus KR15	LB	55	42
S. albus MP63	LB	61	31
S. albus J1074	TSB	54	21
S. albus J1074	LB	27	12

The yields obtained from small-scale fermentations are not indicative for large-scale fermentations. The follow-up large-scale fermentations performed for most of the strains exhibited nonuniform production properties and yields. Possible reasons for this behavior are the high sensitivity of the host strain to small changes in the fermentation environment and the possible phenotype differences of the bacteria used for inoculation.

In conclusion, it is obvious that the different mutant strains produce very different amounts of secondary metabolites and need different fermentation conditions for the expression, despite the fact that the host bacteria used for the expression are the same. The mutations on the expressed gene cluster and the

produced metabolites influence the growth and the expression behavior of the host bacteria strongly.

3.1.3 Gene Deletion Strains of the Griseorhodin A Cluster

In the work of A. Li *et al.* a strain containing the entire *grh* cluster, termed *S. albus* MP31, was constructed.[15] In addition, four gene deletion strains, *S. albus* MP66, *S. albus* MP36, *S. albus* MP70 and *S. albus* MP63, of the *grh* cluster were prepared by using restriction sides in the gene regions. The genes *grhO6*, *grhI+O1*, *grhR2* and *grhO10* were deactivated in that study. These strains were used for initial experiments during this PhD thesis. The list of the mutant strains prepared by A. Li are in Table 3.3.

Table 3.3 List of all gene deletion strains prepared by A. Li.

Number	*S. albus* mutants	Deleted gene region	Proposed function of the missing protein
1	*S. albus* MP31	Entire *grh* cluster	----
2	*S. albus* MP70	Δ*grhR2*	SARP gene (Regulatory protein)
3	*S. albus* MP66	Δ *grhO6*	FAD-dependent monooxygenase
4	*S. albus* MP36	Δ*grhI+*Δ*grhO1*	GrhI: unknown, GrhO1: Covalently bond FAD-dependent oxygenase
5	*S. albus* MP63	Δ *grhO10*	3-Oxoacyl-ACP reductase

S. albus MP70 is a mutant with a deactivated *grhR2* gene region. GrhR2 was thought to have a regulatory function. However, deactivation of the gene did not affect the production of griseorhodin A **(5).** Hence it was concluded that *grhR2* was not directly involved in the biosynthesis steps. The putative oxidoreductase GrhO10 was supposed to be a tailoring enzyme. Biosynthesis did not occur properly and no pigments were produced during the expression of the strain with the deactivated *grhO10* gene. This is evidence that this gene has a more essential role in biosynthesis than a mere tailoring function. The strains *S. albus* MP66 and *S. albus* MP36 produce colored pigments different from those of *S. albus* MP31, which expresses griseorhodin A **(5)** as a red colored pigment. The

successful expression observed for the mutant strains enabled to apply the method of studying the biosynthesis of the compound by deactivating single genes of the cluster and expression in a *S. albus* host strain in order to characterize the accumulating intermediates. This enables to assigne the functions of many tailoring enzymes on the cluster.

In order to realize this goal, K. Reinhardt prepared an additional 17 single gene knockout strains by an advanced and more reliable molecular biological method using recombination sites to delete a specific gene region precisely. Inactivation of the corresponding genes was performed by λ Red-mediated recombination on pMP31.[125] Primers specific for flanking griseorhodin A gene regions and a template plasmid pIJ778, which harbors the spectinomycin resistance gene *aadA*, were used. The prepared recombination cassettes were subsequently electroporated into *E. coli containing* pMP31.[99] The resistance gene was subsequently removed by selection of spectinomycin-resistant clones carrying the *aadA* gene instead of the target gene and subsequent performens FLP-mediated excision or *Spe*I restriction and religation. In this way, deletion of 17 individual genes from the gene cluster was acomplished. Each gene cluster was transferred by conjugation into *S. albus*, which enables a stable integration into the genomic *attB* site. The host strains were grown and used for heterologous polyketide production in the course of the biosynthesis study.[99,110] The details of the molecular biological methods used can be found in the PhD thesis of K. Reinhardt.[125] Besides the strain MP66, new strains were created for expression and gene function studies. The list of the strains obtained and utilized in this PhD thesis is given in Table 3.4. Figure 3.3 displays the clear differences in morphological appearances caused by the different coloration of the produced metabolites.

Table 3.4 List of *S. albus* MP31 containing the entire griseorhodin A **(5)** cluster and all gene deletion strains used for the biosynthetic study and the assumed functions of the deleted genes.

Number	*S. albus* mutants	Deleted gene	Proposed function of the missing protein
1	*S. albus* MP31	----	----
2	*S. albus* KR13	Δ*grhD*	Thioesterase
3	*S. albus* KR5	Δ*grhO1*	FAD-dependent oxygenase
4	*S. albus* KR42	Δ*grhJ*	N-Acetyltransferase (GNAT)
5	*S. albus* KR8	Δ*grhO5*	FAD-dependent monooxygenase
6	*S. albus* MP66	Δ*grhO6*	FAD-dependent monooxygenase
7	*S. albus* KR7	Δ*grhO7*	NADP:quinone oxidoreductase
8	*S. albus* KR40	Δ*grhL*	Methyl transferase
9	*S. albus* KR11	Δ*grhO8*	FAD-dependent monooxygenase
10	*S. albus* KR53	Δ*grhO9*	FAD-dependent monooxygenase
11	*S. albus* KR41	Δ*grhM*	Unknown
12	*S. albus* KR15	Δ*grhP*	Asparagine synthetase
13	*S. albus* MP63	Δ*grhO10*	3-Oxoacyl-ACP reductase
14	*S. albus* KR27	Δ*grhH*	Unknown
15	*S. albus* KR4	Δ*grhI*	Unknown
16	*S. albus* KR39	Δ*grhO2*	2-Oxoacyl-ACP reductase
17	*S. albus* KR43	Δ*grhO3*	Cytochrome P450
18	*S. albus* KR23	Δ*grhN*	Unknown
19	*S. albus* KR61	Δ*grhU*	Unknown
20	*S. albus* KR58	Δ*grhV*	Unknown

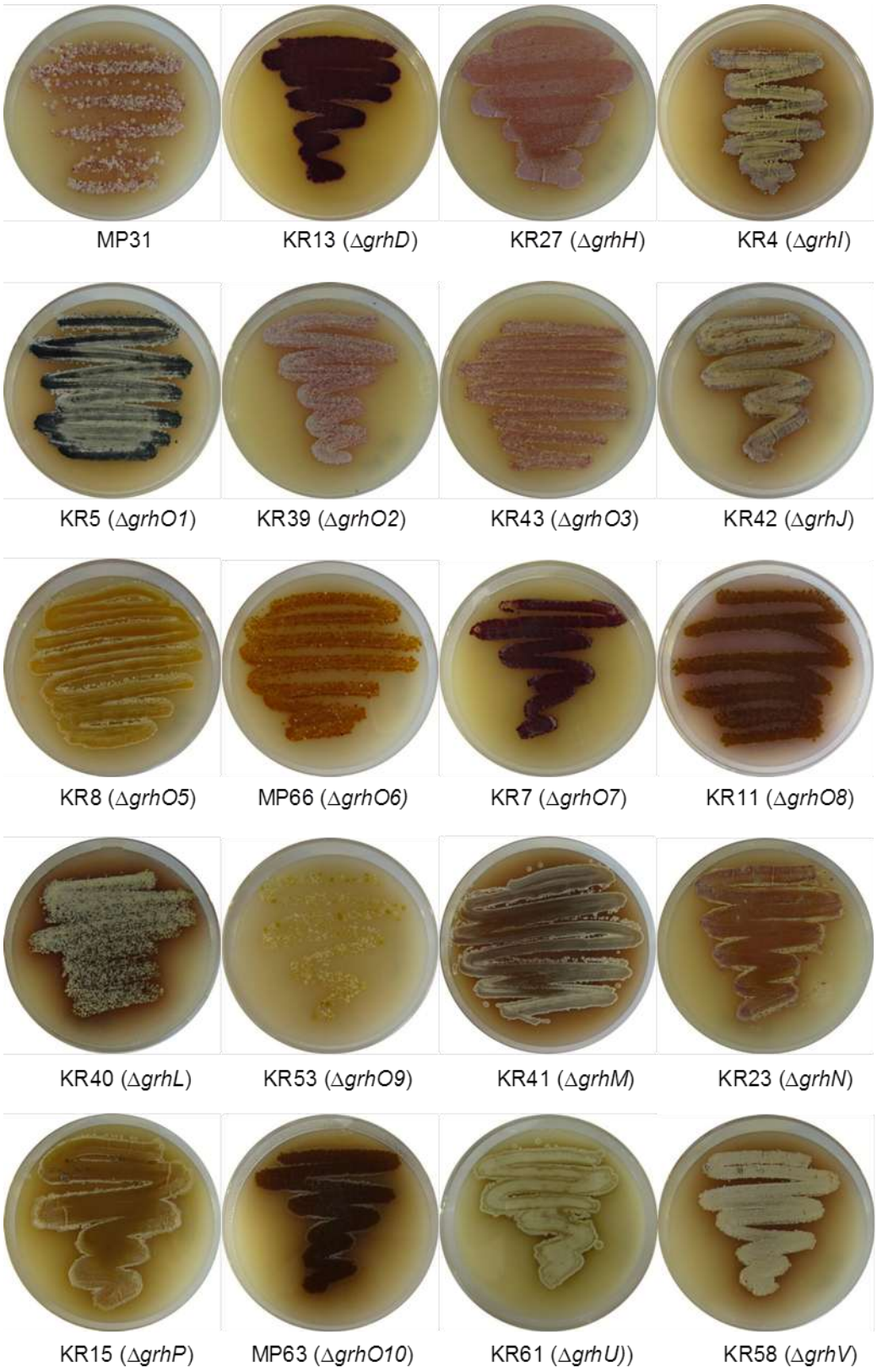

Figure 3.3 Morphological appearances of the mutant strains used for biosynthesis pathway investigation.

After the fermentation of the various strains in liquid medium, as listed in the Table 3.2, the mycelium and the liquid medium were separated by centrifugation as described by Eckardt *et al*. for the isolation of griseorhodin A **(5**).[14] A detailed description of the general extraction can be found in Section 4.1.5.2. Afterwards, these crude extracts were analyzed on HPLC and TLC plates. This analysis revealed that several extractable pigments were produced by the mutant strains that were not produced by the native host strain. These pigments, which might be intermediates of griseorhodin A biosynthesis or a shunt products of the pathway, had to be characterized. After comparing of the TLC fingerprints of the extracts obtained from the mutant strains to the wild type *S. albus* strain, it was found out that new metabolites were produced in addition to the metabolites of the wıld type host strain. This observation showed that the host strain produces metabolites unrelated to the griseorhodin biosynthesis even though the wild-type host strain supposedly does not contain any other polyketide gene clusters. It was observed that these compounds are expressed mostly during the fermentation period in liquid medium. The experiments revealed that these impurities strongly disturb the HPLC and LCMS analysis of the crude extract; furthermore, the impurities prevented the LCMS and HPLC analysis from identifing molecular ions of the new metabolites. To charecterize the compounds, which could be potential intermediates of griseorhodin A biosynthesis, and, which should be isolated from these extracts, another set of experiments were conducted.

It is known that griseorhodin A **(5)** accumulates on the bacteria during the production period. Because of its insolubility in water, similar aromatic intermediates were expected to gather on the mycelium as well. It was found that less complex extracts of the cells could be obtained, when the strains were grown on 2CM and MS agar plates, thus simplifying analysis of the respective pathway. The cell extracts obtained from 2CM agar cultures had the least impurities. In several cases, the precursor compounds and metabolites were observed as single peaks during HPLC analysis, which helped to provide more valuable information for the LCMS measurements of the fermentation extracts. Nevertheless, the amounts of the compounds obtained from agar plate extracts were not sufficient for the isolation of potential intermediates. Therefore, large-

scale fermentations in LB or TSB medium were used for full structural elucidation of the compounds. Figure 3.4 shows the procedure used for the investigation of these extracts in a flow chart.

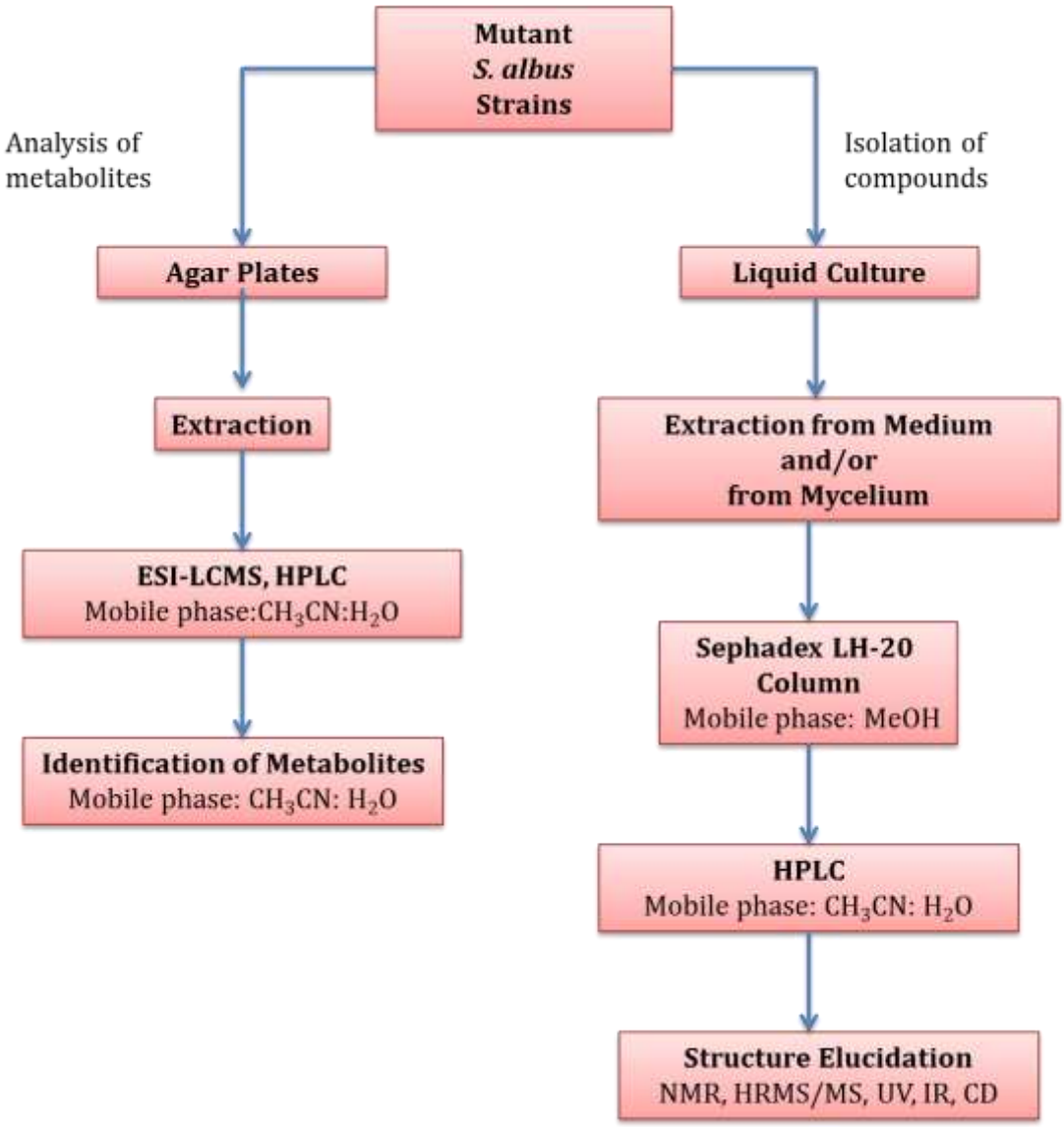

Figure 3.4 The procedure used for the investigation of these extracts in a flow chart.

.

3.2 HPLC and LC-HRMS Analysis of the Strains

To obtain an overview of the metabolites, strains were grown on 2CM agar plates. Details of the cultivation are given in Section 4.1.2.2. The bacteria with pigments were scratched off and extracted for HPLC, LC-MS and TLC analysis. The procedure for the extraction and the details of the procedures for preparing the probes are described in Section 4.1.5.2. The molecular ions of the detected metabolites were determined by LC-HRMS. Figure 3.5 shows the HPLC profile of the griseorhodin A **(5)** producing strain MP31, which contains the entire *grh* cluster for the expression. Figure 3.5 also shows the profiles of the mutant strains with deactivated *grh* genes and the predicted molecular formulae of the compounds according to the molecular ions characterized using LC-HRMS analysis. Table 3.5 shows the predicted molecular formulae according to the molecular ions characterized during LC-HRMS analysis of the single gene deletion mutants. The putative functions of the deactivated genes are also shown in Table 3.5.

These results show that the mutant *S. albus* strains KR13, KR27, KR4, KR39, KR23 still produce the compound griseorhodin A **(5)**. The genes inactivated through deletion from these mutant strains are *grhD, grhH, grhI*, *grhO2 and grhN* respectively. It seems that proteins expressed by these genes are either nonfunctional for the biosynthesis of griseorhodin A **(5)** or other genes on the cluster can take over the functions of the deleted gene so that the biosynthesis of the compound is not interrupted. The effect of the genes involved in tailoring steps can be observed directly from the oxygen and carbon numbers in respective molecular formulae.

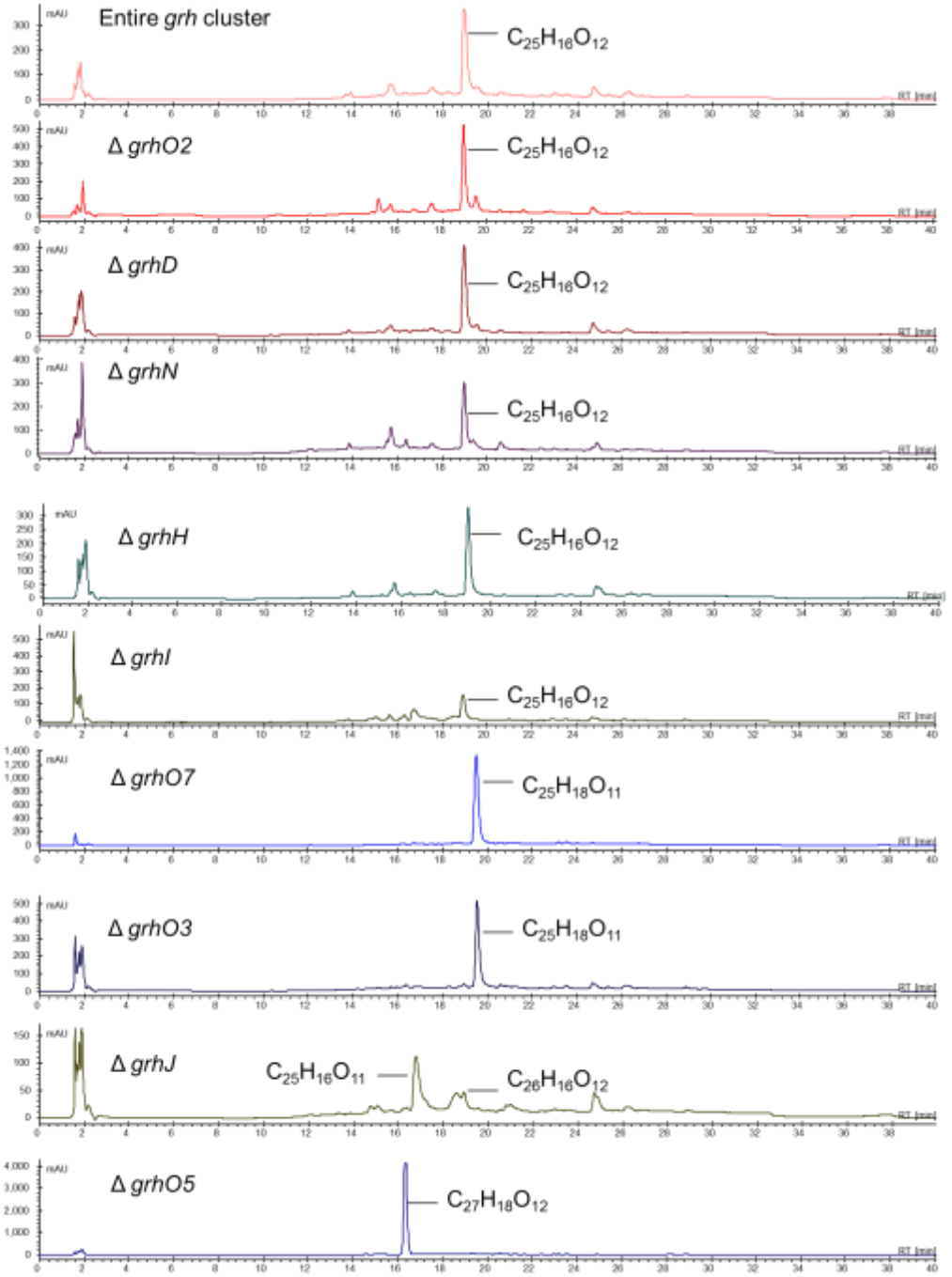
Entire grh cluster
C25H16O12
Δ grhO2
C25H16O12
Δ grhD
C25H16O12
Δ grhN
C25H16O12
Δ grhH
C25H16O12
Δ grhI
C25H16O12
Δ grhO7
C25H18O11
Δ grhO3
C25H18O11
Δ grhJ
C25H16O11
C26H16O12
Δ grhO5
C27H18O12

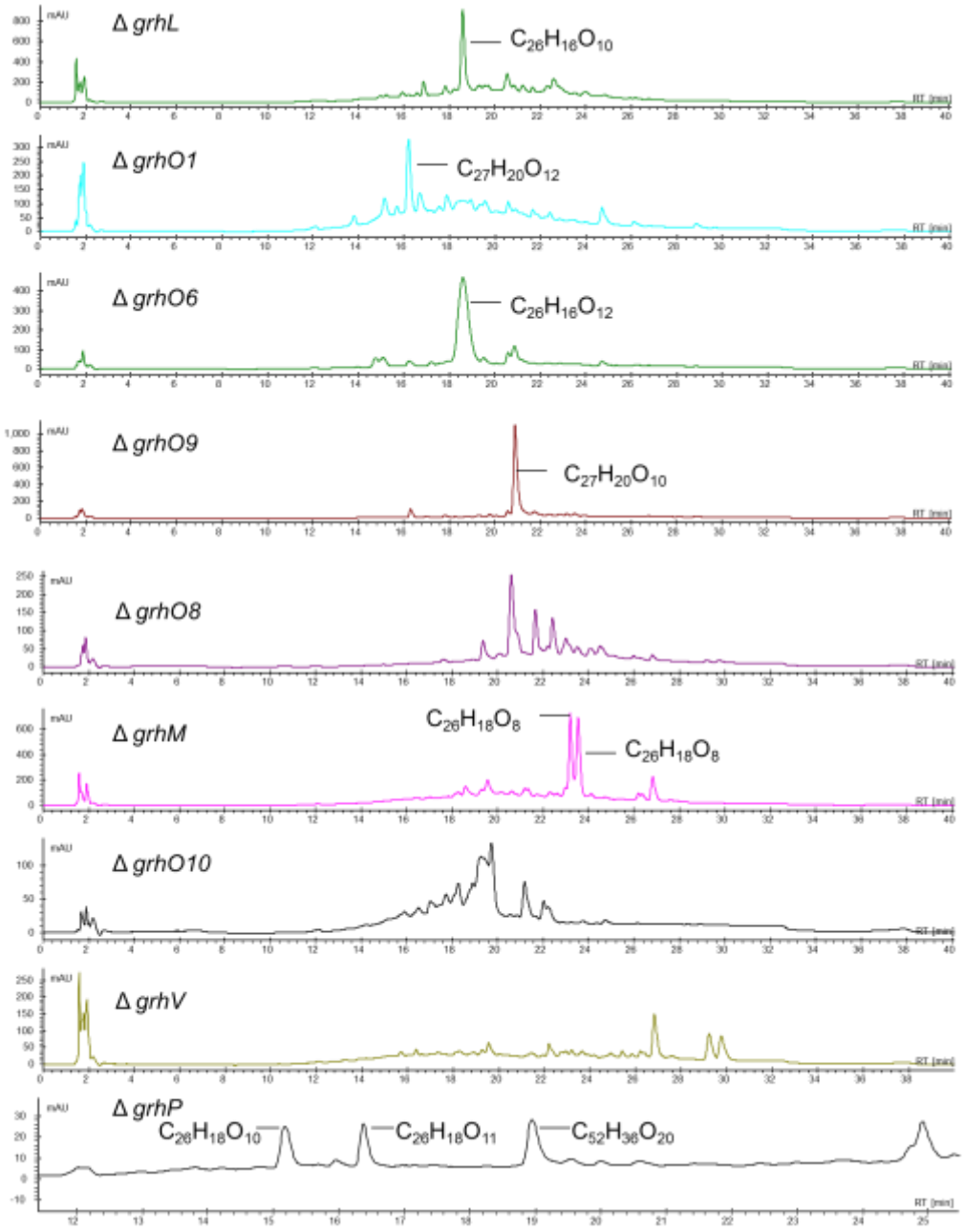

Figure 3.5 HPLC profile of the extracts and the predicted molecular formulae of the compounds according to the molecular ions characterized using LC-HRMS. The first extract is obtained from griseorhodin A (5) producing strain *S. albus* MP31, which contains the entire *grh* cluster for the expression. The HPLC profiles obtained from the extracts of the mutant strains with a deactivated *grh* gene and the predicted molecular formulae of the major compounds are also shown. The bacterial extracts were obtained by cultivation on 2CM agar plates.

Table 3.5 HR-LCMS analysis of the strains. Data are shown for the most prominent compounds observed in the bacterial extract obtained by cultivation on 2CM agar plates.

S. albus **strain**	**Deleted ORF**	**Putative protein function**	**Measured *m/z* [M+H]$^+$**	**Predicted Molecular formula**
JP95[a]	----	----	509.0720	$C_{25}H_{16}O_{12}$
MP31[b]	----	----	509.0720	$C_{25}H_{16}O_{12}$
KR13	*grhD*	Thioesterase	509.0717	$C_{25}H_{16}O_{12}$
KR27	*grhH*	Unknown	509.0720	$C_{25}H_{16}O_{12}$
KR4	*grhI*	Unknown	509.0717	$C_{25}H_{16}O_{12}$
KR39	*grhO2*	Ketoreductase	509.0720	$C_{25}H_{16}O_{12}$
KR23	*grhN*	Unknown	509.0711	$C_{25}H_{16}O_{12}$
KR43	*grhO3*	Cytochrome P450	495.0922	$C_{25}H_{18}O_{11}$
KR7	*grhO7*	NADPH: quinone oxidoreductase	495.0922	$C_{25}H_{18}O_{11}$
KR42	*grhJ*	GCN5-related N-acetyltransferase family	493.0769	$C_{25}H_{16}O_{11}$
			521.0716	$C_{26}H_{16}O_{12}$
			457.0921	$C_{26}H_{16}O_{8}$
MP66	*grhO6*	FAD-dependent oxygenase	337.0550	$C_{15}H_{12}O_{9}$
			521.0720	$C_{26}H_{16}O_{12}$[c]
KR8	*grhO5*	FAD-dependent oxygenase	535.0877	$C_{27}H_{18}O_{12}$
KR53	*grhO9*	FAD-dependent oxygenase	505.1120	$C_{27}H_{21}O_{10}$
KR15	*grhP*	Amido transferase	491.0975	$C_{26}H_{18}O_{10}$
			507.0922	$C_{26}H_{18}O_{11}$
			981.1870	$C_{52}H_{36}O_{20}$
KR11	*grhO8*	FAD-dependent oxygenase	477.1150	$C_{26}H_{20}O_{9}$
KR40	*grhL*	Methyl transferase	489.0785	$C_{26}H_{16}O_{10}$
			471.0695	$C_{26}H_{14}O_{9}$
KR41	*grhM*	Unknown	459.1050	$C_{26}H_{18}O_{8}$
KR5	*grhO1*	Oxygenase with covalently bound FAD	537.1021[c]	$C_{27}H_{20}O_{12}$[c]
MP63	*grhO10*	3-Oxoacyl-ACP reductase	n.d.[d]	n.d.[d]
KR61	*grhU*	Unknown	n.d.[d]	n.d.[d]
KR58	*grhV*	Unknown	n.d.[d]	n.d.[d]

[a]wild-type griseorhodin producer
[b]S.albus carrying the entire grh cluster
[c]modified fermentation and extraction protocol
[d]polyketides bound irreversibly to chromatographic stationary phases or the amount of the expressed compounds in the extract were not enough to obtain a molecular ion.

Due to the postulated biosynthesis that starts with one initial poly-β-keto chain, which is subsequently folded into a pentangular aromatic scaffold and methylated, it was expected to obtain intact intermediates with a molecular scaffolds having up to 26-27 carbon atoms, depending of O-methylation. Molecular ions matching this found could be detrmined in the analysis of the *S. albus* strains KR8, KR53 and KR5, which have the genes for oxygenases *grhO5, grhO9 and grhO1* deactivated, respectively. These compounds have also the highest number of oxygen atoms in their scaffolds. This suggests that these deleted oxygenase genes might be involved in oxidation steps resulting in the elimination of two carbon atoms of intermediates containing 26 or 27 carbon atoms in order to generate the spiroketal compound griseorhodin A **(5)** with 25 carbon atoms. Other interesting compounds were observed in the extract of the *S. albus* strain MP66 and KR42, which contain 26 carbon atoms. The evidence that the extract of the *S. albus* strain MP66 and KR42 contain 26 carbon atoms shows that the enzyme GrhO6 and the protein GrhJ had a function after a step causing the lost of a carbon atom. Extracts of the *S. albus* strain KR7 and KR43 contained a highly oxidized intermediate with 25 carbon atoms and 11 oxygen atoms. The deactivated proteins probably act during the last steps of the biosynthesis. There are compounds in the extracts of the strains KR41 and KR11 containing 26 carbons but a fewer number of oxygen atoms. This situation may indicate an involvement of the deleted proteins in the early oxygenation steps of the aromatic polyketide prepared by cyclases and aromatases. The mutant strains MP63, KR61 and KR58 showed an observable change in the expression on the agar plates in comparison to the wildtype *S. albus* host. However, there were no colorful pigments to observe, and the extracts contained insufficient amounts of compounds to determine molecular ions of the metabolites. The strain KR15 expressed a few colorless compounds, which diffused into the agar. Therefore, the agar was extracted and the molecular ions for the compounds in the extract were determined.

Strains determined by the experiments to produce important metabolites in sufficient amounts were used for large scale fermentations from 12 L up to 20 L, and the detected components were isolated from the fermentation extracts in order to further characterize their structures.

3.3 TLC Analysis of the Fermentation Extracts

In order to compare the components and production of the mutant strains, a TLC analysis of the prepared mycelia and medium extracts were performed as described in Section 4.1.4.3 in detail. The crude extract was dissolved in the mobile phase $CHCl_3$:MeOH (9:1). As a stationary phase, silica plates impregnated with 2 M NaH_2PO_4 or KH_2PO_4 were used. It was better to use impregnated plates, since they simplified the detection of polar compounds. Impregnating the silica material before use prevents the polar aromatic phenolic compounds and griseorhodin type of compounds from attaching on the material. Depending on the pKa value, these compounds become deprotonated, and form strong interactions on silica materials. Impregnation of the silica plates results in full protonation and decrease of polarity of the analytes, thus improving chromatographic behaviour. The same principle also helps during flash chromatographic purification of the extracts containing phenolic aromatic compounds. The procedures of the impregnation and chromatographic applications are elaborated in detail in Section 4.1.4.2 and Section 4.1.4.1. Figure 3.6A shows the TLC analysis of the medium extracts obtained from the fermentation of the strains in the medium mentioned in the Table 3.2. The extracts of mycelium can be seen in Figure 3.6B, which shows that the mycelia contain more compounds and are less complex than the extracts of the fermentation medium shown in Figure 3.6A. The main reason is that the compounds were usually insoluble and stuck on the bacterial cell wall during fermentation. In many cases for purification, the mycelia extract was used since the purification of the compounds from the medium extracts was more time consuming and the yield of the compound was insufficient. It was also observed that most extracts of the mutant strains, which had an oxygenase deactivated, contained red pigments similar to the compound griseorhodin A **(5)**. On the other hand, strains such as *S. albus* KR11, *S. albus* KR41, *S. albus* MP63 and *S. albus* KR15 produced rather darker pigments, which were not retained on the silica material. *S. albus* MP63 and *S. albus* KR15 did not produce a metabolite in adequate yields which could be purified further by these chromatographic methods.

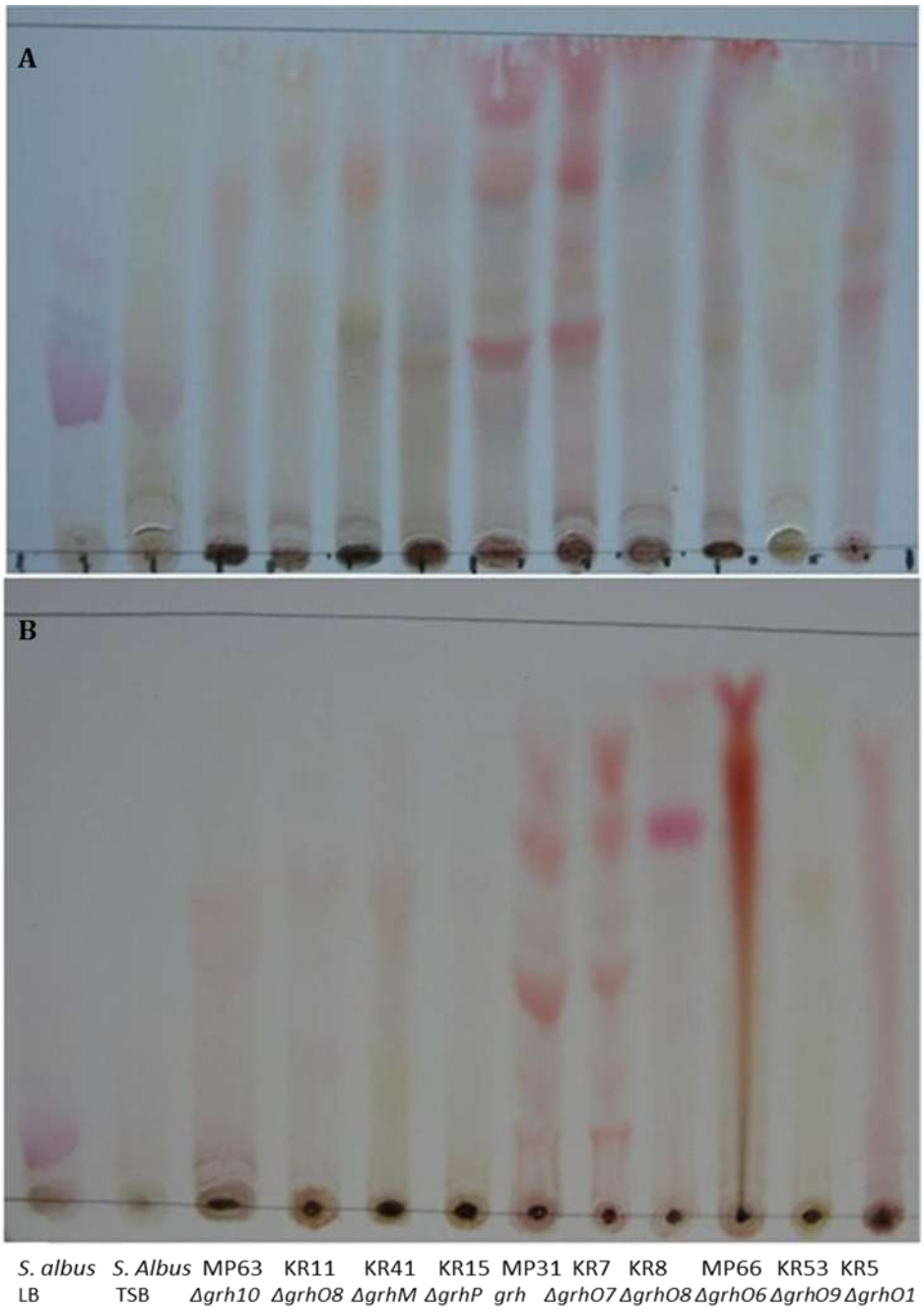

Figure 3.6 TLC analysis of the fermentation extracts. The bacterial extracts were obtained using fermentation in liquid medium. As stationary phase, NaH_2PO_4 impregnated silica was used and the mobile phase used was CH_3Cl:MeOH (9:1). A. The medium extract of the griseorhodin A (5) producing strain *S. albus* MP31, which uses the entire *grh* cluster for the expression, and the medium extract of the mutant strains with a deactivated *grh* gene were compared. B. The mycelium extract of the griseorhodin A (5) producing strain *S. albus* MP31, which uses the entire *grh* cluster for the expression, and the mycelia extracts of the mutant strains with a deactivated *grh* gene were compared. The first and second spots are the extracts of the host strain *S. albus* expressed in LB and TSB growth medium.

3.4 Isolation and Characterization of Compounds

The metabolites identified by HRMS as potential intermediate had to be isolated in order to elucidate their structure. For measurements and bioactivity assays at least 10 mg of compound was necessary. Therefore strains had to be fermented in liquid medium. The griseorhodin A **(5)** producer strain *S. albus* MP31 and the mutant strains *S. albus* KR7, *S. albus* KR8, *S. albus* MP66, *S. albus* KR5, *S. albus* KR53, *S. albus* KR41 and *S. albus* KR11 were fermented in suitable media. The general procedure for the isolation a griseorhodin type metabolite is in Section 4.1.5.4. However, regarding to the properties of the extracts and compounds, this procedure was customized according to the properties of the metabolites and compounds to be isolated. These customized procedures are described further in the Section 4.1.5.

3.4.1 Isolation and Determination of Absolute Configuration of Griseorhodin A (5)

3.4.1.1 Isolation of Griseorhodin A (5)

Griseorhodin A **(5)** was first isolated as a red water insoluble pigment by Eckard *et al.* Tressolt *et al.* and Zeeck *et al.* worked on completing the structure elucidation.[98,112,113] However, its absolute configuration was not determined. For the determination of the absolute configuration as well as potential biological and pharmacological activities, the compound was isolated from the fermentation extracts of the expression strain *S. albus* MP31, which contained the entire griseorhodin A cluster.

For the identification of the compound, the molecular ion was measured by HR-ESI-MS analysis with a predicted molecular formula $C_{25}H_{16}O_{12}$ (509.069 measured $[M+H]^+$, 509.072 calculated $[M+H]^+$). Figure 3.7 shows the HPLC trace of the strain extract from which the compound was isolated, as well as the UV absorption spectrum and the total ion current of the peak belonging to griseorhodin A **(5).**

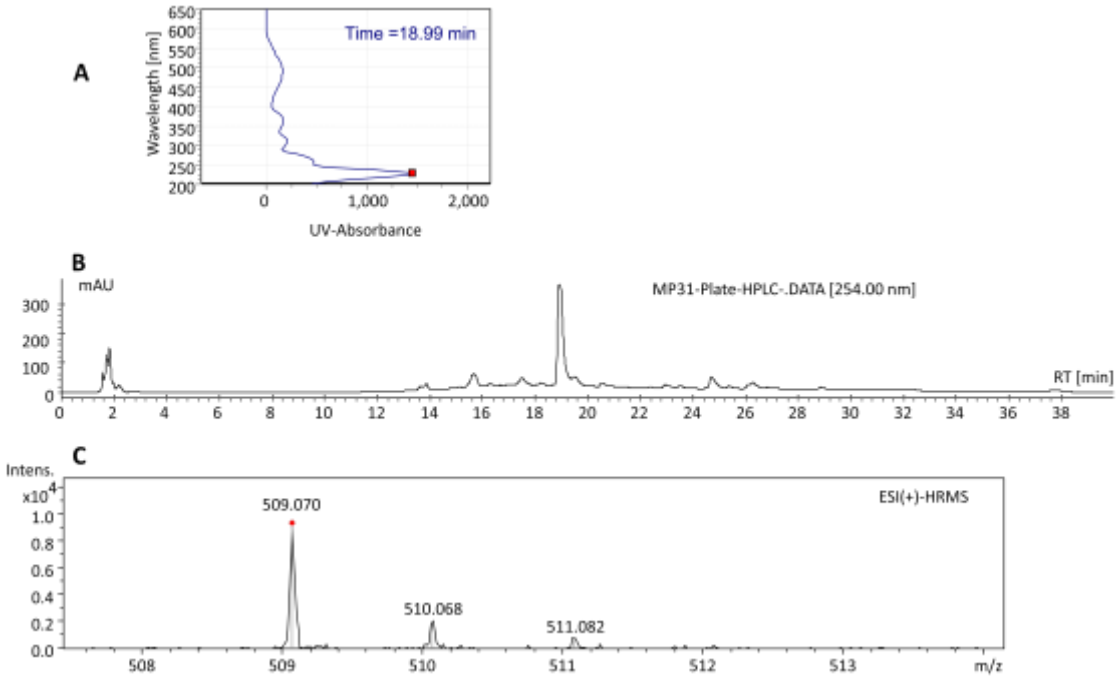

Figure 3.7 HPLC trace, UV absorption and the LC-HRMS data of griseorhodin A (5). A. UV bsorption of the compound. B. HPLC trace of the mycelia extract obtained from *S. albus* MP31 cultivated on 2CM agar plates. C. The molecular ion $[M+H]^+$ observed at ESI-HRMS.

The isolation procedure to obtain griseorhodin A **(5)** is given in Chapter 4.1.5.6. The yield of the isolation was 17 mg from 9 L of fermentation. The identity of the compound was confirmed by ^{1}H-NMR analysis in DMSO-d_6 and HRMS data. The spectral data were found to be identical with the published data in the literature. Figure 3.9 shows the ^{1}H-NMR spectrum of the isolated compound whereas Figure 3.8 provides the published ^{1}H-NMR data by Tresselt *et a.*[113]

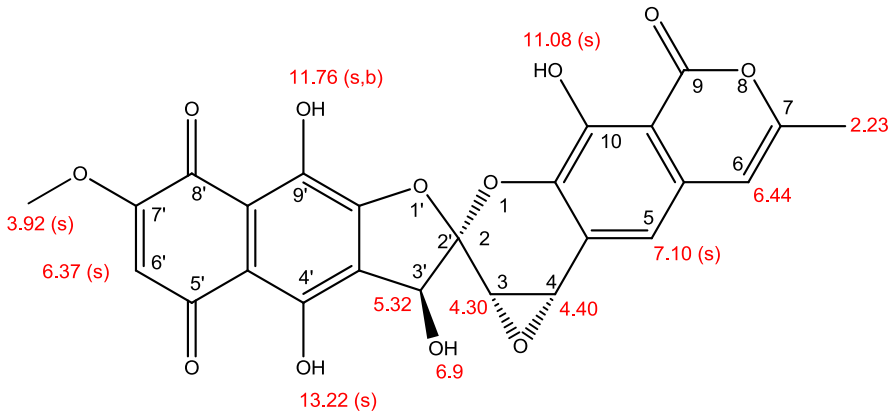

Griseorhodin A (5)

Chemical Formula: $C_{25}H_{16}O_{12}$

Exact Mass: 508.064

Figure 3.8 Structure and ^{1}H-NMR data provided by Tressolt *et al.*of griseorhodin A (5).

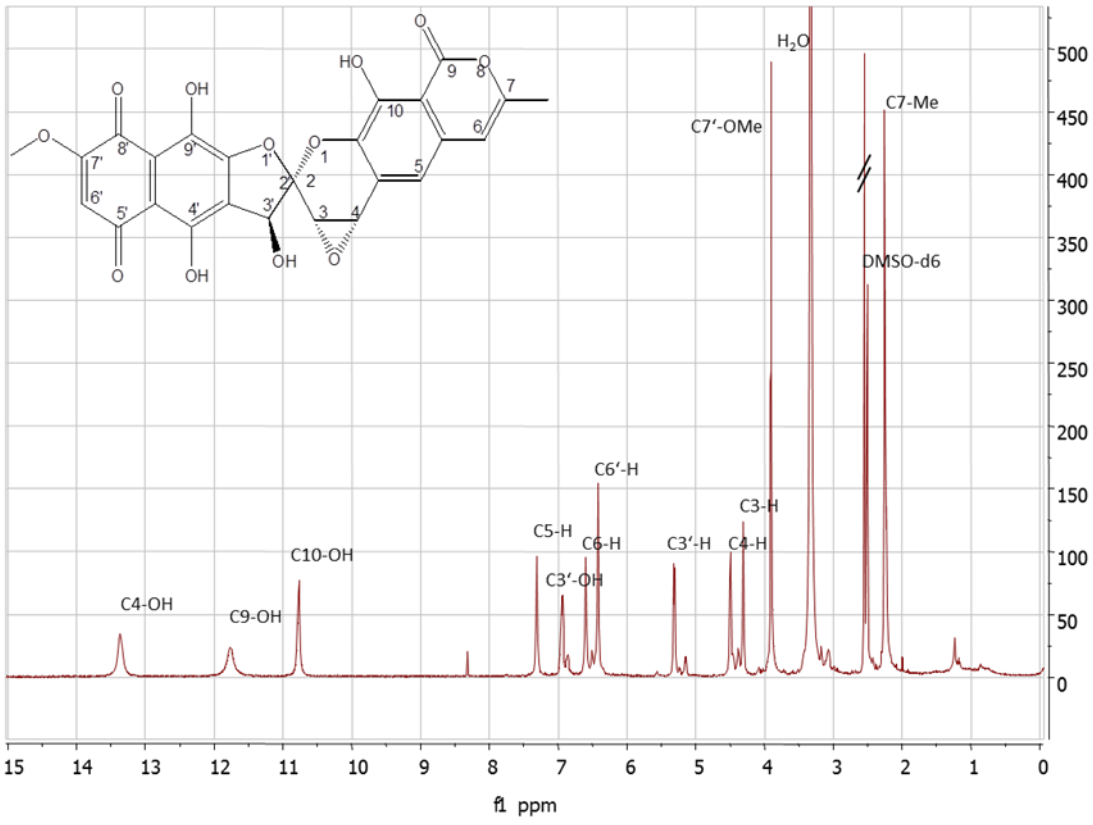

Figure 3.9 ^{1}H-NMR spectrum of the isolated griseorhodin A (5).

3.4.1.2 Determination of the Absolute Configuration

In the previous derivatization experiments, Eckardt *et al.* had established the relative configuration.[112] In order to obtain the entire stereochemical information about the compound, a reliable method was used based on comparison of quantum chemical calculation results with measured CD spectra. Interestingly, work on the stereochemistry of the griseorhodin A **(5)** congeners heliquinomycin **(39)** and γ-rubromycin **(37)** using quantum chemical CD calculation had demonstrated that the spiro centers are configured differently in these closely related compounds. In the course of our work, the absolute configuration of griseorhodin A **(5)** was successfully determined in cooperation with Prof. Dr. Bringmann and Dr. Torsten Bruhn and published.[99] For the measurements approximately 4 mg of pure compound was used .The CD spectrum was measured and compared to the calculated theoretical CD data, which were calculated of the possible stereo-isomers by Dr. Torsten Bruhn. The calculated and measured CD spectra and the determined absolute configuration of the compound are shown in the Figure 3.10. Comparison of the theoretical spectra with the experimental one revealed an excellent agreement with the theoretical CD curve of the (2'*S*,3'*S*,2*S*,3*S*) isomer, while the spectrum calculated for the (2'*R*,3'*R*,2*R*,3*R*) enantiomer showed an inverted curve. The (*S*)-configuration of the spiro center in griseorhodin A **(5)** is therefore identical with that of ?-rubromycin **(37)** and opposite to that of heliquinomycin **(39)**.

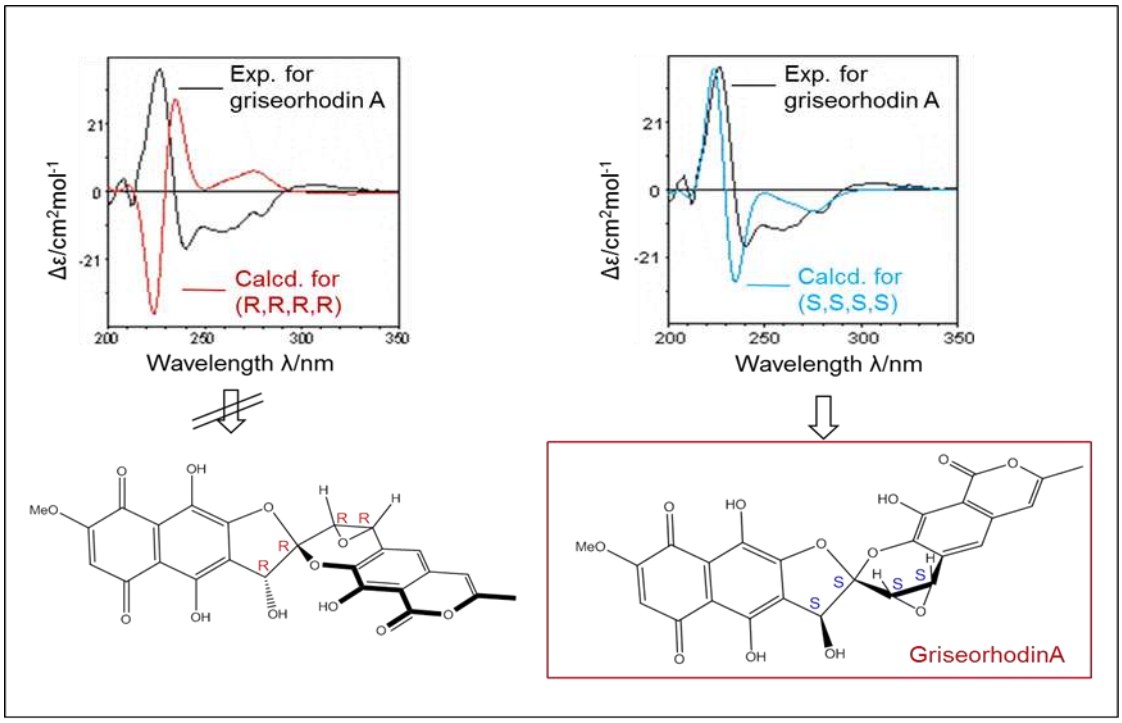

Figure 3.10 Calculated and measured CD spectra and the determined absolute configuration of griseorhodin A (5).

3.4.2 Isolation and Identification of Didesoxygriseorhodin C (46)

This compound was identified as a red pigment in two different oxygenase knockout strains *S. albus* KR7 and *S. albus* KR43, which seemed to produce the same metabolite. *S. albus* KR7 with a deactivated NADP:quinone oxidoreductase GrhO7 and *S. albus* KR43 with a deactivated cytochrome P450 family oxygenase produced a single main metabolite. *S. albus* KR7 produced the pigment in adequate yield, and was therefore chosen for fermentation in order to isolate the compound. Figure 3.11 shows the comparison of HPLC traces of the plate-extracts of *S. albus* KR7 and *S. albus* KR43 strains as well as the UV spectrum of the compound at RT= 19.5 min.

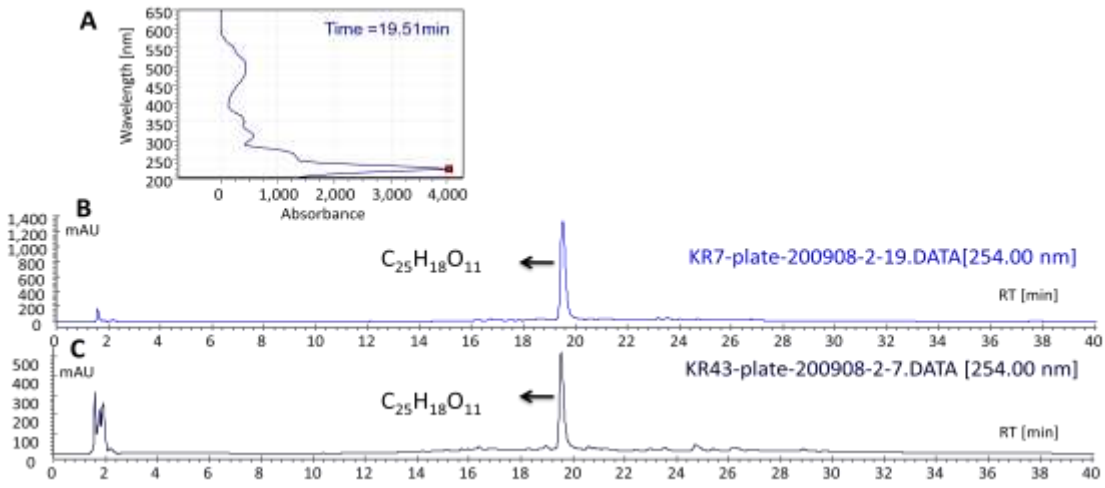

Figure 3.11 HPLC trace, UV absorption of dideoxygriseorhodin C. A. UV absorption of the compound. B. HPLC trace of the mycelia extract obtained from *S. albus* KR7 cultivated on 2CM agar plates. C. HPLC trace of the mycelia extract obtained from *S. albus* KR43 cultivated on 2CM agar plates.

To verify whether the compounds are indeed identical, an LC-MS/MS experiment was performed. The HRMS and the ESI-MS/MS fragmentation of the compounds from *S. albus* KR7 and *S. albus* KR43 extracts did not differ from each other, establishing that the strains produced the same compound. Figure 3.12A shows the HRMS of the compounds extracted from *S. albus* KR7, and Figure 3.12B shows the HRMS of the compounds extracted from *S. albus* KR43. The Figures 3.12C and 3.12D show the ESI-MS/MS fragmentation of the molecular ions.

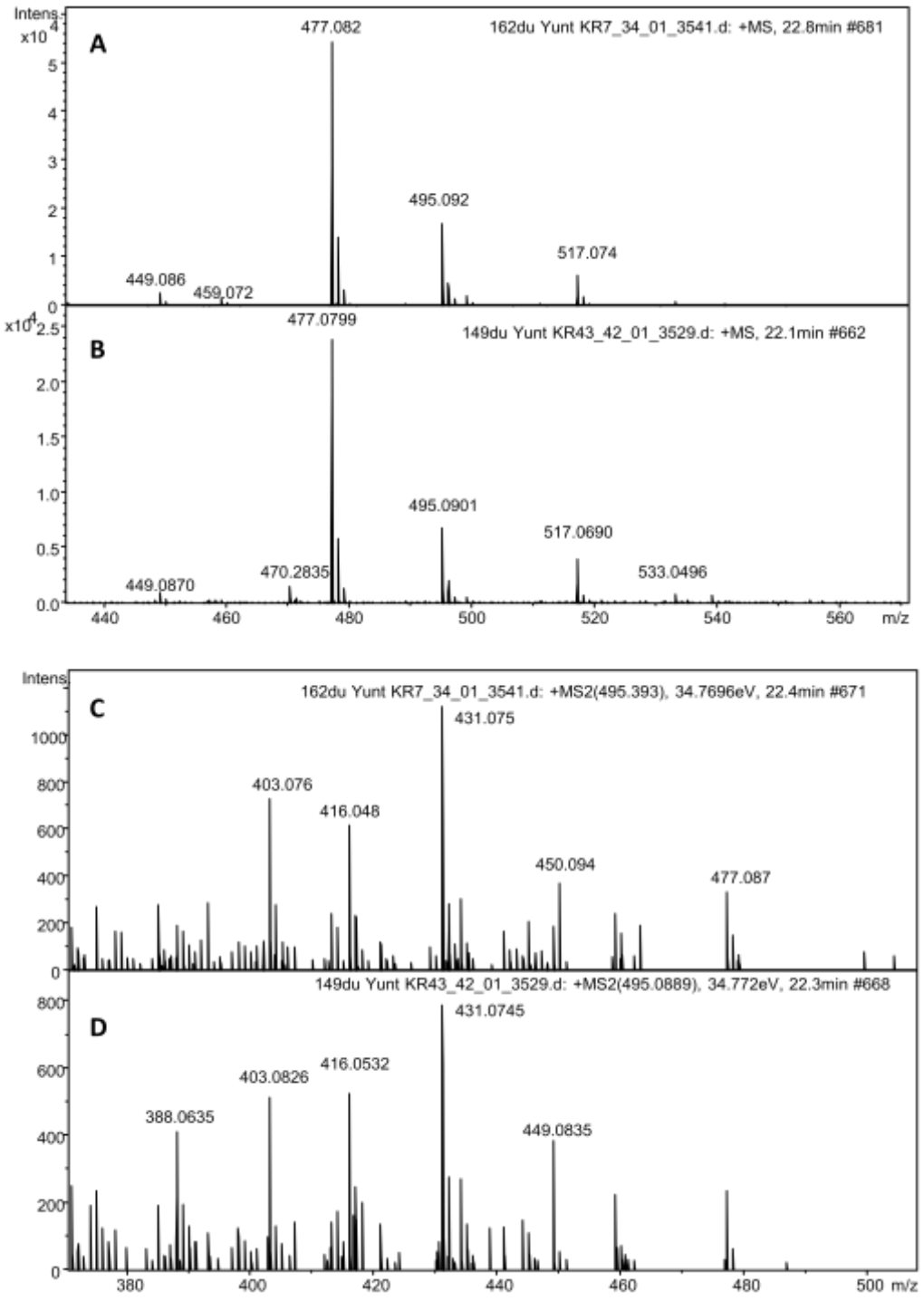

Figure 3.12 HRMS/MS data of the compounds in the extracts of *S. albus* KR7 and *S. albus* KR43 A. ESI-HRMS data of the compound in the extract of *S. albus* KR7 B. ESI-HRMS data of the compound in the extract of *S. albus* KR43. C. ESI-HRMS/MS fragmentation of the compounds in the extract of the strains. *S. albus* KR7 D. ESI-HRMS/MS fragmentation of the compounds in the extract of *S. albus* KR43.

The molecular formula was deduced by ESI-HRMS analysis as $C_{25}H_{18}O_{11}$ (495.089 measured for the molecular ion $[M+H]^+$, 495.085 calculated $[M+H]^+$).

For the isolation of the compound, *S. albus* KR7 was fermented. The conditions for the fermentation and the details of the isolation are provided in Section 4.1.5.7. The yield of the isolation was 16 mg from 6 L of fermentation. The identity of the compound was confirmed by one- and two-dimensional NMR analysis in DMSO-d_6 and AN-d_3 Measured ^{1}H-, ^{13}C-, HMBC and HMQC NMR spectra are provided in Appendix 2, Figure 2.1-2.6.

The carbon NMR spectra of the compound showed 25 carbon atoms as expected from the molecular formula of the compound $C_{25}H_{18}O_{11}$. The presence of a quinone carbonyl group is deduced from the carbon signals at 185.37 ppm and 179.86 ppm in the ^{13}C-NMR spectrum. Another carbonyl signal was observed at 165.64 ppm. Three aromatic protons at 6.41 ppm, 6.45 ppm, 6.49 ppm were observed in the ^{1}H-NMR spectrum. These hydrogens correlated in the HMQC spectra with the carbon atom signals at 110.14, 114.86, and 103.72 ppm, respectively. However, no coupling among these protons was observed. A methoxy group attached to an aromatic ring with a characteristic signal at 56.97 ppm was observed in the ^{13}C-NMR spectrum and the three methoxy protons showed a singulet signal at 3.92 ppm in the ^{1}H-NMR spectrum. The presence of three OH signals at 13.27, 11.84 and 10.78 ppm in the ^{1}H-NMR spectrum showed the presence of three kinds of phenolic OH groups forming hydrogen bonds. Two carbon atoms at 21.22 and 23.12 ppm showed two methylene groups on the ^{1}H-NMR and ^{13}C-NMR-spectra. An additional methyl group at 18.63 ppm in the ^{13}C-NMR spectrum and at 2.24 ppm in the ^{1}H-spectrum could be determined.

The HMBC correlation of the aromatic proton at 6.41 ppm to the two quinone carbonyl groups and the methoxy attached carbon atom at 160.2 ppm and additional correlations of the hydroxyl groups forming a hydrogen bond implied the partial structure 1a. (Figure 3.13)

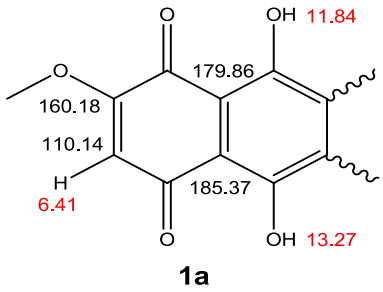

Figure 3.13 Partial structure 1a of didesoxygriseorhodin C (46).

The HMBC correlations of the methyl group at 2.24 ppm and methine protons at 6.49 and 6.85 ppm were observed. However, no couplings among these two protons were observed. Additional couplings of the two methylene protons to the aromatic proton at 6.85 ppm implied the Western part of the molecule with the partial structure 1b. (Figure 3.14)

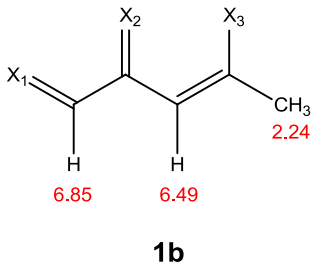

Figure 3.14 Partial structure 1b of didesoxygriseorhodin C (46).

The carbonyl signal at 165.64 ppm can not belong to an ester but an unsaturated lactone structure having a hydrogen bond to the hydroxyl group at 152.14 ppm. The HMBC correlations of the hydroxyl group at 10.78 ppm proved the unsaturated lactone structure 1c. Together the partial structures 1b and 1c make up the Eastern part of the molecule 1d. (Figure 3.15)

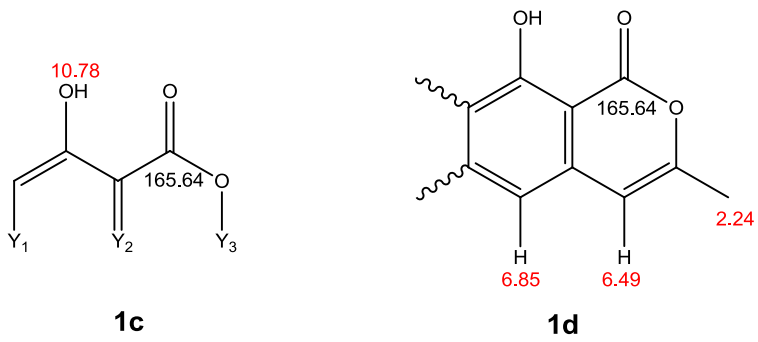

Figure 3.15 Partial structure 1c and 1d of didesoxygriseorhodin C (46).

The unassigned partial structures are: one -CH_2CH_2 unit, one quaternary carbon at 114.16 ppm, one CH at 74.06 ppm, one H and three O atoms. The chemical shifts of the carbons of the methylene group are 21.22 ppm and 23.12 ppm. One has more downfield shift and the protons have a HMBC correlation to the C atom at 104.6 ppm. The carbon atom at 74.04 ppm has HMBC correlation to the Western part of the molecule and the attached proton correlates with the carbon atom at 104.16 ppm. The structure of the molecule was therefore predicted as 1e. (Figure 3.16)

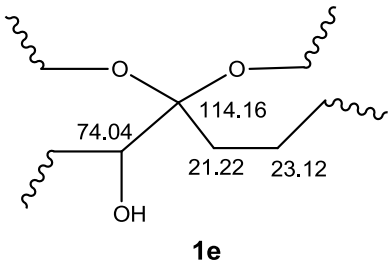

Figure 3.16 Partial structure 1e of didesoxygriseorhodin C (46).

The compound identified as didesoxygriseorhodin C **(46)**. The examination of long range ^{1}H-^{13}C correlations and the molecular formula obtained from HRMS experiments further established the structure. Figure 3.17 shows the important HMBC correlations of the compound.

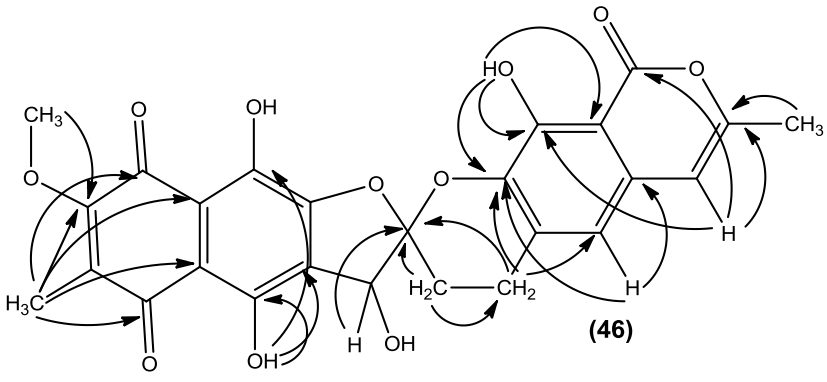

Figure 3.17 HMBC data of didesoxygriseorhodin C (46).

A literature survey showed that didesoxygriseorhodin C **(46)** was isolated before by Suetsuna *et al*. from *Streptomyces* sp. 76. All spectral data were identical with the published data.[126-128] Figure 3.18B shows the published NMR data of the compound. Table 3.6 shows the measured ^{1}H-NMR and ^{13}C-NMR data obtained in DMSO-d_6.

Table 3.6 ^{1}H- and ^{13}C-NMR data of didesoxygriseorhodin C **(46).**

Didesoxygriseorhodin C (46) (In DMSO-d_6, 500 MHz)					
Position	**^{13}C-NMR [ppm]**	**^{1}H-NMR [ppm]**	**Position**	**^{13}C-NMR [ppm]**	**^{1}H-NMR [ppm]**
1	179.86		9a	137.69	
2	160.18		10	103.72	6.49
3	110.14	6.41(s)	11	113.12	
4	185.37		13	165.64	
4a	106. 35		13a	132.35	
5-OH		13.27(s)	14-OH		10.78
5	157.14		14	152.14	
5a	130.18		14a	146.79	
6-OH		6.45 (b)	16a	148.58	
6	74.04	5.15(s)	17-OH		11.84
6a	114.16		17	153.96	
7	21.22	2.20-2.22(m)	17	153.96	
8	23.12	2.50-2.44(m)	17a	114.01	
8a	124.02		18	18.63	2.24
9	114.86	6.85(s)	2-OCH3	56.97	3.92

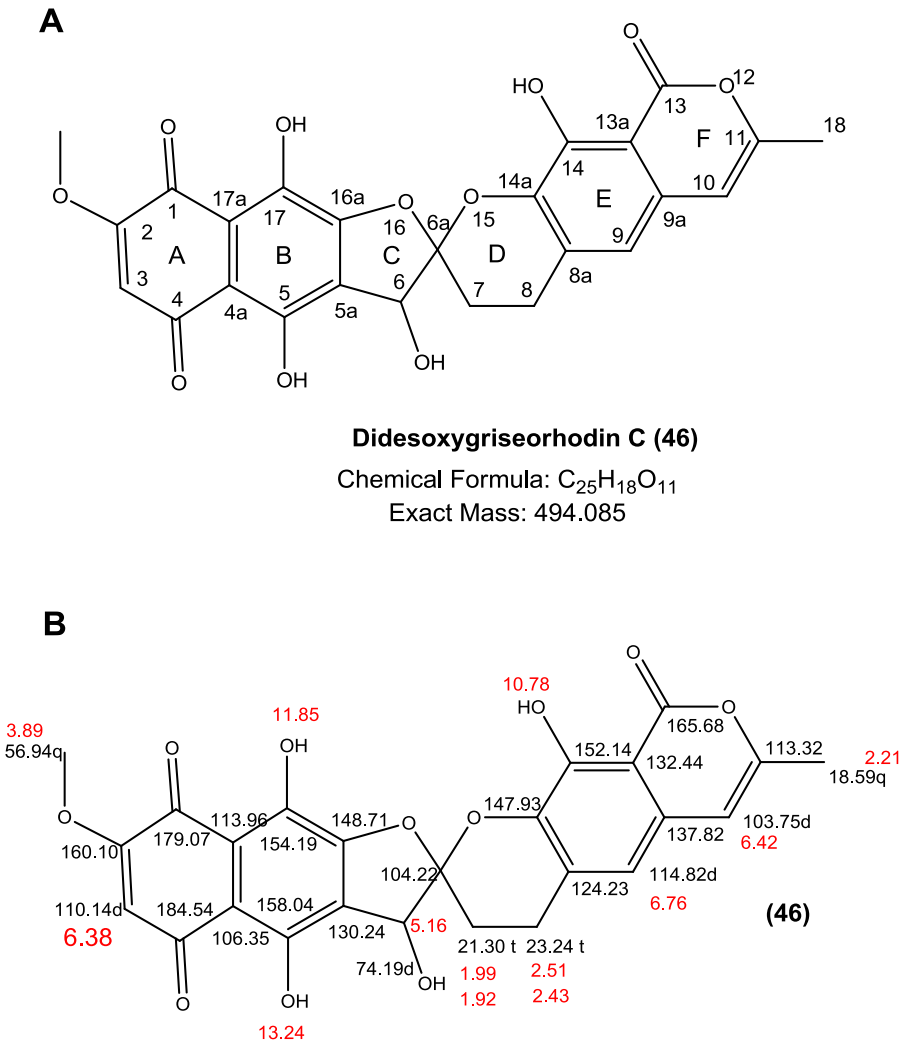

Figure 3.18 A. Structure of didesoxygriseorhodin C (46). B. Published NMR data of the compound by Suetsuna *et al.* [126-128]

As a result both enzymes GrhO7 and GrhO3 are involved in the formation of the epoxied function on the ethylene group at C-7 and C-8. It is a rare case of an epoxidation reaction starting on a saturated C-C bond. Figure 3.19 shows the proposed involvement of GrhO7 and GrhO3 in griseorhodin A **(5)** biosynthesis.

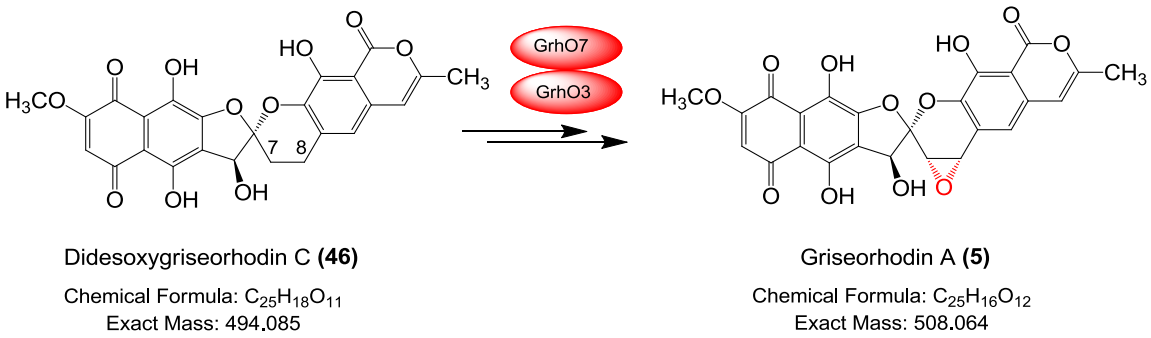

Figure 3.19 Proposed functions of GrhO7 and GrhO3 in the biosynthesis of griseorhodin A (5).

In order to obtain more information about the suggested function of GrhO3 and GrhO7 sequence homologies with other tailoring enzymes were investigated by BLAST (Basic Local Alignment Search Tool) analysis by Kathrin Reinhardt. Table 3.7 shows the BLAST (Basic Local Alignment Search Tool) results of the enzymes.[125]

Table 3.7 Homologous proteins to GrhO3 and GrhO7 by the BLAST analysis results[125]

Protein	Amino Acids	Proposed function	Sequence Similarity (Protein, Origin)	Similarity/ Identity [%]
GrhO3	416	Cytochrom P450	PteD/ *Streptomyces avermitilis* MA-4680[129]	71/55
			I36-105-2/ *Streptomyces griseolus* (Unpublished)[125]	70/56
GrhO7	325	NADPH:quinone oxidoreductase	Med-Orf9/ *Streptomyces* sp. AM-7161[130]	61/46
			ActVI Orf2/ *Streptomyces coelicolor* A3(2)[131]	59/43

GrhO3 shows sequence homology to the cytochrome P450 family of oxygenases. Although cytochromes P450 usually generate epoxides from alkenes,[132,133] examples of the formation of cyclic ethers from saturated precursors have been reported, such as the epoxidase OleP from oleandomycin biosynthesis [134] and aureothin P450 AurH, which closes a tetrahydrofuran ring by 1,5-

dehydrogenation of an alcohol precursor.[135] GrhO7 shows homology to NADPH:quinone oxidoreductases of medium-chain dehydrogenase/reductase superfamily (MDR), which take part in electron transfer reactions. An involvement at an epoxidation reaction was unexpected. The closest homologues of GrhO7 are the enoylreductases Med-Orf9[130] and ActVI-Orf2[131] in the medermycin and actinorhodin biosynthesis, respectively. They are involved in stereospecific reduction of the double bond at C14-C15 positions of (S)-DNPA **(47)** (4-dihydro-9-hydroxy-1-methyl-10-oxo-3-H-naptho-[2,3-c]-pyran-3-(S)-acetic acid) shown in Figure 3.20.

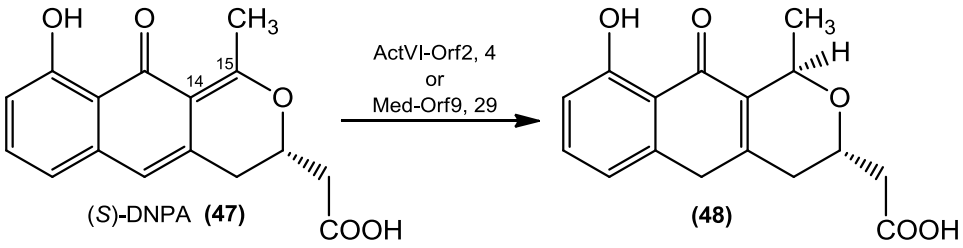

Figure 3.20. The involvement of Med-Orf9 and ActVI-Orf2 in medermycin and actinorhodin biosynthesis.[130,131]

The formation of identical products in both deletion mutants suggests that GrhO7 and GrhO3 jointly participate in epoxide formation. A possible explanation might be that the two enzymes are forming a complex to epoxidize the olefinic carbon bond. This would suggest that the epoxidation would not occur in the absence of either GrhO3 or GrhO7. Another possible explanation is that GrhO3 is capable to perform the epoxidation of the olefinic carbon bond alone and GrhO7 might be responsible for the reductive recycling of olefinic shunt products that arise from an eliminative side reaction. The investigation of the monooxygenase gene *styAB* from *Pseudomonas sp.* VLB120 showed that the rate of epoxidation is depending on the present amount of NADPH.[136] This would also suggest that GrhO7 belonging to a NADPH:quinone oxidoreductases might be involved at the effective regeneration of the coenzyme for the oxygenase GrhO3 belonging to cytochrome P450 family. For further investigation of the epoxidation on the compound functional enzyme assays with GrhO3 and GrhO7 can be suggested.

3.4.3 Isolation and Identification of Collinone (41)

The compound was observed as a pink pigment in the extract of the oxygenase knockout strain *S. albus* KR8. The deleted oxygenase of the cluster GrhO5 is a predicted FAD-dependent oxygenase, and the only observed metabolite of the strain has a molecular formula $C_{27}H_{18}O_{12}$. The compound has the largest number of carbon and oxygen atoms compared to other stable metabolites. Figure 3.21 shows the HPLC trace, the UV spectrum and LC-HRMS data of the compound.

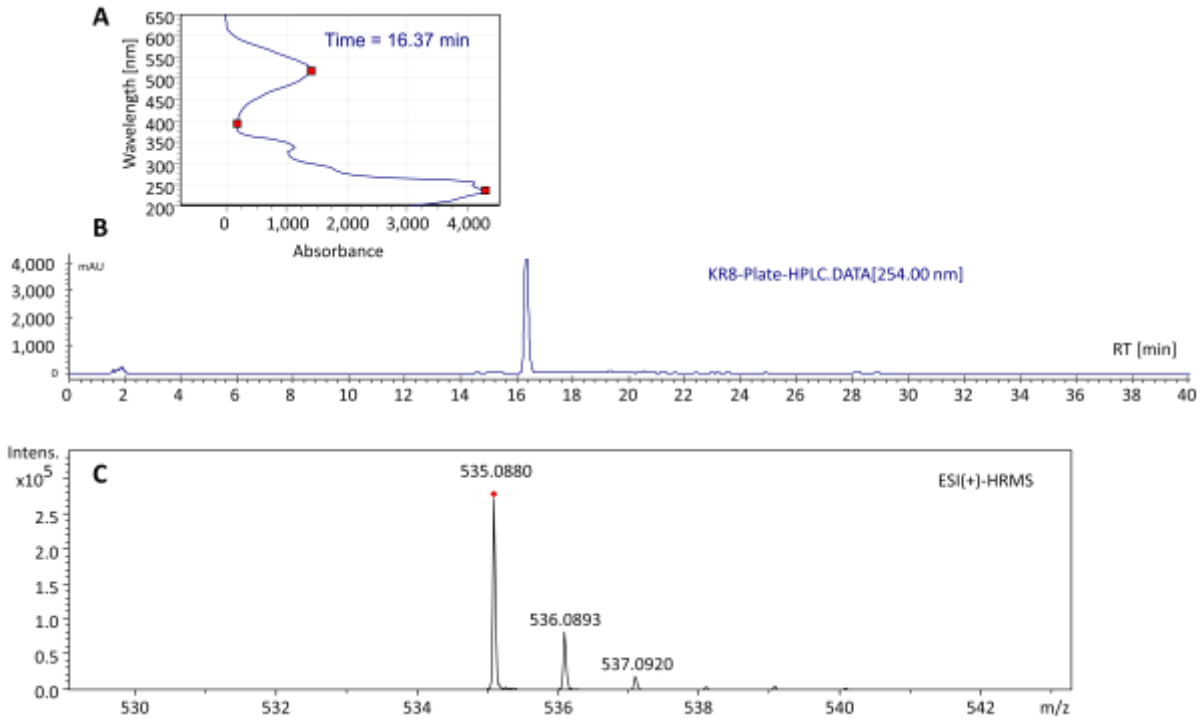

Figure 3.21 HPLC trace, UV spectrum and the LC-HRMS data of collinone (41). A. UV spectrum of the compound. B. HPLC trace of the mycelia extract obtained from *S. albus* KR8 cultivated on 2CM agar plates. C. The molecular ion $[M+H]^+$ observed at ESI-HRMS.

For the isolation of collinone **(41)**, *S. albus* KR8 was fermented in TSB medium, and the compound was isolated from the mycelia extract. The conditions for the fermentation and the detailed procedure for the isolation are in Section 4.1.5.8. The yield of the isolation was 8 mg from 6 L of fermentation. The identity of the compound was confirmed by ESI-MS analysis (*m/z*: 557.067 $[M+Na]^+$) and NMR analysis in $CDCl_3$. Measured ^1H-, ^{13}C-, HMBC and HMQC NMR spectra of the compound are shown in Appendix 2, Figure 2.7-2.11.

The carbon spectra of the compound showed 27 carbon atoms as expected from the molecular formula of the compound $C_{27}H_{18}O_{12}$. The presence of a quinone carbonyl group is deduced from the carbon signals at 194.3, 191.01, 188.14 and 182.65 ppm in the ^{13}C-NMR spectrum. Another carbonyl signal was observed at 166.51 ppm. Three aromatic protons at 6.54, 6.15 and 6.07 ppm were observed, which correlated in the HMQC spectrum with the carbon signals at 115.8, 110.78 and 104.9 ppm, respectively. However, no couplings among these protons were observed. A methoxy group attached to an aromatic ring with a characteristic signal at 57.17 ppm was observed in the ^{13}C-NMR spectrum, and the three methoxy protons showed a singulet signal at 3.89 ppm in the ^{1}H-NMR spectrum. The presence of three OH signals at 13.52, 12.58 and 11.58 ppm in the ^{1}H-NMR spectrum showed the presence of three kinds of phenolic OH groups forming hydrogen bonds. Two carbon atoms at 26.1 and 27.3 ppm showed methylene groups on the DEPT and ^{13}C-NMR spectra. An additional methyl group at 2.15 ppm in the ^{1}H-NMR spectrum and at 19.45 ppm in the ^{13}C-NMR spectrum could be determined. Collinone **(41)** has an unsaturation index of 19, and as the NMR data suggest the presence of 5 carbonyl groups and 8 carbon-carbon double bounds, the data indicate a hexacyclic structure. Structure elucidation was complicated by the presence of no less than 18 non protonated carbons, but careful examination of long range ^{1}H-^{13}C correlations established the structure. The HMBC correlations of the methoxy group at 3.89 ppm to the carbon atom at 160.74 ppm and a weak correlation to the adjacent carbon atom at 110.78 ppm indicated the presence of methyl enol ether, and this is also supported by the chemical shift of the double bound carbons. The strong HMBC correlations of the aromatic proton at 6.15 ppm to the carbon atoms at 160.74, 182.65, 188.14, 116.7, and 115.9 ppm and the HMBC correlations of the hydroxyl protons at 13.48 ppm to the quarternary carbons at 155.6, 130.9, 128.6, 115.9 and 115.9 ppm supported a dihydroxymethoxy1,4-napthoquinone structure 2a for the Western part of the molecule. (Figure 3.22)

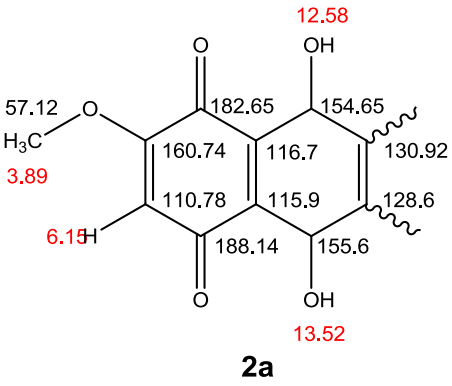

Figure 3.22 Partial structure 2a of the compound collinone (41).

For the Eastern part of the molecule, a 3-methyl substituted isocoumarin moiety 2b is indicated by the strong HMBC couplings of the methyl group to the carbon atoms 155.12 and 104.09 ppm. Additional couplings of the aromatic proton at 6.07 ppm to the carbon atoms at 155.12, 103.48 and 159.5 ppm support the conclusion as well. The carbonyl signal at 166.51 ppm belongs to the unsaturated lactone because of its hydrogen bond to the hydroxyl group at 11.58 ppm and HMBC couplings with the aromatic hydrogen atom at 6.07 ppm. It is an. HMBC correlations of the hydroxyl group at 11.58 ppm and the aromatic proton at 6.54 ppm with the aromatic carbon atoms on the isocoumarin moiety establishes the substructure 2b. (Figure 3.23)

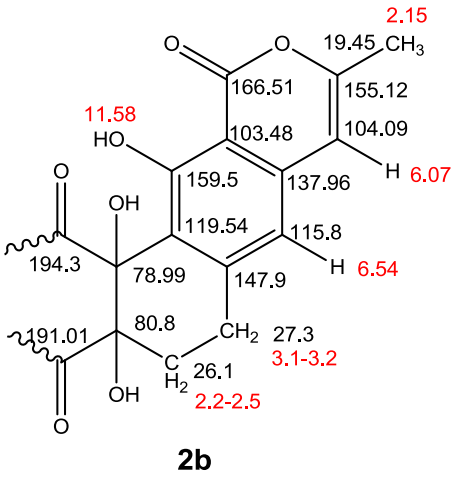

Figure 3.23 Partial structure 2b of the compound collinone (41).

Two methylene units both showed strong correlations to the Eastern part of the molecule. The methylene protons at 2.4-2.5 ppm (m) had HMBC correlations to the carbonyl group at 191.01 ppm and 194.03 ppm in the Western part of the molecule. The quarternary atoms at 80.8 ppm and 78.7 ppm correlated with the methylene protons as well. HMBC correlations of the methylene groups enables to close the six member ring structure adjacent to the isocoumarin system 2b and attaches the Western part to the Eastern part of the molecule, resulting in a pentangular moiety. The chemical shift of the two quaternary carbon atoms at 78.99 and 80.8 ppm can not be an epoxy group, since the chemical shift of the carbon atoms of an epoxy group at this position is usually expected at 60-70 ppm. The molecular formula of the compound and the chemical shift of the carbon atoms at C-5 and C-18 supports that two hydroxyl groups are substituted at these positions. The identified compound and the correlations observed in HMBC experiments are summarized in Figure 3. 24.

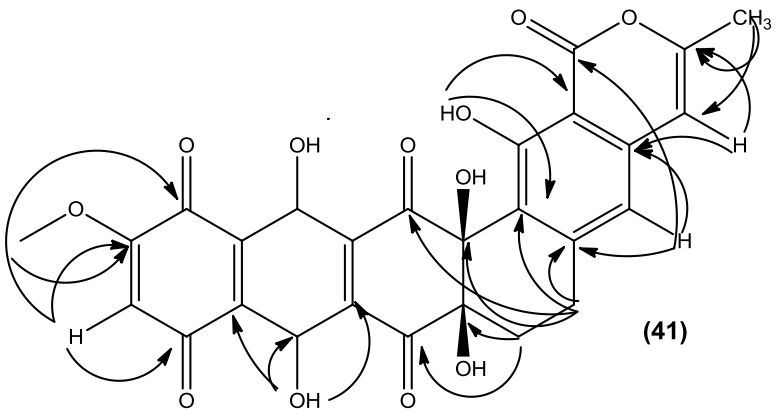

Figure 3.19 HMBC data of the compound collinone (41).

The hydroxyl groups at the positions C5 and C18 could not be observed, because $CDCl_3$ was used for the NMR measurements. DMSO-d_6, as well as other solvents and combinations of solvents, were not suitable for NMR measurements with collinone **(41),** because the ^{13}C-NMR signals for the dihydroxy-methoxy-1,4-naphthoquinone system could not be observed. This may be caused by a rapid interchange between the 1,4-quinone and 1,4-hydroquinone functionalities.[137] The partial structures obtained from the NMR spectra and HRMS data indicate the structure of collinone **(41)**.

All spectral data were found to be identical with published data .[137] Figure 3.25A shows the structure of collinone **(41).** Figure 3.25B shows the published NMR data of collinone **(41).** Table 3.8 shows the measured ^{1}H-NMR and ^{13}C-NMR data.

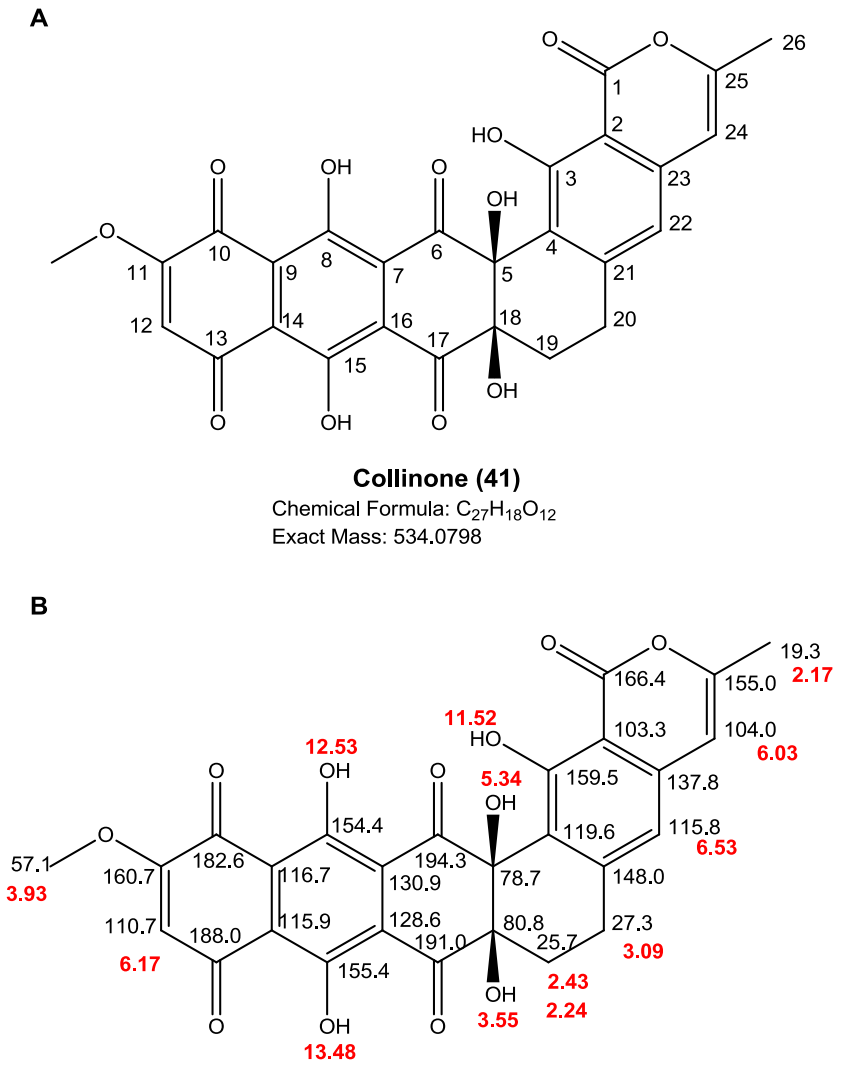

Figure 3.20A. Structure of collinone (41). 3.25B. The published NMR data of collinone (41).[137]

Table 3.8 ^{1}H- and ^{13}C- NMR data of collinone **(41)**.

Collinone(41)(In $CDCl_3$, 300 MHz)					
Position	**^{13}C-NMR [ppm]**	**^{1}H-NMR [ppm]**	**Position**	**^{13}C-NMR [ppm]**	**^{1}H-NMR [ppm]**
1	166.508		15	155.6	
2	103.481		16	128.6	
3	159.5		17	191	
4	119.54		18	80.8	
5	78.99		19a	26.1	2.4-2.5 (m)
6	194.3		19b	26.1	2.2-2.3 (m)
7	130.92		20a,b	27.3	3.1-3.2 (m)
8	154.65		21	147.9	
9	116.7		22	115.8	6.54 (s)
10	182.65		23	137.96	
11	160.74		24	104.09	6.07 (s)
12	110.78	6.15 (s)	25	155.12	
13	188.14		26	19.45	2.15 (s)
14	115.9		27-OMe	57.17	3.89
3-OH		11.58 (s)	8-OH		12.58
			15-OH		13.52

Collinone(**41)** is a heavily oxidized angular hexacyclic compound containing an unusual 1,4,5,8(2H,3H)-anthracenetetrone moiety only reported in the glycoside antibiotics SF2446A1, A2, A3, B1, B2 (isolated from *Streptomyces sp*.), SF2446 and the antibiotic tetracyclic quinone glycoside polyketomycin (produced by *Streptomyces diastatochromogenes* Tu6028).[137] The absolute configuration of collinone **(41)** was not determined in the previous studies, but the relative stereochemistry of C-5/C-18 bridge is suggested to be *cis*.[137] The absolute configuration of the compound was determined in cooperation with Anu Schaumlöffel in the group of Prof. Dr. Gerhard Bringmann, who compared CD spectra from theoretical quantum chemical calculations with the measured CD spectrum. For the CD measurements, 2 mg of the compound was provided. The experiment showed that the hydroxyl groups are in *cis* position and the determined configuration is (5*S*,18*R*)**.** Figure 3.26 shows the results of these experiments and the determined absolute configuration of the compound.

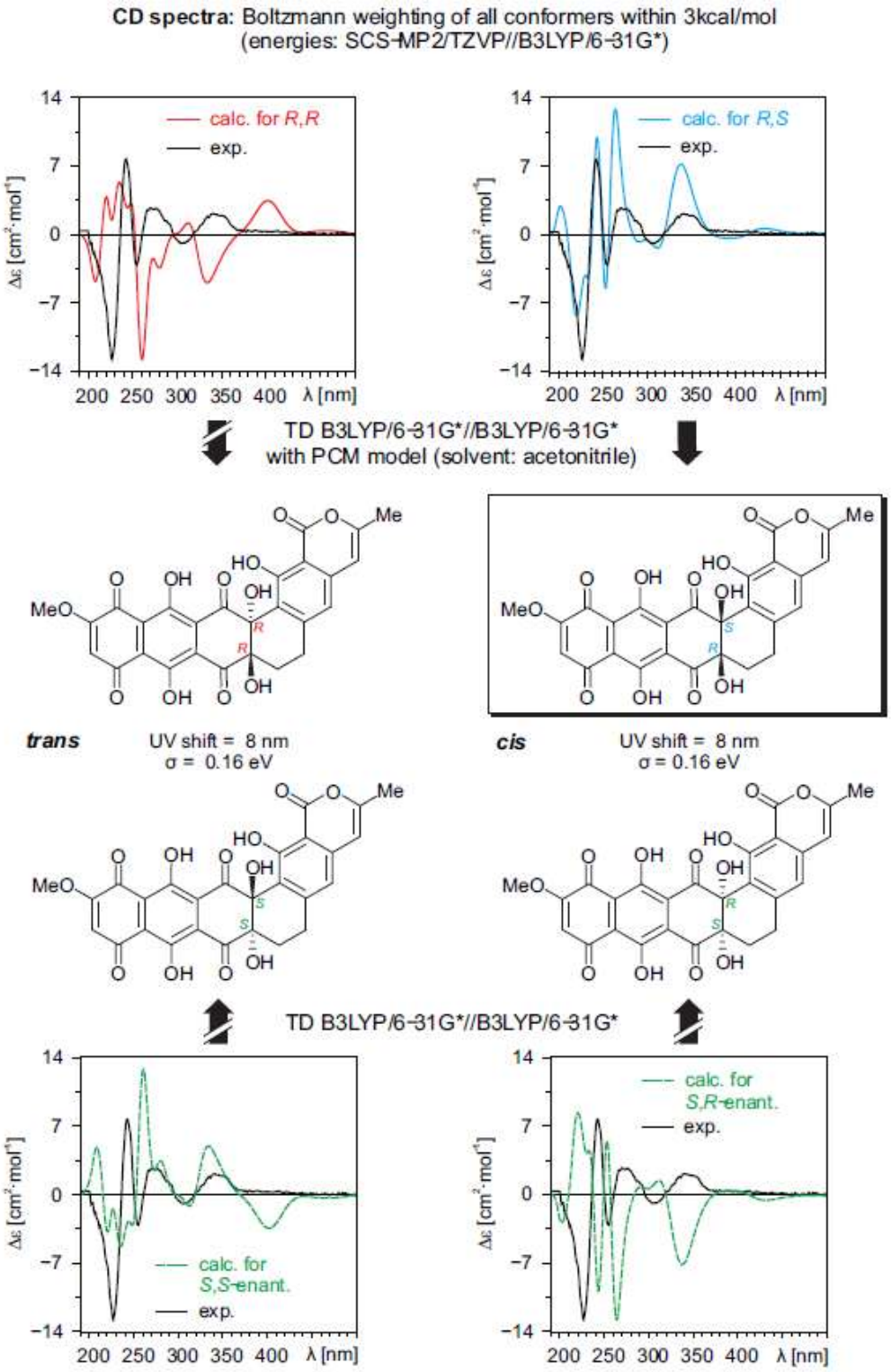

Figure 3.21 Data of the calculated and measured CD spectra and the determined absolute configuration of collinone (41).

The group of Minas, Bailey, and coworkers had previously reported the compound.[137] They produced the compound by heterologous expression using randomly chosen 30-50 kb sized genomic DNA fragments of the strain *S. collinus* DSM 2012, which contains a putative rubromycin cluster, using *S. coelicolor* CH999 as a host. However, their results could not exclude the possibility that the expressed DNA belonged to another pathway unrelated to rubromycin biosynthesis. Their investigations suggested that the rubromycins might have a tridecaketide precursor in their biosynthetic pathway. [137]

The characterization of this compound in the extract of the mutant strain *S. albus* KR8 proves the hypothesis that griseorhodin A **(5)** is built from a single polyketide chain and that there exists a pentangular aromatic precursor in the biosynthesis of griseorhodin-type aromatic spiroketal polyketides.[110] The structure shows that at least three carbon-carbon cleaveges are necessary for spiroketal formation shown in Figure 3.27. This result clearly suggests that GrhO5 initiates the cleavage sequence by using collinone as a substrate.

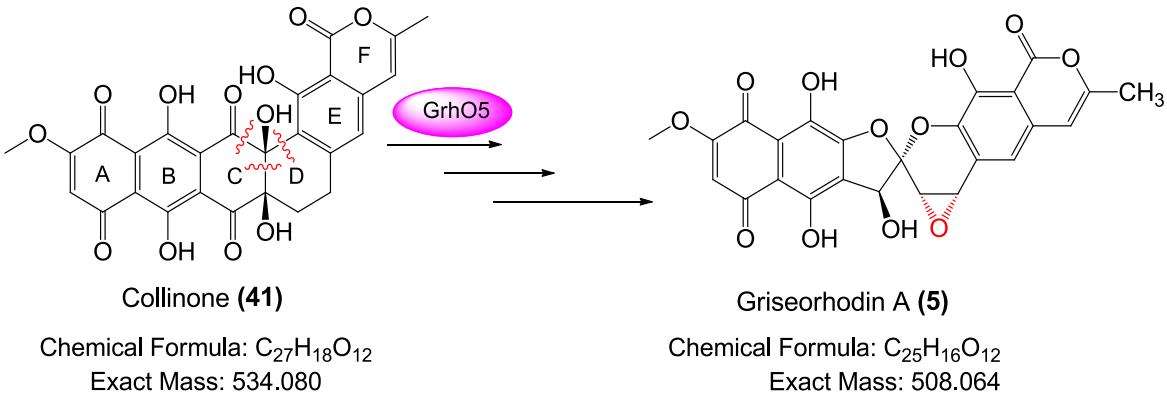

Figure 3.27 Predicted cleavages necessary for the formation of griseorhodin A **(5)** starting with the suggested intermediate collinone **(41)**.

To get more insights in to the possible function of GrhO5, sequence homology of GrhO5 was investigated by BLAST (Basic Local Alignment Search Tool) by Kathrin Reinhardt. Table 3.9 shows the BLAST results of the protein.[125]

Table 3.9. Homologous proteins to GrhO5 determined by the BLAST analysis.[125]

Protein	Amino Acids	Proposed function	Sequence Similarity (Protein, Origin)	Similarity/ Identity [%]
GrhO5	537	FAD-dependent monooxygenase	RubL/ *Streptomyces collinus* (Unpublished)[125]	76/69
			GrhO8/ *Streptomyces* sp. JP95[15]	58/45
			GrhO9/ *Streptomyces* sp. JP95[15]	58/44
			DntB/ *Burkholderia* sp. DNT[138]	57/44
			TcmG/ *Streptomyces glaucescens*[139]	56/41

The enzyme GrhO5 shows similarity to FAD-dependent monooxygenases GrhO8 and GrhO9 of the *grh* cluster.[125] Another enzyme showing sequence homology is DntB.[138] DntB (4-methyl-5-nitrocatechol (4M5NC **(49)**) monooxygenase) from *Burkholderia* sp. catalyzes the second step of 2,4-dinitrotoluene degradation by converting 4M5NC **(49)** to 2-hydroxy-5-metylquinone **(50)** with the concominant removal of the nitro group, which is shown in Figure 3.28.[138] DntB is a flavoprotein that has a very narrow substrate range. [138,140]

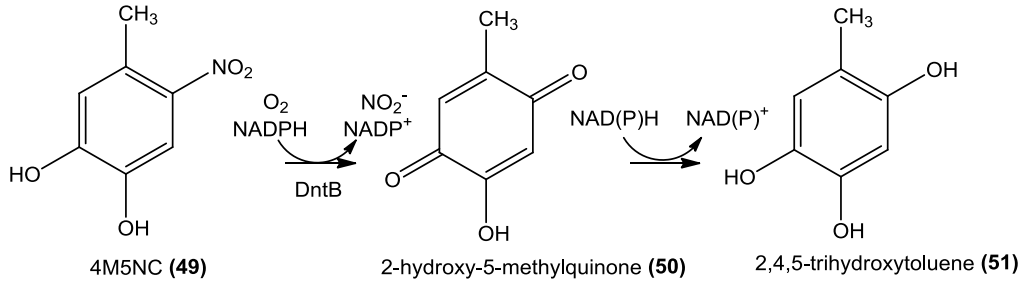

Figure 3.28 The involvement of DntB in the catalysis of 2,4-dinitrotoluene degradation by converting 4M5NC (49) to 2-hydroxy-5-metylquinone (50).[140]

The hydroxylase TcmG is an oxygenase in the biosynthesis of the bacterial polyketide tetracenomycin C **(52).** TcmG hydroxylates tetracenomycin A2 **(51)** at positions C-4, C-4A, and C12A to generate tetracenomycin C **(52)**.[139] Figure 3.29 shows the involvement of TcmG in tetracenomycin C biosynthesis, catalyzing triple hydroxylation of tetracenomycin A2 **(51)** to tetracenomycin C

(52). The sequence homology of GrhO5 to TcmG suggests that GrhO5 might be involved in a hydroxylation reaction on an aromatic ring or a multiple hydroxylation reaction leading to carbon-carbon cleavages.

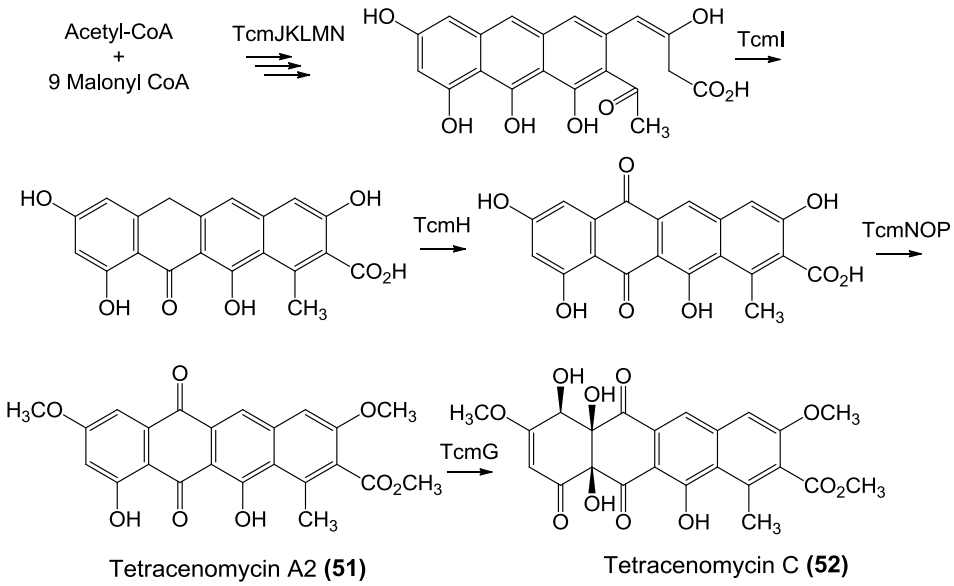

Figure 3.29 The involvement of TcmG in tetracenomycin biosynthesis catalyzing triple hydroxylation of tetracenomycin A2 (51) to tetracenomycin C (52).[139]

3.4.4 Isolation and Characterization of Lenticulone (53) and ZY1 (54)

In the extracts of the FAD-dependent oxygenase GrhO6 knockout strain *S. albus* MP66, MP66a was observed as a purple pigment. The gene *grhO6* showed amino acid sequence similarity to Baeyer-Villiger oxygenase MtmOIV.[141] The molecular ion detected for this major compound was at *m/z*: 521.0720 for $[M+H]^+$ suggesting a molecular formula $C_{26}H_{16}O_{12}$ with a calculated exact mass 521.0716 for $[M+H]^+$ Another strain, *S. albus* KR42 with a deleted *grhJ* gene that has sequence similarities to GNAT (GCN5-related N-acetyltransferase family) genes also produced metabolites suggesting the same molecular formula.[125] The measured molecular ion for the suggested molecular formula $C_{26}H_{16}O_{12}$ in the *S. albus* KR42 extract was at *m/z*: 521.0716 for $[M+H]^+$. In Figure 3.30, a comparison of agar plate extracts from *S. albus* MP66 to *S. albus* KR42 based on their HPLC traces is shown. It was observed that extracts *of S. albus* KR42

belonging to the strain grown on agar produces a major metabolite with a suggested molecular formula $C_{25}H_{16}O_{11}$ with a measured molecular ion at *m/z*: 493.0769 for $[M+H]^+$ and calculated exact mass 493.0769 for $[M+H]^+$. Additionally, two minor metabolites MP66a and MP66a' with the same molecular formula $C_{26}H_{16}O_{12}$ were produced. Later investigations of the compound MP66a, which was renamed lenticulone **(53)** after structure elucidation, showed that the metabolite MP66a' occurs also after keeping MP66a in solutions over pH 7 as described in Chapter 4.1.6. In order to prove that the extracts contain the same compound MP66a, an ESI-HRMS tandem MS/MS experiment was carried out. Figure 3.31A and B shows that the ESI-MSMS measurements of the compound MP66a in the extracts of both strains are identical.

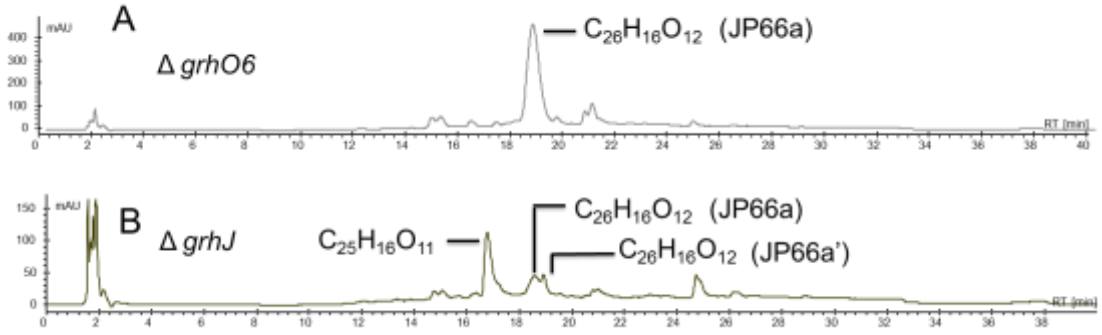

Figure 3.30 HPLC traces of the strains containing compound MP66a in extracts. A. HPLC traces of *S. albus* MP66. B. HPLC traces of *S. albus* KR42.

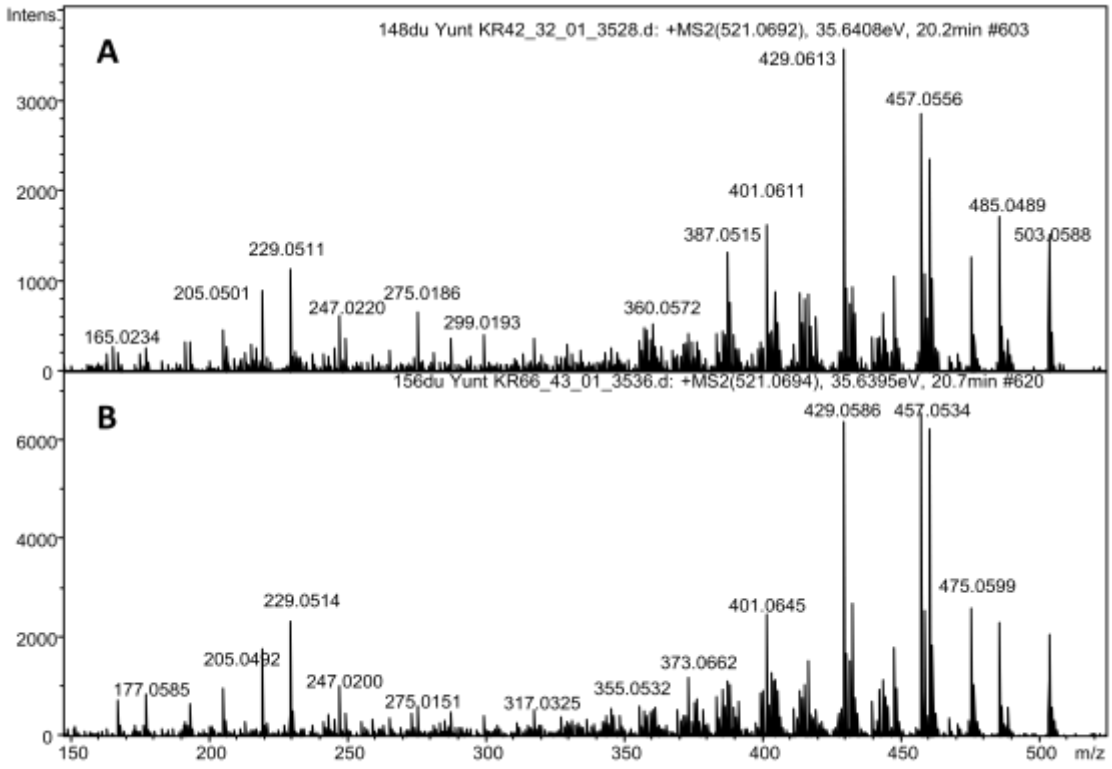

Figure 3.31 ESI-MSMS fragmentation comparison of the peak at RT= 19 min of *S. albus* MP66 to *S. albus* KR42. A ESI-MSMS fragmentation comparison of the compoundat RT= 19 min of *S. albus* MP66. B ESI-MSMS fragmentation comparison of the compoundat RT= 19 min of *S. albus* KR42.

Investigation of the metabolites of *S. albus* MP66, and structure elucidation of MP66a was carried out in this work. Further investigation of the metabolites from *S. albus* KR42 was carried out by Kathrin Reinhardt for her PhD. work. [125]

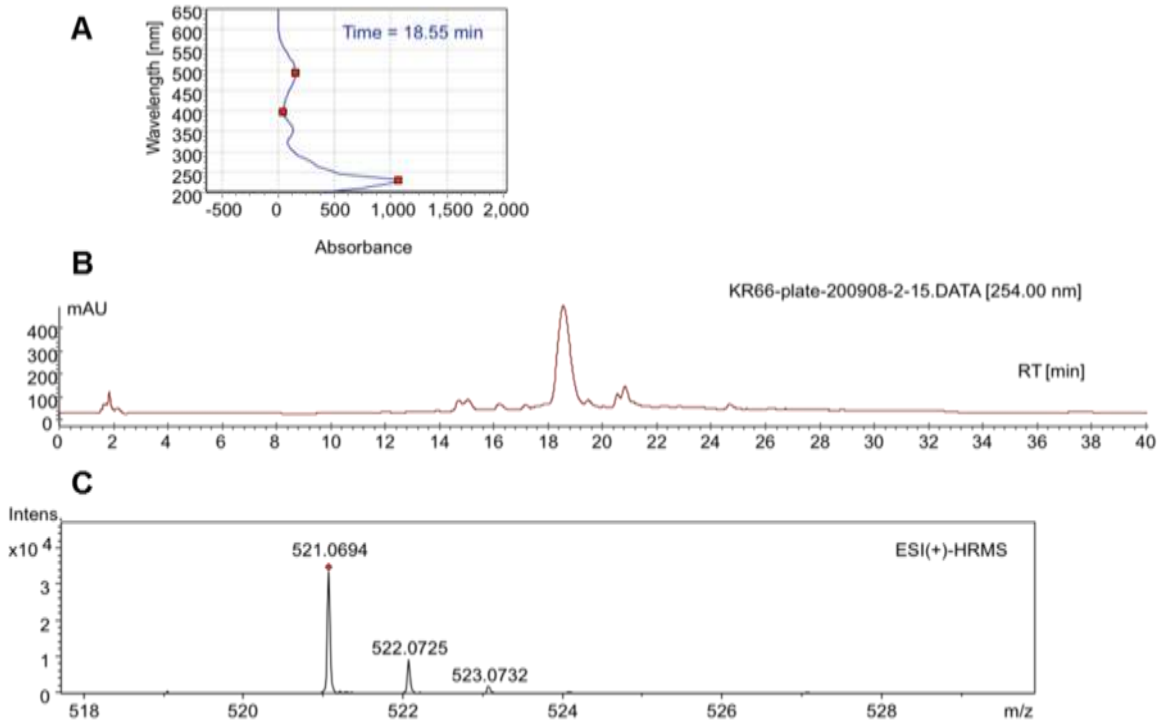

Figure 3.32 HPLC trace, UV spectrum and the LC-HRMS data of lenticulone (48). A. UV of the compound. B. HPLC trace of the mycelia extract obtained from *S. albus* MP66 cultivated on 2CM agar plates. C. The molecular ion $[M+H]^+$ observed by ESI-HRMS.

Figure 3.32 shows the HPLC trace, UV spectrum and LC-HRMS data of MP66a produced by *S. albus* MP66, which was cultivated on 2CM agar plate. For the isolation of the metabolites of *S. albus* MP66a, a similar protocol for the isolation of griseorhodin A **(5)**, as described in Chapter 4.1.5.5 was applied. However, another compound was observed during the first isolation attempt, which was called MP66b. During the isolation steps, it became obvious that MP66a was instable even in the presence of small amounts of methanol, especially at acidic conditions. During the extraction and also after the chromatographic purification with chloroform:methanol (9:1) on impregnated silica plates a rapid decomposition was observed. During the first purification attempts the compound MP66b, which was named as ZY1 **(54)**, was obtained. The isolation procedure of compound ZY1 **(54)** is described in Chapter 4.1.5.10. The yield of the isolation was 6 mg from 12 L of fermentation. The molecular ion was determined at ESI-(+)-HRMS as *m/z:* 337.055 for $[M+H]^+$ suggesting a molecular formula $C_{15}H_{12}O_9$ with a calculated exact mass 337.056 for $[M+H]^+$. Figure 3.33 shows the HPLC trace and UV spectrum of the compound.

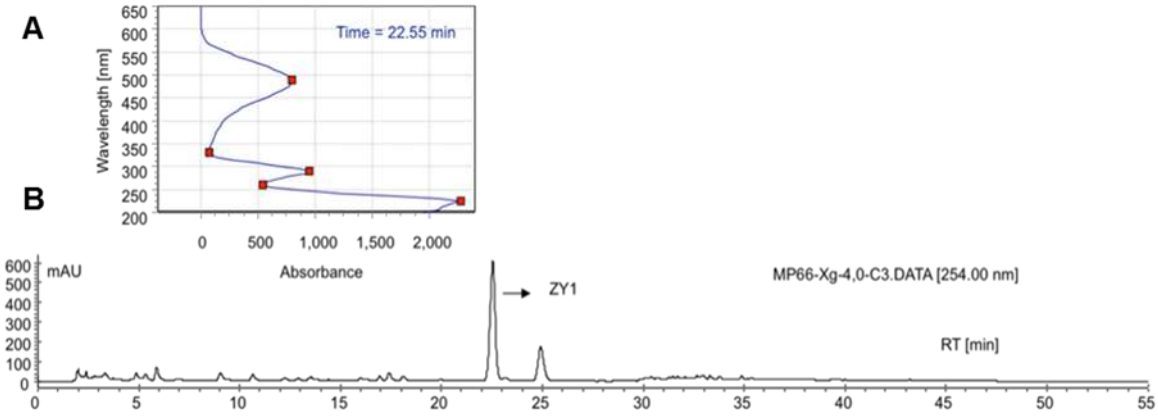

Figure 3.33 HPLC trace, UV spectrum of ZY1 (54). A. UV of the compound. B. HPLC trace of the compound mycelia extract obtained from *S. albus*MP66 fermentation.

UV absorption maxima in acetonitrile were observed at 490, 362, 310, and 260 nm. The NMR measurements for structure elucidation were performed by LC-NMR in AN-d_3 at the University of Greifswald by Dr. Michael Lalk. Measured ^{1}H-, ^{13}C-, HMBC and HMQC NMR spectra of the compound are shown in Appendix 2, Figure 2.12-2.16.

The NMR spectra of the compound showed an aliphatic impurity. But the unrelated peak integrals on the ^{1}H-NMR spectra and HMBC correlations of the impurity were distinguishable from the dominating signals of the compound ZY1 **(54).**

The ^{13}C-NMR showed 14 carbon signals in the lower field of 100 ppm. Two signals at 184.35 and 190.13 ppm showed the presence of two quinolic carbonyl groups. The signals at 164.82, 164.76 and 162.4 ppm showed the presence of carbonyl groups. Two strong methoxy signals at 58.38 and 54.01 ppm showed the presence of at least two methoxy groups. In the upper field of the ^{13}C-NMR spectra and the HMBC spectra from 10 up to 40 ppm aliphatic carbon atoms were observed, which only coupled in the HMBC spectra to the carbon atoms at 174 and 130.59 ppm in the lower field of the ^{13}C-NMR spectra. These two carbon atoms were not correlating with the hydroxy group at 12.86 ppm and the proton at 6.34 ppm. The data of the aliphatic carbons showed that a commercially prevalent used phthalic acid chain ester derivative was present as

inpurity. However, the HMBC and HMQC data were clear enough to allow for an evaluation of the structure.

The presence of two OH signals at 12.87 and 12.16 ppm in the ^{1}H-NMR spectra showed the presence of two phenolic OH groups forming hydrogen bonds. One methoxy signal at 3.94 ppm and two overlapping methoxy signals at 3.86 ppm suggested the presence of three methoxy groups in the compound. Integral of the phenolic proton at 6.34 ppm was used as reference for a hydrogen peak.

The HMQC spectrum showed an aromatic proton attached to a carbon atom at 111.53 ppm. The methoxy group at 3.94 ppm was attached to a carbon at 58.8 ppm and the other two methoxy groups were attached at an overlapping carbon signal at 53.82 ppm. HMBC correlations of the hydrogens allowed for further structure elucidation of the compound.

The methoxy group at 3.94 ppm had HMBC correlation to the carbon atom at 162.4, and a week correlation to the adjacent carbon atom at 111.53 ppm indicating the presence of a methyl enol ether. This is also supported by the chemical shift for the double bond carbons at 162.4 and 111.53 ppm. Strong HMBC correlations of the aromatic proton at 6.34 ppm to the carbon atoms at 162.4, 184.35, 190.13 and 153.12 ppm and couplings to the quaternary carbon atoms at 114.52 and 115.10 ppm indicated a naphtoquinone structure. HMBC correlations of the hydroxyl proton at 12.87 ppm to the carbon atoms at 153.12, 130.77, and 114.52 ppm established the dihydroxymethoxy-1,4-naphtoquinone structure of the molecule, similar to the Western part of the previously isolated molecule collinone **(41)**. The methoxy groups had HMBC couplings with the carbon atoms at 164.82 and 162.44 ppm, which indicates the involvement of two methyl ester groups to the structure and fulfills the molecular formula $C_{15}H_{12}O_9$. The attachment of the two methylester groups on the dihydroxymethoxy-1,4-naphtoquinone structure completed the structure of ZY1 **(54)**. Figure 3.34 shows the HMBC correlations of the compound.

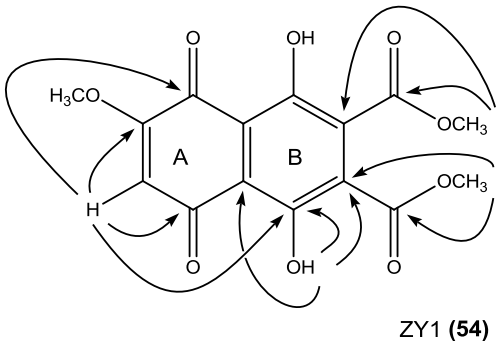

Figure 3.34 HMBC data of ZY1 (54).

Figure 3.35 shows the structure of ZY1 **(54)** whereas an overview of the NMR data is shown in Figure 3.36. Table 3.10 shows the measured ^{1}H-NMR, ^{13}C-NMR and HMBC data obtained. After the structural elucidation was completed the literature survey showed that this compound has not been published.

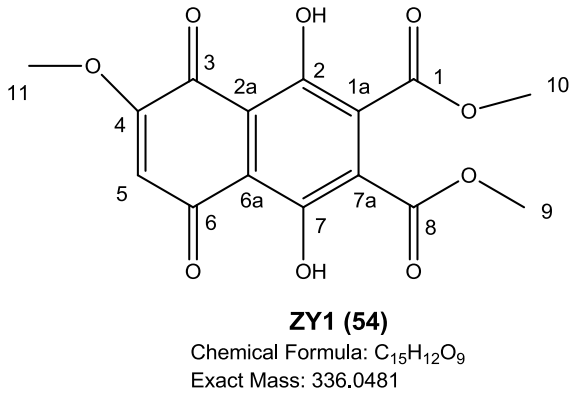

Figure 3.35 Structure of ZY1 (54).

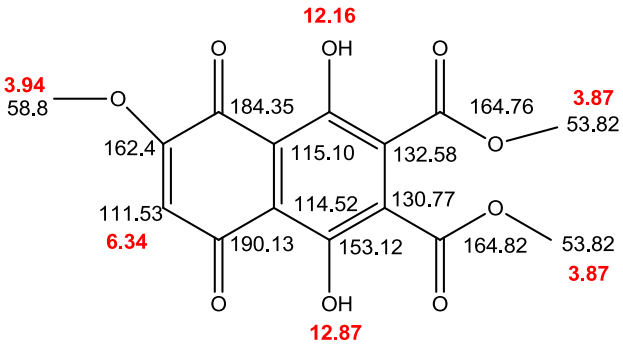

Figure 3.36 ^{1}H-NMR and ^{13}C-NMR data of the compound ZY1 (54).

Table 3.10 ^{1}H- and ^{13}C- NMR Data of ZY1**(54).**

ZY1 (54) (in AN-d_3), 500MHz, LC-NMR			
Position	**^{13}C-NMR[ppm]**	**^{1}H-NMR [ppm]**	**HMBC**
1	164.76	-	
1a	132.58	-	
2-OH	-	12.16	
2	154.06	-	
2a	115.1	-	
3	184.35	-	
4	162.44	-	
5	111.53	6.34	3; 4; 5; 6; 7
6	190.13	-	
6a	114.52	-	
7-OH	-	12.87	6a; 7; 7a
7	153.12	-	
7a	130.77	-	
8	164.82	-	
9- OMe	53.82	3.87	7a; 8
10- OMe	53.82	3.87	1; 1a
11-OMe	58.18	3.94	3; 4; 5

To enable the isolation and increase the yield of the isolated MP66a, lenticulone **(53),** the work-up procedure was modified. In order to avoid the use of acetic acid, TFA was tried. Although TFA had a stronger acidity it was prefered, since the boiling point is 78 °C. It was easier to remove acid during evaporation of ethyl acetate, which has a boiling point of 77 °C. Another essential change needed was a better mobile phase mixture in order to purify the compound by column chromatography with minimum loss. In order to avoid the use of methanol a mobile phase of chloroform:ethyl acetate (5:1) on impregnated silica was used. For the isolation lenticulone **(53),** *S. albus* MP66 was grown in LB medium. The yield of the isolation was 20 mg from 12 L of fermentation. The description of the isolation procedure is in Section 4.1.5.9. The identity of the compound was confirmed by ESI-HRMS analysis for $[M+H]^+$ as $C_{26}H_{16}O_{12}$: *m/z* = 521.0714, calculated $[M+H]^+$ *m/z* = 521.0720, and NMR analysis in $CDCl_3$. Measured ^{1}H-, ^{13}C-, HMBC and HMQC NMR spectra of the compound are shown in Appendix 2, Figure 2.17-2.24.

The carbon NMR of MP66a showed 26 carbon atoms as expected from the molecular formula $C_{26}H_{16}O_{12}$. DEPT spectra and HMQC spectra showed aromatic protons at 110.20, 114.21 and 104.81 ppm connected to the protons at 6.29, 6.61 and 6.17 ppm, respectively. The signal at 57.33 ppm in the ^{13}C-NMR, and DEPT and an aromatic methoxy signal at 4.01ppm in the ^{1}H-NMR showed the presence of an aromatic methoxy group on the molecule. The presences of three quinone carbonyl groups are indicated by the carbon signals at 188.78, 181.6, and 182.81 ppm in the carbon NMR. An additional carbonyl signal was observed at 166.6 ppm. Three OH signals at 13.37, 12.74 and 10.98 ppm in the ^{1}H-NMR spectrum showed the presence of three phenolic OH groups forming hydrogen bonds. Two secondary carbon atoms at 20.59 and 23.96 ppm in the ^{13}C-NMR, DEPT and HMQC spectra showed the presence of two CH_2 groups. An additional methyl group at 19.30 ppm in the ^{13}C-NMR spectrum and at 2.24 ppm in the ^{1}H-spectrum could be determined. The structure was established by examination of long range ^{1}H-^{13}C correlations in the HMBC spectra. The HMBC correlation of the aromatic proton at 6.17 ppm with the two quinone carbonyl groups at 188.78 and 181.67 ppm, and its correlations with the methoxy attached carbon atom at 161.15 ppm together with the additional correlations of the hydroxyl groups at 13.37 and 12.74 ppm forming a hydrogen bond, showed a dihydroxymethoxy-1,4-naphtoquinone structure similar to the compounds didesoxygriseorhodin C **(46)**, collinone **(41)** and ZY1 **(54)** for the Western part of the molecule. Hydroxyl protons at 13.37 and 12.74 ppm showed weak couplings to the carbonyl carbon at 182.81 and 158.28 ppm. These HMBC correlations implied the partial structure 3a for the Western part the molecule. (Figure 3.37)

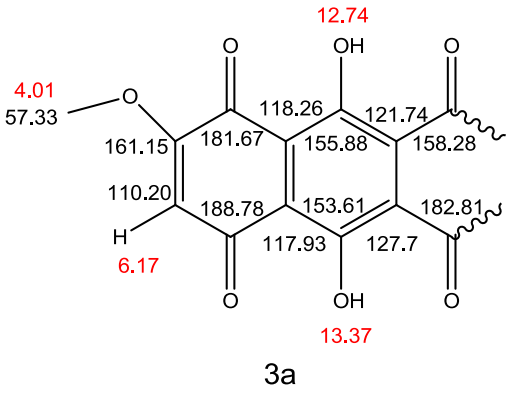

Figure 3.37 Partial structure 3a of lenticulone (48).

For the Eastern part of the molecule, a 3-methyl substituted isocoumarin moiety, similar to the Eastern part of the molecule didesoxygriseorhodin C **(46),** was demonstrated by the strong HMBC correlations of the methyl group with the carbon atoms at 152.85, 104.01 and 114 ppm. Additional couplings of the aromatic protons at 6.29 and 6.61 ppm with the carbon atoms at 166.66, 150.15, 105.08, 137.14, 132.09, 152.85 and 19.30 ppm proved the aromatic structure. HMBC correlations of the hydroxyl group at 10.98 ppm forming hydrogen bond to the quinone carbonyl group oxygen at 166.66 ppm, established the unsaturated lactone ring of the methylated isocoumarin moiety Figure 3.38 shows the partial structure 3b for the Eastern part of the molecule.

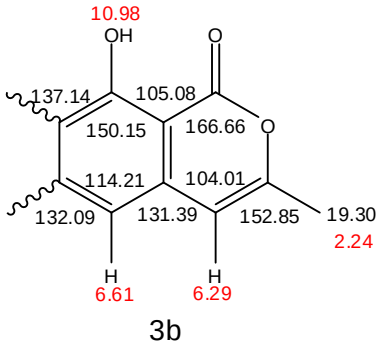

Figure 3.38 Partial structure 3b of lenticulone (53).

Ethylene carbon atoms at 20.59 and 23.96 ppm correlated with the aromatic protons in the Eastern part of the molecule at 6.61 ppm and with the quinone carbonyl group at 182.81 ppm on the Western part of the molecule. Both ethylene protons coupled to the carbon atom at 99.08 ppm. The latter shift is characteristic for a (hemi)acetal function, suggesting that the compond has a spiro system at a position analogous to the spiro center in griseorhodin A **(5)**. The presences of a carbonyl signal at 158.28 ppm and an additional carbonyl signal occurring with a downfield shift at 182.81 ppm indicated an adjacent keto function to the acetal carbon. HMBC couplings of the ethylene group showed that the Western part and the Eastern part of the molecule are connected over an unusual spiro center as shown in the partial structure 3c. (Figure 3.39).

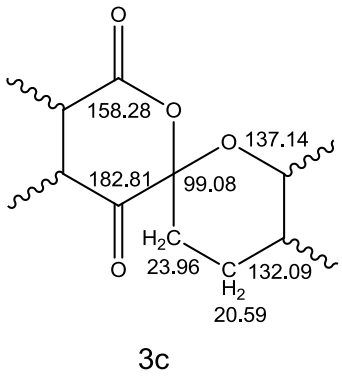

3c

Figure 3.39 Partial structure 3c of lenticulone (53).

The structure of MP66a was estimated and the new compound was renamed lenticulone **(53)**. Figure 3.40 shows the important HMBC correlations of the compound lenticulone **(53)**.

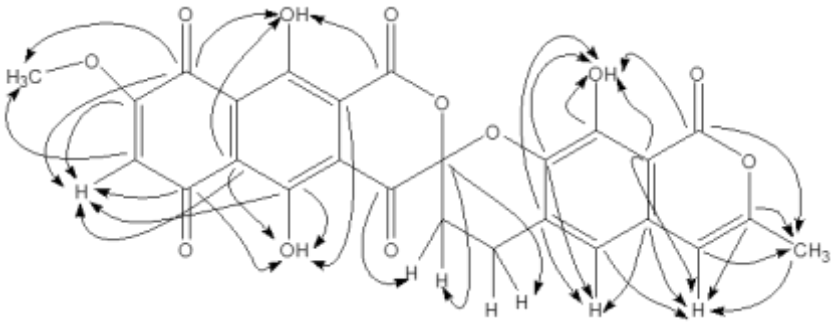

Figure 3.40 Important HMBC correlations of lenticulone (53).

Figure 3.41 shows lenticulone **(53)**. Figure 3.42 shows an overview of the NMR data obtained for lenticulone **(53)**. Table 3.11 shows the measured ^{1}H-NMR, ^{13}C-NMR data and the observed HMBC correlations.

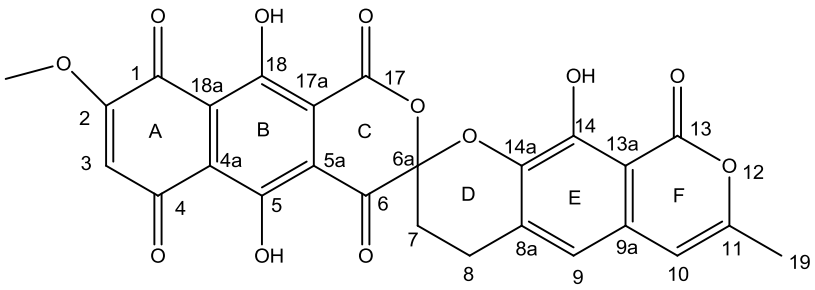

Lenticulone (53)

Chemical Formula: $C_{26}H_{16}O_{12}$

Exact Mass: 520.0642

Figure 3.41 Structure of lenticulone (53)

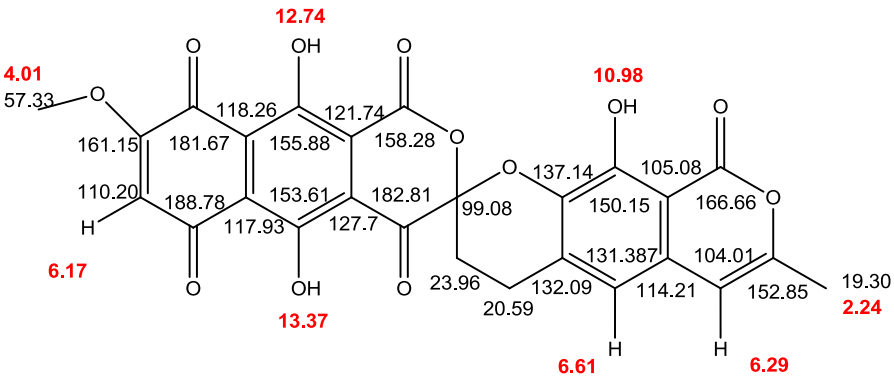

Figure 3.42 ^{1}H-NMR and ^{13}C-NMR data of lenticulone (53).

Table 3.11 ^{1}H- and ^{13}C- NMR Data of lenticulone **(53)**.

Lenticulone (53) (In $CDCl_3$-d), 500 MHz			
Position	**^{13}C-NMR [ppm]**	**^{1}H-NMR [ppm]**	**HMBC**
1	181.67	-	
2	161.15	-	
3	110.20	6.29 (s, H)	1; 2; 4; 4a; 5; 18
4	188.78	-	
4a	117.93	-	
5	153.61	-	
5a	127.7	-	
6	182.81	-	
6a	99.08	-	
7	23.96	2.4-2.5 (m, $H_{a,b}$)	6; 6a; 8; 8a; 9; 17
8	20.59	3.25 (m, H_a);	6a; 7; 8a; 9; 9a; 13a; 14; 14a
8	20.59	2.85 (ddd, H_b)	6a; 7; 8a; 9a; 14
8a	132.09	-	
9	114.21	6.61 (s, H)	7;8; 8a; 9; 10; 13; 13a; 14; 14a
9a	131,387	-	
10	104.01	6.17 (d, H)	8a; 9a; 11; 13a; 14; 19
11	152.85	-	
13	166.66	-	
13a	105.08	-	
14	150.15	-	
14a	137.14	-	
17	158.28	-	
17a	121.74	-	
18	155.88	-	
18a	118.26	-	
19-Me	19.30	2.24 (d, 3H)	8a; 9; 9a; 10; 11; 13; 14; 14a
2-Ome	57.33	4.01 (s, 3H)	1; 2; 4
5-OH	-	13.37 (s, H)	4; 4a; 5; 5a; 17; 17a
14-OH	-	10.98 (s, H)	8a; 13; 13a; 14; 14a
18-OH	-	12.74 (s, H)	1; 18

Lenticulone **(53)**, with the HRMS for $[M+H]^+$as $C_{26}H_{16}O_{12}$ (*m/z* :521.0714, calcd. 521.0720) was fragmented to further analyze its constitution by HR-ESI-MS/MS. The result of the fragmentation is shown in Figure 3.43 and table 3.12 which was carried out with the help of Dr. Engeser. Collision-induced dissociation of the sodium adduct ion $[M+Na]^+$ yielded one major fragment with an exact mass difference of Δm = 204.0372. This indicating a loss of $C_{11}H_8O_4$. and was assigned to a cleavage of ring D (Figure 3.43, fragmentation path A) resulting in the formation of the ion $[I+Na]^+$. In addition fragmentation product

$[II+Na]^+$ (*Δm* = 316.0155; loss of $C_{15}H_8O_8$). was observed in smaller abundance. Two further fragmentation products could be assigned to a cleavage of ring C of the compond (Figure 3.43, path B**)**: loss of $C_{13}H_6O_7$ (III, *Δm* = 246.0362) and $C_{13}H_{10}O_5$ (IV, *Δm* = 274.0054). This fragmentation pattern had a diagnostic value for the structure of the compound. An MS^3 experiment with the main product ion $[I+Na]^+$ only showed water expulsion. Therefore, a hypothetical alternative formation of $[III+Na]^+$ by subsequent fragmentation of $[I+Na]^+$ could be ruled out. Direct fragmentation of lenticulone **(53)** can lead to $[III+Na]^+$ only if the constitution of ring C is the one shown in Figure 3.43, i.e., the carbonyl function at C-12 must be connected to ring B. Thus, the MS^n data confirmed that lenticulone **(53)** is a novel spiroketal that contains an expanded ring C in comparison to griseorhodin A **(5)**. The HR-ESI-MS/MS spectra is shown in Appendix 1, Figure 1.3.

Table 3.12 Fragmentation of lenticulone **(53)**: HR-ESI-MS/MS of $[M+Na]^+$

m/z		**relative intensity**	**Δm_{exp}**	**Δm_{calc}**
525	$M+Na^+-H_2O$	8	18.0098	18.0106
515	$M+Na^+-CO$	4	27.9935	27.9949
499	$M+Na^+-CO_2$	28	43.9886	43.9898
481	$M+Na^+-CO_2-H_2O$	3	61.9952	62.0004
339	$M+Na^+-C_{11}H_8O_4$ (D)	100	204.0372	204.0423
321	$M+Na^+-C_{11}H_8O_4-H_2O$	56	222.0478	222.0528
311	$M+Na^+-C_{12}H_8O_5$	3	232.0209	232.0371
297	$M+Na^+-C_{13}H_{10}O_5$ (B)	2	246. 0362	246.0528
269	$M+Na^+-C_{13}H_6O_7$ (A)	4	274.0054	274.0114
227	$M+Na^+-C_{15}H_8O_8$ (C)	12	316.0155	316.0219
181	$M+Na^+- C_{16}H_{10}O_{10}$	32	362.0317	362.0274

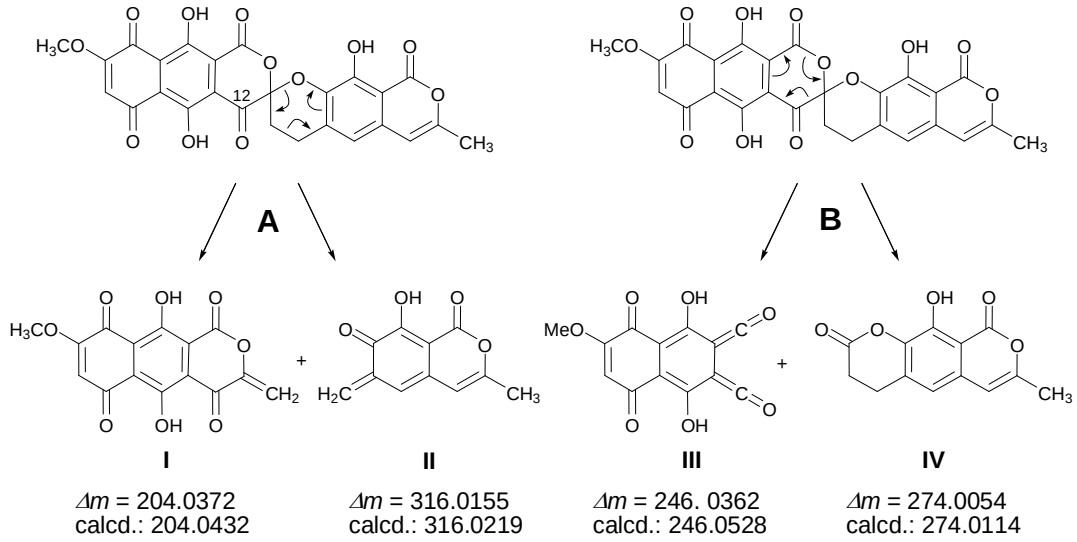

Figure 3.43 ESI-MS/MS fragmentation path of the compound lenticulone (53).

The characterization of lenticulone **(53)** in the extract of the mutant strain *S. albus* MP66 and later in *S. albus* MP42 shows that GrhO6 and GrhJ catalyzea key reaction in the biosynthesis of the spiroketal moiety. GrhO6 and GrhJ have the function of cleaving the C17-C17a bond to generate the spiroketal moiety as shown in Figure 3.44. The presemce of lenticulone **(53)** and additional metabolite with a molecular formula $C_{25}H_{16}O_{11}$ in the extract of *S. albus* MP42 suggested the involvement of GrhJ in this transformation of the compound. The investigation of the GrhJ mutant strain by Kathrin Reinhardt resulted with a postulated metabolite 7, 8 dideoxy-6-oxygriseorhodin C **(55)** for the compound with a molecular formula $C_{25}H_{16}O_{11}$.[125] This metabolite was not observed in the extract of MP66. This compound with one less oxygen atom and one less carbon atom suggested that GrhJ together with GrhO6 catalyzes the final steps of spiroketal formation. Figure 3.44 shows the postulated involvement of GrhO6 and GrhJ in the griseorhodin A **(5)** biosynthesis.

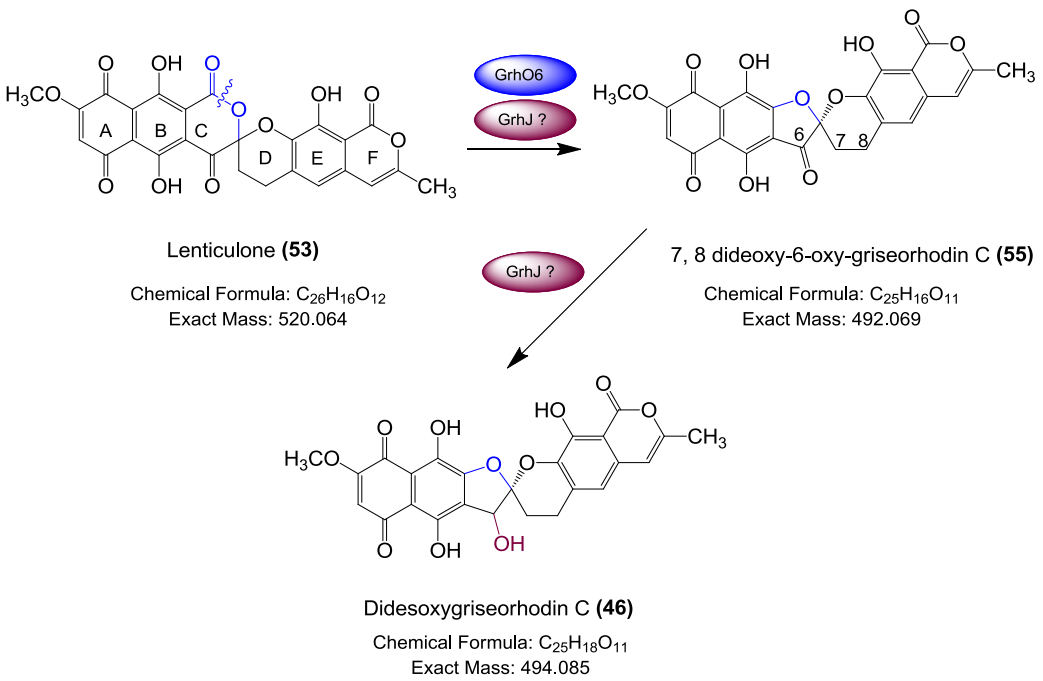

Figure 3.44 Proposed functions of GrhO6 and GrhJ in the biosynthesis of griseorhodin A (5).

In order to obtain further information about GrhO6 and GrhJ, sequence homology of GrhO6 and GrhJ were investigated by BLAST analysis by Kathrin Reinhardt.[125]. Table 3.13 shows the BLAST analysis results and the enzymes showing homologies to GrhO6 and GrhJ.

Table 3.13. BLAST analysis results for GrhO6 and GrhJ.[125]

Protein	Amino Acids	Proposed function	Sequence Similarity (Protein, Origin)	Similarity/ Identity [%]
GrhO6	520	FAD-dependent monooxygenase, Baeyer-Villigerase-type oxygenase	RubN/ *Streptomyces collinus* (unpublished)[125]	84/76
			PokO4/ *Streptomyces diastatochromogenes* Tü6028[142]	59/45
			CmmOI/ *Streptomyces griseus*[143]	58/45
			MtmOIV/ *Streptomyces argillaceu*[141]	56/45
GrhJ	295	*N*-Acetyl-transferase (GNAT)	*-/Salinispora arenicola* CNS-205 (unpublished)[125]	42/29
			-/ Salinispora tropica CNB-440 (unpublished)[125]	41/29
			Dra0019/ *Deinococcus radiodurans*[15]	41/31

Investigations of sequence homologies of GrhO6 showed high protein similarity with two Baeyer-Villigerases, CmmOI and MtmOIV in the chromomycin and mithramycin biosynthesis, respectively.[141,143] However, GrhO6 would be an unusual example of a monooxygenase acting on an ester instead of a ketone. Flavin-containing Baeyer-Villiger monooxygenases employ NADPH and molecular oxygen to catalyze the insertion of an oxygen atom into a carbon-carbon bond of a carbonylic substrate.[144] MtmOIV cleaves a C-C bond, essential for the conversion of biologically active inactive precursor, premithramycin B **(56)**, into the active drug mithramycin **(23)**. Figure 3.45 shows the involvement of MtmOIV in the biosynthetic pathway to mihtramycin **(23)**.[69,144]

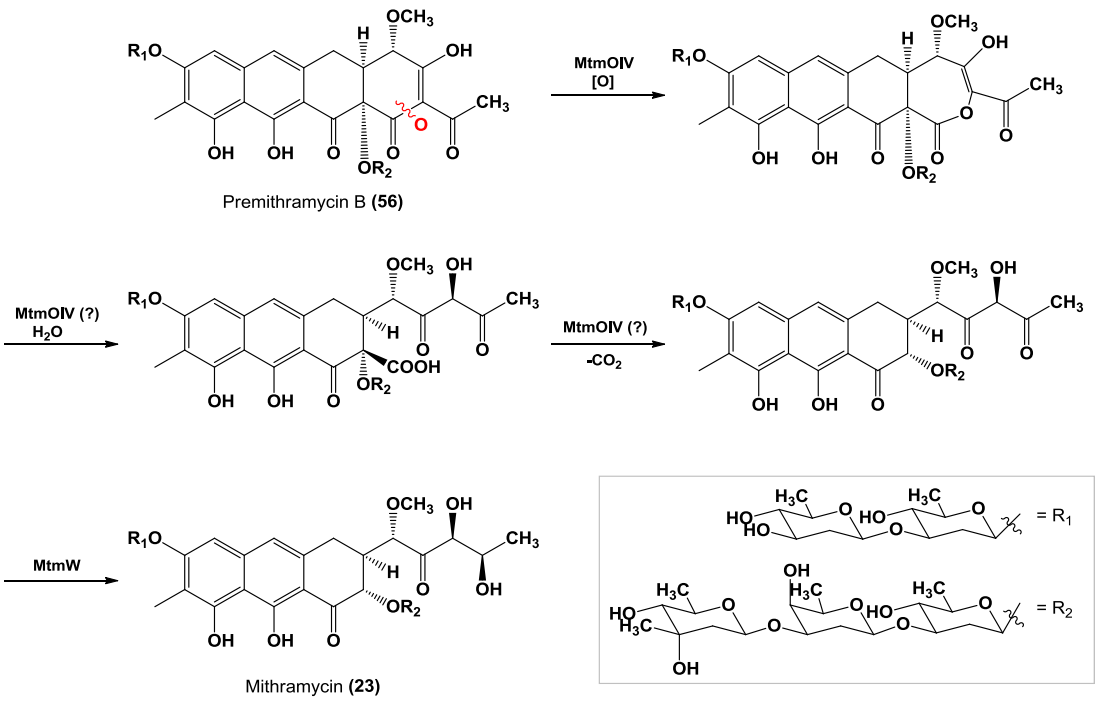

Figure 3.45 The involvement of Baeyer-Villiger monooxygenase MtmOIV in the biosynthesis of mitramycin (23).[69]

Another possibility for the catalytic carbon-carbon cleavage mechanism of GrhO6 could be a ring hydroxylation and subsequent fragmentation aided by rearomatization. In that case GrhO6 would act as a hydroxylase. For the oxygenase OtcC from *Streptomyces rimosus* in the oxytetracyclin biosynthesis, which shows a sequence similarity to GrhO6, a hydroxylation reaction of the antracyclin moiety was assigned.[145] The position of hydroxylation is shown in Figure 3.46. A related mechanism has been proposed for 4-hydroxybenzoate hydroxylase of *Candida parapsilosis* CBS604 on the basis of inhibitor studies and molecular orbital considerations. [146]

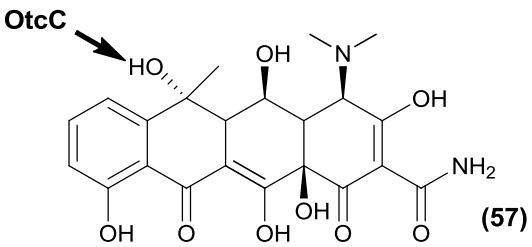

Figure 3.46 The position of hydroxylation of OtcC in the oxytetracyclin biosynthesis.[145]

These investigations for the function of GrhO6 suggest two alternative routes for the reaction mechanism at the generation of the spiroketal moiety that are shown in Figure 3.47. (Only the BCD rings are shown). The first possibility is that GrhO6 acts as a Baeyer-Villigerase on the ester moiety of lenticulone **(53)**, resulting in decarboxylation. The second possibility is that GrhO6 acts as a hydroxylase and hydroxylates the ester α-position, and decarboxylation results from rearomatization.

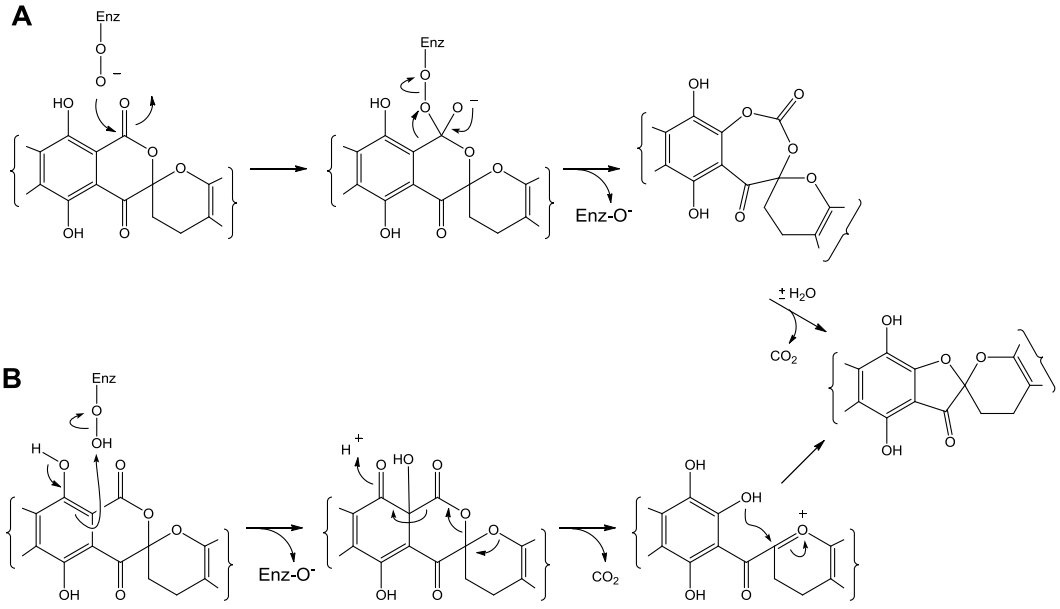

Figure 3.47 Two possible pathways for the final carbon-carbon bond cleavage in griseorhodin A biosynthesis (only the BCD rings are shown). A: GrhO6 acts as a Baeyer-Villigerase on the ester moiety, resulting in decarboxylation. B: GrhO6 hydroxylates the ester α-position, and decarboxylation results from rearomatization.

GrhJ shows homology to GCN-5 related N-acetyltransferases (GNATs). It is reported that typeI PKSs sometimes use GNATs to incorporate acetyl starter-unit into complex polyketides.[147] Examples of such polyketide clusters are known from pederin, onnamide, rhizoxin and myxovirescin biosynthesis.[147,148] Therefore, GrhJ was suspected to play a similar role in griseorhodin A biosynthesis initially. However, the examination of the *grhJ* gene deletion strain by Kathrin Reinhard for her PhD work implied the presence of a suggested intermediate 7,8-dideoxy-6-oxygriseorhodin C **(55)** in addition to lenticulone **(53)**. Unfortunately, the amounts produced were not enough for a

characterization of the metabolite by NMR.[125] This compound with one less oxygen atom and one less carbon atom suggested that GrhJ together with GrhO6 catalyzes the final steps of spiroketal formation.

In order to examine the carbon-carbon cleavage mechanism an *in vitro* assay with the overexpressed GrhO6 was conducted. The experiments could not prove an *in vitro* activity of GrhO6 using lenticulone **(53)** as a substrate at the assay conditions. The results of the *in vitro* assay with the overexpressed GrhO6 are described and discussed further in Section 3.5.

3.4.5 Isolation and Characterization of Precollinone (58)

The metabolite precollinone **(58)** was observed as a yellow compound in the extract of the oxygenase knockout strain *S. albus* KR53. The mutant strain has a *grhO9* gene deletion on the griseorhodin A cluster. The encoded enzyme at this deleted gene is predicted as an FAD-dependent monooxygenase. Figure 3.48 shows the HPLC trace, UV spectrum and LC-HRMS data of the plate-extracted compound produced by *S. albus* KR53.

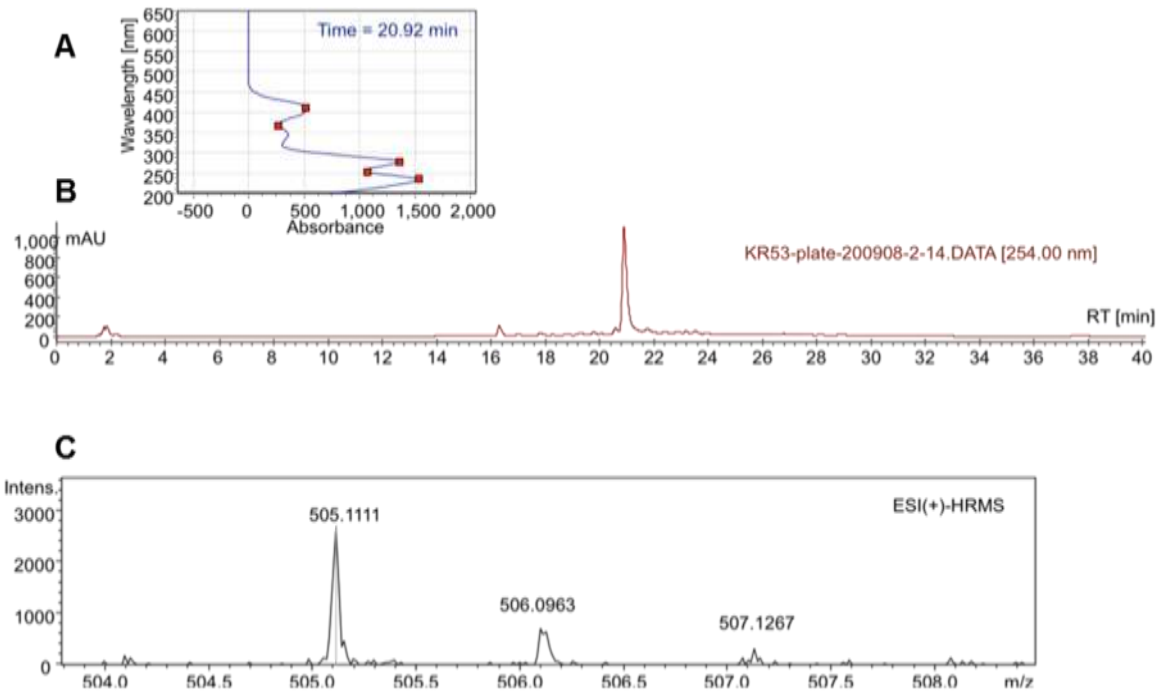

Figure 3.48 HPLC trace, UV spectrum and the LC-HRMS data of precollinone (58).A. UV of the compound. B. HPLC trace of the mycelia extract obtained from *S. albus* KR53 cultivated on 2CM agar plates. C. The molecular ion $[M+H]^+$ observed at ESI-HRMS.

For the isolation of the compound *S. albus* KR53 was fermented in LB medium, and the compound was isolated as described in the Section 4.1.5.11. The yield of the isolation was 18 mg from 9 L of fermentation. The molecular ion detected for this major compound was at *m/z*: 505.1111 for $[M+H]^+$ suggesting a molecular formula $C_{27}H_{20}O_{10}$ with a calculated exact mass *m/z*: 505.1135 for $[M+H]^+$. The structure of the compound was established by ESI-HRMS data and NMR analysis in DMSO-d_6. Measured ^{1}H-NMR, ^{13}C-NMR, HMBC and HMQC spectra of the compound are shown in Appendix 2, Figure 2.25-2.29.

The carbon spectra of the compound showed 27 carbon atoms as expected from the molecular formula $C_{27}H_{20}O_{10}$ of the compound. The ^{1}H-NMR and HMQC spectra showed the presence of five aromatic protons at 7.75, 7.14, 6.61, 6.57 and 6.17 ppm attached to the carbon atoms at 118.44, 102.67, 116.10, 103.88 and 104.06 ppm respetively. A methoxy signal at 3.86 ppm in the ^{1}H-NMR and at 56.09 ppm in the ^{13}C-NMR spectra was observed. An additional methyl group at 2.06 ppm in the ^{1}H-NMR and at 19.15 ppm in the ^{13}C-NMR spectra was detected. The presence of the quinone carbonyl group is deduced with the carbon signals at 198.96 and 197.71 ppm in the ^{13}C-NMR spectrum. The presence of the OH signal at 11.36 ppm in the ^{1}H-NMR indicated a phenolic hydroxyl group forming a hydrogen bond. Two carbon atoms at 28.05 and 23.76 ppm showed a ethylene group in the ^{13}C-NMR spectra. Additional two quaternary carbon atoms at 77.99 ppm and 80.85 ppm similar to those in collinone **(41)** were observed.

For the Western part of the molecule, a 1,8-dihydroxy-3-methoxy naphthalene partial structure was indicated. HMBC coupling of the methoxy group with the carbon atom at 163.20 ppm was observed. Strong HMBC correlations of the two aromatic protons at 7.14 and 7.75 ppm with the carbon atoms at 163.20, 159.17, 164.40, 140.42, 111.02, 131.45, 106.92 and 103.88 ppm implied a naphthalene moiety. The aromatic protons at 7.14 and 7.75 ppm showed a typical ^3J-coupling of 0.5 Hz for a 1,8- naphtalene substitution. The aromatic proton at 6.57 ppm did not show any couplings with the protons at 7.14 and 7.75 ppm. HMBC correlations of the aromatic proton at 6.57 ppm with the carbon atoms at 140.42, 102.67, 164.40 and 106.92 ppm together with the corellations of aromatic protons at 7.14 and 7.75 ppm established the structure

of the naphthalene moiety. Aromatic protons at 7.75 ppm showed HMBC correlations with the two quinolic carbonyl carbons at 197.71 and 198.96 ppm. This implied the presence of two quinone carbonyl groups in the Western part of the molecule. (Figure 3.49)

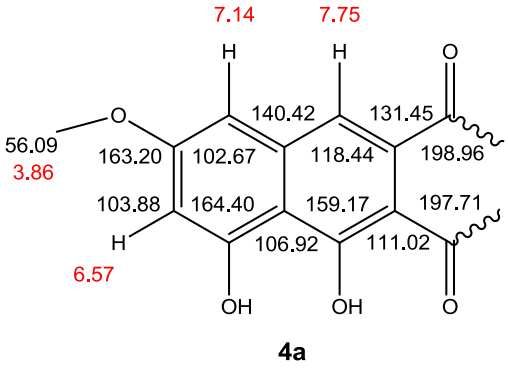

Figure 3.49 Partial structure 4a of precollinone (58).

NMR data for the Eastern part of the molecule has strong similarities to those of collinone **(41)**, which indicates a 3-methyl substituted isocoumarin moiety. Strong HMBC couplings of the methyl group with the carbon atoms 155.17 and 104.06 ppm indicated a methyl substituted aromatic ring. Additional couplings of the aromatic proton at 6.17 ppm to the carbon atoms at 155.17, 103.03 and 159.08 ppm support the conclusion as well. The carbonyl signal at 166.71 ppm belongs to an unsaturated lactone forming a hydrogen bond to the hydroxyl group at 11.36 ppm, which is attached to the carbon atom at 159.08 ppm. HMBC correlations of the hydroxyl proton at 11.36 and the aromatic proton at 6.61 ppm establish the isocoumarin moiety 4b. (Figure 3.50)

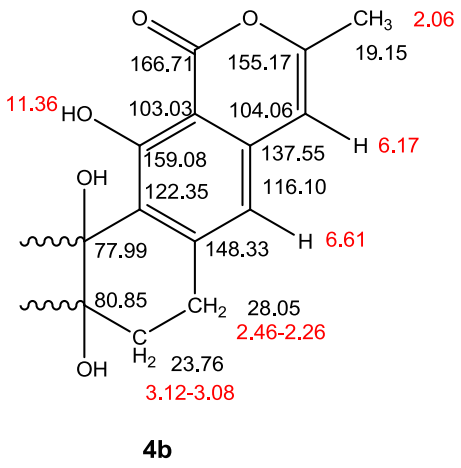

Figure 3.50 Partial structure 4b of precollinone (58).

Two methylene hydrogens both showed strong correlations with the Eastern part of the molecule. The ethylene protons at 2.3-2.5 ppm (m) had HMBC correlations with the carbonyl groups at 197.71 and 198.96 ppm and the carbonyl group at 194.03 ppm in the Western part of the molecule. Quarternary atoms at 80.85 and 77.99 ppm correlated with the ethylene protons as well. The HMBC correlations of the metylene groups enables to close the six member ring structure adjacent to the isocoumarin system 4b and attaches the Western part to the Eastern part of the molecule, resulting in a pentangular moiety. The chemical shift of two quaternary carbon atoms at 78.99 and 80.8 ppm can not belong to an epoxy group, since the chemical shift of the carbon atoms of an epoxy group at this position is usually expected at 60-70 ppm. Additional to that, the NMR measurements were carried out in DMSO-d_6 and this enabled to observe 4 hydroxyl signals in three wide singulets at 14.02, 10.2 and 4.1 ppm. The molecular formula of the compound and the chemical shift of carbon atoms C-5 and C-18, supported that two hydroxyl groups are substituted at these positions of the molecule. The new compound was named precollinone **(58)**. The correlations observed in HMBC experiments are summarized in Figure 3.51. Figure 3.52 shows the structure of precollinone **(58)**. Figure 3.53 and Table 3.14 shows the measured ^{1}H-NMR, ^{13}C-NMR and HMBC data.

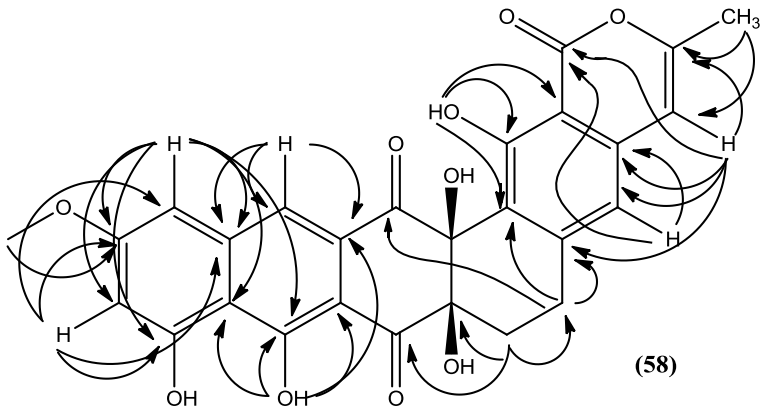

Figure 3.51 HMBC data of precollinone (58).

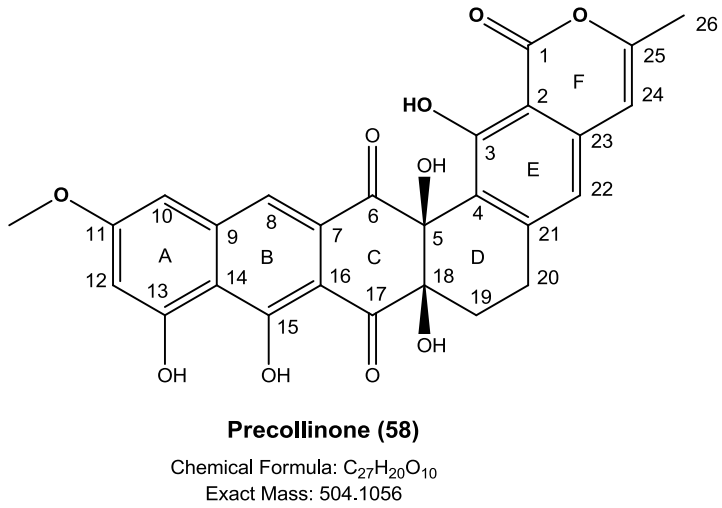

Figure 3.52 Structure of precollinone (58).

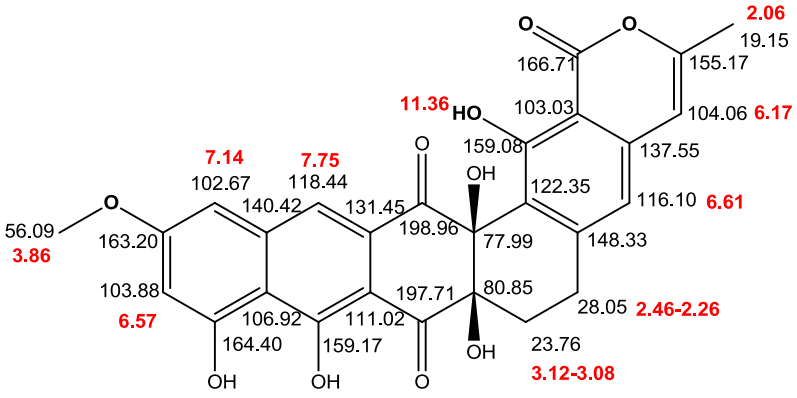

Figure 3.53 ^{1}H-NMR and ^{13}C-NMR data of precollinone (58).

Table 3.14 ^{1}H- and ^{13}C- NMR and HMBC data of precollinone **(58).**

Precollinone (58) in DMSO-d_6			
Position	**^{13}C-NMR [ppm]**	**^{1}H-NMR [ppm]**	**HMBC**
1	166.71	-	-
2	103.03	-	-
3	159.08	-	-
4	122.35	-	-
5	77.99	-	-
6	198.96	-	-
7	131.45	-	-
8	118.44	7.75(s,H)	6,7,9,10,11,14,15,16,17
9	140.42	-	-
10	102.67	7.14(s,H)	8,9,11,12,13,15,16
11	163.20	-	-
12	103.88	6.57(s,H)	9,10,11,13
13	164.40	-	-
14	106.92	-	-
15	159.17	-	-
16	111.02	-	-
17	197.71	-	-
18	80.85	-	-
19	23.76	2.46-2.26(m,H)	5,17,18,20,21
20	28.05	3.12-3.08(m,H)	4,5,18,19,21,22
21	148.33	-	-
22	116.10	6.61(s,H)	1,2,3,4,20,21,23,24
23	137.55	-	-
24	104.06	6.17(s,H)	2,23,25,26
25	155.17	-	-
26	19.15	2.06(s,3H)	2,22,23,24,25
11-OMe	56.09	3.86(s,3H)	11
13-OH	-	14.17(bs,H)	-
15-OH	-	10.09(bs,H)	-
3-OH	-	11.36(s,H)	-

The relative and absolute configuration of the compound was determined in cooperation with Anu Schaumlöffel in the group of Prof. Gerhard Bringmann. As for griseorhodin A **(5)** and collinone **(41),** the method was to compare the calculated CD spectra of all four possible stereo isomers with the measured CD spectrum. For the CD measurements 2 mg of the compound was used. Figure 3.54 shows the results of the method and the determined absolute configuration of precollinone **(58).** The compound was used as an example for a further UV calculation experiment, which resulted in a (5S,18R) precollinone **(58)**

configuration as well. The configurations of the stereocenters of precollinone **(58)** are identical with collinone **(41).**

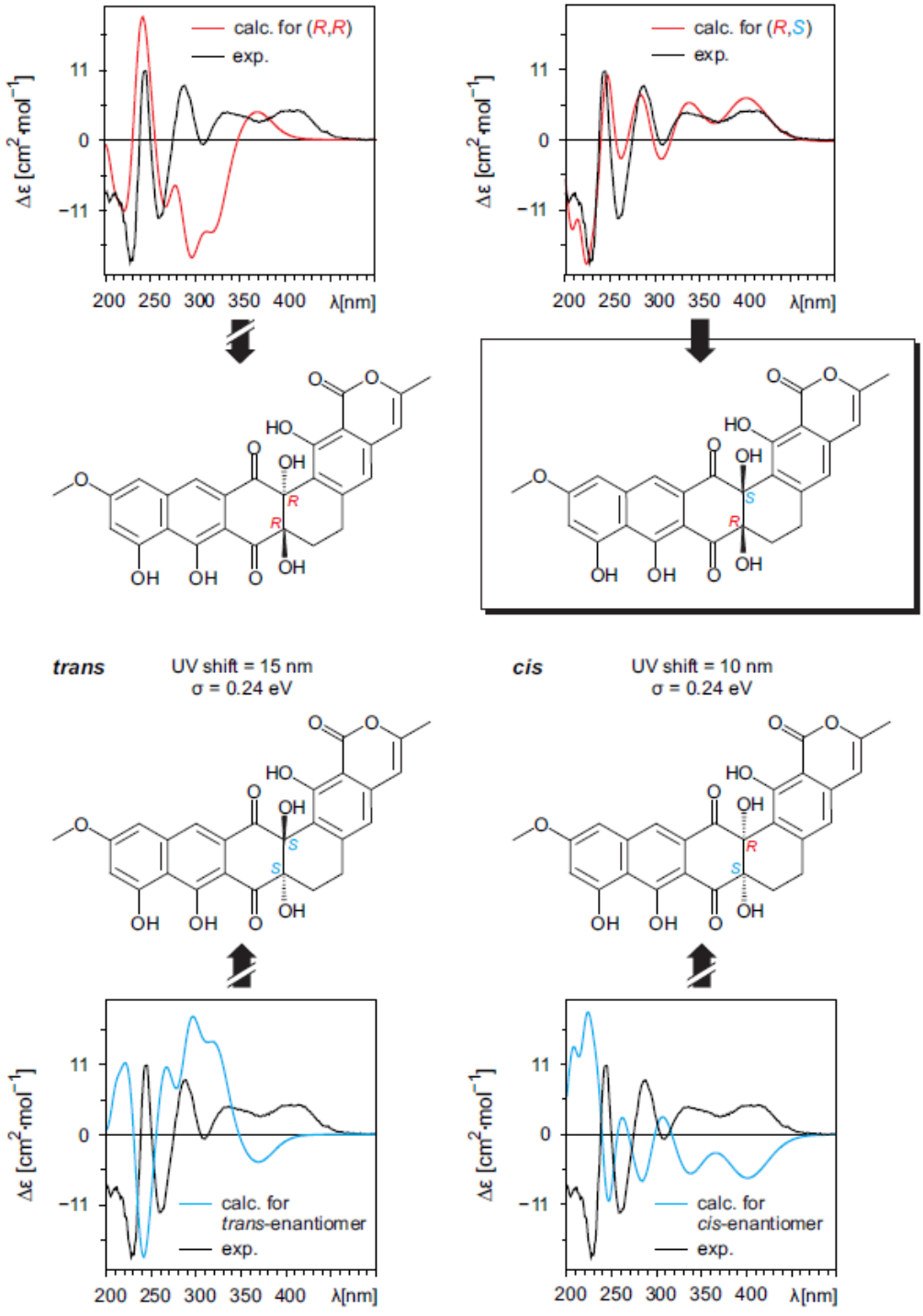

Figure 3.54 Data of the calculated and measured CD spectra and the determined absolute configuration of precollinone (58).

The structure of precollinone **(58)** shows great similarities to collinone **(41)**. Two oxidation steps at ring A and ring B are missing. The compound is the major metabolite of the mutant strain and occurs as a single peak of the HPLC

trace of the plate extract. This shows clearly that GrhO9 acts on the oxidation of the first and second ring. These oxidation steps are occurring after methylation of the aromatic hydroxyl group at C-11 and lactonization of the ring F. But the mechanism of the oxidation, which might start by the hydroxylation of the first or second ring and the role of GrhO9 at the formation of the quinolic functions on the first ring of collinone **(41)**, needs to be investigated further by functional studies. Figure 3.55 shows the suggested oxidation steps catalyzed by GrhO9.

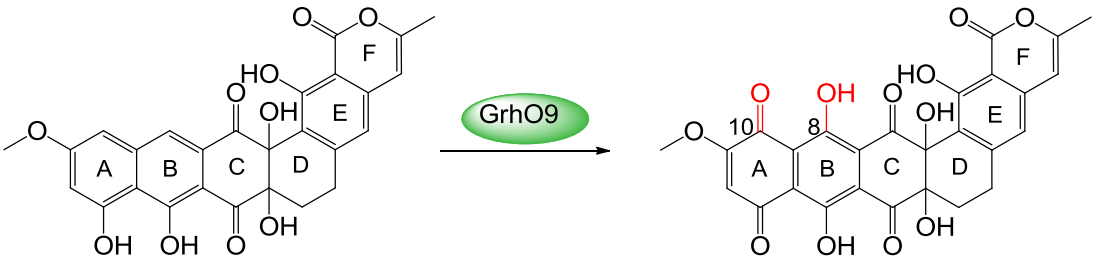

Figure 3.55 Proposed function of GrhO9 in the biosynthesis of griseorhodin A (5).

To get more insights in to the possible function 0f GrhO9, the sequence homology of GrhO9 was investigated by BLAST analysis by Kathrin Reinhardt. Table 3.15 shows the BLAST results of the protein.

Table 3.15. Homologous proteins to GrhO9 determined by the BLAST analysis results[125].

Protein	Amino Acids	Proposed function	Sequence Similarity (Protein, Origin)	Similarity/ Identity [%]
GrhO9	529	FAD-dependent monooxygenase	RubP/ *Streptomyces collinus* (Unpublished)[125]	72/78
			GrhO8/ *Streptomyces* sp. JP95[15]	63/46
			DntB/ *Burkholderia* sp. DNT[138]	58/45
			TcmG/ *Streptomyces glaucescens*[139]	55/42

The protein sequence shows similarity to the oxygenases GrhO8, TcmG and DntB. DntB (4-methyl-5-nitrocatechol (4M5NC **(49)**) monooxygenase) from *Burkholderia* sp. catalyzes the second step of 2,4-dinitrotoluene degradation by converting 4M5NC **(49)** to 2-hydroxy-5-metylquinone **(50)** with the concominant removal of the nitro group as shown in Section 3.4.3 and Figure 3.28.[138] The hydroxylase TcmG is an oxygenase in the biosynthesis of the bacterial polyketide tetracenomycin C **(52)**. TcmG hydroxylates tetracenomycin A2 **(51)** at positions C-4, C-4A, and C12A to give tetracenomycin C **(52)** as shown in Section 3.4.3 and Figure 3.29.[139]

3.4.6 Isolation and Characterization of Secocollinone-1 (59)

The metabolite KR5a was observed as a dark blue pigment on the mycelium of *S. albus* KR5, which changes its color in acidic conditions to pink. The deleted gene *grhO1* was predicted to be a rare FAD dependet oxygenase carrying their cofactor covalently attached to the enzyme. The blue compound was not only water insoluble but also insoluble in several common organic solvents such us $CHCl_3$, MeOH, acetone or ethyl acetate. After acidifying the bacteria up to pH 3 by re-suspending in an aqueous solution with TFA, the color turned to pink and the compound became soluble in ethyl acetate. Nevertheless, an unusual feature of the compound was that it attached strongly to almost every stationary phase used for chromatographic purposes, such as silica, impregnated silica, C18 material and Sephadex LH-20 material, so that it was not possible to further purify the extract. It was therefore necessary to derivatize the polar functions on the molecule. In order to elucidate the structure of KR5a, through a derivatization a reaction was conducted.

To determine the molecular weight of the native metabolite in the crude extract was also difficult, because the metabolites did not appear as defined peaks by RP-HPLC and LC-HRMS measurements. As a result, the mass could not be obtained using common HPLC solvents. Therefore the extract was dissolved in DMSO. This is uncommon for HPLC analysis, since DMSO can also dissolve components of the RP-18 HPLC column material. Nevertheless, the extract was injected for LC-HRMS analysis and the molecular weight was determined. The molecular ion detected for this major compound was at *m/z*: 537.102 for

$[M+H]^+$ suggesting a molecular formula $C_{27}H_{22}O_{12}$ with a calculated exact mass *m/z*: 537.103 for $[M+H]^+$. Figure 3.56 shows the HPLC trace, the UV spectrum and LC-HRMS data of the compound KR5a.

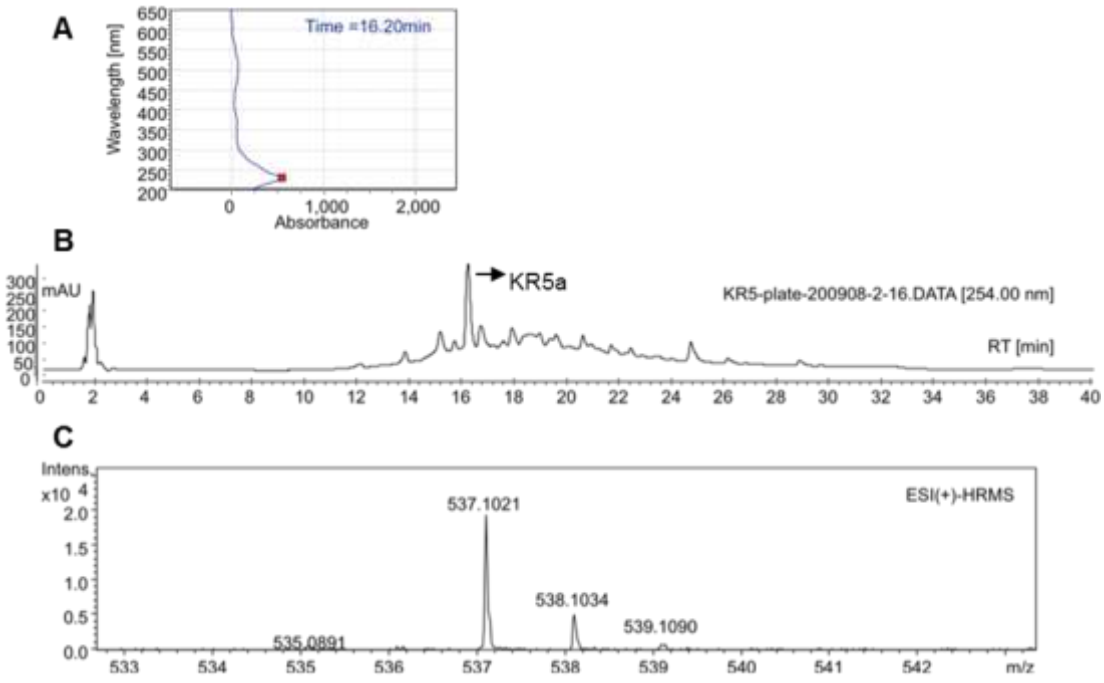

Figure 3.56 HPLC trace, UV spectrum and the LC-HRMS data of KR5a produced by *S. albus* KR5. A. UV of the compound. B. HPLC trace of the mycelia extract obtained from *S. albus* KR5 cultivated on 2CM agar plates. C. The molecular ion $[M+H]^+$ observed at ESI-HRMS.

In order to determine the function of the oxygenase GrhO1, derivatives of the metabolite needed to be investigated. Acetylations and methylations are common derivatization reactions for aromatic phenolic compounds. Several reaction protocols were tested with a commercially available aromatic compound, quinalizarin, in order to find an appropriate reaction with a good yield. It had to be considered that derivatisation reactions of *S. albus* crude extracts are problematic beacuse the yield of the products are considerably law and the result can be a wild mixture of different substances. Test reactions using the crude of extract of *S. albus* KR5 for acetylation and methylation with dimethylsilyl diazomethane did not work well. However, the methylation reaction with dimethylsulfate (DMS) was promising. The result was a single major product, after adapting a reaction from Falc *et al.*[149] Prolongation of the

reaction time provided a total methylation and a single product that allowed for obtaining the necessary amount of substance for further structur elucidation after the purification steps. The reaction procedure for the derivatization is described in the Section 4.1.5.13. Figure 3.57 shows the results of the derivatisation reaction. The compound was named KR5-a-meth.

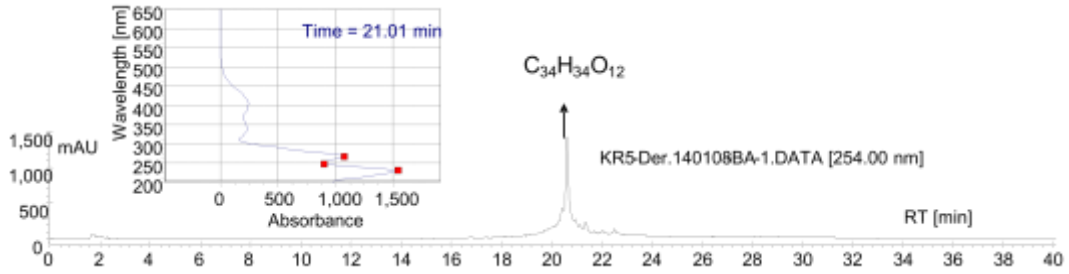

Figure 3.57 HPLC trace and UV spectrum and of KR5a-meth.

For the derivatisation reaction, *S. albus* KR5 was fermented several times in TSB medium. 500 mg brown crude extract was obtained from 12 L of fermentation broth. The procedure for the extraction is described in Chapter 4.1.5.12. The extract was dried overnight in vacuum and used for the methylation reaction with dimethyl sulfate (DMS) as described in 4.1.5.13. The yield of the methylated KR5a, which was named KR5a-meth was 13 mg. The molecular ion of the compound was identified by ESI-HRMS analysis as *m/z*: 635.222 $[M+H]^+$, and the calculated *m/z*: 635.2129 for $[M+H]^+$ for the predicted molecular formula $C_{34}H_{34}O_{12}$. The structure elucidation of KR5a-meth was carried out with NMR analysis in DMSO-d_6 (Figure 3.58). Measured ^1H-, ^{13}C-, HMBC and HMQC NMR spectra of the compound are given in Appendix 2, Figure 2.30-2.35.

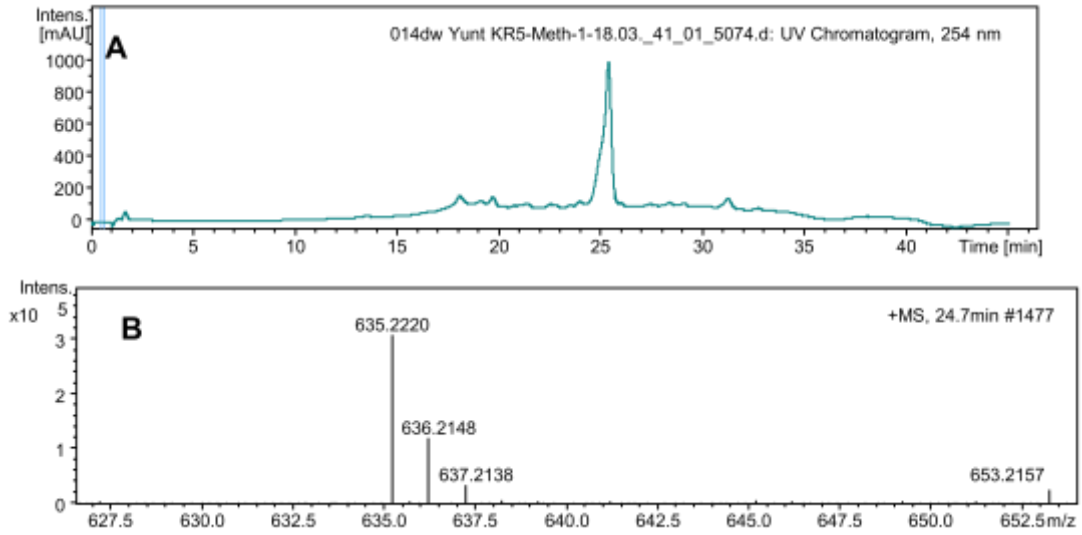

Figure 3.58 HPLC trace and LC-HRMS data of KR5a-meth.

The carbon spectrum of the compound showed 34 carbon atoms as expected from the molecular formula $C_{34}H_{34}O_{12}$. The presence of quinone carbonyl is suggested by the carbon signals at 184.01 and 181.12 ppm in the ^{13}C-NMR spectrum. Additionally, a carbonyl signal at 158.96 ppm was detected. Evidence for 8 methoxy groups was provided by singulet signals at 3.93, 3.90, 3.88, 3.82 (double), 3.81, and 3.80 ppm in the ^{1}H-spectrum and at 63.51, 62.45, 62, 62.04, 61.94, 61.87, 57.56 and 57.31 ppm, respectively. Additionally, a methyl group at 2.18 ppm in the ^{1}H-spectrum and at 19.69 ppm in the ^{13}C spectrum was observed. The presence of aromatic protons at 7.08, 7.02 and 6.43 ppm in the ^{1}H-spectrum was observed. HMBC secondary correlations and DEPT spectra of these aromatic protons showed their attachments to the carbon atoms at 122.26, 103.14 and 103.63 ppm, respectively. Two ethyl carbons had signals at 31.52 and 26.0 ppm in the ^{13}C-NMR and DEPT spectra.

The structure of the Eastern part of the molecule was deduced from the HRMS correlations of the aromatic protons and the methyl group as a 3-methyl substituted isocoumarin moiety, which had similarities of the compounds before. The methyl group showed strong correlations with the carbon atoms at 154.26 and 103.63 ppm and a weak coupling with the quaternary carbon atom at 135.79 ppm. Strong HMBC and HMQC correlations of the aromatic protons at 6.43 and 7.08 ppm allowed establishing the substructure. The attachment of the

two methoxy groups at 3.81 and 3.87 ppm to the 3-methyl substituted isocoumarin moiety 5a, shown in the Figure 3.51, could be established by the HMBC correlations with the carbon atoms at 154.30 and 151.44 ppm. (Figure 3.59)

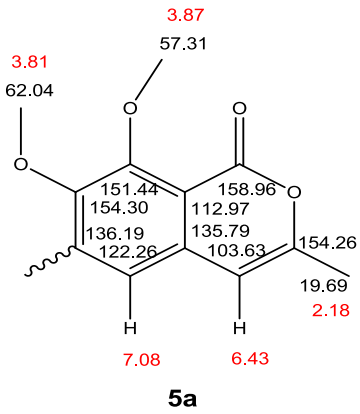

Figure 3.59 Partial structure 5a of KR5a-meth.

For the elucidation of the Western part of the structure, HMBC correlation of the ethylene hydrogen signals at 2.80-2.85 ppm at C-11 and at 2.90-2.95 ppm at C-12, and the additional aromatic hydrogen at 7.02 ppm aat C-19 were used. The hydrogen atom at 7.02 pm showed a HMBC correlation with the quinone carbonyl at 181 ppm and strong correlations with the three methoxy substituted carbon atoms at 156.76, 158.87 and 140.80 ppm. Additional couplings with the two quaternary carbons at 116.03 and 130.79 ppm established the substructure 5b. (Figure 3.60)

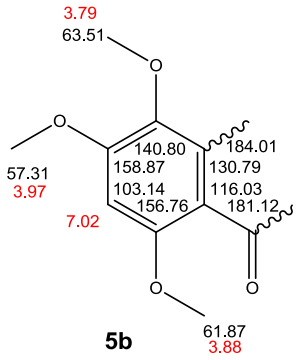

Figure 3.60 Partial structure 5b of KR5a-meth

Two ethylene hydrogens at 2.90-2.95 ppm had correlations with three methoxy attached carbon atoms at 151.44 (on the Eastern part of the molecule), 154.84, 156.83 ppm, with a quaternary aromatic proton at 144.81 ppm and with the methylene carbon at 31.52 ppm. Two ethylene hydrogens at 2.90-2.95 ppm showed HMBC correlations with the carbon atoms in the Eastern part of the structure at 122.26, 136.19, 154.30 and 151.44 ppm, with a quaternary aromatic proton at 144.81 ppm and with the methylene carbon at 26.02 ppm. These correlations showed a connection between the Western part and the Eastern part of the molecule *via* an ethylene Bridge. The substructure 5c was obtained. (Figure 3.61)

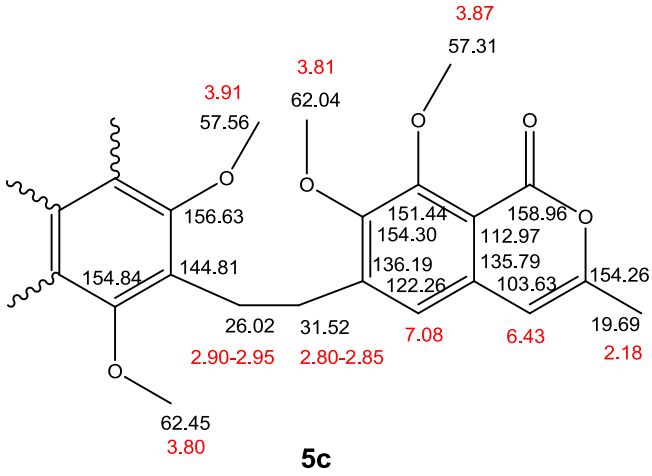

Figure 3.61 Partial structure 5c of KR5a-meth.

The unassigned carbon atoms were: a quinone carbonyl at 184.01 ppm, a methoxy-substituted aromatic carbon at 147.83 ppm and two quaternary aromatic carbons at 129.25 and 125.20 ppm. Important HMBC correlations of the compound are shown in Figure 3.62.

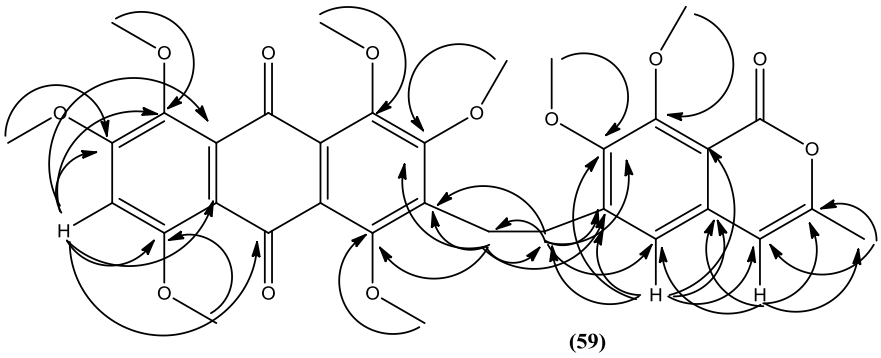

Figure 3.62 Important HMBC correlations KR5a-meth.

However, the partial structures obtained, the unassigned carbon atoms in the spectral data and the molecular formula $C_{34}H_{34}O_{12}$ imply two possible structures for the compound. The position of the quinolic carbonyl group at C-23 and the methoxy substitution at position C-25 can not to be proved by the obtained HMBC data. Therefore the possibility of structure **59b** needed to be excluded. Figure 3.63 shows the possible structures **59** and **59b** of the compound KR5a-meth.

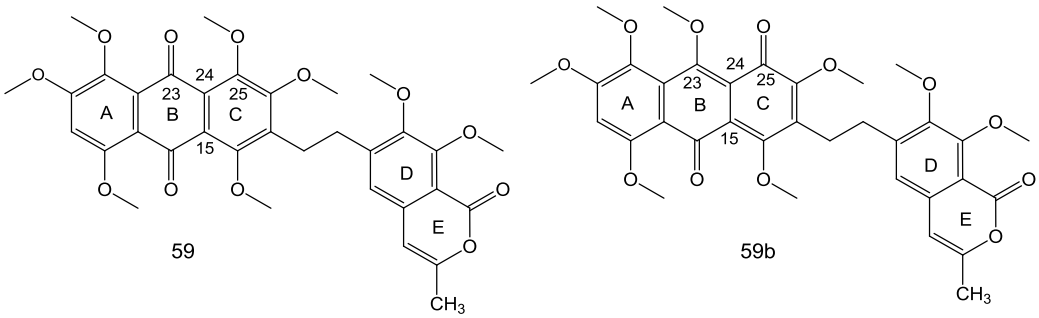

Figure 3.63 Possible structures 59 and 59b of the compound KR5a-meth. 59b is a chemically unlikely variant due to the interrupted aromatic system.

To obtain more information and to distinguish between the large amount of methoxy groups and the quarternary carbon atoms, EI- and ESI-MS/MS fragmentation experiments were performed, but the fragmentations did not provide further information to prove any of the two possible structure. EI-MS and ESI-MS/MS spectra of the compound are presented in Appendix 1, Figure 1.1 and Figure 1.2. An NMR experiment to obtain NOE correlations of the methoxy groups was attempted but the amount of the substance needed for this

experiment using the infra-structure of the institute could not be obtained. An NMR prediction experiment with the NMR program MestreNova was carried out. The NMR prediction results supported structure **59**, which has at the unassigned quinone carbonyl at 184.01 ppm at position C-23 and the methoxy-substituted aromatic carbon at 147.83 ppm and two quaternary aromatic carbons at 129.25 and 125.20 ppm. The obtained NMR predictions for the possible structures 59 and 5b are shown in Appendix 2, Figure 2.36-2.39.

Figure 3.64A shows the elucidated structure of KR5a-meth, which was renamed as secocollinone-1 **(59)** and an overview of the NMR data is shown in Figure 3.64B. Table 3.16 shows the measured. ^{1}H-NMR, ^{13}C-NMR and HMBC data.

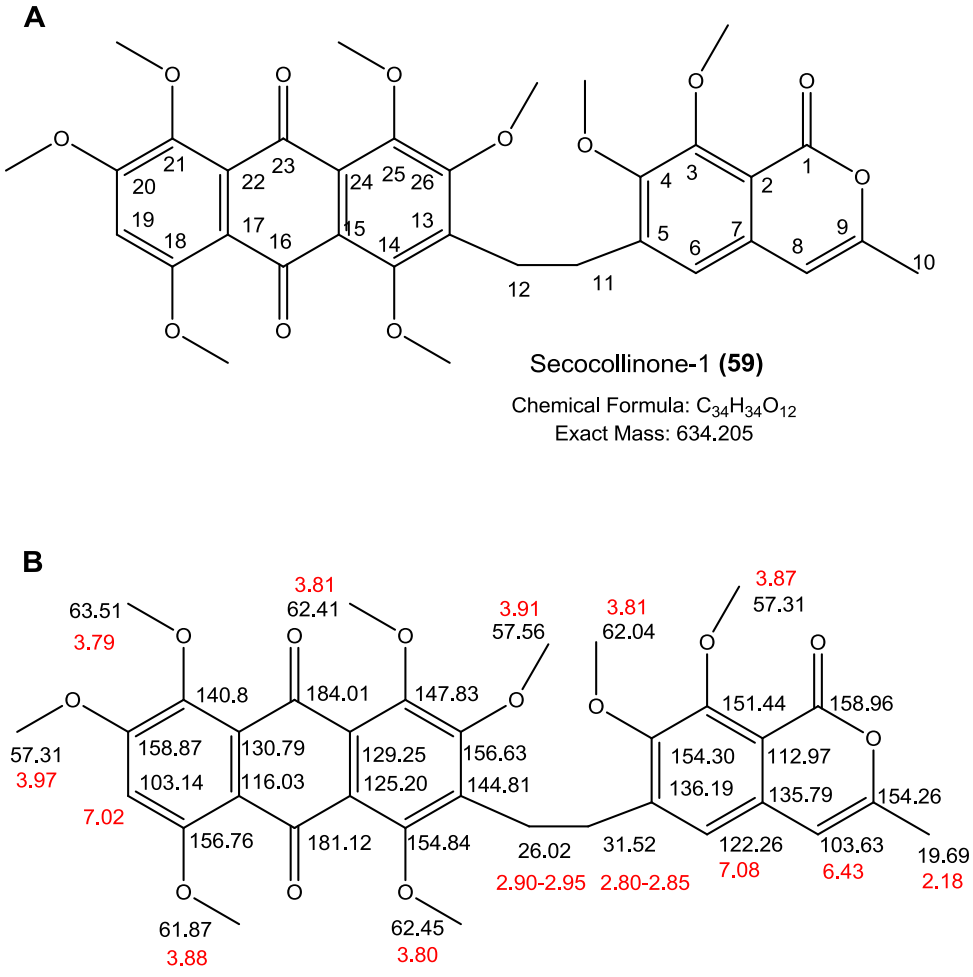

Figure 3.64 A Structure of secocollinone-1 (59) .B ^{1}H-NMR and ^{13}C-NMR data of secocollinone-1 (59).

Table 3.16 ^{1}H- and ^{13}C-NMR and HMBC data of secocollinone-1 **(59).**

Secocollinone-1 (59) in DMSO-d_6			
Position	**^{13}C–NMR [ppm]**	**^{1}H-NMR [ppm]**	**HMBC(Nr. of C)**
C1	158.96		
C2	112.97		
C3	151.44		
C4	154.30		
C5	136.19		
C6	122.26	7.08 (s)	2,3,4,5,7,8,11,12
C7	135.79		
C8	103.63	6.43 (s)	2,6,7,9,10
C9	154.26		
C10	19.69	2.18	1,2,6,7,8,9
C11	31.52	2.80-2.85 (m)	3,5,6,12,19
C12	26.02	2.90-2.95 (m)	4,5,6,11,13,14,26
C13	144.81		
C14	154.84		
C15	125.20		
C16	181.12		
C17	116.03		
C18	156.76		
C19	103.14	7.02 (s)	16,17,18,20,21,22,23
C20	158.87		
C21	140.80		
C22	130.79		
C23	184.01		
C24	129.25		
C25	147.83		
C26	156.63		
C3-OMe	57.31	3.87 (s)	3
C4-OMe	62.04	3.81 (s)	4
C14-OMe	62.45	3.80 (s)	14
C18-OMe	61.87	3.88 (s)	18
C20-OMe	57.31	3.97 (s)	20
C21-OMe	63.51	3.79 (s)	21
C25-OMe	62.41	3.81 (s)	25
C26-OMe	57.56	3.91 (s)	26

The characterized structure of methylated KR5a, secocollinone-1 **(59),** indicates for the structure of KR5a, a related structure to the highly oxidized metabolite collinone **(41)**. The metabolite KR5a was renamed as secocollinone-2 **(60)** and the structure is shown in Figure 3.65.

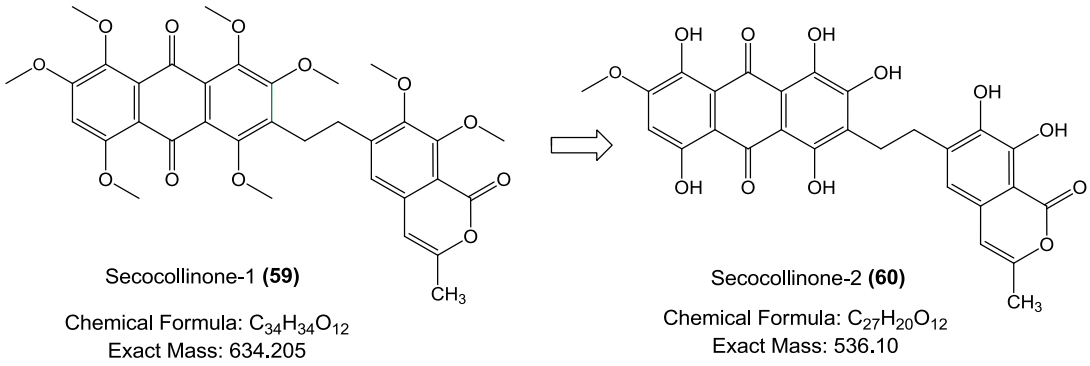

Figure 3.65 Structure of secocollinone-1 (59) and secocollinone-2 (60).

The structure of secocollinone-2 **(60)** suggests that GrhO1 acts after another oxidation reaction, which opens ring D of collinone **(41).** GrhO5 was suggested to initiate reactions leading to three C-C bond cleavages. In that case GrhO1 should act after GrhO5 during the biosynthesis. In this case, the metabolite secocollinone-2 **(60)** is very unlikely a substrate of GrhO1 because the substrate of the enzyme GrhO1 should be in a higher oxidation state than collinone **(41)** after the first bond cleavage reaction of collinone **(41)**. But the ring C of collinone **(41)** is reduced and aromatization of the ring C is observed, which is much unexpected. Therefore the structure of secocollinone-2 **(60)** suggests that this metabolite is a reduced derivative of an intermediate in the pathway for the generation of the spiroketal function of griseorhodin A **(5)**. A possible explanation for the reduction might be that the native intermediate is reduced with the involvement of another enzyme of the host bacterium *S. albus*. Another possibility is that the native metabolite reacts further immediately after expression by the mutant strain, which makes difficult a detection of the native metabolite in a higher oxidation state than collinone **(41).** A reduction reaction as a side reaction during the methylation procedure is rather unexpected. In order to obtain an explanation if and how the enzyme might involve in the spiroketal formation, an oxidized derivative of secocollinone-2 **(60)**, secocollinone-3 **(61)** is suggested as a possible intermediate as shown in Figure 3.66.

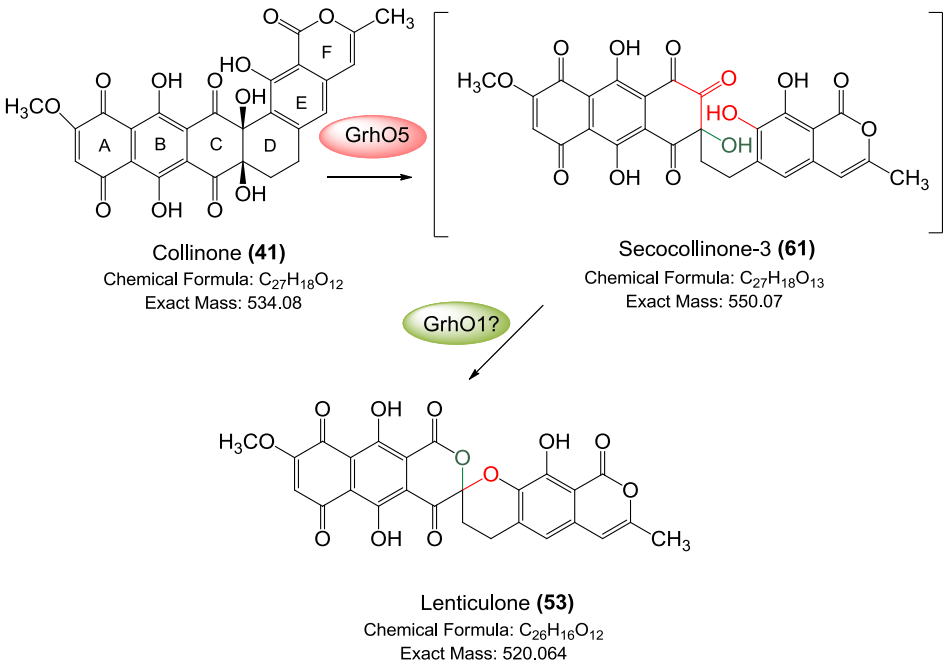

Figure 3.66 Postulted biosynthesis step of GrhO1 and GrhO5 leading to the generation of lenticulone (53) using the suggested intermediate secocollinone-3 (61). Postulated structure secocollinone-3 (61) is shown in paranthesis.

The plate extract of *S. albus* KR5 was reinvestigated and a metabolite with a molecular ion at *m/z*: 551.079 for $[M+H]^+$ suggesting a molecular formula $C_{27}H_{18}O_{13}$ with a calculated exact mass *m/z*: 551.082 for $[M+H]^+$ was detected in small amounts. This metabolite has the same molecular formula with the postulated intermediate secocollinone-3 **(61)** and supports the possibility of a higher oxidized metabolite as a native intermediate for GrhO1.

These investigations for the function of GrhO1 and the postulated intermediate secocollinone-3 suggested a mechanism for the first C-C bond cleavage performed by GrhO5, shown in Figure 3.67 (Only the CDE rings are shown). The function of GrhO1 might be the subsequent biosynthetic decarboxylation reaction of the postulated intermediate **(61)**, leading to the generation of lenticulone **(53)** as shown above in Figure 3.66.

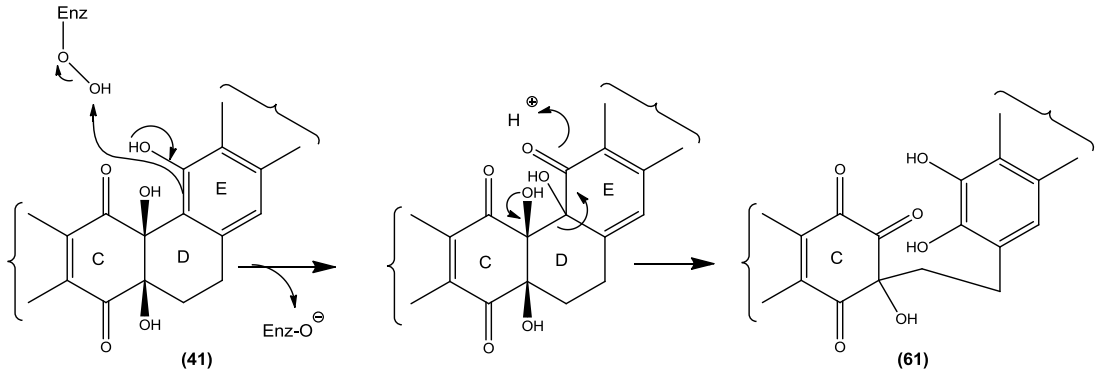

Figure 3.67 Suggested mechanisms for the first C-C bond cleavage generating the postulated intermediate secocollinone-3 (61).

The literature survey showed the presence of an intermediate that is similar but not identical to the suggested intermediate secocollinone-3 **(61** in the fredericamycin A **(26)** carbaspirocyle formation.[150] Deletion of the oxygenase FdmE resulted in a spiro[4.5]decane scaffold characterized by a cyclohexa-1,2,4-triketone moiety **(63)**, serving as a missing link between FDM B **(62)**, and FDM A **(26).**[150] The isolation of relatively unstable metabolite FDM E **(63)**, supports a biosynthetic benzilic acid-like rearrengment leading to a decarboxylation for fredericamycin A **(26)** biosynthesis. Figure 3.68 shows the postulated involvement of the enzyme Fdm E in the fredericamycin A **(26)** biosynthesis.[150]

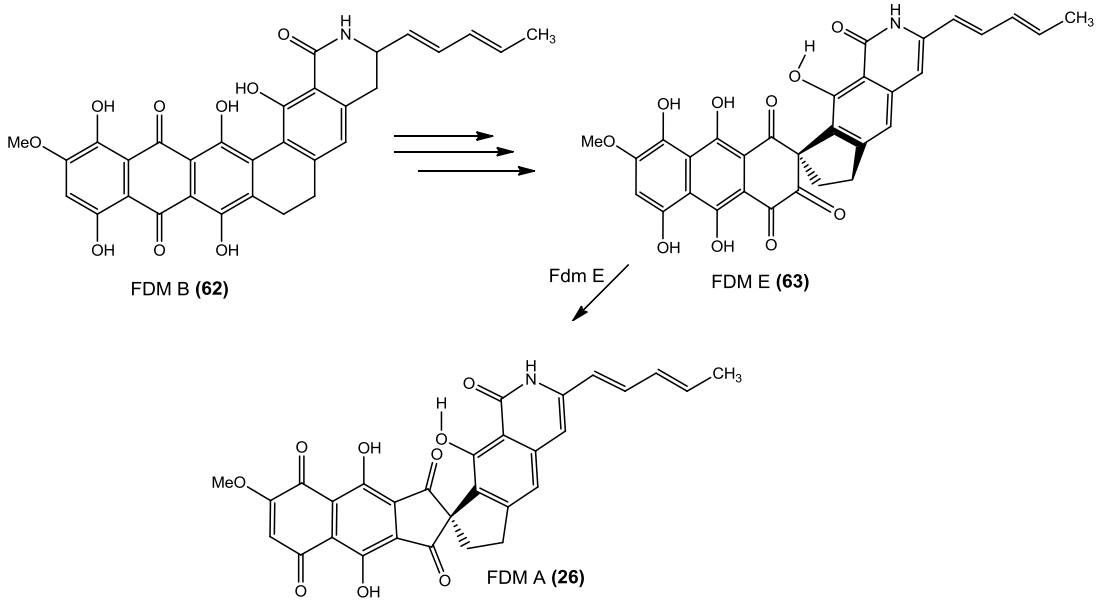

Figure 3.68 Postulated involvement of FdmE in fredericamycin biosynthesis. [150]

In order to obtain more information about the suggested function of GrhO1, sequence homology to other tailoring enzymes were investigated by BLAST analysis by Kathrin Reinhardt. (Table 3.17).[125]

Table 3.17. BLAST analysis results for GrhO1.[125]

Protein	Amino Acids	Proposed function	Sequence Similarity (Protein, Origin)	Similarity/ Identity [%]
GrhO1	475	FAD-dependent oxygenase	RubI/ *Streptomyces collinus* (Unpublished)[125]	72/68
			MitR/ *Streptomyces lavendulae*[118]	57/44
			SACE_4040/ *Saccharopolyspora erythrae* NRRL 2338[151]	55/44

The deleted gene *grhO1* was predicted to encode a rare FAD-dependent oxygenase carrying their cofactor covalently attached to the enzyme. These types of oxygenases are involved in unusual oxidative C-C bond cleavages, such as EncM in the enterocin biosynthesis shown in Figure 1.20 in Section 1.5.3.[63] GrhO1 showed homologies to the proteins MitR and SACE_4040, but the functions of the proteins are unknown yet.[118,151]

3.4.7 Isolation of Compounds Produced by *S. albus* KR41 and Structure Elucidation of the Compound KS-619-1 (64).

The metabolites of the knockout strain *S. albus* KR41, which has the gene *grhM* deleted, were observed as an orange pigment on the mycelium on 2CM agar plate growing cultures. In the beginning of the research, the function of the gene *grhM* could not be predicted as an oxygenase because it sequence does not show any similarities to any other oxygenase with an identified function. Later publications, such as the investigation of the oxygenases FdmM and FdmM1 in the fredericamycine A **(26)** biosynthesis showed that the protein might have a function as an oxygenase.[152] The HPLC traces and the UV spectra of the metabolites in the plate extract of *S. albus* KR41 are shown in the Figure 3.69. Two major components are observed and named as KR41c and KR41c'. Both compounds had the same UV spectra, the same ESI-HRMS molecular ion *m/z*: 459.1050 $[M+H]^+$ and *m/z*: 459.1069 $[M+H]^+$ and the same deduced molecular formula $C_{26}H_{19}O_8$ (calculated $[M+H]^+$=459.1074 for $[C_{26}H_{19}O_8]^+$), which implies that the two compounds peaks are isomers of each other. Figure 3.69 shows the HPLC trace of the extract and UV spectra of the metabolites KR41c and KR41c'. Figure 3.70 shows the HRMS data of both metabolites.

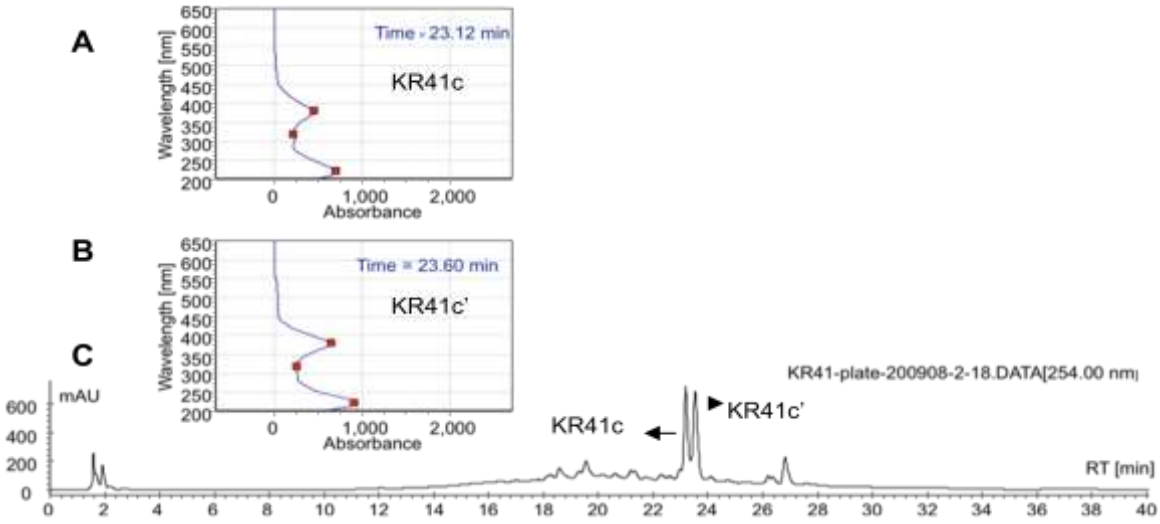

Figure 3.69 HPLC trace of the plate extract from *S. albus* KR41 with UV spectra and LC-HRMS data of the two major compounds KR41c and KR41c'.

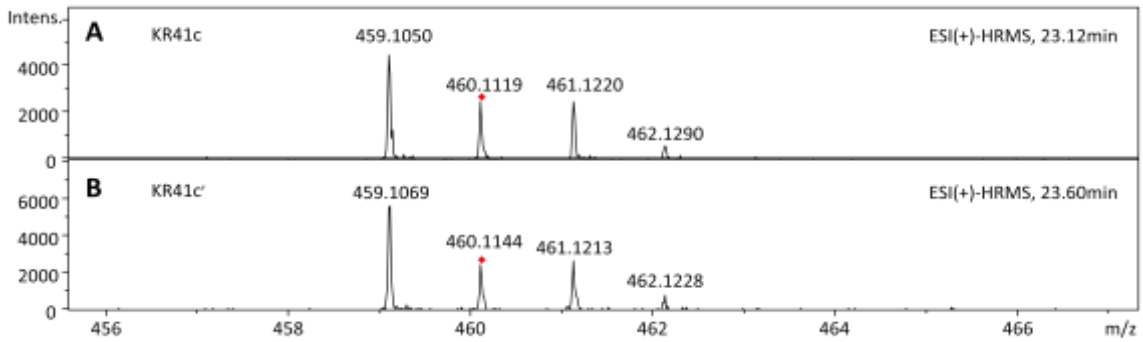

Figure 3.70 ESI-HRMS molecular ions observed for the peaks KR41c and KR41c'.

For the isolation of KR41c and KR41c', *S. albus* KR41 was fermented in TSB medium. The bacterial mycelium and the growth medium were extracted separetly. The detailed procedure for the fermentation and extraction are presented in Section 4.1.4.14 and 4.1.4.16. HPLC traces and molecular ions detected by ESI-HRMS at *m/z*: 459.104 for $[M+H]^+$ and at *m/z*: 459.107 for $[M+H]^+$ supporting a molecular formula for both compounds $C_{26}H_{18}O_8$ (calculated $[M+H]^+$=459.1074 for $[C_{26}H_{19}O_8]^+$) shows that KR41c and KR41c' are produced in the liquid culture as well. Extracts of the liquid culture contained additional compounds. Figure 3.71 shows the HPLC traces of the fermentation extracts obtained from the mycelium (Figure 3.71A) and medium (Figure 3.71B.). An interesting new component was KR41a, which also occurred in the fermentation extract of the GrhO8 oxygenase knockout *S. albus* KR11. GrhO8 enzyme predicted to be a FAD-dependent monooxygenase. Detailed investigation of *S. albus* KR11 and the characterization of their metabolites are explained further in Section 3.4.8.

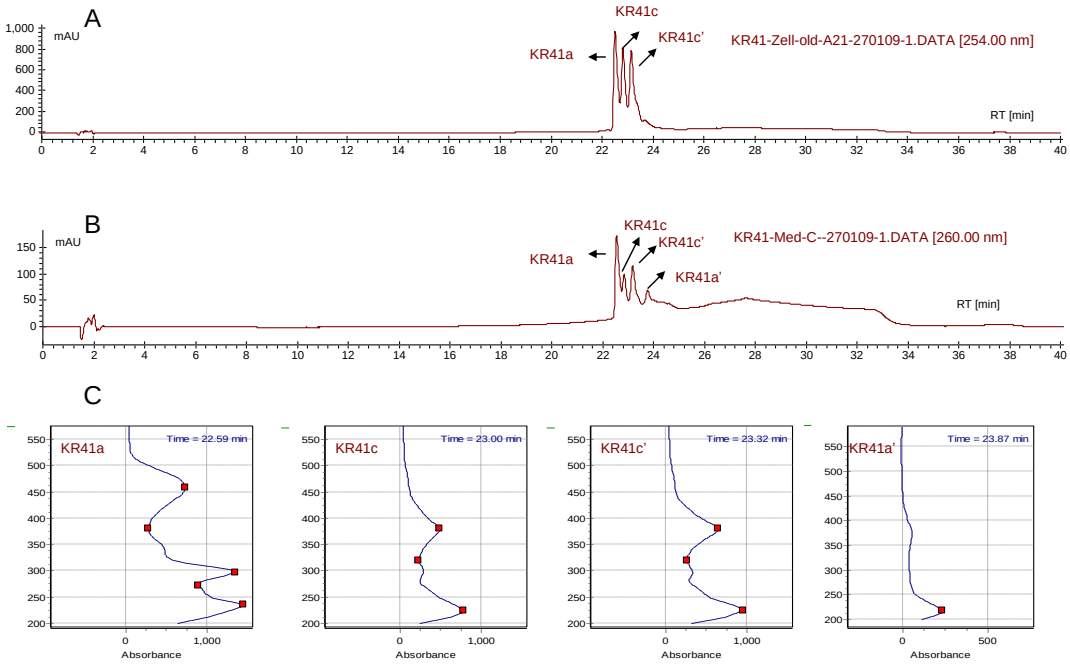

Figure 3.71. HPLC trace of the fermentation extract of *S. albus* KR41. A. HPLC trace of the mycelium extract. B. HPLC trace of the medium extract. C. UV spectra of the observed metabolites KR41a, KR41c, KR41c', KR41a'.

KR41a was analyzed by ESI-HRMS. The molecular ion for KR41a was measured as *m/z*: 475.100 $[M+H]^+$. This suggests $C_{26}H_{18}O_9$ as the molecular formula for KR41a with a calculated $[M+H]^+$=475.1024 for $[C_{26}H_{19}O_9]^+$. Another compound KR41a' has the same suggested molecular formula as KR41a, thus being an isomer of KR41a. A red pigment, observed in small amounts, was named KR41b. The molecular formula of KR41b was suggested as $C_{26}H_{18}O_{10}$ with a measured *m/z*: 491.099 for $[M+H]^+$ by ESI-HRMS analysis, and a calculated *m/z*: 491.097 for $[M+H]^+$. Figure 3.72 shows the ESI-LC-HRMS data of KR41a, KR41c, KR41b, KR41c', and KR41a' obtained from the fermentation extract.

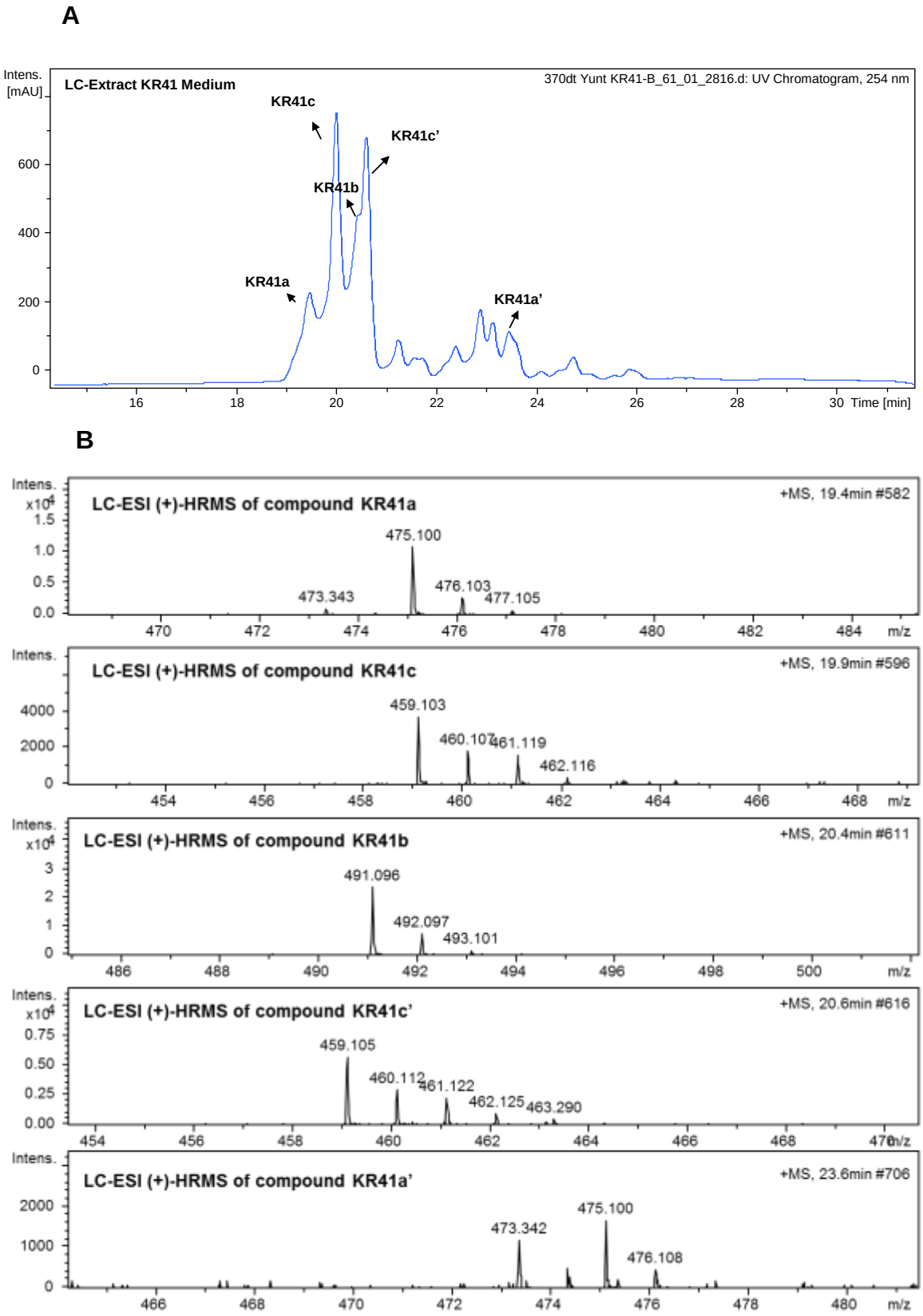

Figure 3.72 HRMS data of the compounds of the fermentation extract from *S. albus* KR41A. A. LC trace of the metabolites in the extract. B. LC-ESI-HRMS data of the observed molecular ions for the detected metabolites.

For the isolation of the compounds, *S. albus* KR41 was grown in 19 L TSB medium which was distributed to 1 L baffled flasks, so that each flask contained 400 mL fermentation culture. After incubation at 220 rpm for 4 days at 30 °C the bacteria were harvested by centrifugation and suspended in 50 mL H_2O and subsequently freeze-dried. The mycellia extract contains the yellow compounds KR41c and KR41c' as major components that have a characteristic UV absorption at 360 nm. The extract was used for the isolation of KR41c as described in the section 4.1.4.16. The yield of the isolation was 12 mg from 19 L of fermentation. During the purification steps it was observed that the two compounds were always occurring together even after several separation steps. The fraction of KR41c and KR41c' were rather in an equilibrium state instead of occurring as a single peak. KR41c was purified by HPLC several times and was used for the NMR measurements. The first attempt to measure NMR spectra in DMSO-d_6 failed because of decomposition to a green unidentified mixture. The color of the compound changed during measurement to green, suggesting degradation. The isolation procedure was repeated, and the obtained 10 mg of the compound were dissolved in AN-d_3. The obtained ^{1}H-NMR, ^{13}C-NMR, HMBC and HMQC spectra of the compound are shown in Appendix 2, Figures 2.40-2.43)

The carbon spectra showed 22 carbon atoms. The ^{1}H-NMR and HMQC spectra showed the presence of two aromatic protons at 6.19 and 6.75 ppm attached to the carbon atoms at 107.11 and 123.63 ppm, respectively. Signals in the ^{1}H-NMR at 11.93 and 11.85 ppm showed the presence of two aromatic hydroxyl groups forming hydrogen bonds. Four wide singulets observed at 12.3, 7.4, 5.9 and 3.3 ppm might belong to additional hydroxyl groups on the compound. One methyl group at 1.77 ppm, one ethylene group as a multiplet in the region 2.5 to 3 ppm and one hydrogen proton at 4.35 ppm were detected in ^{1}H-NMR. The carbon atoms observed in ^{13}C-NMR spectra were one quinone carbonyl at 189.99 ppm, one ester carbonyl at 170.08 ppm, 16 carbon atoms in the aromatic reagion from 100 up to 168 ppm, one CH at 54.33 ppm attached to the hydrogen atom at 4.35 ppm, one methylene group at 29.27 ppm, and a methyl carbon at 19.02 ppm. However, the correlations in the HMBC spectra did not allow establishing any partial structure of the compound. Low solubility of the

compound in the NMR solvents and insability might be a reason for the missing spectral data necessary for a further investigation.
Attempts to derivatize KR41c and KR41c' with DMS or by acetylation, in order to produce a more stable and better soluble derivative, resulted in brown colored compound mixtures without any specific product in sufficient amounts, which would help for further structure elucidation. The procedure of the methylation attempt is described in the Section 4.1.5.17.

Other metabolites in the *S. albus* KR41 extract were further investigated. KR41a and KR41b with the suggested molecular formulae $C_{26}H_{18}O_9$ and $C_{27}H_{22}O_{12}$ were isolated. Both compounds have a characteristic UV absorption maximum at 470 nm indicating to a quinolic aromatic structure. The compounds were isolated as described in Section 4.1.5.14. The medium extract contained KR41a, KR41b, KR41b' and KR41c. The yellow compounds KR41c and KR41c' with UV absorption maximum at 360 nm were separated from KR41a and KR41b by subjecting the extract to Sephadex LH20 column chromatography using methanol as mobile phase. Further purification of the compounds KR41a and KR41b was carried out by preparative HPLC. The yield of the isolation for KR41a was 17 mg and for KR41b 4 mg from 19 L of fermentation. ^{1}H-NMR of KR41b showed that the amount and the purity of the compound was not sufficent to use for further NMR experiments. For KR41a, ^{1}H-NMR, ^{13}C-NMR, HMBC and HMQC spectrum were completely measured. However, it was unusual to see that a set of peaks was doubled. The data allow for establishing the Western part of the molecule but HMBC correlations of the Eastern part did not show correlations for a full structure elucidation. The NMR spectra of KR41a is shown in Appendix 2, Figure 2.44-2.48.
The ^{1}H-NMR spectra showed the presence of four aromatic protons at 8.52, 6.76, 7.05 and 6.45 ppm. The aromatic hydrogens at 8.52 and 6.45 ppm occurred as dublets. The hydrogens at 7.05 and 6.45 ppm gave split signals with a coupling constant 2.2 Hz. The HMQC spectra revealed the connection of the hydrogens at 7.05 and 6.45 ppm to the carbon atoms at 108.99 and 107.66 ppm, respectively. Two hydroxyl groups at 12.40 and 11.98 ppm in the ^{1}H-NMR showed the presence of two aromatic hydroxyl groups forming hydrogen bonds. An additional aromatic hydroxyl group forming a hydrogen bond at 12.24 ppm

was detected. However the integral of the peak was 1/3 of an assigned hydroxyl group. Two wide singulets on 11.42 and 3.61 ppm showed the presence of additional hydroxyl groups on the compound. One CH_3 group at 2.4 ppm, two CH_2 groups as a multiplet between 2.72 to 2.75 ppm, and, one CH group at 3.3 ppm were detected in the ^{1}H-NMR spectrum. A methylene group was observed at 49.07 ppm in the DEPT, HMBC and HMQC spectra. ^{13}C-NMR spectrum showed 26 carbon atoms as expected for the predicted molecular formula $C_{26}H_{18}O_9$. ^{13}C-NMR and DEPT spectra showed the presence of two quinone carbonyls at 189.38 and 180.92 ppm, one ester carbonyl at 169.11 ppm, 18 carbon atoms in the aromatic region from 106 up to 165 ppm, one CH group at 49.07 ppm, two CH_2 groups at 19.52 and 28.27 ppm and a methyl group at 2.4 ppm. The measured ^{1}H-NMR, ^{13}C-NMR, HMQC, DEPT and HMBC spectra are shown in Appendix 2, Figures. 2.44-2.48.

The correlations in the HMBC spectra allowed establishing the partial structure KR41a-partial **(6c)** for the Western part of the compound, which is shown in Figure 3.73.

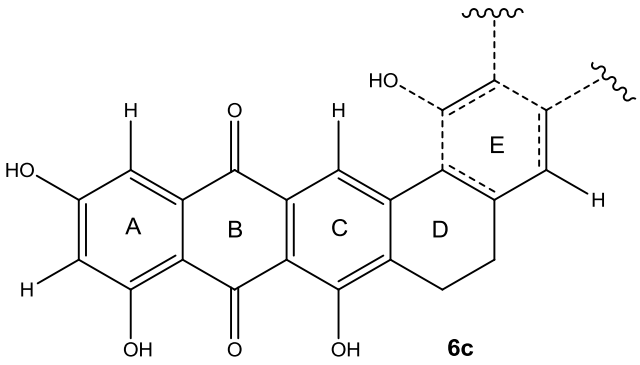

Figure 3.73 The substructure KR41a-partial (6c). (Dashed lines of ring E assigns bonds with missing HMBC corelations of the missing substituents causing uncertainity in characterizing of the configuration.)

The aromatic protons at 6.45 and 7.05 ppm showed a *meta* coupling. The HMBC correlations of these protons and the correlations of the hydrogen-bonded hydroxyl group at 11.98 ppm did allow establishing the structures of the ring system AB fully and the positions of the quinone carbonyl groups. HMBC correlations of the aromatic proton at 8.52 ppm and the hydrogen-bonded

hydroxyl group at 12.40 ppm were used to confirm the antrachinone structure of the ring ABC. Hydrogens of two CH_2 groups occurring at 2.72-2.75 ppm coupled with the carbon atoms of ring C. Additionally, the ethylene carbon atoms coupled with the hydrogen-bonded hydroxyl group at 12.40 ppm and aromatic protons at 6.76 ppm connected to ring E. These HMBC correlations allowed establishing ring D. However, the suggested hydrogen-bonded hydroxyl group at 12.40 ppm showed an uncomplete peak integral of 1/3 of an assigned hydrogen atom. HMBC correlations of this hydroxyl proton with the carbon atoms at 106.32, 118.45, 138.68 and 159.40 ppm in ring E, with a carbonyl carbon at 169.11 ppm and an unassigned carbon atom at 148.15. .The aromatic proton at 6.76 ppm occured as a splitted one in the ^{1}H-NMR spectrum. This proton is not coupling with any other aromatic proton on the antraquinone part of the molecule. It showed HMBC correlations with the ethylene carbon atoms and the aromatic carbon atoms at 106.32, 138.68, 139.96 and 159.40 ppm in ring E, with a carbonyl carbon at 169.11 ppm and an unassigned carbon atom at 148.15. It can be expected to have a hydrogen bond causing substitution on the ring E, which would lead to the occurring of the hydrogen bonded hydroxyl group at 12.24 ppm. The carbon signal at 169.11 ppm suggets that a lactone ring might be attached to ring E, but the HMBC correlations of the unassigned carbons at 148.15, 49.07, 37.47 and 22.18 ppm did not provide the data to prove the structure of ring E further. DEPT spectra showed a CH_2 group at 37.47 ppm. The HMQC spectra showed the connection of this carbon atom to a proton at the region 3.2-3.1 ppm but the peak integral in the ^{1}H NMR spectrum was ½ of an assigned CH_2 signal. Although, the CH_2 group at 37.47 ppm showed HMBC coupling with the aromatic hydrogen at 6.76 ppm in the ring E. But the spectral data did not provide the certain positions of these carbon atoms. The substructure for the Eastern part of the molecule could not be established with the NMR data obtained.

The problems occurring with the integrals and the split signals of the peaks on ring E might have been evidence, that the molecule was not stable but in an equilibrium state causing double peaks and umcomplete peak integrals in the ^{1}H-NMR spectral data. Therefore a temperture experiment was conducted. The ^{1}H-NMR spectrum of the compound was measured from 20 °C up to 60 °C in

order to observe spectrals, which can prove a temperature depended equilibrium. The ^{1}H-NMR measurements were repeated with continuous scanning under stepwise increase in temperature up to 60 °C, but any changes on the could not be observed. The NMR of the temperature experiments are shown in Appendix 2, Figure 2.49. ^{1}H-NMR and ^{13}C-NMR data of KR41a-partial **(6c)** for the compound KR41a is shown on Figure 3.74. HMBC correlations of the substructure are shown in the Figure 3.75. Table 3.18 shows the NMR data obtained for KR41a.

Figure 3.74 The ^{1}H-NMR and^{13}C-NMR data of the partial structure for the compound KR41a-partial (6c). (Dashed lines of ring E assigns bonds with missing HMBC corelations of the missing substituents causing uncertainity in characterizing of the configuration)

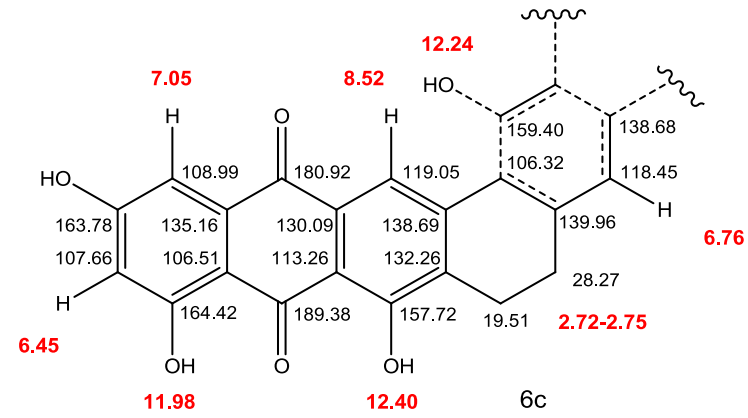

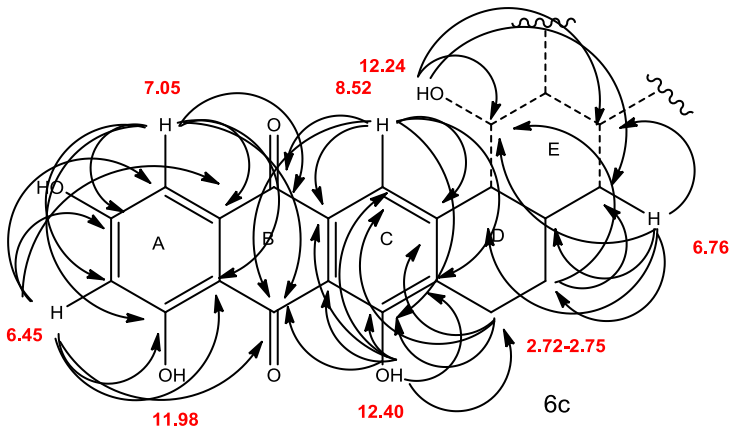

Figure 3.75 The HMBC data of the partial structure for the compound KR41a-partial (6c).

Table 3.18. Overview of the NMR data obtained for the compound KR41a.

KR41a (In DMSO-d_6)					
Nr.	**^{13}C-NMR [ppm]**	**1H-NMR [ppm]**	**Nr.**	**^{13}C-NMR [ppm]**	**^{1}H-NMR [ppm]**
1	189.38		17	113.26	
2	180.92		18	108.99	7.05 (d,H,CH, J_3=2.2 Hz)
3	169.11		19	107.66	6.45 (d,H,CH, J_3=2.2 Hz)
4	164.42		20	106.51	
5	163.78		21	106.32	
6	159.40		22	49.07	3.3 (H)
7	157.72		23	37.47	3.2-3.1 ((1/2)CH_2)**
8	148.45		24	28.27	2.72-2.75(m,2H,CH_2)
9	139.96		25	22.18	2.4 (3H,CH_3)
10	138.69		26	19.52	2.72-2.75(m,2H,CH_2)
11	138.68				
12	135.16				12.40 (OH)*
13	132.26				12.24 (1/3 OH)**
14	130.09				11.98 (OH)*
15	119.05	8.52(H,CH)*			11.42 (bs, OH)
16	118.45	6.76(H,CH) *			3.61 (bs, 2OH)

*^{1}H-NMR peaks are occurring as dublets.

^{1}H-NMR peaks have incomplete integrals but HMBC couplings with the substructure KR41a-partial **(6c).

A literature survey showed that the obtained spectral data and the physical properties of the compound showed high similarities to a polyketide already reported in the literature as KS-619-1 **(64),** a phosphodiesterase inhibitor with the same molecular formula as $C_{26}H_{18}O_9$.[153] Figure 3.76 shows the reported structure and the NMR data of KS-619-1 **(64)** reported by Sano *et al*. [153]

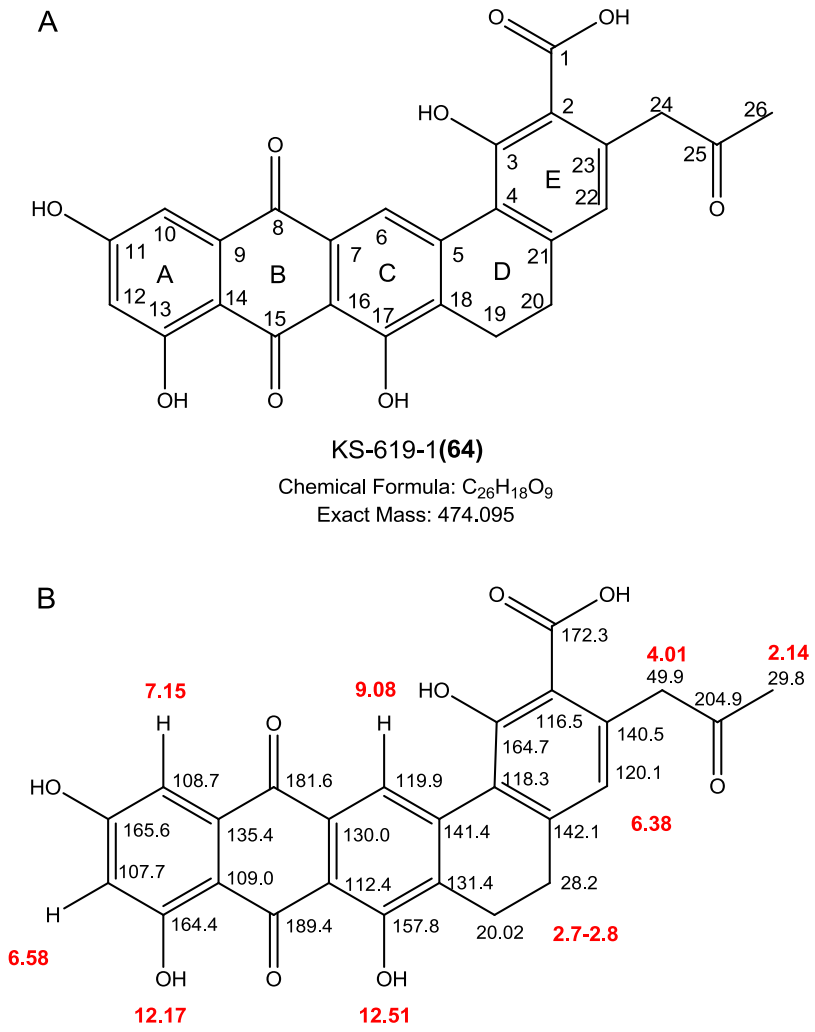

Figure 3.76 A.The structure of the polyketide KS-619-1 (64). B. ^{1}H and ^{13}C NMR data of KS-619-1 by Sano *et al* .[153]

The NMR data and the antraquinone part of the molecule KS-619-1 **(64)** showed high similarities to KR41a-partial 6c. However, the carbon signals of an aldehyde carbonyl and the carbon signals for the methyl group of KS-619-1 **(64)** were not observed in the NMR data of KR41a-partial 6c. It was suggested that the structure of the Eastern part of KR41a-partial 6c may be a lactone or another ring structure. It was expected to have a hydrogen bond causing substitution on the ring E, which would lead to the occurring of the hydrogen bonded hydroxyl group at 12.24 ppm. The carbon signal at 169.11 ppm suggest that a lactone ring might be attached to ring E, as well. Although with the possibility to have the molecular formula $C_{26}H_{19}O_8$ and a pentangular structure, as it can be seen by the structure of KR41a-partial 6c, it is very unusual to have

problems to see the substituents on ring E. A suggested reason might be that the suggested Eastern Part of the molecule is influenced by a intramolecular equilibrium. A suggestion for such equilibrium is shown in Figure 3.77.

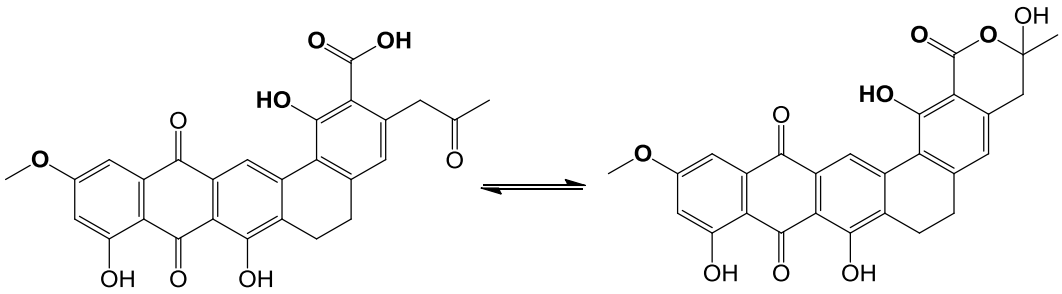

Figure 3.77 A suggested intramolecular equilibrium as the disturbance of the NMR measurements of KR41a.

It was reported that applying a methylation reaction with diazomethane enabled the structural elucidation of the compound KS-619-1 **(64)**. The product of the derivatisation reaction KS-619-2 was used for the further structural elucidation.[153] The compound KS-619-2 was a methylated derivative with four methoxy groups and a free hydroxyl group at position 9. According to this evidence, a methylation reaction of the compound KR41a it was suggested that this could help to obtain more information about the structure of the metabolite KR41a and enable elucidating the structure of KR41a.

KR41a was methylated with dimethyl sulfate (DMS). The procedure for the experiment is described in Section 4.1.5.15. The molecular ions detected for the resulting compounds by ESI-HRMS analysis were at *m/z*: 545.1869 $[M+H]^+$, 543.1677 $[M+H]^+$, 531.1699 $[M+H]^+$ .The suggested molecular formulae for the derivatives are $C_{31}H_{29}O_9$, $C_{31}H_{26}O_9$, and $C_{30}H_{26}O_9$ with a calculated molecular ion for *m/z*: 545.1806, *m/z*: 543.1649, and *m/z*: 531.1649 for $[M+H]^+$, respectively. Figure 3.78 shows the HPLC trace of the products after methylation and the detected ESI-HRMS molecular ion of the compounds.

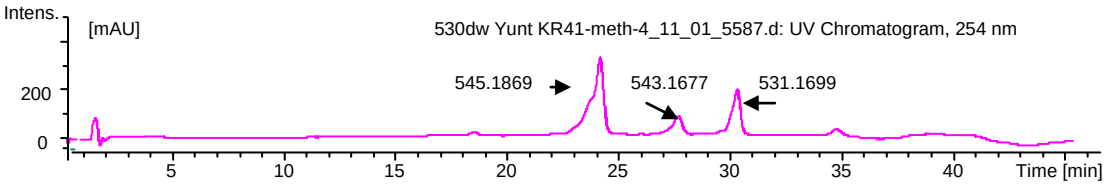

Figure 3.78 HPLC trace of the methylation reaction of the compound KR41a and the ESI-HRMS molecular ion of the major derivatives.

The reported methylated derivative of KS-619-1, KS-619-2, with a molecular formula $C_{30}H_{26}O_9$ was suggested to be among the derivatisation products of KR41a. However the amount of the compound was not sufficant for further NMR experiments. The yield of another major derivative with a molecular formula $C_{31}H_{28}O_9$ was 6 mg. The molecular ion detected for this compound was at *m/z*: 545.187 for $[M+H]^+$ The major product of the derivatisation reaction was characterezied by ^{1}H-NMR, ^{13}C-NMR and DEPT NMR analysis in $CDCl_3$. KS-619-2 has four methyl groups and the compound with the suggested molecular formula $C_{31}H_{29}O_9$ has five methyl groups, which implies an additional methylation of the compound KS-619-1. The compound was named KS-619-3 **(65)**.The spectral data found to be almost identical to the published data of the literature KS-619-2. However, there was a difference regarding a methoxy group at C-9 instead of the hydroxyl group at the compound KS-619-2. This was evident from extra methoxy group signals in the NMR, as well as from chemical shifts of the carbon atoms in the ring C, which were slightly different due to the less polar methoxy substituent. The structure of KS-619-3 **(65)** is shown on Figure 3.79. The measured ^{1}H-NMR and ^{13}C-NMR spectra and DEPT data are shown in Appendix 2, Figures 2.50-2.54. Table 3.19 shows the obtained ^{1}H-NMR and ^{13}C-NMR data for KS-619-3 **(65)**.

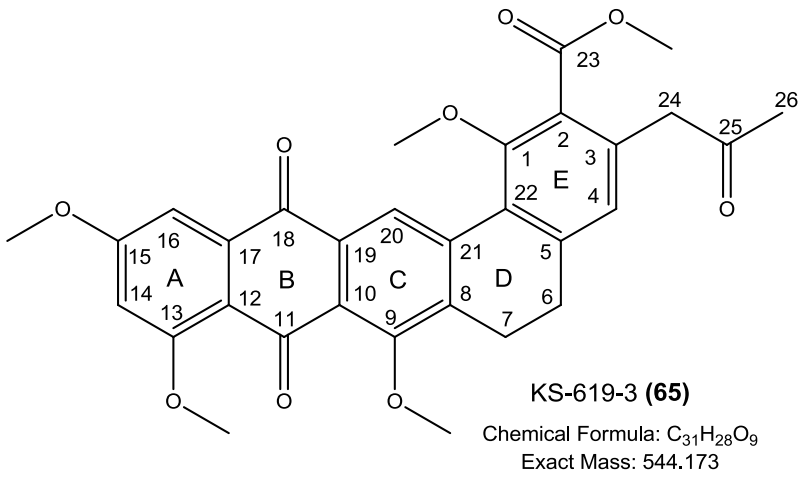

Figure 3.79 .Structure of KS-619-3 (65).

Table 3.19 ^{1}H-NMR and ^{13}C-NMR data for KS-619-3 **(65)**.

KS-619-3 (65). (In $CDCl_3$)					
Position	**^{13}C-NMR[ppm]**	**^{1}H-NMR [ppm]**	**Position**	**^{13}C-NMR [ppm]**	**^{1}H-NMR [ppm]**
1	156.61		17	137.06	
2	128.62		18	183.73	
3	132.99		19	125.65	
4	126.16	6.97(s,H)	20	122.46	9.01(s,H)
5	143.04		21	140.38	
6	29.09	3-3.5(m,2H)	22	126.29	
7	21.70	2.8-2.6(m,2H)	23	168.33	
8	134.18		24	48.52	3.77 (s,2H)
9	157.01		25	205.26	
10	118.81		26	29.88	2.24 (s,3H)
11	181.94		1-OMe	62.02	3.69 (s,3H)
12	118.57		15-OMe	56.66	4.00 (s,3H)
13	162.01		13-OMe	56.03	4.01 (s,3H)
14	105.29	6.82(s,H)	9-OMe	62.11	4.03 (s,3H)
15	164.49		23-COOMe	52.53	3.98 (s,3H)
16	102.42	7.41(s,H)			

As a result, the structure of the metabolite KR41a with the molecular formula $C_{26}H_{18}O_9$ from *grhM* deleted strain *S. albus* KR41 was identified as KS-619-1 **(64)**. The metabolites KR41c and KR41c' showed no quinone absorbence at UV spectra in the quinolic region 470 nm to 490 nm. The metabolites KS-619-1

(64) and KR41b showed UV absorption maxima at 475 nm, which indicates aromatic quinone absorption of an antraquinone-type substructure. The structure of the quinolic metabolite KR41a, which was identified as KS-619-1 **(64)** suggests that the structures of the other quinolic metabolite in the liquid culture, KR41b, with a molecular formula $C_{26}H_{18}O_{10}$ might be a structurally related pentangular polyketide.

However, the structures of both KR41c and KR41c', which are suspected to be tautomers or configuration isomers with a molecular formula $C_{26}H_{18}O_9$, could not be obtained. The structure of the quinolic metabolite KR41a with an additional oxygen atom, identified as KS-619-1 **(64)** might suggest that the structure of the intermediates KR41c and KR41c' are structurally related pentangular polyhydroxyl aromatic polyketides. It is possible that the metabolite KR41c and KR41c' converted to oxidized species KR41a and KR41b during fermentation. However, it can not be excluded that the polyketide metabolites produced by *S. albus* KR41 in liquid medium and on agar plates are structurally unrelated, since the metabolite KS-619-1 **(64)** and KR41b were only observed in liquid cultures.

The identification of the metabolite KS-619-1 **(64)** provides clear evidence that the protein GrhM functions in an early oxidation reaction of pentangular biosynthesis intermediates.

In order to obtain more information about the suggested function of GrhM sequence homologies with other tailoring enzymes were investigated by BLAST analysis and the results were provided by Kathrin Reinhardt. Table 3.20 shows the BLAST results of the enzymes.[125]

Table 3.20 Homologous proteins to GrhM by the BLAST analysis results[125]

Protein	Amino Acids	Proposed function	Sequence Similarity (Protein, Origin)	Similarity/ Identity [%]
GrhM	150	Oxygenase	RubQ/ *Streptomyces collinus* (Unpublished)[125]	85/77
			LlpQ/ *Streptomyces tendae* (Unpublished)[125]	60/50
			FdmM/ *Streptomyces griseus*[152]	54/46
			LlpB/ *Streptomyces tendae* (Unpublished)[125]	48/37
			BenG/ *Streptomyces* sp. A2991200[52]	50/32

Homologs of GrhM can be found in biosynthetic gene clusters of many other aromatic polyketides ranging from dodecaketides to pentadecaketides. These includes RubQ in γ-rubromycin **(37)**, LlpQ and LlpB in lysolipin X, [125] FdmM in fredericamycin A **(26)**,[152] and BenG in the benastatin A biosynthetic pathways.[52] Investigation of FdmM and FdmM1 mutant strains showed that the enzymes perform early hydroxylations on C-6 and C-8 in the fredericamycin biosynthesis, as shown in Figure 3.80.[152] The *ΔfdmM* mutant strain accumulated three compounds FDM M-1 **(66)**, FDM M-2 **(67)** and FDM M-3 **(68)** whereas FDM M-2 **(67)** and FDM M-3 **(68)** were reported as shunt products of the rapidly oxidizing FDM M-1 **(66).** The *ΔfdmM1* mutant strain produced FDM1-1 **(66)** which reacts further to FDM C **(70)**. Figure .3.80 shows the postulated involvement of the monooxygenases FdmM and FdmM1 in the fredericamycin biosynthesis.

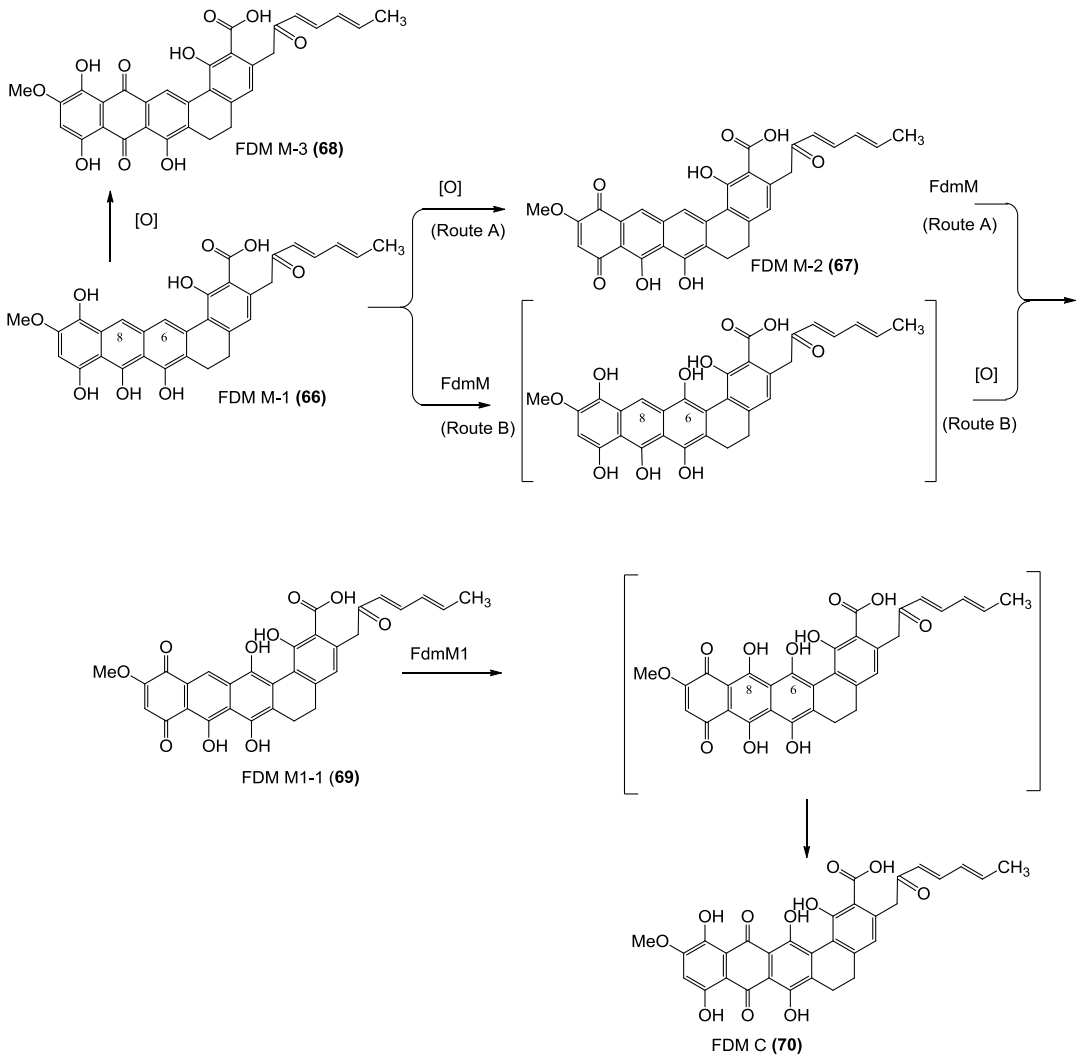

Figure 3.80 The postulated involvement of the monooxygenases FdmM and FdmM1 in the fredericamycin biosynthesis.[152]

The homology of GrhM to FdmM suggests a function for GrhM in the hydroxylation of ring C of an aromatic pentangular intermediate. Additionally, the presence of the metabolite KS-619-1 **(64)** in the extract of another mutant strain that has the *grh08* gene deleted allows suggesting that the two oxygenases work simultaneously or in series which is discussed further in Section 3.4.8 and Section 3.7. Figure 3.81 shows the suggested reactions for GrhM. The enzyme GrhM is suggested to be responsible for the hydroxylation of ring C of the compound KS-619-1 **(64)** or a previously suggested intermediate **(71).**

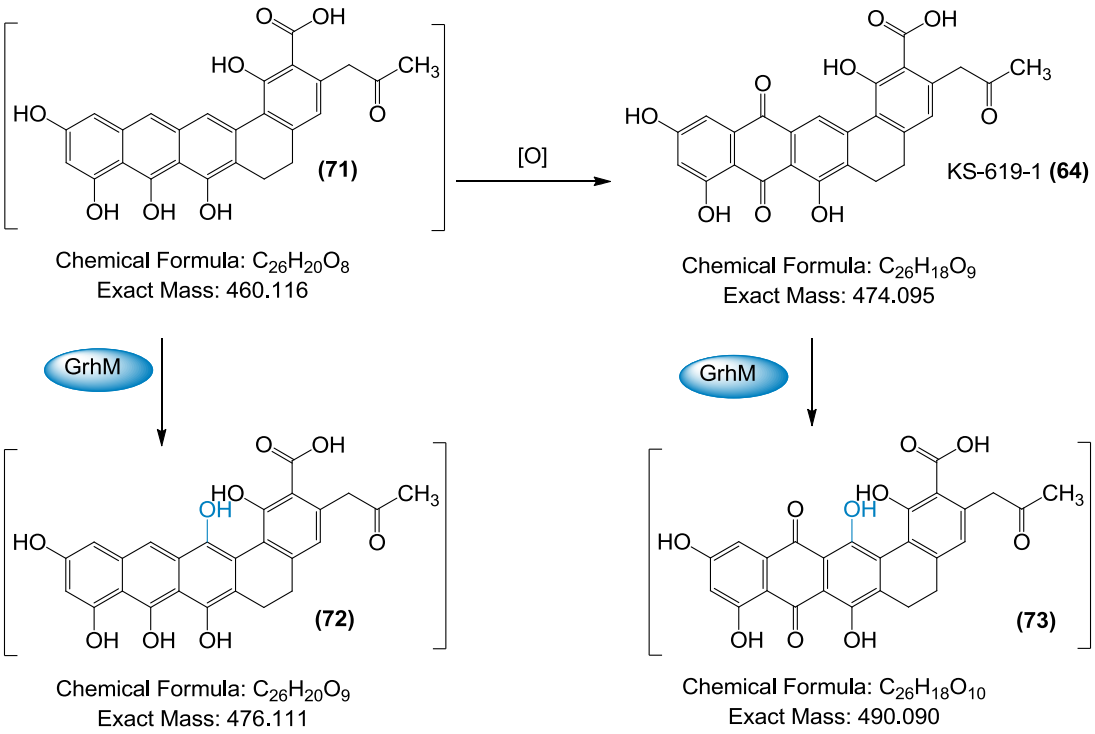

Figure 3.81 The postulated involvement of the oxygenase GrhM in the griseorhodin A biosynthesis.

3.4.8 Compounds Produced by *S. albus* KR11

The knockout strain *S. albus* KR11 has the gene *grhO8* deleted. This gene is supposed to be a FAD-dependent monoxygenase. The metabolites of the knockout strain *S. albus* KR11 were observed after 2 days cultivation on agar plates as a yellow pigment, which changed the color to dark brown on the third day. The initial compounds observed after 2 days cultivation were extracted from the agar plates by using acidic ethyl acetate and measured immediately by HPLC and LC-HRMS in order to obtain molecular ions. During extraction, a fast colour change in 15 to 20 minutes of the extract to brown was observed, which showed that the compounds were highly unstable. It was not possible to prevent its degradation either after extraction or during growth in the incubator. Figure 3.82A shows the UV spectra, Figure 3.82B the HPLC trace of the fresh extract measured, from a plate incubated for 2 days. The measured

molecular ion for the initially observed yellow major compound KR11x before degradation is shown in Figure 3.82C.

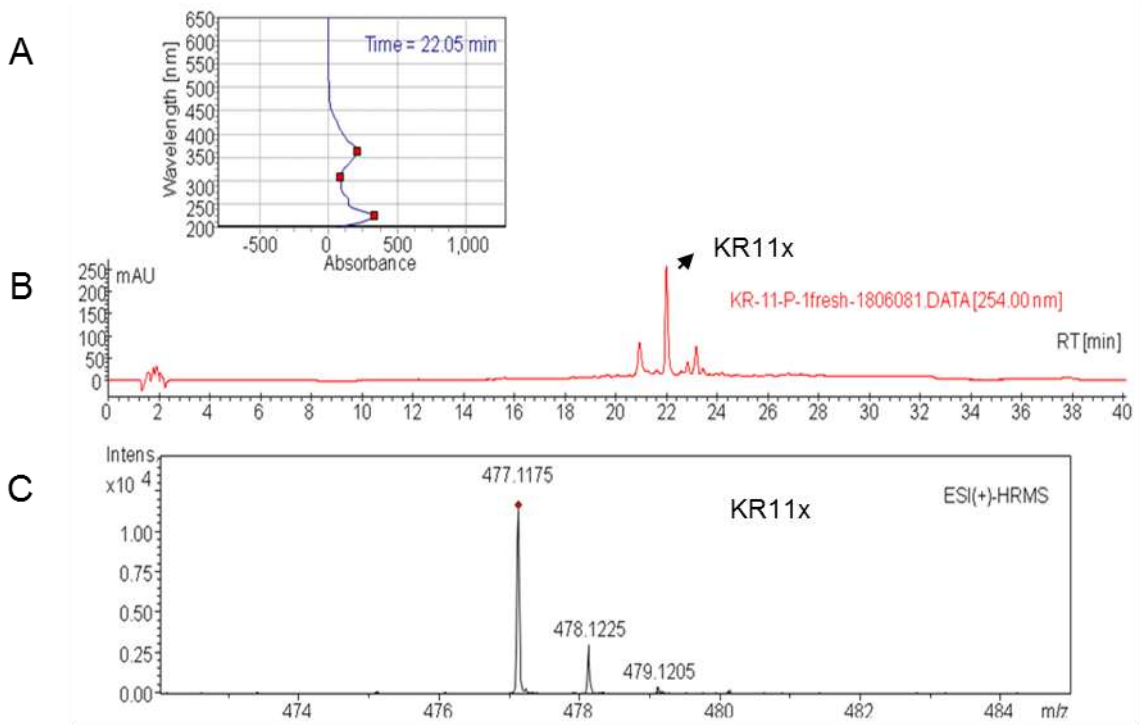

Figure 3.82 UV spectra, HPLC and ESI-HRMS of KR11x of *S. albus* KR11.

The molecular ion for the metabolite KR11x was measured as *m/z*: 477.1175 $[M+H]^+$ and the suggested molecular formula $C_{26}H_{20}O_9$ with the calculated *m/z*: 477.1180 for $[M+H]^+$ was obtained. Figure 3.83 compares HPLC traces of the fresh extract (A), the same extract after 40 minutes (B), and the extract from a plate culture incubated a day longer (C). The Figure 3.83 shows that the compound is unstable after extraction and even during incubation in the dark. This means the metabolite KR11x is very sensitive to the oxygen in the air.

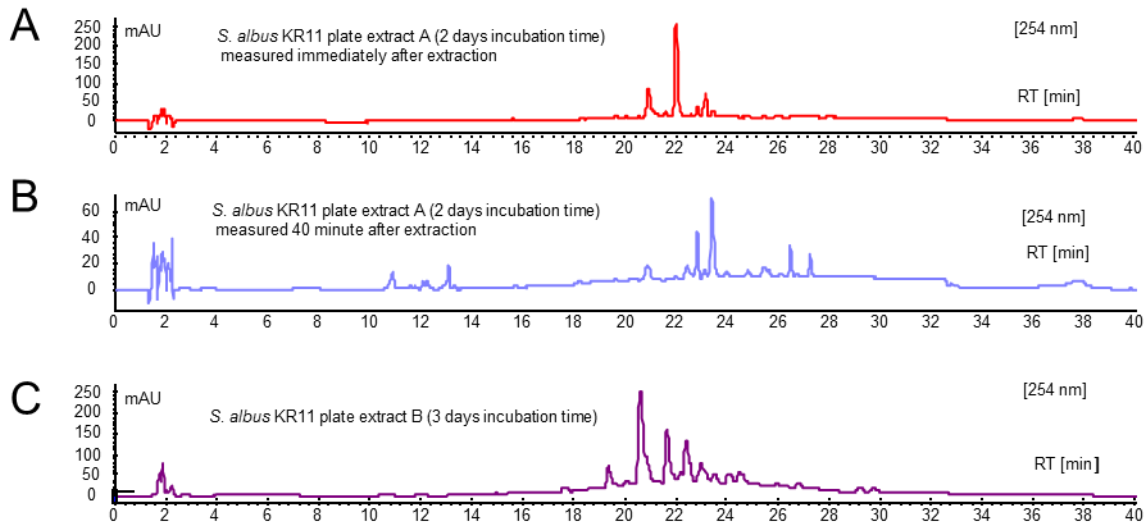

Figure 3.83 A. HPLC trace of the initial metabolites in the plate extract of *S. albus* KR11 after 2 days of incubation B. HPLC trace of the plate extract of *S. albus* KR11 after 40 min. C. HPLC trace of the metabolites in the plate extract of *S. albus* KR11 after 3 days of incubation.

Liquid cultivation of the mutant strain in TSB medium provided another set of metabolites with predominating green polymeric pigments on the mycelium and brown compounds in the medium. During fermentation, the lipophilic absorption material amberlite XAD7 (Sigma-Aldrich, Seelze) was used to test whether the instable compounds would be extracted more efficiently but none significant improvement was observed. In order to prevent the degradation of the produced metabolites, the incubator was covered up to minimize light exposure during fermentation but any change in the fermentation broth was not obtained. This showed that the isolation of the initially produced substance KR11x from the liquid fermentation procedure was inefficient. However, further investigation of the extract was performed, with the hope to isolate a structurally related degradation product of the compound, in order to obtain insights, about the structure of the initial metabolites. Therefore, the fermentation medium was acidified to pH 3 and extracted with ethyl acetate. The compound KR11a was isolated by the procedure described in Section 4.1.5.18. Figure 3.84B shows the HPLC trace of isolated yellow compound KR11a with a molecular ion in the MS analysis at *m/z*: 475.1077 $[M+H]^+$ matching a calculated molecular formula $C_{26}H_{18}O_9$ with the calculated $[M+H]^+$ *m/z*: 475.1024 for $[M+H]^+$. The UV spectrum, HPLC retention time and the

molecular formula of the compound were identical with the identified as KS-619-1 **(64)** in the Δ*grhM* mutant strain *S. albus* KR41, which was described in Section 4.2.7 in detail. Figure 3.84A shows the HPLC trace of the fermentation extract of *S. albus* KR41 showing KR41a, which was identified as KS-619-1 **(64)**, in order to compare the trace of the isolated compound KR11a from Δ*grh08* mutant strain *S.albus* KR11. Figure 3.84B shows the HPLC trace of the metabolite KR11a. UV spectra of the metabolites KR41a and KR11a are shown in Figure 3.84C and 3.84D.

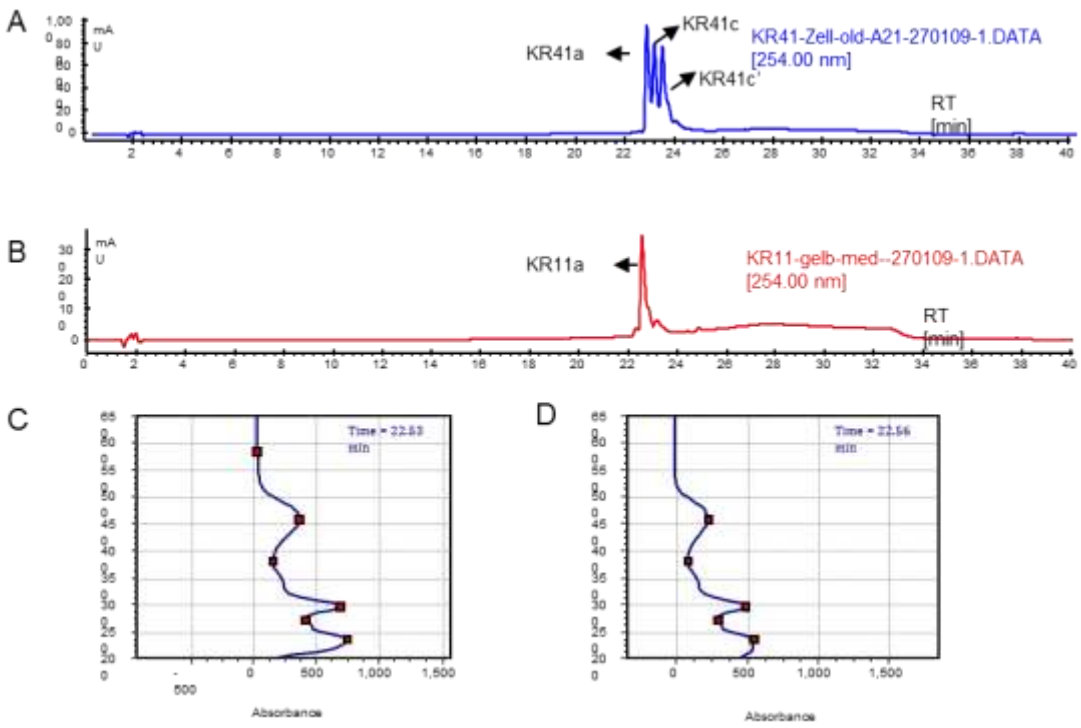

Figure 3.84 A. HPLC trace of the extract from *S. albus* KR41 B. HPLC trace of KR11a isolated from *S. albus* KR41 C. UV spectra of KR41a identified as KS-619-1 (64) and KR11a. D. UV spectra of KR11a identified as KS-619-1 (64) and KR41a

For the isolation of KR11a, *S. albus* KR11 was grown in 18 L TSB medium. The yield of the isolation was 12 mg from 18 L of fermentation. The NMR data of the compound were acquired in DMSO-d_6. The NMR spectra had great similarity with the NMR spectra of KS-619-1 **(64)**. The problem for structural characterization was the same with the previous structure elucidation attempts, that the NMR correlations of the Western part of the molecule could be

observed but not the NMR correlations of the Eastern part. Based on the available data, KR11a suggested being identical to KS-619-1 **(64).** To verify these assumptions, LC-MS/MS data of the compounds were compared. Figure 3.85 shows the HPLC and ESI-HRMS data KS-619-1 **(64)** and KR11a. The ESI-MS/MS fragmentations were identical.medium and mycelium contained insoluble green pigments. The medium was extracted and the compound KR11a was isolated with the procedure as described in Section 4.1.5.18.

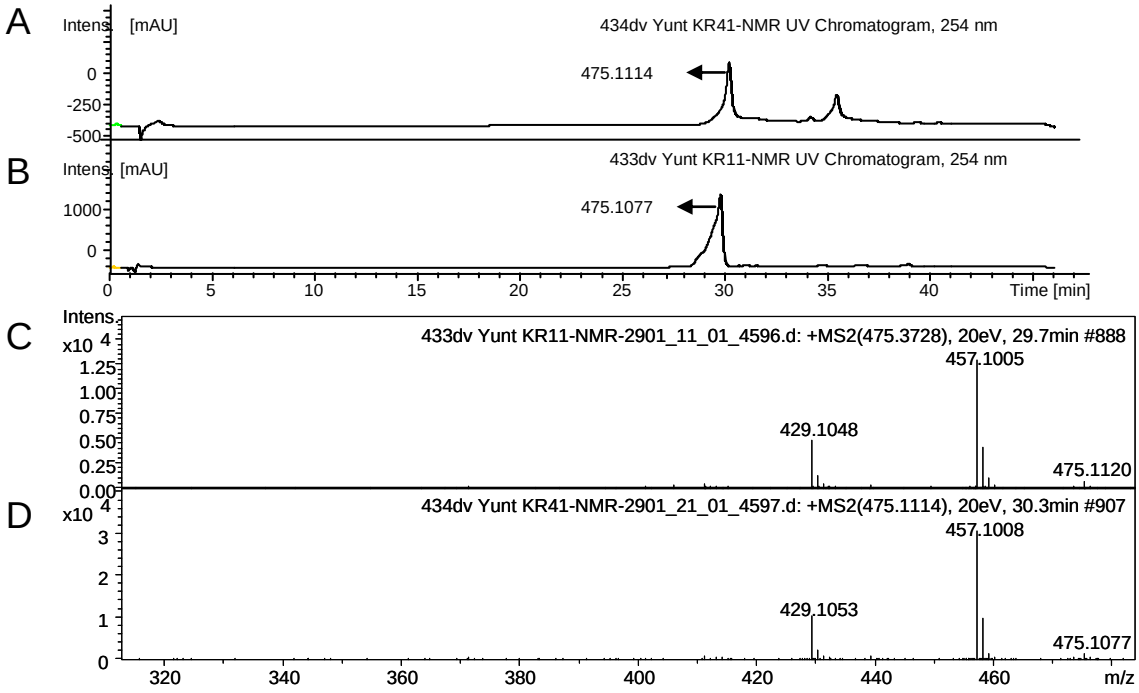

Figure 3.85 The HPLC and ESI-HRMS data of KS-619-1 (64) that was identified in the mutant strain *S. albus* KR41 and KR11a from the mutant strain *S. albus* KR11.

For a further prove, KR11a was derivatized with DMS as previously described for KS-619-1 **(64)**. The procedure of the methylation is described in detail at Section 4.1.4.19. For the reaction 12 mg of KR11a was used. The yield of the isolated methylated compound was 3 mg. The identity of the compound was determined by comparing the ESI-MS/MS fragmentation pattern KS-619-1 **(64)** to that of KR11a. The HPLC traces of the methylation reaction of KS-619-1 **(64)** and KR11a are shown in Figure 3.85. The ESI-MS/MS fragmentation pattern of the two compounds KS-619-1 **(64)** and KR11a are shown in Figure 3.85. The differences at the retention times of the compounds are because of the changing

pressure conditions on the HPLC used for the LCMS mashine, which caused a deletion in the retention times due to this defect. However, the high resolution molecular ions of the derivatisation products and the MS/MS fragmentations of the obtained molecular ions proved that the methylated compound KR11a and KR41a showed identical methylated derivatives, such as KS-619-3 **(65)**. Figure 3.86 shows the products of the methylation reactions of KR41a and KR11a. Figure 3.87 shows the identical MS/MS fragmentation proving the presence of the same compound KS-619-3 **(65)** as a product of the methylation reactions of the metabolites KR41a and KR11a. The identity and structure of KS-619-3 **(65)** is described in detail in Section 3.4.7.

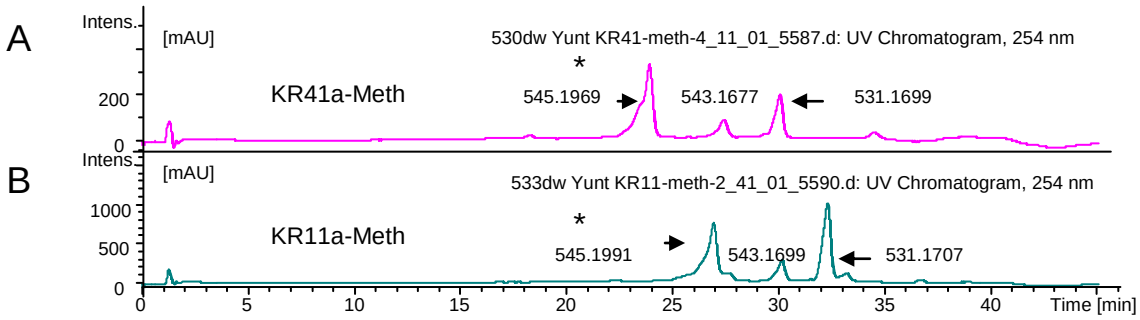

Figure 3.86 HPLC traces of the products obtained from the methylation reactions of KR41a and KR11a. The compound with an asterix is identified as KS-619-3 (65).

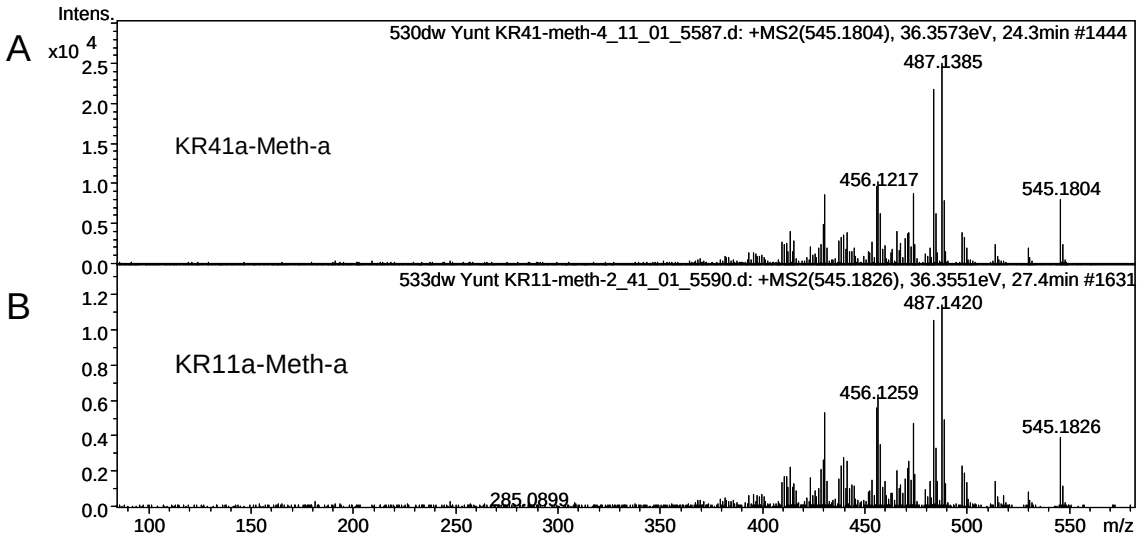

Figure 3.87 ESI-MS/MS fragmentation showing the presense of KS-619-3 (65) in both products obtained from the methylation reactions of KR41a and KR11a.

The fermentation broth of *S. albus* KR11 also contained a characteristic green pigment KR11b, which was also observed in the fermentation broths of the Δ*grhP* and Δ*grhL* mutant strains. The gene *grhP* has sequence similarities to asparagine synthetases, and the gene *grhL* suggested being a methyl transferase. The green pigment was insoluble in all tested polar and unpolar organic solvents. All attempts to isolate this compound were unsuccessful and the structure of this green pigment could not be identified.

In order to obtain KR11b, the bacteria were freeze-dried and stored under argon. The only successful method to remove this green pigment from the bacterial mycelium was using a mixture of 90% acetone and 10% saturated $NaHCO_3$ solution. After filtration of the mycelium and removal of the solvent with a rotary evaporator, the crude extract obtained was eluted over silica with methanol. However, the compounds bound irreversibly on silica, impregnated silica, Sephadex LH-20 material and also reverse phase (C18) silica. With the crude extract, a methylation reaction with DMS was also carried out. The protocol of the methylation reaction is described in Section 4.1.4.20. The product had several green components, but none of the green pigments were retained on C18 silica as a definite peak. After purification attempts with Sephadex LH-20 using methanol as a mobile phase and subsequent purification on silica column chromatography with a mobile phase methanol:ethyl acetate (5:1) a green fraction was collected, but the ^{1}H-NMR of the compound showed rather a mixture of compounds, which could not be used for further structure elucidation experiments. HRMS and EI measurement of the fraction did not provide a molecular ion peak. These investigations suggested that the green fraction was a mixture of components. It might be also a product of a polymerization reaction of an unstable phenolic aromatic intermediate, reacting during the fermentation process.

As a result, the investigation of the extracts from the strain *S. albus* KR11 proved that KR11a from *S.albus* KR11 is identical to KR41a from *S.albus* KR41 and both metabolites are identified as KS-619-1 **(64)**. The presence of identical metabolites in both extracts implies that the substrates of GrhM and the oxygenase GrhO8 might be related. However, their function is not identical. The unstable metabolite with a molecular formula $C_{26}H_{20}O_9$ that was observed in the

extract of the Δ*grhO8* mutant strain was not in the extract of the Δ*grhM* mutant strain. Additionally, the intermediates with the molecular formula $C_{26}H_{18}O_8$ that are observed in the extract of the Δ*grh*M mutant strain were not in the extract of the Δ*grh*O8 mutant strain. However, the GrhO8 and GrhM gene deletion strains both have the aromatic pentangular compound KS-619-1 **(64)** with a molecular formula $C_{26}H_{18}O_9$ in their extract. The molecular formula of the metabolites with an additional oxygen atom KR11x and KS-619-1 **(64)** suggests that GrhO8 functions after the oxygenase GrhM and before GrhO9. It can also be suggested that the methylation and lactonization reactions are occurring in a later stage of the biosynthesis.

In order to investigate the possible function of GrhO8, sequence homologies of GrhO8 were investigated. The results of the BLAST are provided by Kathrin Reinhardt. Table 3.21 shows the BLAST results of the protein.[125]

Table 3.21. Homologous proteins of GrhO8 determined by the BLAST analysis results[125].

Protein	Amino Acids	Proposed function	Sequence Similarity (Protein, Origin)	Similarity/ Identity [%]
GrhO8	534	FAD-dependent monooxygenase	GrhO9/ *Streptomyces* sp. JP95[15]	63/46
			RubL/ *Streptomyces collinus* (Unpublished)[125]	60/46
			RubP/ *Streptomyces collinus* (Unpublished)[125]	59/46
			GrhO5/ *Streptomyces* sp. JP95[15]	57/45
			DntB/ *Burkolderia* sp. DNT[138]	56/40
			TcmG/ *Streptomyces glaucescens*[139]	57/38

The protein sequence of GrhO8 shows similarities to the oxygenases GrhO9 and GrhO5 in griseorhodin A biosynthesis[125], RubL and RubP in γ-rubromycin biosynthesis,[125] TcmG in tetracenomycin biosynthesis,[139] and DntB.[138] DntB (4-methyl-5-nitrocatechol (4M5NC **(49)**) monooxygenase) from *Burkholderia* sp. catalyzes the second step of 2,4-dinitrotoluene degradation by converting

4M5NC **(49)** to 2-hydroxy-5-metylquinone **(50)** with the concominant removal of the nitro group **)** as shown in Section 3.4.3 and Figure 3.28.[138] The hydroxylase TcmG is an oxygenase in the biosynthesis of tetracenomycin C **(52)**. TcmG hydroxylates tetracenomycin A2 **(51)** at positions C-4, C-4A, and C12A to give tetracenomycin C **(52)** as shown in Section 3.4.3 and Figure 3.29 .[139]

The isolated pentagular metabolite shows that the initial substrate of GrhO8 is an intermediate of the early tailoring steps. This suggests that GrhO8 is a hydroxylase. Since the function of the other monooxygenases GrhO9 and GrhO5 could be predicted by the isolated metabolites collinone **(41)** and precollinone **(58)** GrhO8 is the last possible candidate among the griseorhodin A cluster tailoring enzyms in respect to the sequence homology analysis, which could perform the hydroxylation reactions at the carbon atoms at C-6 and C-17 of the compounds collinone **(41)** and precollinone **(58)**. Figure 3.88 shows the suggested reactions for the enzymes GrhO8 and GrhM.

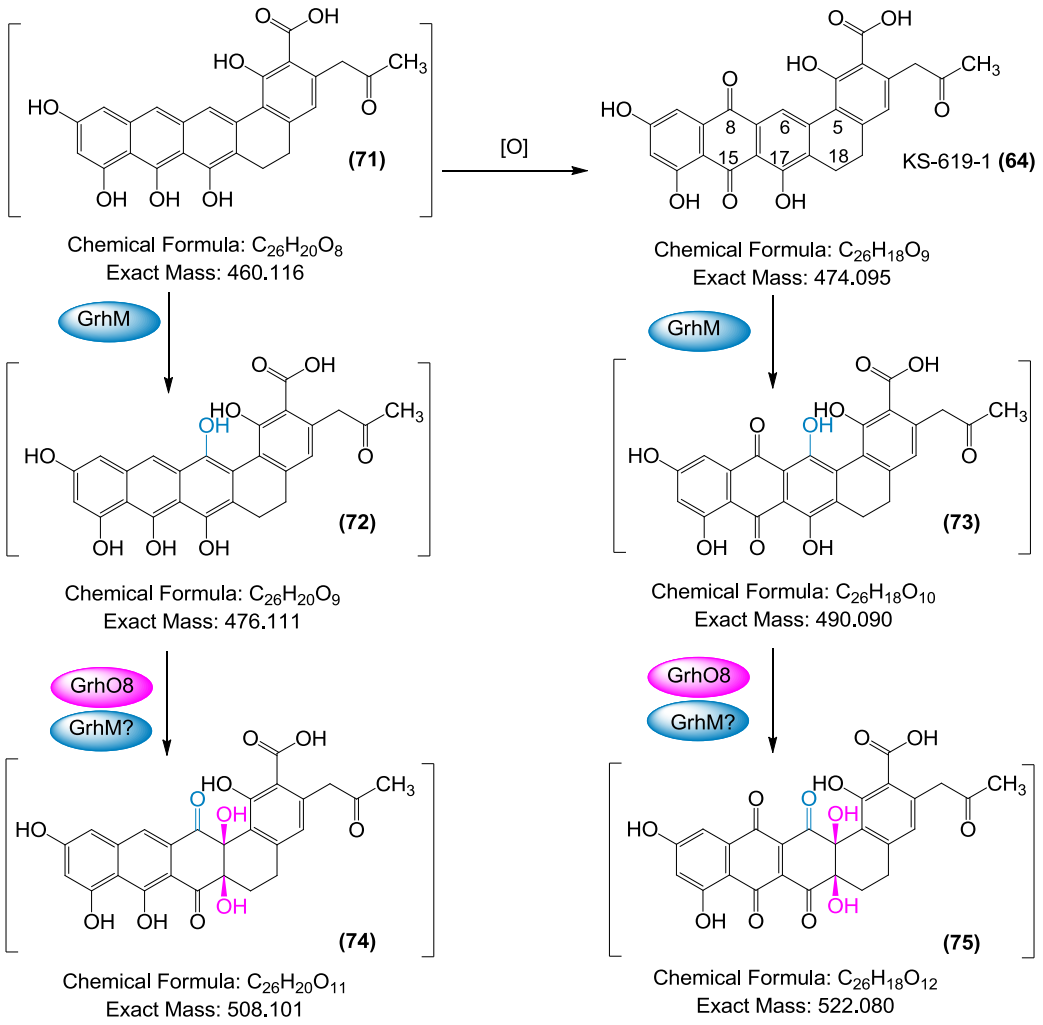

Figure 3.88 The postulated reactions of GrhM and GrhO8 in the griseorhodin A biosynthesis.

A literature survey revealed a similar dihydroxylation reaction that was published by Daum *et al*. for the monooxygenase PokO2 in the polyketomycin **(76)** biosynthesis.[142] Figure 3.89 shows the involvement of the oxygenases PokO1 and PokO2 in the polyketomycin biosynthesis. In this case, PokO1 hydroxylates the position C-4. Subsequently, PokO2 performs a dihydroxylation at C-4a and C-12a as shown in Figure3.89. The dihydroxylation reaction will be initiated by a proposed epoxidation reaction with a subsequent ring opening with addition of a water molecule those results in *cis* configuration of the hydroxyl groups at C-4a and C-12a.[142] Further experiments sing gene deletion mutants of *ΔpokO1*, *ΔpokO2* and *ΔpokO1/ ΔpokO2* showed that the enzyme PokO1 can take over the function of PokO2.[142]

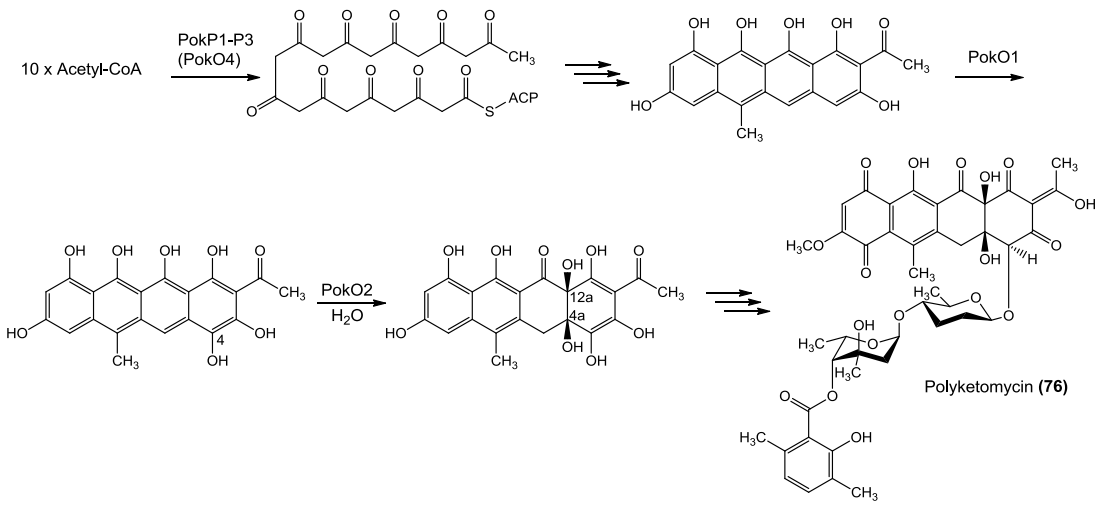

Figure 3.89 Proposed involvement of the oxygenases PokO1 and PokO2 in the biosynthesis of polyketomycin (76).[142]

3.4.9 Compounds Produced by Other Mutant Strains

After incubation of the Δ*grhP* and Δ*grhL* mutant strains on MS agar plates and subsequent HRLC-MS analysis, new metabolites were determined. Figure 3.90 shows the HPLC traces of the *ΔgrhL*, *ΔgrhP* and *ΔgrhV* mutant strains and the predicted molecular formulae for the observed metabolites.

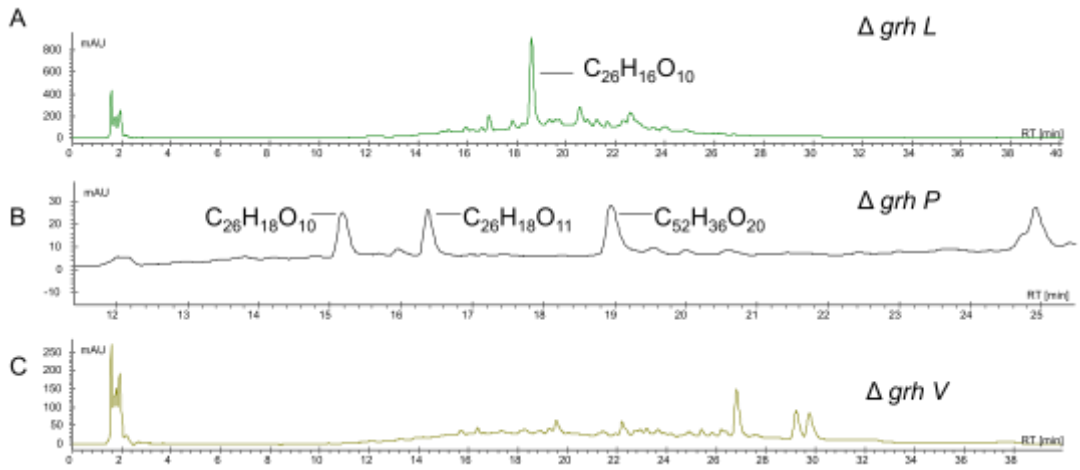

Figure 3.90 A. HPLC trace of the extract from Δ*grhL* mutant *S. albus* KR40 B. HPLC trace of the extract from Δ*grhP* mutant *S. albus* KR15 C. HPLC trace of the extract from Δ*grhV* mutant *S. albus* KR58.(The molecular formulae of the metabolites could not be determined by HR-LCMS.)

The mutant strain Δ*grhP* with a deleted amidotransferase gene produced major metabolites with the predicted molecular formulae $C_{26}H_{18}O_{10}$ (for $[M+H]^+$

measured *m/z*: 491.0975, calculated *m/z*: 491.0973), $C_{26}H_{18}O_{11}$ (for $[M+H]^+$ measured *m/z*: 507.0922, calculated *m/z*: 507.0922) and $C_{52}H_{36}O_{20}$ (for $[M+H]^+$ measured *m/z*: 981.1870, calculated *m/z*: 981.1873). The mutant strain Δ*grhL* with a deleted methyl transferase gene produced major metabolites with predicted molecular formulae $C_{26}H_{14}O_9$ (for $[M+H]^+$ measured *m/z*: 471.0695, calculated *m/z*:471.0711), and $C_{26}H_{16}O_{10}$ (for $[M+H]^+$ measured *m/z*: 489.0785, calculated *m/z*: 489.0816). In both strain extracts, several additional metabolites with 26 carbon atoms were observed. However, the fermentation broth of these strains contained also rather green and black unidentified pigments, which did not allow isolation of a metabolite in proper amounts for further structure elucidation. The observed metabolites indicate intermediates with 26 carbon atoms as the detected metabolites in the mutant strain Δ*grhM* and mutant strain Δ*grh08*. All intermediates observed indicate an involvement of GrhP and GrhL in early tailoring steps. The investigation of the extracts from these strains suggested that these compounds might be polyketides with an unmethylated pentangular aromatic moiety, but these unmethylated metabolites are not stable enough to permit isolation for structure elucidation. The lack of the enzymatic methylation on ring A and the lactonization of the ring F might be a reason for the observation of instable metabolites and the dominantly produced green and black pigments, which might be polymerization products initiated by radicalic reactions or oxidations during fermentation.

The mutant strains *S. albus* KR61 and *S. albus* KR58 with a single gene deletion of *grhU* and *grhV*, respectively, had extremely low production of metabolites. Further investigations for a better production of GrhU and GrhV gene deletion strains and the produced metabolites of GrhU and GrhV gene deletion strains were performed by Kathrin Rheinhardt and Minna Eklund in the group of Prof. Piel.

In order to assign possible functions of the enzymes for which structures could be obtained, sequence homology to other tailoring enzymes were investigated. The BLAST results for the sequence homology of GrhL, GrhP, GrhU and GrhV were carried out by Kathrin Reinhardt. Table 3.22 shows the homology to the enzymes to other polyketide tailoring enzymes.[125]

Table 3.22. Homologous proteins to GrhL, GrhP, GrhU and GrhV determined by the BLAST analysis results[125].

Protein	Amino Acids	Proposed function	Sequence Similarity (Protein, Origin)	Similarity/ Identity [%]
GrhL	343	Methyl transferase	TcmO/ *Streptomyces glaucescens*[123]	60/47
			LlpMII/ *Streptomyces tendae* (Unpublished)[125]	60/46
			PdmT/ *Streptomyces griseus*[154]	54/46
			CmmMI/ *Streptomyces* griseus[143]	58/46
GrhP	625	Asparagin-synthetase	RubR/ *Streptomyces collinus* (Unpublished)[125]	84/76
			Orf1/ *Streptomyces refuienes* subsp. *thermotolerans*[156]	62/48
			LlpA/ *Steptomyces tendae* (Unpublished)[125]	62/49
GrhU	107	Unknown	RubH/ *Streptomyces collinus* (Unpublished)[125]	83/72
			LlpOIII/ *Steptomyces tendae* (Unpublished)[125]	80/60
			PdmH/ *Actinomadura hibisca*[154]	73/63
GrhV	102	Unknown	RubT/ *Streptomyces collinus* (Unpublished)[125]	78/70
			FdmQ/ *Streptomyces griseus*[42]	66/45
			LlpOII/ *Steptomyces tendae* (Unpublished)[125]	66/47
			BenJ/ Streptomyces sp. A2991200[52]	65/47

The protein sequence of GrhL shows homology to *O*-methyl transferases. Homologs of GrhL can be found in biosynthetic gene clusters of other aromatic polyketides TcmO in tetracenomycin[123], LlpMII and LlpMI in lysolipin X[125], PdmT in pradimicin[154], and CmmMI in chromomycin[143] biosynthetic pathways.

Griseorhodin A **(5)** has one methoxy group at ring A, which suggests the function of the only metyltransferase homolog GrhL. The importance of the investigation of the enzyme was to determine at which stage the methylation occurs. The molecular formula $C_{26}H_{16}O_{10}$ of the major metabolite suggests that the methylation occurs to the unmethylated backbone of the compound precollinone **(58)** with a molecular formula $C_{27}H_{20}O_{10}$. The major metabolites of the *ΔgrhO8* and *ΔgrhM* gene deletion strains provided metabolites with less than ten oxygen atoms and 26 carbon atoms. The major metabolites of the *ΔgrhP* gene deletion mutant strain that might be involved at the generation of lactone function of ring F provided metabolites with 26 carbon atoms and 10 to 11 oxygens. This suggests that the lactonization occurs before methylation with a loss of water and the following methylation leads to formation of the metabolites with 27 carbon atoms, such as collinone **(41)** and precollinone **(58)**.

The protein sequence of GrhP shows homology to asparagine synthetases B. These enzymes are glutamine-amido transferases and catalyze an ATP-dependent transformation of asparaginic acid to asparagin with the usage of glutamine as a nitrogen source. This kind of enzymes can also be found in biosynthetic gene clusters of other aromatic polyketides such as RubR in the γ-rubromycin,[125] LlpA in the lysolipin X,[125] PdmD in the pradimicin,[154] and FdmV in the fredericamycin A[42] biosynthetic pathways. Fredericamycin A **(26)** and pradimicin **(29)** have lactam rings in their scaffold. However, rubromycins and griseorhodin A **(5)** have lactone rings. Recent work of Chen *et al.* proved the function of FdmV as a tailoring enzyme that is responsible for the generation of the amide bond formation for the lactam ring.[155] FdmV converts FDM M-3 **(66)** to the corresponding amide FDM M-6 and FDM C **(70)** to the corresponding amide FDM B by utilizing L-Asn, L-Gln, or free amine, as a nitrogen source for the lactamization generating the last ring.[155] The sequence homology of GrhP to FdmV suggests an involvement of GrhP in the lactonization of ring F in the griseorhodin A biosynthesis. The metabolite KS-619-1 **(51)** in the extracts of *ΔgrhM* and *ΔgrhO8* mutant strains indicates that the lactone formation of ring F occurs after the oxidation steps of GrhM and GrhO8, as a tailoring step. This

assumption needs to be proven by further investigation of the enzyme or the metabolites.

Homologs of GrhV can be found in biosynthetic gene clusters of other aromatic polyketides. RubT in the γ-rubromycin,[125] FdmQ in the fredericamycin A,[42] LlpOII in the lysolipin X,[125] and BenJ in the benastatin A[52] biosynthetic pathways are homologous proteins. Up to now, the functions of these homologous enzymes are not clear. to GrhV. The investigation of the mutant strain Δ*grhV* by Kathrin Reinhardt provided metabolites with predicted molecular formulae $C_{23}H_{22}O_{10}$ (for $[M+H]^+$ measured *m/z*: 459.1319, calculated *m/z*: 459.1286), and $C_{25}H_{18}O_7$ (for $[M+H]^+$ measured *m/z*: 431.1108, calculated *m/z*: 431.1125). The amount of carbon atoms less than 26 and large amount of hydrogens in the predicted molecular formulae indicates that the enzyme might act in the early biosynthesis as an early oxygenase or cylase.

Another enzyme with an unassigned function is GrhU. The mutant strain produces extremely small amounts of metabolites. This enzyme shows homology to RubH in the γ-rubromycin,[125] FdmQ in the fredericamycin A,[42] LlpOIII in the lysolipin X,[125] and PdmH in the pradimicin[154] biosynthetic pathways. The investigations for the function of monooxygenase PdmH in pradimicin biosynthesis showed that the enzymes PdmH, and the two cyclases PdmK and PdmL are working in synergistic actions to generate the ring C and D of the molecule.[157] In the absence of one of these enzymes random cyclication products are observed. The reason for this is suggested that sequential binding and tailoring of long poly-β-ketone by individual enzymes may not be fast enough to prevent spontaneous cyclization of the reactive backbone. While an individual tailoring enzyme can only bind a portion of the extended polyketide chain, a multienzyme complex can effectively span the entire length of the uncyclized polyketide to lock the backbone in place and to suppress aberrant cyclizations.[157] Figure 3.91 shows the postulated early steps of pradimicin A biosynthesis.

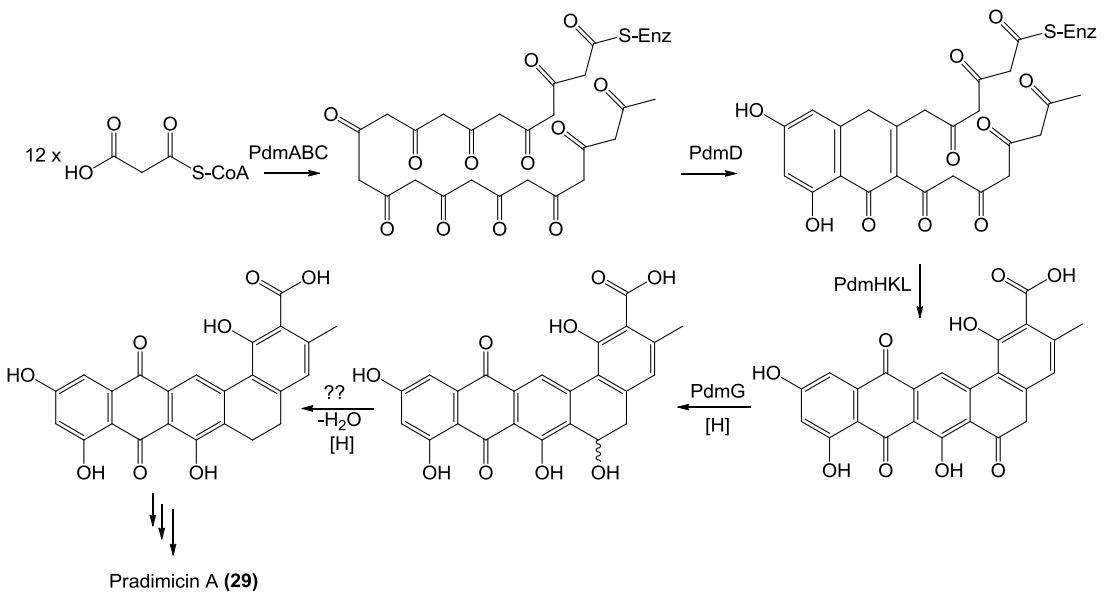

Figure 3.91. **Postulated early steps of pradimicin A biosynthesis.** [157]

Further functional investigation of the enzymes GrhU and GrhV are necessary to assign the oxidation step of these enzymes. At this point it would be necessary to remind a successful attempt of Kathrin Reinhardt to obtain a hybrid product, benarhodin A **(78)**, of the polyketides griseorhodin A **(5)** and benastatin A **(77)**.[125] For this combinatorial approach the minimal PKS of the *grh* cluster was replaced by the minimal PKS of benastatin A cluster. This experiment showed that the early oxygenases of *grh* cluster are able to perform tailoring reactions on the polyketide backbone produced by benastatin A minimal PKS. Figure 3.92 shows the structures of griseorhodin A **(5)**, benastatin A **(77)** and the combinatorial product benarhodin A **(78)**.[125]

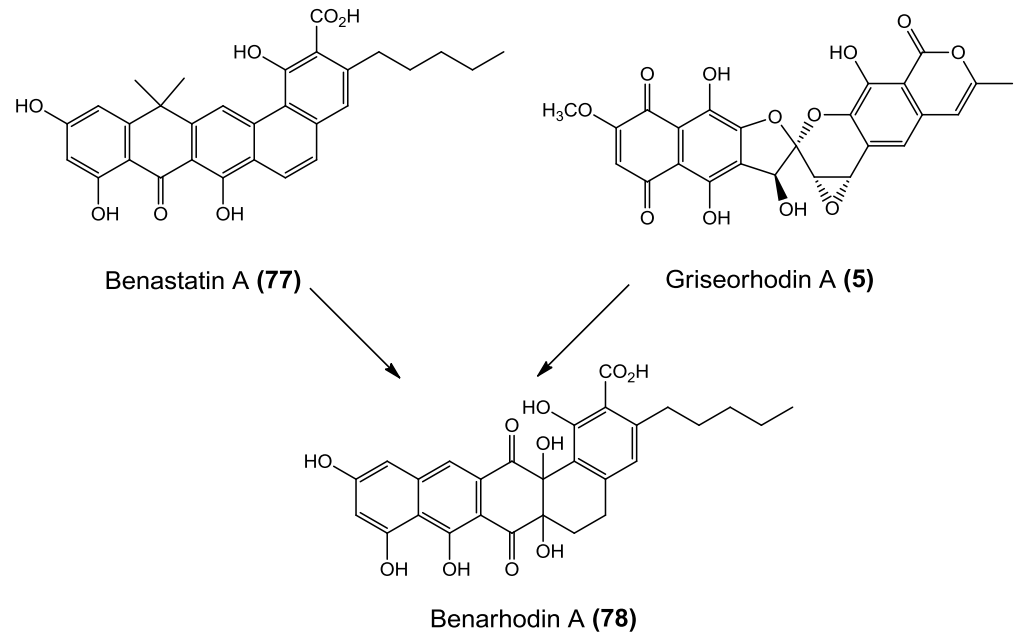

Figure 3.92. Griseorhodin A (5), benastatin A (77) and the combinatorial product benarhodin A (78) of the griseorhodin A tailoring enzymes and benastatin A minimal PKS .[125]

This result suggests that the early tailoring enzymes of the grh cluster are able to use wide range of substrates for their tailoring reactions. These features of the early tailoring enzymes might also be in usage at the griseorhodin A biosynthesis and usage of alternative substrates during the early biosynthesis could be an option for the early biosynthetic pathway.

3.5 *In Vitro* Enzyme Assay for the Overexpressed Oxygenase GrhO6

To obtain more information about GrhO6 an *in vitro* activity assay was conducted with the isolated compound lenticulone **(53)**. Lenticulone **(53)** was isolated from the extracts of the *grhO6* deletion mutant *S. albus* MP66 as described in Section 4.1.5.9. The compound was a good candidate to be an important biosynthesis intermediate and a substrate of GrhO6. Investigations of sequence homology of the FAD-dependent monooxygenase GrhO6 showed high protein similarity with two Baeyer-Villigerases, CmmOI and MtmOIV in the chromomycin and mithramycin biosynthesis, respectively.[141,143] MtmOIV is a Baeyer-Villiger oxygenase in the biosynthesis of the aromatic polyketide mithramycin **(23)**, as shown in Figure 3.45, Section 3.4.4. The crystal structure of MtmOIV and the kinetic characterization of the enzyme were achieved successfully by the group of Prof. Jürgen Rohr.[69,144,158] For the kinetic characterization of MtmOIV an *in vitro* assay was performed by using an isolated mithramycin precursor, premithramycin **(56)** (Figure 3.45), on an optimal pH of 8.25.[69] The procedure for the *in vitro* activity assay reported by Rohr and coworkers *Gibson et. al* was applied for the compound lenticulone **(53)** and GrhO6, in order to find out whether the enzyme accepts this compound as a substrate and if the enzyme acts in a similar way as MtmOIV.[69] Additionally, the experiment was an option to obtain possible products of the oxygenation reaction of GrhO6.

A first important aspect for the assay was to find suitable conditions for the optimal activity of GrhO6 *in vitro*. Second, the stability of the compound was investigated because some of the griseorhodin biosynthesis intermediates and metabolites detected are not stable at basic conditions, especially lenticulone **(53)**. It was an additional challange that in comparison to lenticulone **(53)** in comparison to premithramycin **(56)**, the former precursor used in the *in vitro* assay studies for MtmOIV, is a less stable compound.[69] Therefore, optimal pH conditions for the assay were to be determined through examining the stability of the compound over a range from pH 6 up to pH 8.5. Meanwhile the expression, kinetics and the stability of Grh06 were investigated as a part of the

PhD work of K. Rheinhardt and H. Niederkrüger, and is described in details in their PhD thesis.[125] Determination of an optimal pH, monitoring the assay and chemical investigation of the resulting products, which was the analytical part of the assay, were done in the context of this work.

3.5.1 Optimal pH Determination

The test substance lenticulone **(53)** was dissolved in Tris buffer at pHs 6; 6.5; 7; 8.25; 8.5 and 9 to test the stability of the compound. This was monitored by HPLC. MtmOIV is functioning in slightly basic solution at pH 8.25 but the test substance GrhO6 is instable at pH 7 and higher. Figure 3.93A shows the HPLC trace of lenticulone **(53)** dissolved in acetonitrile after isolation procedure described in Section 4.1.5.9. The occurrence of lenticulone **(53)** peak is marked with an asterix. Figure 3.93B shows the compound redissolved in Tris buffer at pH 6.5 and Figure 3.93C shows the compound redissolved in Tris buffer at pH 8.25. The compound is unsatbleand at pH values higher than 7 leading to the occurrence of a second substance with the same molecular weight. Therefore, an assay condition between at pH 6 and pH 7 was preferred.

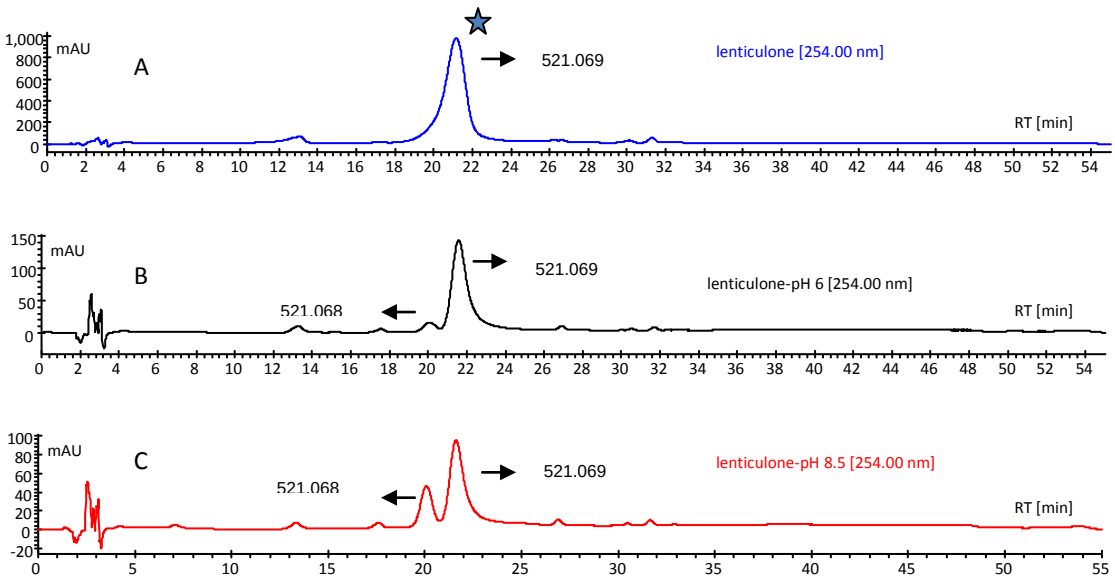

Figure 3.93A. HPLC trace of lenticulone (53) dissolved in acetonitrile. B. HPLC trace of lenticulone (53) redissolved in Tris buffer at pH 6. C. HPLC trace of lenticulone (53) redissolved in Tris buffer at pH 8.25. The occurrence of lenticulone (53) peak is marked with an asterix.

3.5.2 Assay 1:

For the first assay the reaction was performed in an open 50 ml Falcon tube at 30 °C at 250 rpm with a total volume of 2 ml. The assay was carried out in 1 M Tris buffer at pH 6 with 1 mM NADPH and 10 μM FAD as co-factor for a total of 4 hours reaction time as described in Section 4.1.6.1. 150 μL of 1 mM enzyme was added to the prepared mixture and every 30 min 400 μL of the solution was removed and extracted with 250 μl ethyl acetate. Subsequently, the organic phase was evaporated on a speed evaporator. The extract was dissolved in 50 μL acetonitrile and subjected to RP-HPLC with a mobile phase of acetonitrile/water (40:60 to 100:0). In parallel to this reaction a positive control reaction without enzyme and a negative control reaction without substance were also performed. During the reaction a light precipitation was observed. The detailed procedure of the reaction is described in Section 4.1.6.1. Figure 3.94 shows the monitored results of assay 1 and the control reaction monitored for assay 1. The control reaction did not contain the enzyme but all other components of the assay mixture.

As a result, the first assay at pH 6 and at 30 °C did not show any differences between the test reaction and the control reactions. The additional compound at the retention time of 11 min, which was mentioned in the degradation of the compound in the pH determination, was observed again. This assay leads to the assumption that the change in composition was due to the natural degradation but not the activity of the enzyme.

In order to observe more metabolites the assay was performed at larger scale and the reaction conditions were slightly changed. of the extraction For monitoring the composition of the assay better, the extraction procedure was additionally improved.

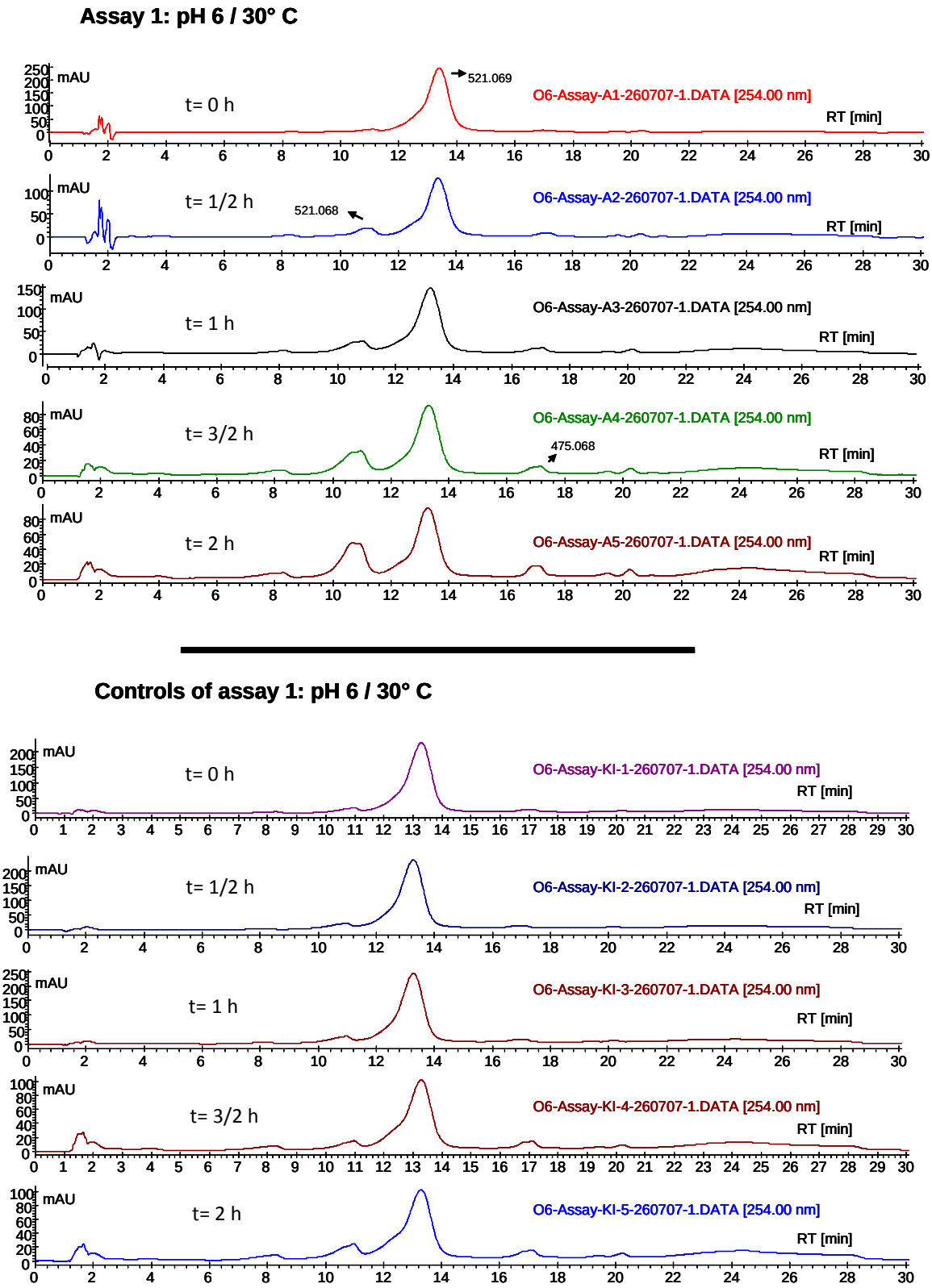

Figure 3.94 HPLC traces of assay 1 at pH 6 and the control reaction. The assay on the top was performed for a period of 4 hours and the composition was monitored by taking samples every hour. Meanwhile a control assay without enzyme was monitored, which is shown at the bottom.

3.5.3 Assay 2:

The reaction was performed in an open 50 ml Falcon tube at 30 °C at 225 rpm. The total volume of the reaction was 5 ml. The assay was performed in 1 M Tris buffer at pH 6 and 7 as assay 2a and 2b, respectively. It was performed with 1 mM NADPH and 10 μM FAD as co-factor for a total of 4 hours reaction time. The detailed procedures for the assays 2a at pH 6 and 2b at pH 7 are in Section 4.1.6.2. For the assay, freshly purified GrhO6 was used. A light precipitation during the assay and strong precipitation during the extraction procedure was observed. Figure 3.95 shows the results of assay 2a at pH 6 and the results of the control reaction for the assay 2a. Figure 3.96 shows the results of the assay 2b at pH 7 and the results of the control reaction for the assay 2b.

As a result, in the second assay at pH 6 at 30 °C, the assay mixture contained the same compounds as the compounds in the control reaction. The presence of enzyme did not result in a formation of a new product. However, the concentrations of the compounds in the first assay differed from the concentrations observed in the control assay. The likely main cause for this observation might be the protein precipitation in the reaction mixture effecting the extraction of the components and the yield of the compounds changes due to the extraction method used. Analysis of 2a at pH 6 showed that the change of the substrate due to the natural degradation of the compound but not the activity of the enzyme. Analysis of 2b at pH 7 at 30 °C showed the same results as 2a. The presence of enzyme did not cause formation of a new product at the chosen pH conditions.

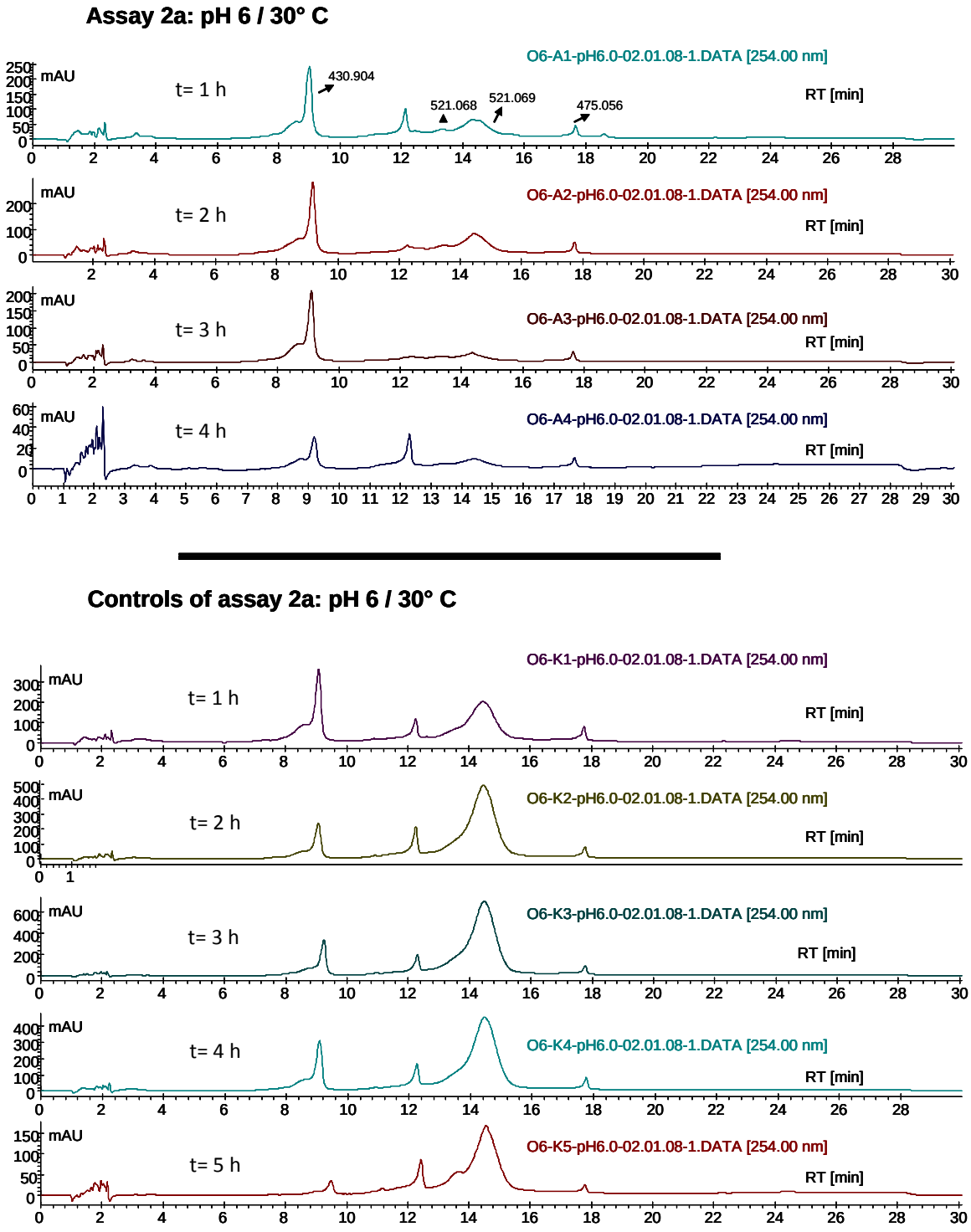

Figure 3.95 HPLC traces of assay 2a at pH 6 and the control reaction. The assay on the top was performed for a period of 4 hours and the composition was monitored by taking samples every hour. Meanwhile a control assay without enzyme was monitored, which is shown at the bottom.

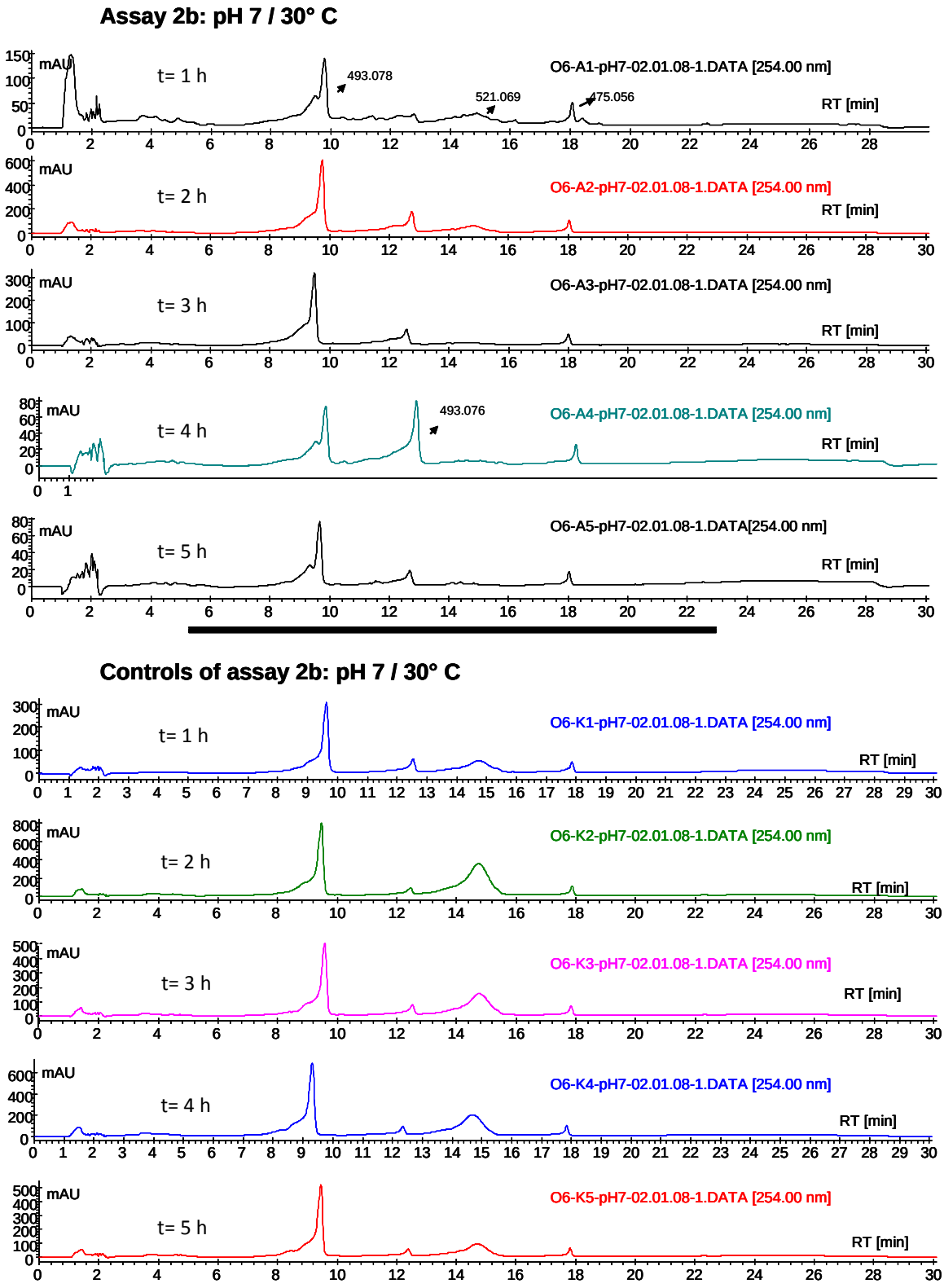

Figure 3.96 HPLC traces of assay 2b at pH 6 and the control reaction. The assay on the top was performed for a period of 4 hours and the composition was monitored by taking samples every hour. Meanwhile a control assay without enzyme was monitored, which is shown at the bottom.

3.5.4 Assay 3:

In order to obtain better conditions for the enzyme activity and stability, in another assay at the temperature was lowered to 27 °C and the pH 8.25 was tested, although the risk of substance degradation of lenticulone **(53)** was higher. The rationale was here that the enzyme might function better at this basic pH.

The reaction was performed in 1 M Tris buffer at pH 7 and 8.25 with 1 mM NADPH and 10 μM FAD as co-factor in a total of 4 hours reaction time. The detailed procedure is as described in the Section 4.1.6.3. The extraction procedure for the metabolites was slightly changed. The changes applied were that the solution taken out every hour was acidified before proceeding with the extraction with ethyl acetate. The compound was not soluble in organic solvents without being protonated; therefore samples of the assays at pH 7 were diluted with an equal amount of 0.025 % TFA solution and then extracted. The samples of the assays at pH 8.5 were diluted with 2 ml of the 0.025 % TFA solution. Figure 3.97 and 3.98 shows the observed metabolites during the assay at pH 7 and 8.25. Figure 3.97 shows the monitored composition of the assay 3a at pH 7 and the control solution without enzyme. Figure 3.98 shows the monitored composition of the assay 3b at pH 8.25 and the control solution without enzyme.

As before, assays at both pH values did not yield any compounds different from the ones observed in the control assays without enzyme. Thus it was concluded that the products of the assays were again a result of a spontaneous degradation of the initial substrate lenticulone **(53)**.

In summary, *in vitro* enzyme assays for the overexpressed GrhO6 oxygenase were investigated for the acidic pH 6, for pH 7, and for the basic pH 8.25 and compared to the control assay without enzyme. There was no difference observed to the natural degradation of the compound. The reason for these results might be that the substrate lenticulone **(53)** is not the natural substrate of the enzyme or the assay conditions found in the literature is not applicable for this substrate. The substrate lenticulone **(53)** is less stable than the substrates used in other assays, such as premithramycin **(56)**. Additionally,

lenticulone **(53)** has low solubility in aqueous solutions; therefore small amount of DMSO was added to increase the solubility of the compound and to avoid a precipitation of the compound, which might have a negative effect on the enzyme function. Another possibility is that the overexpressed GrhO6 enzyme was not active at the chosen *in vitro* assay conditions. At that point it is important to recall, that the metabolic analysis of the mutant strains suggested an involvement of the protein GrhJ at the processing of the candidate substrate lenticulone **(53)**. GrhO6 and GrhJ might therefore form a complex and lenticulone **(53)** might not be oxygenated in the absence of GrhJ.

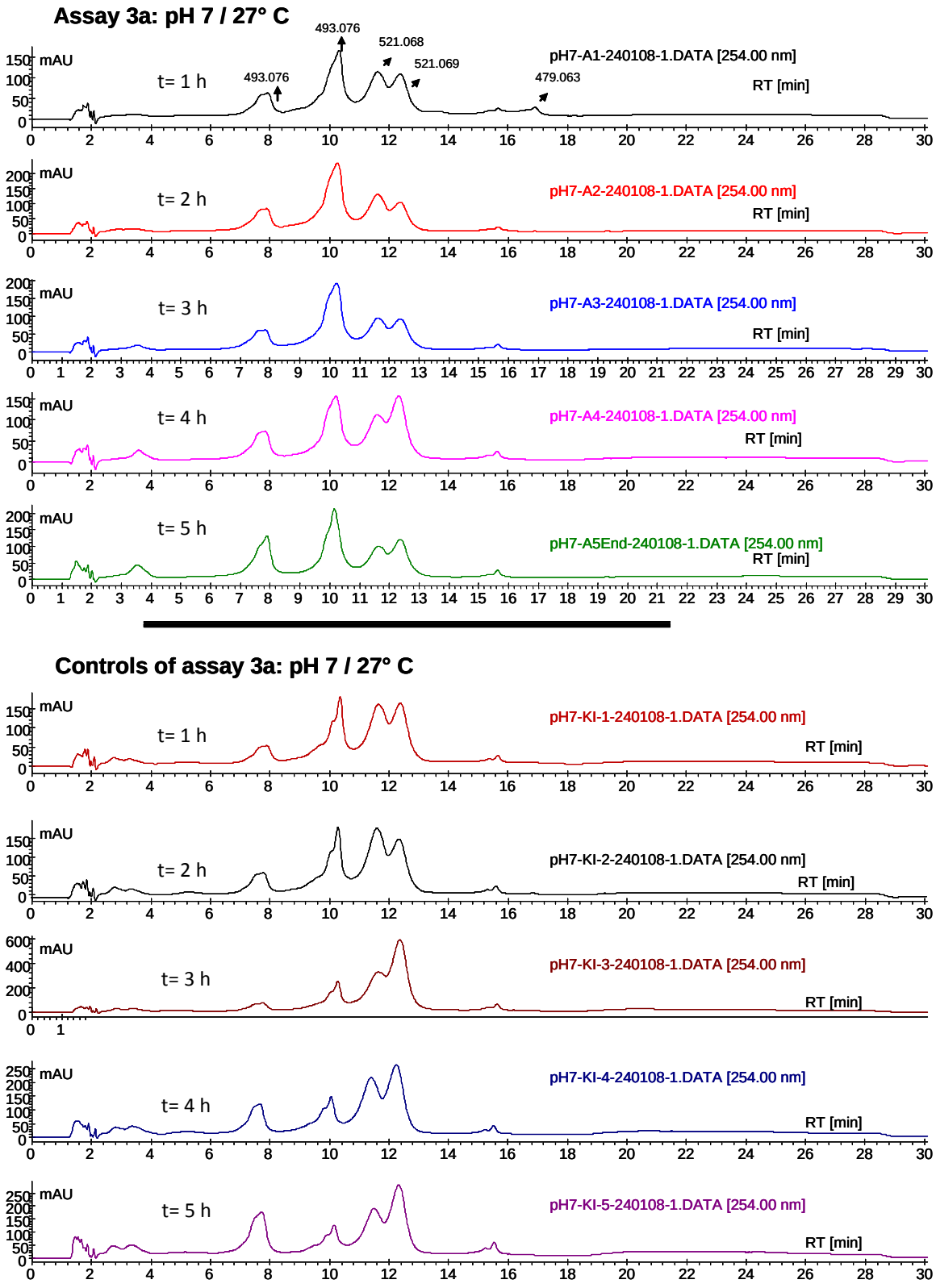

Figure 3.97 HPLC traces of assay 3a at pH 6 and the control reaction. The assay on the top was performed for a period of 4 hours and the composition was monitored by taking samples every hour. Meanwhile a control assay without enzyme was monitored, which is shown at the bottom.

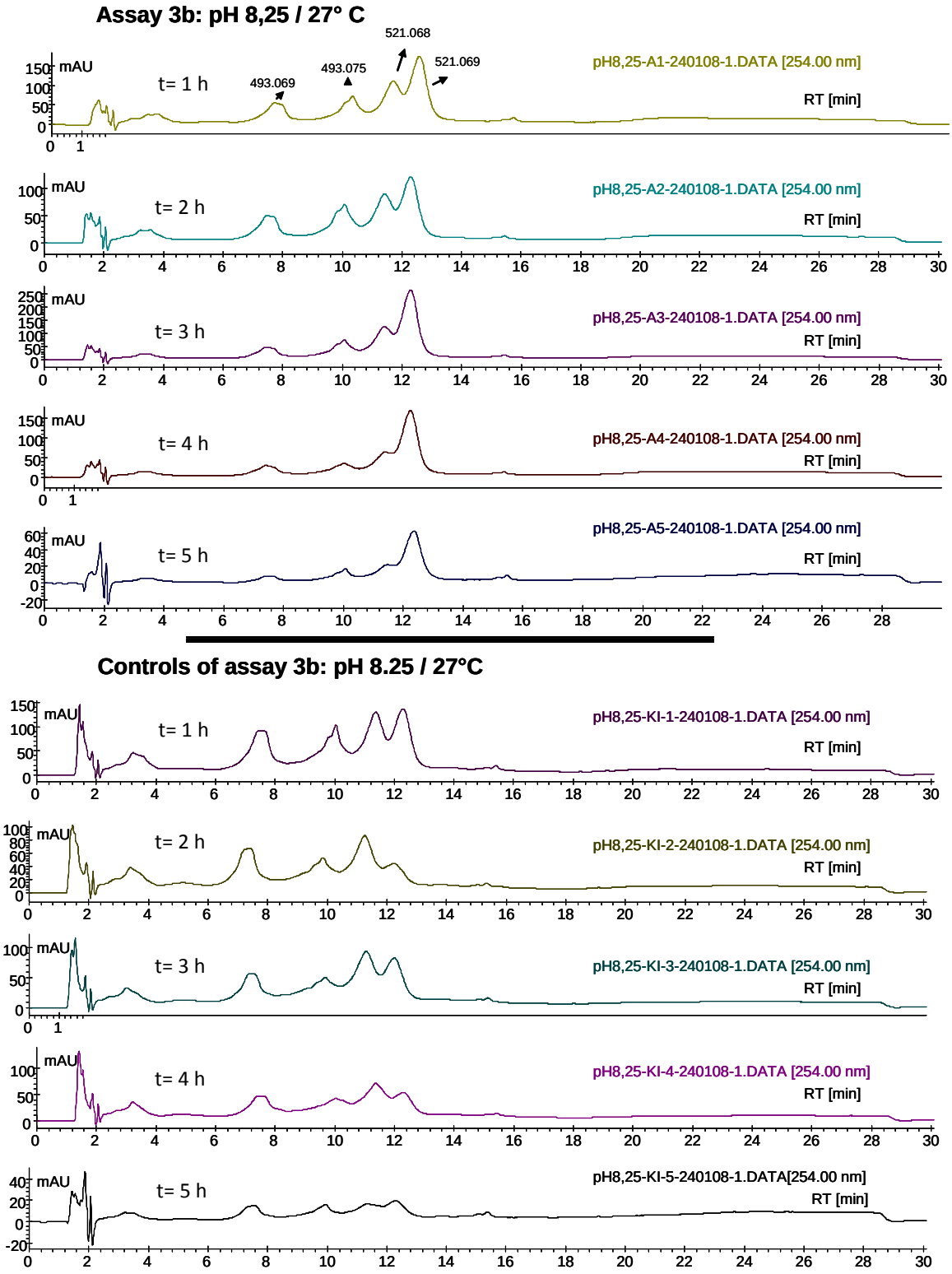

Figure 3.98 HPLC traces of assay 3b at pH 6 and the control reaction. The assay on the top was performed for a period of 4 hours and the composition was monitored by taking samples every hour. Meanwhile a control assay without enzyme was monitored, which is shown at the bottom.

3.6 Assays For Determining The Bioactivity of Isolated Compounds

To determine the bioactivity of the isolated compounds, the antibacterial activity of pure polyketides and some of the crude extracts were tested. In order to determine the impact of the oxidative modifications occuring during griseorhodin A **(5)** biosynthesis on the bioactivity of the metabolites, antiproliferative and cytotoxic properties of the compounds were tested in cooperation with the group of Hans Martin Dahse in HKI, Jena.

It was reported that some oxaheterocylic natural products are known to inhibit serine proteases. Examples are the inhibition of trypsin by flavonids and of thrombin by triterpene lactones from *Lantana camara*. [159] The substances of the griseorhodin family, which carries a lactone ring attached to the aromatic spiro moiety, were never tested for such an activity. Therefore, serine protease inhibiting activity of the isolated compounds and some extracts were tested in the group of Michael Gütschow.

3.6.1 Assays for Determining Antibacterial Activity

To determine the antibacterial activity of the compounds and metabolites in the extracts, two assays were performed. For the compound collinone **(41)**, an antibacterial activity for Gram-positive and Gram-negative bacteria has been reported in the former studies.[82] The first assay was an agar diffusion assay, which was performed on agar plates. For compounds showing an activity, a second assay was performed to determine the minimal inhibition concentration (MIC). This assay is for determination of the concentration range of growth inhibition on the test bacteria.

3.6.1.1 Agar Diffusion Assay

Water-soluble molecules can diffuse through the agar. The compound can be applied to a well that is cut into the agar. Alternatively, a cellulose disk with the compound applied on it can be used to place the substance on the agar. The compound will tend into the agar depending on its solubility. Before placing the substance on the agar plate, a bacterial test strain without antibiotic resistance

has to be spread on the plate, so that the growth inhibition of the strain can be observed after an overnight incubation. The principle is that the antibiotic will diffuse out of the disk into the agar and in the surrounding area of active compounds, generating a zone without bacterial growth. The radius of the area can then be measured, providing the *inhibition zone* of the compound for the chosen strain. This version of agar diffusion assay is known as the Kirby-Bauer disk diffusion assay.[160,161] Isolated substances and some of the crude extracts were used for this assay to observe the ones with an inhibition activity and to proceed further with a MIC assay. The compounds and some of the crude extracts obtained from the mutant strain were tested against the test bacterial strains below, which were available in our labarotories.

- *Escherichia coli* DH5α (Gram-)
- *Staphylococcus carnosus* DSH 20501 (Gram+)
- *Bacillus amyloliquefaciens* (Gram+)
- *Pseudomonas fluorescens* DSH 50090T (Gram-).

The aromatic polyketides used for the assay had very low water solubility. In order to achieve a better solubility, a little amount of DMSO was used to increase diffusion properties. The diffusion was few and unsymmetrical. Therefore the inhibition zone could not be determined as a value, but the growth inhibition on the disc surface and borders was an evidence for an antibacterial activity. A detailed procedure of the assay carried on is given in Section 4.1.7.1.

For the assay, the compounds griseorhodin A **(5)**, dideoxygriseorhodin C **(46)**, lenticulone **(53)**were used, which have differently configured spiro centers. Additionally, the compounds collinone **(41)** and precollinone **(58)** with a pentangular aromatic moiety were tested. For all compounds the procedure for isolation are given in Chapter 3.4. The crude extract of the mycelium obtained from the strains *S. albus* KR5 and *S. albus* KR11 and the extract of the medium from the fermentation of *S. albus* KR11 were also used for this assay. The extracts of these strains contained compounds that could not be characterized

without derivatisation reactions. In order to see if the original metabolite mixture contains active compounds, the test with these crude extracts was performed. The procedures of the extraction are provided in Chapter 3.4, as well. The substances with an assumed activity against test bacteria were assayed further to determine the MIC values as described in Section 3.6.2 in detail. Results of the agar diffusion assay are listed in Table 3.23. Figure 3.99 shows pictures of the assay plates.

Table 3.23 Results for agar diffusion assay. Presence of an inhibition zone is remarked as (+) and upsence of an inhibition zone is remarked as (-).

Bacterial strains	**Tested compounds on agar diffusion assay**			
	Lenticulone (53)	**Collinone (41)**	**Griseorhodin A (5)**	**Dideoxygriseorhodin C (46)**
Escherichia coli	-	+	-	-
Staphylococcus carnosus DSH 20501	+	+	+	+
Bacillus amyloliquefaciens	+	+	+	+

Bacterial strains	**Tested compounds and extracts on agar diffusion assay**			
	***S. albus* KR11 Medium-Crude extract**	***S. albus* KR11 Mycellium-Crude extract**	***S. albus* KR5 Mycellium Crude extract**	**Precollinone (58)**
Escherichia coli DH5α	-	-	-	-
Staphylococcus carnosus DSH 20501	+	-	-	+
Bacillus amyloliquefaciens	+	-	-	+
Pseudomona fluorescens DSH 50090T	-	-	-	-

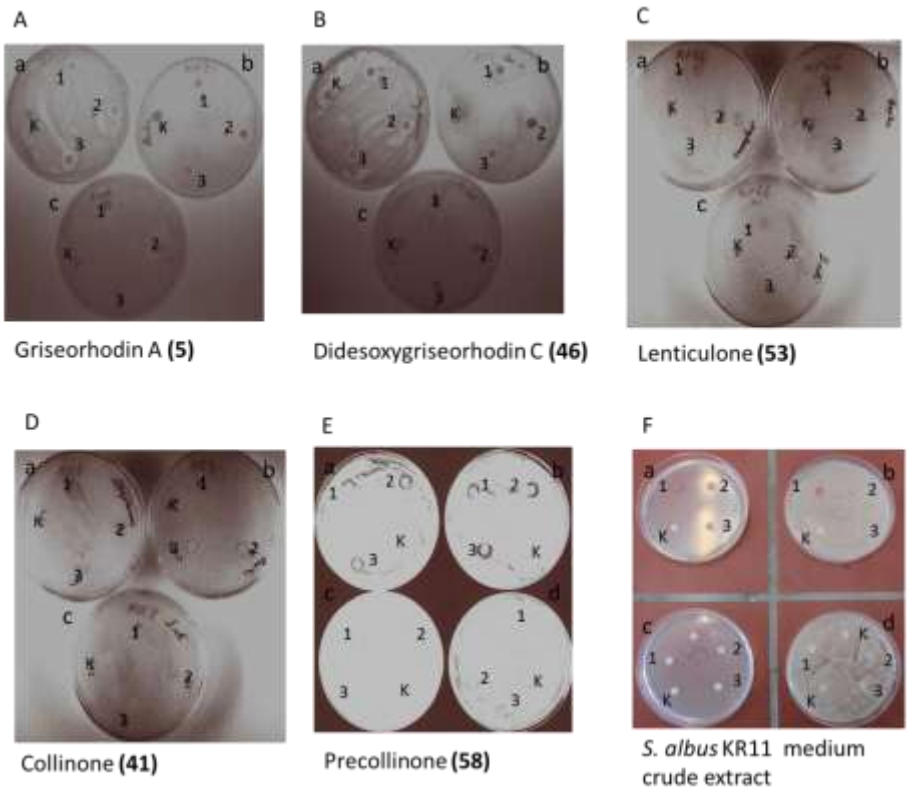

Figure 3.99 Results for agar diffusion assay. Pictures A, B, C, D show the agar diffusion assays of griseorhodin A (5), didesoxygriseorhodin C (46), lenticulone (53), and collinone (41) to the strains *Staphylococcus carnosus* DSH 20501, *Bacillus amyloliquefaciens* DSH 50090T and *Escherichia coli* DH5α shown as a, b and c, respectively. Pictures E and F show the agar diffusion assays of precollinone (58) and the extract of the medium from the fermentation of *S. albus* KR11 to the strains *Staphylococcus carnosus* DSH 20501, *Bacillus amyloliquefaciens* DSH 50090T, *Escherichia coli* DH5α and *Pseudomonas fluorescens* DSH 50090T shown as a, b, c and d, respectively. (K= Control disk without compound, 1, 2 and 3 = disks with 20, 10 and 5 µg test substance, respectively. For the assay F, 1, 2 and 3 = Disks with 40, 20 and 10 µg test extract, respectively.)

As a result of the agar diffusion assays for the antibacterial activity, it is concluded that lenticulone **(53)**, griseorhodin A **(5)**, didesoxygriseorhodin C **(46)**, precollinone **(58)** and collinone **(41)** inhibit the growth of the two Gram+ strains, *Staphylococcus carnosus* DSH 20501 and *Bacillus amyloliquefaciens* DSH 50090T. It was also observed that collinone **(41)** inhibits also the growth of the Gram- strain *Escherichia coli* DH5α. The crude extract of the mycelium obtained from *S. albus* KR5 and *S. albus* KR11 showed no activity. The extract of the medium from the fermentation of *S. albus* KR11 tested showed low inhibition of

the two Gram+ strains, *Staphylococcus carnosus* DSH 20501 and *Bacillus amyloliquefaciens* DSH 50090T.

3.6.1.2 Minimum Inhibitory Concentration (MIC) Assay

This method is used to determine the minimum concentration of a potential antibiotic compound at which the growth of a selected test organism is inhibited. A set of tubes with decreasing amount of the test compound is prepared in a growth medium and is inoculated with the test organism. For an active compound, growth diminishes as the concentration of antibiotic increases and a minimal concentration can be observed at which growth does not occur. This concentration is the MIC value. A detailed procedure of the assay carried on is is in Section 4.1.7.2. For all the used compounds the procedure for isolation are given in Chapter 4.1.4. The compounds obtained from the mutant strain were tested against the bacterial strains below.

- *Staphylococcus carnosus* DSH 20501 (Gram+)
- *Bacillus subtilis* (Gram+)

The list of the determined MIC values for the test compounds griseorhodin A **(5)**, didesoxygriseorhodin C **(46),** lenticulone **(53),** precollinone **(58)** and collinone **(41)** are listed in Table 3.24.

Table 3.24 Results for MIC assays.

Tested Substances	**MIC value for *Staphylococcus carnosus* [µg/ml]**	**MIC value for *Bacillus subtilis* [µg/ml]**
Griseorhodin A **(5)**	1.44	0.013
Lenticulone **(53)**	22.25	5.56
Collinone **(41)**	5.38	2.69
Didesoxygriseorhodin C **(46)**	0.23	0.004
Precollinone **(58)**	3.92	3.92

As a result of the MIC assays, it is concluded that the spiroketal compounds griseorhodin A **(5)**, didesoxygriseorhodin C **(46)** and the spiro compound lenticulone **(53)** have higher antibiotic activity against both Gram-positive strains in comparison to the pentangular aromatic polyketides precollinone **(58)** and collinone **(41).** The exact mechanism of the inhibition is not known but the spiro structures might play an important role at the antibacterial activity of these aromatic compounds. On the other hand, the lower solubility of these aromatic spiro compounds in water is a disadvantage for the use of their high activity as an antibiotic.

3.6.2 Antiproliferative Activity and Cytotoxicity

Organisms are utilizing against oxidative damage polyphenolic compounds, such as quercetin and myricetin and it is suggested that they may have the same role in humans.[162,163] Their features include antitumoral, antiviral, antibacterial, cardioprotective and anti mutagenic activities. They may play a role at different stages of malignant tumors by protecting DNA from oxidative damage.[164,165] Inactivation of carcinogens by inhibiting the expression of mutogenic genes; inactivation of the enzymes activating procarcinogenes and activation of the systems responsible for the detoxification of xenobiotics are some properties observed among these compounds which makes them an important tool for the life prolongation of organisms. [166,167]

For some polyphenolic compounds, such as flavanones, it is known that the antiproliferative activity and the cytotoxicity can be strongly influenced by the oxidation degree of the compounds.[166] Cytotoxicity compounds are toxic to cells and antiproliferative compounds are toxic to certain tumoral cells. It is important for a potential drug candidate compound to obtain low cytotoxicity, whilst also conserving the neccesary pharmacological activity in order to achieve an *in vivo* application as a drug.

To determine how the degree of oxidative modification during griseorhodin biosynthesis affects bioactivity, collinone **(41)**, griseorhodin A **(5)**, lenticulone **(53)**, and didesoxygriseorhodin C **(46)** were tested in antiproliferative and

cytotoxicity assays in the facilities of the HKI, Jena, by Hans Martin Dahse. Table 3.25 shows the determined activity of the compounds.

As a result, in general, the activity of all those compounds were in the same range, with didesoxygriseorhodin C **(46),** being slightly less active in all assays and lenticulone **(53)** showing decreased activity only in the Huvec assay.

Table 3.25 Antiproliferative activity and cytotoxicity of the compounds obtained from the mutant strains.

	Antiproliferative activity		**Cytotoxicity**
Compound	**Huvec** GI_{50} **[µg/mL]**	**K-562** GI_{50} **[µg/mL]**	**HeLa** CC_{50} **[µg/mL]** (CC_{10} **[µg/mL])**
Collinone **(41)**	22.6	19.4	30.7 (8.6)
Griseorhodin **(5)**	42.8	36.5	38.5 (14.2)
Lenticulone **(53)**	34.2	19.8	33.8 (12.4)
Didesoxygriseorhodin C **(46)**	>50	18.4	47.0 (21.8)

3.6.3 Protease Inhibiting Activity

A protease is an enzyme that breaks down proteins and initiates the protein catabolism by hydrolysis of the peptide bonds. Proteases can either break specific peptide bonds or break down a complete peptide to amino acid monomers depending on the sequence of a protein. Proteases can be classified regarding to the amino acids at the peptide bond they break as serine, threonine, cysteine, asparagine and glutamic acid proteases.[168] Alternatively, proteases may be classified by the optimal pH in which they function optimal such as acid, neutral or basic proteases or the structural features can also be used for classification such as metalloproteases.[168]

Proteases naturally occur in all organisms. They are involved in many physiological reactions. These reactions can be found in digestion or highly regulated cascades such as blood cloting, apoptosis, and the complement system.[168] They determine the lifetime of other proteins playing important

physiological roles like hormones, antibodies or other enzymes. In organizms these enzymes are used as one of the fastest switching tool for the regulatory mechanism.[168,169]

Bacteria also secrete proteases to digest proteins.[168] They can utilize these enzymes as exotoxins to destroy extracellular structures or as virulence factors in bacterial pathogenesis. Some viruses, such as HIV, are dependable on the activity of specific proteases in their reproductive cycle. They are Protease inhibitors investigated and developed for antiviral activity. One example of protease inhibition is the serpin superfamily.[168-170]

3.6.3.1 Serine-Protease Inhibiting Activity

To determine whether the metabolites of mutant *S. albus* strains show any activity against serine proteases, an enzyme inhibition assay for the serine proteases trypsin, chemotrypsin and human leukocyte elastase (HLE) were performed in the group of Prof. Michael Gütschow by Stephanie Hautmann using the crude extracts. The assays were carried out *in vitro*. The assays for chymotrypsin and trypsin inhibiting activity were performed with 25 ng/mL enzyme and 50 µg/mL test extract. Changes in the relative enzyme activity were monitored with a UV spectrometer. For the assay with human leukocyte elastase (HLE), 20 µg/mL of each extract was used and the activity of the enzyme was monitored by the concentration changes of the substrate para-nitroaniline (pNA) at 405 nm. The crude extracts do not show trypsin and chymotrypsin inhibitin activity. Inhibition of the enzyme human leukocyte elastase (HLE) was observed and was investigated further.

3.6.3.2 Elastase-Inhibiting Activity:

Elastase is an enzyme from the class of proteases. Human elastase breaks down elastin. Elastin fibers and collagen determine the mechanical properties of connective tissue. It cleaves the peptide bonds on the carboxy side amino acids such as glycine, alanine, and valine. Other features of these enzymes are to break down the outer membrane protein of Gram-negative bacteria, and also to break down Shigella virulence factors. [171-173]

Organisms such as *P. aeruginosa* also produce specific elastases, that are considered as virulence factors.[174] Some bacterial elastase has been shown to damage tissue, break down cytokines and alpha proteinase inhibitors, disturbing the complement system and decrease the ability of neutriphiles to kill bacteria by phagocytosis and contribute to human pathology. [171]

In order to determine extracts containing potential HLE inhibitors, a preassay was carried out by the group of Prof. Gütschow at the Pharmaceutical Institute in the University of Bonn. Table 3.26 shows the provided extracts for the assay and the effects of the extracts on the relative enzyme activity. The crude extracts of the strains *S. albus* KR4, *S. albus* KR5, *S. albus* KR7 *S. albus* KR8, *S. albus* KR13 and *S. albus* MP70 showed activity in the HLE screening.

Table 3.26 Effects of the compounds in the crude extracts of the mutant *S. albus* strains on the activity of human leukocyte elatase (HLE) screening. Active extracts are marked with an asterisk.

Crude extract of the strain	**Concentration used [µg/mL]**	**Relative activity of the enzyme (HLE) in %**
S. albus KR4★	20	18
S. albus KR5★	100	16
S. albus KR7★	20	17
S. albus KR8★	20	20
S. albus KR13★	20	46
S. albus MP31	20	40
S. albus MP36	20	64
S. albus MP63	20	71
S. albus MP66	20	31
S. albus MP70★	20	26

The crude extracts of the strains *S. albus* KR4, *S. albus* KR5, *S. albus* KR7, *S. albus* KR8, *S. albus* KR13 and *S. albus* MP70 were further used to determine the IC_{50} values for the concentration of HLE inhibition. The obtained values for the crude extracts are listed in the Table 3.27.

Table 3.27 IC_{50} values of the crude extracts for the inhibition of the HLE enzyme.

Crude extract of the strain	**Consentration range tested**	**IC_{50} [µg/mL]**
S. albus KR4	6.67-26.67 µg/mL	6.63± 0.63 µg/mL
S. albus KR5	25-100 µg/mL	9.21±2.05 µg/mL
S. albus KR7	6.67-26.67 µg/mL	3.10±0.83 µg/mL
S. albus KR8	6.67-26.67 µg/mL	7.41±1.48 µg/mL
S. albus KR13	10-40 µg/mL	16.3±0.5 µg/mL
S. albus MP70	6.67-26.67 µg/mL	14.4±2.7 µg/mL

The extracts were further investigated and the major compounds in the extracts were determined and isolated. Griseorhodin A **(5)** is the major component of the extracts from *S. albus* KR4, *S. albus* KR13, and *S. albus* MP70. Didesoxygriserhodin C **(46)** is the major component of the extract from *S. albus* KR7. The strain *S. albus* KR8 produces the compound collinone **(41)** as a major metabolite. The major metabolite of *S. albus* KR5 could not be obtained without derivatisation reactions and was not used for further experiments. Lenticulone **(53)** was isolated from *S. albus* MP66 and was also provided for further investigation of the active compounds. The IC_{50} values for the compounds were determined in the group of Prof. Gütschow. The details of the test methods were used are published. [13] Table 3.28 shows the obtained IC_{50} values for the compounds.

Table 3.28 The obtained IC_{50} values for the active compounds.

Compound	**IC_{50} [µg/mL]**
Collinone **(41)**	4.763±1.040
Griseorhodin **(5)**	0.957±0.086
Lenticulone **(53)**	1.396±0.308
Didesoxygriseorhodin C **(46)**	0.690±0.160

As a result of these assays, the spiro structure of the compounds directly influences the inhibiting activity for the HLE enzyme. Didesoxygriseorhodin C **(46)** showed a considerable activity, and it became the first reported aromatic

polyketide inhibiting the HLE enzyme strongly.[99] Additionally, the spiro compounds griseorhodin A **(5)** and lenticulone **(53)** exhibited stronger inhibitors than the pentangular aromatic compound collinone **(41).** These compounds are the first reported aromatic polyketides with high HLE inhibitory activity. An important achievement of this investigation is that it opens the way for a new class of HLE-inhibiting substances containing aromatic spiro moietys.

3.7 Summary and Discussion of Griseorhodin A Biosynthesis

Griseorhodin A **(5)** is the most heavily oxygenated member of the rubromycin family of aromatic polyketides with a unique epoxyspiroketal moiety. Many rubromycins, such as γ-rubromycin **(37)**, purpuromycin **(38)**, and griseorhodin A **(5)** are inhibitors of human telomerase and β-rubromycin shows inhibiting activity of retroviral reverse transcriptases, such as HIV.[97] They possess a non-planar structure due to the presence of this spiroketal moiety. Telomerase inhibition depends on the presence of the spiroketal moiety.[97] Therefore, the study of the biosynthesis of the spiroketal moiety is important for the development of more potent and selective inhibitors.

The compound is synthesized by a type II PKS. The initial steps of the biosynthesis are the synthesis of a poly-β-keto chain by the minimal PKS GrhABC initiated with an acyl-CoA starter and the iterative condensation of 12 malonyl-CoA extender units for the chain elongation of the chain. Reduction of the poly-β-keto chain intermediate at C-19 by a ketoreductase and catalytic cyclization reactions directed by the cyclases generate a pradimicin-type pentangular aromatic core that is further converted by the tailoring enzymes into griseorhodin A **(5)**.[15] The biosynthetic steps in the generation of the aromatic core were not investigated during the course of this work. However, sequence homology of GrhU, GrhQ and GrhS to the cyclases PdmHKL in the pradimicin biosynthesis suggest that GrhU, GrhQ and GrhS act early in the biosynthesis of the pradimicin-type aromatic core.[154,157] The focus of this work is the tailoring steps that generate the spiroketal pharmacophore in the biosynthesis of griseorhodin A **(5)**. This section provides an overview of the studies performed to gain deeper insights into the complex biosynthesis of the compound, and discusses the postulated biosynthesis pathway suggested by the results obtained from the investigations of the griseorhodin A cluster.

In general, a heterologous expression system has to be created in order to simplify studies on the biosynthesis of griseorhodin A **(5)** and rubromycin-type spiroketal compounds. Such an expression system was created by Aiying Li.[15]

The expression strain *S. albus* MP31, which carried the entire griseorhodin A gene cluster integrated into its genome, was constructed by using the host strain *S. albus* J1074. For further functional investigation of the genes and the biosynthetic pathway, 20 genes of the cluster were individually deleted by Kathrin Rheinhardt via λ-red-mediated recombination on the plasmid pMP31 containing the entire griseorhodin A cluster. Subsequently, the resultant mutant clusters were heterologously expressed after conjugation into the *S. albus* J1074 host strain.[99,125]

To achieve the major objective of this thesis, the chemical investigation of these mutant strains was performed and the determination of the functions of the encoded enzymes of the deleted genes was attempted. To characterize the metabolites resulting from the single gene knockout experiments, the mutant strains were grown on 2CM agar plates; metabolites were extracted and were analyzed by TLC, HPLC and HRLC-MS. The isolation of sufficient amounts of metabolites for structure elucidation required time-consuming large-scale fermentations of the knockout strains. During this thesis work, isolation and characterization of the produced metabolites, performance improvements in strain fermentations, and development of isolation methods for potential intermediates were accomplished. In addition, derivatization procedures were developed for the unstable metabolites. Isolation and characterization of the derivatization products provided further information for the possible biosynthesis intermediates.

Initially, chemical investigations focused on the 10 oxygenases and a methyl transferase, suspected to be involved in the tailoring steps. However, the HRMS analysis of the provided 20 gene deletion mutants showed that additional genes with unknown functions were involved in the tailoring steps of griseorhodin A **(5)**. During the course of this work, besides the compound griseorhodin A **(5)**, seven metabolites, which were present in the extracts of fourteen mutant strains, were identified. Three mutant strains did not produce detectable amount of metabolites, and two strains did not produce sufficient amounts for structure elucidation of the detected metabolites at the tested fermentation conditions. Table 3.29 summarizes the most important data obtained and used

to propose a biosynthesis pathway. Table 3.29 includes the names of the mutant strains; the putative function of the deleted genes, the HRMS analysis results, the suggested molecular formulae of the observed metabolites, and in the last column contains the numbers corresponding to the structures in Figure 3.100. Figure 3.100 shows the structures obtained from the chemical investigation of the mutant strains. The structure of KS-619-1 **(64)** is shown in parenthesis, because the structure was identified indirectly using the structure elucidation of a fully methylated derivative KS-619-3 **(65)** as described in Section 3.4.7. The compound secocollinone-2 **(60)** could be identified in the extract of *S. albus* KR5. Similarly, the identification of the metabolite was performed indirectly via structure elucidation of a fully methylated derivative, secocollinone-1 **(59)** as described in Section 3.4.6**.** Therefore, its structure is shown in parenthesis, too.

Investigation of the gene deletion strains in Table 3.29 by HRMS provided further information about the functions of the genes in the biosynthesis. The mutant *S. albus* KR39 with a deleted GrhO2 oxygenase gene still produces griseorhodin A **(5)**. The unaffected biosynthesis of the compound in the absence of GrhO2 suggests that GrhO2 has no function or the function of GrhO2 can be performed by another enzyme. Similarly, the deletions of the genes *grhD*, *grhH*, *grhI*, and *grhN* with unknown functions did not affect the production of griseorhodin A **(5)** by the mutants *S. albus* KR13, *S. albus* KR27, *S. albus* KR4, *S. albus* KR23, respectively. Additionally, in the absence of *grhJ*, *grhP*, *grhM*, *grhU*, and *grhV* genes with an unassigned function, the single gene deletion mutants could not produce griseorhodin A **(5)** but small amont of several other metabolites which are used for further investigation of the biosynthesis. The analysis of the metabolites produced by the mutants proves the necessity of these genes for the generation of griseorhodin A **(5)**.

The mutants with *grhO10, grhV*, and *grhU* gene deletions produced extremely small amounts of various unidentified metabolites even though the growth conditions were altered to increase the yields. The presence of griseorhodin A **(5)** in the extracts was not confirmed for these cases. The absence of the compound shows that these genes are crucial for the biosynthesis, but it is difficult to propose functions for these genes without analyzing any metabolites.

It is thought that these genes affect the early steps of the biosynthesis generating pradimicin-type metabolites as oxidoreductases or cyclases because aromatic polyketide metabolites are produced in extremely low quantities in the absence of these genes. These genes are further investigated by Minna Eklund in the group of Piel.

The function of *grhJ* in the construction of the spiro moiety is identified using the metabolites lenticulone **(53)** and didesoxygriseorhodin C **(54)** detected in the extracts of the mutant strain as described in Section 3.4.4. The function of GrhJ is suggested as a oxygenase and the function is described further at the discussion of the generation of the spiroketal moiety in this section.

In the extract of the *grhP* gene deletion mutant, major metabolites with 26 carbon atoms were detected, which suggested the involvement of the protein in the tailoring steps of the pradimicin-type core. The gene *grhP* has homology to an enzyme from oxytetracycline biosynthesis (OxyD)[38] that is responsible for the synthesis of the malonamate starter unit. Additionally, *grhP* has homology to amidotransferase genes, which are responsible for the transfer of an amide function to the polyketide core of the compounds such as fredericamycin (FdmV)[42] and lysolipin (LlpA).[175] The function of FdmV as a tailoring enzyme at the generation of the lactam ring F in the biosynthesis of fredericamycin A **(26)** is proven.[155] Since the compound griseorhodin A **(5)** does not have any amide or lactam group, the involvement of the protein GrhP in the biosynthesis needs to be proven. Unfortunately, the isolation and structure elucidation of the metabolites produced by the mutant strain could not be achieved due to the mutant strain producing insufficient amounts. However, the metabolite KS-619-1 **(51)** in the extracts of *ΔgrhM* and *ΔgrhO8* mutant strains indicates that the lactone formation of ring F occurs after the oxidation steps of GrhM and GrhO8, as a tailoring step.

In the extract of the mutant formed after *grhM* gene deletion, two major metabolites with an identical suggested molecular formula $C_{26}H_{18}O_8$ were detected. Additionally the metabolite KS-619-1 **(64)** was identified as described in Section 3.4.7. This shows the involvement of this gene in the early tailoring

steps as an oxygenase as described further at the discussion of the postulated early tailoring steps in this section.

An insightful finding of the HRMS analysis was that some metabolites carry 27 carbon atoms. Note that griseorhodin A **(5)** has only 25 carbon atoms. The additional carbon atoms support the hypothesis that the biosynthesis of griseorhodin A **(5)** is completed after the loss of two carbon atoms from a highly oxidized polycylic core. The compound collinone **(41)** that was discovered by *Minas et al*. as described in Section 3.4.3, was also detected in the extracts of the mutant strain *S. collinus* DSM 2012, which contains a putative rubromycin cluster, using *S. coelicolor* CH999 as a host.[137] Previously the compound was suggested as a possible intermediate of the rubromycins.

In this work, this hypothesized intermediate collinone **(41),** which is a pink-colored stable solid with the molecular formula $C_{27}H_{18}O_{12}$, was identified and isolated in the extract of *S. albus* KR8, a mutant that lacked the FAD-dependent oxygenase GrhO5. The isolation and identification of this compound from *S. albus* KR8 proved the hypothesis that griseorhodin A **(5)** is built from a single tridecaketide chain and that a pentangular aromatic precursor exists in the biosynthesis of rubromycin-type aromatic spiroketal polyketides.[110]

Table 3.29 Metabolites observed in HRMS analysis of the mutant strains created in order to study the functions of tailoring enzymes via single gene deletions. (n.d: The strain did not produce secondary metabolites in sufficient amounts.)

Strain	ΔORF	Putative protein Function	Measured *m/z* $[M+H]^+$	Predicted Molecular Formula	Structure Nr.
MP31	----	----	509.0720	$C_{25}H_{16}O_{12}$	**5**
KR5	*grhO1*	Oxygenase with covalently bound FAD	537.1021	$C_{27}H_{20}O_{12}$	**60**
KR39	*grhO2*	Ketoreductase	509.0720	$C_{25}H_{16}O_{12}$	**5**
KR43	*grhO3*	Cytochrome P450	495.0922	$C_{25}H_{18}O_{11}$	**46**
KR8	*grhO5*	FAD-dependent oxygenase	535.0877	$C_{27}H_{18}O_{12}$	**41**
MP66	*grhO6*	FAD-dependent oxygenase	337.0550	$C_{15}H_{12}O_9$	**54**
			521.0720	$C_{26}H_{16}O_{12}$[c]	**53**
KR7	*grhO7*	NADPH: quinone oxidoreductase	495.0922	$C_{25}H_{18}O_{11}$	**46**
KR41	*grhM*	Unknown oxygenase	459.1050	$C_{26}H_{18}O_8$	n.d
			459.1069	$C_{26}H_{18}O_8$	n.d
			475.1114	$C_{26}H_{18}O_9$	**64**
KR11	*grhO8*	FAD-dependent oxygenase	477.1150	$C_{26}H_{20}O_9$	n.d
			475.1077	$C_{26}H_{18}O_9$	**64**
KR53	*grhO9*	FAD-dependent oxygenase	505.1120	$C_{27}H_{20}O_{10}$	**58**
MP63	*grhO10*	3-Oxo-acyl-ACP reductase	n.d.	n.d.	n.d.
KR15	*grhP*	Amidotransferase	491.0975	$C_{26}H_{18}O_{10}$	n.d
			507.0922	$C_{26}H_{18}O_{11}$	n.d
			981.1870	$C_{52}H_{36}O_{20}$	n.d
KR40	*grhL*	Methyl transferase	489.0785	$C_{26}H_{16}O_{10}$	n.d.
			471.0695	$C_{26}H_{14}O_9$	n.d.

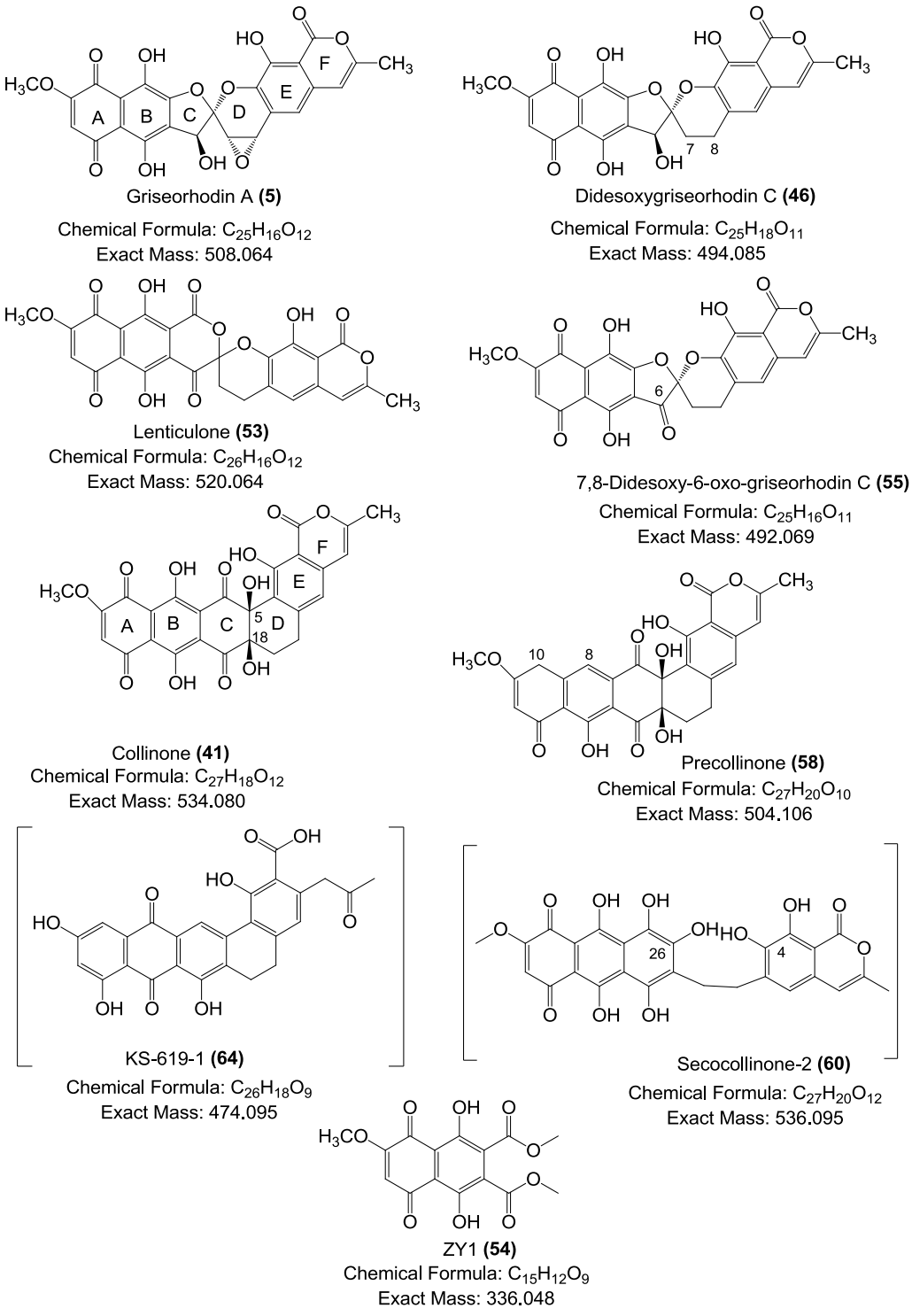

Figure 3.100 Structures of possible intermediates and metabolites isolated during the chemical investigation of the 20 gene deletion strains. Structures shown in parenthesis are possible intermediates suggested by the isolated methylated derivative of the native metabolites.

The biosynthesis of griseorhodin A **(5)** can be analyzed in two parts. The first part is the oxidation of an initial intact pradimicin-type intermediate to the highly oxidized collinone **(41)** (Collinone **(41)** has the largest number of carbon and oxygen atoms compared to the other metabolites.) and the second part is the construction of the spiro system of griseorhodin A **(5).** The tailoring enzymes involved in this biosynthesis are therefore separated into two groups based on their relationships to this intermediate collinone **(41)**. The enzymes, which are involved in the early biosynthetic steps leading to collinone **(41)**, constitute the first group and enzymes responsible for the construction of the complex epoxy spiroketal structure constitute the second group.

In this section, first the functions of the enzymes in the second group are discussed because of their unique role in the construction of the pharmacologically significant epoxyspiroketal group. Then, the functions of the enzymes in the first group are discussed.

Figure 3.101 shows the enzymes involved in the biosynthesis starting with the compound collinone **(41)** and ending with griseorhodin A **(5)**. GrhO5 is a FAD-dependent monooxygenase. *S. albus* KR8, a mutant with a *grhO5* gene deletion, produces the compound collinone **(41)** as a single metabolite. This clearly suggests that GrhO5 initiates the cleavage sequence steps by using collinone **(41)** as a substrate. *S. albus* KR5 which lacks the covalently bound FAD-dependent oxygenase GrhO1 produces metabolites with 27 carbon atoms as well but it does not produce collinone **(41)**. Further investigation of metabolites of *S. albus* KR5 provided secocollinone-2 **(60)**. This compound indicates that the substrate of GrhO1 had already a bond cleaved at the ring D. This suggests that GrhO5 together with GrhO1 act in the cleavage of three carbon bonds. Ring D of the collinone **(41)** would lose a carbon atom, which leads to the generation of the suggested intermediate lenticulone **(53)**. The absence of collinone **(41)** in the extracts of the *grhO1* gene knockout strain suggests that the two enzymes are not acting simultaneously, but in series to form lenticulone **(53)**.

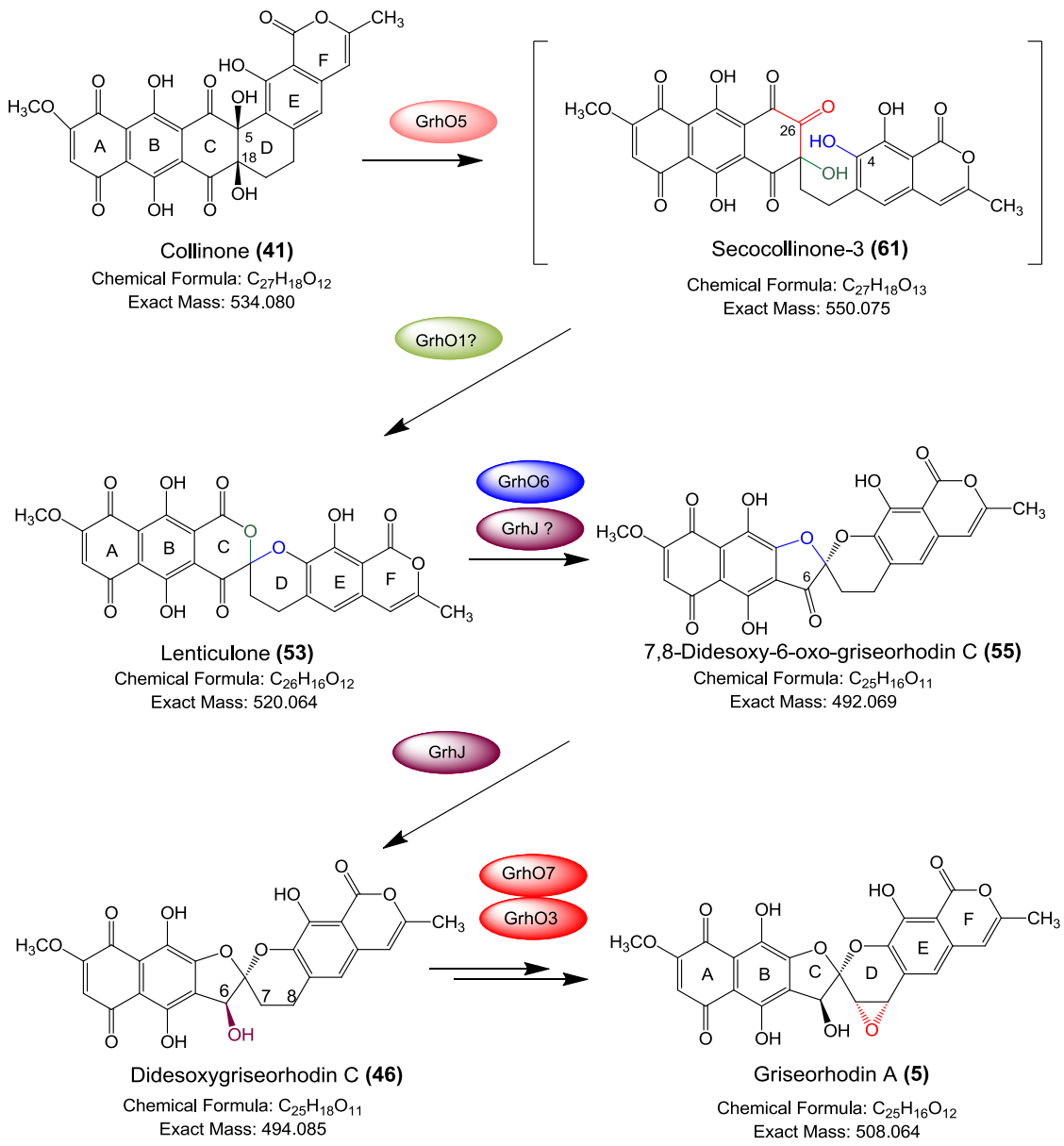

Figure 3.101 Enzymes involved in the tailoring steps after the formation of collinone (41). Structures in parenthesis are proposed intermediates implied by the compounds obtained via derivatization reactions.

Secocollinone-2 **(60)** was detected in the crude extract of *S. albus* KR5 but to elucidate the structure, the crude extract was methylated as described in Chapter 3.4.6 and the fully methylated derivative secocollinone-1 **(59)** was used for structure elucidation. The structure of the methylated derivative shows clearly that the native intermediate produced by the strain is an open ring form of collinone **(41)**. This suggest that the enzyme GrhO1 acts after a bond cleavage

reaction catalyzed by GrhO5, which should open ring D. (Figure 3.76A). However, the structure of the possible metabolite obtained based on the isolated derivative is in a reduced state compared to the postulated biosynthesis intermediate. This is rather unlikely for a reaction catalyzed by an oxygenase. A possible explanation for the aromatization on ring C is that secocollinone-2 **(60)** is a reduced derivative of an unstable intermediate. In this case an enzymatic or spontaneous reduction of the native intermediate during the fermentation, isolation or derivatization reactions could cause the generation of the compound secocollinone-2 **(60)**. For the biosynthetic pathway, a predicted intermediate secocollinone-3 **(61)** is suggested as a substrate for the enzyme GrhO1 based on the obtained metabolite secocolline-2 **(59)**. An intermediate related to the structure **(61)** would also explain the generation of the isolated metabolite lenticulone **(53)** as described in Section 3.4.6.

Lenticulone **(53)** was isolated from the extracts of *S. albus* MP66, a mutant with a *grhO6* gene deletion. In basic solutions the compound is not stable, and in the presence of acids and methanol the compound decomposes to ZY1 **(54)**. Lenticulone **(53)** and ZY1 **(54)** were isolated and characterized during this study as new compounds from the stain *S. albus* MP66.[99]

A surprising result related to *S. albus* KR42 is that GrhJ, which has a homology to a GCN5-related N-acetyltransferase (GNAT) family enzyme, acts like a tailoring enzyme. Lenticulone **(53)** was also observed as a minor component in extracts of this strain *S. albus* KR42, a mutant with a *grhJ* gene deletion. The main compound produced by *S. albus* KR42 plate extracts had been previously suggested in the work of K. Rheinhardt as 7,8-didesoxy-6-oxo-griseorhodin C **(55)** with a molecular formula $C_{25}H_{16}O_{11}$.[125,176] The presence of the same metabolite in both extracts suggests that the oxygenases GrhO6 and GrhJ are responsible for the formation of the suggested metabolite 7,8-didesoxy-6-oxo-griseorhodin C **(55)** that has one carbon atom less than lenticulone **(53)**. However, the extracts of the GrhO6 deletion mutant did not contain 7,8-didesoxy-6-oxo-griseorhodin C **(55).** This suggests that the enzymes GrhO6 and GrhJ act together in the oxidation reactions in which a fourth bond cleavage and loss of another C atom occurs. In addition, GrhJ might be involved in the

downstream reactions converting 7,8-didesoxy-6-oxo-griseorhodin C **(55)** to the next isolated intermediate didesoxygriseorhodin C **(46).**

The enzyme sequence of GrhO6 shows sequence homology to the Baeyer-Villigerase-type oxygenases, such as MtmOIV in mithramycin **(23)** biosynthesis.[141] This homology and the structure of the potential substrate lenticulone **(53)** suggest that GrhO6 might act as a Baeyer-Villigerase on the ester moiety of the compound resulting in decarboxylation. However, an alternative mechanism could not be excluded, in which GrhO6 hydroxylates the ester α-position, and the subsequent decarboxylation results from rearomatization as discussed in Section 3.4.4.

In order to obtain more insight into the enzyme function and to test whether GrhO6 directs the second oxidative decarboxylation by itself, an *in vitro* enzyme assay with the over-expressed enzyme GrhO6 and the compound lenticulone **(53)** as a substrate was performed. GrhO6 did not function as expected at the chosen conditions of the *in vitro* assay. A possible reason might be that the substrate is unstable in the basic conditions over pH 7. The poor water solubility of lenticulone **(53)** and the enzyme at the assay conditions might also be a reason that the assay did not provided further results about the reaction of GrhO6. Another reason might be that the enzyme does not function properly in the absence of the protein GrhJ as suggested before. The details of the assays are described in Section 4.1.6 and discussed in Chapter 3.5.

S. albus KR7 with a deactivated NADPH:quinone oxidoreductase enzyme GrhO7 and *S. albus* KR3 with a deactivated cytochrome P450 family oxygenase GrhO3 both produced a single main metabolite characterized as didesoxygriseorhodin C **(46)** with a molecular formula $C_{25}H_{18}O_{11}$. This result implies an unusual involvement of these oxygenases in the epoxidation of didesoxygriseorhodin C **(46)**. Although cytochrome P450 enzymes usually use alkenes to generate epoxides, they are few examples of the formation of cyclic ethers from saturated precursors have been reported. The epoxidase OleP from oleandomycin biosynthesis[134] and the aureothin P450 AurH that closes a tetrahydrofuran ring by 1,5-dehydrogenation of an alcohol precursor can be found as an example.[135] To our knowledge, this is the first case reported that a NADPH:quinone

oxidoreductase participates in the epoxidation reaction of a polyketide. The production of the same substance by the two mutant strains, GrhO3 and GrhO7 was unexpected. In the case that the compound didesoxygriseorhodin C **(46)** is the true substrate of GrhO3 and GrhO7, a possible explanation would be that the two enzymes form a complex, which is inactive if one component is absent. This suggests that GrhO7 and GrhO3 jointly participate in epoxide formation. Another possible explanation is that GrhO3 is capable of the epoxidation of the olefinic carbon bond alone and GrhO7 might be responsible for the reductive recycling of olefinic shunt products that arise from an eliminative side reaction. The investigation of the monooxygenase gene *styAB* from *Pseudomonas sp. VLB120* showed that the rate of epoxidation depends on the amount of NADPH present.[136] This would also suggest that GrhO7, a member of the NADPH:quinone oxidoreductases, might be involved in the effective regenerating of the coenzyme for the oxygenase GrhO3, a member of the cytochrome P450 family. For further investigation of the epoxidation on didesoxygriseorhodin C **(46)**, functional enzyme assays with GrhO3 and GrhO7 can be performed.

In summary, the isolated and characterized compounds, collinone **(41)**, secocollinone-2 **(60)**, lenticulone **(53)**, didesoxygriseorhodin C **(46)** and the suggested metabolite 7,8-didesoxy-6-oxo-griseorhodin C **(55)** provide deeper insights to the functions of the oxygenases GrhO1, GrhO3, GrhO5, GrhO6, GrhO7 and the protein GrhJ in the construction of the epoxyspiroketal moiety of griseorhodin A **(5)** via four complex bond cleavages and the loss of two carbon units.

The investigation of the metabolites for the first part of the biosynthesis showed that the early intermediates are very unstable. Metabolites in the plate extracts of the knockout strains of suggested early oxygenases were different from the metabolites obtained from their fermentation extracts. Large amounts of green and black unidentified pigments in the fermentation extracts of the strains *S. albus* KR11, *S. albus* KR40 and *S. albus* KR15 prevented the isolation of the metabolites detected by HRMS analysis. Therefore the functions of *grhO8*, *grhL*, and *grhP* could not be determined exactly. However, structures of two isolated

metabolites from the extracts of *grhM, grhO8* and *grhO9* gene deletion strains, the amounts and the molecular formulae of the metabolites detected by HRMS analysis and sequence homology results provided additional information that enabled the suggestion of a preferred biosynthetic pathway for the early tailoring steps of griseorhodin A **(5)**. Figure 3.102 shows the proposed early tailoring steps and the participation of enzymes in the early oxygenation reactions.

The presence of the metabolite KS-619-1 **(64)** in the fermentation extracts of *grhM* and *grhO8* mutants could be proven as described in Section 3.4.7 and 3.4.8. The structure of KS-619-1 **(64)** implies that the two oxygenases GrhM and GrhO8 act prior to the lactonization and methylation reactions. The metabolite has an antraquinone Western part due to an oxidation at ring B, which might be a result of a spontaneous oxidation of an unstable pradimicin type intermediate. Analysis of the structure of KS-619-1 **(64)** suggests structure **(71)** as an earlier intermediate. However, the possibility of an enzymatic oxidation cannot be excluded. In that case, KS-619-1 **(64)** would be an early intermediate of an alternative oxidation cascade. The other two metabolites predominantly produced by the *grhM* mutant strain with a molecular formula $C_{26}H_{18}O_8$ and fewer oxygen atoms than the metabolites produced by the *grhO8* mutant strain indicate that the two oxygenases act rather in series than simultaneously.

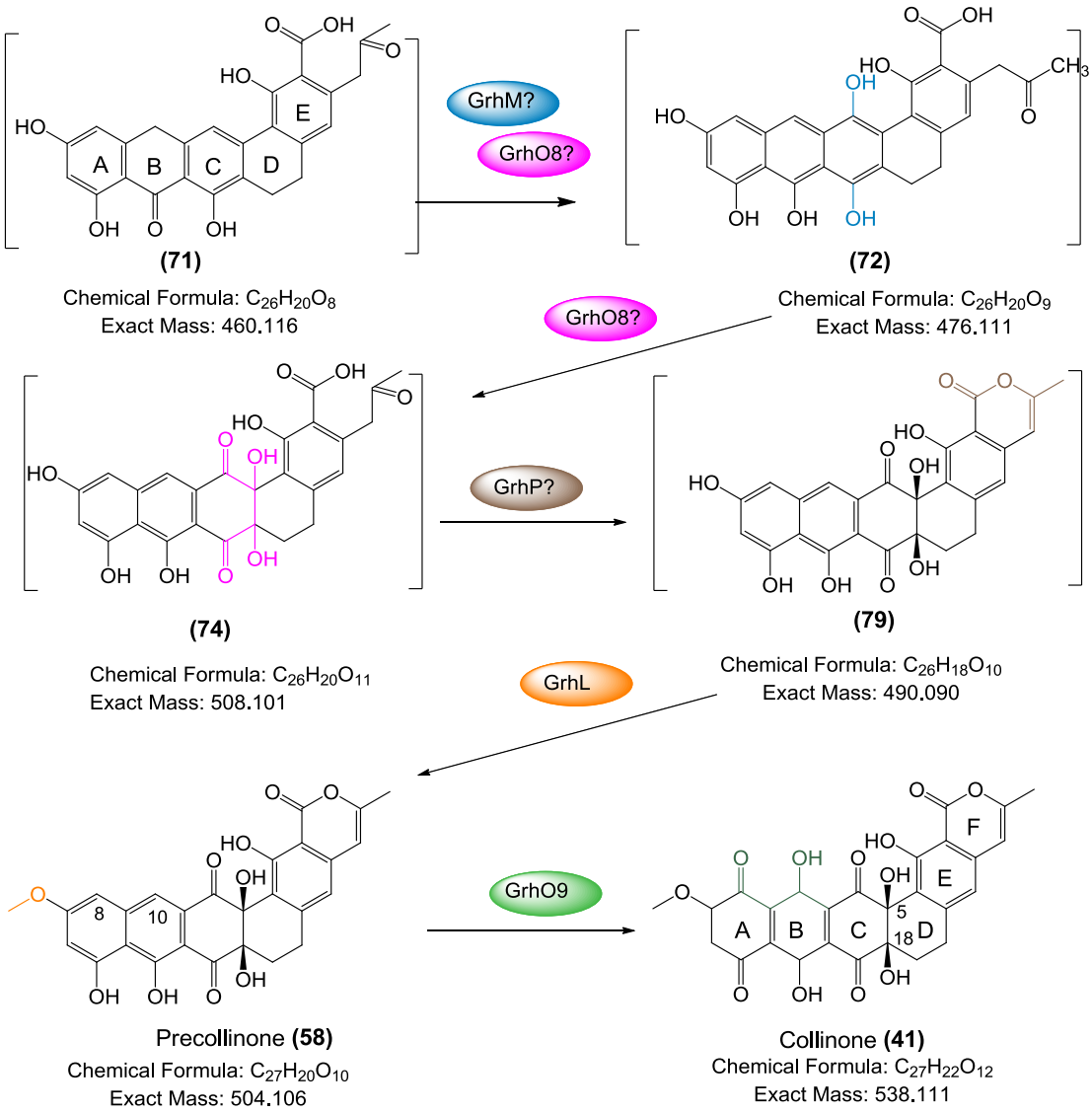

Figure 3.102 A. Proposed early oxidation steps leading to the formation of collinone **(41)** starting with the pradimicin-type intermediates. The structures in the parentheses are suggested intermediates.

The investigation of the early tailoring steps of the aromatic polyketide fredericamycin A **(26)** showed that two aromatic hydroxylases, FdmM and FdmM1, which have high sequence similarities to the oxygenases GrhM and GrhO8, are acting in series and add three hydroxyl groups to the aromatic pentangular core. FdmM is an aromatic hydroxylase and stabilizes the substrates of the oxygenase FdmM1 during the early biosynthesis steps of fredericamycin A **(26)** as described in Section 3.4.7 (Figure 3.80).[152] The structure of the isolated intermediate KS-619-1 **(64)** and the sequence

homology of GrhM and GrhO8 allow suggesting that the two oxygenases act as hydroxylases like FdmM and FdmM1 at the rings C and D. In that case, GrhM would first hydroxylate ring C and GrhO8 would perform the oxidation reactions on ring D. A similar dihydroxylation reaction was published by Daum *et al*. for the monooxygenase PokO2 in polyketomycin **(76)** biosynthesis.[142] In that case PokO1 hydroxylates ring C. Subsequently, PokO2 performs a dihydroxylation at ring D. The dihydroxylation reaction is initiated by a proposed epoxidation reaction with a subsequent ring opening with addition of a water molecule that results in a *cis* configuration of the hydroxyl groups at ring D as described in Section 3.4.8 (Figure 3.89).[142] Further experiments with thegene deletion mutants of *ΔpokO1*, *ΔpokO2* and *ΔpokO1*/ *ΔpokO2* showed that the enzyme PokO1 can take over the functıon of PokO2.[142]

The predominant metabolites produced by the *grhP* and *grhL* mutant strains with the suggested molecular formulae $C_{26}H_{18}O_{11}$ and $C_{26}H_{16}O_{10}$, respectively, imply that the lactonization of ring F takes places before the methylation reaction at ring A. Both strains produced large amounts of unidentified green and brown pigments during fermentation. These pigments prevented the isolation of any metabolites from the fermentation extracts as described in Section 3.4.9. Investigations of the extracts point to the presence of random polymerization products of easily oxidized metabolites. GrhL is the only methyl transferase gene found in the cluster. Therefore it is very likely that GrhL is responsible for the methylation at ring A. GrhP does not show homology to oxygenases. However, its sequence has sequence homology to several putative and proven asparagine synthetases, such as RubR in γ-rubromycin, LlpA in lysolipin X, OxyD in oxytetracyclin, PdmD in pradimicin, and FdmV in fredericamycin A biosynthetic pathways. Proposed function of PdmD and FdmV is transfer of an amine function of an amino acid to the polyketide scaffolds of pradimicin. The function of FdmV as a tailoring enzyme at the generation of the lactam ring F in the biosynthesis of fredericamycin A **(26)** has been demonstrated.[155] Both polyketides have a lactam ring in their scaffolds. However, rubromycins and griseorhodin A **(5)** have lactone rings. The sequence homology to the lactam generating PdmD and FdmV suggests a function of GrhP in the lactonization of ring This assumption needs to be proven by further

investigation of the enzyme GrhP and/or the metabolites that were produced in miniscul amounts.

Precollinone **(58)** was produced by the *grhO9* mutant strain as a major metabolite during the early tailoring steps. The compound was produced both in plate and fermentation extracts as a stable metabolite. This indicates that the methylation of ring A and the lactonization of ring F, which stabilizes the intermediates of early tailoring enzymes, are key reactions for the stability of the aromatic pentangular metabolites. Precollinone **(58)** is hydroxylated at rings C and D, but not at rings A or B. This shows that GrhO9 participates in the oxidation of rings A and/or B on route to collinone **(41)**. The structures of precollinone **(58)** and KS-619-1 **(64)** raise questions about the oxidation sequence at rings A, B, C.

One possible explanation is that GrhO9 and several other tailoring enzymes can utilize alternative metabolites and substrates leading to the generation of collinone **(41),** and the metabolite precollinone **(58)** is the predominant substrate produced in the absence of GrhO9. In this case many early tailoring enzymes would not act on specific substrates and oxygenation reactions of the early oxygenases would provide several products, which could be further processed by alternative oxygenation cascades on the multienzyme complex. This would also explain the numerous metabolites observed in the early tailoring steps leading to the compound precollinone **(58)**. However, further functional investigation of these particular oxygenases is necessary to determine their substrate specificity and/or substrate range.

At this point it would be necessary to mention a successful attempt of Kathrin Reinhardt to obtain a hybrid product, benarhodin A **(78)**, of the polyketides griseorhodin A **(5)** and benastatin A **(77)** as described in Section 3.4.9 (Figure 3.92) .[125] For this combinatorial approach the minimal PKS of the *grh* cluster was replaced by the minimal PKS of benastatin A cluster. This experiment showed that the early oxygenases of *grh* cluster are able to perform tailoring reactions on the polyketide backbone produced by benastatin A minimal PKS. This indicates that the early tailoring enzymes might have a larger substrate range.

Another possible explanation for the oxidation at the aromatic core of KS-619-1 **(64)** is that KS-619-1 **(64)** is a spontaneous oxidation product of an unstable pradimicin-type metabolite, such as **(71)**. Excessive production of diverse pigments during fermentation described at Section 3.4.8 and 3.4.9 also suggests that the substrates of the early enzymes might undergo spontaneous reactions during fermentation, such as oxidation and polymerization. In this case the possibility of a preferred pathway leading to the generation of collinone **(41)** as postulated in Figure 3.102 could be expected. However, it is extremely difficult to identify intermediates for the biosynthetic steps up to the formation of the relatively stable compound precollinone **(58)** due to the unstable and diverse metabolites produced by the mutant strains. In addition, further investigation of the tailoring enzymes GrhU and GrhV, which could not be related to the biosynthetic steps yet, might reveal further insights into the early biosynthetic steps.

The results presented in this thesis provide deeper understanding of the complex tailoring steps and enzymes taking part in the biosynthesis of griseorhodin A **(5)** and related rubromycin-type spiroketal compounds. These new insights to the griseorhodin A biosynthesis also contribute to the ongoing research in utilizing polyketide tailoring enzymes to create novel polyketide libraries to obtain new polyketide lead-structures via combinatorial biosynthesis. However, additional functional assays and combinatorial studies using genes with suspected cooperative activity need to be conducted to obtain further information about the individual mechanism and substrate specificities of these numerous interesting tailoring enzymes.

4 MATERIALS AND METHODS

4.1 Molecular Biological Materials and Methods

4.1.1 Solutions and Media

The following ingredients were purchased for the preparation of broth and media; Tryptone (Becton Dickinson, Heidelberg), yeast extract (Becton Dickinson, Heidelberg), soja flour (Bacto Saitone, Becton Dickinson, Heidelberg), tryptic soy broth (Difco, USA), beef extract (Roth, Karlsruhe), acid casein hydrolysate (Roth, Karlsruhe) potato starch (Sigma-Aldrich, Seelze), agar-agar (Roth, Karlsruhe).

4.1.1.1 LB - (Luria Bertani) Medium and Agar

10 g NaCl, 10 g tryptone, 5 g yeast extract were dissolved in 1 L of distilled water. The pH of the LB medium was adjusted to 7 with 1 N NaOH solution. The mixture was autoclaved for 20 min at 120 °C.

To prepare LB agar, 1 L of LB medium was prepared, and 15 g agar-agar was added into it. The mixture for the agar was autoclaved 20 min at 120 °C.

To prepare both LB-Apr^{10} medium and agar containing the antibiotic apramycin, the mixtures for both the medium and agar were both autoclaved and cooled down to 50-60 °C. 1 mL of the apramycin stock solution with a concentration 10 mg/mL was added both to a total volume of 1 L of LB medium and to agar.

4.1.1.2 TSB Medium

30 g Tryptic soy broth was dissolved in 1 L of distilled water. The mixture was autoclaved 20 min at 120 °C.

4.1.1.3 MS Agar

For the preparetation of 1 L of MS agar, 20 g agar-agar, 20 g mannitol, 20 g soja flour (Bacto Saitone) were used, and distilled water was added to a total volume

of 1 L. 5 mL of a 2 M $MgCl_2$ solution were added to the mixture and the mixture was autoclaved twice at 120 °C for 15 min.

To prepare both MS-Apr[10] medium and agar containing the antibiotic apramycin, the mixtures for both the medium and agar were autoclaved and cooled down to 50-60 °C. 1 mL of an apramycin stock solution with a concentration 10 mg/mL was added to the 1 L of the mixture.

4.1.1.4 2CM Agar

20 g agar-agar, 10 g soluble potato starch, 2 g tryptone, 1 g NaCl, 2 g $(NH_4)_2SO_4$, 1 g K_2HPO_4, 2 g $CaCO_3$, 2 g $MgSO_4 \cdot 7H_2O$ were used, and distilled water was added to achieve a total volume of 1 L. 1 mL Inorganic salt solution was added into the mixture and the mixture was autoclaved for 20 min at 120 °C. For preparing 2CM -Apr[10] agar containing the antibiotic apramycin, the mixtures for both the medium and agar were autoclaved and cooled down to 50-60 °C. 1 mL of an apramycin stock solution with a concentration 10 mg/mL was added to 1 L of the both mixtures.

Ingredients for the inorganic solution needed to prepare 2CM agar

1 g $FeSO_4 \cdot 7H_2O$, 1g $MgCl_2 \cdot 6H_2O$, 1g $ZnSO_4 \cdot 7H_2O$ were used and distilled water was added to achieve a total volume of 1 L. The mixture was autoclaved for 20 min at 120 °C.

4.1.1.5 MM Agar (Müller Minton Agar)

2 g Beef extract, 17.5 g acid casein hydrolysate, 1.5 g potato starch, 17 g agar were used, and distilled water was added to achieve a total volume of 1 L. The mixture was autoclaved for 20 min at 120 °C.

4.1.2 Methods for the Storage and Cultivation of the *S. albus* Strains

4.1.2.1 Storage of Strains

For long-term storage of *S. albus* strains, spores were suspended in a solution of 20% (v/v) glycerol and stored at -80 °C. For storage of the strains up to 3

months, strains were grown overnight in 200 mL of LB medium and the culture was transferred into 50 mL Falcon tubes to harvest the bacteria by centrifuging at 5000 rpm. Bacteria were washed twice with a sterile 10.3% (w/v) sucrose solution. Subsequently, bacteria were resuspended in 10 mL of the sucrose solution, transferred into 10 mL Falcon tubes and stored at -20 °C.

4.1.2.2 Cultivation on Agar Plate

S. albus strains were plated on 2CM and MS agar plates. Also 2CM-Apr^{10} and MS-Apr^{10} agar plates were used in cases where the cultures were contaminated with other bacteria. Sterile toothpicks were used to pick single colonies. To obtain a larger amount of bacteria for extractions, bacteria were plated with a sterile cotton bud on the agar plates, and depending on the growth and expression of the strain, plates were incubated up to 6 days.

4.1.2.3 Cultivation and Fermentation of Mutant Strains in Liquid Medium

S. albus strains were fermented in LB, TSB and MS media. For fermentation baffled flasks of volume up to 2 L were used. The medium occupies 20% of the flask volume to provide the bacteria enough oxygen supply needed during fermentation. For inoculation of the larger scale fermentations with several flasks, an overnight culture of the strain was used and distributed in equal amounts to the flasks containing the medium.

4.1.2.4 Freeze-Drying for Storage and Extraction of Mycelium

Bacteria obtained from fermentation were harvested by centrifugation. The obtained mycelia were resuspended in 100 mL of distilled water and were transferred into 1 L round flasks. The suspension was frozen with liquid nitrogen. The flasks were left to dry overnight in the freeze drier. Subsequently, flasks were filled with argon gas to avoid the decomposition of the compounds on the dry mycelia during their storage.

4.1.3 Methods for the Storage and Cultivation of the Strains Used for the Antibacterial Activity Assays

Strains chosen for the tests are following:

- *Escherichia coli*-DH5α (Gram-)
- *Staphylococcus carnosus*-DSH 20501 (Gram+)
- *Bacillus amyloliquefaciens* (Gram+)
- *Bacillus subtilis* (Gram+)
- *Pseudomonas fluorescens*-DSH 50090T (Gram-).

4.1.3.1 Storage of Strains

For the long-term storage of strains, 750 µL of overnight cultures in LB medium were mixed with a 750 µL of 30% (v/v) glycerol solution. The mixture was frozen with liquid nitrogen and was stored at -80 °C.

4.1.3.2 Cultivation of the Strains for the Antibacterial Assay

For the antibacterial assay, strains were grown on MM agar and incubated at 37 °C over night. For the MIC assay, bacteria were grown on LB medium and incubated at 37 °C at 220 rpm over night.

4.1.4 Analytical and Chemical Materials and Methods

4.1.4.1 Thin Layer Chromatography and Column Chromatography

For the thin layer chromatography, silica gel 60 F_{254} 20x20 cm plates (layer thickness 0.2 mm, Merck) were used. Dipping in a 2 M NaH_2PO_4 solution impregnated the plates as discriebed in Section 4.1.4.2. For the column chromatography, a silica gel 60, 40-63 µm (Roth) material was used. For the impregnation of the silica plates, 2 M NaH_2PO_4 solution was used. The silica material, which was used for column chromatography was impregnated with a 2 M NaH_2PO_4 solution as well.

4.1.4.2 Procedure for Impregnation

200 mL of silica were stirred overnight in 400 mL of 2 M NaH_2PO_4 solution. The gel was poured into glass plates and left to dry in a dry oven at 100 °C overnight. Impregnation of the silica gel was necessary for the chromatographic separation of polar phenolic compounds. Depending on the pK_a value, these compounds become deprotonated and form strong interactions on silica materials. Impregnation of the silica plates results in full protonation and decrease of polarity of the analytes, thus improving chromatographic behaviour. For the chromatography, a mobile phase either chloroform:methanol (9:1) or chlorofom:ethyl acetate (4:1) was preferred. The NaH_2PO_4-impregnated silica material can be used for a mobile phase up to 25% of methanol. Higher percentages of methanol should be avoided because of the elution of salts during chromatography.

4.1.4.3 Sephadex LH-20 Gel Chromatography

Sephadex material (Sephadex LH-20, Bead size: 25-100 µm, Sigma) was used for gel chromatographic separation. Gel chromatographic separation takes plates according to the mechanism that the analytes with higher molecular weight elute slower than the analytes with smaller molecular weight. Sephadex LH-20 powder purchased was made to swell overnight in methanol without stirring. The obtained Sephadex LH-20 gel was pured in glass columns and used for chromatographic separation of the compounds in the extracts. As a mobile phase methanol was used.

4.1.4.4 Analytical and Semipreparative HPLC

For the LC-HRMS measurements, a Jasco 2000 Plus series HPLC device with a Jasco pump PU-2080 and a Jasco autosampler AS2050 was used. For the analysis of the extracts, an PerfectChrom 100 C18 reverse-phase analytic column (250 mm × 4 mm, 5 μm) at a flow rate of 1 mL min^{-1} was used. As mobile phase, acetonitrile:water containing 0.1% TFA was used. For the purification of the substances, extracts were subjected on a PerfectChrom 100 C18 reverse-phase semipreparative column (250 mm × 8 mm, 5 μm) at a flow rate of 6 mL min^{-1} and a mobile phase acetonitrile:water containing 0.1% TFA was used. The

compounds were detected with a Jasco MD-2015 PDA detector. The UV spectra was recorded between 220 and 600 nm. The unsaturated compounds were detected at 254 nm. As characteristic absorption maxima the wavelengths of 360 nm was selected for detection of polyaromatic phenols, and the wavelangth of 488 nm for aromatic quinone compounds. The fact that aromatic compounds having a quinone structure in their scaffold have a specific absorption maximum at 488 nm helped to identify the compounds in the extracts, related to griseorhodin A **(5).** The gradients used for the separation are as described below.

For the LC-HRMS measurements, an Agilent 1200 Series HPLC device and a Nucleodur 100-5 C18 column (100 mm × 4 mm, 5 μm) with a flow 0.4 mL/min were used. For the detection of the compounds a Bruker micrOTOF-Q time-of-flight mass spectrometer and an Agilent 4000 UV spectrometer, which makes detection at the wavelength 254 nm, was used. LC Methods and solvents were the same as the methods used for the HPLC. The only difference was that the flow rate had to be reduced to adapt to the LC column.

4.1.4.5 HPLC Methods

Analytical method 1: A 10-90 % to 95-5% AN:H_2O + 0.1% TFA gradient was used over 20 min at a flow rate of 1.5 mL min^{-1}.

Analytical method 2: A 10-90% to 95-5% MeOH:H_2O gradient was used over 20 min at a flow rate of 1 mL min^{-1}.

Analytical method 3: A 20-80% to 100-0% AN:H_2O + 0.1% TFA gradient was used over 15 min at a flow rate of 1 mL min^{-1}.

Preparative method 1: A 25-75% to 100%-0% AN:H_2O + 0.1% TFA gradient was used over 25 min at a flow rate of 6 mL min^{-1}.

Preparative method 2: A 60-40% to 100%-0% MeOH:H_2O gradient was used over 25 min at a flow rate of 4 mL min^{-1}.

Preparative method 3: A 60-40% to AN:H_2O + 0.1% TFA gradient was used over 25 min at a flow rate of 6 mL min^{-1}.

4.1.4.6 UV Spectrometry

The compounds' UV spectra were recorded with a Jasco MD-2015 PDA detector at the wavelengths ranging from 220 nm to 600 nm.

4.1.4.7 IR Spectrometry

The compounds' IR spectra were recorded as a film on a Nicolet 380 FT-IR spectrometer (Thermo Scientific). Measured IR spectra are in Appendix 3.

4.1.4.8 Optical Rotation

Polarimetric measurements were performed with a Perkin-Elmer 340 polarimeter at the wavelength of 589 nm at 20 °C. 1 dm long cuvettes were used to measure the samples. A solution with a concentration up to $5x10^{-3}$ g/100 mL of the compounds with the solvent $CHCl_3$ was used for the measurement.

4.1.4.9 CD Spectrometry

CD spectrometry of the compounds and the quantum chemical calculation of the spectral data were performed by the group of Prof. Bringmann at the University of Würzburg as described in the literature. [13]

4.1.4.10 Mass Spectrometry

ESI-HRMS (Electrospray high-resolution mass spectra) and collision-induced dissociation (CID) MS^n spectra were recorded on a Bruker micrOTOF-Q time-of-flight mass spectrometer and a Bruker APEX IV Fourier-transform ion cyclotron-resonance (FT-ICR) mass spectrometer with a 7.05 T magnet. Both instruments were equipped with an Apollo electrospray ion source. Analyte solutions in acetonitrile were introduced into the ion source with a syringe pump (Cole-Parmers Instruments, Series 74900) at flow rates of 3 to 4 µL min^{-1} or with an Agilent HPLC pump (1200 series) at a flow rate of 50 µL/min. Ion transfer into the first of three differential pump stages in the ion source occurred through a glass capillary with 0.5 mm inner diameter and nickel coatings at both ends.

For the (CID) MS^n measurements, fragmentation of the compounds was achieved, in which the molecule ions were accelerated in an electrical potential and fragmented through collision with the utilized inert gas argon in the gas phase. The fragment ions were analyzed by a Bruker APEX IV Fourier-transform ion cyclotron-resonance (FT-ICR) mass spectrometer.

ESI-MS/Tandem–MS (MS/MS)/MS^n measurements were recorded on a Bruker micrOTOF-Q time-of-flight mass spectrometer (Bruker, Carlsruhe, Germany) For the ESI-MS/Tandem–MS (MS/MS)/MS^n measurements, observation of the charged molecular ions and fragments are achieved, in which the compounds are dispersed by electrospray into an aerosol using acetonitrile and water, thus enabling ionization to positive or negative charged molecular ions depending on the properties of the compound.

For the HR-LCMS measurements, an Agilent 1200 Series HPLC device and a Nucleodur 100-5 C18 column (100 mm × 4 mm, 5 μm) at a flow rate of 0.4 mL/min were used. For the detection of the compounds a Bruker micrOTOF-Q time-of-flight mass spectrometer and an Agilent 4000 UV spectrometer at the wavelength of 254 nm were used. For the calibration, sodium formiate was used as an internal standard.

LC methods applied to separate the compounds were adapted from the analytical HPLC methods in the section for HPLC analysis.

4.1.4.11 NMR-Spectrometry

^{1}H-NMR and ^{13}C-NMR, DEPT, HMBC, HMQC spectra were recorded on a Bruker ADVANCE DPX 400 and DRX 500 device at 400 MHz and 500 MHz, respectively, in either DMSO-d_6 or $CDCl_3$ (if not indicated otherwise) using the solvent signals as the reference. Measured IR spectra are in Appendix 2.

NMR measurements for collinone **(41),** and the compounds less than 5 mg were carried out in a cooperation with Dr. Harald Gross at the Pharmaceutical Institute at University of Bonn on a Bruker device at 300 MHz. The temperature experiments were also done in the same facility.

LC-NMR measurement for the compound ZY1 **(54)** was performed at a Bruker ADVANCE DPX 400 device in cooperation with Michael Lalk at the University of Greifswald.

4.1.5 Procedures for the Isolation

4.1.5.1 Determination of the Growth and Production Curve of *S. albus* MP66

1 liter of LB medium inoculated with *S. albus* MP66 was prepared and distributed into ten 250 mL baffled Erlenmeyer flasks so that each flask contained 100 mL of culture. The bacteria were incubated at 30 °C in a shaker at 220 rpm. During a period of five days, one of the Erlenmeyer flasks containing 100 mL culture was taken out, and the time of incubation was noted two times a day, in the morning and in the afternoon. Bacteria and culture medium were separated by centrifugation at 10000 rpm for 10 minutes. To measure growth, the bacteria were freeze-dried and weighed in order to determine the changes of the biomass in each Erlenmeyer flasks. To measure secondary metabolite production, the absorption of the culture medium at 488 nm was used, since most produced metabolites have a characteristic absorption at 488 nm.

4.1.5.2 Extraction of *S. albus* Strains for HPLC, HRMS and TLC Analysis

To obtain an overview of the metabolites, strains were incubated 2-3 days at 30 °C on 2CM agar plates. The bacteria with pigments were scratched off, extracted eather with EtOAc:MeOH:AcOH (95:5:1) or acetonitrile with 0.1% TFA. An ultrasound bath was used to obtain better solubility and to destroy the bacterial wall. The bacterial residues were removed by centrifugation, and subsequently, the solvents were removed by a SpeedVac concentrator. The remaining crude extract was solved in 0.5 mL ethyl acetate to use for the TLC analysis.

For the HPLC and LCMS analysis, the prepared cell extract was dissolved in 0.5 mL of AN, and the HPLC method 1 (Section 4.1.4.5) was used. The molecular weight of the compounds were determined by LC-HRMS after the same bacterial extract was dissolved in MeOH or AN. ESI-HRMS and ESI-MS/Tandem-(MS/MS)

spectra were recorded on a Bruker microTOF-Q time of flight mass spectrometer.

4.1.5.3 General Procedure for the Extraction of *S. albus* Liquid Cultures

After the fermentation of the various strains in liquid medium, the mycelium and the liquid medium were separated by centrifugation, as described by Eckardt *et al*. for the isolation of griseorhodin A **(5)**.[85] The separated mycelium was extracted with a mixture of EtOAc:MeOH:AcOH (95:5:1). The solvent was removed. After acidification to pH 4 with 2 N HCl the separated medium was extracted with ethyl acetate. The organic phase was dried with Na_2CO_3. The solvent was removed at a rotary evaporator.

4.1.5.4 General Procedure for the Chromatographic Analysis and Purification of the Liquid Culture Extracts of *S. albus* Strains

For the TLC analysis of the prepared bacterial extracts, the crude extract was dissolved in the mobile phase $CHCl_3$:MeOH (9:1). As stationary phase, impregnated silica plates with 2 M NaH_2PO_4 or KH_2PO_4 were used. It was advantageous to use impregnated plates since they simplified the separation of polar compounds. Impregnating the silica material before use prevents the polar aromatic phenolic compounds to attach on the material. Depending on the pK_a value, these compounds become deprotonated and form strong interactions on silica materials. Impregnation of the silica plates results in full protonation and decrease of polarity of the analytes, thus improving chromatographic behaviour. The same principle also helps during flash chromatographic purification of the extracts containing phenolic aromatic compounds. The procedure of the impregnation is given in 4.1.4.2 in detail.

4.1.5.5 General Procedure for the Isolation and Characterization of the Compounds

For structure elucidation purposes, approximately 10 mg of compound was needed. Therefore, fermentation of the strains in liquid medium rather than on plates was performed to obtain this amount. The inoculates used for the fermentations were frozen stocks of strains kept in the -80 °C freezer or frozen

cultures in 10.3% sucrose solution stored at -20 °C. These procedures used for storing *S. albus* strains are given in the Section 4.1.2. The strains were tested for a suitable growth medium and fermented 4 to 6 days. The fermentation broth was centrifuged, and the mycelium was extracted separately from the fermentation broth. The aromatic pigments produced by the strains were usually accumulating on the surface of the bacterial cell wall so that most of the interesting compounds were isolated from mycelium extract. To increase the solubility of the compounds, the cells were acidified with an acidic solution of water to pH 3-4, left in ultrasound bath for 20 minutes and later extracted several times with ethyl acetate. The growth medium was also acidified to pH 3-4 and extracted several times with ethyl acetate as well. After removing the solvent at a rotary evaporator, the crude extract was purified using flash silica and Sephadex LH-20 column chromatography depending on the characteristic of the extract. Final purification was performed with HPLC.

4.1.5.6 Procedure for the Isolation of Griseorhodin A (5)

For the isolation of griseorhodin A **(5)**, *S. albus* MP31 spores were inoculated into 100 mL of LB medium and grown overnight. This seed culture was used to inoculate 9 L of LB medium, which was distributed to fifteen 1 L baffled flasks. Flasks were incubated at 220 rpm for 5 days at 30 °C. For compound isolation, the mycelia were harvested by centrifugation and suspended in 300 mL of H_2O. The pH of the mixture was adjusted to 3-4 with TFA. After extraction with 200 mL of EtOAc for 3 times, the combined extracts were fractionated by flash column chromatography on impregnated silica with a mobile phase $CHCl_3$:MeOH (9:1). Further fractionation was done by Sephadex LH-20 gel filtration and the substances were eluted with methanol. Fractions containing griseorhodin A **(5)** were combined, dried, and further purified by semipreparative HPLC on a MN-Nucleodur-100 RP18 column with a gradient CH_3CN:H_2O +0.1% TFA (25:75) to CH_3CN:H_2O +0.1% TFA (90:10) in 25 min. The yield of the isolation was 17 mg. The identity of the compound was confirmed by both ^{1}H-NMR analysis in DMSO-d_6 and HRMS data. The molecular ion $[M+H]^+$ of griseorhodin A **(5)** with the molecular formula $C_{25}H_{16}O_{12}$ was detected in the

HRMS analysis at 509.0691 (509.072 is calculated $[M+H]^+$). Spectral data found to be identical with the spectral data in the literature.[14,112]

^{1}H-NMR spectrum was recorded on a Bruker ADVANCE DPX 400 device. A Jasco MD-2015 PDA HPLC detector was used to obtained the UV spectrum of the compound. The IR spectrum was recorded as a film on a Micolet 380 FT-IR spectrometer. Polarimetric measurement of the compound was performed with a Perkin-Elmer 340 polarimeter at 589 nm at 20 ˚C.

4.1.5.7 Procedure for the Isolation of Didesoxygriseorhodin C (46)

For the isolation of the compound, *S. albus* KR7 spores were inoculated into 100 mL of LB medium and grown overnight. The resulting seed culture was used to inoculate 6 L of LB medium, which was distributed to fifteen 1 L baffled flasks, so that each flask contained 400 mL culture. These were incubated at 220 rpm for 6 days at 30 °C. For the isolation, the mycelia were harvested by centrifugation and suspended in 300 mL of H_2O. The pH of the mixture was adjusted to 3-4 with TFA. After extraction with 200 mL of EtOAc for 3 times, the combined extracts were fractionated by flash column chromatography on impregnated silica with a mobile phase $CHCl_3$:MeOH (9:1). Fractions containing didesoxygriseorhodin C **(46)** were combined, dried, and further purified by semipreparative HPLC on a RP18 column with a gradient CH_3CN:H_2O+0.1%TFA (25:75) to CH_3CN:H_2O+0.1% TFA (90:10) in 25 min. This procedure yielded 16 mg of pure compound. The molecular formula was deduced by ESI-HRMS analysis as $C_{25}H_{18}O_{11}$ (494.089 measured $[M+H]^+$, 494.085 calculated $[M+H]^+$). The identity of the compound was confirmed by one- and two-dimensional NMR analysis in DMSO-d_6. A literature survey showed that didesoxygriseorhodin C **(46)** was isolated formerly by Suetsuna *et al*. All spectral data were identical with the published data. [126-128]

^{1}H-NMR, ^{13}H-NMR, HMBC and HMQC spectra were recorded on a Bruker ADVANCE DPX 400 device. A Jasco MD-2015 PDA HPLC detector was used to obtain the UV spectrum of the compound. The IR spectrum was recorded as a film on a Micolet 380 FT-IR spectrometer. Polarimetric measurement of the

compound was performed with a Perkin-Elmer 340 polarimeter at 589 nm at 20 ˚C.

4.1.5.8 Procedure for the Isolation of Collinone (41)

For the isolation of collinone **(41)**, *S. albus* KR8 spores were inoculated into 100 mL of TSB medium and grown overnight. The resulting culture was used to inoculate 6 L of TSB medium, which was distributed to 500 mL Erlenmeyer flasks with a stainless steel spring, so that each flask contained 200 mL medium for production. Flasks were incubated in shaker for 4 days at 30 °C at 200 rpm. For the extraction of the compounds, the mycelia were harvested by centrifugation and the acidity was adjusted to pH 2 with a 2 N HCl solution. Afterwards, the mixture was extracted with ethyl acetate for 3 times. The combined extracts were fractionated by flash chromatography on NaH_2PO_4-impregnated silica gel column eluted with a mobile phase $CHCl_3$:MeOH (9:1). The compound was detected via TLC and HPLC in column fractions and fractions needed were combined and dried. Further purification was carried out by preparative HPLC using a PerfectChrom 100 C18 reverse-phase semipreparative column (250 mm x 8 mm, 5 μm) with UV detection at 254 nm and 488 nm using a Jasco MD-2015 PDA detector. A 25%-75% to 40%-60% CH_3CN:H_2O+0.1% TFA gradient was used over 22 min at a flow rate of 6 mL min^{-1}. As a result 8 mg of pure collinone **(41)** was obtained. The identity of the compound was confirmed both by ESI-HRMS analysis (*m/z*: 557.067 $[M+Na]^+$) and by one- and two-dimensional NMR analysis in $CDCl_3$. All spectral data were found to be identical with published data. [137]

^{1}H-NMR, ^{13}H-NMR, HMBC and HMQC spectra were recorded on a Bruker DPX 300 device. A Jasco MD-2015 PDA HPLC detector was used to obtain the UV spectrum of the compound. The IR spectrum was recorded as a film on a Micolet 380 FT-IR spectrometer. Polarimetric measurement of the compound was performed with a Perkin-Elmer 340 polarimeter at 589 nm at 20 ˚C.

4.1.5.9 Procedure for the Isolation of Lenticulone (53)

For the isolation of the compound MP66a, which was later renamed as lenticulone **(53)**, *S. albus* MP66 was grown in 12 L of LB medium which was

distributed to 1 L baffled flasks, so that each flask contained 400 mL culture. After incubation at 220 rpm for 4 days at 30 °C, the bacteria were harvested by centrifugation and suspended in 400 mL of H_2O. The solution was acidified to pH 3-4 with TFA and extracted for 3 times with 300 mL of ethyl acetate. To prevent decomposition of the compound during solvent removal, most of the TFA was back extracted with H_2O for 2 times. The crude extract was fractionated by flash column chromatography on impregnated silica with a mobile phase $CHCl_3$:EtOAc (5:1). Fractions containing the compound were combined and dried, and further purification was carried out by preparative HPLC using a PerfectChrom 100 C18 reverse-phase semipreparative column (250 mm x 8 mm, 5 μm) with UV detection at 254 nm and 488 nm using a Jasco MD-2015 PDA detector. A 25%-75% to 100%-0% CH_3CN:H_2O+0.1% TFA gradient was used over 25 min at a flow rate of 6 mL min^{-1}. The yield of the isolation was 20 mg of lenticulone **(53)**. The identity of the compound was confirmed by both ESI-HRMS/MS analysis for the molecular ion $[M+H]^+$ as $C_{26}H_{16}O_{12}$ (*m/z* = 521.0714, calcd. 521.0720) and one- and two-dimensional NMR analysis in $CDCl_3$.

^{1}H-NMR, ^{13}H-NMR, HMBC and HMQC spectra were recorded on a Bruker ADVANCE DPX 400 device. A Jasco MD-2015 PDA HPLC detector was used to obtain the UV spectrum of the compound. The IR spectrum was recorded as a film on a Micolet 380 FT-IR spectrometer. Polarimetric measurement of the compound was performed with a Perkin-Elmer 340 polarimeter at 589 nm at 20 °C.

4.1.5.10 Procedure for the Isolation of ZY1 (54)

For the isolation of ZY1 **(54)**, *S. albus* MP66 was grown in 12 L of LB medium, which was distributed to 500 mL flasks with stainless-steel springs, so that each flask contained 200 mL culture. Flasks were incubated at 200 rpm for 4 days at 30 °C. Mycelia were harvested by centrifugation and suspended in 400 mL of H_2O. After adjustment to pH 2 with 2 N HCl, the mixture was extracted with 300 mL of EtOAc:MeOH:AcOH (95:5:1) for 3 times. The combined extracts were fractionated by flash column chromatography on impregnated silica with a mobile phase $CHCl_3$:MeOH (9:1). Fractions containing the compound were

combined, dried, and further purification was carried out over Sephadex LH-20 with MeOH as mobile phase. The solvent was removed on a rotary evaporator. The yield of the isolation for the compound ZY1 **(54)** was 6 mg. The molecular ion for the new compound was determined by ESI-HRMS as $[M+H]^+$ of $C_{15}H_{12}O_9$: *m/z* = 337.055, calcd. 337.056. One- and two-dimensional NMR analysis were carried out in AN-d_3.

^{1}H-NMR, ^{13}H-NMR, HMBC and HMQC spectra were recorded on a Bruker ADVANCE DPX 400 device in the LC-NMR facilities of the University Greifswald by Michael Lalk. A Jasco MD-2015 PDA HPLC detector was used to obtain the UV spectrum of the compound.

4.1.5.11 Procedure for the Isolation of Precollinone (58)

For the isolation of the compound, spores of *S. albus* KR53 were inoculated into 100 mL of LB medium and grown overnight. The resultant seed culture was used to inoculate 9 L of LB medium, which was distributed to fifteen 1 L baffled flasks. Flasks were incubated at 220 rpm for 3 days at 30 °C. Subsequently, the mycelia were harvested by centrifugation and freeze-dried overnight. The biomass was suspended in 500 mL of MeOH. After filtering the cell residues, MeOH was removed by a rotary evaporator. 500 mL of water with 0.1% TFA was added to the brown-yellow crude extract. The mixture was stirred for 30 min and extracted for 3 times with 200 mL of ethyl acetate. The combined extracts were filtered on C18-silica before being fractionated on Sephadex LH-20 material with methanol as mobile phase. Fractions containing the compound were combined, dried, and further purification was carried out by preparative HPLC using a PerfectChrom 100 C18 reverse-phase semipreparative column (250 mm x 8 mm, 5 μm) with UV detection at 254 nm and 360 nm using a Jasco MD-2015 PDA detector. A 40-60% to 60-40% CH_3CN:H_2O+0.1% TFA gradient was used over 25 min at a flow rate of 6 mL min^{-1}. The yield of the isolated new compound precollinone **(58)** was 18 mg. The identity of the new compound with the molecular formula C27H20O10 was confirmed by both ESI-HRMS analysis for the molecular ion *m/z* = 505,111 for $[M+H]^+$, calcd. 505.116, and one- and two-dimensional NMR analysis in DMSO-d_6.

^{1}H-NMR, ^{13}H-NMR, HMBC and HMQC spectra were recorded on a Bruker ADVANCE DPX 400 device. A Jasco MD-2015 PDA HPLC detector was used to obtain the UV spectrum of the compound. The IR spectrum was recorded as a film on a Micolet 380 FT-IR spectrometer. Polarimetric measurement of the compound was performed with a Perkin-Elmer 340 polarimeter at 589 nm at 20 °C.

4.1.5.12 Procedure for the Extraction of KR5a

For the extraction of the compound, *S. albus* KR5 spores were inoculated into 100 mL of TSB medium and grown overnight. The resultant seed culture was used to inoculate 12 L of LB medium, which was distributed to fifteen 1 L baffled flasks. Flasks were incubated at 220 rpm for 4 days at 30 °C. For the isolation, the mycelia were harvested by centrifugation and freeze-dried overnight. The dry bacteria were suspended in 500 mL of H_2O with TFA at pH 3. After 10 to 15 minutes, 500 mL of EtOAc was added and stirred overnight in RT. After filtering the solution the EtOAc phase was separated and dried with Na_2CO_3. After removal of solvent in vacuum, 500 mg brown crude extract was obtained from a total of 12 L of fermentation broth.

4.1.5.13 Procedure for the Methylation of KR5a

To a stirred suspension of 500 mg crude extract of *S. albus* KR5 and 10 g anhydrous K_2CO_3 (72.46 mmol) in 90 mL of dry acetone, 14 mL of dimethyl sulfate (DMS) (144.29 mmol) was added dropwise. The mixture was stirred at RT for an hour and then heated under reflux for 24 h at 40 °C. Afterwards the mixture was cooled down to room temperature and diluted with 100 mL of H_2O. After stirring for further 30 min, the mixture was extracted with 300 mL of $CHCl_3$. The organic phase was washed with water to remove the remaining salt. and the solvent was removed to obtain the dry extract. The combined extracts were fractionated by flash chromatography with a mobile phase of $CHCl_3$:EtOAc (1:1). Fractions containing the compound were detected via TLC (Rf: 0.63) and HPLC. Further purification was carried out by preparative HPLC using a PerfectChrom 100 C18 reverse-phase semipreparative column (250 mm x 8 mm, 5 μm) with UV detection at 254 nm and 488 nm using a Jasco MD-2015

PDA detector. A 60-40% to 100-0% CH_3CN:H_2O gradient was used over 25 min at a flow rate of 6 mL/min. Next, a second purification on preparative HPLC was carried out using methanol/water. A method with a 60-40% to 100-0% MeOH:H_2O gradient was used over 25 min at a flow rate of 4 mL/min. The isolated yield of secocollinone-1 **(59)** was 13 mg. The molecular ion of the compound was determined by ESI-HRMS analysis (*m/z*: 635.222 $[M+H]^+$). The structure was confirmed by one- and two dimensional NMR analysis in DMSO-d_6.

^{1}H-NMR, ^{13}H-NMR, HMBC and HMQC spectra were recorded on a Bruker ADVANCE DPX 400 device. A Jasco MD-2015 PDA HPLC detector was used to obtain the UV spectrum of the compound. The IR spectrum was recorded as a film on a Micolet 380 FT-IR spectrometer. Polarimetric measurement of the compound was performed with a Perkin-Elmer 340 polarimeter at 589 nm at 20 °C.

4.1.5.14 Procedure for the Isolation of KR41a

For the isolation of the compound, spores of *S. albus* KR41 were inoculated in 19 L of TSB medium, which was distributed to 1 L baffled flasks, so that each flask contained 400 mL culture. After incubation at 220 rpm for 4 days at 30 °C the bacteria were separated and removed by centrifugation. The medium was extracted with EtOAc . The aqueous phase was acidified to pH 3-4 with a 2 mL/L TFA solution and extracted 3 for times with 300 mL of EtOAc. To prevent the decomposition of the compounds during solvent removal at rotary evaporator, the organic phase was back extracted with 100 mL of H_2O to remove remaining TFA. The crude extract was fractionated by flash column chromatography on impregnated silica with a mobile phase $CHCl_3$:MeOH (9:1). The combined extracts were applied to a Sephadex LH-20 column with methanol as mobile phase. Further purification of the compounds KR41a was carried out by preparative HPLC using a PerfectChrom 100 C18 reverse-phase semipreparative column (250 mm x 8 mm, 5 μm) with UV detection at 254 nm and 475 nm using a Jasco MD-2015 PDA detector. A 60-40% to 100-0% CH_3CN:H_2O+0.1% TFA gradient was used over 25 min at a flow rate of 6 mL/min. The isolated yield of KR41a was 17 mg. The molecular formula was

determined via ESI-HRMS analysis for the molecular ion $[M+H]^+$ as $C_{26}H_{19}O_9$: *m/z* = 475.100 calcd. 475.1029 . One- and two-dimensional NMR analysis of the compound were carried out in DMSO-d_6.

^{1}H-NMR, ^{13}H-NMR, HMBC and HMQC spectra were recorded on a Bruker ADVANCE DPX 400 device. A Jasco MD-2015 PDA HPLC detector was used to obtain the UV spectrum of the compound.

4.1.5.15 Procedure for the Methylation of KR41a

2 ml dimethyl sulfate (21.08 mmol) was added dropwise to a suspension of 17 mg of KR41a and 2 g of anhydrous K_2CO_3 (14.47 mmol) in 15 mL of dry acetone. The mixture was stirred at room temperature for an hour and later heated under reflux for 15 h. The mixture was cooled down to room temperature and diluted with 100 mL of H_2O. After stirring for further 30 min, the mixture was extracted with 100 mL of $CHCl_3$. The organic phase was washed with water and the solvent was removed in vacuum. A yellow crude product was obtained. In the TLC analysis with a mobile phase of $CHCl_3$:MeOH (9:1) at RT a spot was observed with an R_f value of 0.73. Further purification was carried out by preparative HPLC using a PerfectChrom 100 C18 reverse-phase semipreparative column (250 mm x 8 mm, 5 μm) with UV detection at 254 nm and 488 nm using a Jasco MD-2015 PDA detector. A 60-40% to 100-0% CH_3CN/H_2O gradient was used over 25 min at a flow rate of 6 mL/min. Subsequently a second purification was carried out on preparative HPLC using a 60-40% to 100-0% MeOH/H_2O gradient over 25 min at a flow rate of 4 mL/min. The yield of the compound, KS-619-3 **(65),** was 5 mg. The molecular formula of the compound was obtained by ESI-HRMS analysis for the molecular ion $[M+H]^+$ as $[C_{31}H_{29}O_9]^+$: *m/z* =545.1969 $[M+H]^+$ (calcd. 545.1812). The identity of the compound was confirmed by ^{1}H-NMR and ^{13}H-NMR analysis in $CDCl_3$.

^{1}H-NMR and ^{13}H-NMR spectra were recorded on a Bruker ADVANCE DPX 400 device. A Jasco MD-2015 PDA HPLC detector was used to obtain the UV spectrum of the compound. The IR spectrum was recorded as a film on a Micolet 380 FT-IR spectrometer.

4.1.5.16 Procedure for the Isolation of KR41c

For the isolation of the compound, *S. albus* KR41 was grown in 19 L of TSB medium, which was distributed to 1 L baffled flasks, so that each flask contained 400 mL culture. After incubation at 220 rpm for 4 days at 30 °C, the mycelium was harvested by centrifugation, suspended in 50 mL of H_2O and freeze-dried. 250 mL of MeOH was added to the dry mycelium to extract the metabolites, and after stirring for at least an hour, the bacterial residue was removed by filtration. Methanol was removed at a rotary evaporator. The crude extract was washed with $CHCl_3$ and EtOAc to avoid the presence of non-polar lipids during further purification. The residue was acidified with water containing 3 mL/L TFA and extracted for 3 times with 300 mL of EtOAc. To prevent the decomposition of the compounds during solvent removal, TFA was back extracted with H_2O from the organic phase, and the ethyl acetate was removed at the rotary evaporator. The mycelium extract contained mainly the compounds KR41c and KR41c' with a characteristic UV absorption at 360 nm. The extract was dissolved in AN, filtered, and further purification was carried out by preparative HPLC using a PerfectChrom 100 C18 reverse-phase semipreparative column (250 mm x 8 mm, 5 μm) with UV detection at 254 nm and 360 nm using a Jasco MD-2015 PDA detector. The isolated yield of KR41c was 12 mg. The molecular formula was confirmed by the determined molecular ion by ESI-HRMS analysis for $[M+H]^+$ as $[C_{26}H_{19}O_8]^+$: m/z = 459.1050 calcd. 459.1074. One- and two-dimensional NMR analysis was carried out in AN-d_3.

^{1}H-NMR, ^{13}H-NMR, HMBC and HMQC spectra were recorded on a Bruker ADVANCE DPX 400 device. A Jasco MD-2015 PDA HPLC detector was used to obtain the UV spectrum of the compound.

4.1.5.17 Procedure for the Methylation of KR41c

Into a stirred suspension of 10 mg of KR41c and 2 g anhydrous K_2CO_3 (14.47 mmol) in 15 mL of dry acetone, 2 mL dimethyl sulfate (21.08 mmol) was added dropwise. The mixture was stirred at room temperature for an hour, heated under reflux for 15 h, cooled down to room temperature and diluted with 100 mL of H_2O. After stirring further for 30 min, the mixture was extracted with 50

mL of $CHCl_3$, washed with water and the solvent was remived. TLC analysis with a mobile phase of $CHCl_3$:MeOH (9:1) and HPLC analysis of the product showed that the reaction did not yield sufficient amount of substance to carry out a characterization.

4.1.5.18 Procedure for the Isolation of KR11a

For the isolation of the compound KR11a, *S. albus* KR11 was grown in 18 L of TSB medium which was distributed to 1 L baffled flasks, so that each flask contained 400 mL culture. After incubation at 220 rpm for 4 days at 30 °C, the mycelia were harvested by centrifugation and suspended in 50 mL of H_2O and freeze-dried for further investigation.

The fermentation medium, which had been obtained after the centrifugation, was extracted with 300 ml of EtOAc and subsequently acidified to pH 3-4 with TFA. Next, the acidified mixture was extracted for 3 times with 300 mL of EtOAc. To prevent decomposition of the compounds during solvent removal, TFA was back extracted with H_2O. The extract contained the yellow compound KR11a with an characteristic UV absorption maximum at 470 nm. The crude extract obtained from the medium was fractionated by flash column chromatography on impregnated silica with a mobile phase $CHCl_3$:MeOH (9:1). Fractions containing the compound were combined and dried, and further purification was carried out by semipreparative HPLC with a gradient: 25% to 100% CH_3CN in H_2O+ 0.1% TFA over 25 min. The isolated yield of KR11a was 12 mg. The identity of the compound was confirmed by ESI-HRMS analysis for the molecular ion $[M+H]^+$ as $[C_{26}H_{19}O_9]^+$: *m/z* = 475.1077 calcd. 475.1029 . One- and two-dimensional NMR analysis was carried out in DMSO-d_6.

^{1}H-NMR, ^{13}H-NMR, HMBC and HMQC spectra was measured on a Bruker ADVANCE DPX 400 device. A Jasco MD-2015 PDA HPLC detector was used to obtain the UV spectrum of the compound.

4.1.5.19 Procedure for the Methylation of KR11a

Into a stirred suspension of 12 mg of the yellow compound KR11a and 2 g anhydrous K_2CO_3 (14.47 mmol) in 15 mL of dry acetone, 2 mL dimethyl sulfate (21.08 mmol) was added dropwise. The mixture was stirred at room

temperature for an hour and then heated under reflux for 15 h, cooled down to room temperature and diluted with 100 mL of H_2O. After stirring further for 30 min, the mixture was extracted with 100 mL of $CHCl_3$, washed with water and the solvent was removed. A yellow solid compound was obtained. By using TLC with a mobile phase of $CHCl_3$:MeOH (9:1) at RT, a spot was detected at R_f : 0.7. Purification was carried out by preparative HPLC using a PerfectChrom 100 C18 reverse-phase semipreparative column (250 mm x 8 mm, 5 μm) with UV detection at 254 nm and 470 nm using a Jasco MD-2015 PDA detector. A 60-40% to 100-0% CH_3CN:H_2O gradient was used over 25 min at a flow rate of 6 mL min^{-1}. Subsequently a second purification on preparative HPLC was carried out using a 60-40% to 100-0% (MeOH:H_2O) gradient over 25 min at a flow rate of 4 mL min^{-1}. The yield of the isolated methylated compound was 3 mg. The identity of the compound was confirmed by ESI-HRMS analysis for the molecular ion $[M+H]^+$ as $[C_{31}H_{29}O_9]^+$: *m/z* =545.1991 $[M+H]^+$ calcd. 545.1812.

4.1.5.20 Procedure for the Methylation of KR11b

Into a stirred suspension of 1 g of the mycelia crude extract of the *S. albus* KR11 and 10 g anhydrous K_2CO_3 (72.35 mmol) in 90 mL of dry acetone, 12 mL dimethyl sulfate (126.53 mmol) was added dropwise. The mixture was stirred at room temperature for an hour and then heated under reflux for 24 h, cooled down to room temperature and diluted with 100 mL of H_2O. After stirring further for 30 min, the mixture was extracted with 150 mL of $CHCl_3$, washed with water and the solvent was removed at a rotary evaporator. A green solid was obtained. Using a mixture of $CHCl_3$:MeOH (9:1) as a mobile phase, TLC was made and an R_f value of 0.75 was determined for a green component. The product was further purified with column chromatography with the same solvent mixture, and applied on a Sephadex LH-20 column with a mobile phase of methanol. Further purification attempts on RPand Normal-phase HPLC columns with the solvents MeOH, AN and H_2O did not yield any results. Experiments using less polar solvent mixtures with THF, ethanol, and isopropanol were not further pursued due to the technical problems caused by these solvents on the HPLC instrument. ^{1}H-NMR of the partially purified

compound was performed in DMSO-d_6. 10 mg of the green solid was used. The spectrum was not clean enough to use for structure elucidation.

4.1.6 Assays for Determining *In Vivo* Activity of the Oxygenase GrhO6

4.1.6.1 Procedure for Assay 1

For the first assay, the reaction was performed in a 50 mL Falcon tube without lid at 30 °C at 250 rpm. The reaction was carried out factor for a time period of 4 hours in a total volume of 2 mL of 1 M Tris buffer at pH 6 with 1 mM NADPH and 10 μM FAD used as cofactor. Into 630 μL of 0.32 mg/mL lenticulone **(53)**, which was solved with an addition of 10 μL DMSO-d_6 in Tris buffer, 4 μL of FAD solution (0.005 M), 100 μL of NADPH solution (0.02 M) and 1116 μL of Tris buffer were added. To the mixture 150 μL enzyme with a concentration of 1 mM of the enzyme GrhO6 was added and every 30 min 400 μL of the solution was removed into a 1mL Eppendorf tube. The compounds were extracted with 250 μL of ethyl acetate, centrifuged and the organic phase was transferred into another 1 mL Eppendorf tube. During the extraction, the formation of a white precipitate was observed, which made the extraction process more difficult due to the clinging of red pigments on this precipitate. The precipitation is predicted to be caused by the fact that the protein components are insoluble in organic solvents. The ethyl acetate from the extraction was removed on a SpeedVac. The extract was dissolved in 50 μL of acetonitrile and subjected to MN-Nucleodur-100 RP18 HPLC column with a gradient of 40-60% to 100-0% acetonitrile:water at a flow rate 1 mL/min. Simultaneously, a control mixture was incubated. This control mixture contained the identical reaction mixture with the substrate lenticulone **(53)** without the enzyme. The control reaction was incubated in order to see the degradation products of the compound during the assay. A second control mixture contained the identical reaction mixture with GrhO6 but not the assumed substrate lenticulone **(53)** was also incubated in order to tast the effects of components, such as cofactors, and to make sure that such components do not lead to a signal, which might be mistaken for a product of the enzyme reaction.

4.1.6.2 Procedure for Assay 2

Assay 2 investigates the enzyme activity of GrhO6 in two different pH values. The assay fallows a procedure similar to assay 1 described above. The reaction was carried out in a 50 mL Falcon tube without lid at 30 °C at 225 rpm. Assay 2a was carried out at a pH 6 in 1 M Tris buffer at pH 6 and assay 2b was carried out pH7 in 1 M Tris buffer at pH 7. 1 mM NADPH and 10 μM FAD were used as co-factor for a time period of 4 hours. The total volumes of both reactions were increased to 5 mL in order to enable better UV detection of the resulting compounds. Into 4490 μL of Tris buffer, 10 μL of the FAD solution in Tris buffer (0.005 M), 250 μL of NADPH solution in Tris buffer (0.02 M) and 1 mg lenticulone **(53)**, which was dissolved in 50 μL DMSO, were added. To the mixture 200 μL 1.5 mM enzyme was added. Every hour 1 mL of the solution was withdrawn from both mixtures and additional 100 μL enzyme was added into the assay mixtures. The transferred 1 mL solutions were immediately extracted with 0.5 mL of ethyl acetate. Precipitates of the proteins were formed again, therefore ultrasound bath were used in order to get better solubility during extraction this time. The extraction mixture was centrifuged, the organic phase was transferred into an Eppendorf tube and ethyl acetate was removed on the SpeedVac. The extract was dissolved in 50 μL of acetonitrile and subjected to MN-Nucleodur-100 RP18 HPLC column with a gradient of 40-60% to 100-0% acetonitrile:water at a flow rate 1 mL/min. Additionaly to this reaction, a control mixture without GrhO6 and another control mixture without lenticulone **(53)**, were prepared as a control mixture and the procedure for the assay was applied.

4.1.6.3 Procedure for Assay 3

The optimal enzyme activity of a related enzyme MtmOIV was reported to take place at the pH 8.25, therefore the previous assay was repeated in 1 M Tris buffer at pH 7 and at pH 8.25. The assay 3a was performed at pH 7 and assay 3b was performed at pH 8.25. Assay 3 was carried out in a similar manner with assay 2. The reactions were performed in an 50 mL Falcon tube without lid at 27 °C at 225 rpm by addition of 1 mM NADPH and 10 μM FAD as co-factor for a

total time period of 4 hours. Into 4490 μL of Tris buffer, 10 μL of FAD solution in Tris buffer (0.005 M), 250 μL NADPH solution in Tris buffer (0.02 M) and 1 mg lenticulone **(53)**, which was dissolved in 50 μL DMSO, were added. To both mixtures 200 μL of 1.5 mM enzyme was added. Every hour 1 mL of both solutions was withdrawn and a additional 100 μL enzyme was added into assay mixture. The transferred 1 mL solutions were immediately extracted with 0.5 mL of ethyl acetate. A precipitate of the proteins formed again therefore ultra sound bath was used in order to get better solubility during extractions. The only difference of the extraction procedure from the previous ones is that 1 mL solutions taken out every hour is required to be acidified before the extractions with 0.5 mL of ethyl acetate. This is because these compounds are not soluble in organic solvents without being acidified. Therefore the withdrawn samples at pH 7 were diluted with an equal amount of 0.025% TFA solution and then extracted. The withdrawn samples at pH 8.25 were diluted with 2 mL of the 0.025 % TFA solution. The extraction mixtures were centrifuged and the organic phases were transferred into Eppendorf tubes. Afterwards, ethyl acetate was removed on the SpeedVac. The extracts were dissolved in 50 μL of acetonitrile and subjected to MN-Nucleodur-100 RP18 HPLC column with a gradient 40-60% to 100-0% acetonitrile:water at a flow rate 1 mL/min. Additionaly to this reaction, a control mixture without GrhO6 and another control mixture without lenticulone **(53)**, were prepared as a control mixture and the procedure for the assay was applied.

4.1.7 Assays for the Determination of Antibacterial Activity

The isolated compounds lenticulone **(53)**, griseorhodin A **(5)**, collinone **(41)**, precollinone **(58)**, didesoxygriseorhodin C **(46)** and the crude extracts of the mycelia from *S. albus* KR11 and *S. albus* KR5, and also the medium extract of *S. albus* KR11 were tested by the strains below.

4.1.7.1 Agar Diffusion Assay:

Two Gram-positive and two Gram-negative bacterial strains were chosen to test the antibacterial activity of the compounds for this assay. The strains used for the assay are below:

- *Escherichia coli*-DH5α (Gram-)
- *Staphylococcus carnosus*-DSH 20501 (Gram+)
- *Bacillus amyloliquefaciens* (Gram+)
- *Pseudomonas fluorescens*-DSH 50090T (Gram-).

The strains were incubated overnight in TSB medium at 37 °C and plated on MM agarplates (Müller Minton agar). A set of ethyl acetate solutions of the test compounds at the concentrations of 1 mg/mL, 0.5 mg/mL and 0.25 g/mL were prepared in Eppendorf tubes. For the assay with a crude extract, double amount of extract was used. Sterile 6 mm filter paper disks with radius 0.5 cm (Whatman filter paper; Whatman International Ltd.) were prepared and each was soaked with 20 μL of each test solution. A disk was used as negative control by applying only 20 μL of ethyl acetate. The disks were left to dry. Prepared disks with different concentrations and the control disk were placed on the prepared plates; 10 μL of distilled water was dropped on the disc to increase the diffusion of the compounds into the agar plates. The plates with the bacteria and discs on them were incubated overnight at 37 °C. On the next day, the discs with active compounds showed no signs of bacterial growth on the surface and on the borders. However, bacterial growth was observed on the surface and around the control disc without compound. Thus, it was concluded that these compounds inhibited the strains' growth. Although the compounds inhibited the bacterial growth on and around the disk surface, no activity zone could be determined. The inhibition radius was not determined since activity zone was not observed as a symmetric area, in some cases not even as an area. The reason is predicted to be the low water solubility and poor diffusion property of the test substances. Eventhough colorful pigments were used as compounds, low compound concentration prevented the observation of the activity zone by color.

4.1.7.2 Minimum Inhibition Concentration (MIC-Assay)

MIC value was determined for the compounds, which showed antibacterial activity with the two Gram+ strains at the agar diffusion assay explained above. The strains used for the assay are below:

- *Staphylococcus carnosus* (Gram+)
- *Bacillus subtilis* (Gram+)

The assay was carried out in LB medium. The total volume of each test tube was 2.5 mL. All initial solutions of the test compounds in LB medium were prepared in a Falcon tube with a total volume of 10 mL. Each solution had a carefully determined compound concentration in the range of 100 μg/mL. For the preparation of the initial solutions, the test compounds were weighed in an Eppendorf tube and 20 μL DMSO was added to solve these compounds. Next, they were transferred into 10 mL of LB medium. Each initial solution was distributed into two overnight culture tubes so that each tube contained 5 mL of the solution. These tubes were used to prepare two set of test tubes in a concentration row to test each strain. For the prepartion of each concentration row, 2.5 mL of the initial solution was transferred to from the first tube into the next tube. Afterwards, 2.5 mL of LB medium was added into this next tube to obtain a twofold dilution in a total volume of 5 mL. The next tube of the concentration row was prepared by transferring 2.5 mL of the twofold-diluted solution into it and by addition of 2.5 mL of LB medium so that again a total volume of 5 mL was obtained. The solution is a four-fold dilution of the initial solution. This procedure was repeated until there were 8 different concentrations in decreasing order. The final volume of the solutions in the tubes was 2.5 mL. 20 μL DMSO was added to each tube to increase the solubility of the test compound. A control mixture containing only 20 μL DMSO and LB medium without the test compound was also prepared. For the preparation of the strains a day before, bacterial strains were grown overnight at 37 °C in LB medium and used on the following day to inoculate a new culture to achieve a growth maximum of the bacteria (OD_{600} between 0.08 and 0.1). 100 μL of each bacterial cultures was used to inoculate the tubes in the concentration row and

the control tubes. Afterwards, the prepared tubes were incubated overnight at 37 °C in a shaker at 175 rpm. A second control tube without bacteria containing only LB Medium was also incubated to check for any contaminations that might be present in the test medium. On the next day the minimum inhibition concentrations could be determined by observing the tubes with bacterial growth. When the assay result showed no bacterial growth at any concentration another complimentary assay was carried out starting at the low concentration of 5 μg/mL. The procedure of the complimentary assay described above in detail.

4.1.8 Characterization of the Isolated Compounds

4.1.8.1 Griseorhodin A (5)

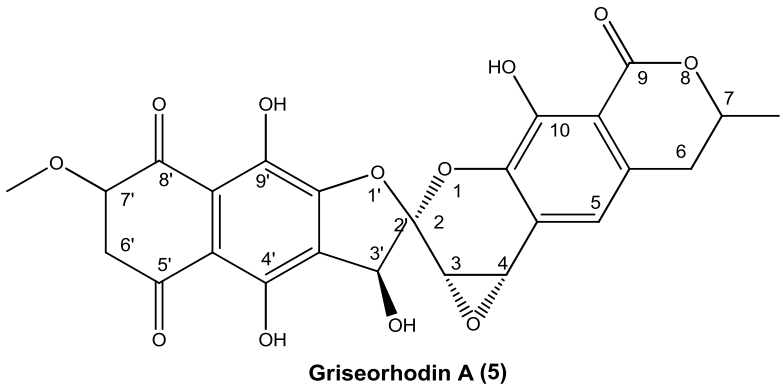

Figure 4.1. Structure of Griseorhodin A (5).

Chemical formula: $C_{25}H_{16}O_{12}$

$[\alpha]_{589}^{20}$= +54 (c=0.015 g/100 mL in $CHCl_3$)

ESI-(+)-HRMS=Measured *m/z*: 509.0691, calculated *m/z*: 509.0720 for $[M+H]^+$.

IR ν[cm^{-1}]=3481, 1687,1649,1604, 1440, 1308, 1159, 1136, 1104, 1077, 1020, 977, 936, 651, 586, 542, 451, 441.

UV (in acetonitrile) λ [nm]=224, 260, 308, 362, 488 nm.

^{1}H-NMR (500 MHz, DMSOd$_6$)=δ 2.23 (s, 3H, CH$_3$-7), 3.92 (s, 3H, OCH$_3$-7'), 4.30 (d, 1H$_a$, *J*^{3} [H$_{a,b}$] =4 Hz, H-3), 4.40 (d, 1H$_b$, *J*^{3} [H$_{b,a}$] =4 Hz, H-4), 5.32 (s, 1H, H-3'), 6.37 (bs, 1H, H-6'), 6.44 (s, 1H, H-6), 6.90 (s, OH, H-3'), 7.1 (s, 1H, H-5),10.80 (s, OH, OH-10), 11.76 (sb, OH, OH-9'), 13.22 (s, OH, OH-4').

4.1.8.2 Didesoxygriseorhodin C (46):

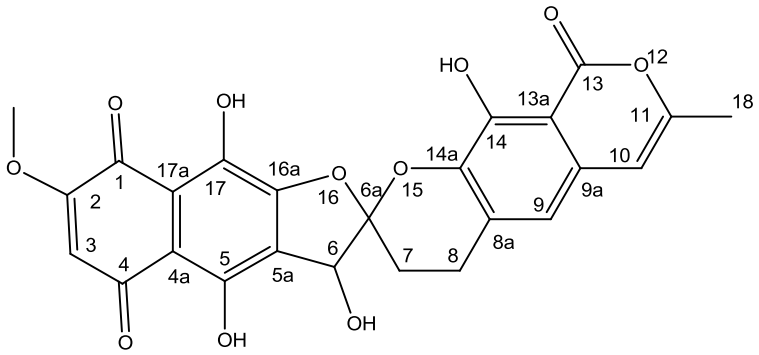

Didesoxygriseorhodin C (46)

Figure 4.2 Structure of didesoxygriseorhodin C (46).

Chemical formula: $C_{25}H_{18}O_{11}$

$[\alpha]_{589}^{20}$=+48 (c=0.015 g/100 mL in $CHCl_3$)

ESI-(+)-HRMS=Measured *m/z*: 495.0911, calculated *m/z*: 495.0927 for $[M+H]^+$.

IR ν[cm^{-1}]=3509, 1687, 1650, 1604, 1439, 1320, 1284, 1195, 1157, 1081, 1041, 121, 983, 929.

UV (in acetonitrile) λ [nm]=224, 254, 314, 356, 494 nm.

^{1}H-NMR (500 MHz, DMSO-d$_6$)=δ 1.8 (3H, s, CH$_3$-18), 2.20-2.22 (4H, m, CH$_2$-7, CH$_2$-8), 5.15 (s, 1H, H-6), 6.41,6.45 (bs, OH, OH-6), 6.49 (s, 1H, H-6), 6.85 (s, 1H, H-6), 10.78 (s, OH, OH-14), 11.84 (s, 1 OH, OH-17).

^{13}C-NMR (400 MHz, DMSO-d$_6$)=δ 18.63 (s, C-18), 21.22 (s, C-7), 23.12 (s, C-8), 56.97 (s,OCH$_3$-2), 74.04 (s, C-6), 103.72 (s, C-10), 104.16 (s, C-6a), 106.35 (s, C-4a), 110.14 (s, C-3), 113.12 (s, C-11), 114.01(s, C-17a), 114.86 (s, C-9), 124.02 (s,

C-8a), 130.18 (s, C-5a), 132.35 (s, C-13a), 137.69 (s, C-9a), 146.79 (s, C-14a), 148.58 (s, C-16a), 152.14 (s, C-14), 153.96 (s, C-17), 157.14 (s, C-5), 160.18 (s, C-2), 165.64 (s, C-13), 179.86 (s, C-1), 185.37 (s, C-4).

4.1.8.3 Lenticulone (53):

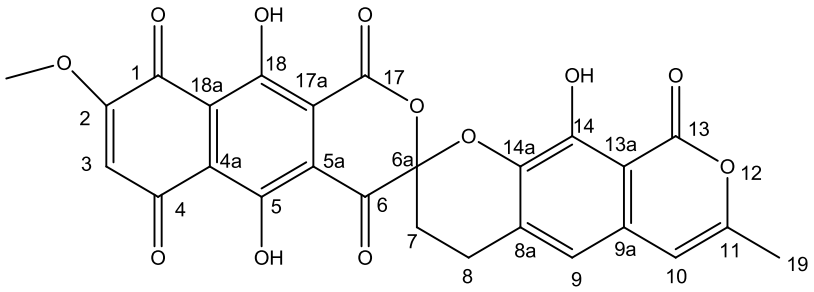

Lenticulone (53)

Figure 4.3 Structure of Lenticulone (53)

Chemical formula: $C_{26}H_{16}O_{12}$

$[\alpha]_{589}^{20}$=+28 (c=0.012 g/100 mL in $CHCl_3$)

ESI-(+)-HRMS=Measured *m/z*: 521.0714, calculated *m/z*: 521.0720 for $[M+H]^+$.

IR ν[cm^{-1}]=2923, 2853, 1686, 1650,1606, 1438, 1403, 1336, 1289, 1234, 1197, 1145, 1069, 1053, 1006, 989, 932, 893, 857, 819, 799, 747, 697, 668, 585, 568, 546, 519, 445, 421, 412 .

UV (in acetonitrile) λ [nm]=230, 355, 494 nm.

^{1}H-NMR (500 MHz, $CDCl_3$)=δ 2.24(3H, s, CH_3-19), 2.4-2.5(2H, m, CH_2-7), 2.85-3.25(2H, m, CH_2-8), 4.01 (3H, s, OCH_3-2), 6.17 (1H, s, H-10), 6.29 (1H, s, H-3), 6.61 (1H, s, H-9), 10.98 (OH, s, OH-14), 12.74 (OH, s, OH -18), 13.37 (OH, s, OH -18).

^{13}C-NMR (400 MHz, $CDCl_3$)=δ 19.30 (s, C-19), 23.96 (s, C-7), 20.59 (s, C-8), 57.33 (s, $CH_3$0-2), 99.08 (s, C-6a), 104.01 (s, C-10), 105.08 (s, C-11), 110.20 (s, C-3),

114.21 (s, C-9), 117.93 (s, C-4a), 118.26 (s, C-18a), 121.74 (s, C-17a), 127.7 (s, C-5a), 131.387 (s, C-9a), 137.14 (s, C-14a), 132.09 (s, C-8a), 150.15 (s, C-14), 152.85 (s, C-11), 153.61 (s, C-5), 155.88 (s, C-18), 158.28 (s, C-17), 161.15 (s, C-2), 166.66 (s, C-13), 181.67 (s, C-1), 182.81 (s, C-6).

4.1.8.4 ZY1 (54):

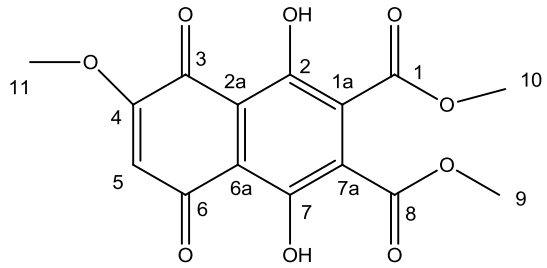

ZY1 (54)

Figure 4.4 Structure of ZY1 (54).

Chemical formula: $C_{15}H_{12}O_9$

ESI-(+)-HRMS=Measured *m/z*: 337.055, calculated *m/z*: 337.056 for $[M+H]^+$.

UV (in acetonitrile) λ [nm]:224, 272, 308, 356, 488 nm.

^{1}H-NMR (400 MHz, $CNCD_3$)=δ 3.87 (6H, s, OCH_3-9, OCH_3-10), 3.93 (3H, s, OCH_3-10), 6.34 (H, s, H-5), 12.16 (OH, s, OH-2), 12.87 (OH, s, OH-7).

^{13}C-NMR (400 MHz, $CNCD_3$)=δ 53.18, 53.82, 53.82, 130.77, 132.58, 111.53, 114.52, 115.10, 132.58, 153.12, 154.06, 162.44, 164.76, 164.82, 184.35, 190.13.

4.1.8.5 Collinone (41):

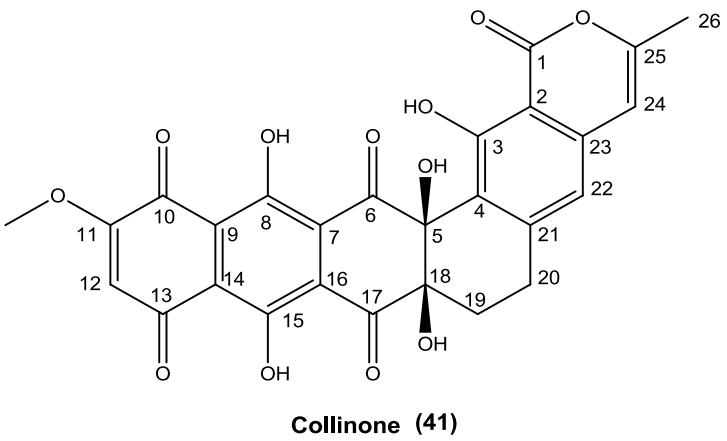

Figure 4.5 Structure of collinone (41).

Chemical formula: $C_{27}H_{18}O_{12}$

$[\alpha]_{589}^{20}$=+39 (c = 0.03 g/100 mL in $CHCl_3$)

ESI-(+)-HRMS= Measured *m/z*: 535.088, calculated *m/z*: 535.088 for $[M+H]^+$.

IR ν[cm^{-1}]=3382, 2920, 2850, 1683, 1616, 1557, 1446, 1403, 1342, 1289, 1231, 1167, 1085, 1013, 984.

UV (in acetonitrile) λ [nm]=236, 290, 338, 510 nm.

^{1}H-NMR (500 MHz, $CDCl_3$)=δ 2.2 (3H, s, CH_3-26), 2.2-2.5 (2H, m, CH_2-19a), 3.1-3.2 (2H, m, CH_2-19b), 6.1 (1H, s, H-24), 6.2 (H, s, H-6), 6.6 (1H, s, H-22), 11.6 (OH, s, OH-3).

^{13}C-NMR (400 MHz, $CDCl_3$)=δ 19.45 (s, C-26), 26.10 (s, C-19a), 27.30 (s, C-20), 78.99 (s, C-5), 80.80 (s, C-18), 103.481 (s, C-2), 104.090 (s, C-24), 110.78 (s, C-12), 115.82 (s, C-22), 115.91 (s, C-14), 119.54 (s, C-4), 128.6 (s, C-16), 130.92 (s, C-7), 147.91 (s, C-21), 154.65 (s, C-8), 155.12 (s, C-25), 155.6 (s, C-15), 159.5 (s, C-3), 160.74 (s, C-11), 166.508 (s, C-1), 182.65 (s, C-10), 188.14 (s, C-13), 191 (s, C-17).

4.1.8.6 Precollinone (58):

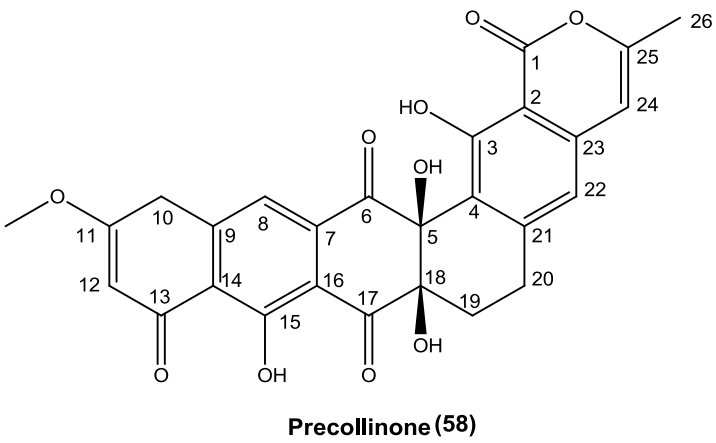

Figure 4.6 Structure of precollinone (58).

Chemical formula: $C_{27}H_{20}O_{10}$

$[\alpha]_{589}^{20}$=+48 (c=0.035 g/100 mL in $CHCl_3$)

ESI-(+)-HRMS=Measured *m/z*: 505.111, calculated *m/z*: 505.114 for $[M+H]^+$.

IR ν[cm^{-1}]=2921, 2851, 1681, 1621, 1425, 1382, 1340, 1253, 1201, 1085, 1040, 811, 755, 720, 668, 657, 569 .

UV (in acetonitrile) λ [nm]=236, 278, 344, 410 nm.

^{1}H-NMR (500 MHz, $CDCl_3$)=δ 2.06 (3H, s, CH_3-26), 2.46-2.26 (2H, m, CH_2-19), 3.12-3.08 (2H, m, CH_2-20), 3.86 (3H, s, OCH_3), 6.17 (1H, s, H-24), 6.57 (1H, s, H-12), 6.61 (1H, s, H-22), 7.14 (1H, s, H-10), 7.75 (1H, s, H-8), 10.09 (OH, s, OH-15), 11.36 (OH, s, OH-3), 14.17 (OH, s, OH-13).

^{13}C-NMR (400 MHz, $CDCl_3$)=δ 19.15 (s, C-26), 23.76 (s, C-19), 28.05 (s, C-20), 56.09 (s, C-11), 77.99 (s, C-5), 80.85 (s, C-18), 102.67 (s, C-10), 111.02 (s, C-16), 116.10 (s, C-22), 103.03 (s, C-2), 103.88 (s, C-12), 104.06 (s, C-24), 106.92 (s, C-14), 118.44 (s, C-8), 122.35 (s, C-4), 131.45 (s, C-7), 137.55 (s, C-23), 140.42 (s, C-9), 148.33 (s, C-21), 155.17 (s, C-25), 159.08 (s, C-3), 159.17 (s, C-15), 163.20 (s, C-11), 164.40 (s, C-13), 166.71 (s, C-1), 197.71 (s, C-17), 198.96 (s, C-6).

4.1.8.7 Secocollinone-1 (59):

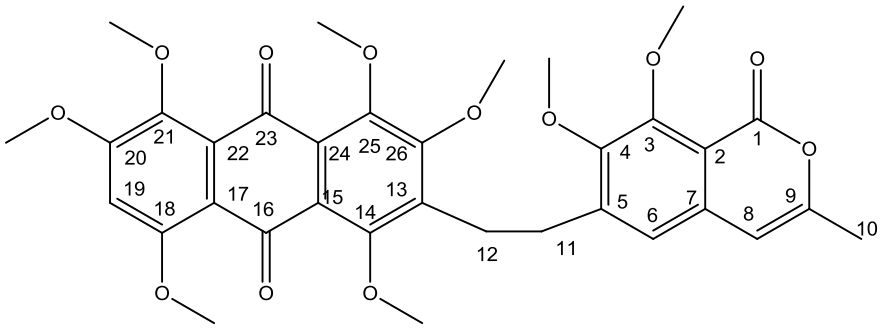

Figure 4.7 Structure of secocollinone-1 (59).

Chemical formula: $C_{34}H_{34}O_{12}$

$[\alpha]_{589}^{20}$=+62 (c=0.05 g/100 mL in $CHCl_3$)

ESI-(+)-HRMS=Measured *m/z*: 634.213, calculated *m/z*: 634.205 for $[M+H]^+$.

IR ν[cm^{-1}]=2920, 1732,1589,1558, 1456,1404,1340, 1257,1209, 1109, 1037,803, 750, 668, 418.

UV (in acetonitrile) λ [nm]=230, 260, 350, 362, 398 nm.

^{1}H-NMR (500 MHz, $CDCl_3$)=δ 2.18 (3H, s, CH_3-10), 2.80-2.85 (2H, m, CH_2-11), 2.90-2.95 (2H, m, CH_2-12), 3.79 (3H, s, OCH_3-21), 3.80 (3H, s, OCH_3-26), 3.79 (3H, s, OCH_3-21), 3.81 (6H, s, OCH_3-4, OCH_3-25), 3.87 (3H, s, OCH_3-3), 3.88 (3H, s, OCH_3-18), 3.91 (3H, s, CH_3-26), 3.97 (3H, s, CH_3-20), 6.43 (H, s, CH-8), 7.02 (H, s, CH-19), 7.08 (H, s, CH-6).

^{13}C-NMR (400 MHz, $CDCl_3$)=δ 19.69 (s, C-26), 26.02 (s, C-26), 31.52 (s, C-26), 57.31 (s, C-26), 57.56 (s, C-26), 61.87 (s, C-26), 62.04 (s, C-26), 62.41 (s, C-26), 62.45 (s, C-26), 63.51 (s, C-26), 103.14 (s, C-26), 103.63 (s, C-26), 112.97 (s, C-26), 116.03 (s, C-26), 122.26 (s, C-26), 125.20 (s, C-26), 129.25 (s, C-26), 130.79 (s, C-26), 135.79 (s, C-26), 136.19 (s, C-26), 140.80 (s, C-26), 144.81 (s, C-26), 147.83 (s, C-26), 151.44 (s, C-26), 154.26 (s, C-26),154.30 (s, C-26), 156.63 (s, C-26), 156.76 (s, C-26), 158.87 (s, C-26), 158.96 (s, C-26), 181.12 (s, C-26), 184.01.

4.1.8.8 KS-619-3 (65):

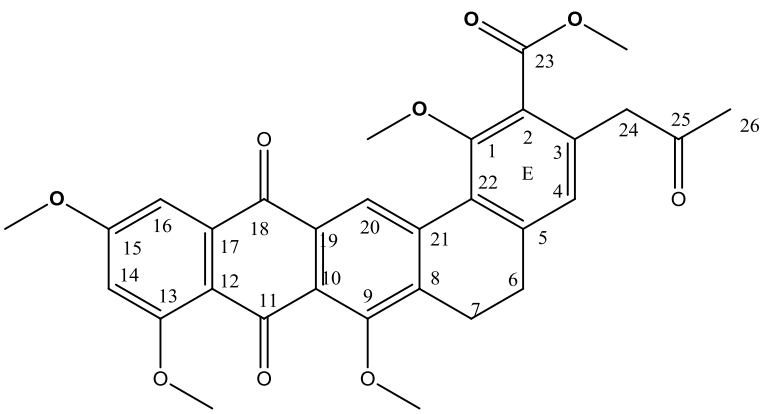

Figure 4.8 Structure of KS-619 (65).

Chemical formula: $C_{31}H_{28}O_9$

$[\alpha]_{589}^{20}$=+23 (c=0.05 g/100 mL in $CHCl_3$)

ESI-(+)-HRMS=Measured *m/z*: 545.1969, calculated *m/z*: 545.181 for $[M+H]^+$.

IR ν[cm^{-1}]=1720, 1661, 1594, 1578, 1460, 1429, 1369, 1304, 1214, 1158, 1134, 1054, 1022, 999, 976, 947, 799, 665, 536, 481, 430.

UV (in acetonitrile) λ [nm]=230, 296, 404 nm.

^{1}H-NMR (500 MHz, $CDCl_3$)=δ 2.19 (3H, s, CH_3-26), 2.8-2.6 (2H, m, CH_2), 2.9-3 (2H, s, CH_2), 3.64 (3H, s, OCH_3-1), 3.72 (3H, s, OCH_3-24), 3.92 (3H, s, OCH_3-23), 3.95 (3H, s, OCH_3-15), 3.96 (3H, s, OCH_3-13), 3.98 (3H, s, OCH_3-9), 6.77 (H, s, H-14), 6.92 (H, s, H-4), 7.42 (H, s, H-16), 8.96 (H, s,H-20).

^{13}C-NMR (400 MHz, $CDCl_3$)=δ 21.89 (s, C-7), 29.29 (s, C-6), 30.08 (s, C-26), 48.71 (s, C-24), 52.85 (s, $COOCH_3$-23), 56.35 (s, OCH_3-13), 56.99 (s, OCH_3-15), 62.22 (s, OCH_3-1), 62.43 (s, OCH_3-9), 102.61 (s, C-16), 105.49 (s, C-14), 118.57 (s, C-12), 118.81(s, C-10), 122.65 (s, C-20), 125.65 (s, C-19), 126.48 (s, C-22), 127.22 (s, C-4), 128.62 (s, C-2), 133.19 (s, C-3), 134.37 (s, C-8), 137.72 (s, C-17), 140.58 (s, C-21), 143.24 (s, C-5), 156.81 (s, C-1), 157.21 (s, C-9), 162.21 (s, C-13), 164.49 (s, C-15), 168.52 (s, C-23), 182.13 (s, C-11), 183.92 (s, C-18), 205.46 (s, C-25).

4.1.9 List of Chemicals and Materials

All chemicals used were standard chemicals of analytical grade from following companies: Across, Fluka, Roth (Karlsruhe), Merck (Darmstadt) and Sigma (Seelze). HPLC grade solvents were purchased from Baker (Deventer,NL), Merck (Darmstadt) and Fischer Scientific (Schwerte). NMR solvents were from Sigma and Euriso-Top.

Table 4.1 Table of Chemicals

Chemicals	**Company, Location**
Acetic acid	Merck, Darmstadt
Acid casein hydrolysate	Roth, Karlsruhe
Agar-agar	Roth, Karlsruhe
Ammonium sulfate	Applichem, Darmstadt
Ampicillin-Sodium salt	Roth, Karlsruhe
Apramycin sulfate	Sigma-Aldrich, Seelze
Beef extract	Roth, Karlsruhe
Calcium carbonate	Roth, Karlsruhe
Calcium chloride	KMF, Lohmar
[D_1] Chloroform ($CDCl_3$)	Euriso-Top, Gif sur Yvette (F)
Dipotasium hydrogenphosphate-dihydrate	Merck, Darmstadt
Dimethyl sulfate (DMS)	Roth, Karlsruhe
Dimethyl sulfoxide (DMSO)	Roth, Karlsruhe
[D_6] Dimethyl sulfoxide (DMSO-d_6)	Euriso-Top, Gif sur Yvette (F)
Disodium hydrogenphosphate-dihydrate	Fluka / Riedel-de-Haën, Seelze
D(+)-Glucose monohydrate	Fluka / Riedel-de-Haën, Seelze
Glycerol	Merck, Darmstadt
Hydrocloric acid	Fluka / Riedel-de-Haën, Seelze
Iron(II)sulfate-heptahydrate	Merck, Darmstadt
Magnesiumchloride-hexahydrate	Fluka / Riedel-de-Haën, Seelze
Magnesiumsulfate-heptahydrate	Roth, Karlsruhe
Mannitol	Roth, Karlsruhe
Potassium carbonate	AppliChem, Darmstadt
Potassium chloride	Acros Organics, Geel (B)
Potassium dihydrogenphosphate	Merck, Darmstadt
Potassium sulfate	Grüssing, Filsum
Potato starch, soluble	Sigma-Aldrich, Seelze
Sodium carbonate	KMF, Lohmar
Sodium chloride	Grüssing, Filsum
Sodium dihydrogenphosphate-dihydrate	Roth, Karlsruhe
Sodium hydroxide	KMF, Lohmar
Sulfric acid	Fluka / Riedel-de-Haën, Seelze
Soja flour (Bacto Saitone)	Becton Dickinson, Heidelberg
Trifluor acetic acid (TFA)	Roth, Karlsruhe
Tris-(hydroxymethyl)-amino methane (Tris)	Roth, Karlsruhe
Trimethyl silyl diazo methan	Roth, Karlsruhe
Tryptic Soy Broth (TSB)	Difco, USA
Tryptic Soy Broth (TSB)	Becton Dickinson, Heidelberg
Trypton	Becton Dickinson, Heidelberg
Yeast extract	Becton Dickinson, Heidelberg
Zinc chloride	Acros Organics, Geel (B)
Zinc sulfate	Merck, Darmstadt

4.1.10 List of Equipments

Table 4.2 Table of equipments

Equipment	Company, Location
Autoklave V65	Systec, Wettenberg
Balance CP225D	Sartorius, Göttingen
Balance 440-47N	Kern, Balingen-Frommern
Balance BP110	Sartorius, Göttingen
Centrifuge Rotina 35R	Hettich, Tittlingen
Centrifuge Z513K	Hermle, Wehingen
Clean bench Biowizard	Kojair, Vilppula (FIN)
Freeze dryer Heto PowerDry LL3000	Thermo, Langenselbold
HPLC-ColumnC18 Nucleodur 100, 125 x 2 mm, 5 µm	Macherey-Nagel, Düren
HPLC-ColumnC18 PerfectChrom 100, 250 x 4 mm, 5 µm	Macherey-Nagel, Düren
HPLC-ColumnC18 PerfectChrom 100, 250 × 8 mm, 5 µm	Macherey-Nagel, Düren
HPLC-Instrument	Jasco, Gross-Umstadt
HPLC-Vials with Cap and Septum	Bio-Rad, München
Inkubator B12	Thermo, Langenselbold
Membrane vakuum pumpe	Vacuubrand, Wertheim
Microcuvettes UltraVette (70-850 µL)	Roth, Karlsruhe
Microwave Lifetec	Medion, Essen
Microcentrifuge Mikro200	Hettich, Tuttlingen
Photometer BioMate 3	Thermo Electron, Cambridge
Pipettes	Gilson, Middleton (USA)
Poly-Prep Column	Bio-Rad, München
Rotation evaporator VV2000	Heidolph, Kelheim
Silica gel 60 (0,040- 0,063 mm)	Merck, Darmstadt
Speedvac / Concentrator 5301	Eppendorf, Hamburg
TLC-Plates silica gel 60 F_{254}	Merck, Darmstadt
TLC-Plates Alugram RP-18 W/UV_{254}	Macherey-Nagel, Düren
Ultrasound homogenisator Sonopuls HD2070	Bandelin, Berlin
Vakuum pump RZ6	Vacuubrand, Wertheim
Vortex-Mixer VTX-3000L	LMS, Tokio (J)
Water bath	GFL, Burgwedel

5 SUMMARY

Griseorhodin A **(5)** is a member of the rubromycins, a group of aromatic polyketides with unique structures. Members of this group such as γ-rubromycin **(37)** and heliquinomycin **(39)** inhibit HIV reverse transcriptase and human telomerase. Both pharmacological activities depend on the presence of a highly unusual spiroketal moiety, but how the bacteria achieve the biosynthesis of this pharmacophore has not been understood completely.

In previous work, the griseorhodin A **(5)** biosynthetic gene cluster (Fig. 1.24) was isolated and sequenced and a heterologous expression system was created to study griseorhodin A biosynthesis 17 mutant strains lacking biosynthetic genes were prepared by Kathrin Reinhardt for her PhD work. The aim of this PhD study was the development of cultivation procedures, the chemical investigation, and the characterization of the metabolites and shunt products from the griseorhodin A pathway, focusing on the function of the 11 griseorhodin A **(5)** tailoring enzymes performing the post-PKS steps and the function as-yet undetermined genes.

Heterologous expression and metabolic analysis of the strains enabled the assignment of most genes to various stages of griseorhodin A biosynthesis, the identification of tailoring enzymes and the study of the pharmacophore generation process. In addition to griseorhodin A **(5)**, seven metabolites, didesoxygriseorhodin C (**46),** collinone **(41),** ZY1 (**54)**, lenticulone **(53),** precollinone **(58)**, KS-619-3 **(65)** and secocollinone-1 **(59)**, were isolated, which are present in the extracts of fourteen producing mutant strains. With the data obtained from the HR-LCMS experiments and structure elucidation, a new biosynthetic pathway for griseorhodin A **(5)** was postulated. (Section 3.7) Among the substances isolated for the biosynthesis studies, the structures of the compounds ZY1 (**54)**, lenticulone **(53),** precollinone **(58)**, KS-619-3 **(65)** and secocollinone-1 **(59)** were identified as new. In addition to biosynthesis studies, an *in vito* enzyme activity assay for the oxygenase GrhO6 with the isolated metabolite lenticulone **(53)** was conducted to stud biosynthesis.

It was also tested, how the degree of oxidative modification during griseorhodin A biosynthesis affects bioactivity. The compounds griseorhodin A **(5),** didesoxygriseorhodin C (**46),** collinone **(41),** precollinone **(58)** and lenticulone **(53)** showed antibacterial activity to Gram-positive bacteria *Staphylococcus carnosus*, *Bacillus amyloliquefaciens* und *Bacillus subtilis*. The MIC values for the inhibitory activity were determined. collinone **(41)** and griseorhodin A **(5)** showed the highest antibacterial activity.

Serine protease-inhibiting activity for the compounds and extracts were tested in the group of Prof. Michael Gütschow, at the University of Bonn. For griseorhodin A **(5),** didesoxygriseorhodin C (**46),** collinone **(41),** and lenticulone **(53)** a considerable inhibiting activity to human leukocyte elastase (HLE) was determined. The highest HLE-inhibiting activity is displayed by didesoxygriseorhodin C **(46).** (IC_{50}=3.10±0.83 μg mL^{-1}) The results impliy that the griseorhodin-type compounds could represent a new class of candidates for HLE inhibitors.

Cytotoxic and antiproliferative activities of griseorhodin A **(5),** didesoxygriseorhodin C (**46),** collinone **(41),** and lenticulone **(53)** were determined in the group of Hans-Martin Dahse in HKI, Jena. In general, the activities of all of these compounds were moderate and in the same range.

In addition, the absolute configuration of griseorhodin A **(5),** collinone **(41)** and precollinone **(58)** was determined by quantum chemical circular dichroism (CD) calculations in combination with experimental CD measurements in the group of Prof. Gerhard Bringmann, at the University of Würzburg.

6 ZUSAMMENFASSUNG

Griseorhodin A **(5)** ist ein Vertreter der Rubromycin-Familie der aromatischen Polyketide. Die Vertreter wie das γ-Rubromycin **(37)** und das Heliquinomycin **(39)** inhibieren HIV reverse Transkriptase und die menschliche Telomerase. Beide pharmakologischen Aktivitäten sind abhängig von der Spiroketal-Einheit der Substanzen. Bislang konnte nicht vollständig aufgeklärt werden, wie die Bakterien dieses Pharmacophore erzeugen.

In früheren Arbeiten wurde der Griseorhodin-Gencluster aus *Streptomyces* sp. JP95 isoliert und ein heterologes Expressionssystem erzeugt. Um die Griseorhodin A Biosynthese zu studieren, wurde von Kathrin Reinhardt in ihrer Dissertation 17 Mutantenstämme generiert, denen Biosynthesegene fehlen. Die Zielsetzung dieser Arbeit ist die Entwicklung effizienter Kultivierung-Protokolle, die chemisch-analytische Untersuchung und Strukturaufklärung der Metaboliten der Mutantenstämme mit Fokus auf der Funktion der 11 Post-PKS Oxygenasen sowie der Enzyme, deren Rollen in der Biosynthese bislang nicht aufgeklärt werden konnte.

Anhand der Ergebnisse war die Zuordnung der meisten Polyketid modifizierenden Enzyme und die Aufklärung der wesentlichen Schritte in der Pharmakophorebiosynthese möglich. Zusätzlich zum Metabolit Griseorhodin A **(5)** wurden Didesoxygriseorhodin C (**46),** Collinon **(41),** ZY1 (**54)**, Lenticulon **(53),** Precollinon **(58)**, KS-619-3 **(65)** und Secocollinon-1 **(59)** isoliert und strukturell characterisiert. Anhand der Ergebnisse der HR-LCMS-Analysen und der aufgeklärten Strukturen konnte ein Verlauf der Biosynthese von Griseorhodin A **(5)** postuliert werden. (Abschnitt 3.7) Unter den Metaboliten, konnten als neue Naturstoffe die Strukturen von ZY1 (**54)**, Lenticulon **(53),** Precollinon **(58)**, KS-619-3 **(65)** und Secocollinon-1 **(59)** identifiziert werden. Zusätzlich zu den Biosynthesestudien wurde eine Untersuchung der *in vitro* Enzymaktivität für die Oxygenase GrhO6 durchgeführt.

In Bioaktivitätsstudien haben Griseorhodin A **(5),** Didesoxygriseorhodin C **(46),** Collinon **(41),** Precollinon **(58)** und Lenticulon **(53)** antibakterielle Aktivitäten

gegen die Gram-positiven Stämme *Staphylococcus carnosus*, *Bacillus amyloliquefaciens* und *Bacillus subtilis* gezeigt. Die MIC-Werte wurden bestimmt. Collinone **(41)** und Griseorhodin A **(5)** haben die höchsten antibakteriellen Aktivitäten gezeigt.

Die Serine-Protease-inhibierende Wirkung der Substanzen und Mutant-extrakte wurde in der Gruppe von Prof. Michael Gütschow am Pharmazeutischen Institut der Universität Bonn untersucht. Griseorhodin A **(5),** Didesoxygriseorhodin C **(46),** Collinon **(41),** und Lenticulon **(53)** besitzen eine hohe hemmende Wirkung gegen die menschliche Leucocyten Elastase (HLE). Die stärkste HLE-Hemmung wurde für Didesoxygriseorhodin C **(46)** nachgewiesen (IC_{50}=3.10±0.83 µg mL^{-1}). Aufgrund dieser Ergebnisse Substanzen der Griseorhodintyps gute Kandidaten für eine neue Klasse von HLE-Inhibitoren sein.

Zytotoxizitäten und antiproliferative Wirkungen der isolierten Substanzen wurden von Hans-Martin Dahse am HKI, Jena, bestimmt. Bei den Substanzen Griseorhodin A **(5),** Didesoxygriseorhodin C **(46),** Collinon **(41),** und Lenticulon **(53)** wurden moderate Zytotoxizitäten und antiproliferative Wirkungen ermittelt.

Außerdem wurde in einer weiteren kooperation die vollständige Strukturaufklärung die absoluten Konfigurationen von Griseorhodin A **(5),** Collinon **(41)** und Precollinon **(58)** durch quantenchemische Circulardichroismus-Kalkulationen in Kombination mit experimentellen Circulardichroismus-Werten in der Gruppe von Prof. Gerhardt Bringmann an der Universität Würzburg bestimmt.

7 APPENDIX

APPENDIX 1: MS Data

APPENDIX 2: NMR Spectra

APPENDIX 3: IR Spectra

7.1 APPENDIX 1: MS Data

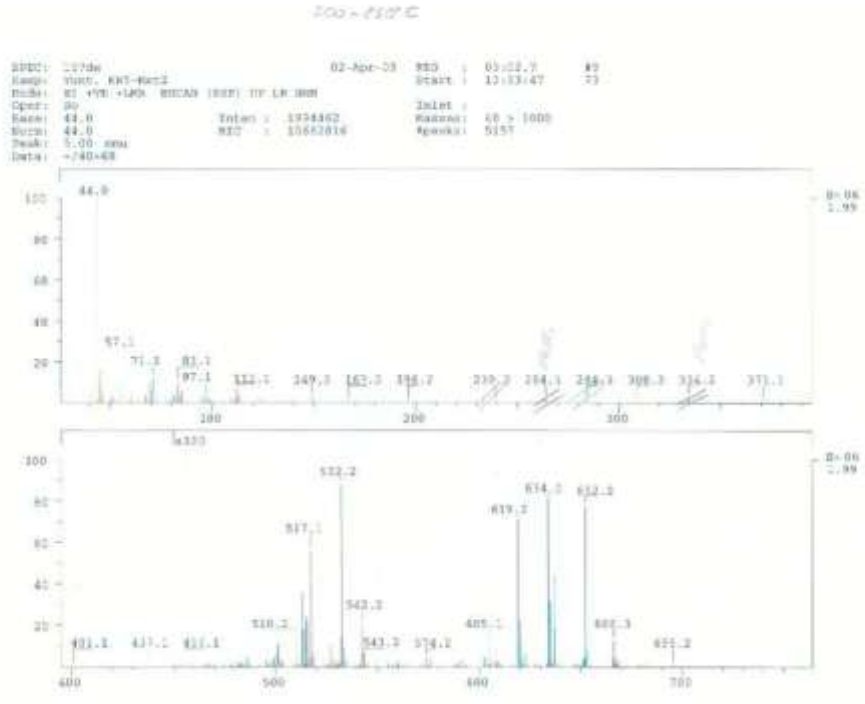

Figure 1.1 EI-MS data of secocollinone-1 (59).

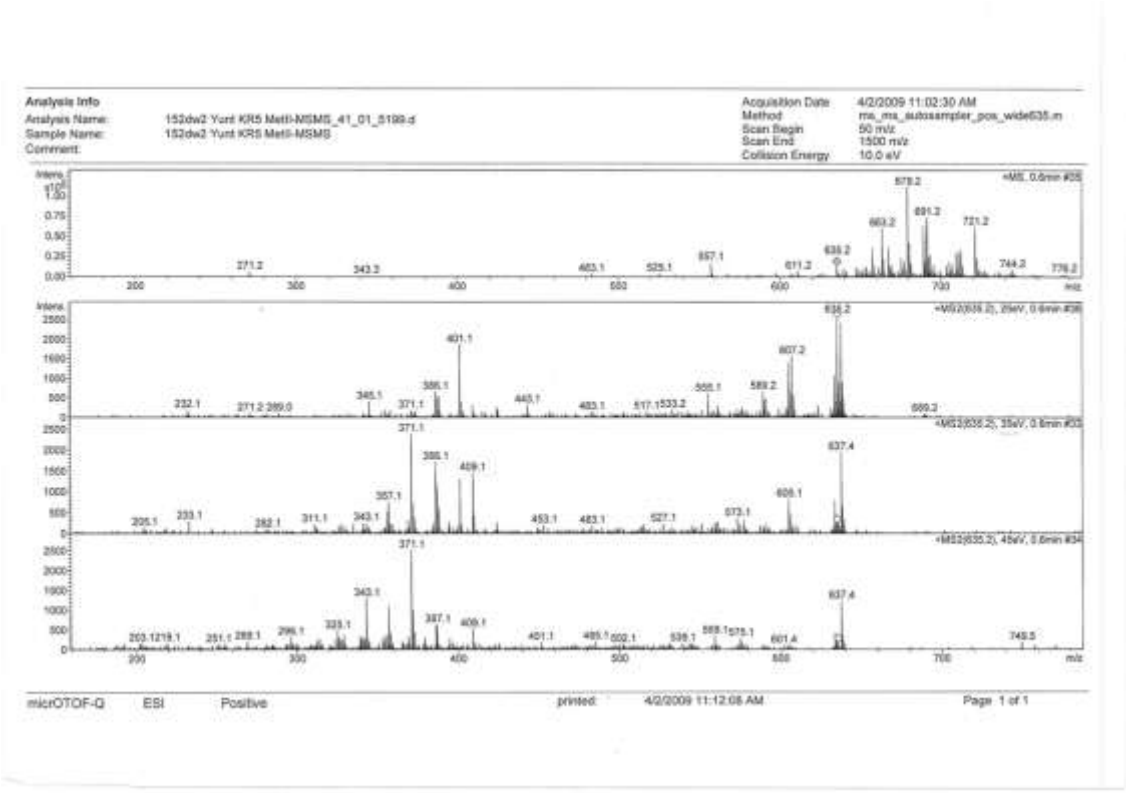

Figure 1.2 ESI-MS/MS of secocollinone-1 (59).

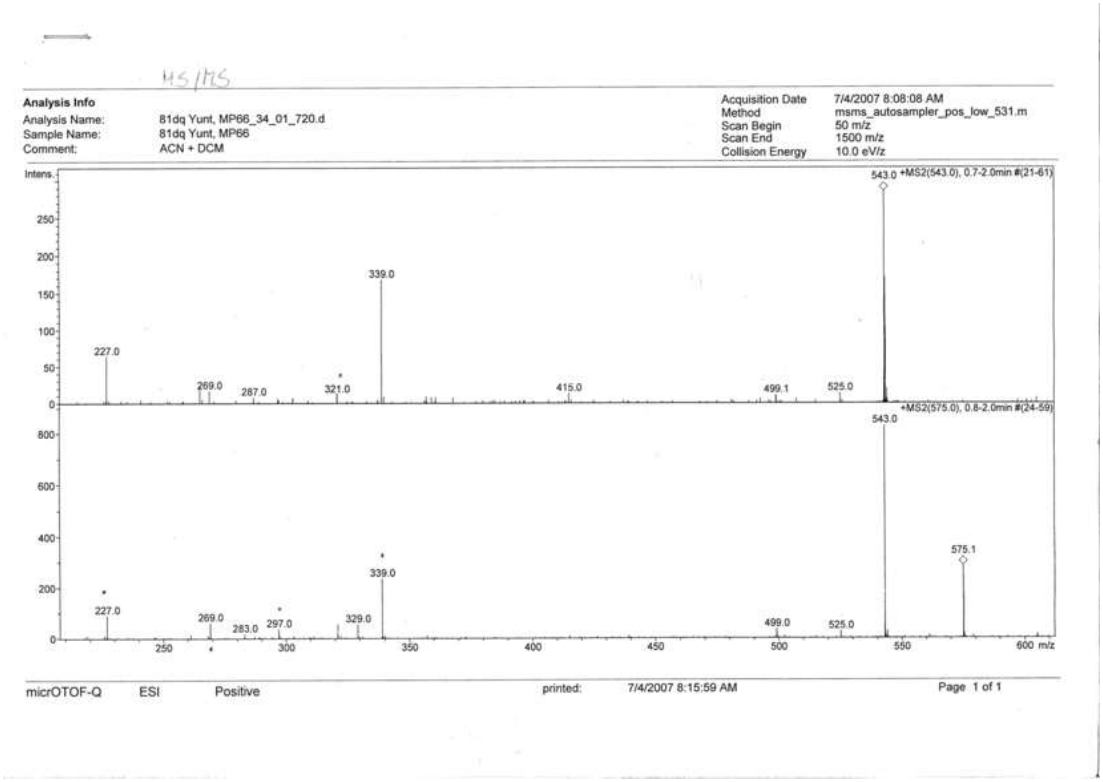

Figure 1.3 ESI-MS/MS of lenticulone (53).

7.2 APPENDIX 2: NMR Spectra

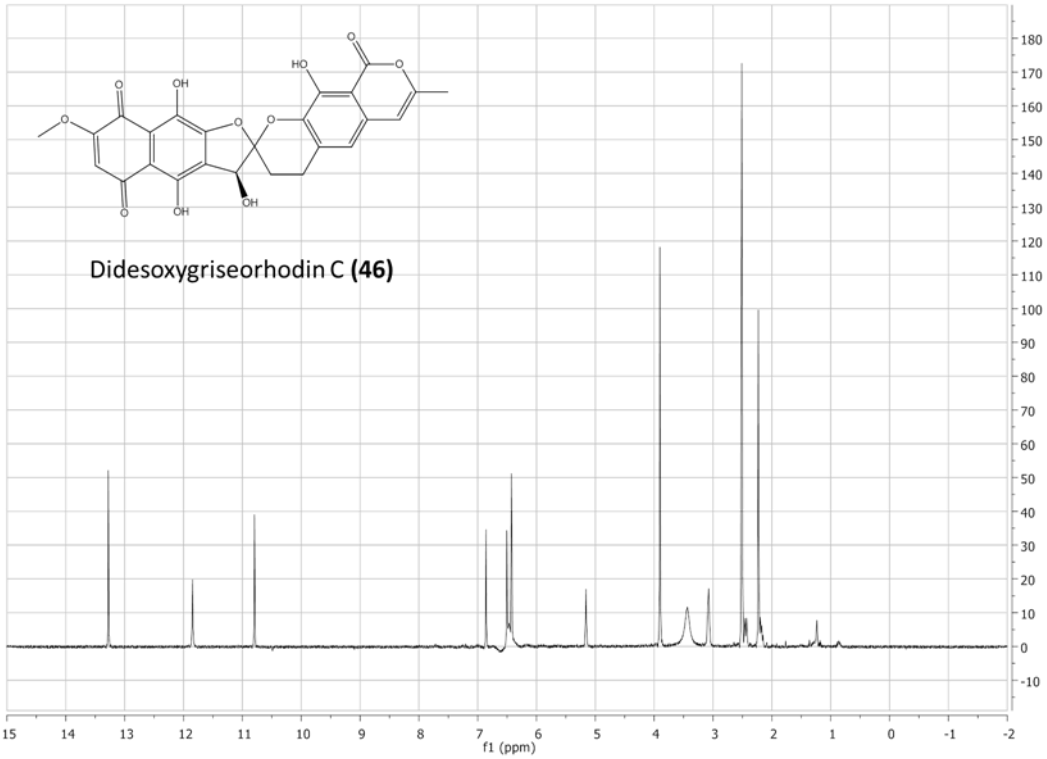

Figure 2.1 ^{1}H-NMR spectrum of didesoxygriseorhodin C (46), in DMSO-d_6, 500 MHz

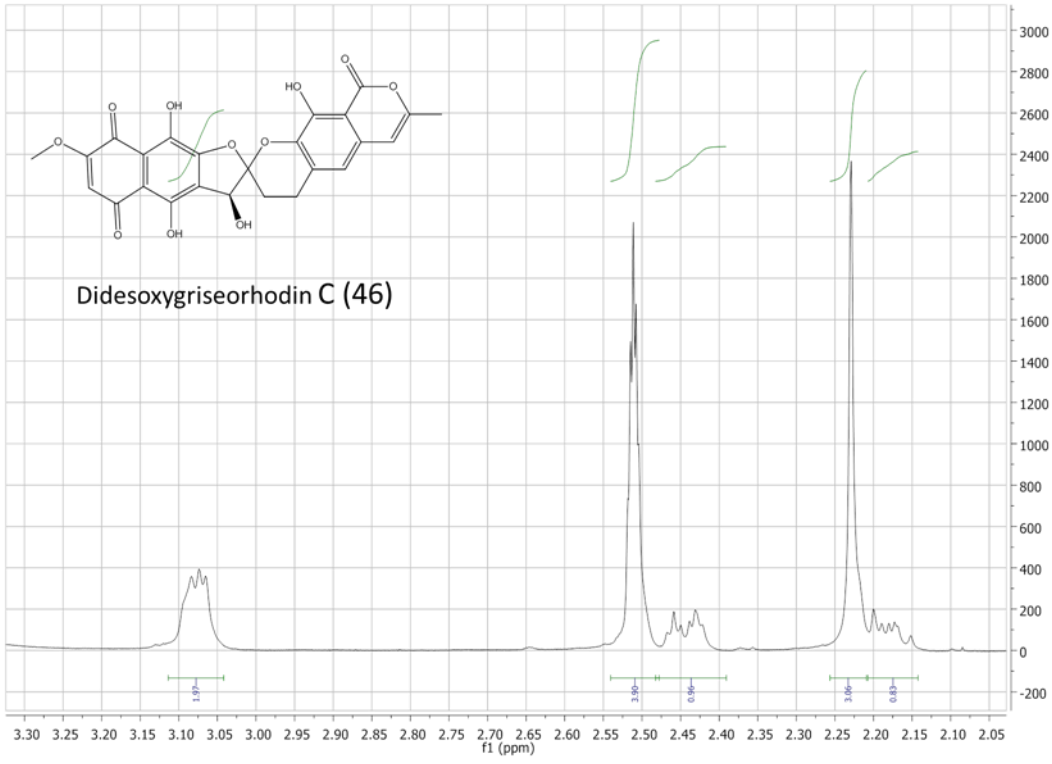

Figure 2.2 ^{1}H-NMR spectrum of didesoxygriseorhodin C (46), in DMSO-d_6, 500 MHz.

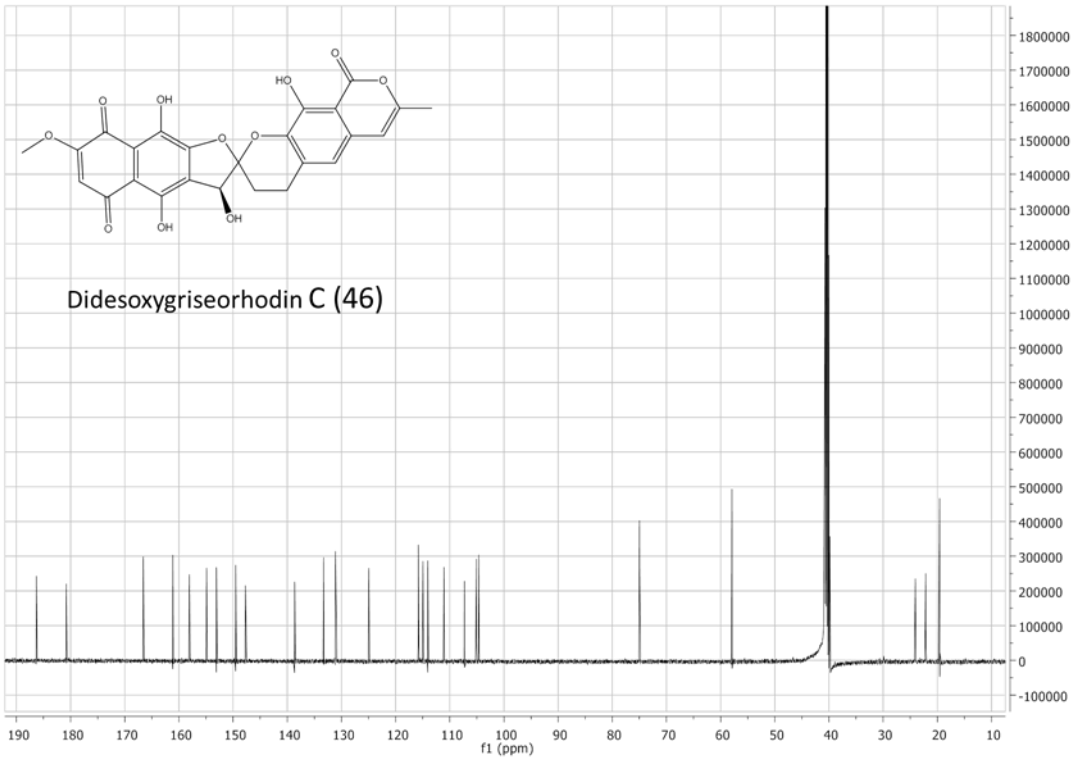

Figure 2.3 ^{13}C-NMR spectrum of didesoxygriseorhodin C (46), in DMSO-d_6, 500 MHz.

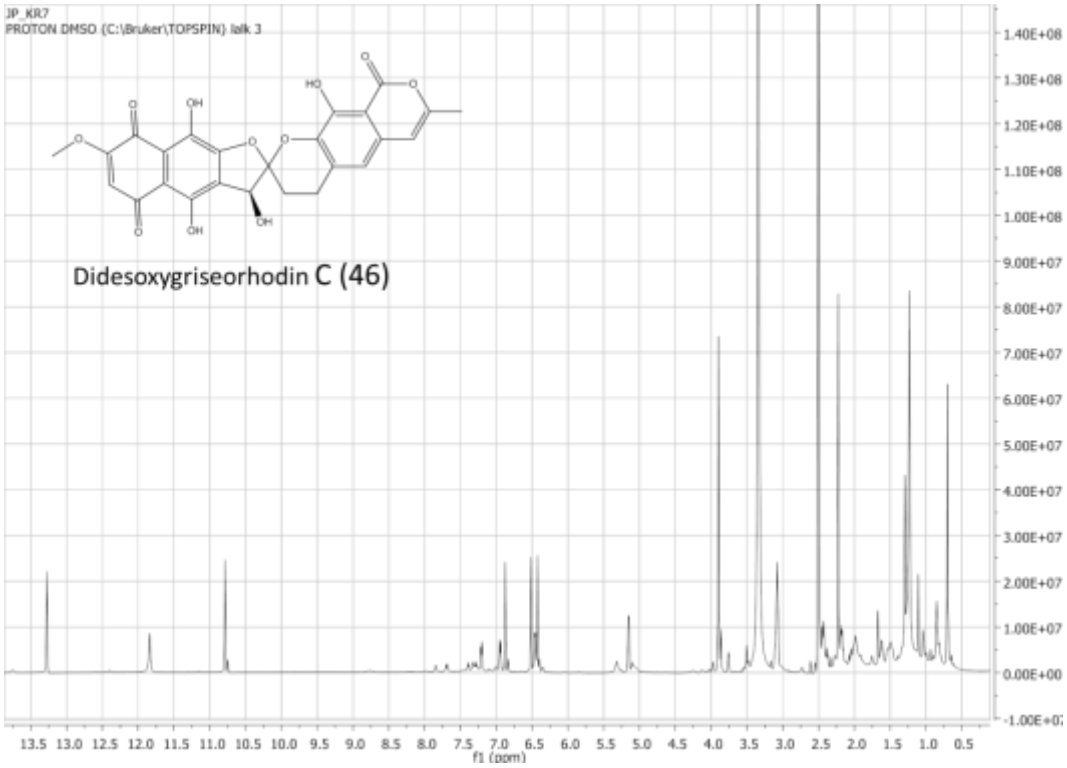

Figure 2.4 LC-^{1}H-NMR spectrum of didesoxygriseorhodin C (46), in AN-d_3, 500 MHz.

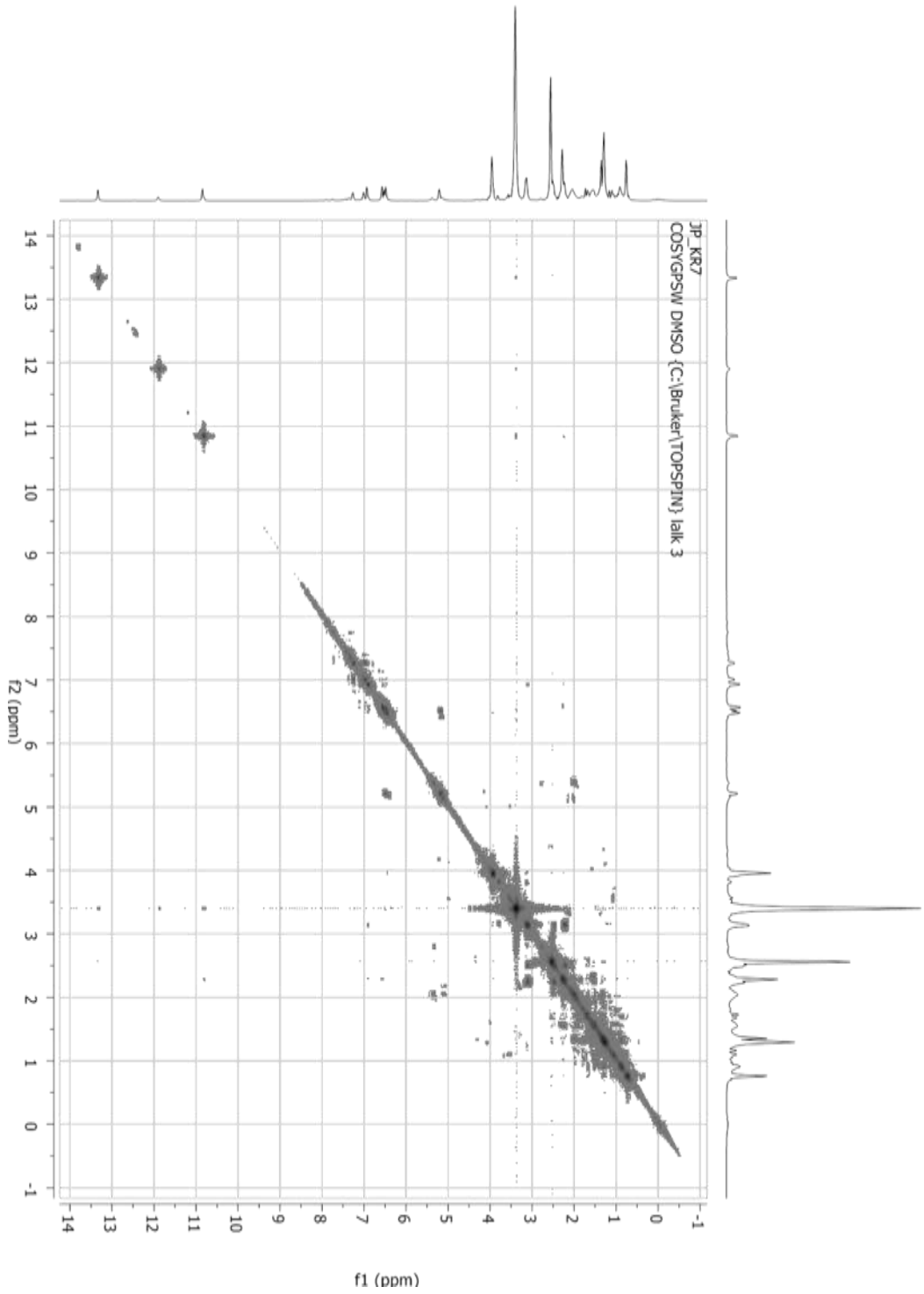

Figure 2.5 LC-HH-COSY-NMR spectrum of didesoxygriseorhodin C (46), in AN-d_3, 500 MHz.

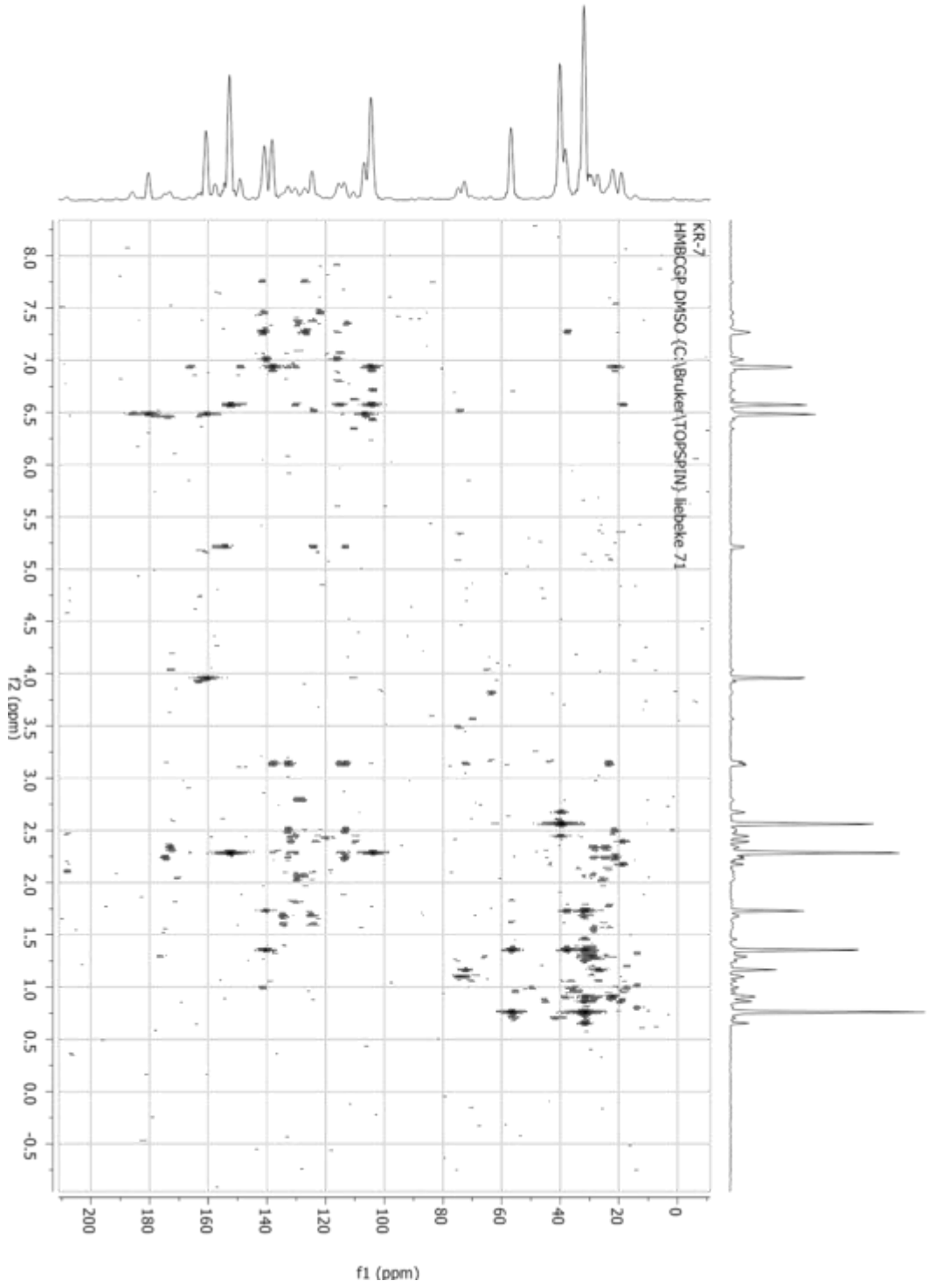

Figure 2.6 LC-HMBC-NMR spectrum of didesoxygriseorhodin C (46), in AN-d_3, 500 MHz.

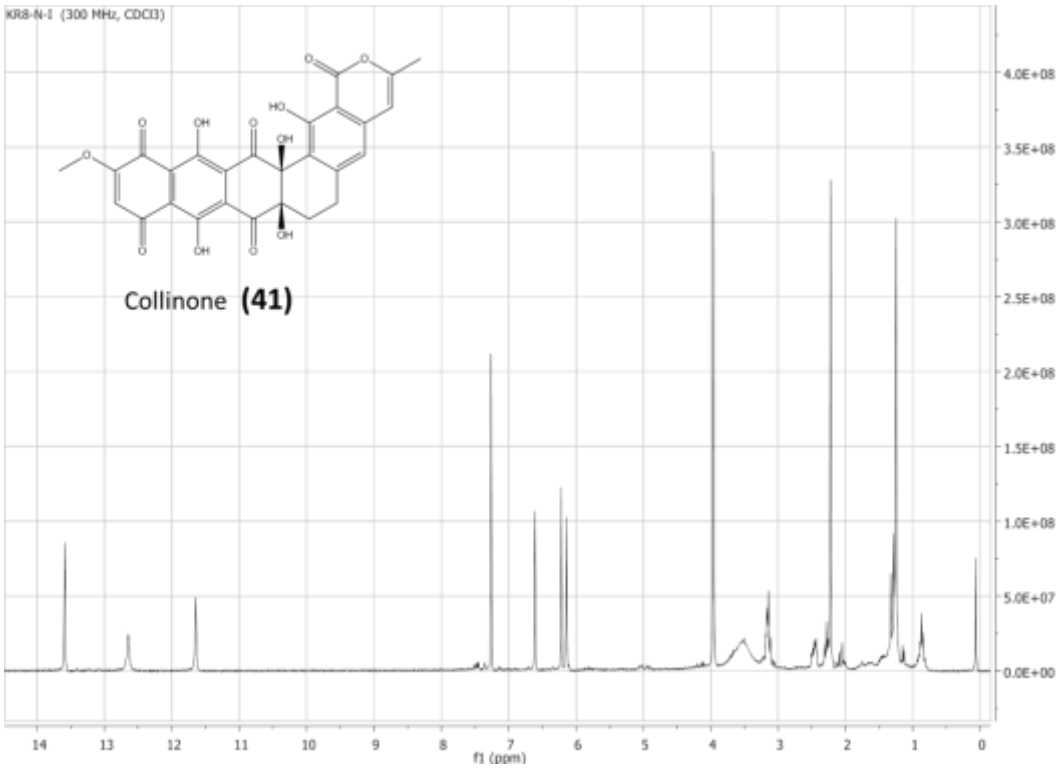

Figure 2.7 ^{1}H-NMR spectrum of collinone (41), in $CDCl_3$, 400 MHz.

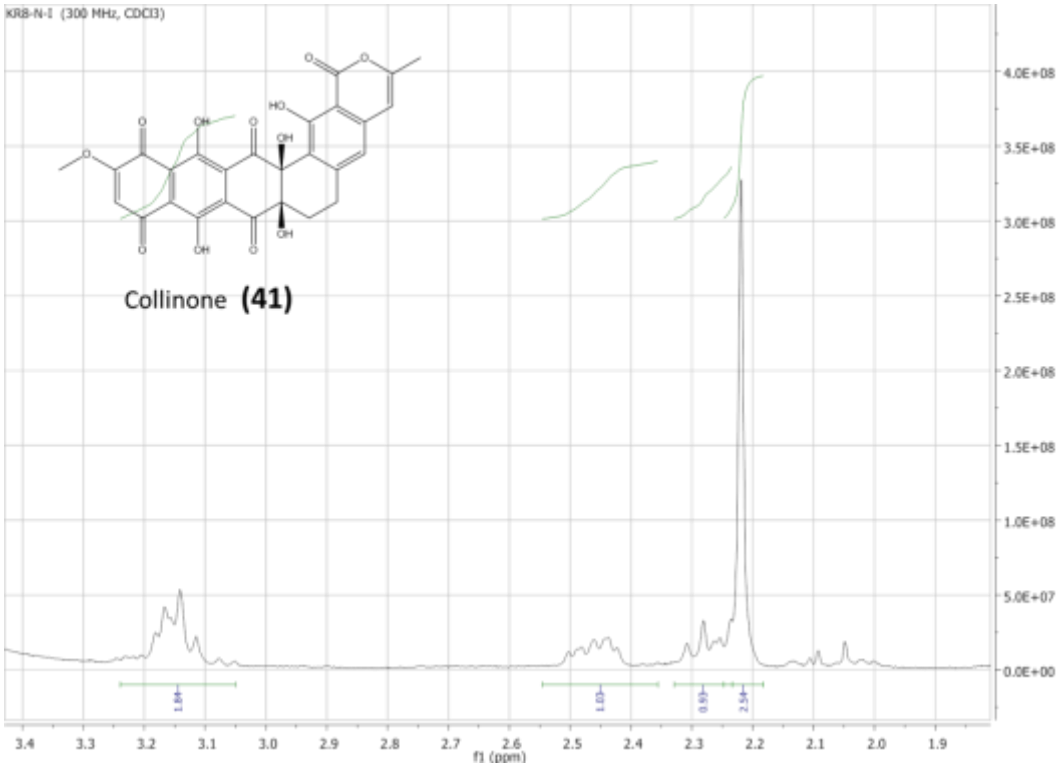

Figure 2.8 ^{1}H-NMR spectrum of collinone (41), in $CDCl_3$, 400 MHz.

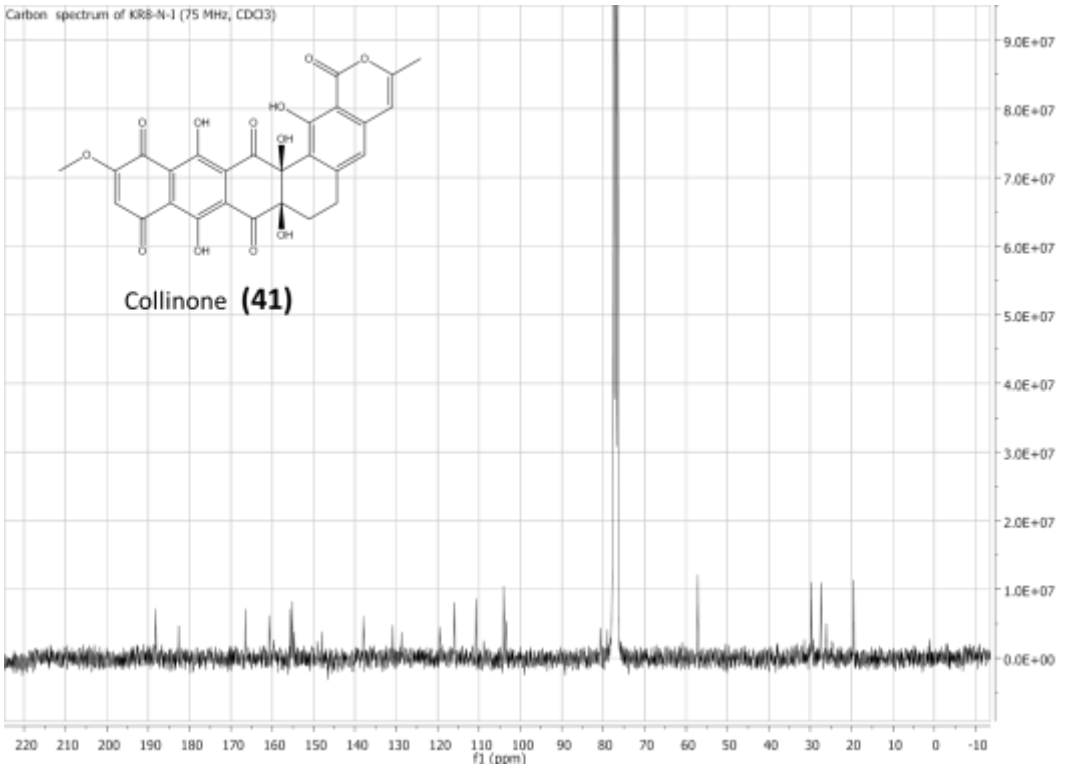

Figure 2.9 ^{13}C-NMR spectrum of collinone (41), in $CDCl_3$, 400 MHz.

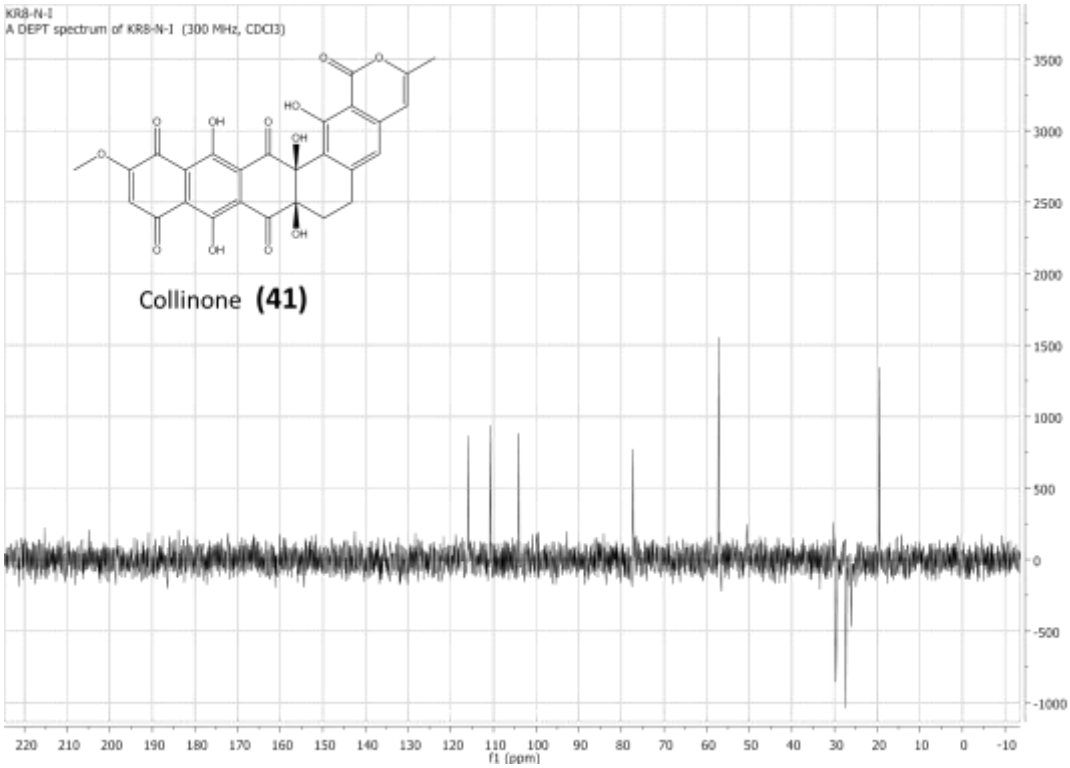

Figure 2.10 DEPT spectrum of collinone (41), in $CDCl_3$, 400 MHz.

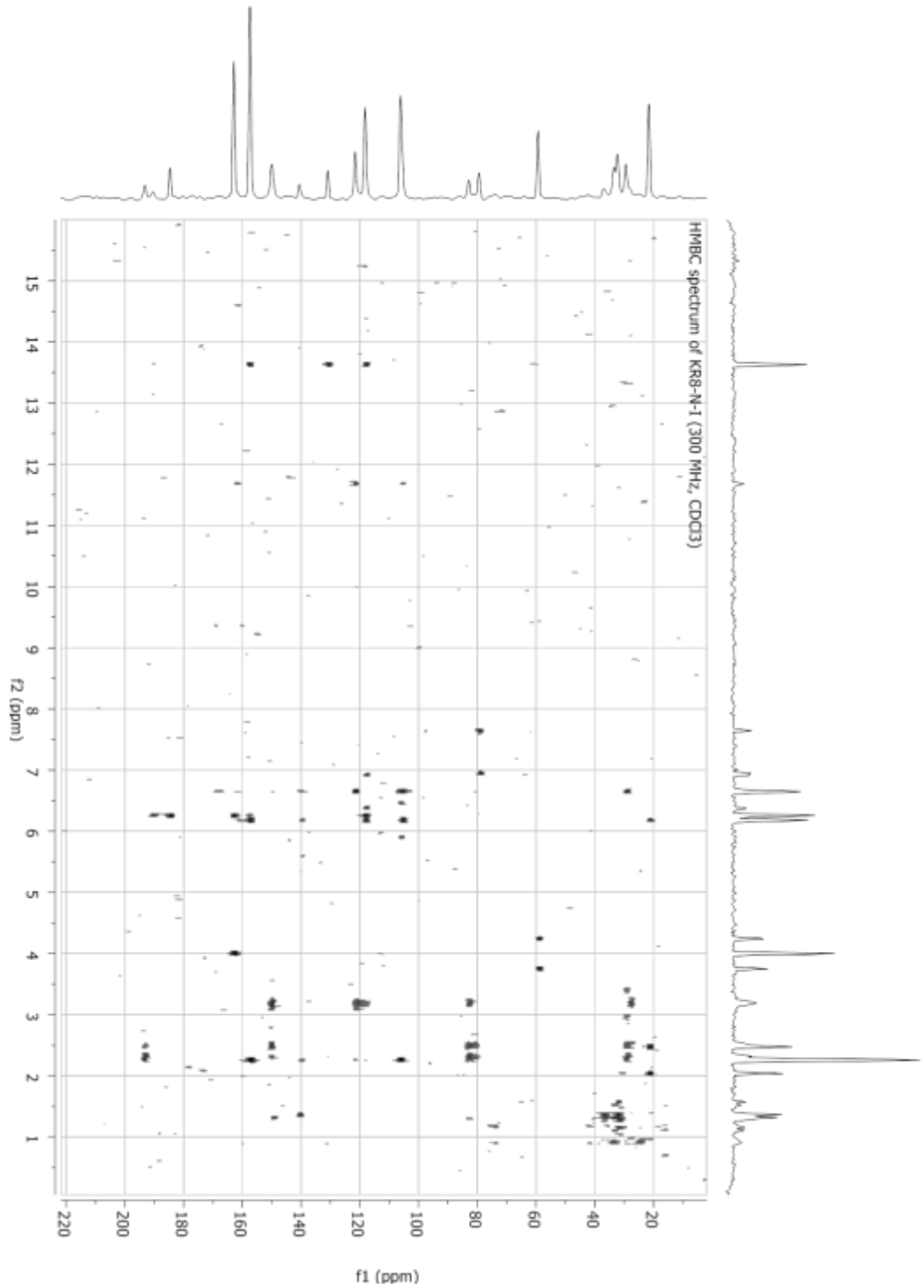

Figure 2.11 HMBC spectrum of collinone (41), in $CDCl_3$, 400 MHz

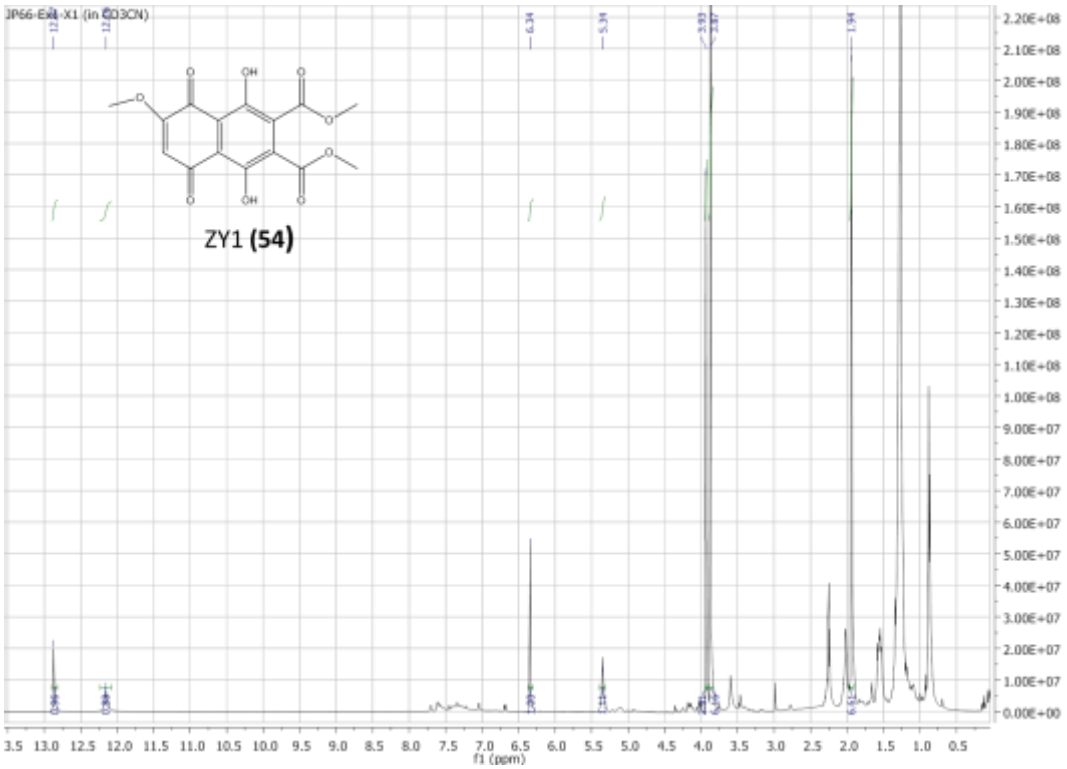

Figure 2.12 LC-^{1}H-NMR spectrum of ZY1 (54), in AN-d_3, 500 MHz

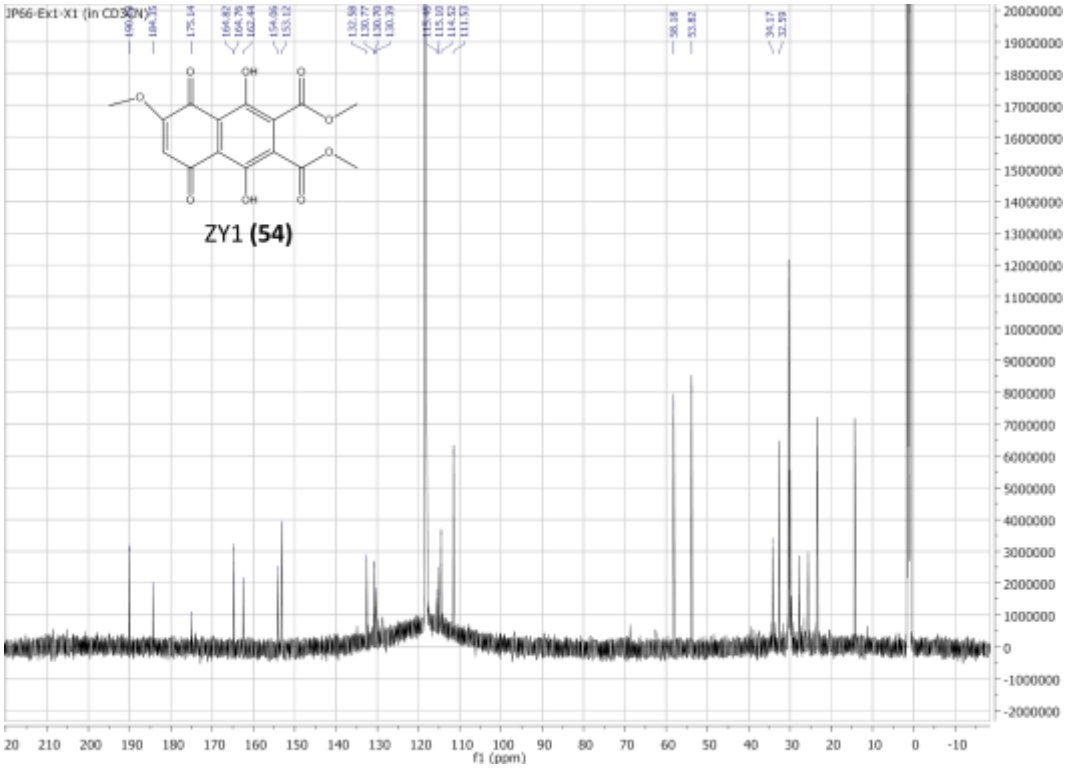

Figure 2.13 LC-^{13}C-NMR spectrum of ZY1 (54), in AN-d_3, 500 MHz

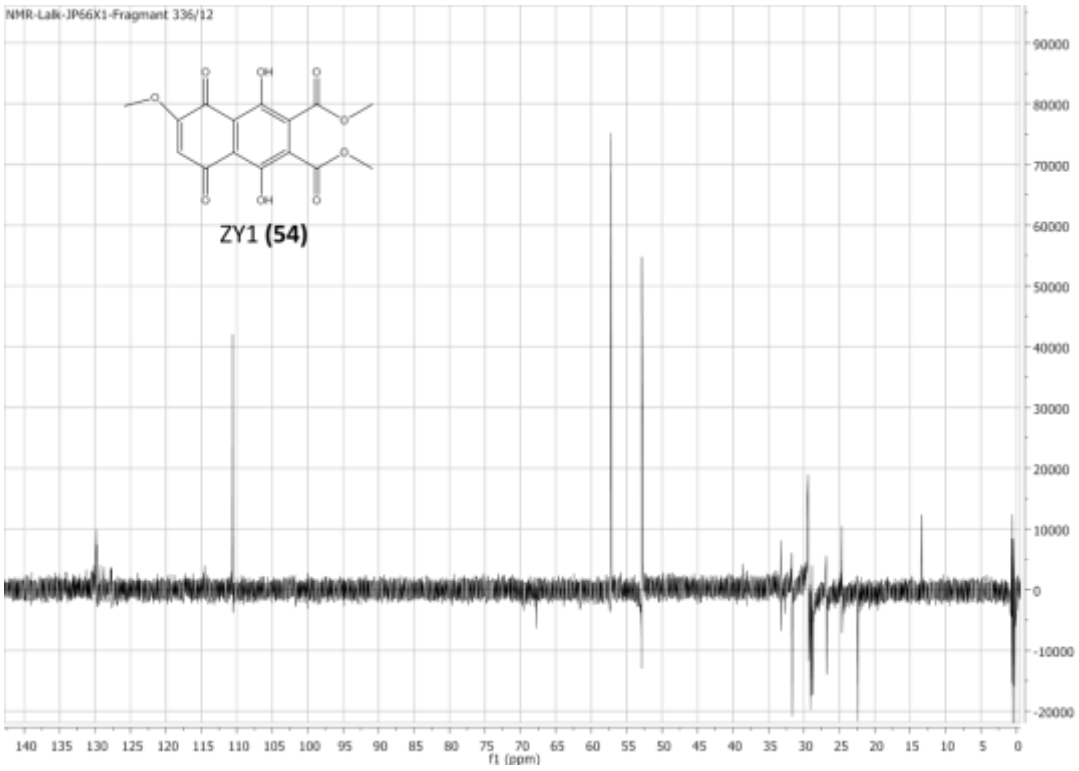

Figure 2.14 LC-DEPT spectrum of ZY1 (54), in AN-d_3, 500 MHz

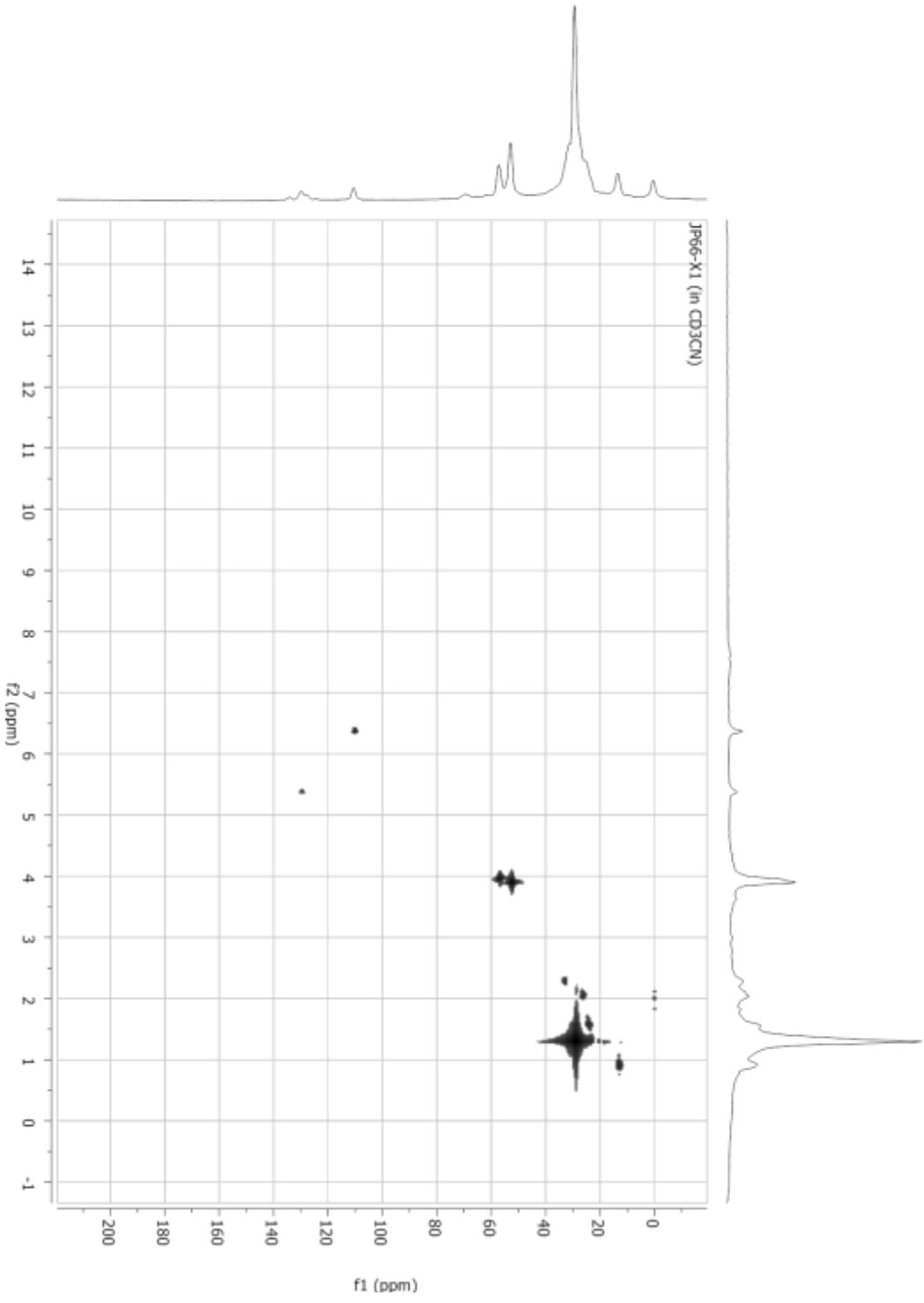

Figure 2.15 LC-COSY spectrum of ZY1 (54), in AN-d3, 500 MHz

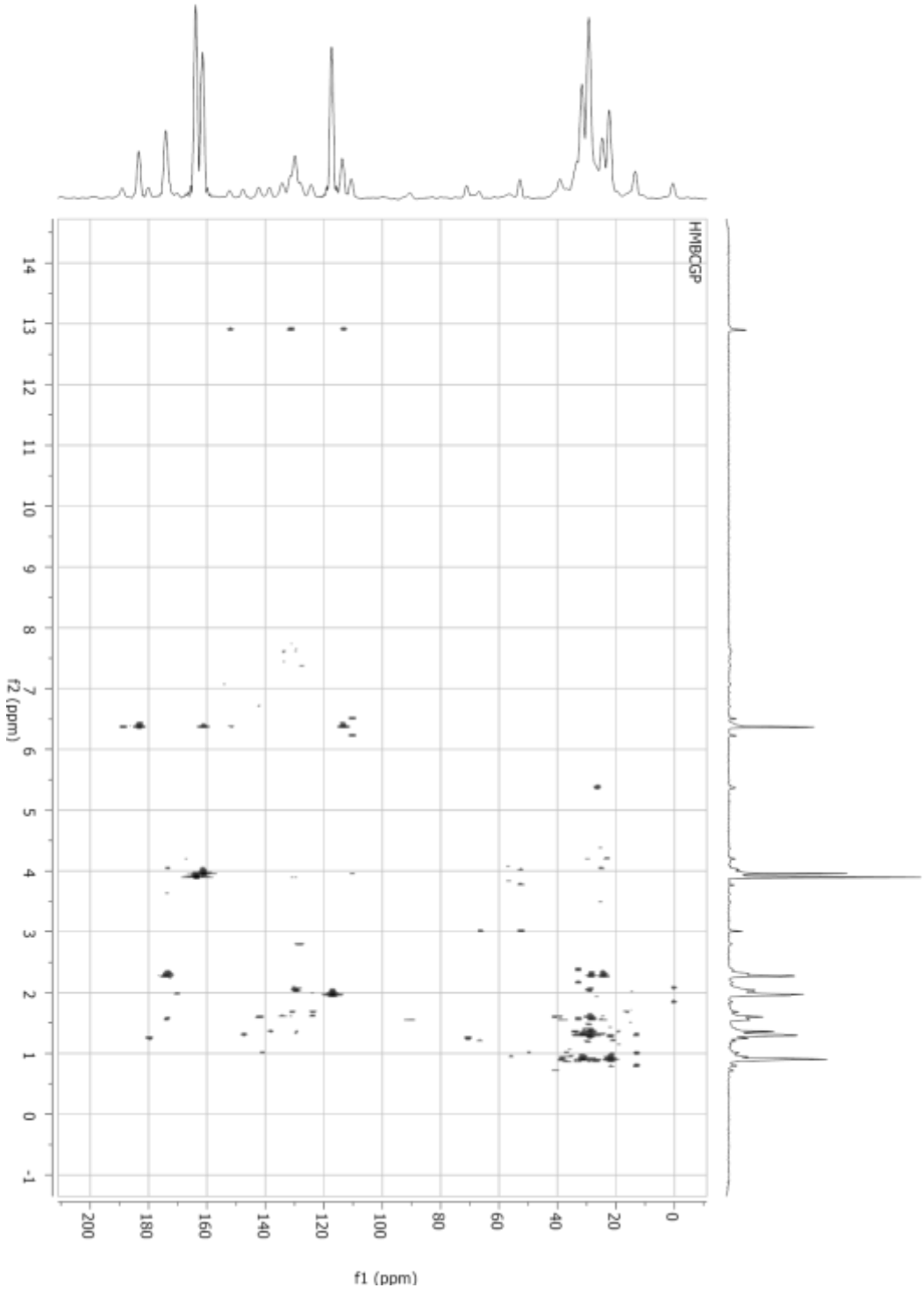

Figure 2.16 LC-HMBC spectrum of ZY1 (54), in AN-d3, 500 MHz

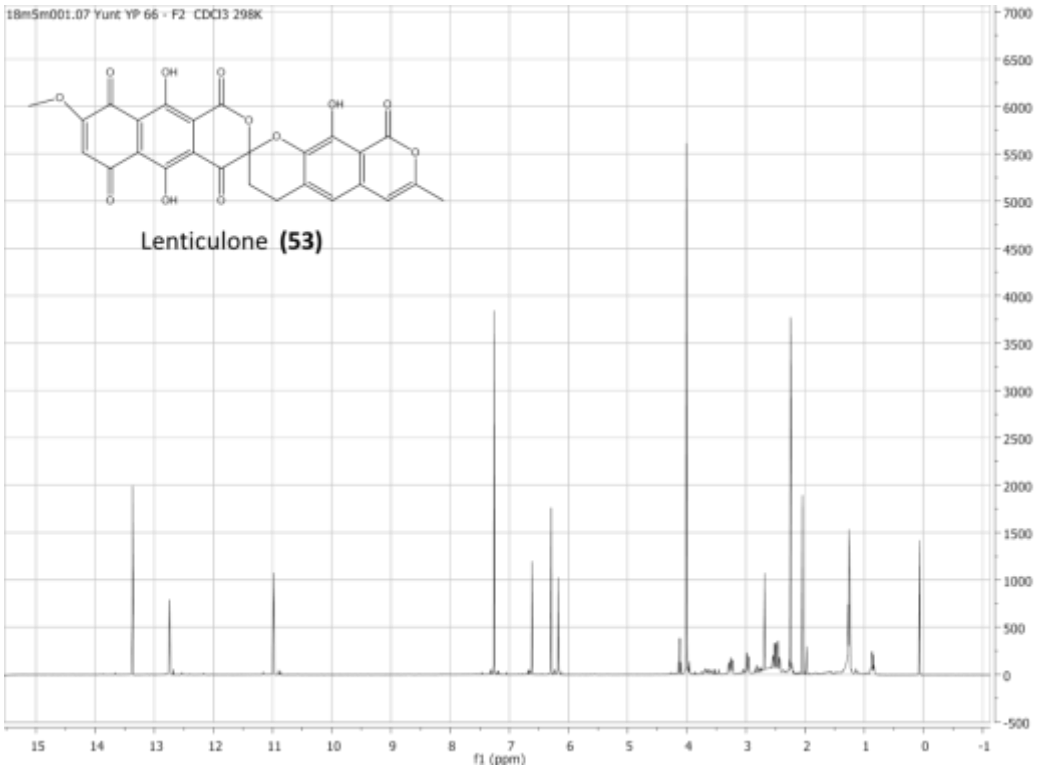

Figure 2.17 ^{1}H-NMR spectrum of lenticulone (53), in $CDCl_3$, 500 MHz.

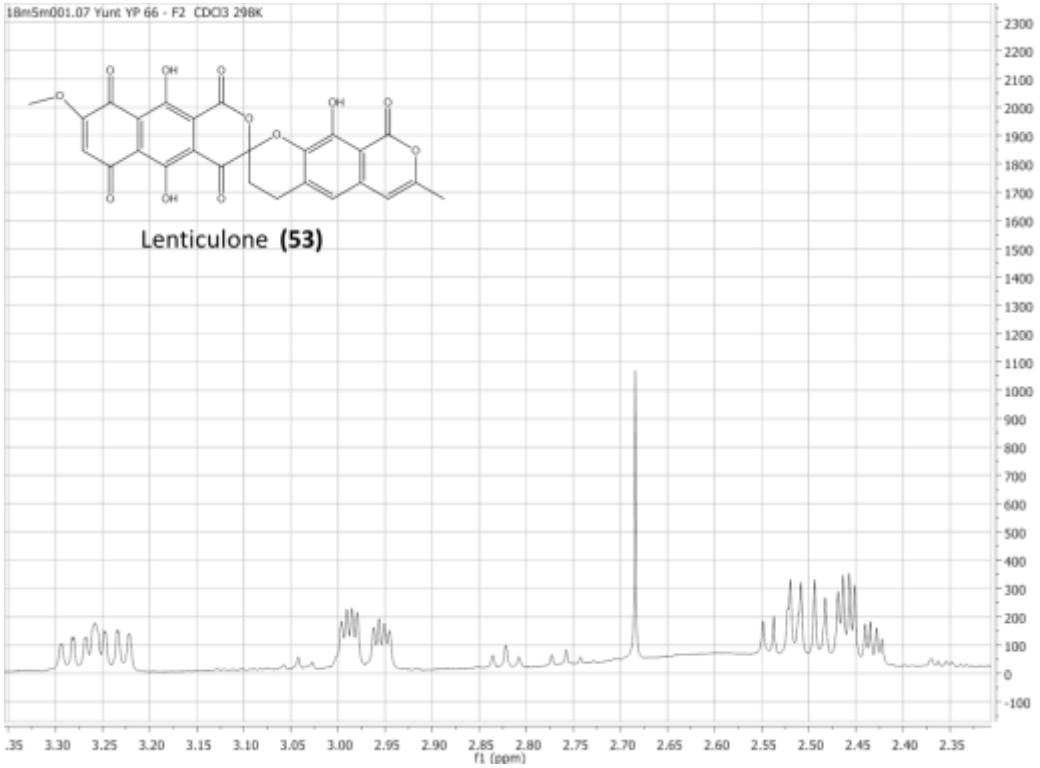

Figure 2.18 ^{1}H-NMR spectrum of lenticulone (53), in $CDCl_3$, 500 MHz.

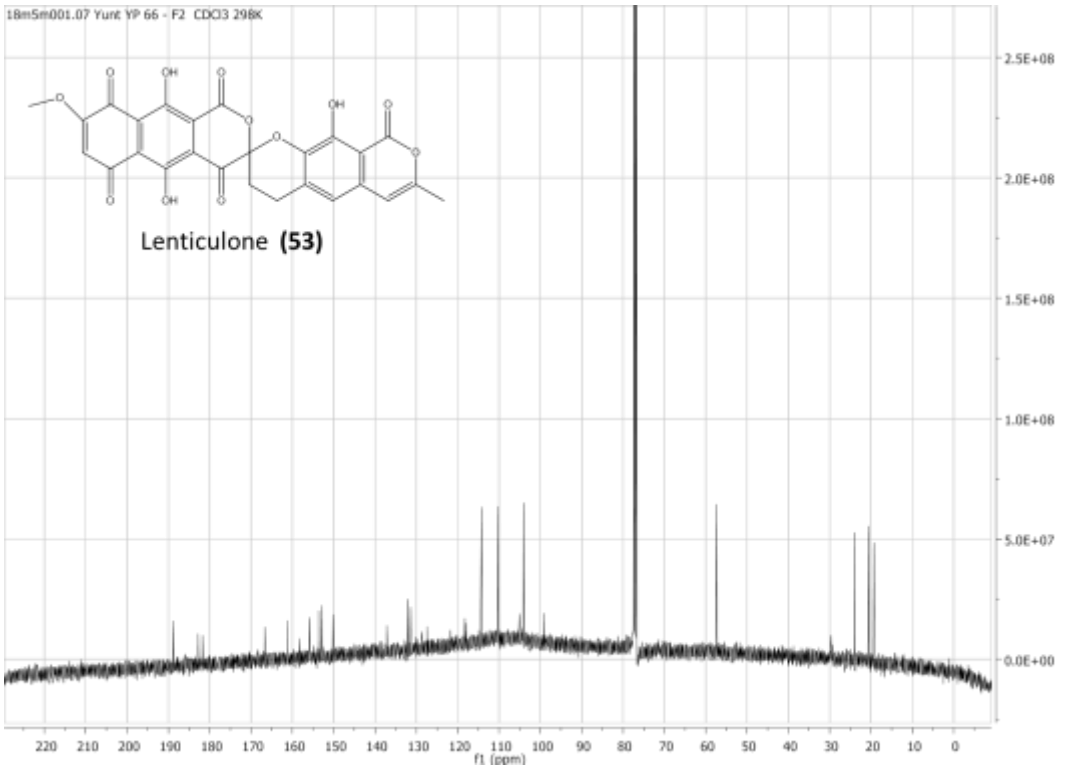

Figure 2.19 ^{13}C-NMR spectrum of lenticulone (53), in $CDCl_3$, 400 MHz.

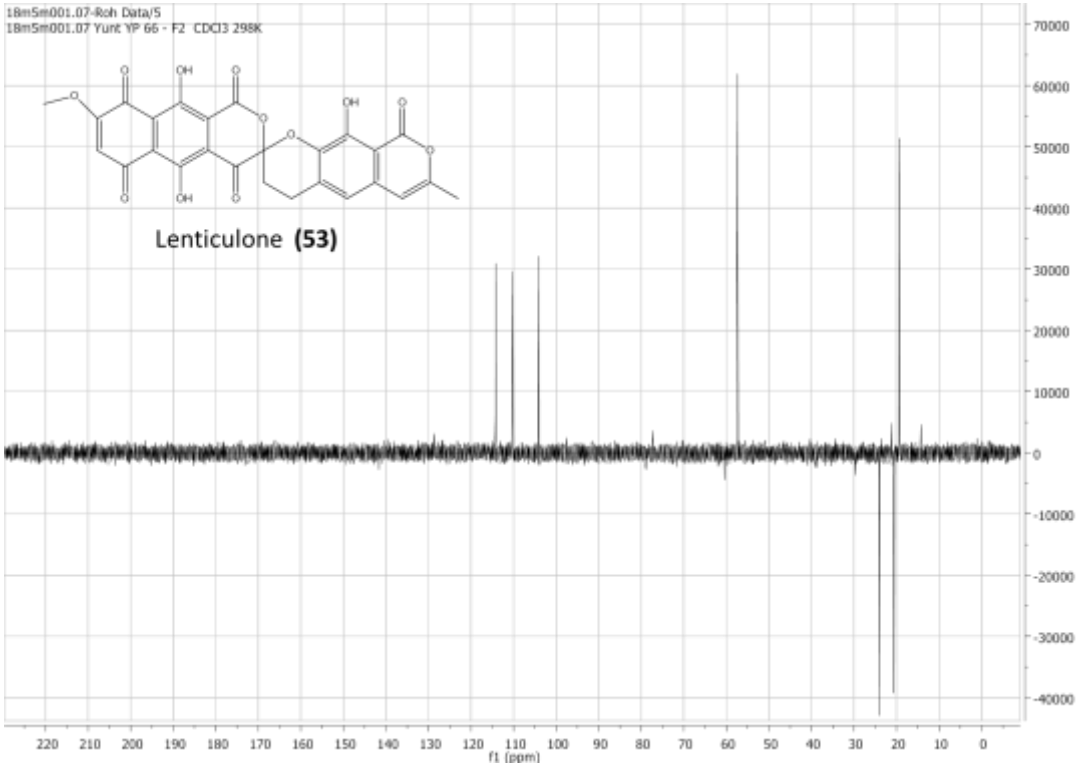

Figure 2.20 DEPT spectrum of lenticulone (53), in $CDCl_3$, 400 MHz.

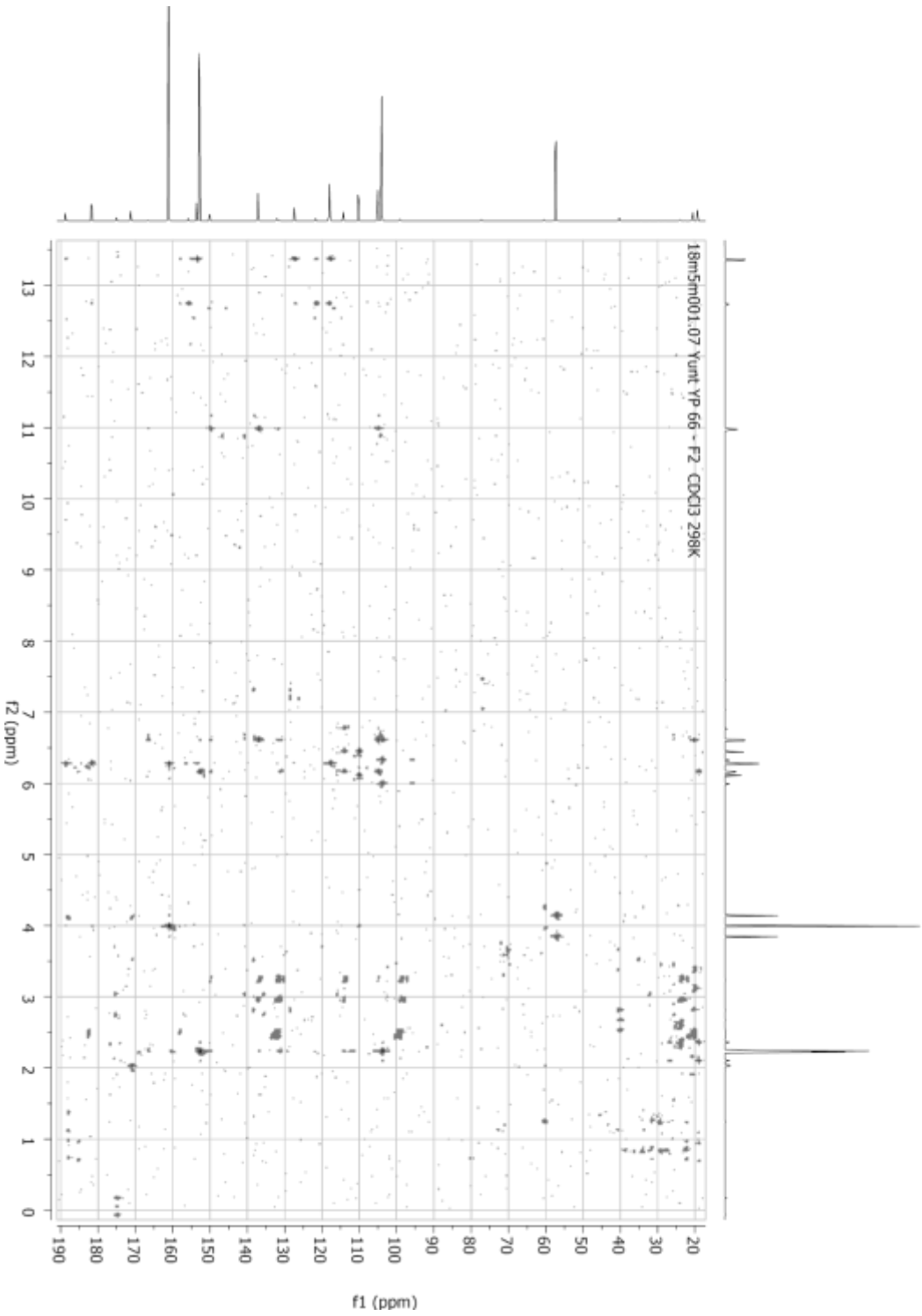

Figure 2.21 HMBC spectrum of lenticulone (53), in $CDCl_3$, 500 MHz.

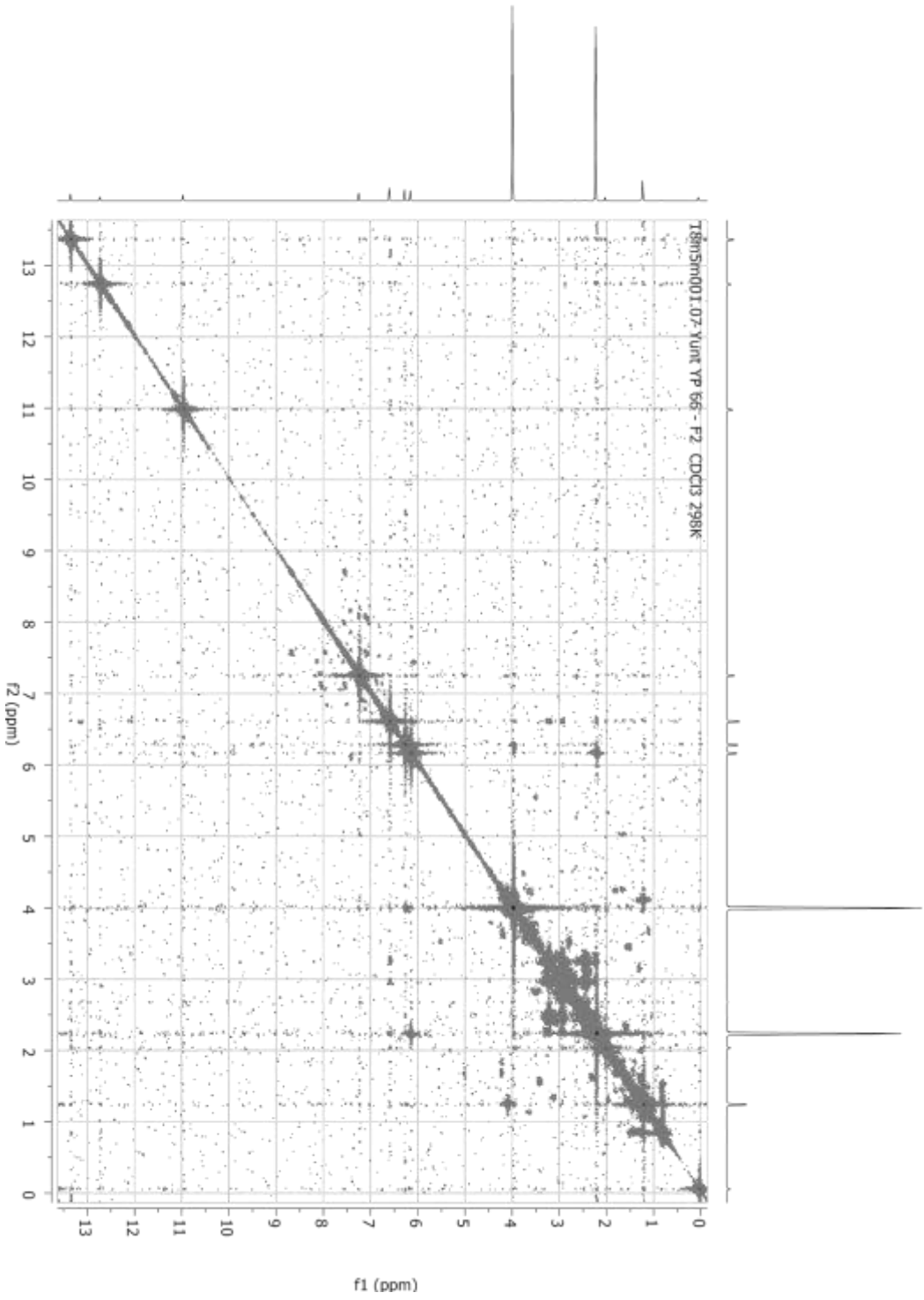

Figure 2.22 H-H-Cosy spectrum of lenticulone (53), in $CDCl_3$, 500 MHz.

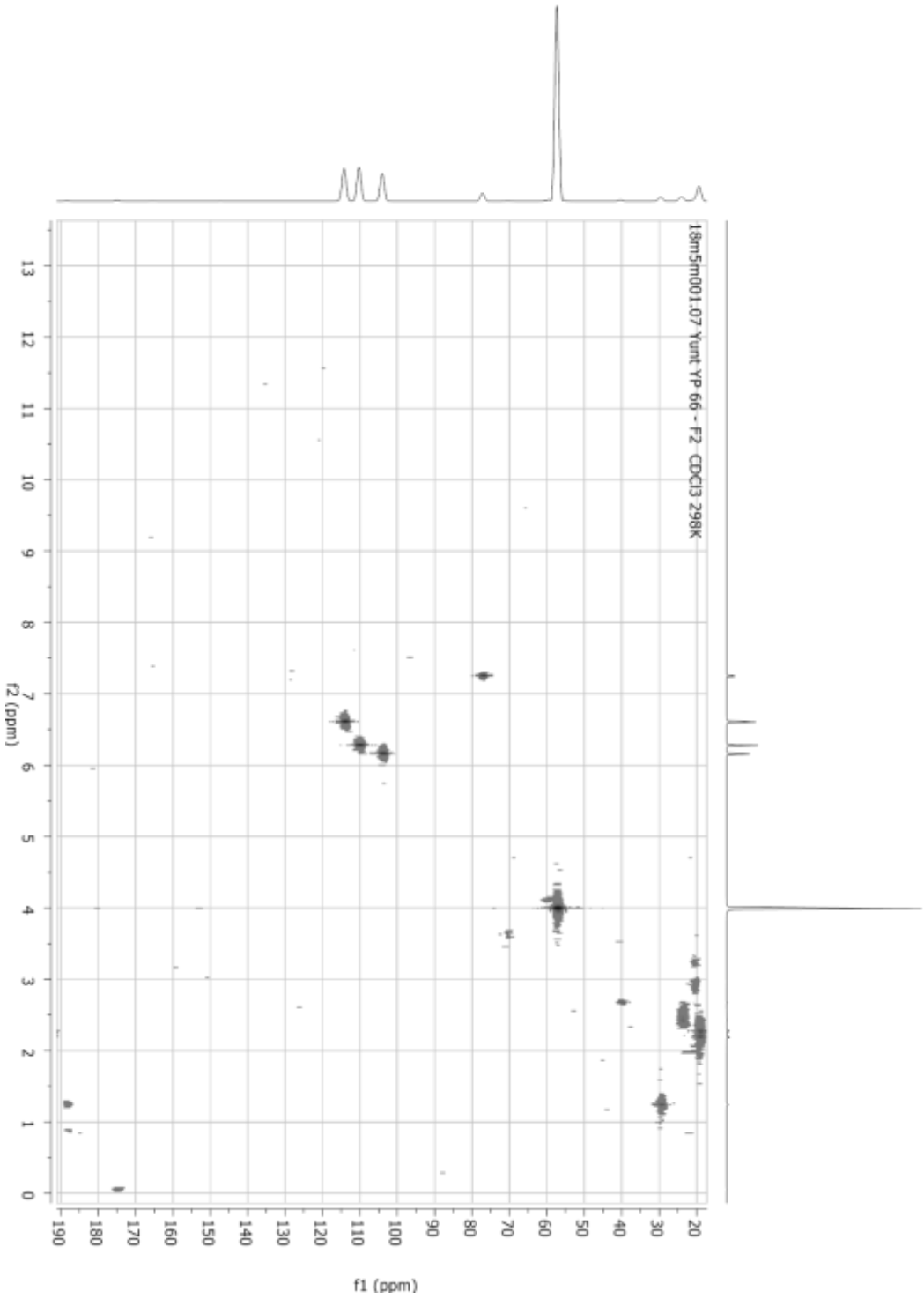

Figure 2.23 HMQC spectrum of lenticulone (53), in $CDCl_3$, 500 MHz.

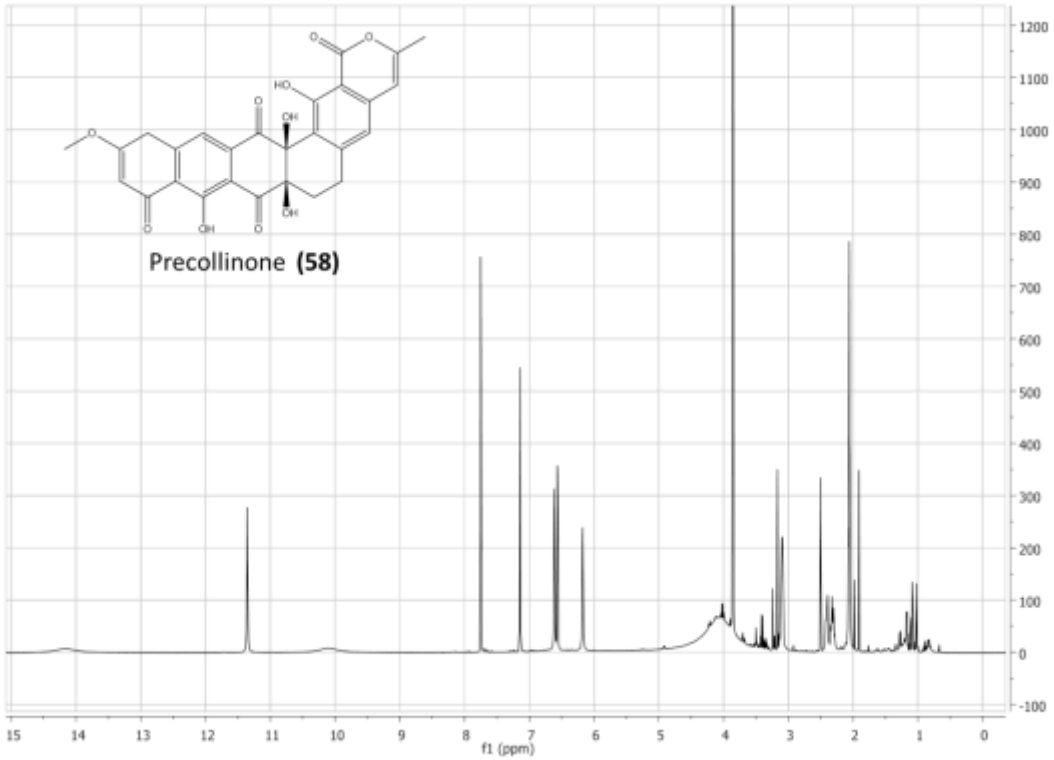

Figure 2.24 ^{1}H-NMR spectrum of precollinone (58), in DMSO-d_6, 500 MHz.

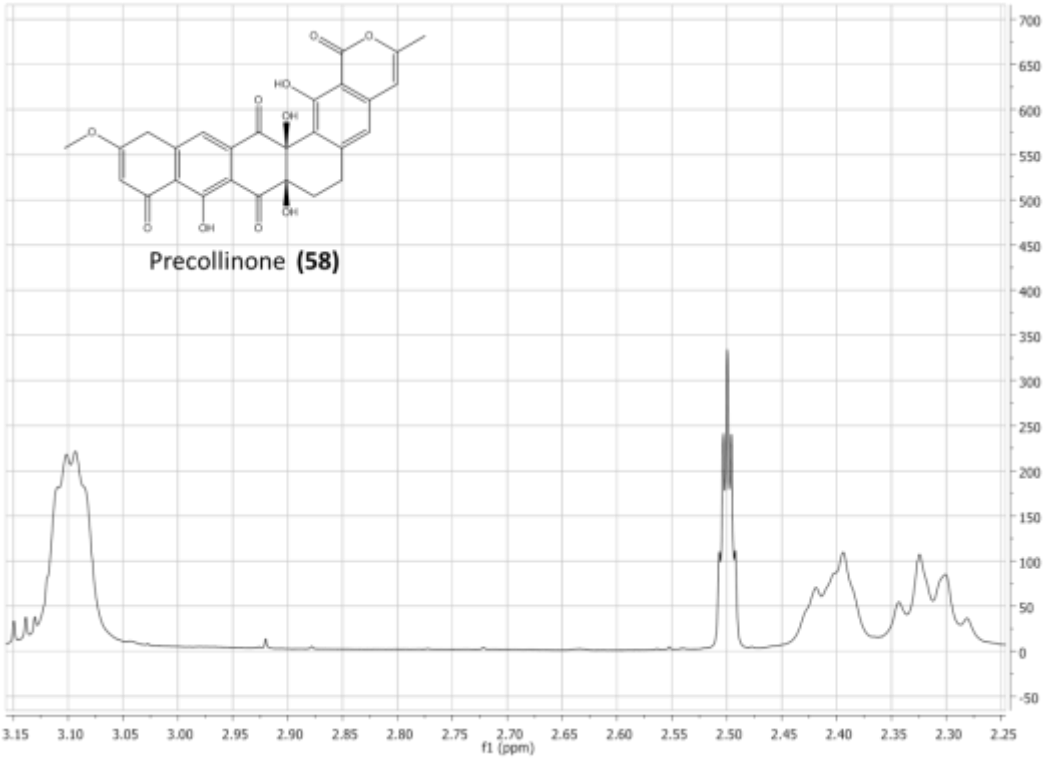

Figure 2.25 ^{1}H-NMR spectrum of precollinone (58), in DMSO-d_6, 500 MHz.

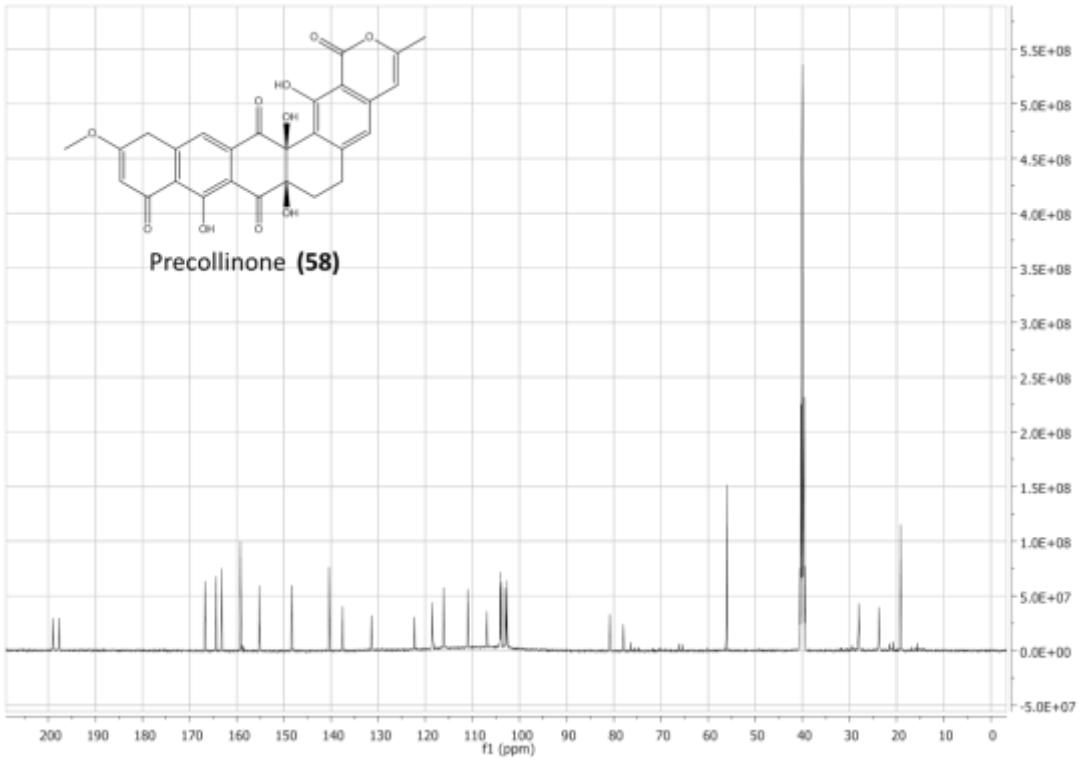

Figure 2.26 ^{13}C-NMR spectrum of precollinone (58), in DMSO-d_6, 400 MHz.

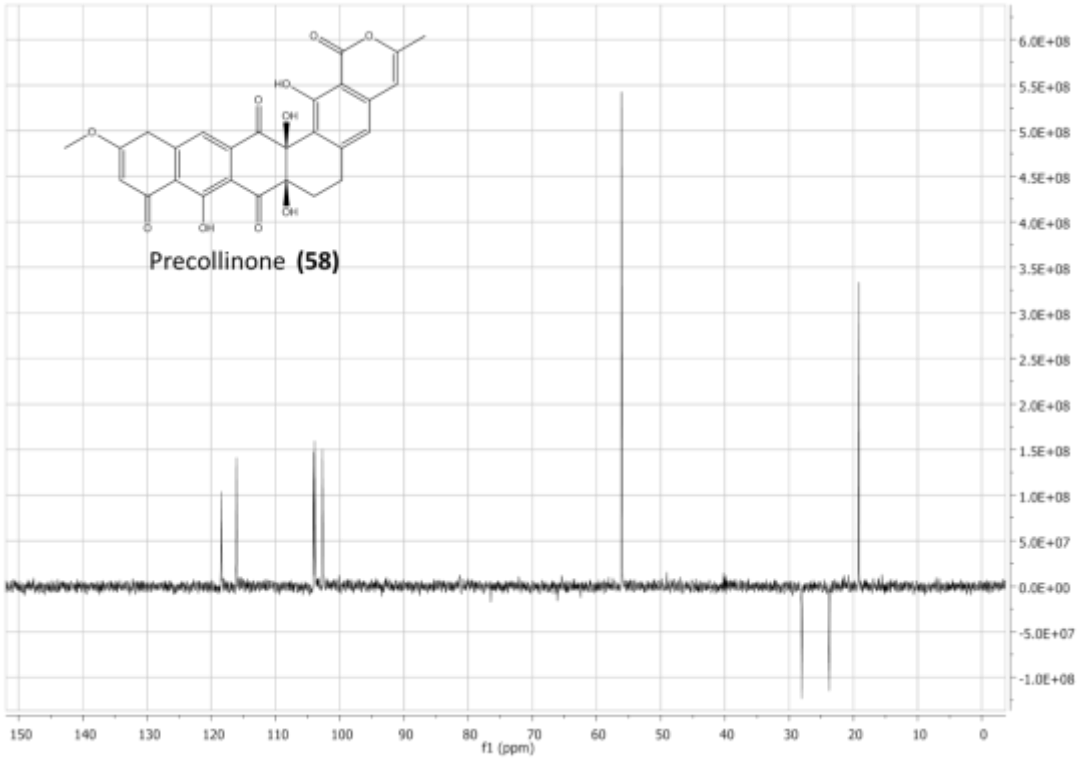

Figure 2.27 DEPT spectrum of precollinone (58), in DMSO-d_6, 400 MHz.

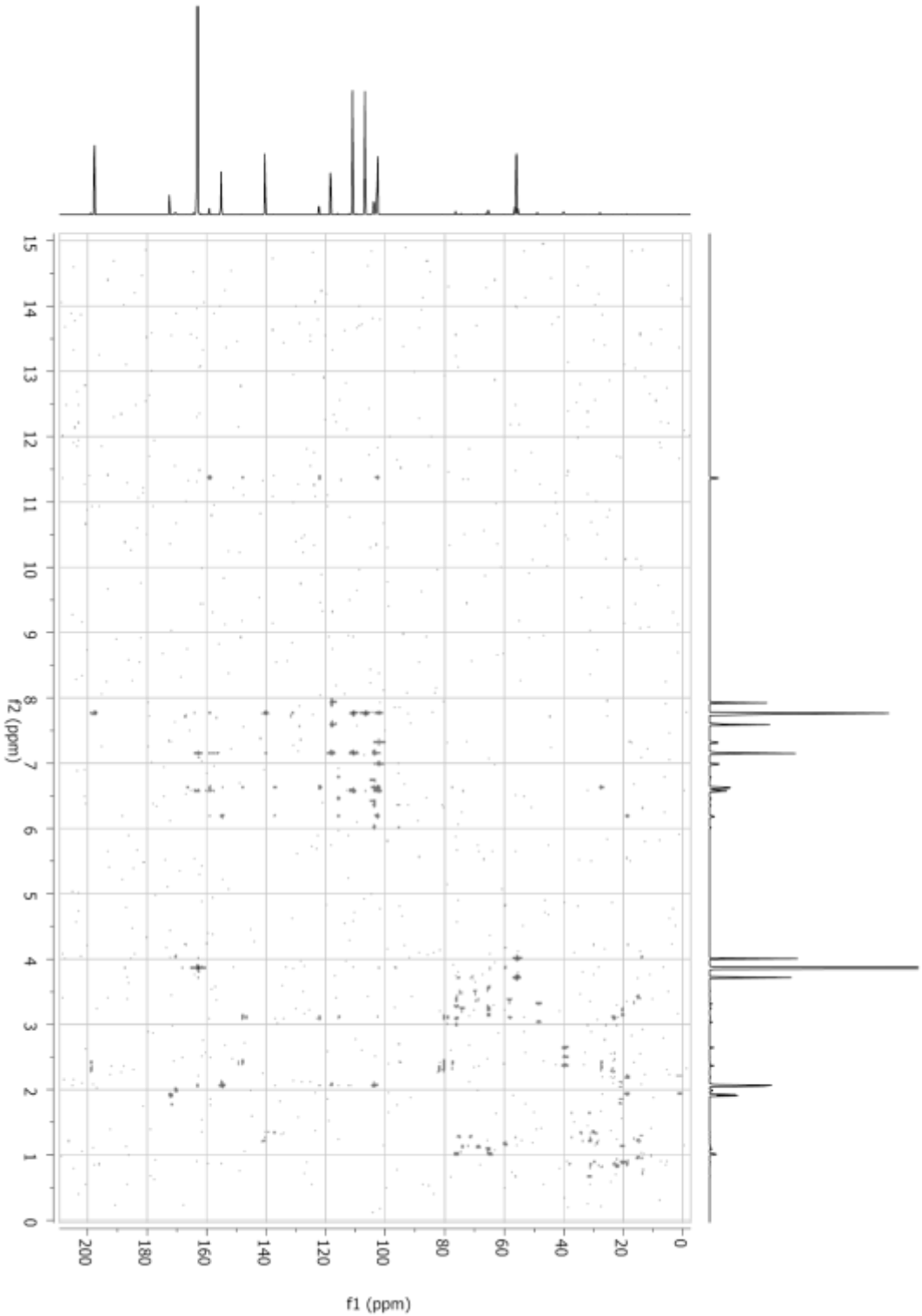

Figure 2.28 HMBC spectrum of precollinone (57), in DMSO-d6, 500 MHz.

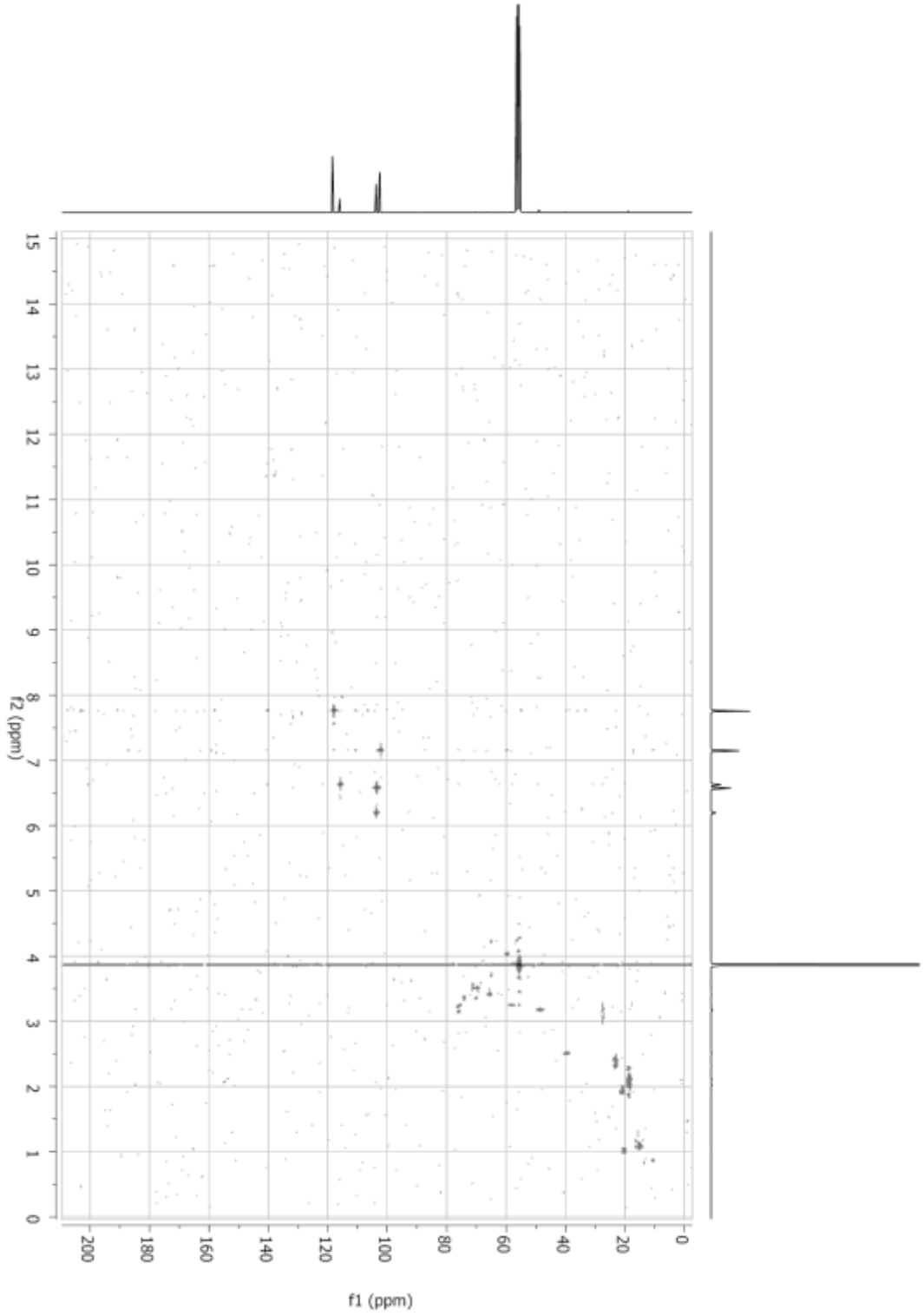

Figure 2.29 HMQC spectrum of precollinone (57), in DMSO-d_6, 500 MHz.

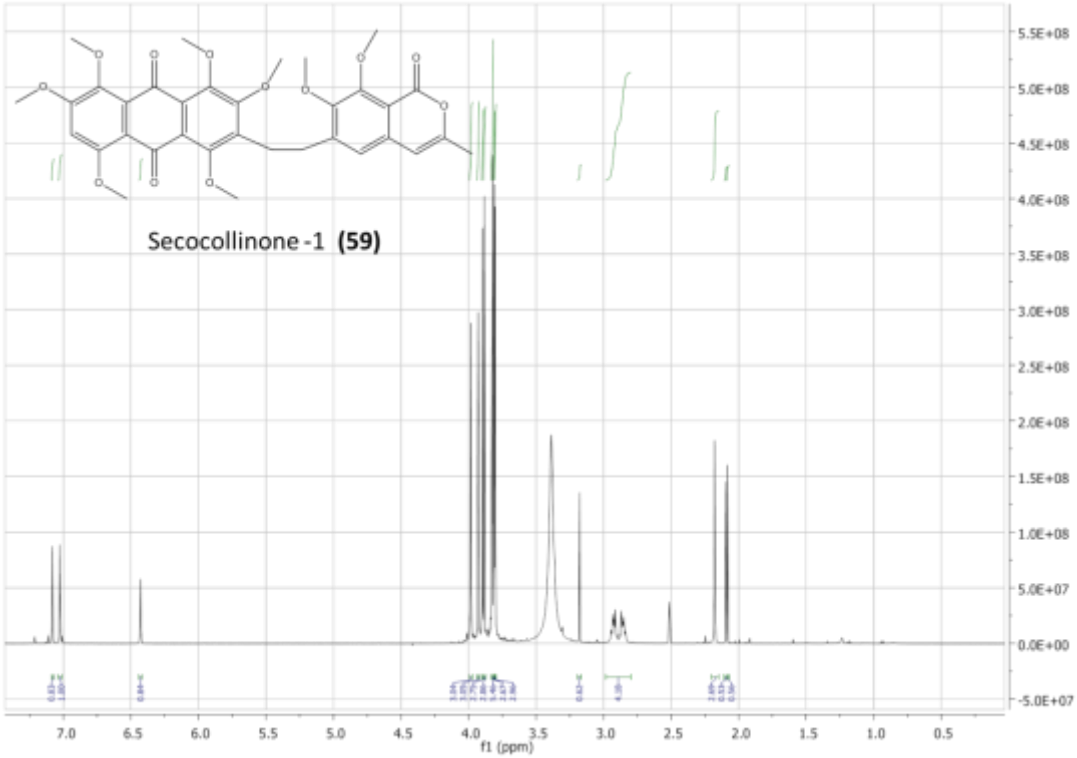

Figure 2.30 ^{1}H-NMR spectrum of secocollinone-1 (59), in DMSO-d_6, 500 MHz.

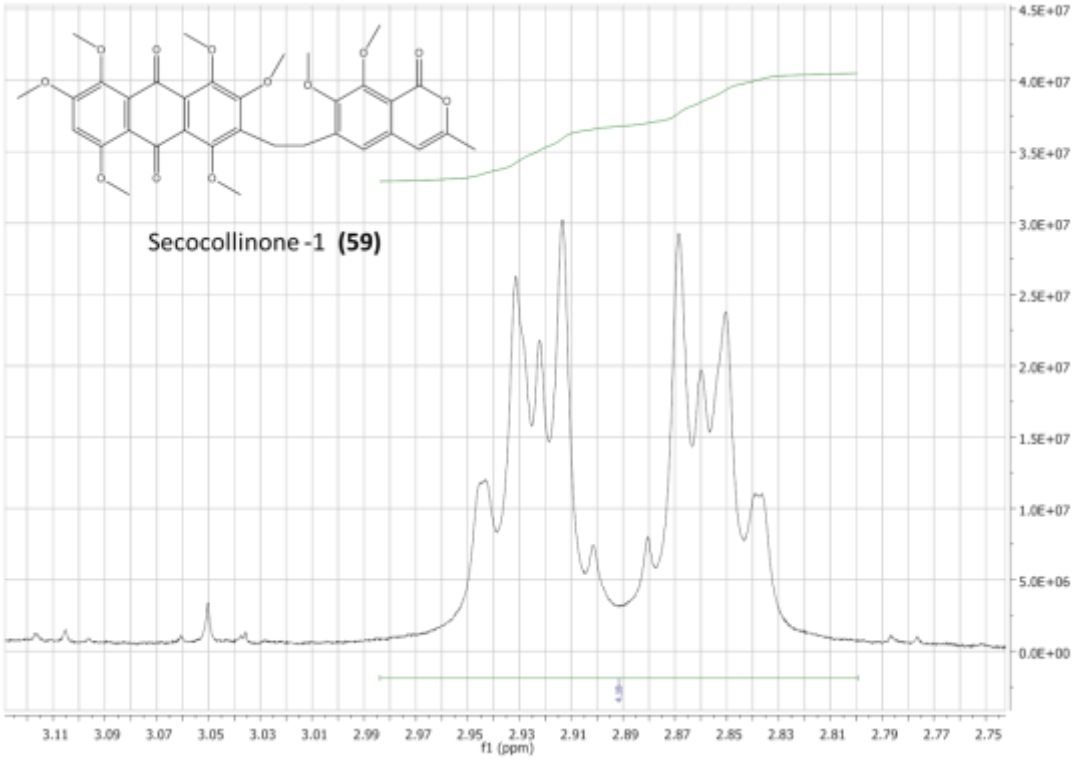

Figure 2.31 ^{1}H-NMR spectrum of secocollinone-1 (59), in DMSO-d_6, 500 MHz.

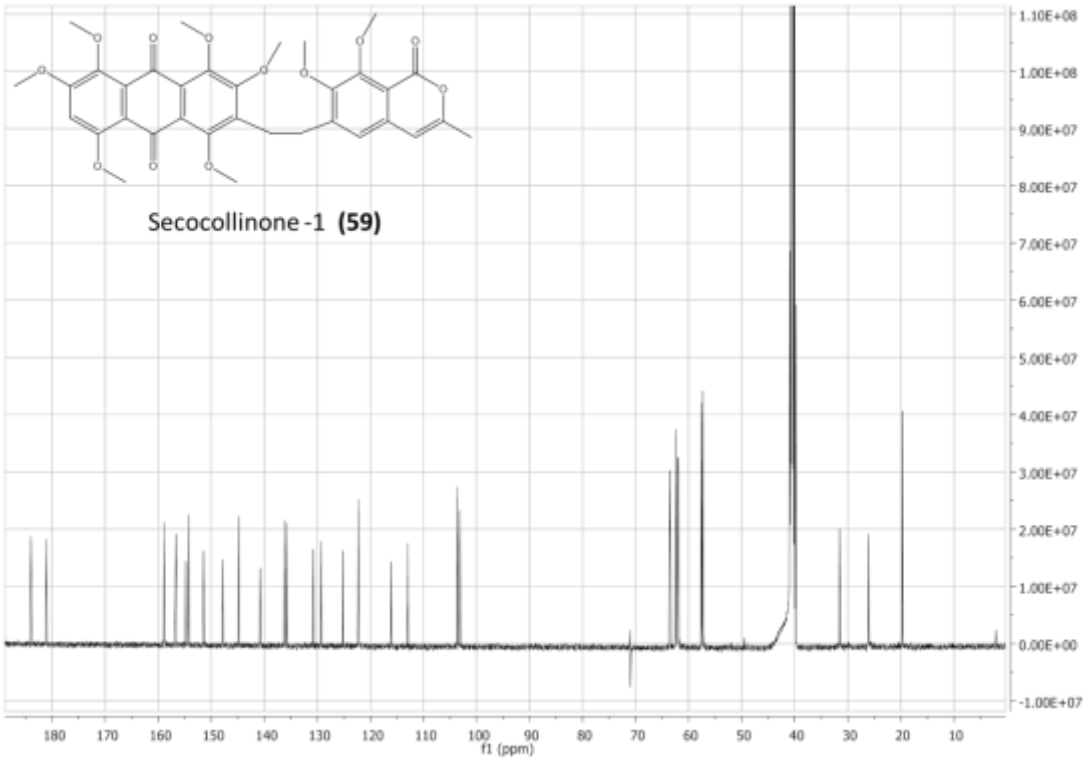

Figure 2.32 ^{13}C-NMR spectrum of secocollinone-1 (59), in DMSO-d_6, 400 MHz.

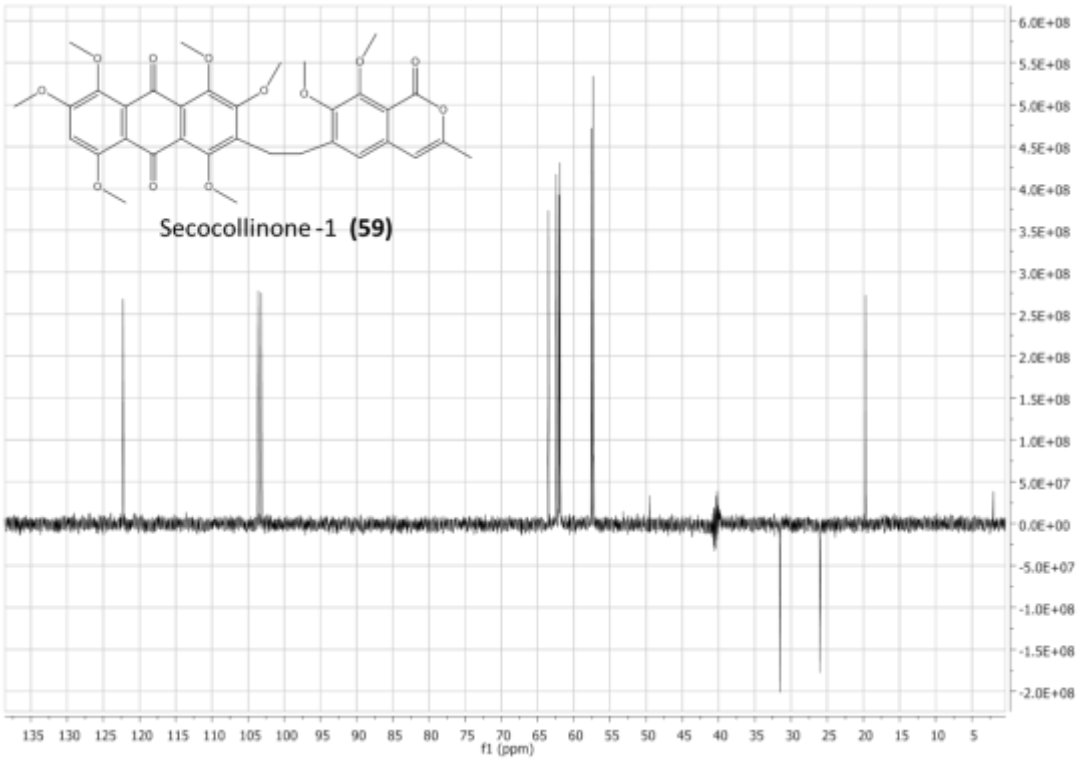

Figure 2.33 DEPT spectrum of secocollinone-1 (59), in DMSO-d_6, 400 MHz.

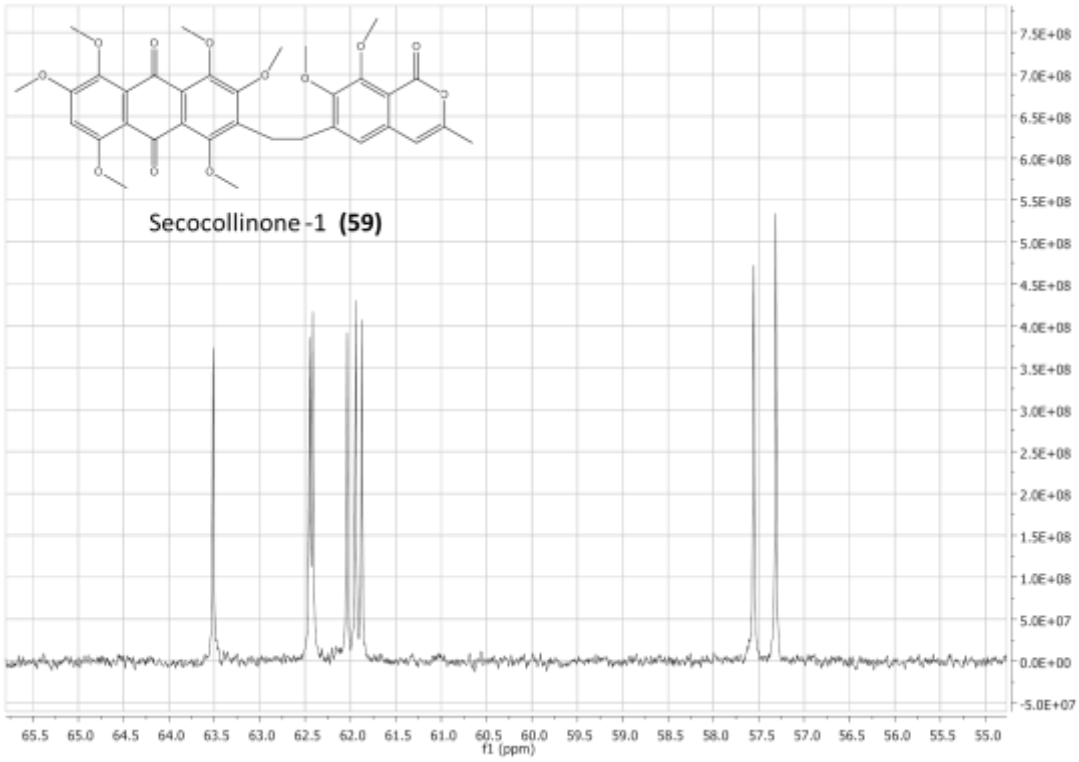

Figure 2.34 DEPT spectrum of secocollinone-1 (59), in DMSO-d_6, 400 MHz.

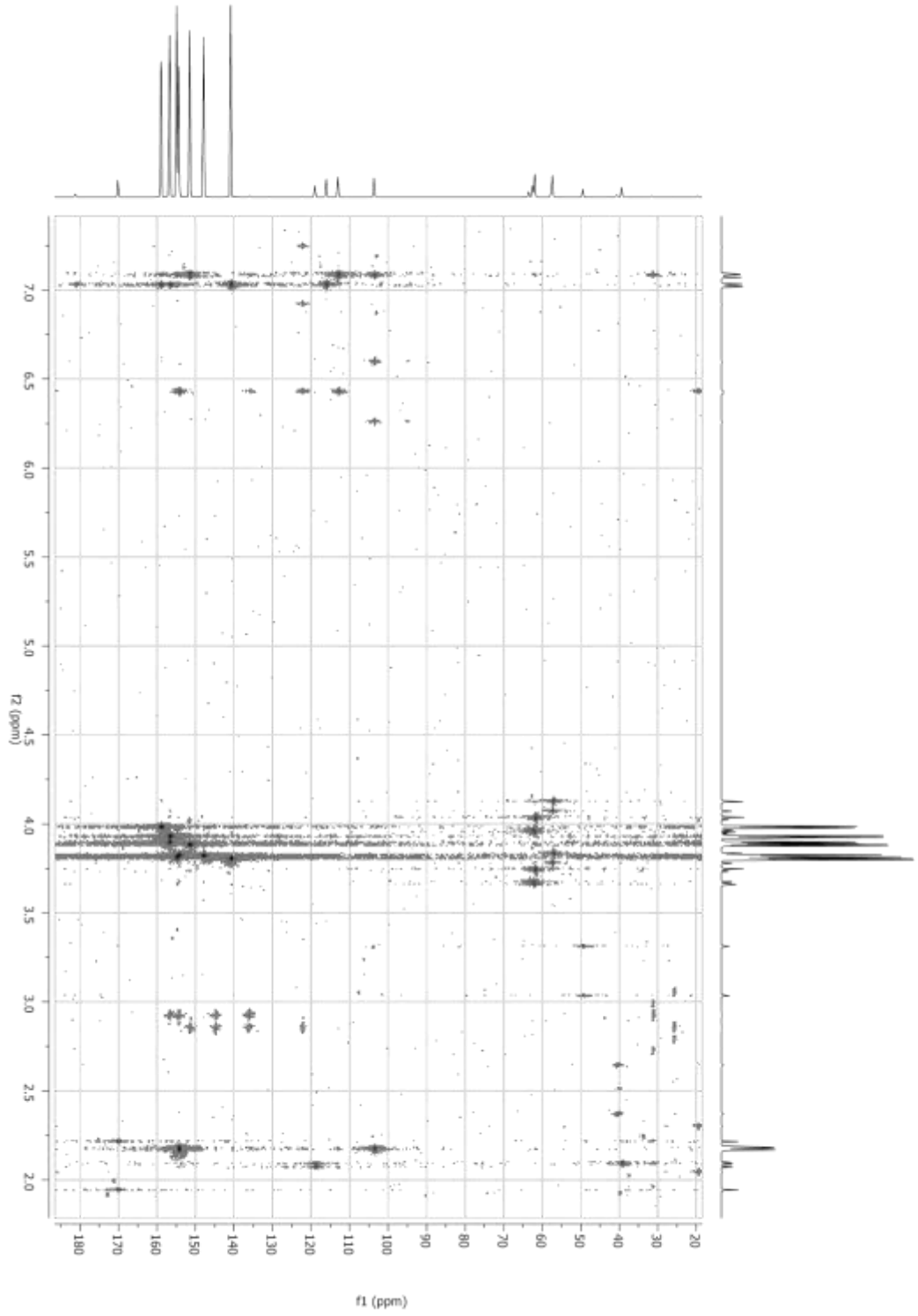

Figure 2.35 HMBC spectrum of secocollinone-1 (59), in DMSO-d_6, 500 MHz.

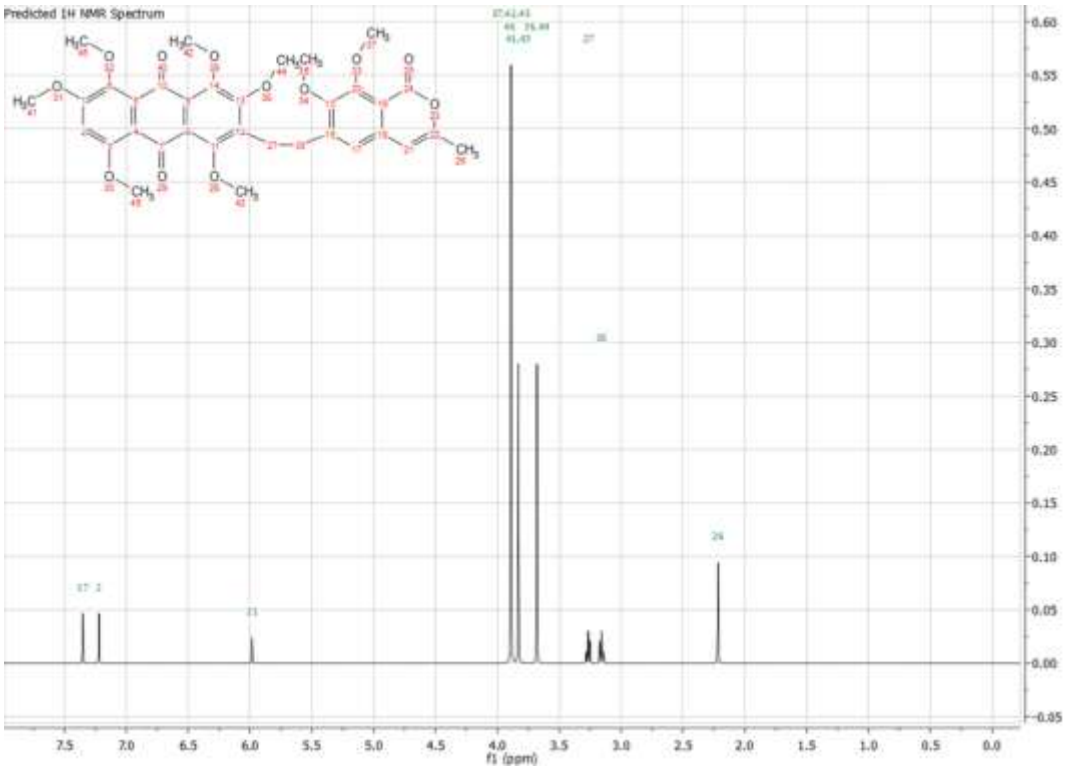

Figure 2.36 Predicted ^{1}H-NMR spectrum of secocollinone-1 (59), in DMSO-d$_6$, 500 MHz

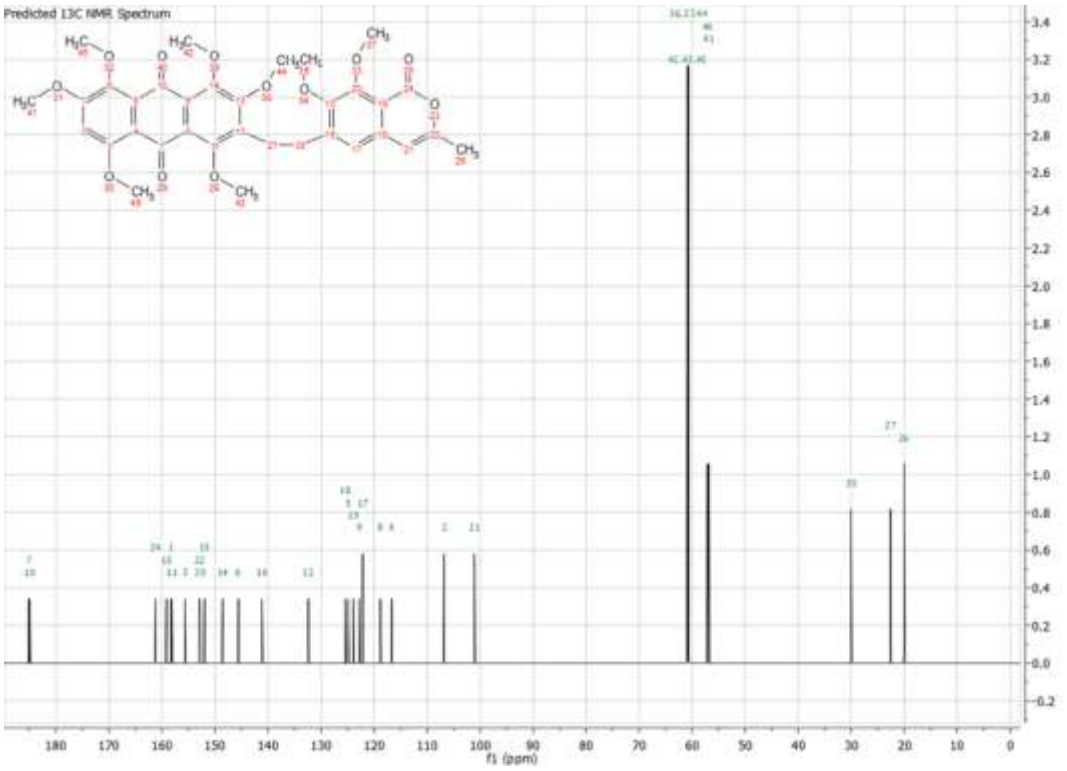

Figure 2.37 Predicted ^{13}C-NMR spectrum of secocollinone-1 (59), in DMSO-d$_6$.

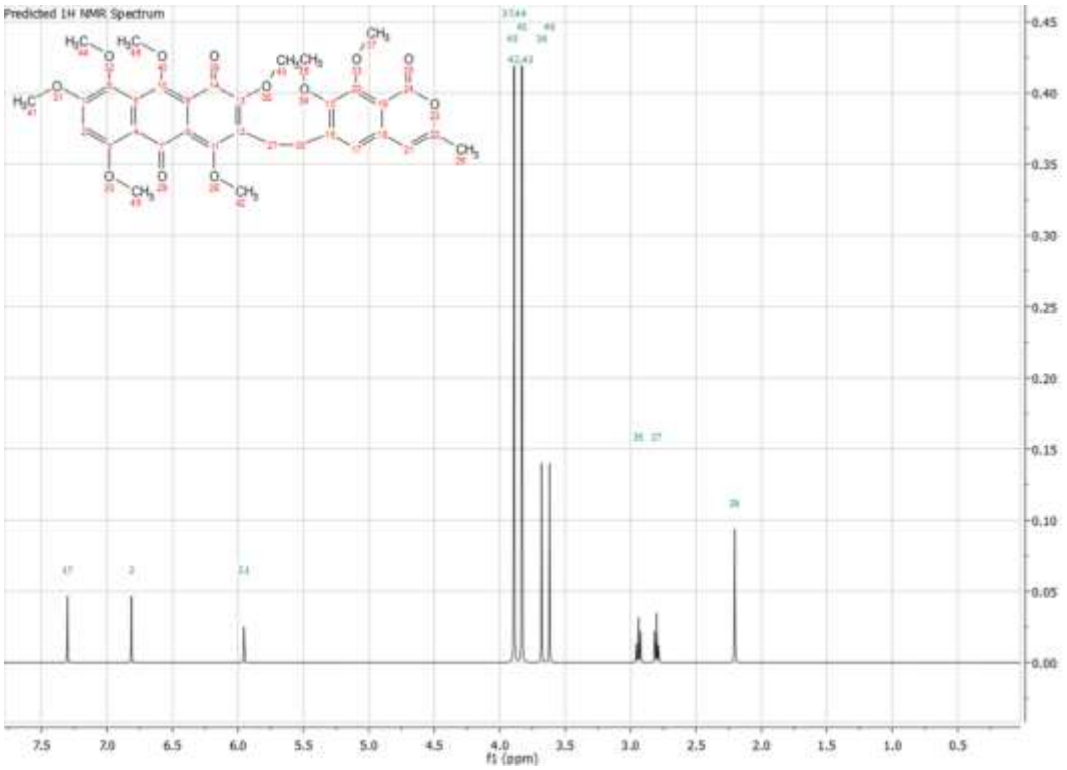

Figure 2.38 Predicted ^{1}H-NMR spectrum of secocollinone (59b), in DMSO-d_6.

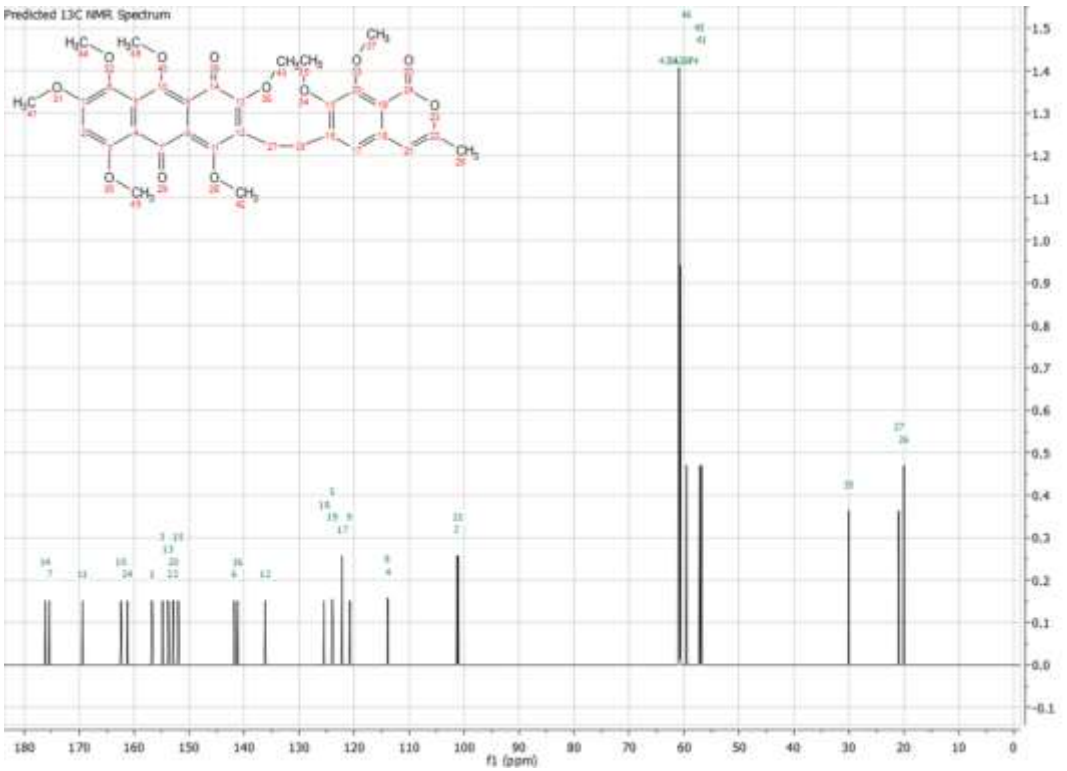

Figure 2.39 Predicted ^{1}H-NMR spectrum of secocollinone (59b), in DMSO-d_6.

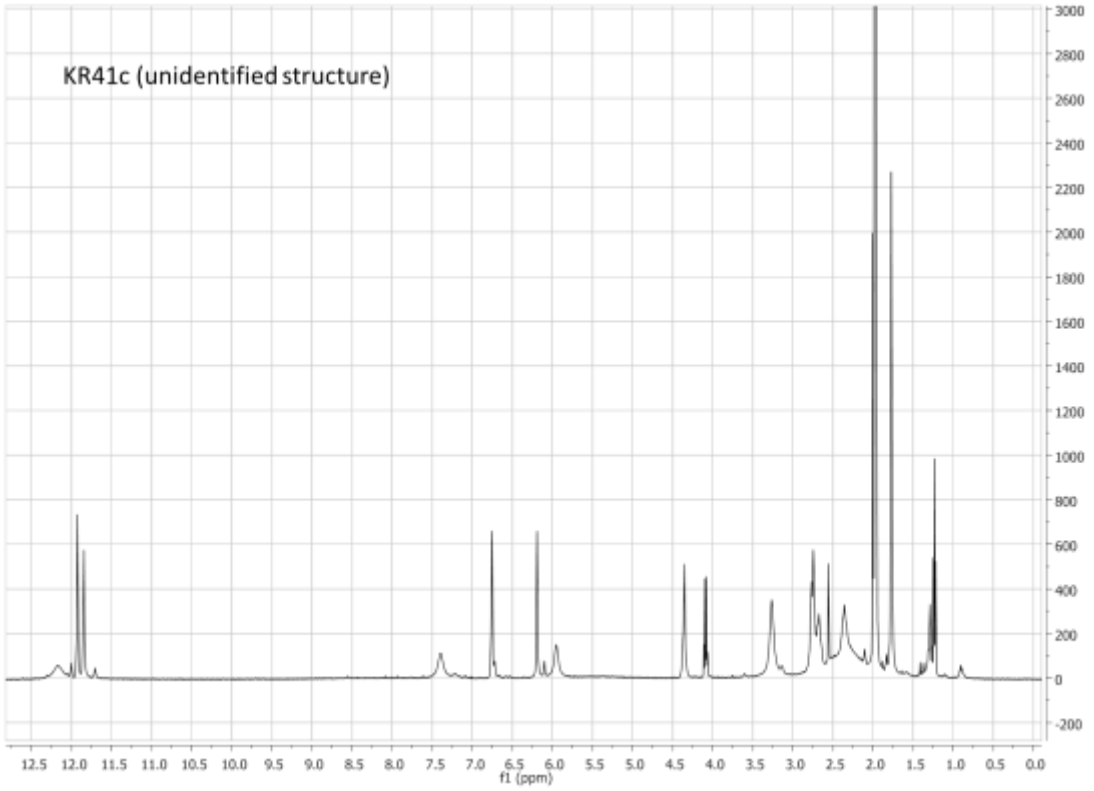

Figure 2.40 ^{1}H-NMR spectrum of KR41c, in AN-d_3, 500 MHz.

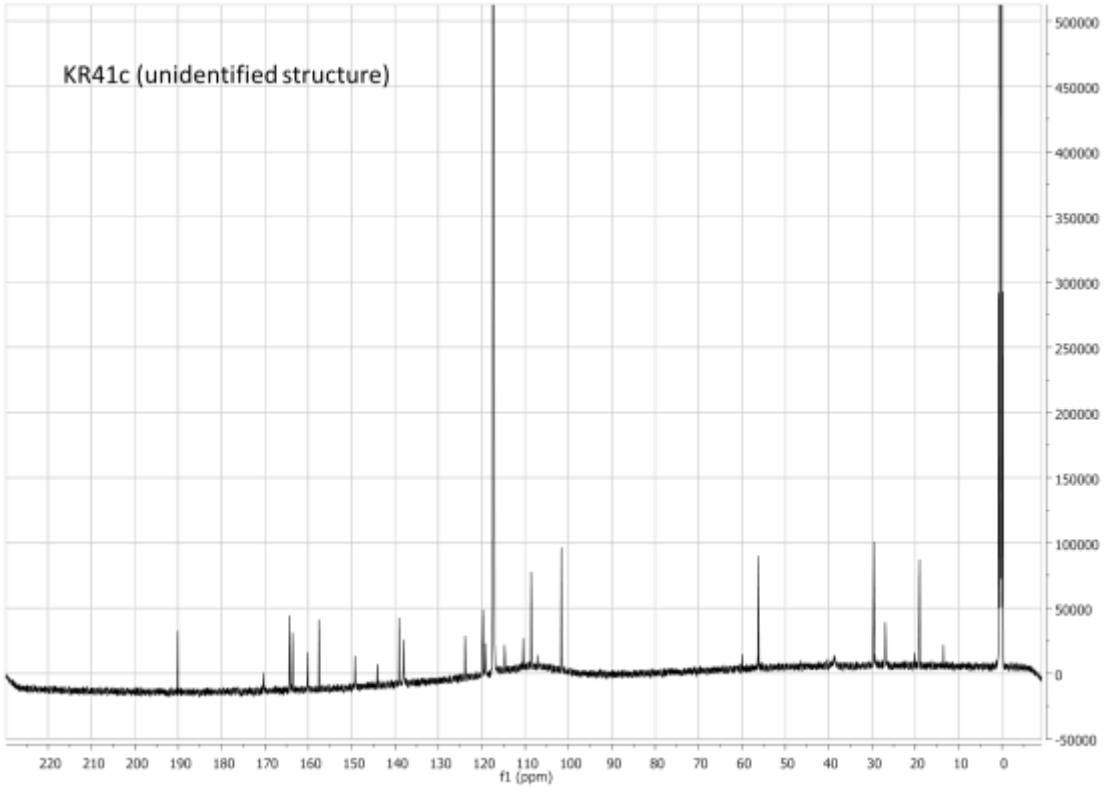

Figure 2.41 ^{13}C-NMR spectrum of KR41c, in AN-d_3, 400 MHz.

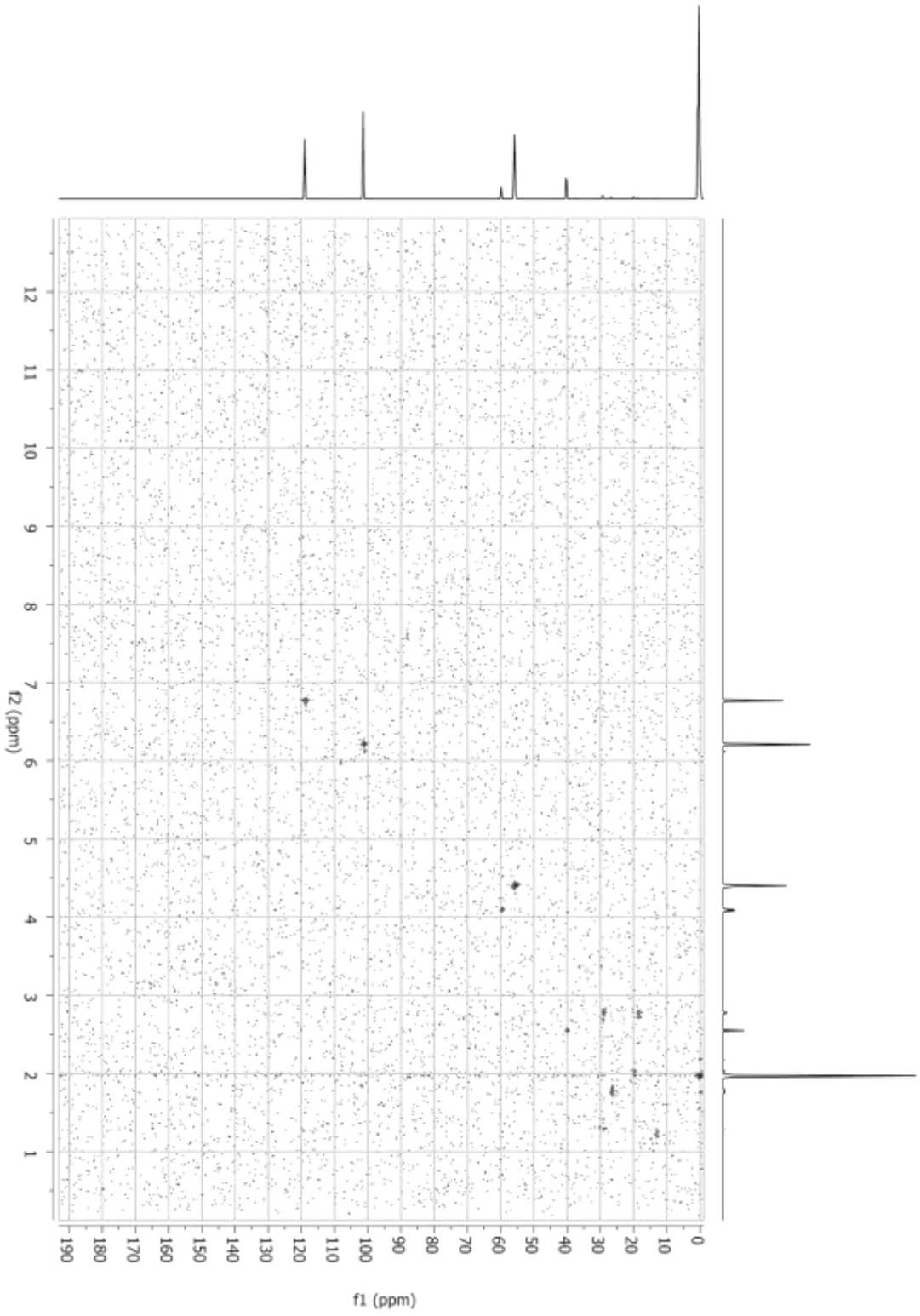

Figure 2.42 HMQC spectrum of KR41c, in AN-d_3, 500 MHz.

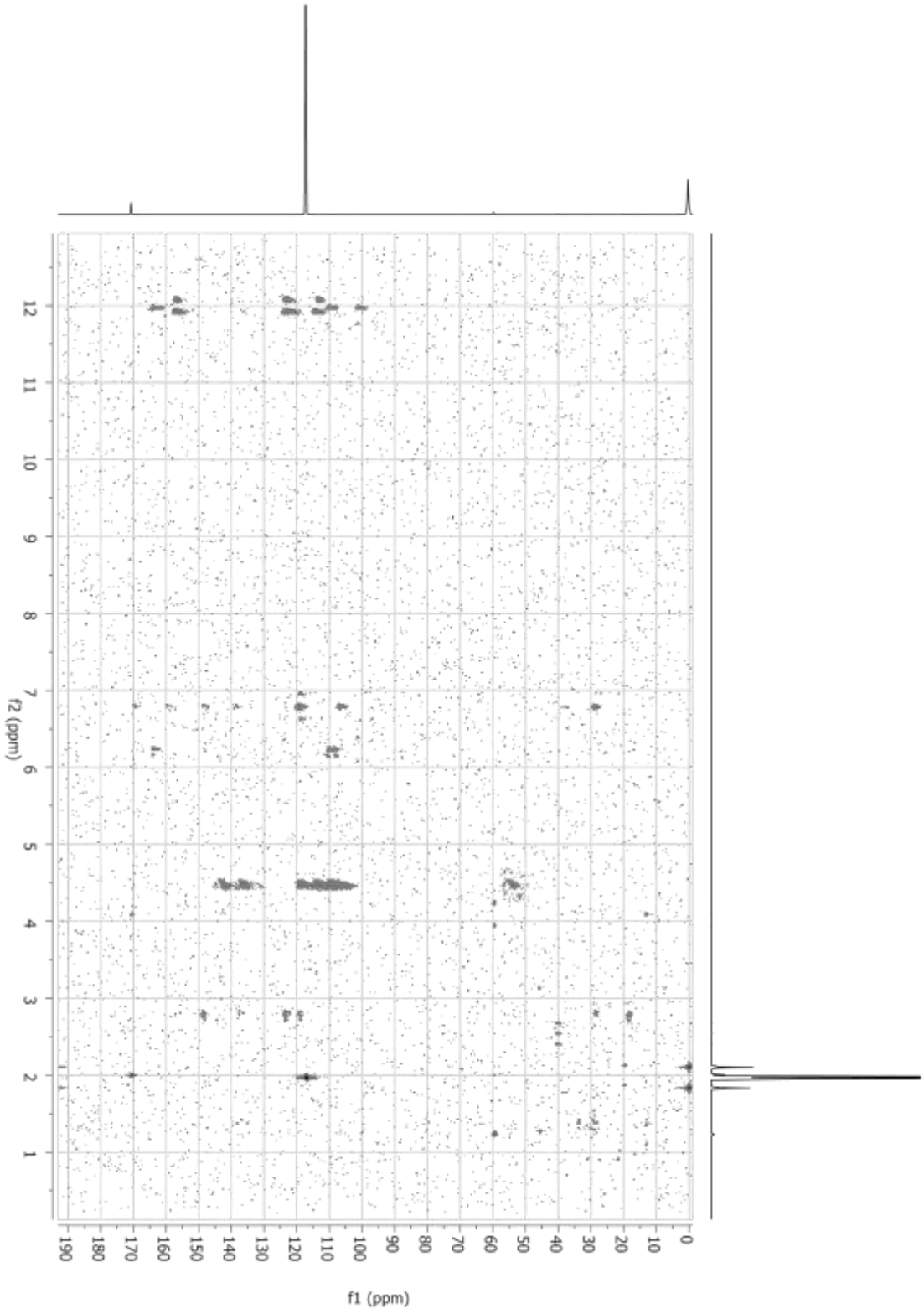

Figure 2.43 HMBC spectrum of KR41c, in AN-d_3, 500 MHz.

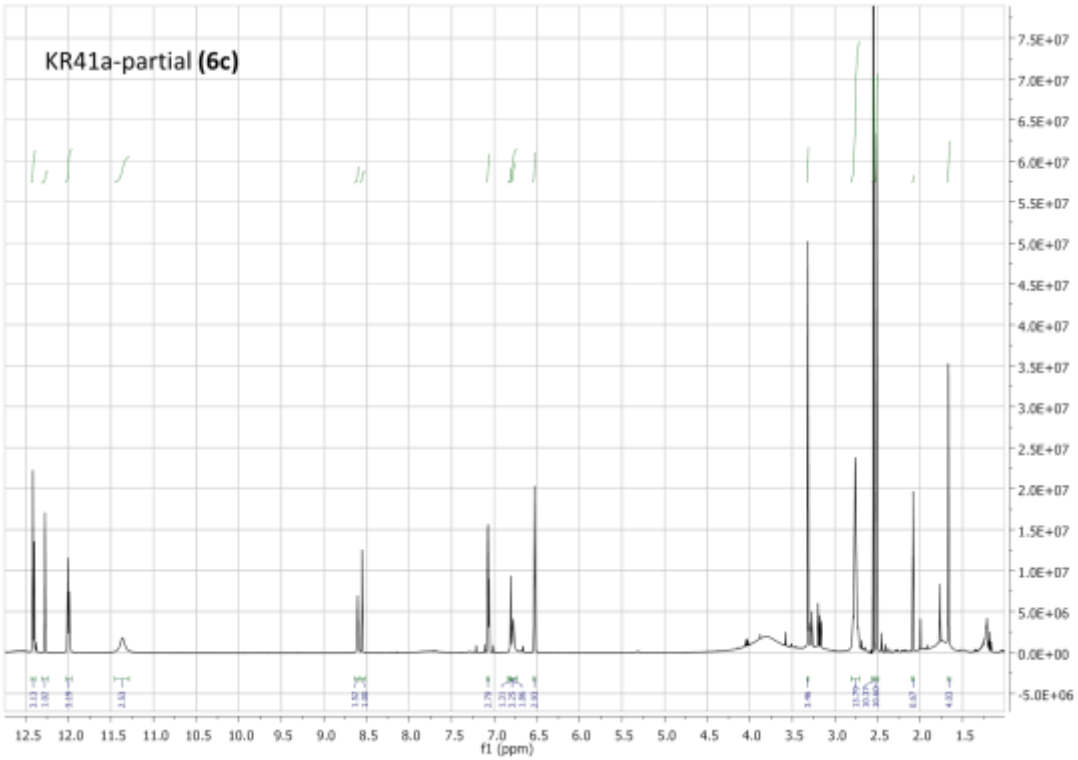

Figure 2.44 ^{1}H-NMR spectrum of KR41a-partial (6c), in DMSO-d_6, 500 MHz.

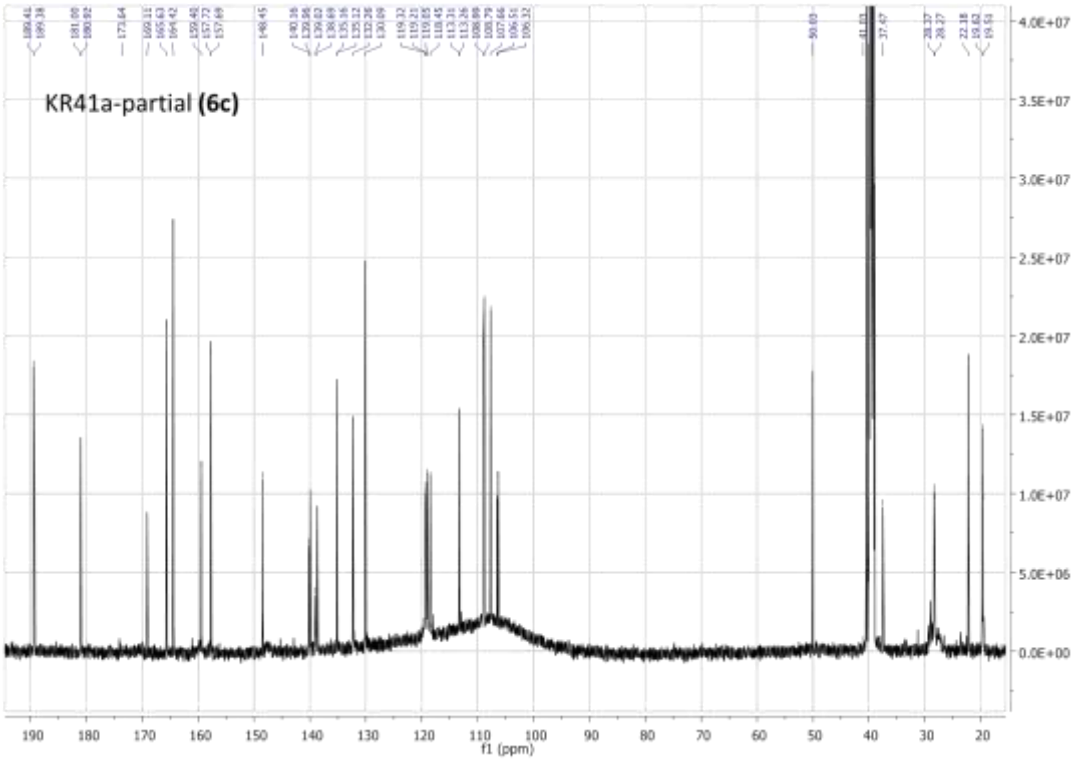

Figure 2.45 ^{13}C-NMR spectrum of KR41a-partial (6c), in DMSO-d_6, 400 MHz.

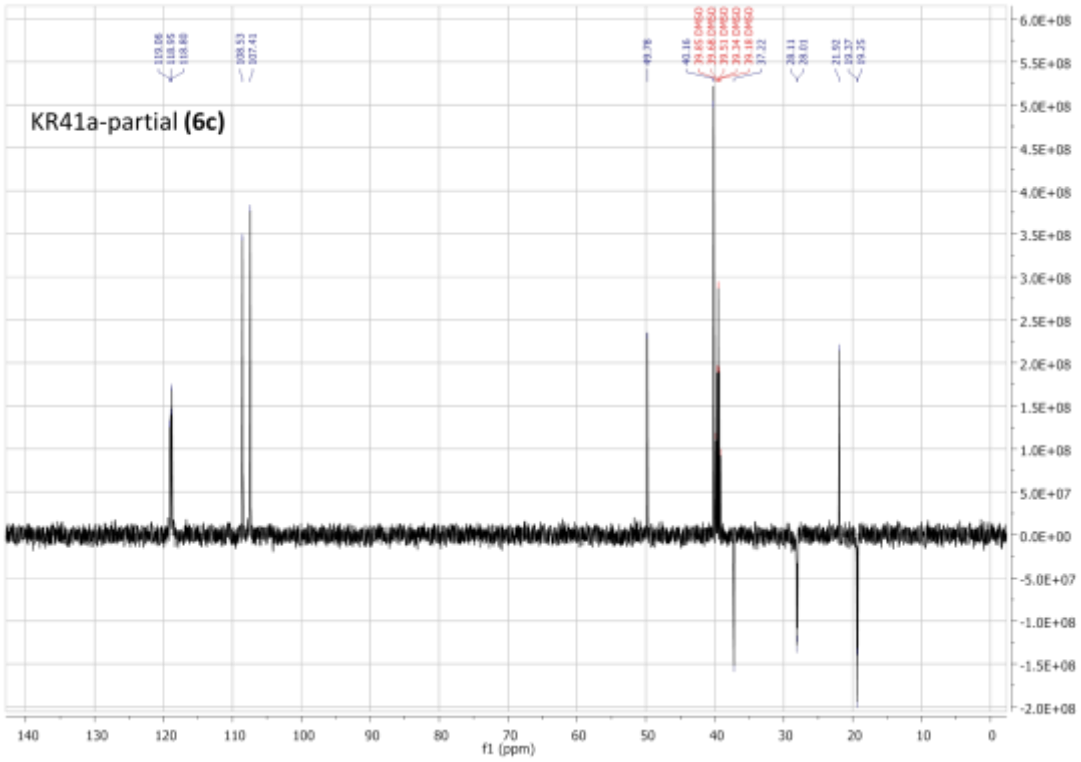

Figure 2.46 DEPT spectrum of KR41a-partial (6c), in DMSO-d_6, 400 MHz.

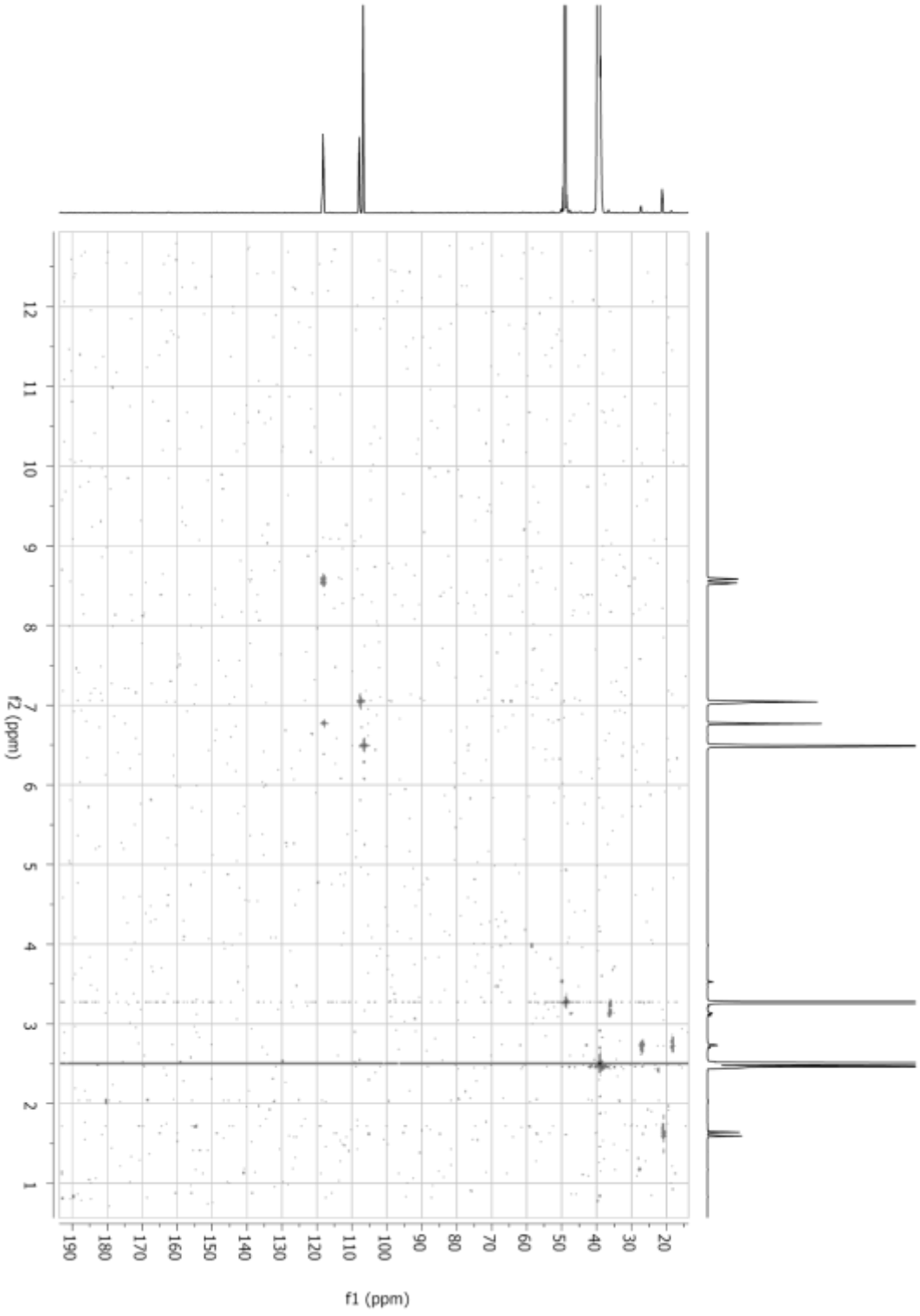

Figure 2.47 HMQC spectrum of KR41a-partial (6c), in AN-d_3, 500 MHz.

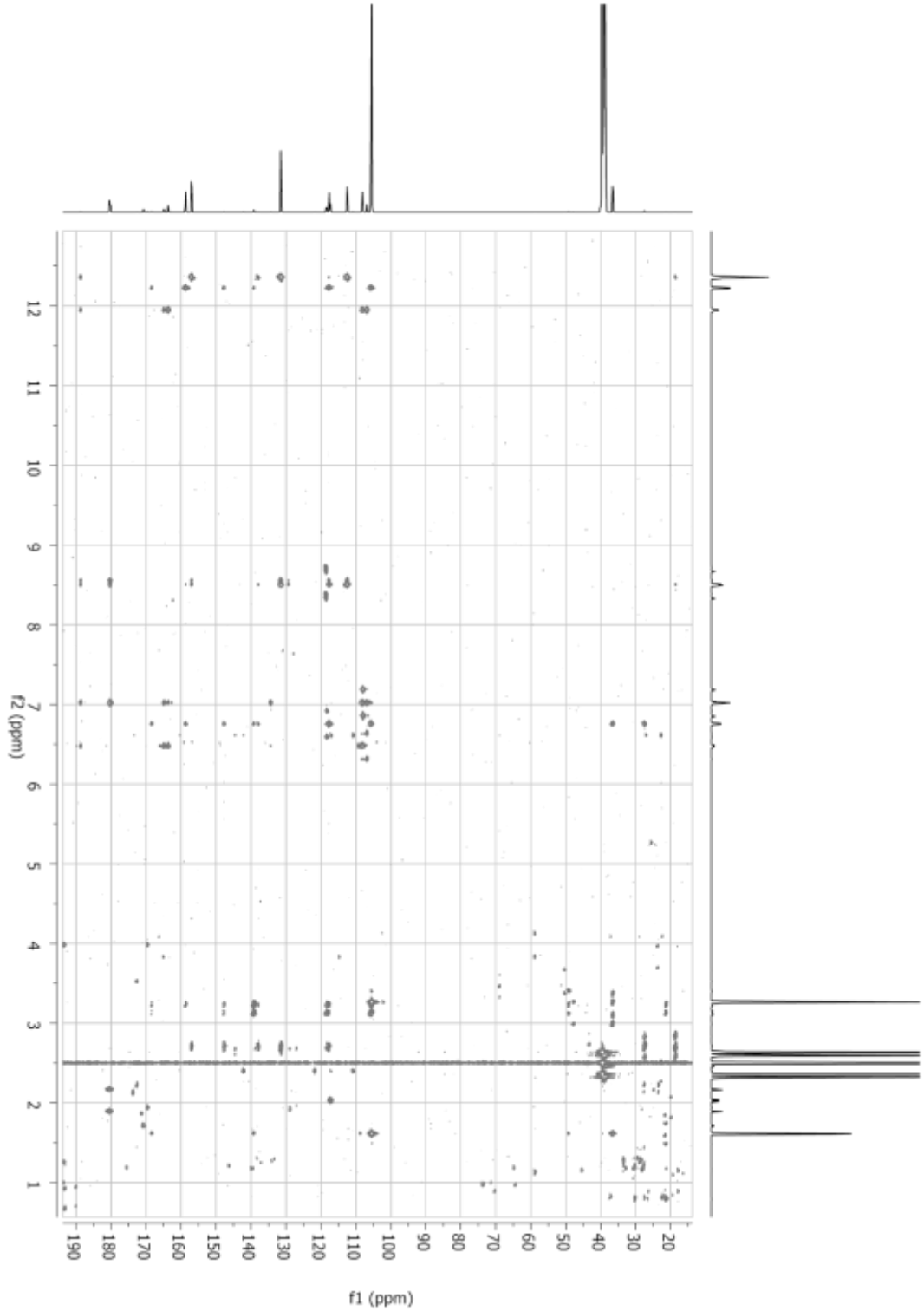

Figure 2.48 HMBC spectrum of KR41a-partial (6c), in AN-d_3, 500 MHz.

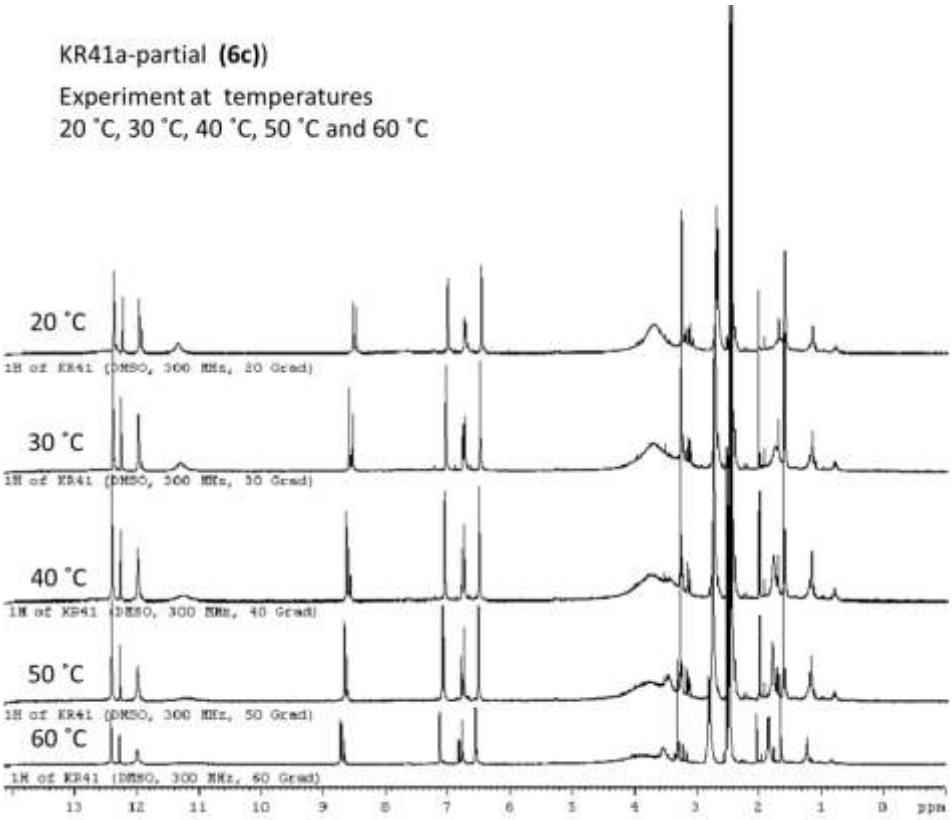

Figure 2.49 ^{1}H-NMR spectra of KR41a-partial (6c), in DMSO-d6, 400 MHz. Experiment at temperatures 20 ˚C, 30 ˚C, 40 ˚C, 50 ˚C and 60 ˚C.

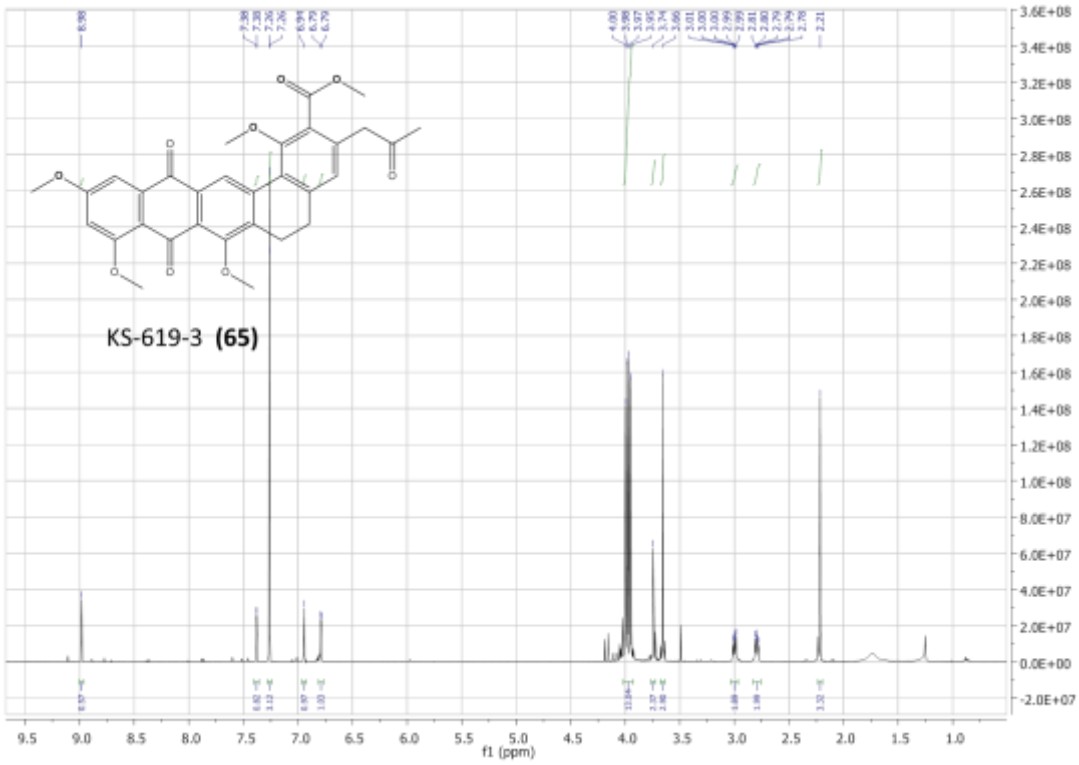

Figure 2.50 ^{1}H-NMR spectrum of KS-619-3 (65), in $CDCl_3$, 500 MHz.

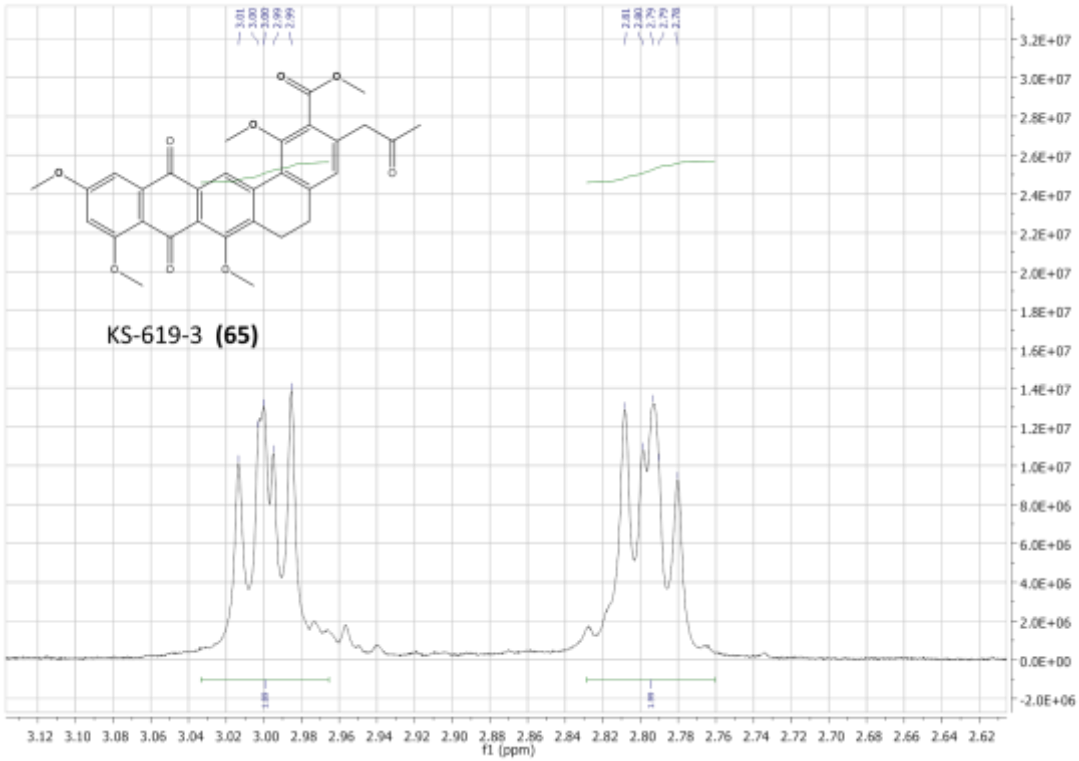

Figure 2.51 ^{1}H-NMR spectrum of KS-619-3 (65), in $CDCl_3$, 500 MHz.

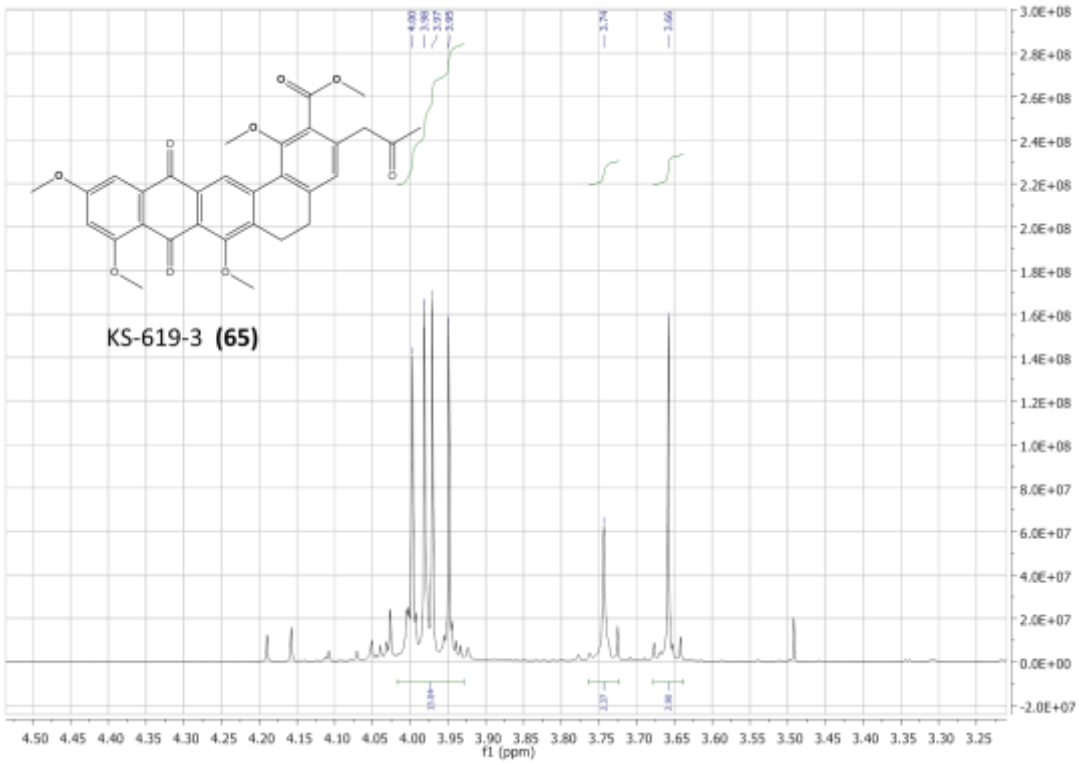

Figure 2.52 ^{1}H-NMR spectrum of KS-619-3 (65), in $CDCl_3$, 500 MHz.

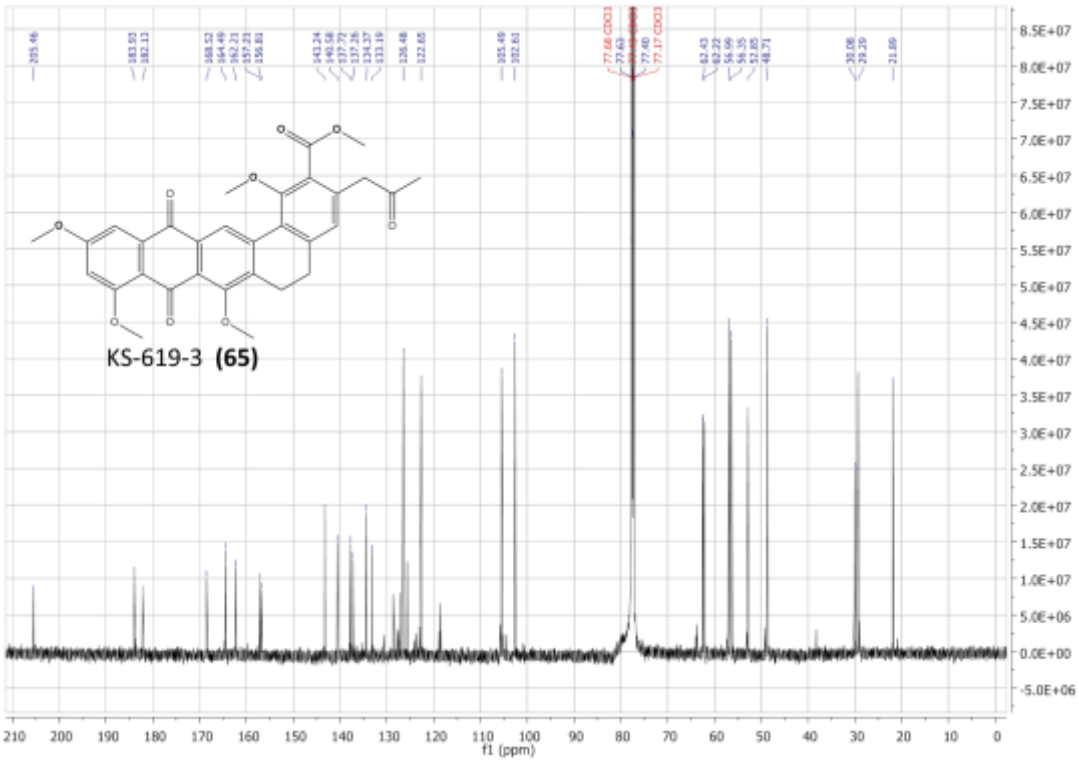

Figure 2.53 ^{13}C-NMR spectrum of KS-619-3 (65), in $CDCl_3$, 400 MHz.

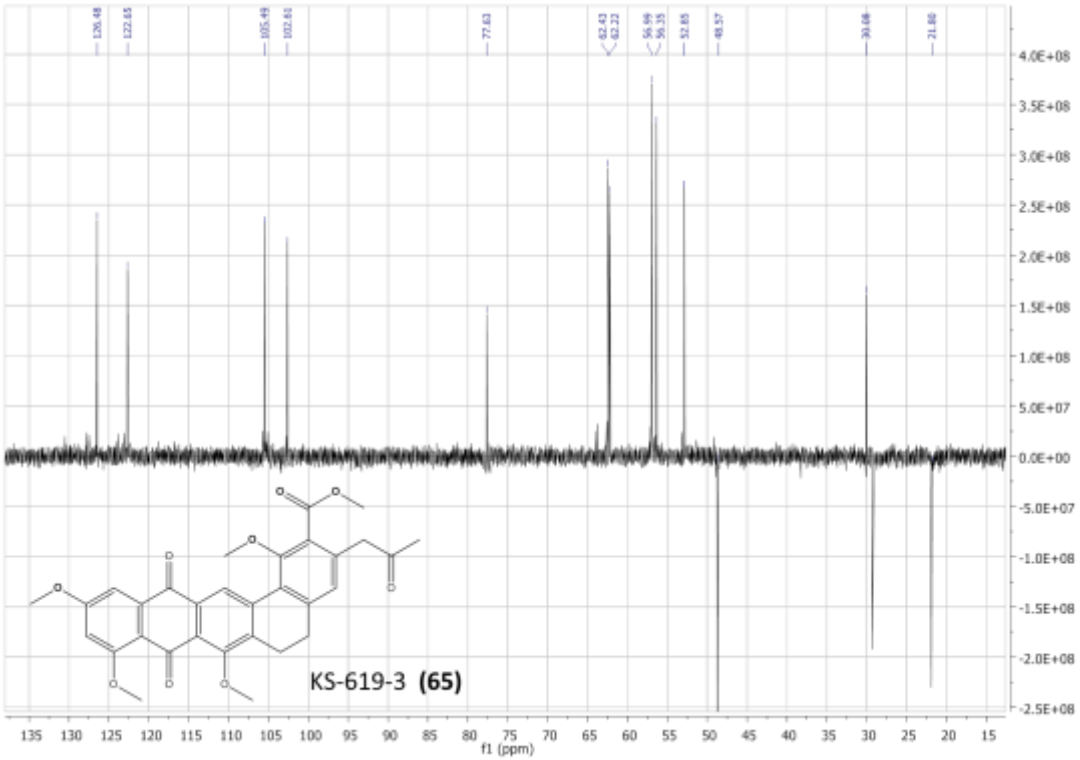

Figure 2.54 DEPT spectrum of KS-619-3 (65), in $CDCl_3$, 400 MHz.

7.3 APPENDIX 3: IR Spectra

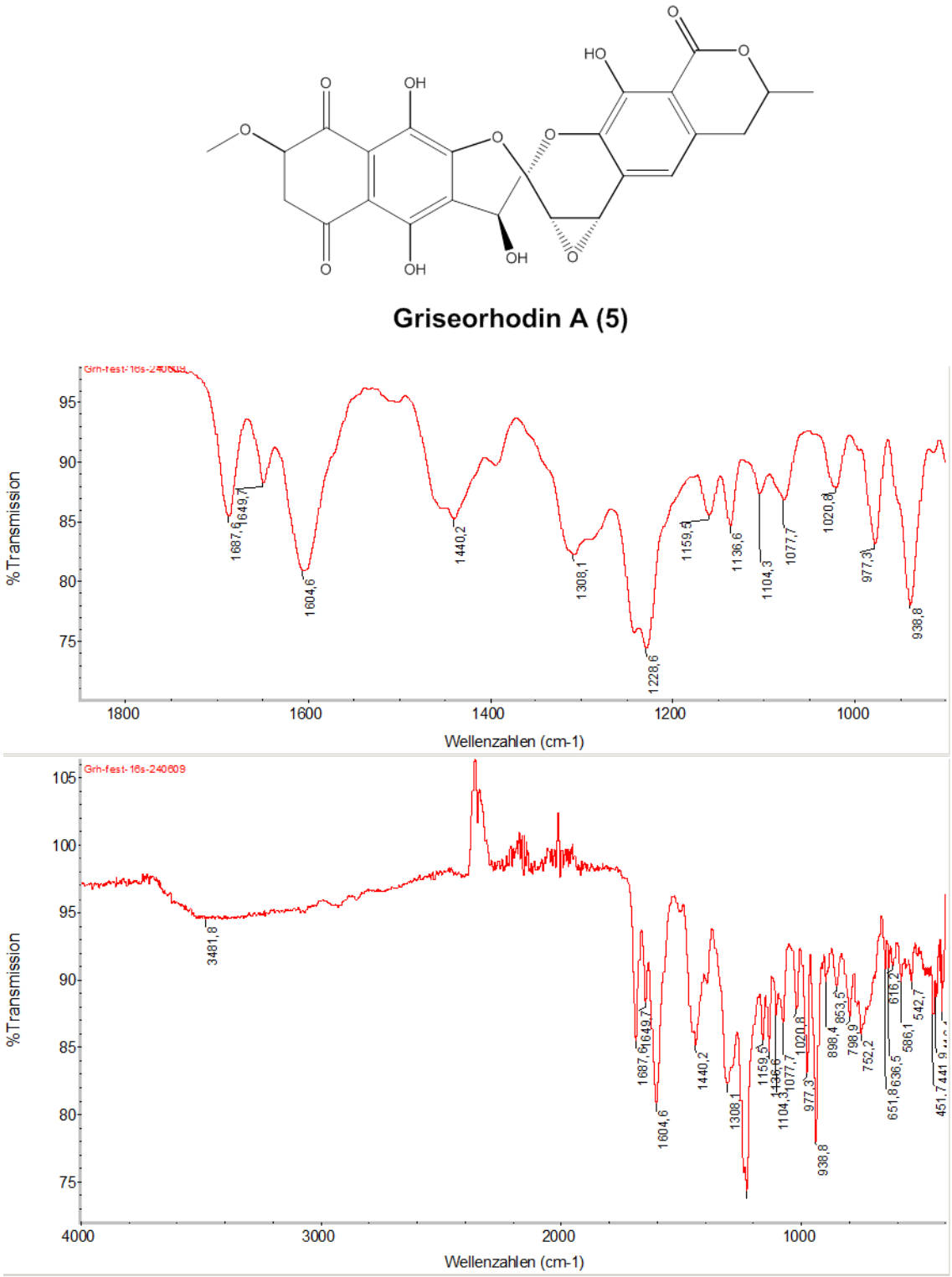

Figure 3.1 IR spectrum of griseorhodin A (5).

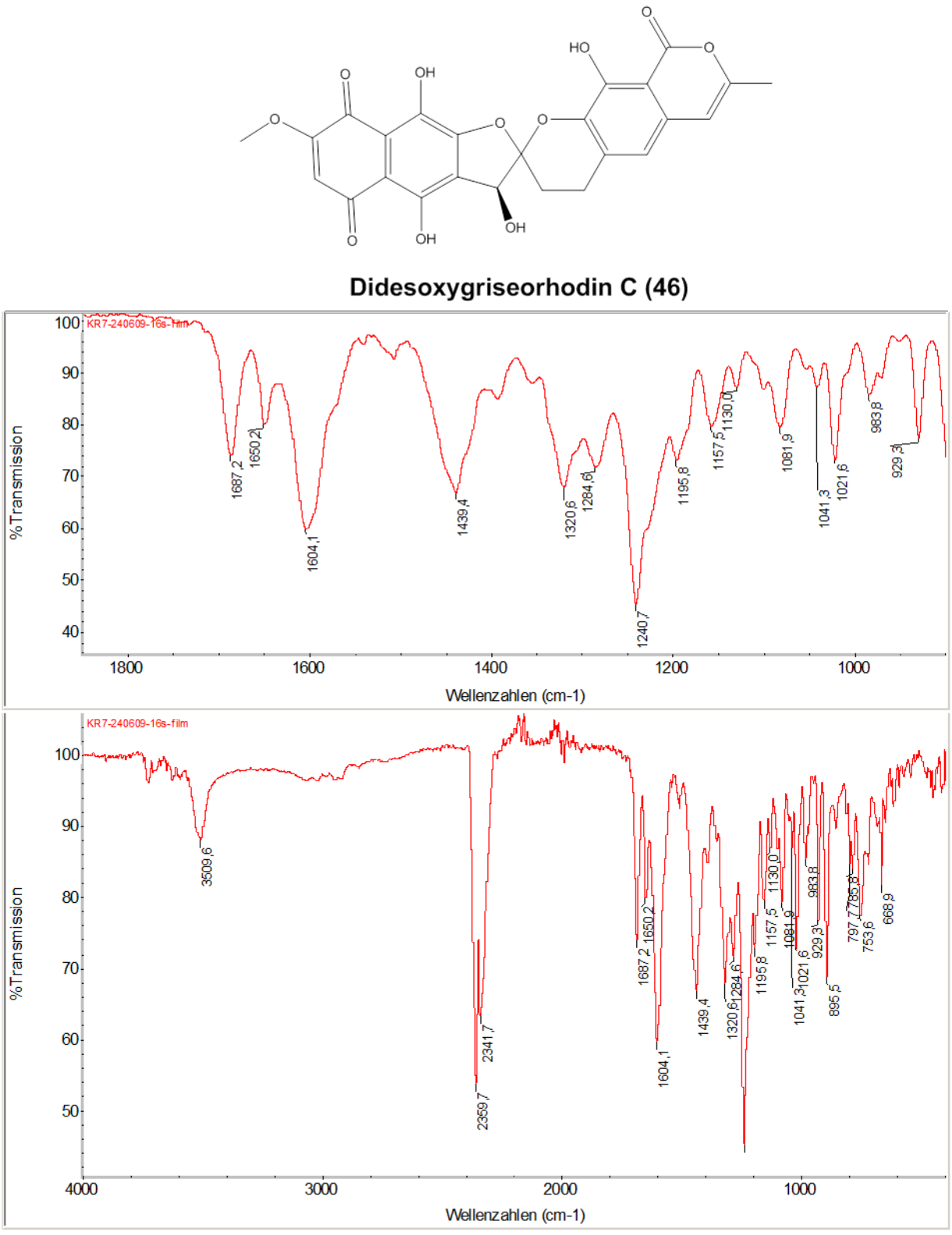

Figure 3.2 IR spectrum of didesoxygriseorhodin C (46).

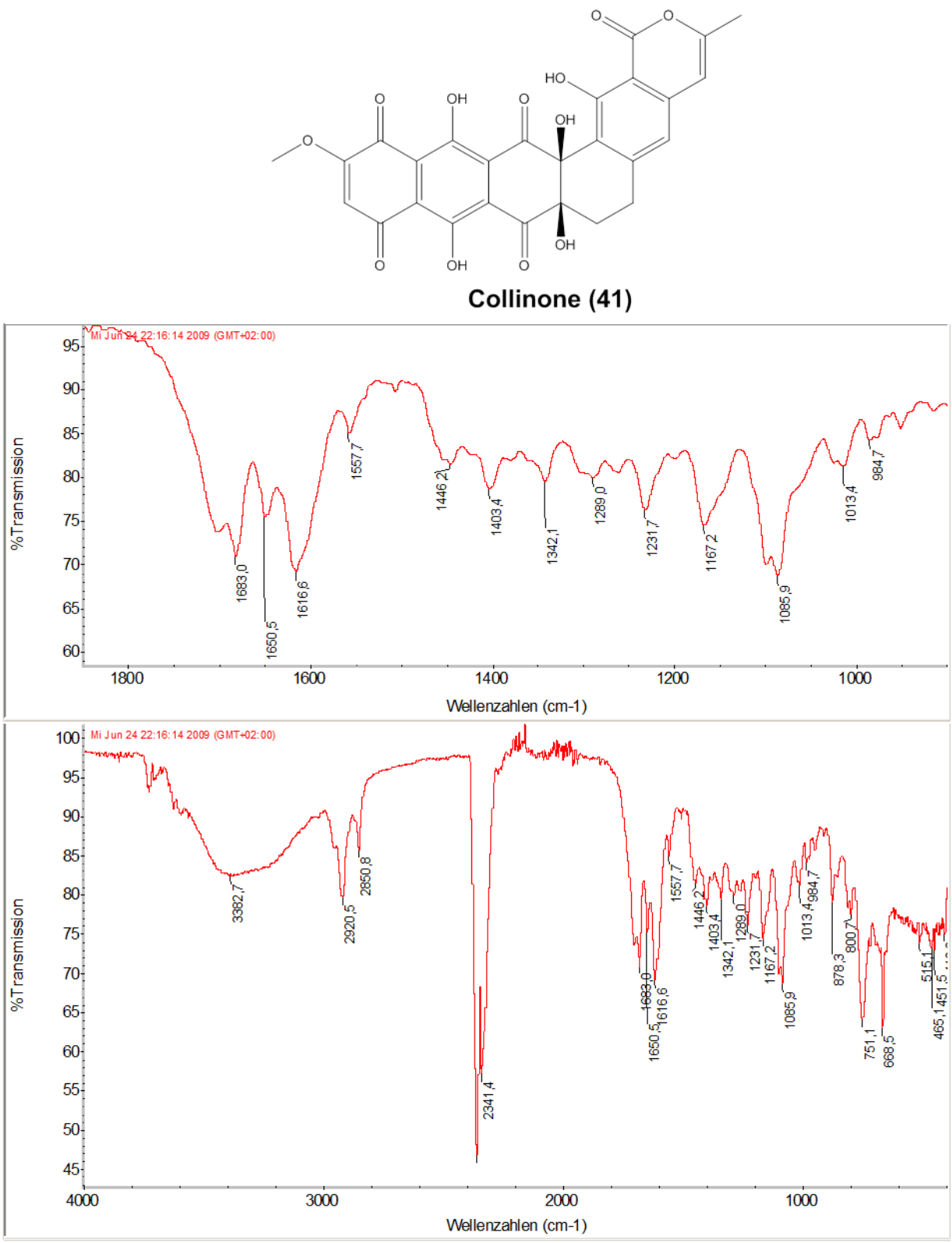

Figure 3.3 IR spectrum of collinone (41).

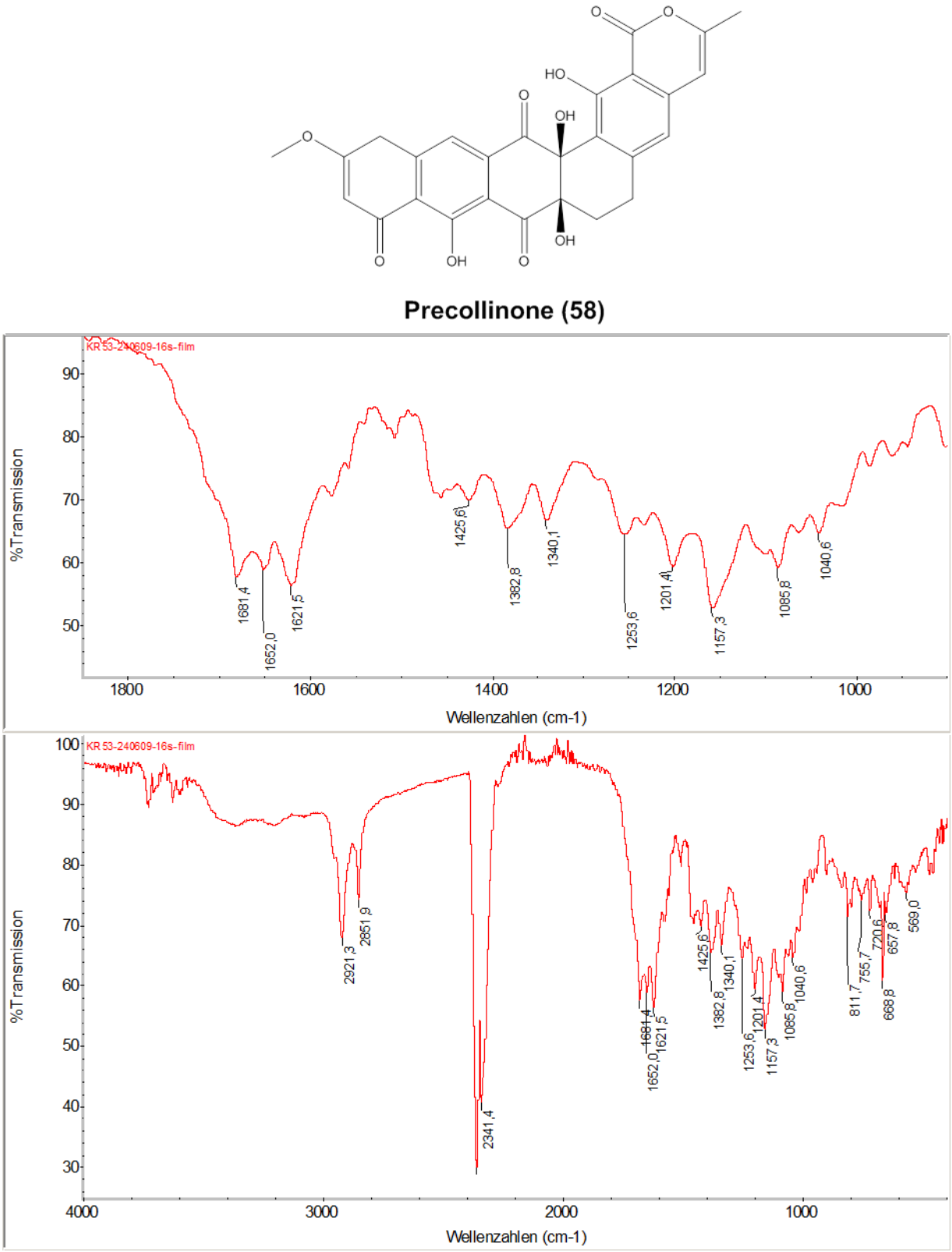

Figure 3.4 IR spectrum of precollinone (58).

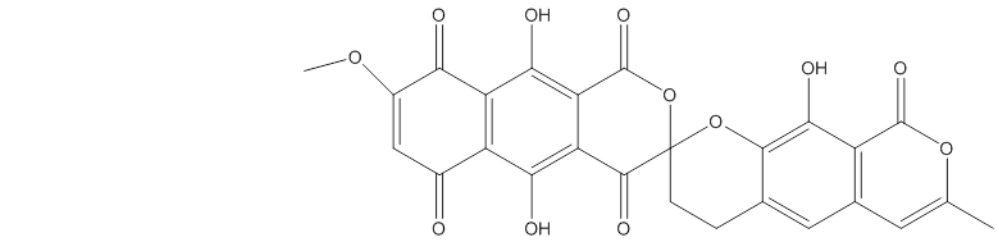

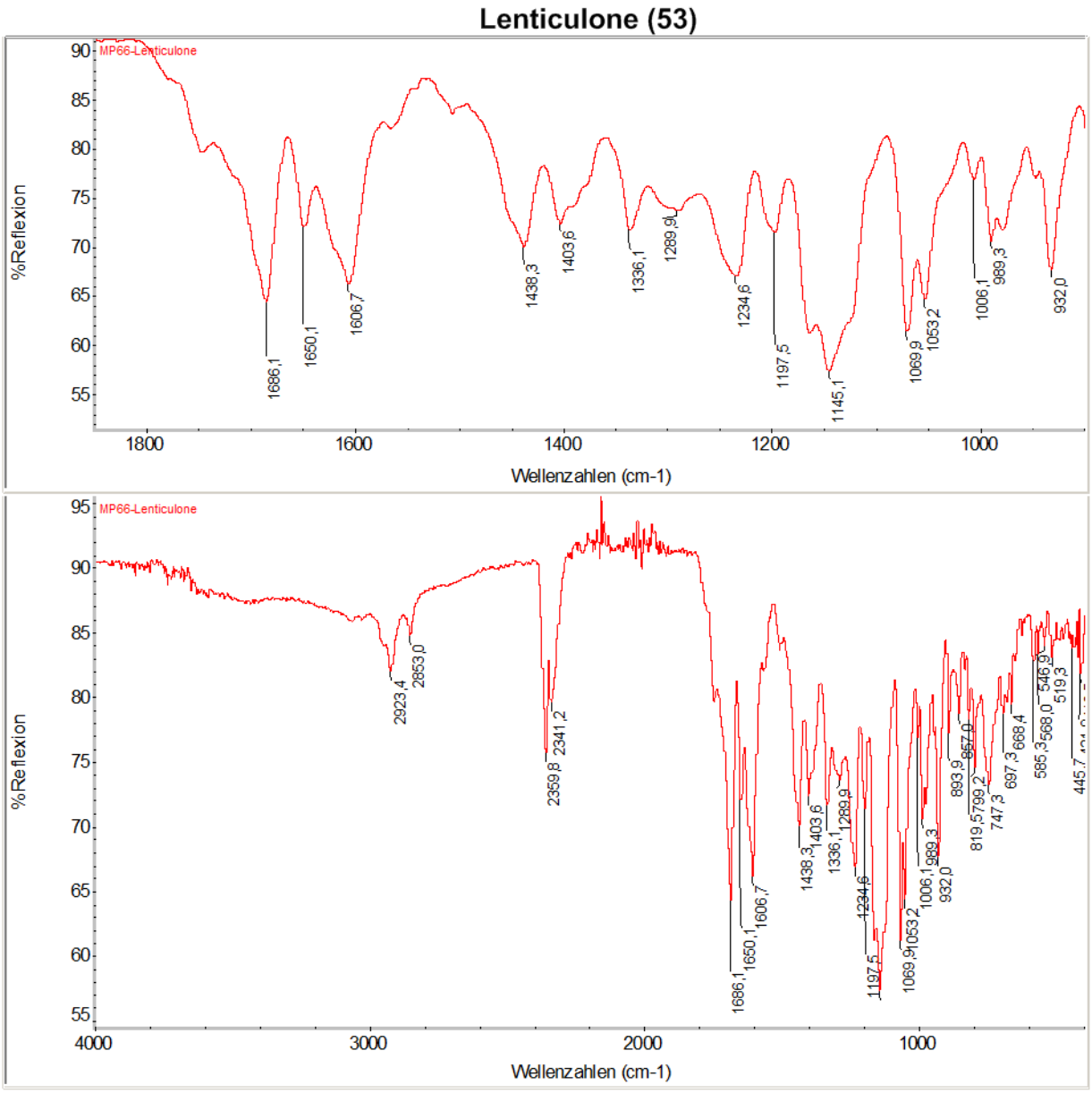

Figure 3.5 IR spectrum of lenticulone (53).

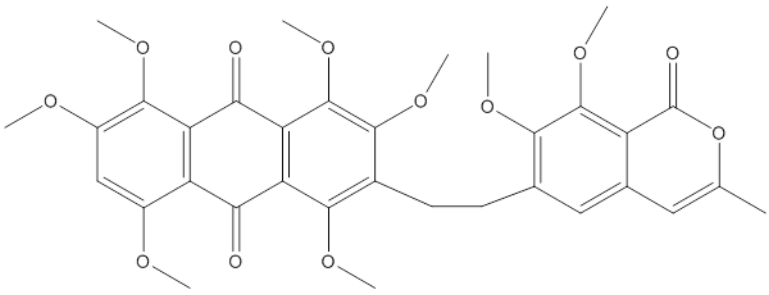

Secocollinone-1 (59)

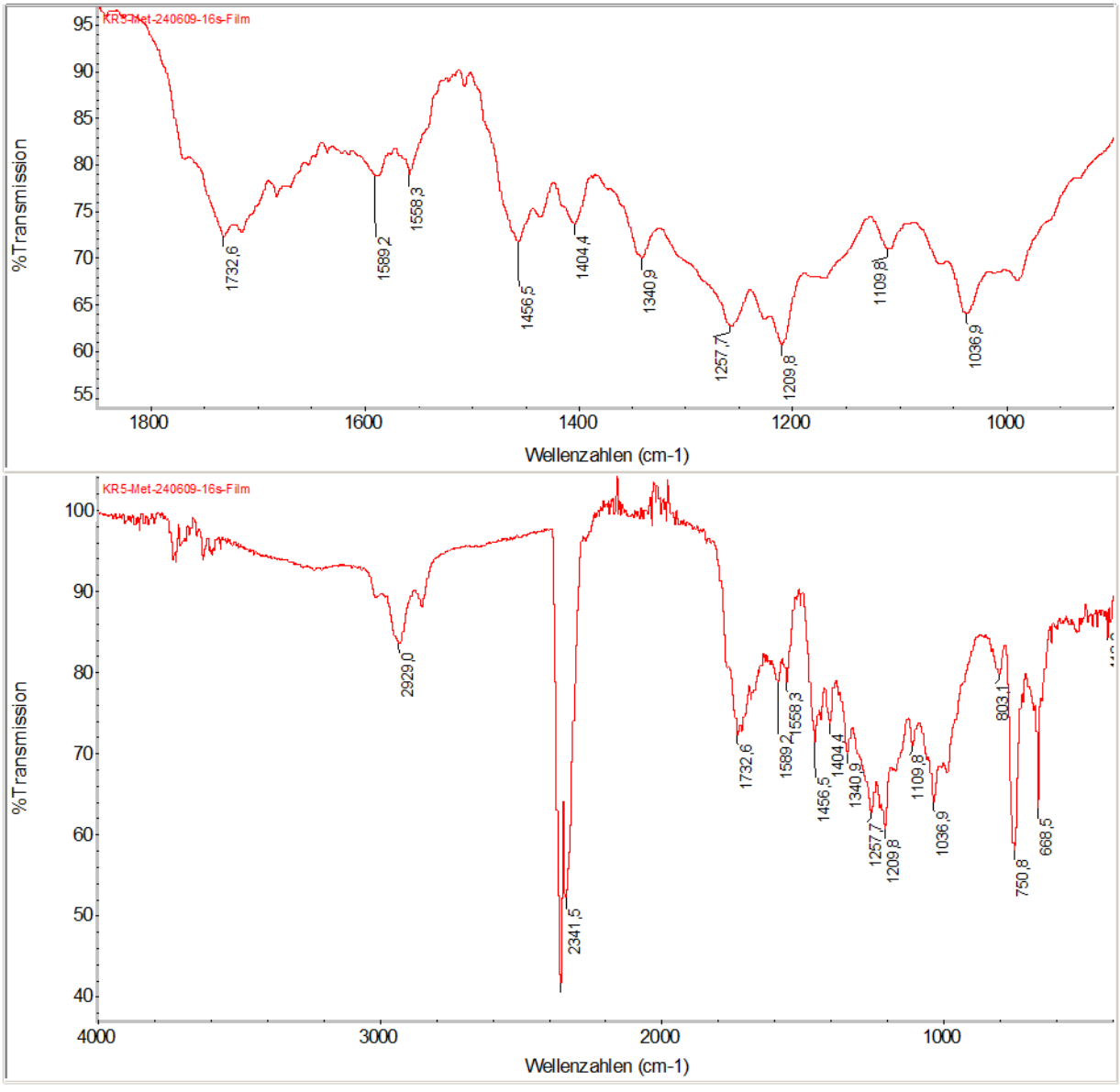

Figure 3.6 IR spectrum of secocollinone-1 (59).

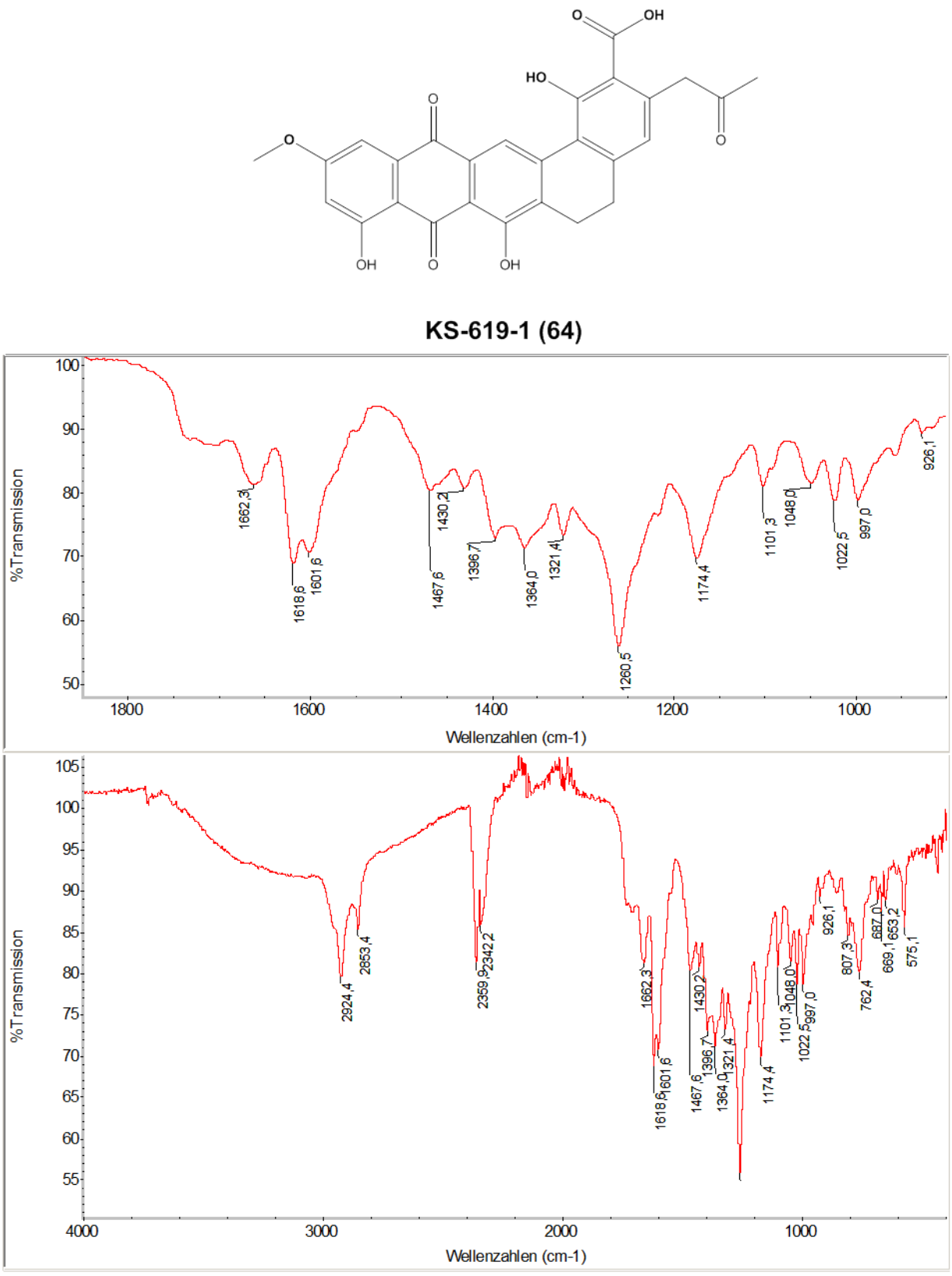

Figure 3.7 IR spectrum of KS-619-1 (64).

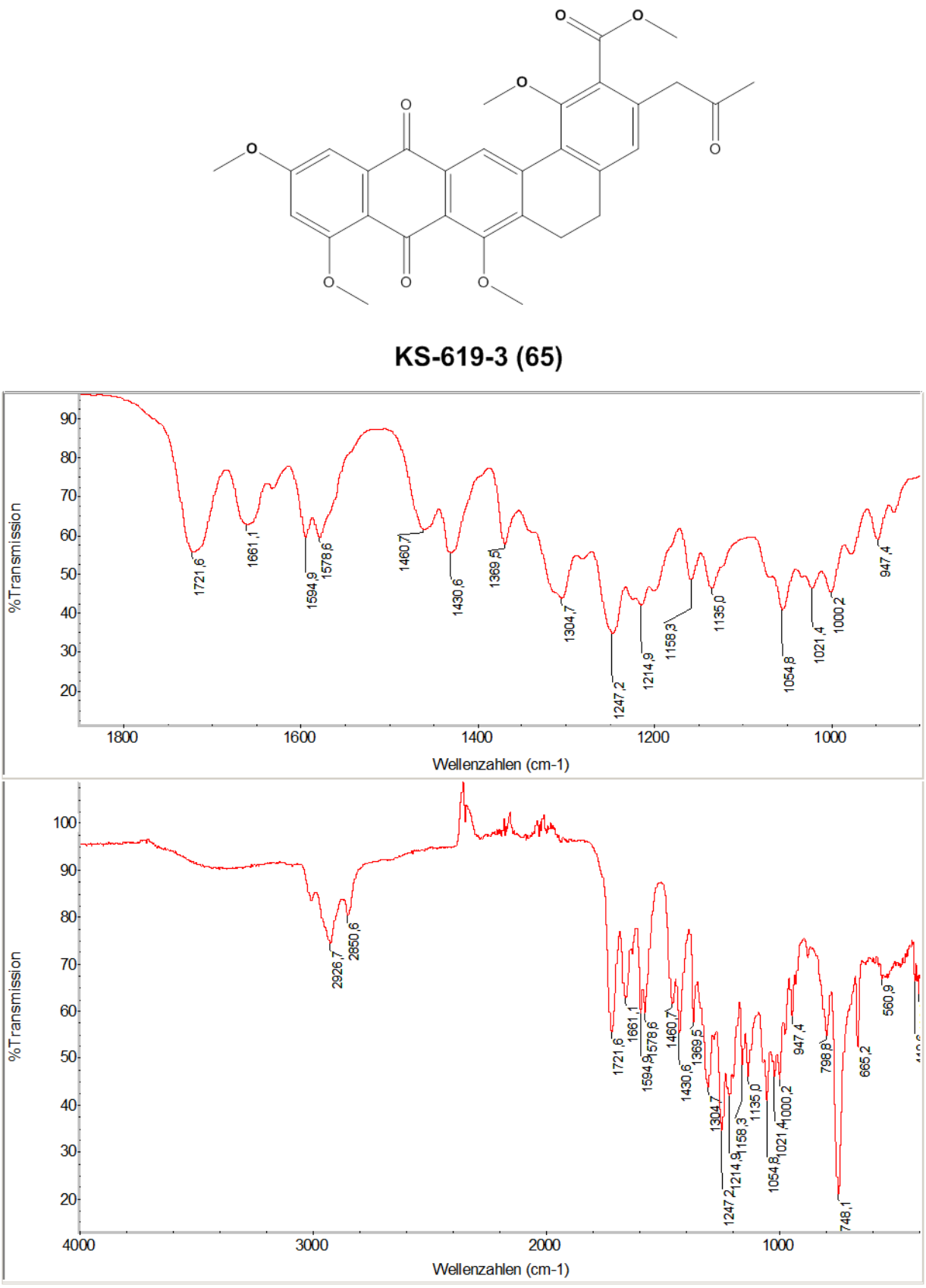

Figure 3.8 IR spectrum of KS-619-3 (65).

8 BIBLIOGRAPHY

(1) Olano, C.; Mendez, C.; Salas, J. A.: Antitumor compounds from marine actinomycetes. *Mar Drugs* **2009**, *7*, 210-48.

(2) Hopwood, D. A.: Cracking the polyketide code. *PLoS Biol* **2004**, *2*, E35.

(3) Wawrik, B.; Kerkhof, L.; Zylstra, G. J.; Kukor, J. J.: Identification of unique type II polyketide synthase genes in soil. *Appl Environ Microbiol* **2005**, *71*, 2232-8.

(4) Weber, T.; Welzel, K.; Pelzer, S.; Vente, A.; Wohlleben, W.: Exploiting the genetic potential of polyketide producing streptomycetes. *J Biotechnol* **2003**, *106*, 221-32.

(5) Thorson, J. S.; Sievers, E. L.; Ahlert, J.; Shepard, E.; Whitwam, R. E.; Onwueme, K. C.; Ruppen, M.: Understanding and exploiting nature's chemical arsenal: the past, present and future of calicheamicin research. *Curr Pharm Des* **2000**, *6*, 1841-79.

(6) Clardy, J.; Walsh, C.: Lessons from natural molecules. *Nature* **2004**, *432*, 829-37.

(7) Hopwood, D. A.; Khosla, C.: Genes for polyketide secondary metabolic pathways in microorganisms and plants. *Ciba Found Symp* **1992**, *171*, 88-106; discussion 106-12.

(8) Hill, A. M.: The biosynthesis, molecular genetics and enzymology of the polyketide-derived metabolites. *Nat Prod Rep* **2006**, *23*, 256-320.

(9) Minotti, G.; Menna, P.; Salvatorelli, E.; Cairo, G.; Gianni, L.: Anthracyclines: molecular advances and pharmacologic developments in antitumor activity and cardiotoxicity. *Pharmacol Rev* **2004**, *56*, 185-229.

(10) Schwecke, T.; Aparicio, J. F.; Molnar, I.; Konig, A.; Khaw, L. E.; Haydock, S. F.; Oliynyk, M.; Caffrey, P.; Cortes, J.; Lester, J. B.; et al.: The biosynthetic gene cluster for the polyketide immunosuppressant rapamycin. *Proc Natl Acad Sci U S A* **1995**, *92*, 7839-43.

(11) Rawlings, B. J.: Biosynthesis of polyketides. *Nat Prod Rep* **1997**, *14*, 523-56.

(12) Weissman, K. J.; Leadlay, P. F.: Combinatorial biosynthesis of reduced polyketides. *Nat Rev Microbiol* **2005**, *3*, 925-36.

(13) Birch, A. W.; Robinson, J. A.: Polyethers. *Biotechnology* **1995**, *28*, 443-76.

(14) Eckardt, K.; Tresselt, D.; Ihn, W.: The structure of the antibiotic griseorhodin C. *J Antibiot (Tokyo)* **1978**, *31*, 970-3.

(15) Li, A.; Piel, J.: A gene cluster from a marine Streptomyces encoding the biosynthesis of the aromatic spiroketal polyketide griseorhodin A. *Chem Biol* **2002**, *9*, 1017-26.

(16) Dewick, P.: Medicinal natural products. *Wiley*- **2005**, *Second Edition*.

(17) Shen, B.; Hutchinson, C. R.: Deciphering the mechanism for the assembly of aromatic polyketides by a bacterial polyketide synthase. *Proc Natl Acad Sci U S A* **1996**, *93*, 6600-4.

(18) Lai, J. R.; Koglin, A.; Walsh, C. T.: Carrier protein structure and recognition in polyketide and nonribosomal peptide biosynthesis. *Biochemistry* **2006**, *45*, 14869-79.

(19) Shen, B.: Polyketide biosynthesis beyond the type I, II and III polyketide synthase paradigms. *Curr Opin Chem Biol* **2003**, *7*, 285-95.

(20) Shen, B.: Biosynthesis of aromatic polyketides. In *Biosynthesis: Aromatic Polyketides, Isoprenoids, Alkaloids*, 2000; Vol. 209; pp 1-51.

(21) Moore, B. S.; Hertweck, C.: Biosynthesis and attachment of novel bacterial polyketide synthase starter units. *Nat Prod Rep* **2002**, *19*, 70-99.

(22) Khosla, C.; Tang, Y.; Chen, A. Y.; Schnarr, N. A.; Cane, D. E.: Structure and mechanism of the 6-deoxyerythronolide B synthase. *Annu Rev Biochem* **2007**, *76*, 195-221.

(23) Khosla, C.; Gokhale, R. S.; Jacobsen, J. R.; Cane, D. E.: Tolerance and specificity of polyketide synthases. *Annu Rev Biochem* **1999**, *68*, 219-53.

(24) Khosla, C.; Kapur, S.; Cane, D. E.: Revisiting the modularity of modular polyketide synthases. *Curr Opin Chem Biol* **2009**, *13*, 135-43.

(25) Leadlay, P. F.: Combinatorial approaches to polyketide biosynthesis. *Curr Opin Chem Biol* **1997**, *1*, 162-8.

(26) Katz, L.; Khosla, C.: Antibiotic production from the ground up. *Nature biotechnology* **2007**, *25*, 428-9.

(27) Hutchinson, C. R.; Kennedy, J.; Park, C.; Kendrew, S.; Auclair, K.; Vederas, J.: Aspects of the biosynthesis of non-aromatic fungal polyketides by iterative polyketide synthases. *Antonie Van Leeuwenhoek* **2000**, *78*, 287-95.

(28) Yabe, K.; Nakajima, H.: Enzyme reactions and genes in aflatoxin biosynthesis. *Appl Microbiol Biotechnol* **2004**, *64*, 745-55.

(29) Rudd, B. A.; Hopwood, D. A.: Genetics of actinorhodin biosynthesis by *Streptomyces coelicolor* A3(2). *J Gen Microbiol* **1979**, *114*, 35-43.

(30) Malpartida, F.; Hopwood, D. A.: Physical and genetic characterisation of the gene cluster for the antibiotic actinorhodin in *Streptomyces coelicolor* A3(2). *Mol Gen Genet* **1986**, *205*, 66-73.

(31) Sankaranarayanan, R.; Saxena, P.; Marathe, U. B.; Gokhale, R. S.; Shanmugam, V. M.; Rukmini, R.: A novel tunnel in mycobacterial type III polyketide synthase reveals the structural basis for generating diverse metabolites. *Nat Struct Mol Biol* **2004**, *11*, 894-900.

(32) Rawlings, B. J.: Biosynthesis of polyketides (other than actinomycete macrolides). *Nat Prod Rep* **1999**, *16*, 425-84.

(33) Hutchinson, C. R.: Drug synthesis by genetically engineered microorganisms. *Biotechnology (N Y)* **1994**, *12*, 375-80.

(34) Hopwood, D. A.; Malpartida, F.; Kieser, H. M.; Ikeda, H.; Duncan, J.; Fujii, I.; Rudd, B. A.; Floss, H. G.; Omura, S.: Production of 'hybrid' antibiotics by genetic engineering. *Nature* **1985**, *314*, 642-4.

(35) Malpartida, F.; Hallam, S. E.; Kieser, H. M.; Motamedi, H.; Hutchinson, C. R.; Butler, M. J.; Sugden, D. A.; Warren, M.; McKillop, C.; Bailey, C. R.; et al.: Homology between Streptomyces genes coding for synthesis of different polyketides used to clone antibiotic biosynthetic genes. *Nature* **1987**, *325*, 818-21.

(36) Hertweck, C.; Luzhetskyy, A.; Rebets, Y.; Bechthold, A.: Type II polyketide synthases: gaining a deeper insight into enzymatic teamwork. *Nat Prod Rep* **2007**, *24*, 162-90.

(37) Malpartida, F.; Hopwood, D. A.: Molecular cloning of the whole biosynthetic pathway of a Streptomyces antibiotic and its expression in a heterologous host. *Nature* **1984**, *309*, 462-4.

(38) Zhang, W.; Watanabe, K.; Wang, C. C.; Tang, Y.: Investigation of early tailoring reactions in the oxytetracycline biosynthetic pathway. *J Biol Chem* **2007**, *282*, 25717-25.

(39) Hutchinson, C. R.: Biosynthetic Studies of Daunorubicin and Tetracenomycin C. *Chem Rev* **1997**, *97*, 2525-2536.

(40) Thompson, T. B.; Katayama, K.; Watanabe, K.; Hutchinson, C. R.; Rayment, I.: Structural and functional analysis of tetracenomycin F2 cyclase from *Streptomyces glaucescens*. A type II polyketide cyclase. *J Biol Chem* **2004**, *279*, 37956-63.

(41) Lomovskaya, N.; Doi-Katayama, Y.; Filippini, S.; Nastro, C.; Fonstein, L.; Gallo, M.; Colombo, A. L.; Hutchinson, C. R.: The Streptomyces peucetius dpsY and dnrX genes govern early and late steps of daunorubicin and doxorubicin biosynthesis. *J Bacteriol* **1998**, *180*, 2379-86.

(42) Wendt-Pienkowski, E.; Huang, Y.; Zhang, J.; Li, B.; Jiang, H.; Kwon, H.; Hutchinson, C. R.; Shen, B.: Cloning, sequencing, analysis, and heterologous expression of the fredericamycin biosynthetic gene cluster from *Streptomyces griseus*. *J Am Chem Soc* **2005**, *127*, 16442-52.

(43) Lombo, F.; Menendez, N.; Salas, J. A.; Mendez, C.: The aureolic acid family of antitumor compounds: structure, mode of action, biosynthesis, and novel derivatives. *Appl Microbiol Biotechnol* **2006**, *73*, 1-14.

(44) Hultin, P. G.: Bioactive C-glycosides from bacterial secondary metabolism. *Curr Top Med Chem* **2005**, *5*, 1299-331.

(45) Xiang, L. K.; Kalaitzis, J. A.; Nilsen, G.; Chen, L.; Moore, B. S.: Mutational analysis of the enterocin Favorskii biosynthetic rearrangement. *Organic Letters* **2002**, *4*, 957-960.

(46) Piel, J.; Hertweck, C.; Shipley, P. R.; Hunt, D. M.; Newman, M. S.; Moore, B. S.: Cloning, sequencing and analysis of the enterocin biosynthesis gene cluster from the marine isolate '*Streptomyces maritimus*': evidence for the derailment of an aromatic polyketide synthase. *Chem Biol* **2000**, *7*, 943-55.

(47) Ishida, K.; Maksimenka, K.; Fritzsche, K.; Scherlach, K.; Bringmann, G.; Hertweck, C.: The boat-shaped polyketide resistoflavin results from re-facial central hydroxylation of the discoid metabolite resistomycin. *J Am Chem Soc* **2006**, *128*, 14619-24.

(48) Fritzsche, K.; Ishida, K.; Hertweck, C.: Orchestration of discoid polyketide cyclization in the resistomycin pathway. *J Am Chem Soc* **2008**, *130*, 8307-16.

(49) Das, A.; Khosla, C.: Biosynthesis of aromatic polyketides in bacteria. *Acc Chem Res* **2009**, *42*, 631-9.

(50) Dreier, J.; Khosla, C.: Mechanistic analysis of a type II polyketide synthase. Role of conserved residues in the beta-ketoacyl synthase-chain length factor heterodimer. *Biochemistry* **2000**, *39*, 2088-95.

(51) Xu, Z.; Metsa-Ketela, M.; Hertweck, C.: Ketosynthase III as a gateway to engineering the biosynthesis of antitumoral benastatin derivatives. *J Biotechnol* **2009**, *140*, 107-13.

(52) Xu, Z.; Schenk, A.; Hertweck, C.: Molecular analysis of the benastatin biosynthetic pathway and genetic engineering of altered fatty acid-

polyketide hybrids. *Journal of the American Chemical Society* **2007**, *129*, 6022-30.

(53) Kantola, J.; Blanco, G.; Hautala, A.; Kunnari, T.; Hakala, J.; Mendez, C.; Ylihonko, K.; Mantsala, P.; Salas, J.: Folding of the polyketide chain is not dictated by minimal polyketide synthase in the biosynthesis of mithramycin and anthracycline. *Chemistry & biology* **1997**, *4*, 751-5.

(54) Liu, W. C.; Parker, L.; Slusarchyk, S.; Greenwood, G. L.; Grahm, S. F.; Meyers, E.: Isolation, characterization, and structure of rabelomycin, a new antibiotic. *J Antibiot (Tokyo)* **1970**, *23*, 437-41.

(55) Yang, K.; Han, L.; Ayer, S. W.; Vining, L. C.: Accumulation of the angucycline antibiotic rabelomycin after disruption of an oxygenase gene in the jadomycin B biosynthetic gene cluster of *Streptomyces venezuelae*. *Microbiology* **1996**, *142 (Pt 1)*, 123-32.

(56) McDaniel, R.; Ebert-Khosla, S.; Hopwood, D. A.; Khosla, C.: Engineered biosynthesis of novel polyketides. *Science* **1993**, *262*, 1546-50.

(57) Jacobsen, J. R.; Hutchinson, C. R.; Cane, D. E.; Khosla, C.: Precursor-directed biosynthesis of erythromycin analogs by an engineered polyketide synthase. *Science* **1997**, *277*, 367-9.

(58) Blanco, G.; Fernandez, E.; Fernandez, M. J.; Brana, A. F.; Weissbach, U.; Kunzel, E.; Rohr, J.; Mendez, C.; Salas, J. A.: Characterization of two glycosyltransferases involved in early glycosylation steps during biosynthesis of the antitumor polyketide mithramycin by *Streptomyces argillaceus*. *Mol Gen Genet* **2000**, *262*, 991-1000.

(59) Lozano, M. J.; Remsing, L. L.; Quiros, L. M.; Brana, A. F.; Fernandez, E.; Sanchez, C.; Mendez, C.; Rohr, J.; Salas, J. A.: Characterization of two polyketide methyltransferases involved in the biosynthesis of the antitumor drug mithramycin by *Streptomyces argillaceus*. *The Journal of biological chemistry* **2000**, *275*, 3065-74.

(60) Rix, U.; Fischer, C.; Remsing, L. L.; Rohr, J.: Modification of post-PKS tailoring steps through combinatorial biosynthesis. *Nat Prod Rep* **2002**, *19*, 542-80.

(61) Blanco, G.; Patallo, E. P.; Brana, A. F.; Trefzer, A.; Bechthold, A.; Rohr, J.; Mendez, C.; Salas, J. A.: Identification of a sugar flexible glycosyltransferase from *Streptomyces olivaceus*, the producer of the antitumor polyketide elloramycin. *Chemistry & biology* **2001**, *8*, 253-63.

(62) Shen, B.; Hutchinson, C. R.: Enzymatic synthesis of a bacterial polyketide from acetyl and malonyl coenzyme A. *Science* **1993**, *262*, 1535-40.

(63) Xiang, L.; Kalaitzis, J. A.; Moore, B. S.: EncM, a versatile enterocin biosynthetic enzyme involved in Favorskii oxidative rearrangement, aldol condensation, and heterocycle-forming reactions. *Proc Natl Acad Sci U S A* **2004**, *101*, 15609-14.

(64) Kendrew, S. G.; Hopwood, D. A.; Marsh, E. N.: Identification of a monooxygenase from *Streptomyces coelicolor* A3(2) involved in biosynthesis of actinorhodin: purification and characterization of the recombinant enzyme. *J Bacteriol* **1997**, *179*, 4305-10.

(65) Chaiyen, P.: Flavoenzymes catalyzing oxidative aromatic ring-cleavage reactions. *Arch Biochem Biophys* **2010**, *493*, 62-70.

(66) Mallick, S.; Chakraborty, J.; Dutta, T. K.: Role of oxygenases in guiding diverse metabolic pathways in the bacterial degradation of low-

molecular-weight polycyclic aromatic hydrocarbons: a review. *Crit Rev Microbiol* **2011**, *37*, 64-90.

(67) Bugg, T. D. H.: Introduction to enzyme and coenzyme chemistry 2nd ed. *Blackwell Publishing: Oxford* **2007**.

(68) Prado, L.; Lombo, F.; Brana, A. F.; Mendez, C.; Rohr, J.; Salas, J. A.: Analysis of two chromosomal regions adjacent to genes for a type II polyketide synthase involved in the biosynthesis of the antitumor polyketide mithramycin in *Streptomyces argillaceus*. *Mol Gen Genet* **1999**, *261*, 216-25.

(69) Gibson, M.; Nur-e-alam, M.; Lipata, F.; Oliveira, M. A.; Rohr, J.: Characterization of kinetics and products of the Baeyer-Villiger oxygenase MtmOIV, the key enzyme of the biosynthetic pathway toward the natural product anticancer drug mithramycin from *Streptomyces argillaceus*. *J Am Chem Soc* **2005**, *127*, 17594-5.

(70) Rix, U.; Wang, C.; Chen, Y.; Lipata, F. M.; Remsing Rix, L. L.; Greenwell, L. M.; Vining, L. C.; Yang, K.; Rohr, J.: The oxidative ring cleavage in jadomycin biosynthesis: a multistep oxygenation cascade in a biosynthetic black box. *Chembiochem : a European journal of chemical biology* **2005**, *6*, 838-45.

(71) Pfeifer, B. A.; Khosla, C.: Biosynthesis of polyketides in heterologous hosts. *Microbiol Mol Biol Rev* **2001**, *65*, 106-18.

(72) Kieser, T., Bibb, M. J., Buttner, M.J., Chater, K. F., Hopwood: *Practical streptomyces genetics*; **2000,** The John Innes Foundation: Norwich, England.

(73) http://microbewiki.kenyon.edu/index.php/Streptomyces.

(74) Flardh K; Buttner MJ. Streptomyces morphogenetics: dissecting differentiation in a filamentous bacterium. *Nat Rev Microbiol,* **2009,** 7, 36-49

(75) Paradkar, A.; Trefzer, A.; Chakraburtty, R.; Stassi, D.: Streptomyces genetics: a genomic perspective. *Crit Rev Biotechnol* **2003**, *23*, 1-27.

(76) Hopwood, D. A.; Chater, K. F.; Bibb, M. J.: Genetics of antibiotic production in *Streptomyces coelicolor* A3(2), a model streptomycete. *Biotechnology* **1995**, *28*, 65-102.

(77) Hutchinson, C. R.; Fujii, I.: Polyketide synthase gene manipulation: a structure-function approach in engineering novel antibiotics. *Annu Rev Microbiol* **1995**, *49*, 201-38.

(78) McArthur M; Bibb MJ. Manipulating and understanding antibiotic production in *Streptomyces coelicolor* A3(2) with decoy oligonucleotides. Proc Natl Acad Sci U S A, **2008**, 105,1020-5.

(79) Malpartida, F.; Hopwood, D. A.: Molecular cloning of the whole biosynthetic pathway of a Streptomyces antibiotic and its expression in a heterologous host. 1984. *Biotechnology* **1992**, *24*, 342-3.

(80) Grimm, A.; Madduri, K.; Ali, A.; Hutchinson, C. R.: Characterization of the *Streptomyces peucetius* ATCC 29050 genes encoding doxorubicin polyketide synthase. *Gene* **1994**, *151*, 1-10.

(81) Kendrew, S. G.; Katayama, K.; Deutsch, E.; Madduri, K.; Hutchinson, C. R.: DnrD cyclase involved in the biosynthesis of doxorubicin: purification and characterization of the recombinant enzyme. *Biochemistry* **1999**, *38*, 4794-9.

(82) Omura, S.; Ikeda, H.; Malpartida, F.; Kieser, H. M.; Hopwood, D. A.: Production of new hybrid antibiotics, mederrhodins A and B, by a genetically engineered strain. *Antimicrob Agents Chemother* **1986**, *29*, 13-9.

(83) Tsoi, C. J.; Khosla, C.: Combinatorial biosynthesis of 'unnatural' natural products: the polyketide example. *Chem Biol* **1995**, *2*, 355-62.

(84) Floss, H. G.: Combinatorial biosynthesis--potential and problems. *J Biotechnol* **2006**, *124*, 242-57.

(85) Hutchinson, C. R.: Combinatorial biosynthesis for new drug discovery. *Curr Opin Microbiol* **1998**, *1*, 319-29.

(86) Oki, T.; Tenmyo, O.; Hirano, M.; Tomatsu, K.; Kamei, H.: Pradimicins A, B and C: new antifungal antibiotics. II. In vitro and in vivo biological activities. *J Antibiot (Tokyo)* **1990**, *43*, 763-70.

(87) Nicholson, T. P.; Winfield, C.; Westcott, J.; Crosby, J.; Simpson, T. J.; Cox, R. J.: First in vitro directed biosynthesis of new compounds by a minimal type II polyketide synthase: evidence for the mechanism of chain length determination. *Chem Commun (Camb)* **2003**, 686-7.

(88) Palmu, K.; Ishida, K.; Mantsala, P.; Hertweck, C.; Metsa-Ketela, M.: Artificial reconstruction of two cryptic angucycline antibiotic biosynthetic pathways. *Chembiochem* **2007**, *8*, 1577-84.

(89) Mendez, C.; Weitnauer, G.; Bechthold, A.; Salas, J. A.: Structure alteration of polyketides by recombinant DNA technology in producer organisms--prospects for the generation of novel pharmaceutical drugs. *Curr Pharm Biotechnol* **2000**, *1*, 355-95.

(90) McDaniel, R.; Ebert-Khosla, S.; Fu, H.; Hopwood, D. A.; Khosla, C.: Engineered biosynthesis of novel polyketides: influence of a downstream enzyme on the catalytic specificity of a minimal aromatic polyketide synthase. *Proc Natl Acad Sci U S A* **1994**, *91*, 11542-6.

(91) Thibodeaux, C. J.; Melancon, C. E.; Liu, H. W.: Unusual sugar biosynthesis and natural product glycodiversification. *Nature* **2007**, *446*, 1008-16.

(92) Salas, J. A.; Mendez, C.: Engineering the glycosylation of natural products in actinomycetes. *Trends Microbiol* **2007**, *15*, 219-32.

(93) Bechthold, A.; Weitnauer, G.; Luzhetskyy, A.; Berner, M.; Bihlmeier, C.; Boll, R.; Durr, C.; Frerich, A.; Hofmann, C.; Mayer, A.; Treede, I.; Vente, A.; Luzhetskyy, M.: Glycosyltransferases and other tailoring enzymes as tools for the generation of novel compounds. *Ernst Schering Res Found Workshop* **2005**, 147-63.

(94) Pelzer, S.; Wohlert, S. E.; Vente, A.: Tool-box: tailoring enzymes for bio-combinatorial lead development and as markers for genome-based natural product lead discovery. *Ernst Schering Res Found Workshop* **2005**, 233-59.

(95) Abel, U.; Simon, W.; Eckard, P.; Hansske, F. G.: Design and semisynthesis of novel fredericamycin A derivatives with an improved antitumor profile. *Bioorg Med Chem Lett* **2006**, *16*, 3292-7.

(96) Goldman, M. E.; Salituro, G. S.; Bowen, J. A.; Williamson, J. M.; Zink, D. L.; Schleif, W. A.; Emini, E. A.: Inhibition of human immunodeficiency virus-1 reverse transcriptase activity by rubromycins: competitive interaction at the template.primer site. *Mol Pharmacol* **1990**, *38*, 20-5.

(97) Ueno, T.; Takahashi, H.; Oda, M.; Mizunuma, M.; Yokoyama, A.; Goto, Y.; Mizushina, Y.; Sakaguchi, K.; Hayashi, H.: Inhibition of human telomerase by rubromycins: implication of spiroketal system of the compounds as an active moiety. *Biochemistry* **2000**, *39*, 5995-6002.

(98) Puder, C. L., S.; Hizi, A.; Zeeck, A.: Structural and biosynthetic investigations of the rubromycins. *Eur. J. Org. Chem.* **2000**, 729 -735.

(99) Yunt, Z.; Reinhardt, K.; Li, A.; Engeser, M.; Dahse, H. M.; Gutschow, M.; Bruhn, T.; Bringmann, G.; Piel, J.: Cleavage of four carbon-carbon bonds during biosynthesis of the griseorhodin a spiroketal pharmacophore. *J Am Chem Soc* **2009**, *131*, 2297-305.

(100) Brockmann, H.; Zeeck, A.: [Rubromycins. 3. The constitution of alpha-rubromycin, beta-rubromycin, gamma-rubromycin, and gamma-iso-rubromycin]. *Chem Ber* **1970**, *103*, 1709-26.

(101) Brockmann, H.; Lenk, W.; Schwantje, G.; Zeeck, A.: [The structure of rubromycin]. *Tetrahedron Lett* **1966**, *30*, 3525-30.

(102) Brockmann, H.; Lenk, W.; Schwantje, G.; Zeeck, A.: [Rubromycin II]. *Chem Ber* **1969**, *102*, 126-51.

(103) Bringmann, G. K., J.; Schmitt, U.; Puder, C.; Zeeck, A. : Determination of the absolute configurations of γ-rubromycin and related spiro compounds by quantum chemical CD calculations. . *Eur. J. Org. Chem.* **2000**, 2729-2734.

(104) Rathwell, D. C.; Yang, S. H.; Tsang, K. Y.; Brimble, M. A.: An efficient formalsynthesis of the humantelomerase inhibitor (+/-)-gamma-rubromycin. *Angew Chem Int Ed Engl* **2009**.

(105) Lowell, A. N.; Fennie, M. W.; Kozlowski, M. C.: A concise synthesis of the naphthalene portion of purpuromycin. *J Org Chem* **2008**, *73*, 1911-8.

(106) Akai, S.; Kakiguchi, K.; Nakamura, Y.; Kuriwaki, I.; Dohi, T.; Harada, S.; Kubo, O.; Morita, N.; Kita, Y.: Total synthesis of (+/-)-gamma-rubromycin on the basis of two aromatic Pummerer-type reactions. *Angew Chem Int Ed Engl* **2007**, *46*, 7458-61.

(107) Xie, X.; Kozlowski, M. C.: Synthesis of the naphthalene portion of the rubromycins. *Org Lett* **2001**, *3*, 2661-3.

(108) Tamiya, M.; Ohmori, K.; Kitamura, M.; Kato, H.; Arai, T.; Oorui, M.; Suzuki, K.: General synthesis route to benanomicin-pradimicin antibiotics. *Chemistry* **2007**, *13*, 9791-823.

(109) Martin, R.; Sterner, O.; Alvarez, M. A.; de Clercq, E.; Bailey, J. E.; Minas, W.: Collinone, a new recombinant angular polyketide antibiotic made by an engineered Streptomyces strain. *J Antibiot (Tokyo)* **2001**, *54*, 239-49.

(110) Lackner, G.; Schenk, A.; Xu, Z.; Reinhardt, K.; Yunt, Z. S.; Piel, J.; Hertweck, C.: Biosynthesis of pentangular polyphenols: deductions from the benastatin and griseorhodin pathways. *Journal of the American Chemical Society* **2007**, *129*, 9306-12.

(111) Treibs, W. E., K. : Über Griseorhodin A, ein neues rotes Antibiotikum aus Actinomyceten. . *Die Naturwissenschaften* **1961**, *48,*, 430.

(112) Eckardt, K. T., D.; Schönecker, B.: Zur Stereochemie der Griseorhodin. *Tetrahedron* **1979**, *35*, 1621-1624.

(113) Tresselt, D. E., K.; Ihn, W. : Antibiotika aus Actinomyceten. Zur chemischen Konstitution des Antibiotikums Griseorhodin A: II. Ableitung der Struktur. . *Tetrahedron* **1978**, *34*, 2693-2699.

(114) Bate, N.; Stratigopoulos, G.; Cundliffe, E.: Differential roles of two SARP-encoding regulatory genes during tylosin biosynthesis. *Molecular microbiology* **2002**, *43*, 449-58.

(115) Suwa, M.; Sugino, H.; Sasaoka, A.; Mori, E.; Fujii, S.; Shinkawa, H.; Nimi, O.; Kinashi, H.: Identification of two polyketide synthase gene clusters on the linear plasmid pSLA2-L in Streptomyces rochei. *Gene* **2000**, *246*, 123-31.

(116) Trefzer, A.; Pelzer, S.; Schimana, J.; Stockert, S.; Bihlmaier, C.; Fiedler, H. P.; Welzel, K.; Vente, A.; Bechthold, A.: Biosynthetic gene cluster of simocyclinone, a natural multihybrid antibiotic. *Antimicrobial agents and chemotherapy* **2002**, *46*, 1174-82.

(117) Ichinose, K.; Bedford, D. J.; Tornus, D.; Bechthold, A.; Bibb, M. J.; Revill, W. P.; Floss, H. G.; Hopwood, D. A.: The granaticin biosynthetic gene cluster of *Streptomyces violaceoruber* Tu22: sequence analysis and expression in a heterologous host. *Chem Biol* **1998**, *5*, 647-59.

(118) Mao, Y.; Varoglu, M.; Sherman, D. H.: Molecular characterization and analysis of the biosynthetic gene cluster for the antitumor antibiotic mitomycin C from *Streptomyces lavendulae* NRRL 2564. *Chemistry & biology* **1999**, *6*, 251-63.

(119) Haigler, B. E.; Suen, W. C.; Spain, J. C.: Purification and sequence analysis of 4-methyl-5-nitrocatechol oxygenase from *Burkholderia* sp. strain DNT. *Journal of bacteriology* **1996**, *178*, 6019-24.

(120) Prado, L.; Fernandez, E.; Weissbach, U.; Blanco, G.; Quiros, L. M.; Brana, A. F.; Mendez, C.; Rohr, J.; Salas, J. A.: Oxidative cleavage of premithramycin B is one of the last steps in the biosynthesis of the antitumor drug mithramycin. *Chemistry & biology* **1999**, *6*, 19-30.

(121) Taguchi, T.; Itou, K.; Ebizuka, Y.; Malpartida, F.; Hopwood, D. A.; Surti, C. M.; Booker-Milburn, K. I.; Stephenson, G. R.; Ichinose, K.: Chemical characterisation of disruptants of the *Streptomyces coelicolor* A3(2) actVI genes involved in actinorhodin biosynthesis. *J Antibiot (Tokyo)* **2000**, *53*, 144-52.

(122) Decker, H.; Haag, S.: Cloning and characterization of a polyketide synthase gene from Streptomyces fradiae Tu2717, which carries the genes for biosynthesis of the angucycline antibiotic urdamycin A and a gene probably involved in its oxygenation. *J Bacteriol* **1995**, *177*, 6126-36.

(123) Summers, R. G.; Wendt-Pienkowski, E.; Motamedi, H.; Hutchinson, C. R.: Nucleotide sequence of the tcmII-tcmIV region of the tetracenomycin C biosynthetic gene cluster of *Streptomyces glaucescens* and evidence that the tcmN gene encodes a multifunctional cyclase-dehydratase-O-methyl transferase. *J Bacteriol* **1992**, *174*, 1810-20.

(124) Dairi, T.; Hamano, Y.; Igarashi, Y.; Furumai, T.; Oki, T.: Cloning and nucleotide sequence of the putative polyketide synthase genes for pradimicin biosynthesis from *Actinomadura hibisca*. *Biosci Biotechnol Biochem* **1997**, *61*, 1445-53.

(125) Reinhardt, K.: Griaeorhodin A: Biosynthesestudien und kombinatorische Biosynthese. Dissertation, Universität Bonn, 2009.

(126) Suetsuna, K.: Structural elucidation of dideoxygriseorhodin-C, a red pigment produced by microbe, and Utility as Pigment-Peptide Complex. *J Jpn Soc Food Sci* **1990**, *37*, 7-14.

(127) Suetsuna, K.; Osajima, Y.: Isolation of structure of dideoxy-griseorhodin-C produced by a *Streptomyces* Sp. *Agr Biol Chem Tokyo* **1989**, *53*, 241-242.

(128) Suetsuna, K.; Seino, A.; Kudo, T.; Osajima, Y.: Production, and biological characterization, of dideoxygriseorhodin-C by a *Streptomyces Sp* and its taxonomy. *Agr Biol Chem Tokyo* **1989**, *53*, 581-583.

(129) Ikeda, H.; Ishikawa, J.; Hanamoto, A.; Shinose, M.; Kikuchi, H.; Shiba, T.; Sakaki, Y.; Hattori, M.; Omura, S.: Complete genome sequence and comparative analysis of the industrial microorganism *Streptomyces avermitilis*. *Nat Biotechnol* **2003**, *21*, 526-31.

(130) Ichinose, K.; Ozawa, M.; Itou, K.; Kunieda, K.; Ebizuka, Y.: Cloning, sequencing and heterologous expression of the medermycin biosynthetic gene cluster of *Streptomyces sp.* AM-7161: towards comparative analysis of the benzoisochromanequinone gene clusters. *Microbiology* **2003**, *149*, 1633-45.

(131) Fernandez-Moreno, M. A.; Martinez, E.; Caballero, J. L.; Ichinose, K.; Hopwood, D. A.; Malpartida, F.: DNA sequence and functions of the actVI region of the actinorhodin biosynthetic gene cluster of *Streptomyces coelicolor* A3(2). *J Biol Chem* **1994**, *269*, 24854-63.

(132) Guengerich, F. P.: Cytochrome P450 oxidations in the generation of reactive electrophiles: epoxidation and related reactions. *Arch Biochem Biophys* **2003**, *409*, 59-71.

(133) Grüschow, S. S., D. H.: *Aziridinnes and Epoxides in Organic Synthesis*; Wiley-VCH: Weinheim, Germany, 2006.

(134) Shah, S.; Xue, Q.; Tang, L.; Carney, J. R.; Betlach, M.; McDaniel, R.: Cloning, characterization and heterologous expression of a polyketide synthase and P-450 oxidase involved in the biosynthesis of the antibiotic oleandomycin. *J Antibiot (Tokyo)* **2000**, *53*, 502-8.

(135) He, J.; Muller, M.; Hertweck, C.: Formation of the aureothin tetrahydrofuran ring by a bifunctional cytochrome p450 monooxygenase. *J Am Chem Soc* **2004**, *126*, 16742-3.

(136) Buhler, B.; Park, J. B.; Blank, L. M.; Schmid, A.: NADH availability limits asymmetric biocatalytic epoxidation in a growing recombinant *Escherichia coli* strain. *Applied and environmental microbiology* **2008**, *74*, 1436-46.

(137) Martin, R.; Sterner, O.; Alvarez, M. A.; de Clercq, E.; Bailey, J. E.; Minas, W.: Collinone, a new recombinant angular polyketide antibiotic made by an engineered Streptomyces strain. *J Antibiot (Tokyo)* **2001**, *54*, 239-49.

(138) Leungsakul, T.; Johnson, G. R.; Wood, T. K.: Protein engineering of the 4-methyl-5-nitrocatechol monooxygenase from *Burkholderia sp*. strain DNT for enhanced degradation of nitroaromatics. *Applied and environmental microbiology* **2006**, *72*, 3933-9.

(139) Shen, B.; Hutchinson, C. R.: Triple hydroxylation of tetracenomycin A2 to tetracenomycin C in *Streptomyces glaucescens*. Overexpression of the tcmG gene in *Streptomyces lividans* and characterization of the tetracenomycin A2 oxygenase. *The Journal of biological chemistry* **1994**, *269*, 30726-33.

(140) Leungsakul, T.; Keenan, B. G.; Mori, M. A.; Morton, M. D.; Stuart, J. D.; Smets, B. F.; Wood, T. K.: Oxidation of aminonitrotoluenes by 2,4-DNT dioxygenase of *Burkholderia sp.* strain DNT. *Biotechnol Bioeng* **2006**, *93*, 231-7.

(141) Lombo, F.; Blanco, G.; Fernandez, E.; Mendez, C.; Salas, J. A.: Characterization of *Streptomyces argillaceus* genes encoding a polyketide

synthase involved in the biosynthesis of the antitumor mithramycin. *Gene* **1996**, *172*, 87-91.

(142) Daum, M.; Peintner, I.; Linnenbrink, A.; Frerich, A.; Weber, M.; Paululat, T.; Bechthold, A.: Organisation of the biosynthetic gene cluster and tailoring enzymes in the biosynthesis of the tetracyclic quinone glycoside antibiotic polyketomycin. *Chembiochem : a European journal of chemical biology* **2009**, *10*, 1073-83.

(143) Menendez, N.; Nur-e-Alam, M.; Brana, A. F.; Rohr, J.; Salas, J. A.; Mendez, C.: Biosynthesis of the antitumor chromomycin A3 in *Streptomyces griseus*: analysis of the gene cluster and rational design of novel chromomycin analogs. *Chemistry & biology* **2004**, *11*, 21-32.

(144) Beam, M. P.; Bosserman, M. A.; Noinaj, N.; Wehenkel, M.; Rohr, J.: Crystal structure of Baeyer-Villiger monooxygenase MtmOIV, the key enzyme of the mithramycin biosynthetic pathway. *Biochemistry* **2009**, *48*, 4476-87.

(145) Peric-Concha, N.; Borovicka, B.; Long, P. F.; Hranueli, D.; Waterman, P. G.; Hunter, I. S.: Ablation of the otcC gene encoding a post-polyketide hydroxylase from the oxytetracyline biosynthetic pathway in *Streptomyces rimosus* results in novel polyketides with altered chain length. *J Biol Chem* **2005**, *280*, 37455-60.

(146) Eppink, M. H.; Boeren, S. A.; Vervoort, J.; van Berkel, W. J.: Purification and properties of 4-hydroxybenzoate 1-hydroxylase (decarboxylating), a novel flavin adenine dinucleotide-dependent monooxygenase from *Candida parapsilosis* CBS604. *Journal of bacteriology* **1997**, *179*, 6680-7.

(147) Gu, L.; Geders, T. W.; Wang, B.; Gerwick, W. H.; Hakansson, K.; Smith, J. L.; Sherman, D. H.: GNAT-like strategy for polyketide chain initiation. *Science* **2007**, *318*, 970-4.

(148) Piel, J.; Wen, G.; Platzer, M.; Hui, D.: Unprecedented diversity of catalytic domains in the first four modules of the putative pederin polyketide synthase. *Chembiochem : a European journal of chemical biology* **2004**, *5*, 93-8.

(149) H. Falk, T. N. H. T.: Synthesis and Properties of an w,w'-Appendend Eighteen Carbon Chains Hypercin Derivative. *Monatshefte für Chemie* **1996**, *127*, 717-723.

(150) Chen, Y.; Luo, Y.; Ju, J.; Wendt-Pienkowski, E.; Rajski, S. R.; Shen, B.: Identification of fredericamycin E from Streptomyces griseus: Insights into fredericamycin A biosynthesis highlighting carbaspirocycle formation. *J Nat Prod* **2008**, *71*, 431-7.

(151) Oliynyk, M.; Samborskyy, M.; Lester, J. B.; Mironenko, T.; Scott, N.; Dickens, S.; Haydock, S. F.; Leadlay, P. F.: Complete genome sequence of the erythromycin-producing bacterium *Saccharopolyspora erythraea* NRRL23338. *Nature biotechnology* **2007**, *25*, 447-53.

(152) Chen, Y.; Wendt-Pienkoski, E.; Rajski, S. R.; Shen, B.: In vivo investigation of the roles of FdmM and FdmM1 in fredericamycin biosynthesis unveiling a new family of oxygenases. *J Biol Chem* **2009**, *284*, 24735-43.

(153) Yasuzawa, T.; Yoshida, M.; Shirahata, K.; Sano, H.: Structure of a novel Ca^{2+} and calmodulin-dependent cyclic nucleotide phosphodiesterase inhibitor KS-619-1. *J Antibiot (Tokyo)* **1987**, *40*, 1111-4.

(154) Kim, B. C.; Lee, J. M.; Ahn, J. S.; Kim, B. S.: Cloning, sequencing, and characterization of the pradimicin biosynthetic gene cluster of *Actinomadura hibisca* P157-2. *Journal of microbiology and biotechnology* **2007**, *17*, 830-9.

(155) Chen, Y.; Wendt-Pienkowski, E.; Ju, J.; Lin, S.; Rajski, S. R.; Shen, B.: Characterization of FdmV as an amide synthetase for fredericamycin A biosynthesis in Streptomyces griseus ATCC 43944. *J Biol Chem* **2010**, *285*, 38853-60.

(156) Hu, Y.; Phelan, V.; Ntai, I.; Farnet, C. M.; Zazopoulos, E.; Bachmann, B. O.: Benzodiazepine biosynthesis in *Streptomyces refuineus*. *Chemistry & biology* **2007**, *14*, 691-701.

(157) Zhan, J.; Watanabe, K.; Tang, Y.: Synergistic actions of a monooxygenase and cyclases in aromatic polyketide biosynthesis. *Chembiochem : a European journal of chemical biology* **2008**, *9*, 1710-5.

(158) Wang, C.; Gibson, M.; Rohr, J.; Oliveira, M. A.: Crystallization and X-ray diffraction properties of Baeyer-Villiger monooxygenase MtmOIV from the mithramycin biosynthetic pathway in *Streptomyces argillaceus*. *Acta Crystallogr Sect F Struct Biol Cryst Commun* **2005**, *61*, 1023-6.

(159) Weir, M. P.; Bethell, S. S.; Cleasby, A.; Campbell, C. J.; Dennis, R. J.; Dix, C. J.; Finch, H.; Jhoti, H.; Mooney, C. J.; Patel, S.; Tang, C. M.; Ward, M.; Wonacott, A. J.; Wharton, C. W.: Novel natural product 5,5-trans-lactone inhibitors of human alpha-thrombin: mechanism of action and structural studies. *Biochemistry* **1998**, *37*, 6645-57.

(160) Bauer, A. W.; Kirby, W. M.; Sherris, J. C.; Turck, M.: Antibiotic susceptibility testing by a standardized single disk method. *American journal of clinical pathology* **1966**, *45*, 493-6.

(161) Bauer, A. W.; Kirby, W. M.; Sherris, J. C.; Turck, M.: Antibiotic susceptibility testing by a standardized single disk method. *Tech Bull Regist Med Technol* **1966**, *36*, 49-52.

(162) Duthie, S. J.; Collins, A. R.; Duthie, G. G.; Dobson, V. L.: Quercetin and myricetin protect against hydrogen peroxide-induced DNA damage (strand breaks and oxidised pyrimidines) in human lymphocytes. *Mutat Res* **1997**, *393*, 223-31.

(163) Skaper, S. D.; Fabris, M.; Ferrari, V.; Dalle Carbonare, M.; Leon, A.: Quercetin protects cutaneous tissue-associated cell types including sensory neurons from oxidative stress induced by glutathione depletion: cooperative effects of ascorbic acid. *Free radical biology & medicine* **1997**, *22*, 669-78.

(164) Sergediene, E.; Jonsson, K.; Szymusiak, H.; Tyrakowska, B.; Rietjens, I. M.; Cenas, N.: Prooxidant toxicity of polyphenolic antioxidants to HL-60 cells: description of quantitative structure-activity relationships. *FEBS letters* **1999**, *462*, 392-6.

(165) Menon, L. G.; Kuttan, R.; Kuttan, G.: Inhibition of lung metastasis in mice induced by B16F10 melanoma cells by polyphenolic compounds. *Cancer letters* **1995**, *95*, 221-5.

(166) Yanez, J.; Vicente, V.; Alcaraz, M.; Castillo, J.; Benavente-Garcia, O.; Canteras, M.; Teruel, J. A.: Cytotoxicity and antiproliferative activities of several phenolic compounds against three melanocytes cell lines: relationship between structure and activity. *Nutr Cancer* **2004**, *49*, 191-9.

(167) Bravo, L.: Polyphenols: chemistry, dietary sources, metabolism, and nutritional significance. *Nutrition reviews* **1998**, *56*, 317-33.

(168) Hooper, N. M.: *Proteases in biology and medicine*; Portland Press: London, 2002.

(169) Hedstrom, L.: Serine protease mechanism and specifitcity. *Chem Rev* **2002**, *102*, 4501-4523.

(170) Chen, H.; Zheng, D.; Davids, J.; Bartee, M. Y.; Dai, E.; Liu, L.; Petrov, L.; Macaulay, C.; Thoburn, R.; Sobel, E.; Moyer, R.; McFadden, G.; Lucas, A.: Viral serpin therapeutics from concept to clinic. *Methods Enzymol* **2011**, *499*, 301-29.

(171) Bieth, J. G.: [The elastases]. *J Soc Biol* **2001**, *195*, 173-9.

(172) Estacio, S. G.; Moreira, R.; Guedes, R. C.: Characterizing the dynamics and ligand-specific interactions in the human leukocyte elastase through molecular dynamics simulations. *J Chem Inf Model* **2011**, *51*, 1690-1702.

(173) Gu, Y.; Lee, H. M.; Simon, S. R.; Golub, L. M.: Chemically modified tetracycline-3 (CMT-3): A novel inhibitor of the serine proteinase, elastase. *Pharmacological research : the official journal of the Italian Pharmacological Society* **2011**.

(174) Clark, C. A.; Thomas, L. K.; Azghani, A. O.: Inhibition of PKC Attenuates Pseudomonas aeruginosa Elastase-induced Epithelial Barrier Disruption. *American journal of respiratory cell and molecular biology* **2011**.

(175) Lopez, P.; Hornung, A.; Welzel, K.; Unsin, C.; Wohlleben, W.; Weber, T.; Pelzer, S.: Isolation of the lysolipin gene cluster of *Streptomyces tendae* Tu 4042. *Gene* **2010**, *461*, 5-14.

(176) Panzone, G.; Trani, A.; Ferrari, P.; Gastaldo, L.; Colombo, L.: Isolation and structure elucidation of 7,8-dideoxy-6-oxo-griseorhodin C produced by *Actinoplanes ianthinogenes*. *J Antibiot (Tokyo)* **1997**, *50*, 665-70.

9 PUBLIKATIONEN

Vortrag

Naturstoffe: Chemie, Biologie und Ökologie: 36. Doktorandenworkshop
10. Oktober 2008, Universität Würzburg
Titel: Biosynthesestudien des Telomeraseinhibitors Griseorhodin A

Veröffentlichungen

Lackner, G.; Schenk, A.; Xu, Z.; Reinhardt, K.; Yunt, Z. S.; Piel, J.; Hertweck, C. Biosynthesis of pentangular polyphenols: deductions from the benastatin and griseorhodin pathways. *J. Am. Chem. Soc.* **2007,** 129, 9306-9312.

Yunt, Z.; Reinhardt, K.; Li, A.; Engeser, M.; Dahse, H.-M.; Gütschow, M.; Bruhn, T.; Bringmann, G.; Piel, J. Cleavage of four carbon-carbon bonds during biosynthesis of the griseorhodin A spiroketal pharmacophore. *J. Am. Chem. Soc.* **2009,** 131, 2297-2305.

Posterpräsentationen

VAAM International Workshop:
4.-6. Oktober 2007, Nonnweiler
Yunt, Z. S.; Reinhardt, K.; Eklund, M.; Xu, Z.; Hertweck, C.; Bruhn, T.; Bringmann, G.; Piel, J.
Titel: Unusual oxidoreductases involved in pharmacophore generation oft he aromatic polyketide griseorhodin A

VAAM International Workshop:
29. September -1. Oktober 2008, Berlin
Reinhardt, K.; Yunt, Z. S.; Engeser, M.; Bruhn, T., Bringmann, G.; Piel, J.
Titel: New insights into the biosynthesis of the griseorhodin A pharmacophore

21. Irseer Naturstofftage:
25.-27. Februar 2009, Irsee
Yunt, Z. S.; Reinhardt, K.; Eklund, M.; Xu, Z.; Hertweck, C.; Bruhn, T.; Bringmann, G.; Piel, J.

Titel: Insights into the biosynthesis of the unusual aromatic polyketide griseorhodin A

6th European Conference on Marine Natural Products:

19.-23. Juli 2009, Porto, Portugal

Reinhardt, K.; Yunt, Z. S.; Eklund, M.; Xu, Z.; Hertweck, C.; Bruhn, T.; Bringmann, G.; Piel, J.

Titel: Griseorhodin A: Biosynthetic Studies and Combinatorial Biosynthesis